NASA TM X- *70812*

APPLICATIONS TECHNOLOGY SATELLITE
ATS-6
EXPERIMENT CHECK-OUT AND CONTINUING
SPACECRAFT EVALUATION REPORT

DECEMBER 1974

GSFC ———— GODDARD SPACE FLIGHT CENTER ————
GREENBELT, MARYLAND

For information concerning availability
of this document contact:

Technical Information Division, Code 250
Goddard Space Flight Center
Greenbelt, Maryland 20771

(Telephone 301–982–4488)

APPLICATIONS TECHNOLOGY SATELLITE

ATS-6

EXPERIMENT CHECK-OUT AND CONTINUING SPACECRAFT

EVALUATION REPORT

DECEMBER 1974

GODDARD SPACE FLIGHT CENTER

Greenbelt, Maryland

APPLICATIONS TECHNOLOGY SATELLITE

ATS-6

EXPERIMENT CHECK-OUT AND CONTINUING SPACECRAFT

EVALUATION REPORT

Prepared by:

In-Depth Analysis Group

W. Moore (Fairchild)
Publication Coordinator

W. Prensky (Fairchild)
Technical Editor

Concurrence:

M. Nachman (Fairchild)
Deputy Director, ATS
Systems Engineering

R. Bartlett (GSFC)
In-Depth Analysis Manager

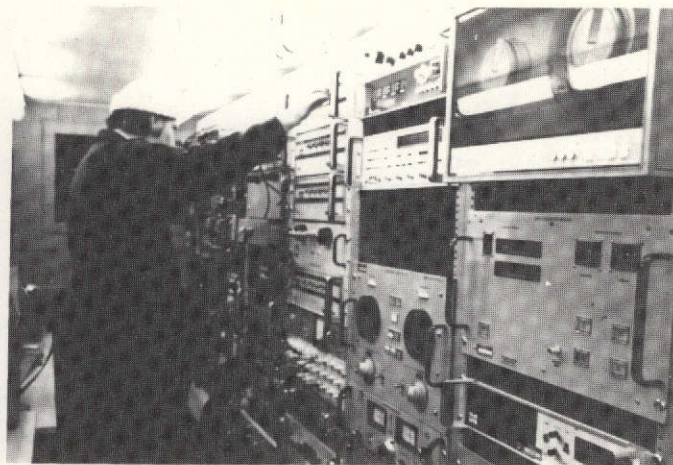PRECEDING PAGE BLANK NOT FILMED

Approved by:

K. Kissin (GSFC)
Mission Operations Director

P. Corrigan (GSFC)
Experiments Manager

Health and Hygiene Lecture for Remote Area in Alaska

Direct Satellite Communications to Isolated Ships at Sea

Improved Aircraft Navigation, Communications and Safety

Medical Services and Training for Rural Areas Via Satellite

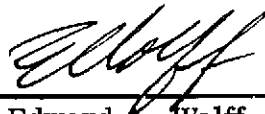Frontispiece — ATS-6, Serving Humanity

PREFACE

ATS-6 has now been on station and operational for several months. The task before us now is to conduct the experimentation on the spacecraft with emphasis on utilization. Based on the spacecraft's performance to date, it seems highly probable that several years of spacecraft operation past the two years design goal are possible.

With this in mind, planning is now under way to explore the uses to which this instrument can be put during its additional years of service. Maximum return in science, technology, and human service will be the goal of this activity.

Because of the flexibility of the spacecraft's design and particularly that of the communications subsystem, many radio, television, and data transmission experiments, which were not originally planned, are possible. ATS-6 represents a unique national asset which will pay substantial dividends. Therefore, it is now incumbant upon us to maximize the return.

Dr. James E. Kupperian
Application Technology Satellite
Project Manager

Dr. Edward A. Wolff
Application Technology Satellite
Project Scientist

APPLICATIONS TECHNOLOGY SATELLITE

ATS-6

EXPERIMENT CHECK-OUT AND CONTINUING

SPACECRAFT EVALUATION REPORT

PRECEDING PAGE BLANK NOT FILMED

FOREWORD

This is the third in a series of reports on the orbital operations of ATS-6 pre-
pared by the In-Depth Analysis (IDA) group. The first two reports were "ATS-6
First Orbit Evaluation," GSFC-X-713-74-177 and "Application Technology
Satellite ATS-6 In-Orbit Checkout Report," GSFC-X-460-74-232.

This report begins a series of quarterly evaluations dealing with the operation
and scheduling of the spacecraft under the direction of Mr. K. Kissin and the
operation and coordination of the scientific and technological experiments under
the direction of Mr. P. Corrigan. The period of time covered by this report
runs from July 1, 1974 through September 30, 1974. Subsequent quarterly reports
will add new spacecraft and experiment evaluations and, if need be, malfunction
analyses. This concept will be extended each quarter for two years resulting in
a series of reports which will be a comprehensive document on the mission of
ATS-6.

Spacecraft performance for the first quarter has been excellent. The only in-
stance of malfunction necessitating the employment of redundant hardware
occurred in the Spacecraft Propulsion subsystem where backup valve heaters
were activated on July 31, 1974 after the SPS 2 primary valve heater circuit
failed.

Four experiments have experienced anomalies. The University of New Hampshire
(UNH) proton measurement experiment generated electromagnetic interference
both times it was operated. Operation of this experiment has been suspended.
One ion engine has been operated, but it was unable to restart after its initial
thrusting. Neither the ion engine or the UNH experiment has yet met its experi-
ment objective. The very high resolution radiometer has ceased to operate, but
its experiment objective was met prior to its failure. One of four travelling
wave tubes in the millimeter wave experiment has failed. However, the experi-
menter is confident that the bulk of the experiment objective can still be met.

The material presented on experiments was either authored or edited by the
following experiment personnel. Since the ATS Project Office is solely re-
sponsible for the operation of the spacecraft and coordination of spacecraft
experimentation, the evaluation of each experiment and the material presented
on each experiment is solely the responsibility of these experimenters.

Experiments	Principal Investigator	Co-Experimenter
AFTE	J. Kirkpatrick (ARS)	P. Brennan (B & K)
ASTP	L. Nicholson	P. Westmoreland (JSC)
Comsat Propagation	G. Hyde (Comsat)	L. King
EME	R. Wales	
Aerospace	G. Paulikas*	
HAC	W. Dunkerly*	
McD	A. Masley*	
NOAA	T. Fritz*	
UCLA	P. Coleman*	R. McPherron*
UCSD	C. McIlwain*	S. DeForest*
U. of Minn.	J. Winckler*	
UNH	R. Arnoldy*	
HET	A. Horley** (DHEW)	E. Volkmer***
Ion Engine	R. Hunter	R. Bartlett
		E. James (EOS)
		R. Worlock (EOS)
MMW	L. Ippolito	A. Straiton (U. of Texas)
		D. Hodge (Ohio)
		C. Bostian (VPI)
		E. Hirschmann
PLACE	A. Ghais	D. Brandel
		D. Brown (ESRO)
		B. Chriswell (USCG)
		J. Chinniek (Canada Dept. Comm.)
		H. Feigleson (Maritime)
		J. Gutwein (DOT)
		R. Hilton (FAA)
QCMB	J. Rogers	
Radio Beacon	K. Davies (NOAA)	R. Grubb (NOAA)
Radiometer	W. Shenk	J. Goldberg
		A. McCulloch
RFI	V. Henry	
SAPPSAC	W. Isley	
SITE	J. Miller	
TDRE (Nimbus)	F. Von Bun	B. Trudell, J. Brown, P. Schmidt

All personnel are located at NASA, Goddard Space Flight Center unless otherwise noted.

*The EME experimenters are from their respective organizations.
**Chairman of Users Committee, no principal investigator.
***Operations Coordinator.

EXPERIMENTER ORGANIZATIONS

AEROSPACE	Aerospace Corporation
ARS	Ames Research Center
B & K	B & K Engineering Inc.
CANADA DPT. COMM.	Canadian Department of Communications
COMSAT	Comsat Corporation
DHEW	Department of Health, Education and Welfare
DOT	Department of Transportation
EOS	Electro-Optical Systems, Division of Xerox Corp.
ESRO	European Spaec Research Organization
FAA	Federal Aviation Administration
HAC	Hughes Aircraft Corporation
JSC	Johnson Space Center
MARITIME	Maritime Administration
McD	McDonnell – Douglas Aircraft Corporation
NOAA	National Oceanic and Atmospheric Administration
OHIO	Ohio State University
UCLA	University of California, Los Angeles
UCSD	University of California, San Diego
UNH	University of New Hampshire
USCG	United States Coast Guard
U of TEX.	University of Texas
VPI	Virginia Polytechnic Institute and State University

The in-depth analysis (IDA) group is responsible for the evaluation of space-craft subsystem performance and generation of resulting documentation. This includes long-term trends and analysis of anomalies as they occur. The members of the IDA group contributing to this report are the following:

FAIRCHILD

J. Blue
P. DeBaylo
M. Frieder
F. Gorsen
D. Heinbuch
R. Karam
W. King
R. Pattishall
W. Sawyer
R. Schrieb
H. Solt
J. Spitzer
J. Wilson

GODDARD

L. Nicholson

OAO Corporation

S. Millikin

Westinghouse

R. Baldridge
H. Hanft
M. Geller

CONTENTS

CONTENTS (Continued)

SECTION 2
REPORT SUMMARIES

CONTENTS (Continued)

SECTION 3
STRUCTURAL SUBSYSTEM

CONTENTS (Continued)

CONTENTS (Continued)

SECTION 8
SPACECRAFT PROPULSION SUBSYSTEM

CONTENTS (Continued)

SECTION 9
COMMUNICATION SUBSYSTEM

CONTENTS (Continued)

CONTENTS (Continued)

CONTENTS (Continued)

SECTION 16
GEOSYNCHRONOUS VERY HIGH RESOLUTION RADIOMETER

SECTION 17
ION ENGINE EXPERIMENT

CONTENTS (Continued)

SECTION 18
ENVIRONMENTAL MEASUREMENTS EXPERIMENTS

SECTION 19
TRACKING AND DATA RELAY EXPERIMENT

CONTENTS (Continued)

SECTION 20
HEALTH EDUCATIONAL TELEVISION EXPERIMENT

SECTION 21
C-BAND RADIO FREQUENCY INTERFERENCE
MEASUREMENT EXPERIMENT

CONTENTS (Continued)

SECTION 22
SATELLITE INSTRUCTIONAL TELEVISION EXPERIMENT
AND
TELEVISION RELAY USING SMALL TERMINALS

SECTION 23
POSITION LOCATION AND AIRCRAFT
COMMUNICATION EXPERIMENT

CONTENTS (Continued)

SECTION 24
RADIO BEACON EXPERIMENT

SECTION 25
SPACECRAFT ATTITUDE PRECISION
POINTING AND SLEWING ADAPTIVE CONTROL

CONTENTS (Continued)

SECTION 1

INTRODUCTION

SECTION 1

INTRODUCTION

1.1 INTRODUCTION

The ATS-6 spacecraft (Figure 1-1), designated as ATS-F prior to launch, was designed and built by the Fairchild Space and Electronics Company, Germantown, Maryland, as prime contractor to the Goddard Space Flight Center, Greenbelt, Maryland, in compliance with NASA Contract NAS5-21100. Other members of the prime team include:

> Philco-Ford, Western Development Labs Division, Palo Alto, California (communications module);
>
> IBM, Gaithersburg, Md. (telemetry, interferometer, and command system);
>
> Honeywell Aerospace Division, St. Petersburg, Fla. (attitude control system);
>
> Lockheed Missile Space Center, Sunnyvale, Calif. (nine-meter parabolic reflector); and
>
> Rocket Research Corp., Redmond, Washington (propulsion system).

Following the completion of the ground test program and launch operations at the Kennedy Space Flight Center, the spacecraft was successfully inserted into synchronous orbit on May 30, 1974 and commenced operations in accordance with its mission plan. The primary purpose of the ATS-6 spacecraft is to evaluate a variety of new space communications concepts requiring the use of a geo-synchronous spacecraft. This involves deployment of a 30 ft diameter parabolic antenna in space, three-axis stabilization and the ability to utilize the high gain of the antenna through accurate pointing and stability.

1.2 PURPOSE

The purpose of this report is to describe the activities of the ATS-6 spacecraft for the 90 day period between July 1, 1974 and September 30, 1974 and to present the results of performance evaluation of its subsystems and experiments.
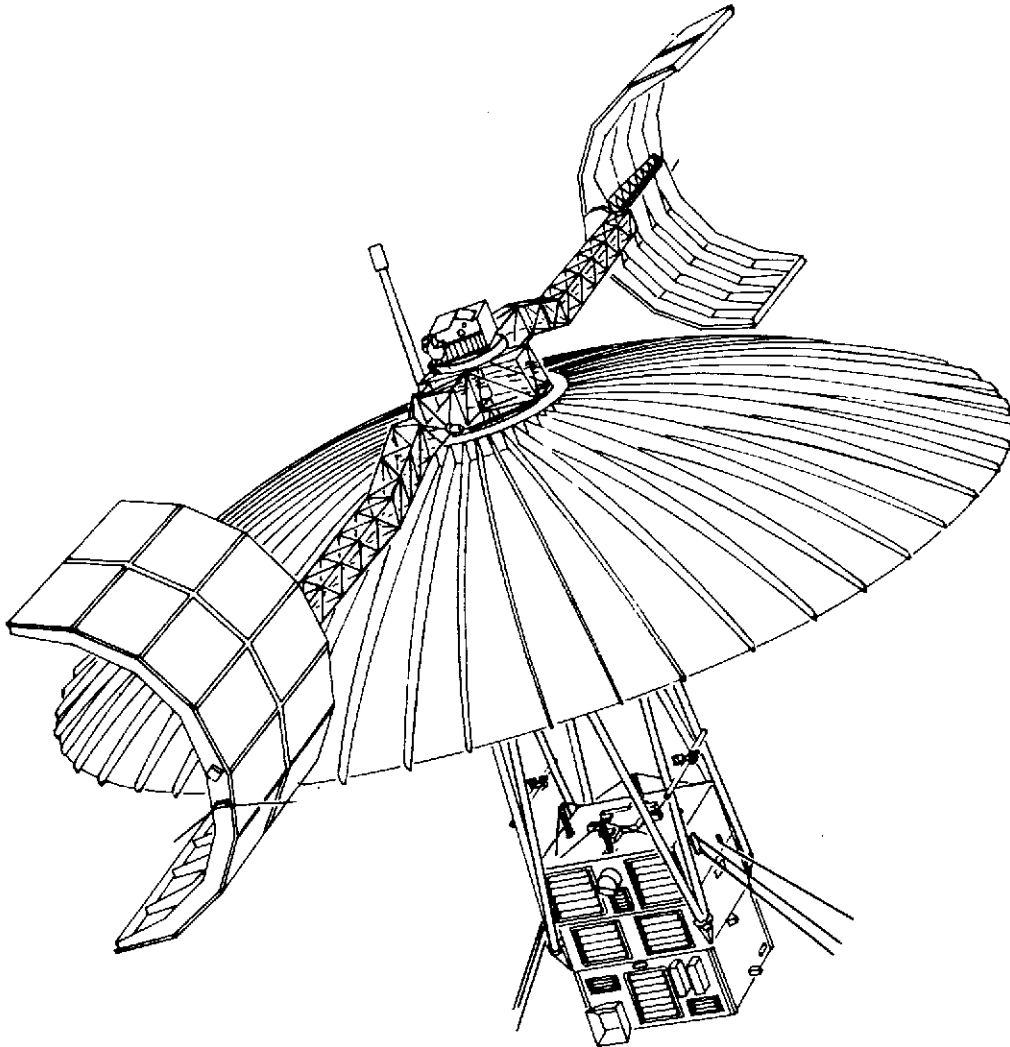
Figure 1-1. ATS-6 Spacecraft

1.3 SCOPE

The scope of this report includes the evaluation of all ATS-6 spacecraft subsystems and components with evaluation of experiments.

1.4 HISTORY OF THE ATS PROGRAM

Prior to development of the Applications Technology Satellite (ATS) program, NASA conducted extensive research with communications satellites at low, intermediate, and synchronous orbital altitudes. These spacecraft included passive reflectors such as the 33-meter (100-foot) diameter Echo balloons and active repeaters such as the Relay and Syncom spacecraft.

Upon the completion of these programs, an Advanced Syncom study was conducted to determine the next step to be taken in communications spacecraft. The ATS program was based on the results of this study and incorporated a number of Syncom techniques. These included spin-stabilized configurations with multi-frequency capability.

The first phase of the ATS program included the development, launch, and utilization of five spin-and gravity gradient-stabilized spacecraft, four of which were to be placed in geostationary orbit. Communication satellites operating from this altitude view about 45 percent of the globe as compared to a 320-kilometer (200-mile) orbit spacecraft which views only about three percent of the globe at one time.

ATS-6 is the next logical step in the program and continues and extends the scope of the experiments conducted by ATS-1 through 5.

ATS-1 (ATS-B before launch)

This spin-stabilized, synchronous-altitude satellite was the first ATS to be launched. Soon after its lift-off on December 7, 1966, from Cape Kennedy, Fla., the satellite was maneuvered into its permanent position over the Pacific Ocean and all its systems checked out as fully operational. Since then, all the experiments have been sending a steady stream of data back to the ground stations. A wide variety of services have been performed by ATS-1 in addition to the large number of technological and scientific experiments.

Educational broadcasting to both Alaska and the Pacific Basin is currently being done through ATS-1. Included are college-level seminars and courses at both primary and secondary levels.

ATS-2 (ATS-A before launch)

The second satellite in the ATS series was launched from Cape Kennedy on April 6, 1967. It was intended that this gravity-gradient-stabilized spacecraft be placed in a medium altitude orbit inclined to Earth's equator, so that it would continuously circle the Earth. A failure in the fuel supply system of the Agena rocket prevented the booster from re-igniting at the crucial point in the satellite trajectory, and the satellite went into a highly elliptical orbit. Large forces, caused by the severe decelerations occurring in this very irregular orbit, proved more than the gravity-gradient stabilization system could overcome, and as a result ATS-2 slowly tumbled and rotated. All the systems and experiments onboard functioned as well as possible under these conditions. The spacecraft reentered Earth's atmosphere on September 2, 1969, and was destroyed.

ATS-3 (ATS-C before launch)

The third satellite in the series, a spin-stabilized spacecraft, was put into synchronous orbit on November 6, 1967, from Cape Kennedy. After a perfect launch, it took up its station over the Atlantic Ocean, and all systems have been operating as expected since then.

A significant achievement of this satellite was the first ground-to-spacecraft-to-aircraft communications link over the Atlantic. This historic event took place on November 21, 1967, during a Pan American flight from New York to London.

Probably the most notable achievement of ATS-3 was its sending the first color photograph of Earth in space, obtained from the multicolor spin-scan cloud camera. Another camera on ATS-3, the image dissector camera (IDCS), also obtained many cloud photographs. The spacecraft continues to monitor severe storms.

ATS-4 (ATS-D before launch)

ATS-4 was a gravity-gradient spacecraft launched from Cape Kennedy on August 10, 1968. The Centaur second ignition was never accomplished. As a result, the spacecraft, with Centaur and apogee motor attached, was left in an approximately 100 by 400 nautical mile orbit. Turn-on of all systems and experiments was accomplished; however, little useful data were obtained because of the extreme anomalistic conditions. ATS-4 reentered Earth's atmosphere and was destroyed on October 17, 1968.

ATS-5 (ATS-E before launch)

ATS-5, another gravity-gradient spacecraft, was launched from Cape Kennedy on August 12, 1969. It has contributed much technical and scientific information although it was not de-spun and therefore never stabilized by the Earth's gravity-gradient.

The auroral particles experiments on ATS-5 have now been operating successfully since 1969 and are continuing to provide a large quantity of useful data.

The NASA/GSFC L-band ranging and position location experiments, being conducted from the Mojave ground station to the ATS-5 satellite, have demonstrated the ability to obtain meaningful range measurements using phase modulation/tone modulation at L-band frequencies.

1.5 SUMMARY OF EXPERIMENTS

The experiments performed with the ATS-6 spacecraft can be divided into four types based upon the objectives of the experiment. These types are: scientific, technological, communications and meteorological. In some cases the experiment is conducted using experiment-unique equipment on-board the spacecraft and in others the experiment utilizes common elements of the spacecraft subsystems. A summary of the experiments conducted with ATS-6 is given in Table 1-1.

1.6 SCIENTIFIC EXPERIMENTS

1.6.1 Environmental Measurements Experiments (EME)

The Environmental Measurements Experiment (EME) package is a group of eight experiments carried onboard the ATS-6 that are designed to study the spacecraft environments of synchronous altitude and to gain information on electromagnetic-ionospheric interactions. Six of the experiments are designed to obtain data on charged particles of several different types and over wide energy ranges. A seventh experiment is to provide magnetic field data, to be used in conjunction with the charged particle measurements to determine the dynamic processes which take place in the synchronous orbit environment. The eighth experiment is a study of solar cell degradation.

The EME will be operated during the entire mission. The scientific data obtained by the experiment will be recorded daily by the ATS ground stations with possible support by STADAN. Data obtained will be recorded at the ground station, processed at GSFC, and sent to the individual experimenters. Also, attitude data and orbital ephemeris data will be provided to EME experimenters to aid in analysis of their data.

1.6.1.1 Low-Energy Proton-Electron Experiment—The low-energy proton-electron experiment measures electrons whose energy is from 2 kev to 25 kev in eleven differential energy windows and proton energy from 20 kev to 500 kev at two differential pitch angles. More specific objectives are:

    a.   To make high-resolution electron measurements for those particles that mirror near the equatorial plane.

    b.   To make a two-point sample of the pitch angle distribution for electrons and protons once every second.

    c.   To study local time dependence of observations.

Table 1-1

ATS-6 Experiments

Experiment	Type of Experiment	Major Objectives
GVHRR	Meteorological	Measure cloud cover Determine wind field Ocean temperatures earth resources
RFI	Communications	Investigate C-band terrestrial noise sources (geographical/noise power distribution)
MMW	Communications	Investigation of atmospheric propagation at MMW frequencies. Feasibility of the application of MMW communications systems
Radio Beacon	Scientific	Ionospheric/exospheric electron content measurements. Study of ionospheric propagation effects
EME	Scientific	Particle measurements. Magnetic field measurement. Solar cell degradation.
SAPPSAC	Technological	Investigation of computer controlled attitude control performance optimization
TRUST	Communications	To advance state-of-the-art in space communications by demonstrating CCIR quality wideband signaling between ATS-6 and inexpensive ground stations
SITE	Communications	To demonstrate the relay by geosynchronous satellite of CCIR quality television from a high-powered program transmitting station to small modified standard TV receivers located throughout rural India and to urban rebroadcast stations.
PLACE	Communications	To develop improved air traffic control communications and techniques
T&DRE	Communications	To demonstrate technology necessary for an operational tracking and data relay satellite system
Cesium Bombardment Ion Engine	Technological	Verify and obtain data on ion microthruster propulsion system. Demonstrate thrust vectoring for attitude control.
COMSAT (13- and 18-GHz)	Technological	Collect data on attenuation due to precipitation. Determine power margins needed in spacecraft communications systems.

Table 1-1 (Cont'd)

ATS-6 Experiments

Experiment	Type of Experiment	Major Objectives
HET	Communications	To evaluate a system that will permit relay of television programs through the satellite to facilities such as schools, CATV systems, and cities.
ATFE	Technological	To evaluate the performance of an advanced thermal control system and to demonstrate its effectiveness in stabilizing temperatures of spacecraft components.
QCM	Technological	To provide data on extremely small mass accretions on the surface of the spacecraft.

d. To study intensity time fluctuations of low-energy electrons and protons when an enhanced solar wind might push the subsolar magnetospheric boundary into the geostationary orbit.

e. To correlate the ATS data with ground, balloon, and rocket studies.

1.6.1.2 Low-Energy Protons Experiment—The low-energy proton experiment measures protons from 20 to 300 kev in six energy ranges. Also, it is the purpose of the experiment to answer the following very important questions:

a. Where in local time are the protons injected into the magnetosphere?

b. Do the protons in the far outer belt follow L in their drift or are they affected by electric fields which permit them to enter and leave the magnetosphere?

c. How closely in time is the injection of protons associated with auroral substorms?

1.6.1.3 Solar Cosmic Ray Experiment—The general objective of this experiment is to conduct a basic study of solar cosmic rays, their entry and propagation within the magnetosphere, and to measure detailed parameters of trapped electrons, both as functions of local time in orbit. Each measurement is performed at two different pitch angles. The measurements will be made with sufficient detail, energy resolution, dynamic intensity range, and time resolution to allow several studies during the period following maximum solar cosmic ray activity. Some of the specific objectives are to:

a) Investigate the mechanism by which low-energy solar cosmic rays gain entry and propagate within the magnetosphere.

b) Investigate the mechanism responsible for cutoff variations during geomagnetic activity.

c) Use the data as a test to evaluate and to improve a recently developed magnetospheric model which includes the tilt of the dipole axis to the solar wind.

d) Compare the time history and development of solar cosmic ray events at $L = 6.6$ Re to the Douglas observatories in the Northern and Southern Polar regions.

e) Study the behavior of trapped electrons as a function of local time and geomagnetic activity in the ATS orbit.

f) Directly compare spectral and intensity changes between two families of particles which traverse vastly different regions of the magnetosphere in order to investigate acceleration and propagation processes during geomagnetic activity and during quiet periods.

Energy ranges are, for alpha particles 1.2 Mev to 180 Mev, for protons 0.2 Mev to 300 Mev and for electrons 50 kev to 800 kev.

1.6.1.4 Auroral Particles Experiment—The scientific objectives of the experiment are as follows:

a) Map the distribution of low-energy (50 ev - 50 kev) electrons and protons on a constant line of force so that correlation studies between these particle fluxes and the visible aurora can be conducted to determine the nature of the accelerating mechanism in the magnetosphere.

b) Make studies of the rapid time variation of the shape of the spectra and location of any peaks in the particle distribution.

c) Compare ATS-6 data with that from other spacecraft.

d) Make detailed studies of the energy balance between particles and fields at their location and relate it to the magnetosphere as a whole.

1.6.1.5 Particle Acceleration Measurements Experiment—The objective of the Particle Acceleration Measurement Experiment is to investigate the origin of the Van Allen trapped radiation. Measurements of the intensity and time variations

of protons and electrons in the vicinity of the synchronous orbit, and detailed analysis of these variations in their relationships to polar and magnetic storms and other perturbations of the magnetosphere will further the knowledge of magnetospheric dynamics of acceleration and modulation processes in several ways:

a) Establish, in a more direct manner, the existence or nonexistence at the geostationary orbit of certain rapidly varying electron fluxes commonly observed in precipitated fluxes.

b) Study the role the protons of these energies play in the dynamics that produce large fluxes of energetic electrons.

c) Study the pitch angle distribution characteristics of protons and electrons during the various modulated activities, such as the quasi-periodic pulsation activity.

d) Study more precisely the dynamic variables that may be affected in transit from the equator to the auroral zone.

Energy ranges are for protons 20 kev to 500 kev and for electrons 20 to 40 kev, 100 to 200 kev, and 1 to 1.5 Mev.

1.6.1.6 Magnetometer Experiment—The primary objective of the Magnetometer Experiment is the study of the magnetic field at synchronous distances along the three orthogonal axes of the spacecraft. The specific goals are as follows:

a) Study the properties of various magnetohydrodynamic phenomena in the magnetosphere, the magnetospheric tail, and the magnetosheath.

b) Study the interaction of the solar wind with the magnetosphere and the magnetospheric tail.

c) Study the properties of the magnetospheric boundary or magnetopause.

d) Study the properties of the magnetosheath.

1.6.1.7 Solar Cell Radiation Damage Experiment—The objective of this experiment is directed primarily toward isolating the predominant degradation mechanism(s) associated with current production solar cells and eliminating anomalous data through increased data points and instrumentation accuracy. A total of 80 solar cells will be individually monitored on the flight experiment with a total of 12 current-voltage points and temperature data for each solar cell transmitted to ground on a real-time basis. Five solar cells of 16 types have been included to provide a statistically meaningful sample size.

1.6.1.8 Omnidirectional Spectrometer Experiment—The purpose of this experiment is to measure the omnidirectional fluxes and spectra of electrons and protons. Four detectors will count protons from 2 or 3 to 10 Mev, 10 to 21 Mev, 20 to 40 Mev, and 40 to 80 Mev. They will also count, respectively, electrons of energies greater than 80 kev and 250 kev, 600 kev, 1.2 Mev, and greater than 4 Mev.

1.6.2 Radio Beacon Experiment (RBE)

The radio beacon experiment (RBE) provides a multifrequency spacecraft-to-ground radio link for investigating particles which affect radio propagation beyond the atmosphere.

There are three carrier frequencies: 40.0160 MHz, 140.0164 MHz and 360.1440 MHz. All radio signals are derived from a common oscillator. Amplitude modulation frequencies are 100 kHz on the 40-MHz and 360-MHz signals, and 1000 kHz on the 40-MHz and 140-MHz signals. The phase reference for the modulation signals is the 100-kHz modulation on the 360.1440-MHz carrier.

The beacon is designed for several types of measurements, principally: Faraday rotation, differential phase (Doppler), phase and amplitude scintillation, and signal amplitude (absorption). Absorption measurements will have to be made on the 40-MHz signal. The other types of measurements are possible with the beacon as presently conceived. The mode of operation calls for continuous emission on all frequencies.

All beacon signals are linearly polarized. Since the spacecraft is attitude controlled, it is possible to define the orientation of the emitted polarization. Differential Faraday measurements are possible using carriers and sidebands.

The phase stability of all modulation signals is ±1°. Correspondingly, when reorienting the satellite, the interferometric effect of displaced phase centers will not be greater than 1°. The absolute (transmitted) phase difference between the 360-MHz reference modulation and the modulation on any other carrier will not be more than 5° and will be known to within 1°. These phase stabilities are necessary for accurate determination of the integrated electron content by modulation phase delay (or content change by differential phase), and must be matched by equal precision of data recording and analysis. The carrier frequency stability is expected to be better than 2 parts in 10^7 per year.

The radio beacon transmitter package is mounted within the communications module and the long whip antennas are mounted on the east and west sides of the EVM. Because of the proximity of some of the RBE carrier frequencies, or harmonics of its carrier frequencies, to the ATS-6 command frequencies, the

RBE will be turned off by the 6-hr clock unless a reset command is given to the 6-hr clock.

Effective radiated powers are sufficient for signal-to-noise (sky and receiver) ratios of 30 dB with bandwidths on the order of 5-Hz and ground antennas with approximately 12-dB gain.

1.7   TECHNOLOGICAL EXPERIMENTS

1.7.1   Spacecraft Attitude Precision Pointing and Slewing Adaptive Control Experiment (SAPPSAC)

The Spacecraft Attitude Precision Pointing and Slewing Adaptive Control (SAPPSAC) experiment is designed to demonstrate a ground-controlled real-time feedback attitude control system for attitude maneuvering and precision pointing of the ATS-6 spacecraft using onboard torquers and sensors with coupling through command and telemetry links.

No special on-board hardware is employed for the SAPPSAC experiment except for a special command decoder called the Ground Attitude Control (GAC) decoder. The experiment is enabled by commands through the Normal decoder which turn on the GAC decoder, select and decouple the on-board torquers (jets or wheels) from the on-board controller (DOC or ABC) and allow the control of the jets or wheels by commands through the GAC decoder. In the event that transmissions from the ground are not received for over three seconds, the GAC decoder is automatically turned off and the spacecraft remains in an open-loop mode. Additional Normal commands are required to reconfigure the spacecraft for normal on-board control.

1.7.2   Cesium Bombardment Ion Engine Experiment

The primary objective of this experiment is to verify and obtain operational data on the utilization of an ion microthruster electric propulsion system. This propulsion system will be used for north-south station keeping orbital maneuvers. A secondary objective is the demonstration of thrust vectoring for attitude control.

The experiment flight hardware consists of two identical cesium bombardment ion microthruster systems. The two systems are mounted on the north and south sides of the Communications Module of the Earth Viewing Module (EVM) and aligned such that their undeflected thrust vectors pass through the spacecraft center of mass, normal to the roll axis. The assumed angle between the thrust vector and the yaw axis requires that the thrust capability of each microthruster be 1.0 mlb. Each microthruster system requires approximately 170 watts of power.

The Ion Engine experiment receives a turn-off command from the 6-Hour Clock which will automatically turn the experiment off every approximately 6 hours unless a reset command to the 6-hour clock is sent by the ground stations.

1.7.3 Propagation Experiment

Occasional severe signal attenuation due to precipitation occurs when radio waves are transmitted through the atmosphere at frequencies above 10 GHz. The theory of precipitation attenuation, although well understood, is only useful for simple atmospheric models as the large number of variables and the general lack of precise knowledge of climatological data prevents a theoretical definition of operational characteristics. Consequently, measurements must be made on a sufficiently large scale to encompass and define all of the situations likely to be encountered in a domestic or regional communications satellite system. The ATS-6 13- and 18-GHz propagation experiment is designed to make such measurements.

1.7.3.1 Objectives of the Experiment—The purpose of the experiment is to collect sufficient long-term data on propagation attenuation caused by precipitation for a large number of locations in the United States to permit determination of minimum power margins needed in spacecraft communications systems operating at frequencies above 10-GHz.

It is expected that the duration of the experiment will be sufficiently long to permit a statistical comparison between the measured attenuation at a site and general meteorological parameters that are routinely collected by the weather bureau, such as rainfall rate, number of thunderstorm days, total precipitation, and weather radar information. This comparison is needed to provide a method for using the data collected in this experiment at other locations and to permit the extrapolation of the data to other periods at the selected location, since there is a great variation in weather conditions at any location from year to year.

To gather statistically significant data, the experiment will be conducted for the longest feasible period of time. The minimum duration of this experiment is estimated to be six months to include the months with greatest occurrences of thunderstorms. During this period, the propagation experiment will be conducted on a 24-hour-a-day, seven-day-a-week basis.

1.7.3.2 Description of the System—The experimental system consists of three main parts:

    a. Fifteen small, widely separated (>100 miles apart) earth stations, each transmitted at approximately 13- and 18-GHz; and nine closely spaced (< 25 miles apart) 18-GHz transmitting terminals.

b. A spacecraft transponder, receiving from the small earth transmitting terminals at approximately 13- and 18-GHz, and retransmitting these signals around 4-GHz. The propagation experiment 4-GHz transmitter uses the C-band transmit earth coverage horn antenna by feeding probes which are orthogonal to the Communications Subsystem probes.

c. A 4-GHz Earth station for receiving and recording the propagation data from the ATS-6 propagation experiment.

1.7.4 Advanced Thermal Control Flight Experiment (ATFE)

The objectives of the experiment are:

a. To evaluate in space the performance of an active, feedback-controlled, variable conductance heat pipe, a thermal diode (one-way heat pipe), and a phase-change heat reservoir or thermal accumulator.

b. To demonstrate the effectiveness of these recently developed thermal control devices in stabilizing the temperature of spacecraft components which undergo marked changes in power dissipation and/or thermal environment.

The temperature-control system proper consists of (1) the equipment shelf and thermal accumulator containing the phase-change material (PCM), (2) the feed-back-controlled heat pipe (FCHP), and (3) the radiator panel. In conjunction with the PCM, the FCHP acts to minimize temperature variations in the equipment shelf under varying heat inputs and/or radiator heat-sink conditions.

In order to avoid the use of spacecraft power to provide heat input, the experiment includes a solar absorber panel and a thermal diode. The solar absorber will be oriented so that, in synchronous orbit, it will be exposed to the full daily range of insolation from 1199 kg-cal per sq meter per hr (442 Btu per sq ft per hr) to zero. When the absorber is in sunlight the absorbed energy will be transmitted to the equipment shelf by the thermal diode; when the absorber is in shadow the one-way nature of the diode will minimize the reverse flow of heat from the shelf to the absorber.

1.7.5 Quartz Crystal Microbalance (QCM) Contamination Monitor

1.7.5.1 Objective of the Experiment—The primary objective of this experiment is to provide data regarding the existence of contaminants on the ATS-6 space-craft. This is done by the use of a quartz crystal microbalance (QCM) which

measures extremely small mass accretions. The ATS-6, being stabilized, permits the QCM to be mounted on a face which views space; therefore, it is designed to run at temperatures around 200°K.

1.7.5.2 Description of QCM Hardware—The experiment flight hardware consists of two parts: a sensor assembly mounted externally on the north face of the earth viewing module, and the electronic unit mounted internally on the same face. The sensor assembly contains the sensing and reference oscillating quartz crystals, heaters, and the electronic driving circuitry for the crystals. The temperature of 200°K for the crystals is obtained by the use of optical solar reflectors for external thermal control, and thermal insulators for mounting structures. The electronic unit contains the signal processing, temperature control, and command circuitry.

1.7.5.3 QCM Operation (Technical Description of the Experiment)—The QCM is a mass measuring device with the relationship between increased mass deposition on the active area of the crystal, Δm, and the change in resonant frequency, Δf, given by

$$\Delta f = -kf^2 \, \Delta m. \tag{1}$$

The Δf is measured as a variation in a beat frequency between a reference and sensing crystal so that changes of parts per 10^3 Hz will be measured with a 1-Hz resolution. The nonlinear relation between the Δm and Δf given in (1) occurs beyond the range of the experiment maximum Δf of 50 kHz. The sensitivity is in the order of 10^{-9} GHz^{-1} using a 10-MHz resonant crystal, thus, allowing detection of less than one equivalent monomolecular layer (eml) of water. Temperature effects on crystal performance are eliminated by active thermal control of the crystals at 200°K ±2°K. Additionally, the reference and sensing crystal are matched so that a maximum of 50-Hz variation will occur during orbital thermal excursions in the event of heater failure. Assuming the thermister also failed, this would amount to an uncertainty of 5 eml.

1.8   COMMUNICATIONS EXPERIMENTS

1.8.1   Position Location and Aircraft Communication Experiment (PLACE)

The Position Location and Aircraft Communication Experiment (PLACE) is an experiment to obtain engineering data and practical experience for determining the operational feasibility of an air traffic control (ATC) satellite system operating in the aeronautical L-band.

The special multiple access capability provides for simultaneous operation of C-band to L-band, and L-band to C-band. To achieve this, the communications subsystem provides a receiver linearity that prevents the multiple carriers from producing significant intermodulation components.

The second objective is to investigate the feasibility and to evaluate the absolute and relative accuracies of several position location techniques using a single satellite. Each of these techniques relays various signals from the aircraft via the satellite to the control center for data processing and position determination.

In-flight performance experiments will be conducted in close cooperation with the FAA and possibly other coexperimenters. These will include actual aircraft flights to determine the effects of multipath, ionosphere, noise environment, and geographic location on both the L-band communications and position location links. Operational experiments including communication link utilization, multiple aircraft tracking, capacity limitations, possible extensions, and ground and cockpit terminals will form an important part of the combined GSFC and FAA research effort.

1.8.2   Satellite Instructional Television Experiment (SITE)

This SITE experiment is a joint experiment between the NASA, the Department of Atomic Energy and the Government of India, entered into formally on September 18, 1969.

The general objectives of the experiment are to:

   a.   gain experience in the development, testing, and management of a satellite-based instructional television system, particularly in rural areas and to determine optimal system parameters

   b.   demonstrate the potential value of satellite technology in the rapid development of effective mass communications in developing countries

   c.   demonstrate the potential value of satellite broadcast TV in the practical instruction of village inhabitants

   d.   stimulate national development in India, with important managerial, economic, technological and social implications.

The experiment will be conducted for a period of one year starting approximately one year after the launch of ATS-6. The ATS-6 spacecraft will be positioned at approximately 35°E Longitude. A frequency modulated TV carrier at 6-GHz will be transmitted to the ATS-6 earth coverage antenna from one of three earth stations: Ahmedabad, Delhi, or Bombay. The signal is processed and retransmitted at 860-MHz.

The 860-MHz downlink will be used to test the concept of a hybrid system involving both direct reception by low-cost augmented TV receivers as well as higher sensitivity earth stations for rebroadcast at VHF to conventional TV receivers. System design parameters are such that an equivalent TASO* grade 1 picture will be received by the direct reception terminal while a CCIR recommended quality signal will be received by the rebroadcast earth station. About 2,000 direct reception and 3,000 conventional sets will be located in 5,000 villages. The direct reception terminals will be located in clusters of about 400 each in various parts of India while the conventional sets will be located in villages near existing or planned VHF TV transmitters.

1.8.3   Television Relay Using Small Terminals (TRUST)

The purpose of the TRUST experiment is to advance and promote the technology of wideband satellite communications to small ground terminals by developing and demonstrating a pilot system using the ATS-6 spacecraft with its high-gain parabolic reflector. Specific program goals are:

a.   To test and evaluate an experimental system for FM relay of black and white and color television signals (and associated sound) between the ATS-6 spacecraft and a UHF receiving facility

b.   To evaluate the performance of the pilot system relative to experiment design objectives and internationally recognized and accepted standards for television transmission systems

c.   To observe the effects of ionospheric dispersion on system performance as a function of electron density, ground station location, and other system variables, and compare with theoretical predictions

d.   To provide interested underdeveloped countries an opportunity to participate in tests and demonstrations of a high EIRP satellite suitable for national ETV using inexpensive receivers, and to provide advice and consultation in the design and implementation of suitable receivers for such systems.

The TRUST experiment basic system will consist of a high-power microwave transmitting terminal for Earth-to-satellite communications, the ATS-6 spacecraft with a microwave-to-UHF communications repeater, and a pilot mobile

---

*TASO—An international standard for grading the quality of television according to signal-to-noise ratio.

UHF ground receiving facility. The Earth-to-satellite communications will be accomplished using existing NASA microwave facilities at Rosman Station, North Carolina, or the Mojave Station near Barstow, California, or both.

1.8.4 Radio Frequency Interference Measurement Experiment (RFIME)

The purpose of the Radio Frequency Interference Measurement Experiment is to provide realistic data on mutual RF interference on C-band between satellite and terrestrial telecommunications systems. This data is needed for optimum use of the frequency spectrum in the design and implementation of advanced communications satellite systems.

The C-band RFIME is designed to measure and evaluate the effect of RF interference in the shared common carrier frequency band of 5929- to 6425-MHz.

The technical objectives of the C-band RFIME are to:

    a.   determine the flux density of 6-GHz interference power at the satellite

    b.   establish practical gain-to-noise ratio limits for the satellite

    c.   establish realistic satellite protection ratios

    d.   determine both geographical and frequency distribution of terrestrial RF noise sources

    e.   investigate the feasibility of establishing mathematical models for predicting RF interference.

The experiment measurement system uses a computer controlled, special purpose spectrum analyzer receiving system and data processor located at the Rosman ground station. The small mobile terminal provides an effective means for calibrating the entire system.

The system is designed to identify 10-dBW interference sources with a frequency resolution of 10-kHz.

1.8.5 Millimeter Wave Propagation Experiment (MMW)

The ATS-6 Millimeter Wave Propagation Experiment (MMW) is designed to evaluate the propagation characteristics of space-to-Earth links centered at 20-GHz and 30-GHz during measured meteorological conditions.

The three primary scientific objectives of the ATS-6 MMW experiment can be described under three areas of investigation:

Propagation - provide the propagation characteristics of space-Earth communication links operating at 20-GHz and 30-GHz under various meteorological conditions and modulation techniques.

Communications - provide engineering data on space-Earth communications links operating at 20-GHz and 30-GHz under various meteorological conditions and modulation techniques.

Prediction - investigate techniques for predicting millimeter wave propagation effects from indirect means such as radiometric sky temperature, and radar backscatter, and establish a model for the millimeter wave channel under defined meteorological conditions.

Three modes of operation are included in spacecraft hardware to provide the measurements needed to meet these objectives;

a)   The multitone (MT) mode consists of nine tones equally spaced out to 720-MHz on both sides of the carrier. This mode provides the major parameters required under the first objective, such as carrier and sideband attenuation statistics, relative sideband phase statistics, coherence bandwidth, fade durations, fade depths, multiple station diversity statistics, and outage time.

b)   The communications (COM) mode consists of a frequency translation transponder with the uplink supplied from the ATS transponder and cross-strapped to 20-GHz and/or 30-GHz downlinks. This mode provides the parameters required under the second objective. The parameters include carrier-to-noise ratio and modulation index for analog modulation schemes, and bit error rates and information rates for digital modulation techniques. The cross-strap capability will also allow a direct comparison of 20-GHz, 30-GHz, and 4-GHz transmissions through the same weather profile.

c)   The carrier only (CW) mode consists of a single downlink test signal at each frequency to provide attenuation measurements for additional locations and multistation diversity studies under the first objective, as well as prediction, correlation and modeling studies under the third objective.

Two antenna beamwidths are available on the satellite: a narrow spot beam (2.3° at 20-GHz and 1.6° at 30-GHz) for communications tests and a continental

1-18

coverage (6° × 8°) horn for more complete coverage during the multitone tests. The spacecraft transmitted power is 2 Watts, maximum, at both frequencies, and fade margins of greater than 60 dB are available for CW propagation measurements during extremely severe weather events. The communications mode provides a 25-MHz clear weather bandwidth capability at either frequency, and digital testing of up to 40 megabits per second is planned.

The Rosman MMW data acquisition system will absorb data which falls into two basic types: experiment propagation data which is interfaced to an analog-to-digital (A/D) converter and multiplexer, and experiment supporting data which will be provided in direct digital form (with one exception) to the data acquisition system. In addition to the propagation parameters, each of the combined ground receiver/radiometer will provide one signal output of apparent sky temperature. This radiometer data and certain meteorological parameters that will be active both in the multitone and CW modes constitute supporting data and are the exceptions to direct digital supporting data mentioned earlier.

1.8.6   Tracking and Data Relay Experiment (TDRE)

The purpose of the experiment is to provide experience and information, using the ATS-6 satellite, which can be used in designing future TDRS systems. The specific objectives are to:

   a)   Determine the extent which the orbit of a low-orbiting spacecraft can
        be established from another higher orbiting spacecraft

   b)   Demonstrate the technology of command and telemetry data trans-
        mission between a low altitude satellite and a ground station using
        a geosynchronous satellite as a communications relay.

The tracking and data relay experiment uses the ATS-6 as a repeater for re-transmission of information between earth and a second satellite such as NIMBUS. This experiment is a duplex link that requires the transponder to transmit and receive on two channels simultaneously. A signal originating on the ground is transmitted to ATS-6 on C-band. The received ground signal is translated to IF, amplified, limited, and switched via an upconverter to S-band. The S-band signal is amplified and transmitted to the satellite NIMBUS. Signals originating in the NIMBUS satellite are transmitted to ATS-6 on S-band, In the transponder they are again translated to IF, amplified, and limited in a manner similar to the received ground signal. The processed signal is translated to C-band and transmitted to the ground. By phase locking the ATS frequency synthesizer to the C-band uplink signal, the output of the transponder is coherent with the ground transmitted signal. This allows direct Doppler rate ranging measurements of the ATS-6 satellite signals and of the NIMBUS signals on the ground.

Single satellite tracking is accomplished by either closed-loop monopulse tracking or open-loop with computed pitch and roll commands based upon the ATS-6 and low-altitude satellite ephemeris data. Before the actual low-altitude satellite transit occurs with open-loop tracking, the ground station must: (1) obtain suitably accurate orbit ephemeris data for the two satellites (low-altitude and ATS-6), (2) transmit this data to the ATS-6 Digital Operational Controller, (3) command the ATS-6 to assume the initial values for the pitch and roll angles, and (4) transmit a start-track command at the appropriate time. When the S-band monompulse system is used, only items 1, 3 and 4 of the above ground station requirements need to be considered.

1.8.7   Health-Education Telecommunications (HET) Experiment

The S-band Health-Education Telecommunications (HET) experiment is a cooperative effort with the Corporation for Public Broadcasting (CPB), the Department of Health, Education and Welfare (HEW), and NASA. The experiment will evaluate the performance and effectiveness of satellite relay of educational programming and health care delivery to facilities such as schools, HEW learning centers, hospitals, clinics, and community antenna television (CATV) distribution systems. ATS-6 is equipped with a two-channel TV transmit capability in the 2.5- to 2.69-GHz band recently allocated to the satellite broadcast service.

High performance reception will be possible with ground receiving systems having at least 7-foot diameter fixed position parabolic antennas of the type currently in use in many instructional television fixed service (ITFS) installations throughout the country. Special receiving equipment including FM-to-AM converters will be required to handle the HET transmissions from ATS-6. Limited talk-back capabilities exist to permit interactive and computer managed communications experiments using existing ATS-6 communications capabilities S-band (2250 MHz).

The basic ATS-6 spacecraft includes a prime focus feed complex having a crossed-array of switchable broadband S-band feed elements. Two of these feed elements will be used for the HET experiment. The two elements selected are the first and second offset elements in the south arm of the crossed array. Spacecraft boresight reorientation is used to shift the fields of view to provide satisfactory illumination of ground terminals participating in the test. No provision is being made for simultaneous operations in nonadjacent areas; therefore, operations outside the footprint will have to be time shared with other coverages with time allowed for moving the spacecraft boresight between transmissions.

1.9 METEOROLOGICAL EXPERIMENT

1.9.1 Geosynchronous Very High Resolution Radiometer (GVHRR)

This experiment is directed toward evaluating:

    a.   The feasibility of new concepts in meteorological and weather data collection and distribution by means of a synchronous weather satellite

    b.   New camera systems aboard stabilized spacecraft.

The radiometer gives both day and night cloud coverage information for the determination of cloud motions, tropical storm life cycles, extratropical storm life cycles, mesoscale phenomena, and cloud climatology studies. It operates in two different frequency ranges, one in the infrared between 10.5 micron and 12.5 micron and one in the visible spectrum between 0.55 micron and 0.75 micron. Operating through an 8-inch Cassegrainian telescope, the instrument generates a picture in 20 minutes with a resolution of 10 km at the subsatellite point. In addition, the radiometer system supplies information used for Earth albedo measurements, Earth resource studies, and ocean temperature studies.

The GVHRR instrument can be commanded to scan the Earth when the spacecraft is pointing at the subsatellite point. An offset capability is also commandable when the spacecraft is pointing at the Rosman ground station. The VHRRE data is transmitted to the ground stations via the Communications Subsystem C-band link.

SECTION 2

REPORT SUMMARIES

SECTION 2

REPORT SUMMARIES

2.1   STRUCTURAL SUBSYSTEM (SECTION 3)

There have been no problems associated with the structural subsystem since the slow deployment of the North Solar Array on Day 150. The Second Motion took approximately 15-1/2 minutes rather than the expected 3 to 7 minutes. The probable cause still cannot be established but additional studies are in progress to evaluate the possibility of interference between panel and boom due to thermal deflections.

2.2   ELECTRICAL POWER SUBSYSTEM (SECTION 4)

The EPS has operated with only one anomaly, high tap voltage on Shunt Dissipator A419, which has had no negative effect on performance. The 90-day degradation of North and South solar panels has resulted in reduction of power output of 4.4% and 5.0% respectively, against 4.25% predicted.

Numerous in-orbit observations have allowed refinements in the Experiment/Mode power profiles which are used in battery state-of-charge predictions.

Battery discharge currents as high as 6.5 amperes per battery have been observed with 77 discharge cycles varying from 10% to 50% in depth-of-discharge.

2.3   THERMAL CONTROL SUBSYSTEM (SECTION 5)

The average temperatures of the Experiment Module, Communications Module and Service Module have varied between 13°C to 28°C, 20°C to 30°C, and 22°C to 26°C respectively. These ranges are well within the specification limits of 5°C to 35°C.

2.4   TELEMETRY AND COMMAND SUBSYSTEM (SECTION 6)

This subsystem has performed without anomalies during the first 90 days of spacecraft operations.

2.5   ATTITUDE CONTROL SUBSYSTEM (SECTION 7)

During the first three months of in-orbit operations, the attitude control subsystem (ACS) met or exceeded specification requirements and, with the aid of a sophisticated software system at ATSOCC, has continued to be relatively easy to monitor and control from the ground.

Several aspects of operation which were not exercised in the first 30 days of flight are reported on. These are the "Local Vertical Orbit Plane East/West" mode, a twenty-hour C-Band monopulse test and the effects of the moon and noise on ESA performance.

Three anomalies are discussed in detail: 1) PSA tracking anomalies, 2) YIRU bias anomaly and 3) DOC command angle anomaly.

2.6   SPACECRAFT PROPULSION SUBSYSTEM (SECTION 8)

The SPS2 valve heater circuit failed on July 31, 1974 but backup heaters were activated and are maintaining proper valve temperatures.

A standard automatic wheel unload procedure is being performed every other day.

Two orbit correction burns have used 0.28 lb of Hydrazine.

2.7   COMMUNICATION SUBSYSTEM (SECTION 9)

Performance of the Communication Subsystem met or exceeded specification requirements during the first 90 days in orbit. The subsystem was used primarily to support communications experiments but extensive investigative tests have yielded substantial performance data in the form of antenna patterns, G/T and EIRP measurements.

2.8   APOLLO-SOYUZ TEST PROJECT (SECTION 10)

The Apollo-Soyuz Test Project (ASTP) is a cooperative effort between NASA and the U.S.S.R. It consists of development, scheduling and test docking between Soyuz and Apollo spacecraft in near-earth orbit. ATS-6 will provide support consisting of real-time relay of telemetry, television and voice communications between the Apollo command-service module and a hybrid terminal on the ground.

2.9   SPACECRAFT CHARGE PHENOMENON (SECTION 11)

A special effort of the In-Depth Analysis Group was organized during the autumnal eclipse season to observe and measure spacecraft charge and any other spacecraft effects caused by the eclipse. The charge phenomenon was observed on fewer than 50% of the eclipse days with voltages less than 10 kilovolts.

2.10 PROPAGATION EXPERIMENT (SECTION 12)

Although the 13 GHz and 18 GHz spacecraft transponders have operated satisfactorily, ground equipment problems and a lack of attitude data on telemetry tapes have prevented scientific evaluation.

2.11 MILLIMETER WAVE EXPERIMENT (SECTION 13)

The MMW Experiment has been very active with most requests for operation during storms being honored. MMW color video tests have shown good picture quality at 20 GHz and 30 GHz.

Hardware operation has been without anomaly except that the 20 GHz horn antenna TWT (H1) will not switch on. Its loss will not impact the basic objectives of the experiment.

2.12 ADVANCED THERMAL CONTROL FLIGHT EXPERIMENT (SECTION 14)

The ATFE has operated almost continuously since launch in its four operational modes. Experiment objectives are being demonstrated except for a daily loss of temperature control around the period of maximum solar input. This is related to elevated radiator temperatures and results in 5 to 10% degradation of experiment objectives.

2.13 QUARTZ CRYSTAL MICROBALANCE CONTAMINATION MONITOR (SECTION 15)

This experiment has operated satisfactorily on a continuous basis since five hours before launch. Data reduction and analysis is continuing to define whether small mass increases noted are related to spacecraft activity.

2.14 GEOSYNCHRONOUS VERY HIGH RESOLUTION RADIOMETER (SECTION 16)

On August 15, operation of the GVHRR was terminated after failure of its chopper motor. Prior to this failure, numerous satisfactory images were collected from the two visible and one IR channels.

Further attempts will be made to start the GVHRR chopper motor.

2.15 ION ENGINE EXPERIMENT (SECTION 17)

Two major ION Engine tests were conducted with the first test starting on day 199 and the second test starting two days later.

The first test, employing the south engine, lasted approximately 1.5 hours. Operation was entirely satisfactory, with telemetered parameters normal. Anomalies associated with spurious counts in the registers controlling X and Y deflections were noted but are not considered a serious problem. No compatibility problems with the communication subsystem were noted.

During the second test, lasting approximately 15 hours, the ion engine high voltage repeatedly cycled off after approximately 1 minute of operation. Additional tests were conducted on days 215, 226, 234, and 235, resulting in the same high voltage problem; however, spacecraft charge data was collected during these trials.

Attempts to operate the thruster will continue.

2.16   ENVIRONMENTAL MEASUREMENTS EXPERIMENTS (SECTION 18)

Of eight experiments, only the University of New Hampshire (UNH) Low Energy Proton Electron Experiment has failed to meet its design goals. The UNH Experiment caused a permanent malfunction in the 64 level subcomutator word #189. All EME experiments use this word and have therefore suffered to some degree.

Minor anomalies have been reported in the Aerospace, UCLA, UMINN and Hughes experiments.

2.17   TRACKING AND DATA RELAY EXPERIMENT (SECTION 19)

Nimbus-F T&DRE tests have indicated signal levels at –98 and –99 dBm, about 2 dB higher than predicted. Tracking modes have indicated range noise to be generally less than 3 meters and range rate noise less than 0.5 mm/sec for 10 second integration periods and less than 4 mm/sec for 1 second integration.

A trilateration test involving Rosman, Mojave and Santiago ground stations achieved good results.

2.18   HEALTH EDUCATIONAL TELEVISION EXPERIMENT (SECTION 20)

The HET flight evaluation tests were started June 11. All equipment functioned well with audio and video signal quality very good.

HET antenna polarization at ground stations was found to be reversed for reception. Corrections were made using field modification kits.

During HET operation while using the spacecraft video transmit frequency channel B (2667.5 MHz), radio astronomy observers using the 140-foot telescope of the National Radio Astronomy Observatory in Green Bank, West Virginia, observed signal spillover into their band (2690 MHz to 2700 MHz) measuring 13 db above the CCIR level of -247 db w/m^2 Hz.

2.19 RADIO FREQUENCY INTERFERENCE EXPERIMENT (SECTION 21)

RFI Experiment Spacecraft activity has been reported for 22 days during this reporting period. Eight of 13 measurement modes have been exercised, of which four modes have been used repeatedly to acquire RFI data from 30 geographic areas in the continental United States, Alaska, and Hawaii.

Computer software failures, and lack of measured in-orbit antenna patterns for the ATS-6 PFF at C-band, have thus far precluded establishing precise geographic location of RFI sources.

2.20 SATELLITE INSTRUCTIONAL TELEVISION EXPERIMENT AND TELEVISION RELAY USING SMALL TERMINALS (SECTION 22)

The received power and ground station antenna gain measurements for TRUST and SITE type installations, as observed at GSFC, have been further refined by more accurate calibration techniques and the use of a revised computer program to account for the actual position of the spacecraft in longitude and latitude.

The test data for the SITE and TRUST antenna indicates gains of 23.4 db and 26.5 db respectively.

No anomalous hardware operation has been observed.

2.21 POSITION LOCATION AND AIRCRAFT COMMUNICATIONS EXPERIMENT (SECTION 23)

Spacecraft operation with PLACE ground and shipboard equipment occurred on 22 different days of this reporting period. The spacecraft PLACE-associated equipment performed well and should adequately support the planned experiments. Special tests related to signal power sharing (PLACE and MARAD), S&R, Voice, Data Channel C/No in both forward and return links, and data channel bit error rate, have furnished data which indicates that the required C/No system performance is achievable.

The tests were involved with the following:

a. Primary Ground Station at Rosman
b. NASA Ground Station at Mojave (Receive Mode)
c. MARAD Station at Kings Point
d. MARAD Ship Terminal at Moorestown
e. TCS Cambridge-USCG Ship Terminal
f. MARAD-COMSAT Modem (Voice and Data)
g. ESRO-EPIRB Buoy Receiving Equipment located at Rosman
h. ROSMAN/MOJAVE Ranging, Voice and Data.

2.22 RADIO BEACON EXPERIMENT (SECTION 24)

The 360 MHz and 140 MHz transmitters are operating as predicted, however, the 40 MHz transmitter shows combinations of anomalies which may indicate a poor antenna match.

The RBE transmitters have been in almost continuous operation since June 2, 1974. While scientific evaluation is still in an early stage, at least two new significant results have been identified. The first pertains to the vertical movement of the ionosphere at dawn, and the second to the height at which additional ionization was produced during a recent large solar flare.

2.23 SPACECRAFT ATTITUDE PRECISION POINTING AND SLEWING ADAPTIVE CONTROL (SECTION 25)

A series of slew and hold maneuvers designed to obtain simultaneous spacecraft attitude sensor data was conducted and the data is being processed for sensor calibration data.

The SAPPSAC PDP-11 computer at Rosman has been employed extensively for on-line attitude determination.

SAPPSAC and interferometer tests performed to date have shown that the C-band and VHF command/telemetry links are of high quality.

The SAPPSAC safety position freeze mode, which fixes the target coordinates at the last computer attitude, was successfully demonstrated during one of the slew maneuver attempts when incorrect position entries were made to the SAPPSAC computer.

SECTION 3

STRUCTURAL SUBSYSTEM

SECTION 3

STRUCTURAL SUBSYSTEM

3.1 INTRODUCTION

During the deployment of the spacecraft following injection into orbit, the north solar array panel failed to complete the second motion of deployment in a normal time span of three to seven minutes, but rather took approximately fifteen and a half minutes. Initial investigations reported in the ATS-6 In Orbit Checkout Report (X-460-74-232) were directed toward establishing a time history of this movement through studies of spacecraft attitude and motion as determined from solar vector aspect angles and spacecraft Rate Gyro Assembly data. This report presents data on telemetry signal polarization and generation of spacecraft electric power from which additional inferences of the time history of the North Solar Array are drawn.

3.2 TELEMETRY SIGNAL STRENGTH VARIATIONS

During the launch of ATS-F and its injection into orbit, two telemetry transmitters (136.23 and 137.11 MHz) were used to transmit data from the spacecraft to the Rosman and Mojave Ground Stations. At Mojave, each signal was received on antennas sensitive to polarization in two orthogonal directions. Each polarization component of the received signal was passed through individual IF circuits having independent automatic gain control (AGC). Figure 3-1 is a plot of the AGC voltages for each of the four IF circuits of the receivers. The fifth trace is a GMT time tick coinciding with the signal. The top two channels were identified as Receiver No. 1 operating on 137.11 MHz. The next two channels were identified as Receiver No. 2, operating on 136.23 MHz. Notations on the graph indicate the times at which spacecraft separation and development events occurred as provided by actuation of event switches and reported via telemetry.

Telemetry data was transmitted from the spacecraft via omni-directional antennas located in the center of the outboard frame of the north and the south solar arrays (referenced to a fully deployed array). Rotation of the antenna with respect to the ground station receiver antenna line of sight causes a change in polarization of the received signal which is reflected in the AGC voltage. For example, note the change in AGC voltage during the period of boom 1st Motion (Ref. time 19:40:00). Similarly, disturbances torques and the resulting spacecraft motion during reflector release at approximately 20:07:00, resulted in significant cahnges in received signal polarization as shown by the AGC voltages. From this, it is believed that the AGC voltages provide a means of identifying solar array motion.
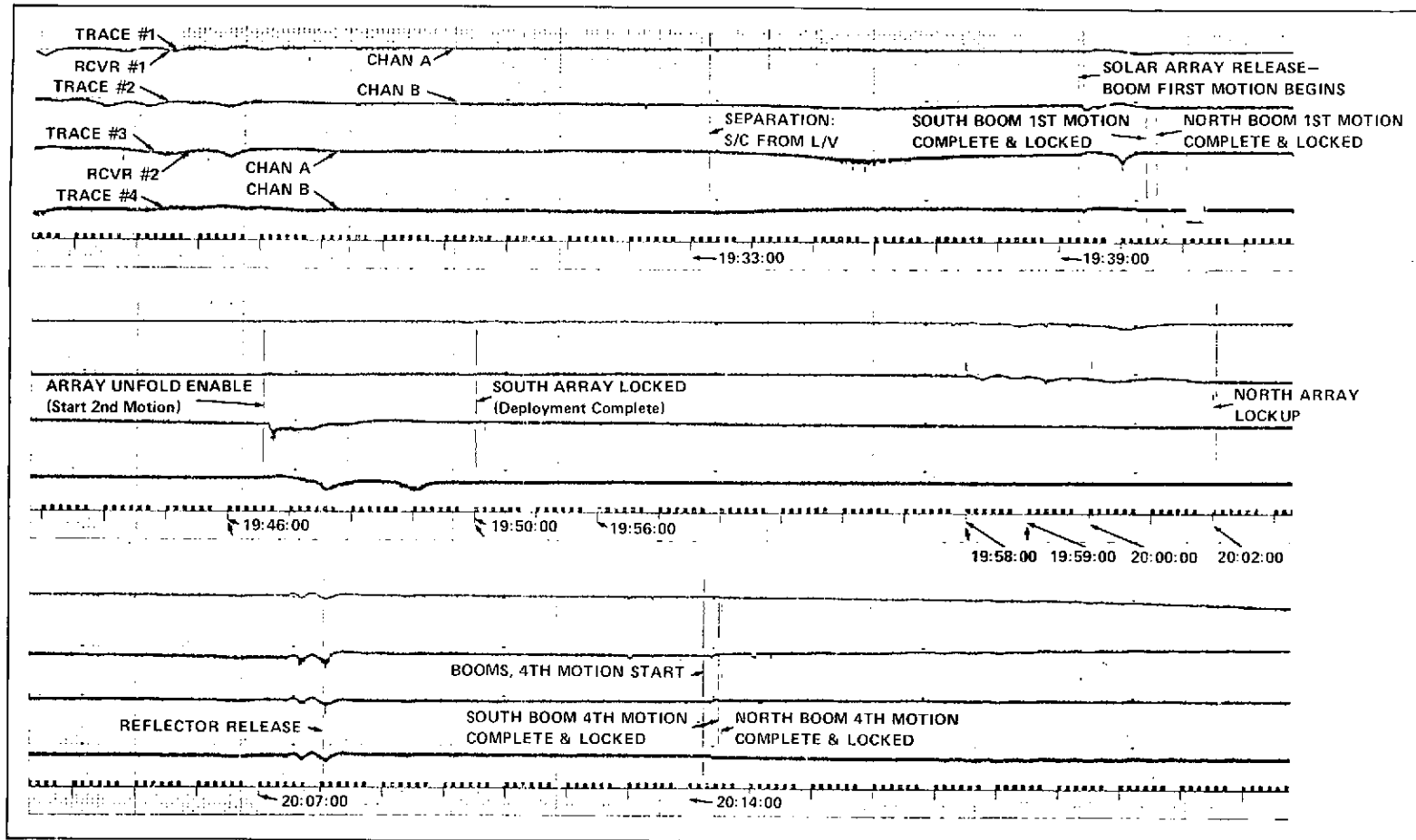
Figure 3-1. AGC Voltages in Ground Station Telemetry Receivers

At approximately 19:46:30, the restraints between the solar array panels and booms were released and the panels were permitted to rotate around the 45° hinge line connecting the panels to the booms (solar array 2nd Motion). From telemetry data, it is known that the south array 2nd Motion lockup mechanism actuated at approximately 19:50:00. Inspection of the AGC voltage traces indicates some motion by the lower two traces in this time span, but the upper traces do not indicate any motion. Beginning at 19:58:00, and continuing through approximately 20:02:00, the upper two traces indicate that some motion was in progress. The array lockup switches indicated via telemetry that north array lockup did occur at 20:02:03.

Spacecraft motion in inertial space with reference to the sun is indicated by sun sensors on board the spacecraft which report the solar vector with respect to the spacecraft axes. These are defined as Z Co-evaluation and Z Azimuth angles. In the ATS-6 In-Orbit Checkout Report (X-460-74-232) Figures 5-2 and 5-3 are plots of the solar vector angles as a function of GMT. From inspection of the Z Az curve, it can be seen that, in the period 19:58:00 to 20:02:00, there was substantial spacecraft motion which can be attributed to something other than spacecraft tumbling velocities. This spacecraft motion coincides with the motion indicated by the AGC voltage variations on Receiver No. 1. Note also that the third and fourth traces, during this period, do not indicate motion of the array.

3.3   VARIATIONS IN SOLAR ARRAY POWER OUTPUT

A study was conducted to determine the solar array power time-history from 2nd Motion release through lockup. Spacecraft electrical loads during this time period are constant and excess solar array power is dissipated by the shunt dissipation components. Since shunt current is reported vis telemetry, it can be used to establish the power generated by the solar arrays.

The predicted power generated is a function of the solar array temperature and the angle of incident solar flux on the individual panel facets of both solar arrays. From concurrent studies reported in the ATS-6 In-Orbit Checkout Report and below, and through consideration of panel/boom/hinge geometry and kinematics, it is believed that panel hangup could most logically occur with the panel in the stowed position, i.e., at the time of release, or at a position reached after 34° of panel rotation about the 45° panel hinge. The latter position coincides with the closest approach of the array edge to the supporting boom during array 2nd Motion. The power profile was predicted for these two conditions, identified as panel position 0° and 34°, respectively (Figures 3-2 and 3-3). It is assumed that the pannel was released at 19:46:34, that the north panel remained at 0° for case I, and that it rotated 34° for case II during the same time period that the south array was deploying (19:46:34 to 19:50:03), that the north panel did not rotate further until 19:58:00 and that panel rotation from start of motion (19:58:00) to
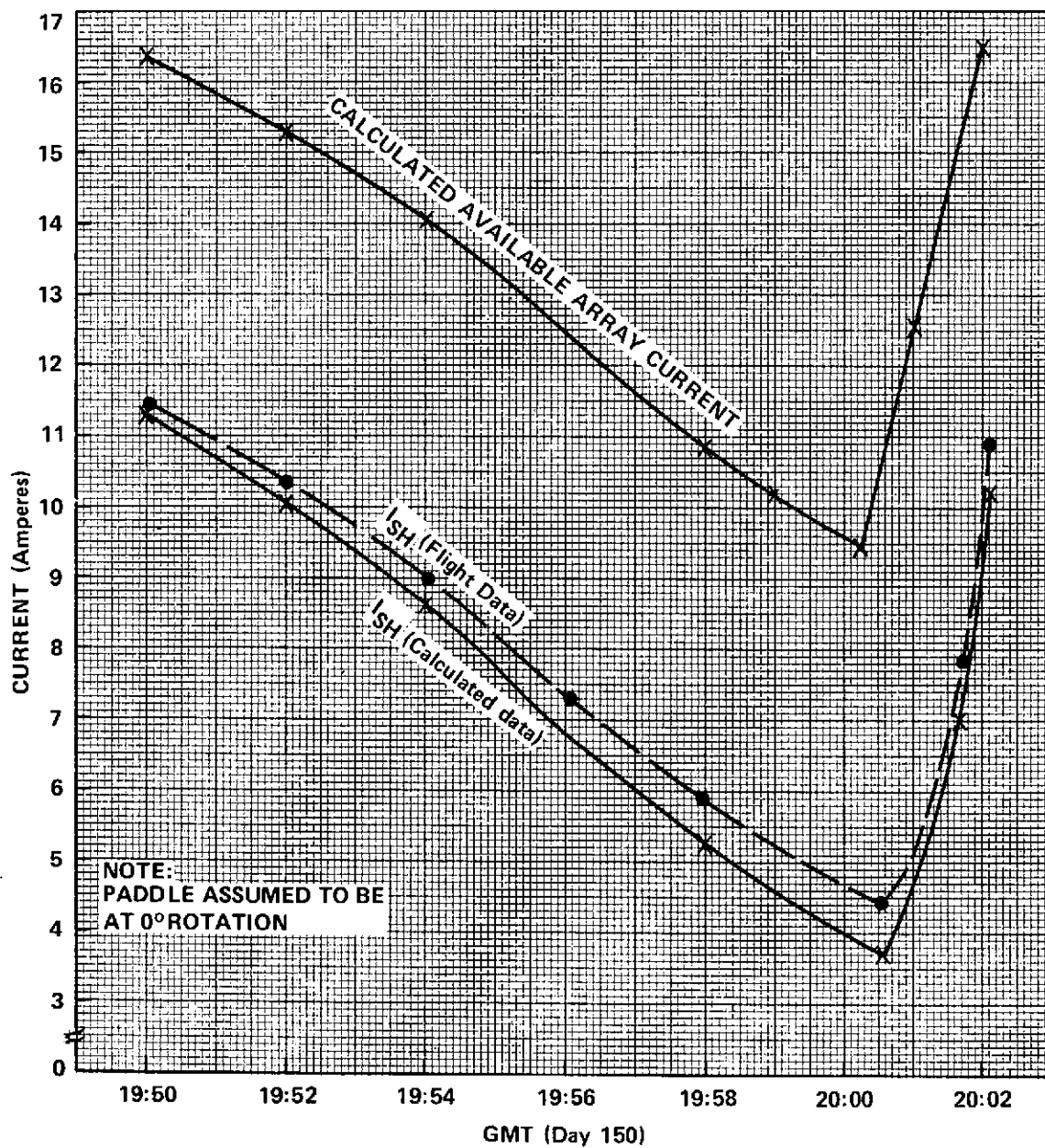
Figure 3-2. Solar Array Currents vs. GMT
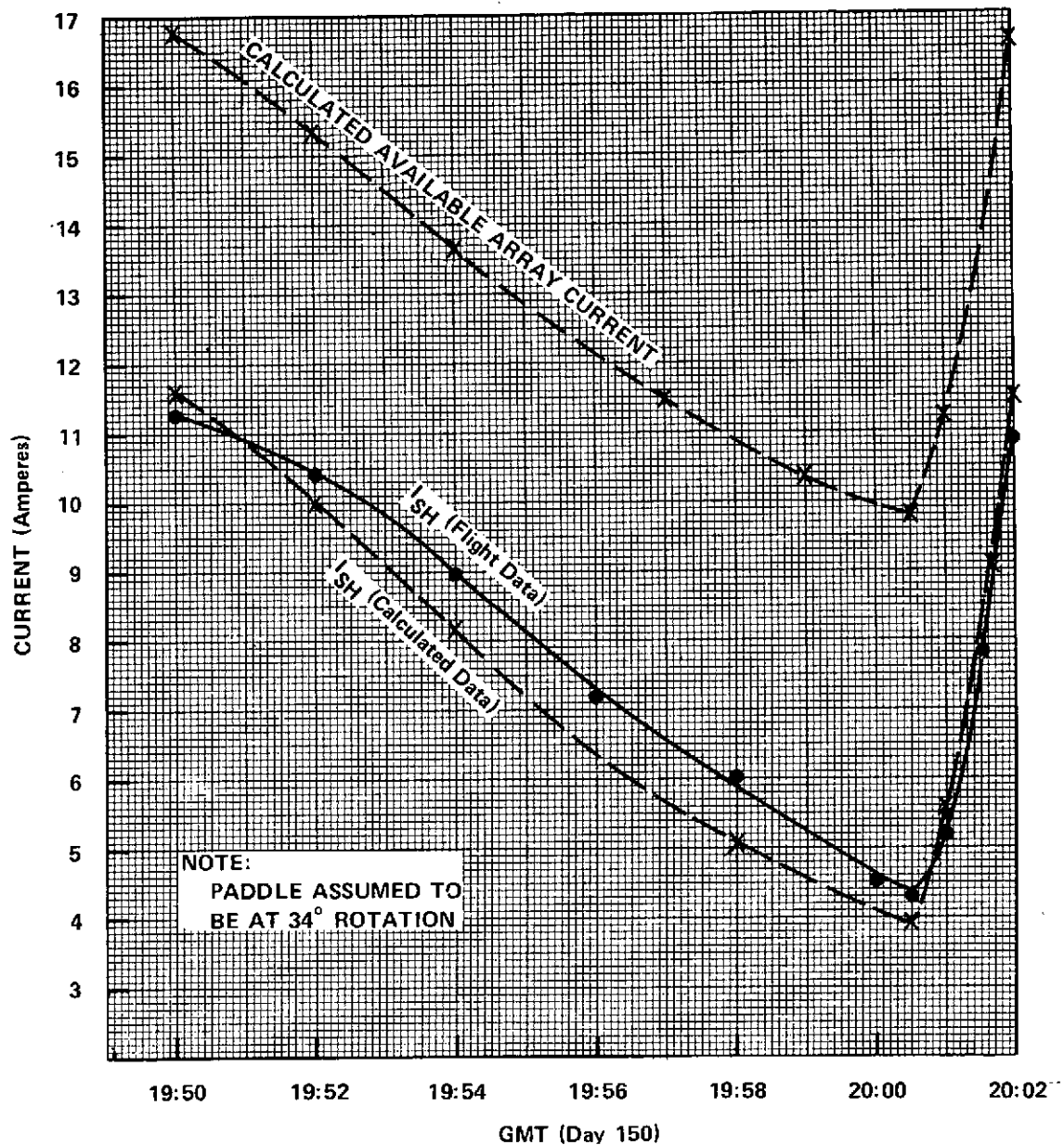
Figure 3-3. Solar Array Currents vs. GMT

lockup (20:02:03) was at uniform velocity. Panel temperatures were predicted based on incident solar flux and a power-generated-time history produced. Predicted and actual flight data shunt currents for these conditions of load and power are shown. Very good agreement does exist between calculated and flight shunt currents.

The relative position of the solar vector was such that practically no change in integrated solar flux occurred during the first 90° of panel rotation. This accounts for the small change in available array current and hence shunt current between 19:58:00 and approximately 20:00:30. The difference between the two curves in the calculated available array currents or in the shunt currents is not significant and is within the tolerance (±7%) of this method of current prediction.

3.4   CONCLUSIONS

This study confirms that the north solar array panel motion occurred primarily during the time period 19:58:00-20:02:03. The results do not define precisely the position of the array panel at hangup, although it is inferred to have occurred before the panel reached 90° of rotation. The change in predicted shunt current from 20:00:30 to 20:02:03 matches the flight data so closely that the assumed angular velocity of the panel is confirmed as being substantially correct. Unless the position of the solar array at hangup can be determined, its probable cause cannot be established with any degree of confidence. Therefore, additional studies are in progress to define the thermal deflections in the north solar array panel during deployment to evaluate the possibility of interference between panel and boom at the 34° position. Another investigation will study the motions of the spacecraft that are induced by deployment of the north array only and will attempt to correlate these predicted motions with the actual motions as reported in the In-Orbit Checkout Report.

SECTION 4

ELECTRICAL POWER SUBSYSTEM

SECTION 4

ELECTRICAL POWER SUBSYSTEM

4.1 INTRODUCTION

The solar array performance during the first 90 days in orbit has been satisfactory with high tap voltage on Shunt Dissipator A419 the only anomaly. The solar array power has been monitored frequently in an effort to determine what degradation if any has occurred.

As explained in the In-Orbit Checkout Report, in order to measure array power degradation, it was necessary to normalize the array power data to a fixed sun elevation (SEL) angle. The array power data presented in Figure 4-1 is normalized to a 20° SEL, so that it may be compared to the data presented in the In-Orbit Checkout Report. The data presented in Figure 4-1 is also segregated with respect to spacecraft local time. This segregation enables determination of the approximate degradation of each solar paddle.

The data indicates approximately 4.4% and 5.0% degradation for the north and south paddles respectively. The anticipated degradation after 90 days in orbit was approximately 4.25%. Taking into account the resolution limitations of the data, the array is behaving as predicted.

Another interesting point observed from the data of Figure 4-1 is that the output power at noon is approximately 10 to 15 watts higher than at 6 A.M. and 6 P.M. This power delta is attributed to the increase in the number of current carrying wires at noon which will diminish the I^2R loss of the harness. The harness impedance of each array paddle is approximately 80 milliohms. At 6 A.M. and 6 P.M. the array power is supplied independently by the south and north paddles respectively. At noon both paddles contribute to the array power and the harness impedance is approximately halved. The following calculations illustrate the harness power delta.

<div align="center">

6 A.M./6 P.M.	Noon
Harness Loss = $I^2 R$	Harness Loss = $I^2 R_2$
$\sim (20)^2 \times .08\,\Omega$	$\sim (20)^2 \times .04\,\Omega$
~ 32 watts	~ 16 watts

</div>

As mentioned previously, the data in Figure 4-1 is normalized to a fixed SEL of 20°. In order to show the actual array output power during the first 90 days
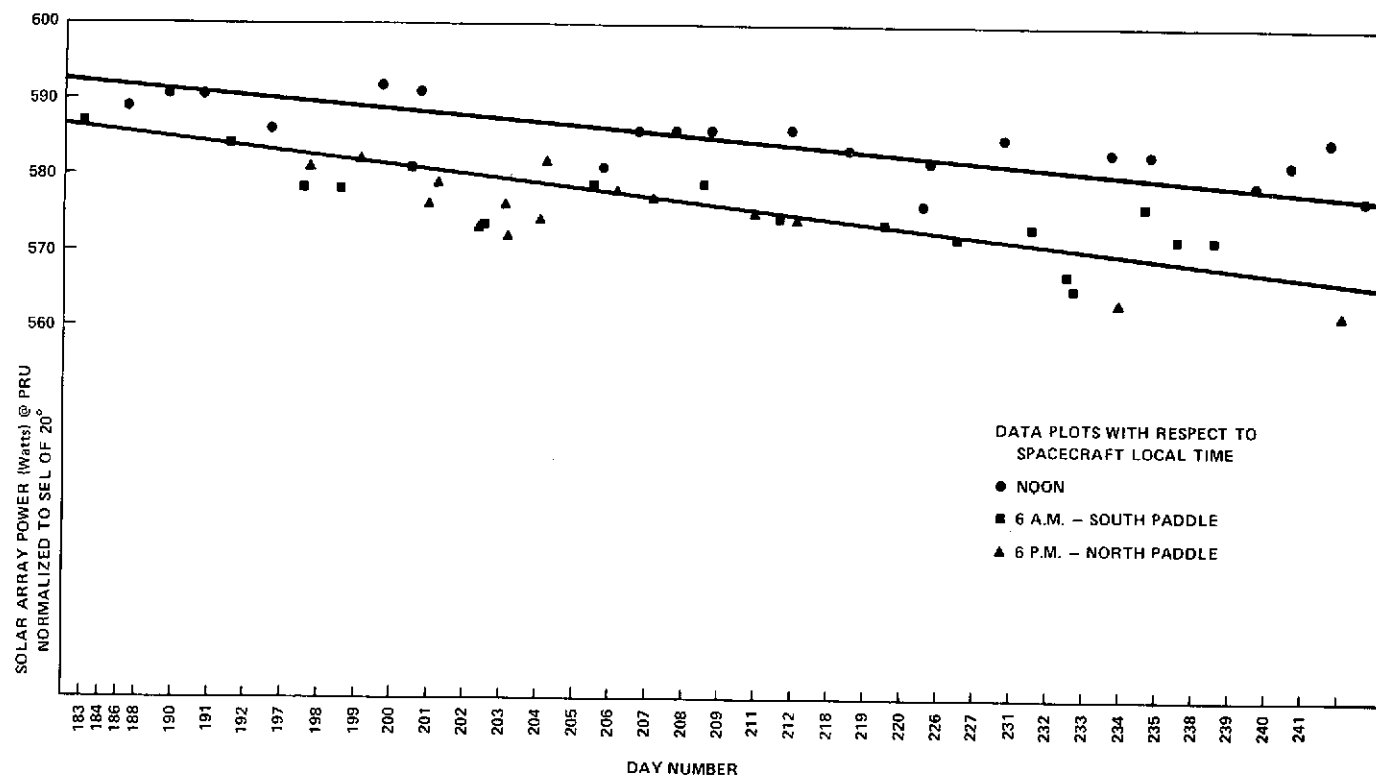
Figure 4-1. Normalized Solar Array Output Power
vs. Day Number

in orbit, a plot of array power versus SEL for various days during the 90-day period is provided in Figure 4-2.

The data in Figure 4-2 indicates that on day 90 the array power was 594 watts which nearly equals the 595 watt power obtained on launch day. The relatively constant power level is attributed to the change from solstice to equinox seasons where the SEL approaches zero.
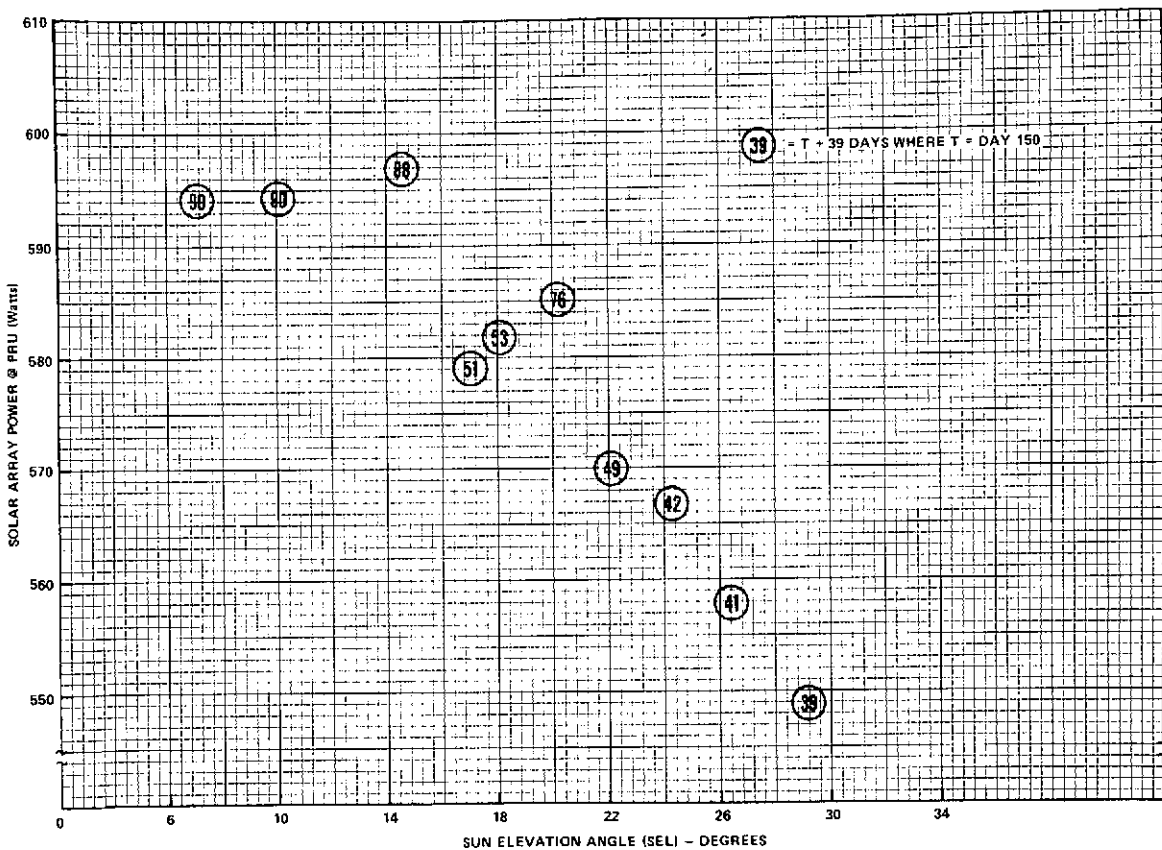
Figure 4-2. Solar Array Output Power
vs. Sun Elevation Angle

4.2 POWER PROFILE

Evaluation of the in-orbit power profile versus the prelaunch power profile was conducted during the first 90 days of flight. Conclusions of this evaluation are: 1) the in-orbit experiment load profile agreed with the prelaunch experiment load profile and 2) the EPS was able to support a greater overall power profile than was planned due to an increase in solar array power output (actual = 595 watts, predicted = 555 watts).

Verification of the experiment load profile was obtained by observing delta changes in the spacecraft load current as the experiments were activated. A comparison of the measured in-orbit data versus prelaunch data for experiment loads is shown in Table 4-1, which indicates good correlation.

Table 4-1

Experiment/Mode Profile Comparison
(In-Orbit vs Prelaunch)

Experiment Mode	Prelaunch COMM + EPS = Total	In-Orbit Δ s/c BUS + COMM STBY = Total
PLACE	237 + 27 = 264 w	235 + 39 = 274 w
HET	242 + 26 = 268	213 + 39 = 252
C-BAND MON	98 + 7 = 105	67 + 39 = 106
TDRE	191 + 18 = 209	183 + 39 = 222
RFI	84 + 7 = 91	70 + 39 = 109
ITV	265 + 26 = 291	254 + 39 = 293
MMW	80	85.8
VHRR	56	60
PROP	13	12
EME	46	50.8
ION ENG	163	165
QCM/ATFE	14	13

A representation of the total spacecraft conditioned power versus spacecraft mode is shown in Figure 4-3. This figure shows that the total conditioned load supported for each spacecraft mode is somewhat greater than prelaunch predictions. This increase in overall profile load is due to increased requirements in the following subsystems:

T&C: DACU 1 and TLM XMTR are left on to provide dwell data

ACS: The YIRU is left on in the monitor mode

COMM: The synthesizer, TCD, DC-DC converter, and 28-volt regulator #1 are left on in the COMM STBY mode.

4.3 BATTERY PERFORMANCE

4.3.1 General

Both of the 15 ampere-hour rated batteries continued to support power requirements exceeding the solar array capability during the second and third months in orbit. Discharge loads of up to 6.5 amperes per battery were exhibited during some of the high power experiments (including HET) and varied continuously with configuration changes and wheel pulsing. Depth-of-discharge was monitored via a computer program and was limited to 50 percent. Battery charge and taper charge performance continued within specification as indicated in the In-Orbit Checkout Report. Fully charged clamp voltages were identical to those previously reported indicating no significant end-of-charge voltage degradation.

4.3.2 Battery Temperature

A partial daily thermal cycle was reviewed and plotted as Figure 4-4. Battery 1 and 2 case temperatures continue to track within a degree centigrade and conform closely to the thermal profile shown in the checkout report.

4.3.3 Battery Operation

Battery 1 and 2 continue to share loads within one-tenth of an ampere and to track terminal voltages during both charge and discharge within one-tenth of a volt. The uniformity of performance is a certain indicator that all cells are performing. A true indicator of battery performance is how it behaves under load. Several plots of data are presented representing HET or similiar mode discharges and are discussed in the following paragraphs.
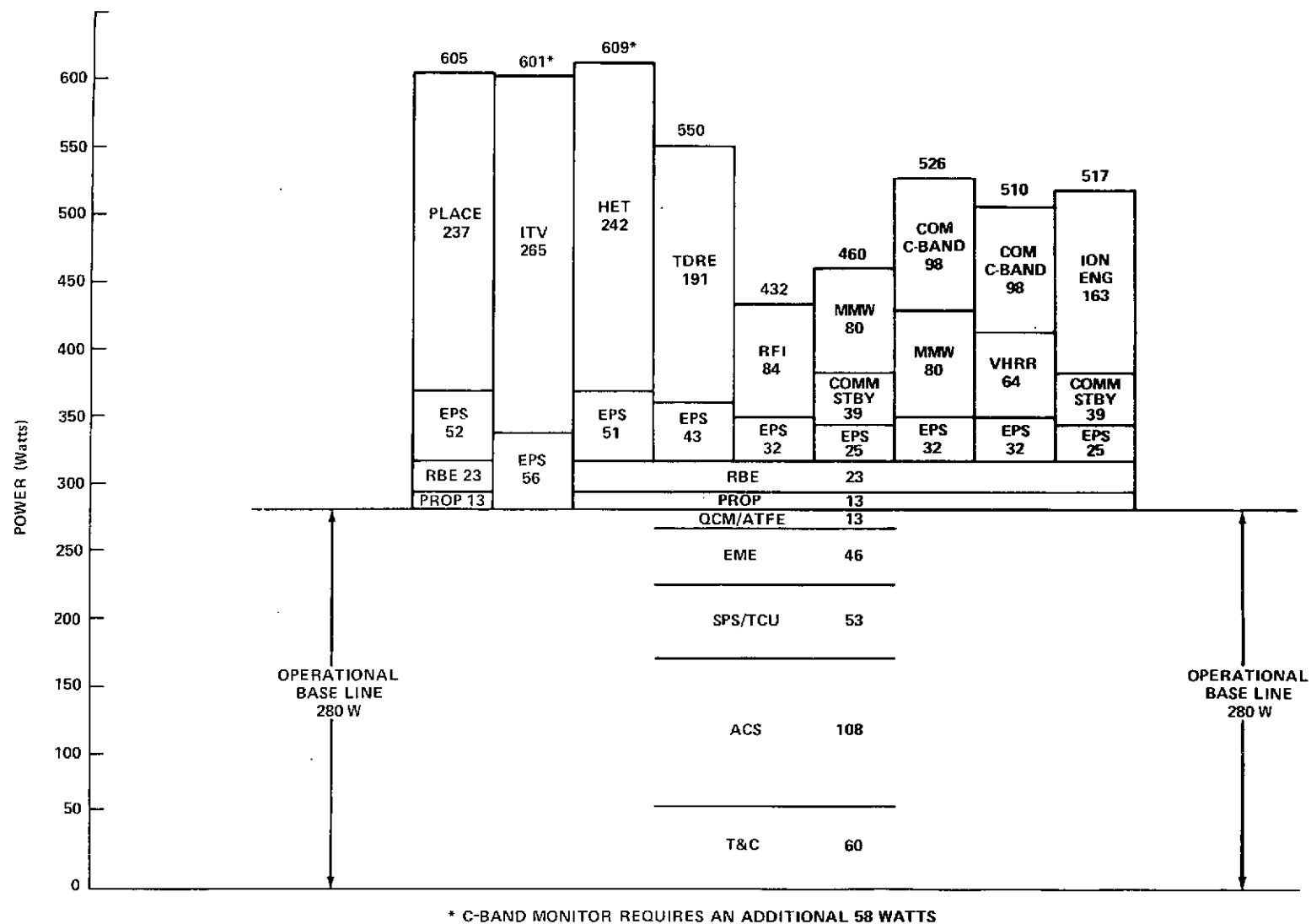
Figure 4-3. Spacecraft Mode Power Requirements
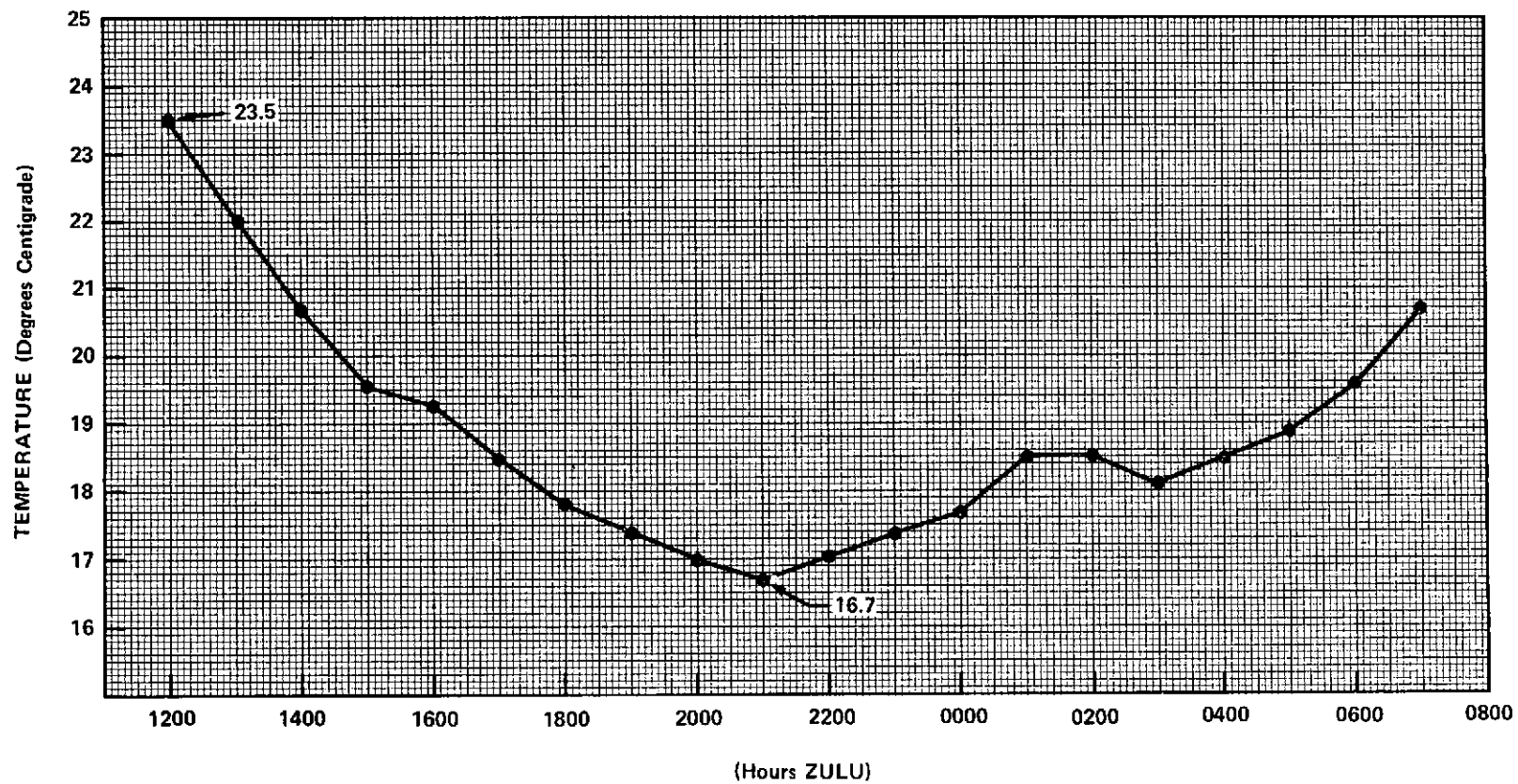
Figure 4-4. Battery 1 Case Temperature
vs. Time (Day 223)

4.3.3.1 Low Current Discharge—Two low-current discharges were plotted in Figure 4-5 for comparison of battery performance over a time span of some 60 days. The first discharge data (day 164) was obtained during a UHF experiment checkout mode and the second (day 224) during one of the HET transmissions. The loads, averaging 0.5 ampere and 0.8 ampere for days 164 and 224 respectively, varied throughout the discharge duration explaining the rise and fall of the terminal voltage. To compare battery performance for these dates, points of equal capacity-out (approximately one ampere-hour) are indicated on the plots. The close terminal voltages of 24.7 volts on day 164 and 24.9 volts on day 224 at these points, coupled with the fact that the lower voltage was obtained during a 3.5°C average higher temperature discharge indicates no noticeable nor significant degradation over this 60-day period. It should be noted, however, that neither depth of discharge was greater than 10 percent.

4.3.3.2 Nominal, Medium Current Discharges—For the HET transmissions as well as some other experiment configurations, typical discharges average between 2 and 4 amperes per battery. Unfortunately for comparisons, each discharge is different. Current loads sometimes start low and increase or vice versa and they often rise and fall with configuration changes. To make matters worse, discharges take place at different times of day, varying the battery temperature and hence the terminal voltage. In addition, the exact state-of-charge at the beginning of the discharge can only be approximated. Several HET discharges were selectively chosen to minimize these variations and were plotted in Figure 4-6 for comparison. The low-current discharges (days 196 to 246) were plotted to exemplify the gross difference in discharge voltage with time that can be observed if the load currents are not matched or if the initial conditions are different. All state-of-charge (SOC) information shown is either recorded computer information or estimated from three-second interval computer data printouts. Looking at days 196 and 246 shows that they reach 93 percent SOC within 10 minutes of each other. Day 196 is characterized by a high initial discharge rate while the day 246 discharge starts out in the tenths of an ampere range and increases to several amps at about T=45 minutes. Comparison of days 169 to 227 is most meaningful if points of equal (approximate) depths-of-discharge are compared. These points reveal close terminal voltages over the 58-day period and show no evidence of gross degradation.

4.3.3.3 High Current Discharge—A battery discharge was observed on day 211 which resulted in a terminal voltage of 22.8v at approximately 50 percent SOC. The accumulated data is plotted in Figure 4-7 representing discharges of 2 to 4 amperes for the major portion of the discharge with pulses up to 6.3 amperes during the last two minutes of discharge. Plotted on the same curve is the final 15°C capacity discharge performed during battery 1 acceptance testing. Comparing terminal voltages at the 50 percent SOC. shows approximately a 0.8 volt
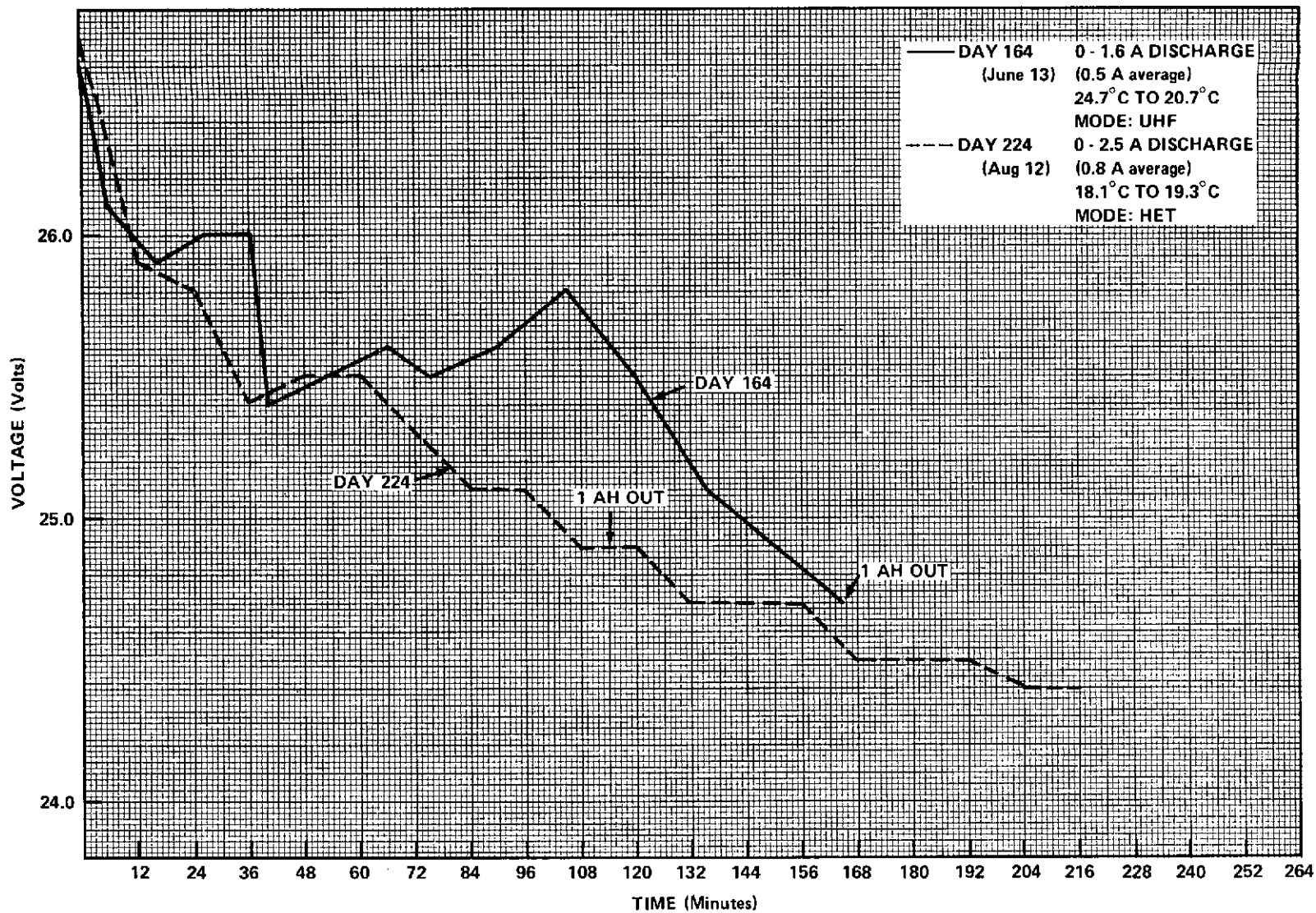
Figure 4-5. Battery 1 Discharges vs. Time
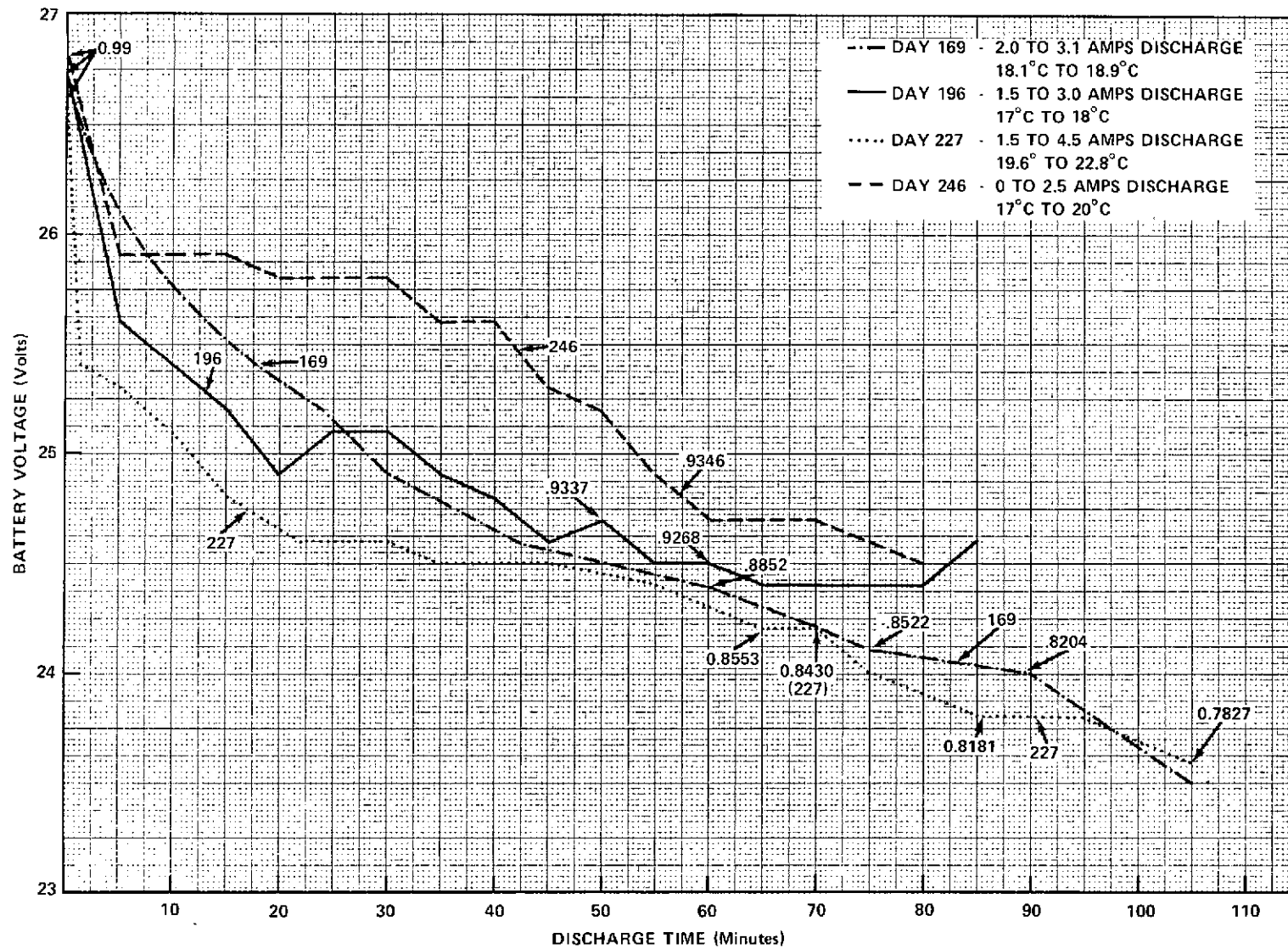
Figure 4-6. Battery 1 Discharges – HET vs. Time
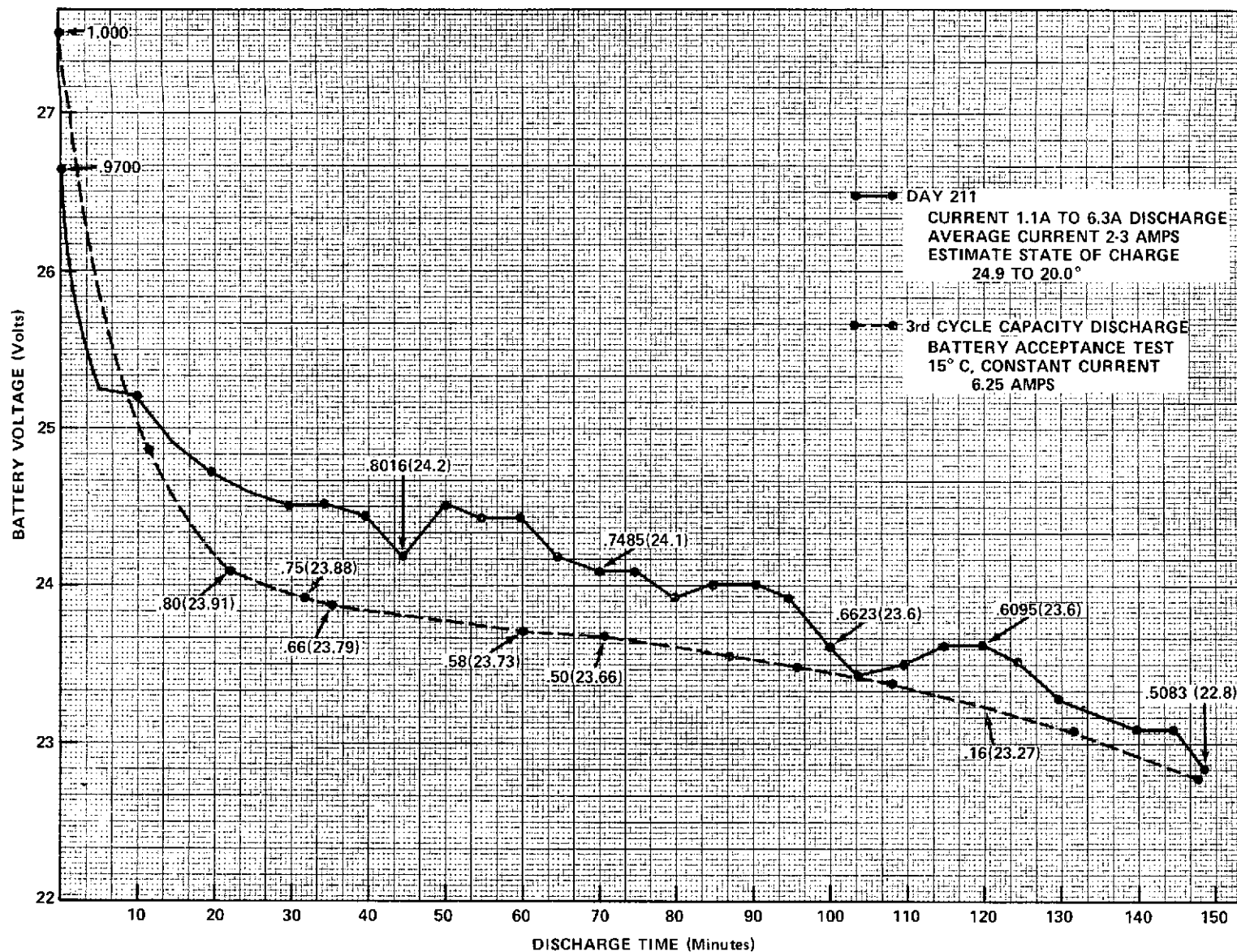
Figure 4-7. Battery 1 Discharge vs. Time

decrease in voltage on day 211 from that seen during ground testing. This effect could have several causes, the two most likely being noncomparable data or voltage degradation. The latter effect is a known phenomenon and is characteristic of NiCd cells.

The high current discharges expected during the occult period will be monitored to further evaluate this condition.

4.3.3.4 Summary of Battery Discharge Cycles—During the first 90 days, approximately 77 battery discharge cycles occurred with depth-of-discharges varying from 4% to 50%. Battery SOC data during the first 66 days was obtained from the EPS log. Data for the remaining 24 days of the quarter was not retrievable from history tapes (SOC is not on the history tape at the present time) and hence had to be estimated from major experiment (HET, PLACE, TRUST) operational periods. Table 4-2 gives the cummulative battery discharge cycle history from launch (day 150) through day 240. Insufficient data is available at the present time to draw any conclusions concerning how battery life will be effected by these discharge cycles. Futher analysis of significant battery parameters will continue so that trends may be observed to develop possible battery life relationships. Battery discharge cycle information (SOC 1 and SOC 2) is presently being monitored and recorded by ATSOCC personnel on a daily basis to assist in this analysis. Additional efforts are also being made to include better SOC information on the history tapes and in the off-line software system.

4.4 ANOMALOUS PERFORMANCE

4.4.1 Solar Array Shunt Tap Voltage for Shunt Dissipator A419

The tap voltage of shunt dissipator A419 has been monitored as suggested in the ATS-6 In-Orbit Checkout Report in an attempt to determine the cause of the high tap voltage observed during share modes of operation at approximately 2200 GMT.

The condition was last observed during the period of 209:22:02 to 209:22:20 when the tap voltage peaked at 25.1 volts. Since that time no unreasonable voltage fluctuations have been observed. There are two probable reasons for the disappearance of the voltage fluctuations: 1) the power system has not normally been in a share mode of operation at 2200 GMT since the conclusion of the spacecraft checkout cycle, and: 2) the SEL has been decreasing with the approach of the equinox period. The decrease in SEL would minimize the shadowing effect of the VHF Omni antenna.

No discernable array power loss has been observed to date which may be associated with this voltage buildup.

Table 4-2

ATS-6 Battery Discharge History

% Depth of Discharge (DOD)	150 (30 Day Checkout)	180	216	240	Totals
10	5	2	5*		12
20	6	8	16*		30
30	4	10	2*		16
40	1	9	2*		12
50	1	4	2*		7
Total Battery Discharge Cycles =					77

*Estimated data

Further monitoring will be required during the next quarter. If the shadowing effect theory is sound, then a similar phenomenon may be observed at approximately 1000 GMT as the winter solstice approaches.

4.4.2 Solar Panel A5 South Temperature/Converter Full Scale Temperature Calibrate Telemetry Failure

On day 210 it was observed that Solar Panel A5 South temperature telemetry was reading 510 counts and the Converter Full Scale Temperature Calibrate voltage was indicating 14.6 volts. This data would indicate that the platinum thermal sensor located on Solar Panel A5 South had developed an open circuit.

The failure was of a cyclic nature for the first seventeen days after it was first observed. Between the hours 1100 to 1500, the temperature sensor functioned properly and the Converter Full Scale Temperature Calibrate indicated a normal value of 15.5 volts. Between the hours of 1500 to 1100 the temperature sensor displayed 510 counts PCM, indicating an open-circuit failure. After reviewing the solar panel 24-hour temperature plots developed during the spacecraft checkout phase, it was seen that the cyclic failure occurred whenever the A5 sensor dropped below 40°C. After day 227 the cyclic failure mode disappeared

and the sensor displayed 510 counts continuously, with the Full Scale Calibrate voltage remaining at 14.5 volts.

The failure of the temperature sensor has no adverse effect on any spacecraft functions with the exception of the external temperature sensors located on other solar panels, the parabolic reflector, the solar array booms, the truss, and the damper panels. The temperature calibration curves for all these monitors will be shifted negatively 28 PCM counts. The calibration curves for these sensors have been revised and incorporated into the ATSOCC data base.

SECTION 5

THERMAL CONTROL SUBSYSTEM

SECTION 5

THERMAL CONTROL SUBSYSTEM

5.1 SUMMARY

ATS-6 thermal control subsystem continues to function satisfactorily during all modes of operation. No serious anomalies have been observed, and the temperatures of all components are being maintained at levels within acceptance and qualification ranges.

The most distinctive indication of the high performance of the EVM thermal subsystem is the relative insensitivity of the individual module temperatures to the various power modes. The average heat pipe wall temperature remains well within the specification requirements range of 20° C ± 15°C. The Experiment Module shows the widest excursion in temperature but mostly due to the spacecraft orientation to the Sun. The average temperature varies between 13°C and 28°C. The Communication Module, where the higher power dissipators are located, shows a maximum temperature of about 30°C (when TWTA's are on) and a minimum value of about 20°C. The Service Module remains at 24°C ± 2°C, almost independent of power variations.

Compilation of data on a periodic basis has continued with special attention paid to the rate of decrease in temperature with the approaching equinox occult. A relationship may exist between emergence of the spacecraft from occult and signal discrepancies in the Polaris Star Tracker. The problem is presently being qualitatively evaluated with respect to possible thermal shock inputs to the solar arrays and solar array booms.

The external SPS temperatures have been observed continuously. It has been elected to limit the valve temperature to no lower than 10°C. This has necessitated turning on the valve backup heaters for about half an hour just before entering occult.

Table 5-1 presents the maximum daily temperature variation of the external SPS components and some outstanding components in the EVM. There is definite repetition of the temperature levels for readings taken 10 days apart. It is expected that only minor deviation from this trend will be observed when the maximum equinox occult occurs.

Typical temperature profiles for sensitive EVM locations and components are shown in Figures 5-1 through 5-5. These profiles coincide with data obtained earlier in the mission thus indicating continuing normal performance. The double peaks appearing in Figures 5-2 and 5-4 are caused by solar eclipse during day number 250 (September 7, 1974).

Table 5-1

ATS Components Daily Temperature Variation

Day:		240	240	250	250
Component	Specification °C	Temperature (°C)			
		Max.	Min.	Max.	Min.
SPS 1					
+ Yaw Valve	5° to 90°	89	35	88	33
− Yaw Valve	5° to 90°	84	32	84	30
Pr West Valve	5° to 90°	80	17	79	14
Bu West Valve	5° to 90°	78	15	78	13
Line, Truss	5° to 90°	58	33	57	35
Line, OCJ	5° to 90°	62	38	62	37
SPS 2					
− Yaw Valve	5° to 90°	79	35	81	33
+ Yaw Valve	5° to 90°	73	30	77	28
Pr East Valve	5° to 90°	84	24	85	21
Bu East Valve	5° to 90°	84	28	85	26
Line, Truss	5° to 90°	62	42	61	41
Line, OCJ	5° to 90°	67	46	66	44
ESA Pitch Head	−7° to 42°	44	2	41	2
ESA Roll Head	−7° to 42°	46	1	43	1
Battery 1	0° to 25°	24	15	24	15
Battery 2	0° to 25°	24	15	24	15
CM North	5° to 35°	26	24	30	20
CM South	5° to 35°	25	22	26	19
SM North	5° to 35°	25	20	25	22
SM South	5° to 35°	24	22	24	22
EM North	5° to 35°	24	16	26	16
EM South	5° to 35°	23	14	28	14
TLM XMTR 1	5° to 35°	34	29	35	28
TLM XMTR 2	5° to 35°	32	30	32	30
TLM XMTR 3	5° to 35°	32	29	32	27
TLM XMTR 4	5° to 35°	28	24	27	24
INTF PV	−20° to 60°	47	7	46	7
INTF RV	−20° to 60°	44	7	42	7
INTF PF	−20° to 60°	41	8	41	7
INTF RF	−20° to 60°	48	−2	48	−2
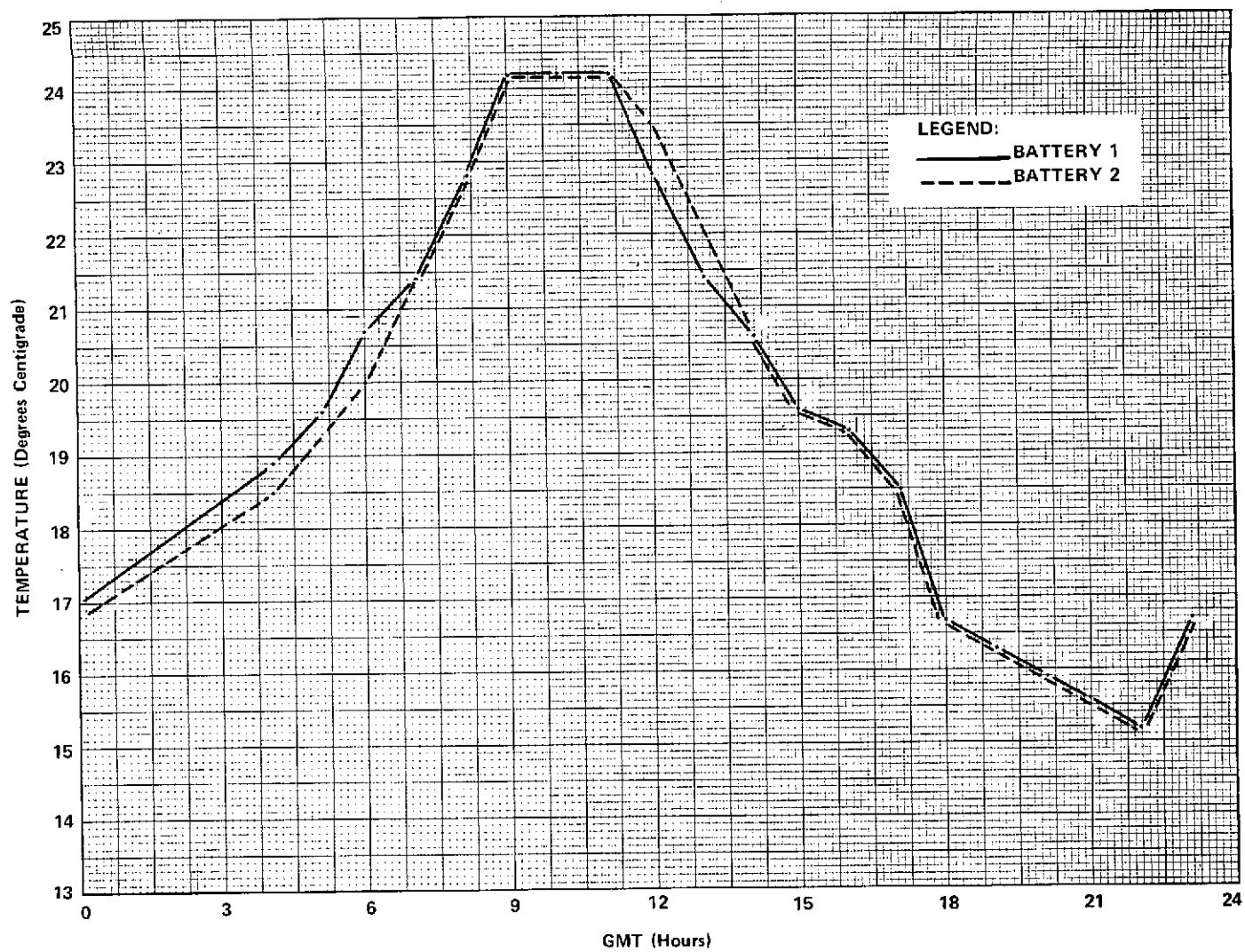
Figure 5-1. Battery Orbital Temperature vs. Time (Day 240)
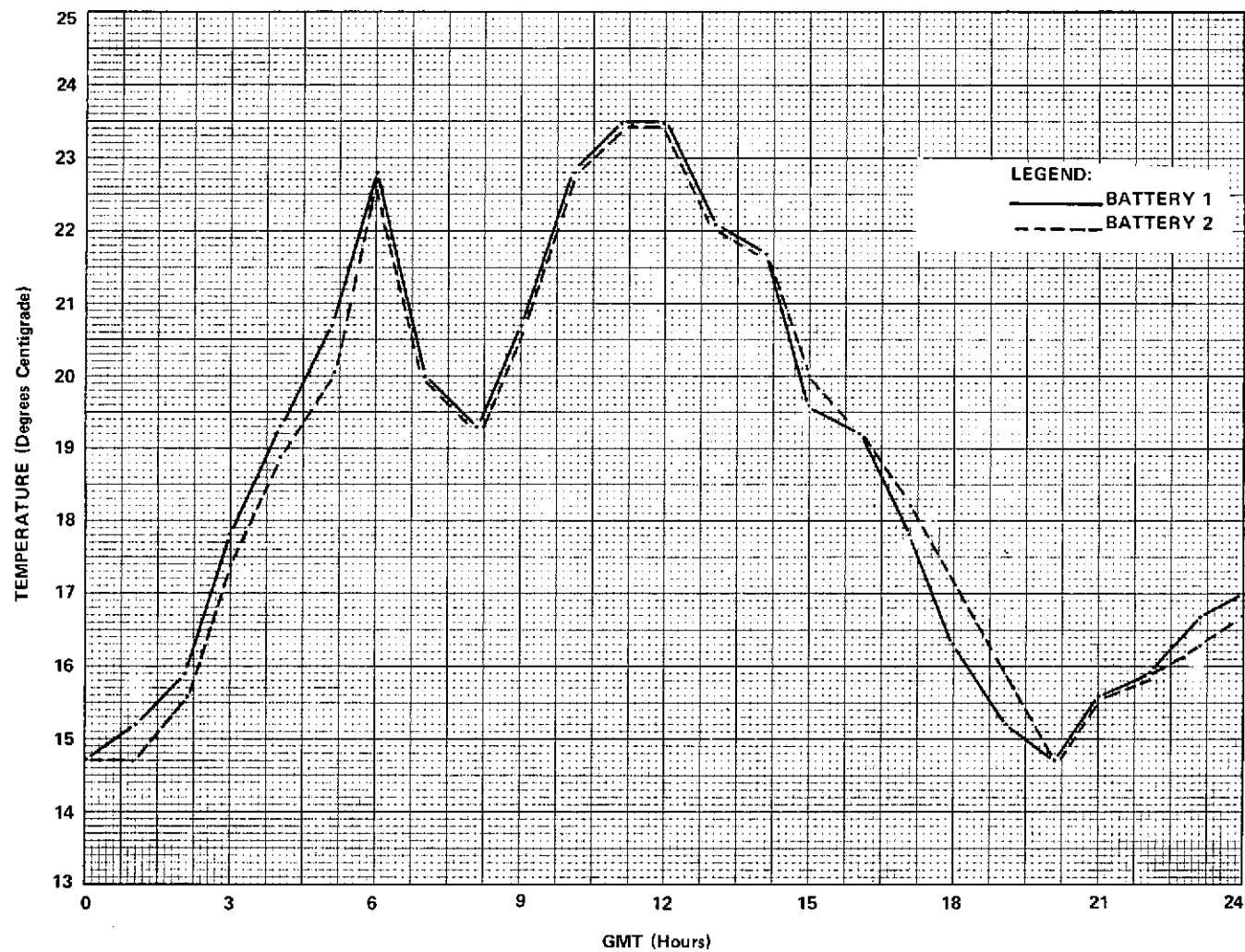
Figure 5-2. Battery Orbital Temperature vs. Time (Day 250)
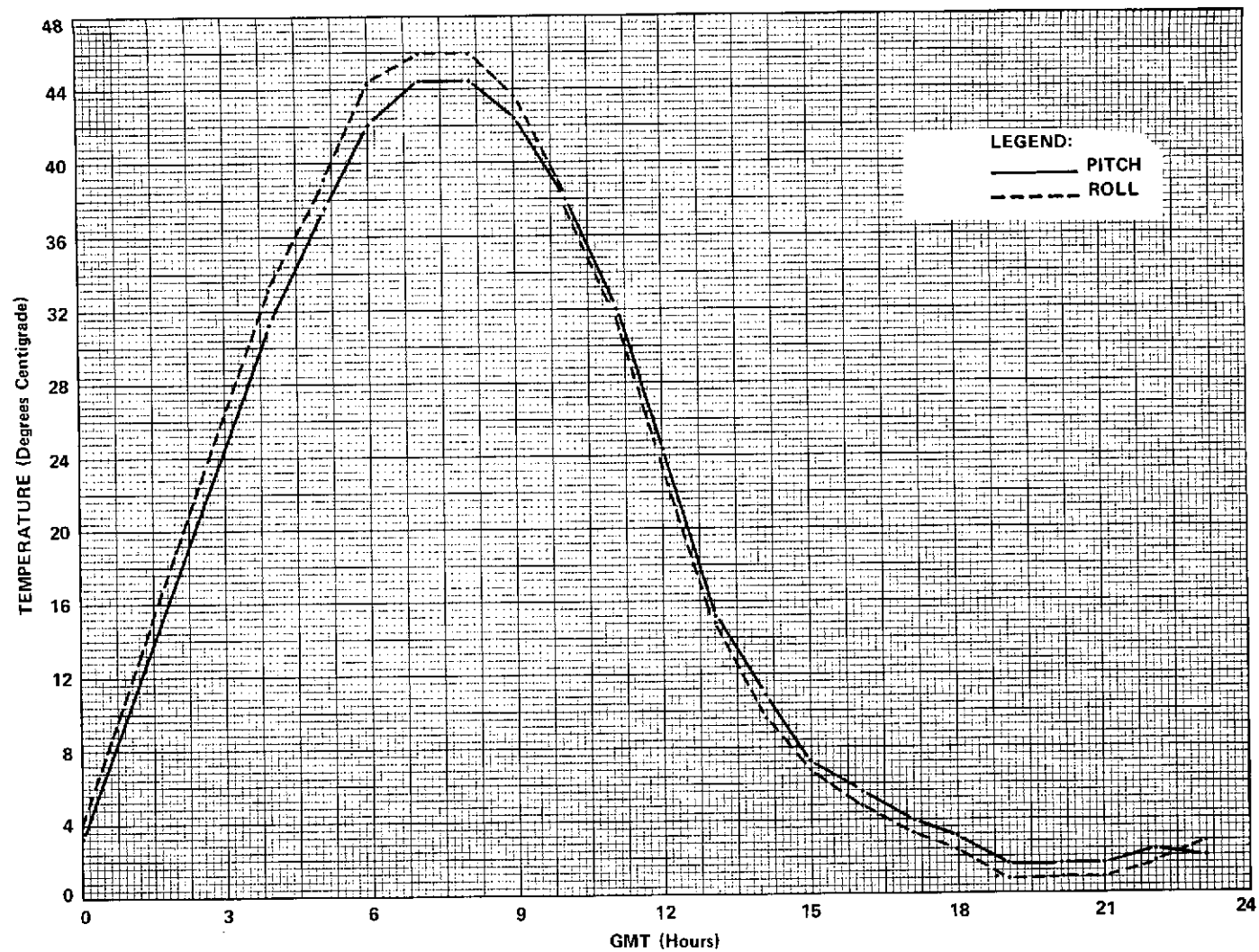
Figure 5-3. Earth Sensor Temperature vs. Time (Day 240)
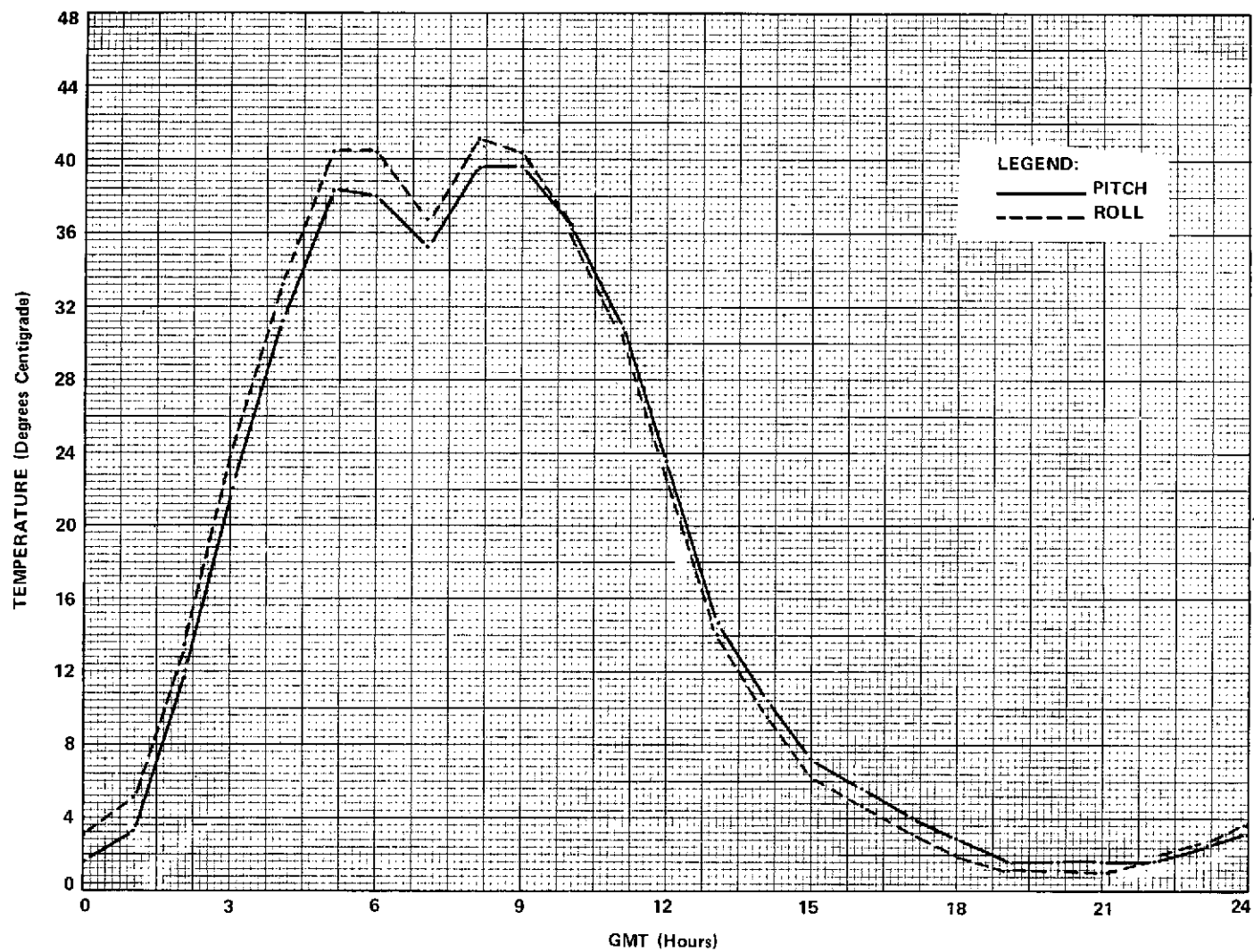
Figure 5-4. Earth Sensor Temperature vs. Time (Day 250)
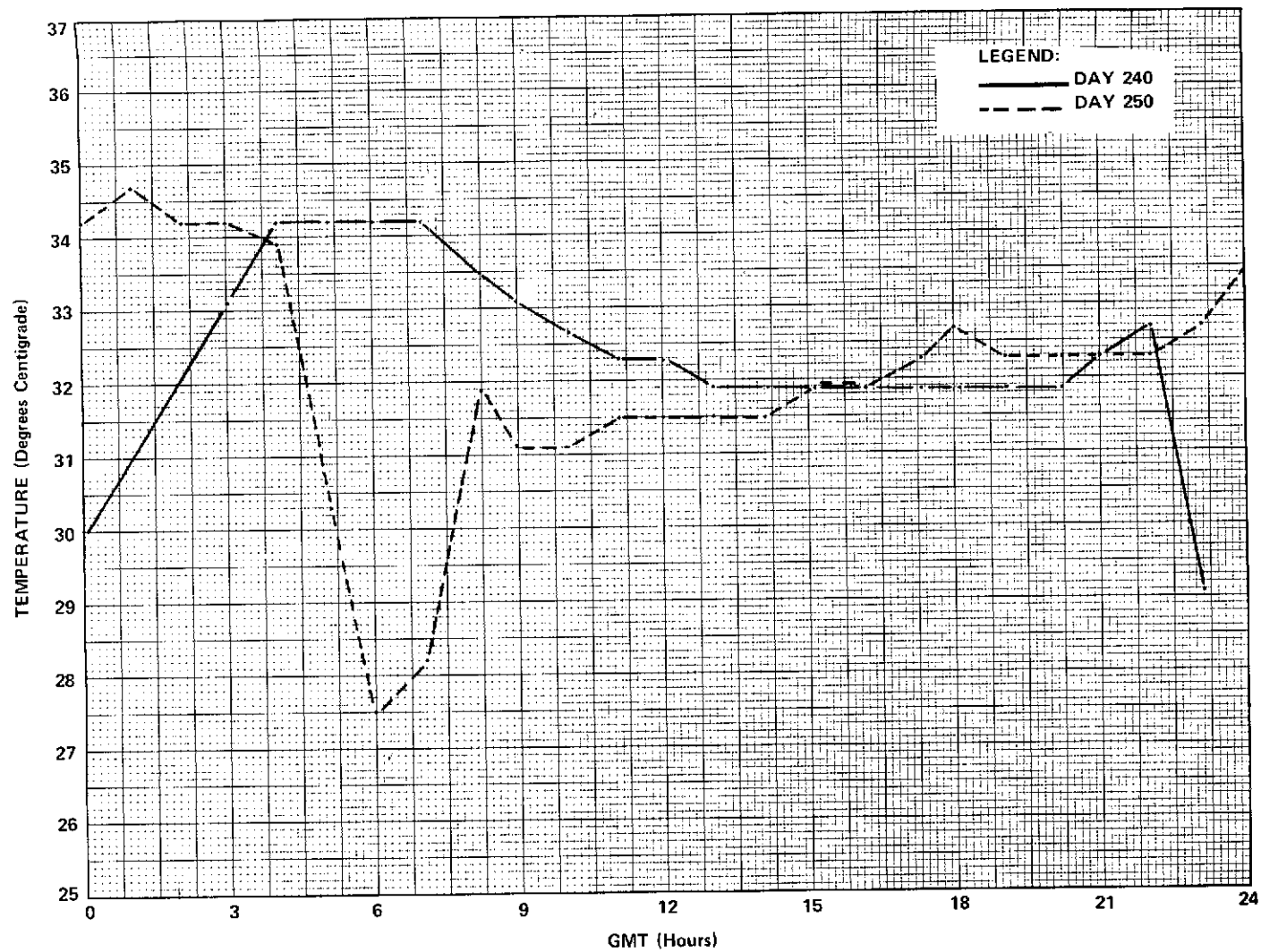
Figure 5-5. TLM XMTR 1 Temperature vs. Time

SECTION 6

TELEMETRY AND COMMAND SUBSYSTEMS

(T&C)

SECTION 6

TELEMETRY AND COMMAND SUBSYSTEM

6.1 INTRODUCTION

The telemetry and command subsystem has performed successfully providing ATS-6 normal telemetry, dwell telemetry, and Environmental Measurements Experiment (EME) telemetry during the last quarter with no anomolies reported. Significant T&C subsystem characteristics monitored during the reporting period are as follows:

    a. Downlink characteristics

        1. Telemetry signal quality including FDM operations

        2. Telemetry time base accuracy

        3. Transmitter power output and frequency

        4. Normal and Dwell DACU operations.

    b. Uplink characteristics

        1. Normal command operations

        2. GAC commond operations

        3. C-band common operations

6.2 SUBSYSTEM CONFIGURATION

The telemetry system configuration (Figure 6-1) used to support ATS-6 operations used the FDM unit to provide both DACU 2 normal and EME telemetry to the A232 telemetry transmitter (137.109 MHz) for downlink transmission via the PFF/30' parabolic antenna. Dwell telemetry was provided via DACU 1 and telemetry transmitter A231 (136.231 MHz) via omni antenna A2. Telemetry transmitter A234 (137.107 MHz) has not been powered on since the 30 day check out and A233 (136.23) has not been on since launch.

The command configuration utilized to support ATS-6 operations is shown in Figure 6-2. The majority of commands uplinked to the spacecraft were sent via the PFF/A242/CDD 2 command link.
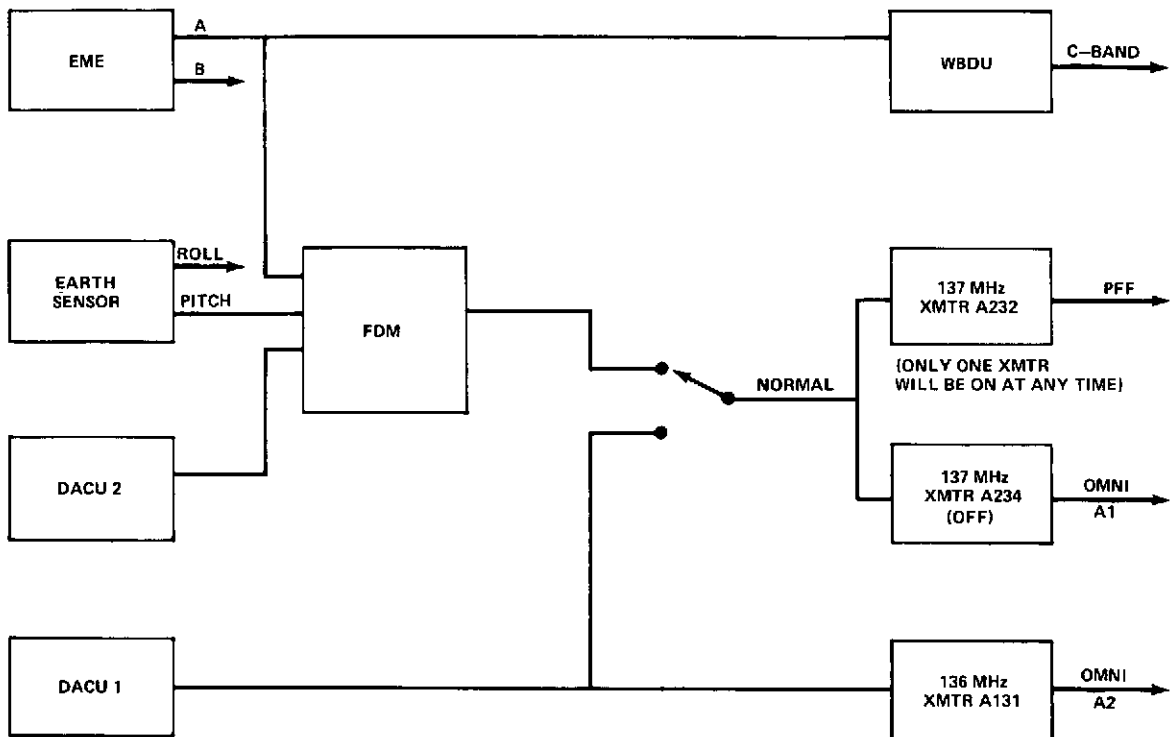
Figure 6-1. TLM RF and Baseband Configuration
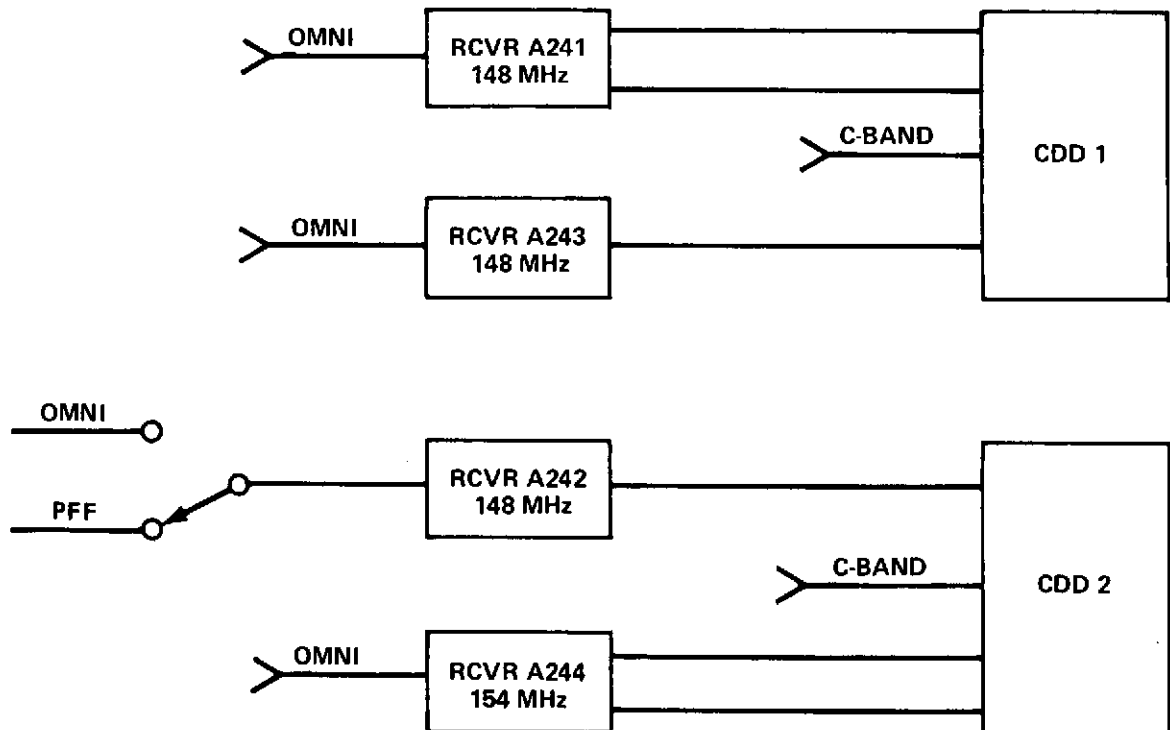
Figure 6-2. Command Configuration

SECTION 7

ATTITUDE CONTROL SUBSYSTEM

(ACS)

SECTION 7

ATTITUDE CONTROL SUBSYSTEM

7.1 INTRODUCTION

During the first three months of in-orbit operations, the attitude control sub-system (ACS) met or exceeded specification requirements and, with the aid of a sophisticated software system at ATSOCC, has continued to be relatively easy to monitor and control from the ground. A summary comparison of ACS performance relative to specification requirements can be found in Table 2-5 of the ATS-6 In-Orbit Checkout Report. In that report, a detailed discussion was given for the following major categories:

a. Launch and Acquisition

    1. Sun Acquisition
    2. Earth Acquisition
    3. Polaris Acquisition
    4. Local Vertical (ABC)

b. Operational Modes (DOC)

    1. Local Vertical Orbit Plane East
    2. Offset Pointing
    3. Station Null Point
    4. Low Jitter
    5. Slewing Maneuvers
    6. Antenna Pattern Maneuvers
    7. Satellite Track

c. Interferometer

d. Inertia Wheel Unload

e. Anomalies

    1. RGA #1 Earth Acquisition Anomaly
    2. PSA Tracking Anomalies
    3. YIRU Bias Anomaly
    4. DOC Command Angle Anomaly
    5. Interferometer AGC IF #2 Anomaly

The following sections of this report will discuss one additional DOC operational mode "Local Vertical Orbit Plane East/West," a twenty-hour C-band monopulse test, and the effects of the moon and noise on the ESA performance. In addition, three anomalies that were discussed in the In-Orbit Checkout Report will also be described further. These anomalies are: 1) PSA tracking anomalies, 2) YIRU bias anomaly, and 3) DOC Command Angle Anomaly.

7.2 REFERENCE ORIENTATION EAST/WEST

Reference Orientation East/West is used to place the spacecraft X axis in the orbit plane with +X pointed east or west, depending on the requirement. The normal flight orientation is with the +X pointed east. The ACS designation for this flight mode, is Local Vertical Orbit Plane East/West.

On day 215, this mode was used to orient the spacecraft +X axis pointed west to allow the use of SPS 1 Orbit Control jets for an orbit correction maneuver. A detailed explanation of why SPS 1 rather than SPS 2 was used for this maneuver is given in the SPS subsystem Section 8 of this report. A rotation of 180 degrees about the yaw axis was made to point the +X axis west. After the maneuver, another 180-degree yaw axis maneuver was made to return to the normal orientation with the +X axis pointed east. The mode was commanded at 215:09:30 GMT using DOC 1 as the controller, the ESA and PSA as sensors, and the wheels as torquers. This configuration was held for 28 minutes. During the period all three axes were limit cycling between ±0.04 degree attitude errors. The performance requirement for this configuration is ±0.1 degree in roll and pitch and ±0.15 degree in yaw.

At 215:09:58, the initial 180-degree yaw-axis maneuver was initiated to point the +X axis west. The maneuver was completed at 215:11:27. The DSS was then selected as the yaw sensor. This configuration was maintained until 215:12:00 at which time the jets were selected as the torquers. The orbit correction maneuver commenced at 215:12:04 and lasted for 5 minutes. The peak attitude errors during the orbit correction maneuver were 0.055, 0.285 and 0.123 degrees in roll, pitch and yaw axis respectively. The specification for attitude errors during orbit correction maneuvers is 0.5 degree in all three axes. At 215:12:10, the second 180-degree yaw axis maneuver was initiated to point the +X axis east. The maneuver was completed at 215:13:35.

7.3 C-BAND MONOPULSE TEST

7.3.1 Introduction

On day 187 (July 6, 1974), a 24-hour test of the C-band monopulse operation was performed. The purpose of this test was to determine the magnitude

of monopulse misalignments with respect to the interferometer, and to determine if any diurnal variation exists in the monopulse misalignments. Test results indicate that misalignments of (-0. 03° to +0. 05°) existed in the monopulse pitch channel. The roll channel exhibited an apparent misalignment of from 0. 05 degree to 0.15 degree. The misalignments are approximately sinusoidal within these limiting values, with a 24 hour period.

Four losses of monopulse control were experienced during the test. Two of these control losses were the result of ground station loss of signal. The two which occurred without apparent loss of ground station power occurred around dawn and dusk spacecraft local time. A possible explanation of these losses of control and the accompanying misalignments, as indicated by interferometer pitch and roll measurements, is that the change in solar incidence across the edge of the reflector resulted in an altered thermal environment for the reflector which in turn caused mechanical distortion of the reflector. After the first of these control losses, the monopulse appears to have acquired control on the antenna side lobes. During the period when the monopulse was controlling on side lobes, the pitch channel appeared to switch from the negative side lobe to the positive side lobe and large errors were observed in the monopulse error signals in both channels. However, no change was observed in AGC level. Additional tests and analysis are recommended to determine the nature of the control loss phenomena and to provide a more precise measurement of monopulse misalignment.

7. 3. 2 Discussion of Test

The twenty-four hour C-band monopulse test was performed controlling the spacecraft on DOC 1 using the monopulse as the roll/pitch control sensor and PSA as the yaw control sensor and using the interferometer error signals to measure the true line-of-sight to the ground transmitter. During the test, an on-line sixteen column printer was used to record monopulse, interferometer and earth sensor outputs. Wheel speed data, AGC levels, and command history data was obtained from off-line telemetry data retrieval.

Figure 7-1 presents monopulse roll and pitch output, wheel direction and DOC 1 control state as a function of time for the test period. Where possible, interferometer data is plotted for comparison. C-band monopulse control was initiated at 187:03:38 and appeared to operate properly until 187:08:36 at which time the Rosman transmitter went down. The loss of the Rosman transmitter is confirmed by the loss of AGC signal on COMM IF 1 and Interferometer IF 1 (Figure 7-2). Figure 7-3 presents the same data as figure 7-2 and is included because it presents all telemetry points (Figure 7-2 is plotted using approximately one data point every 12 minutes) and shows the character of the AGC signals. The data in figure 7-3 appears to have a calibration error of about -4 dBm for
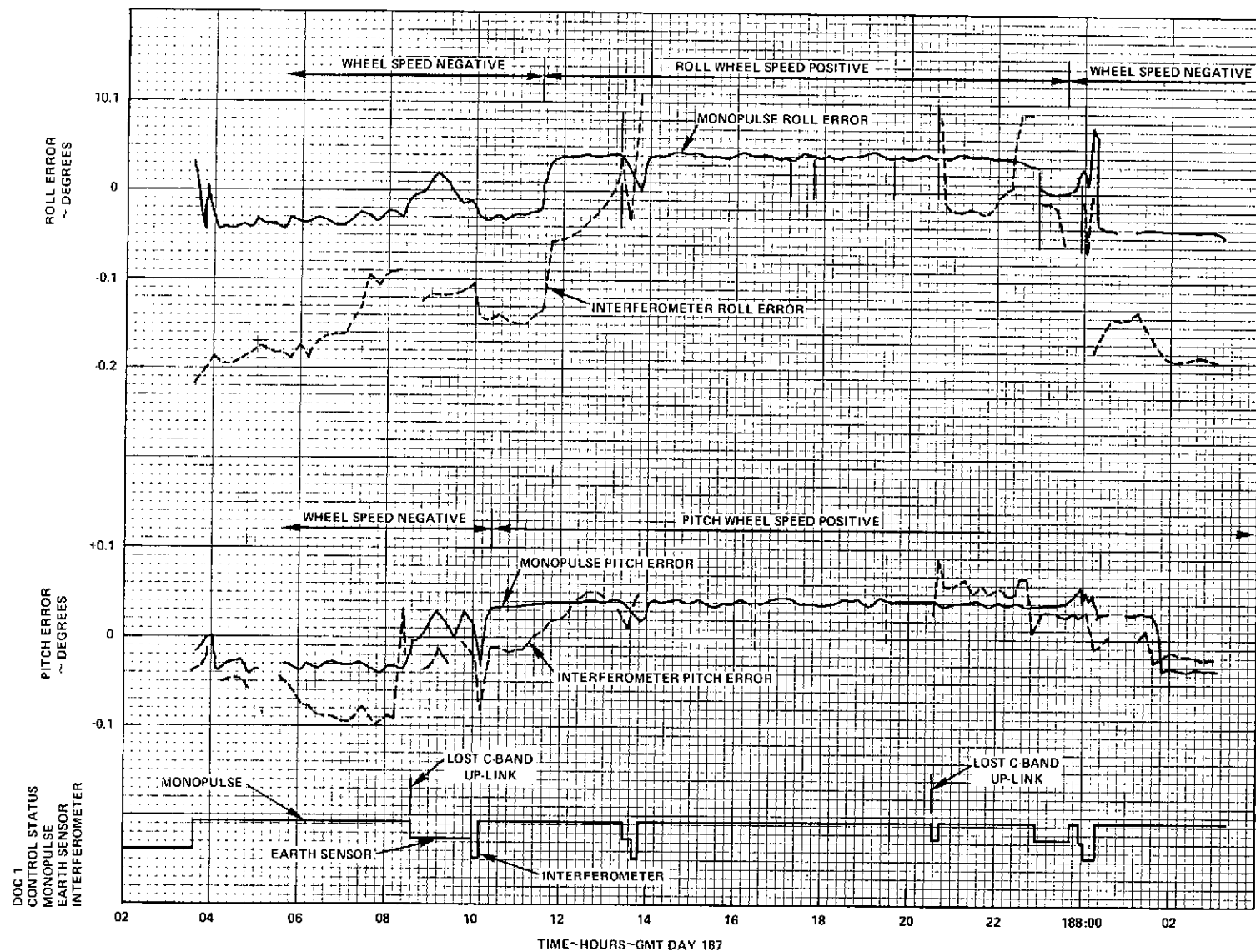
Figure 7-1. Day 187 - Monopulse Errors, Interferometer Errors,
and DOC 1 Control State
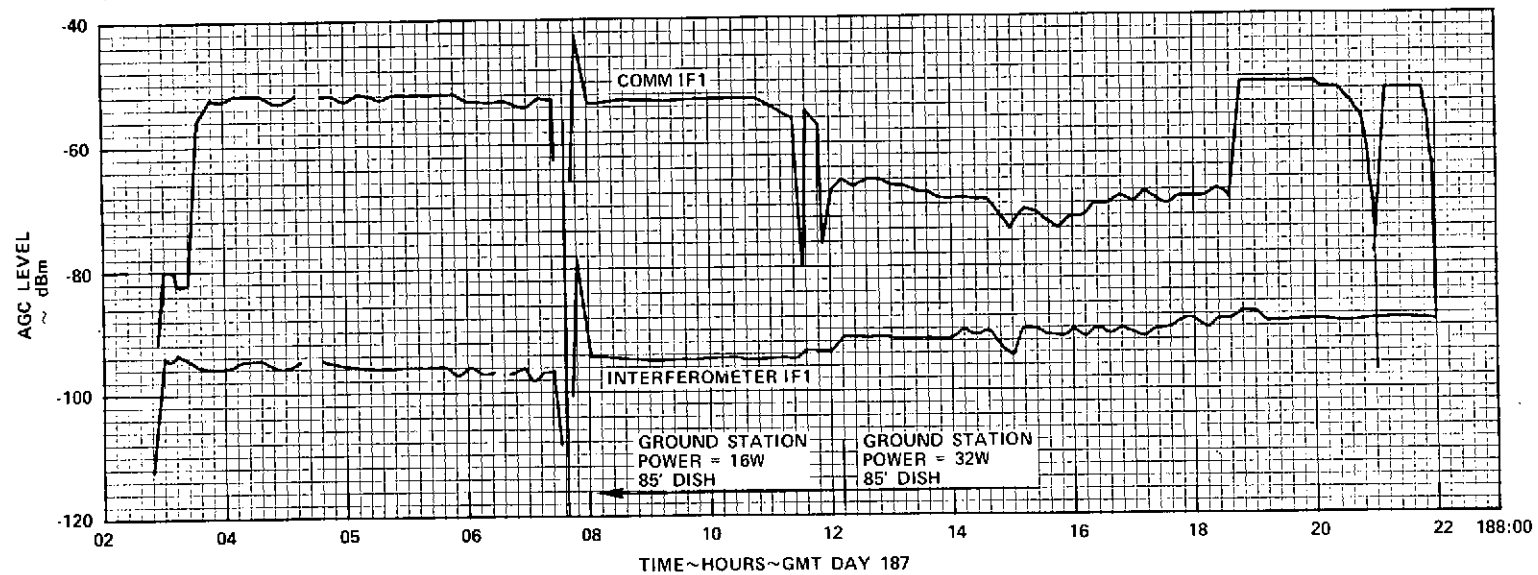
Figure 7-2. Day 187 - AGC Levels
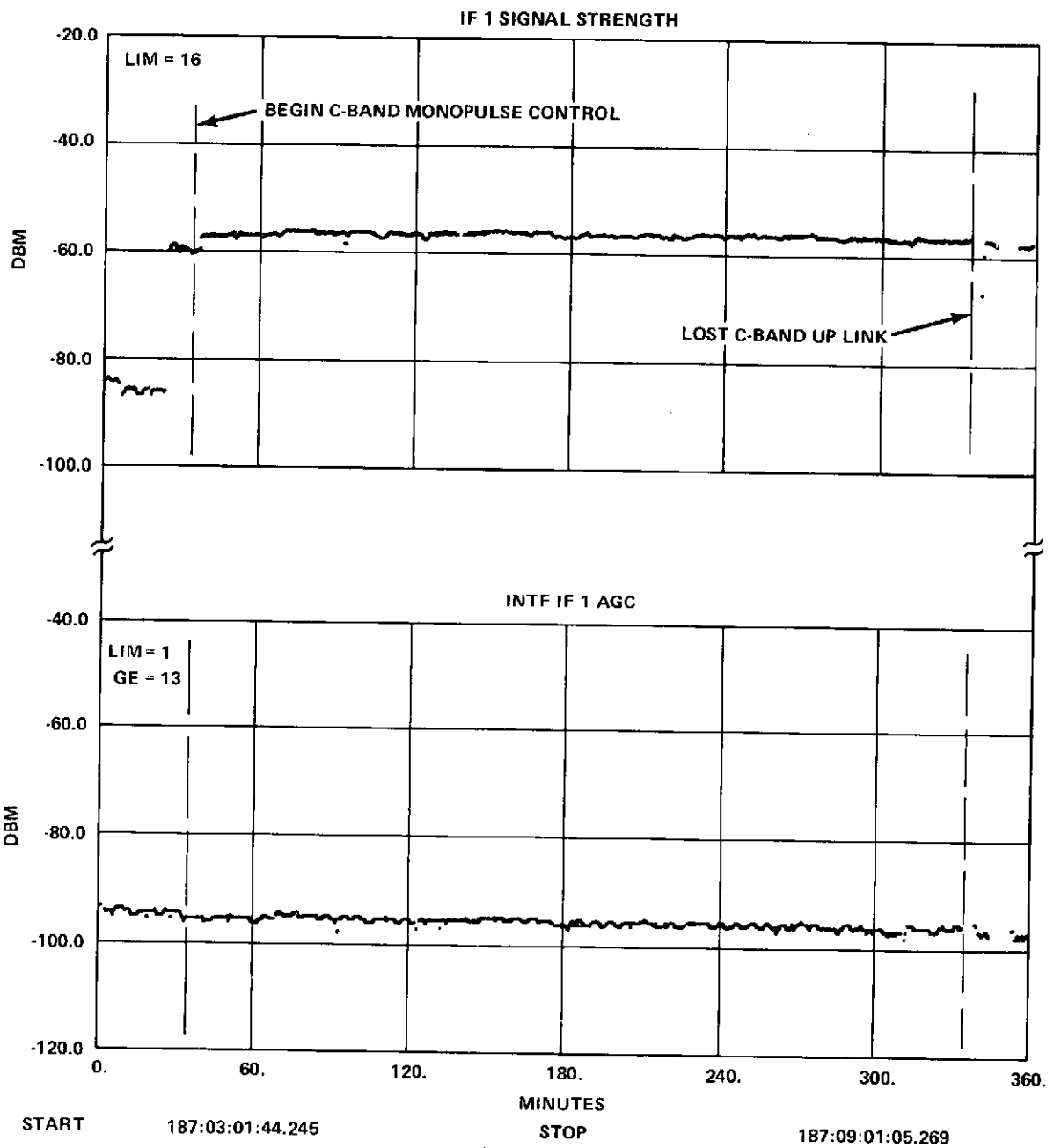
Figure 7-3. Monopulse and Interferometer IF Signal Strength

IF 1 SIGNAL STRENGTH
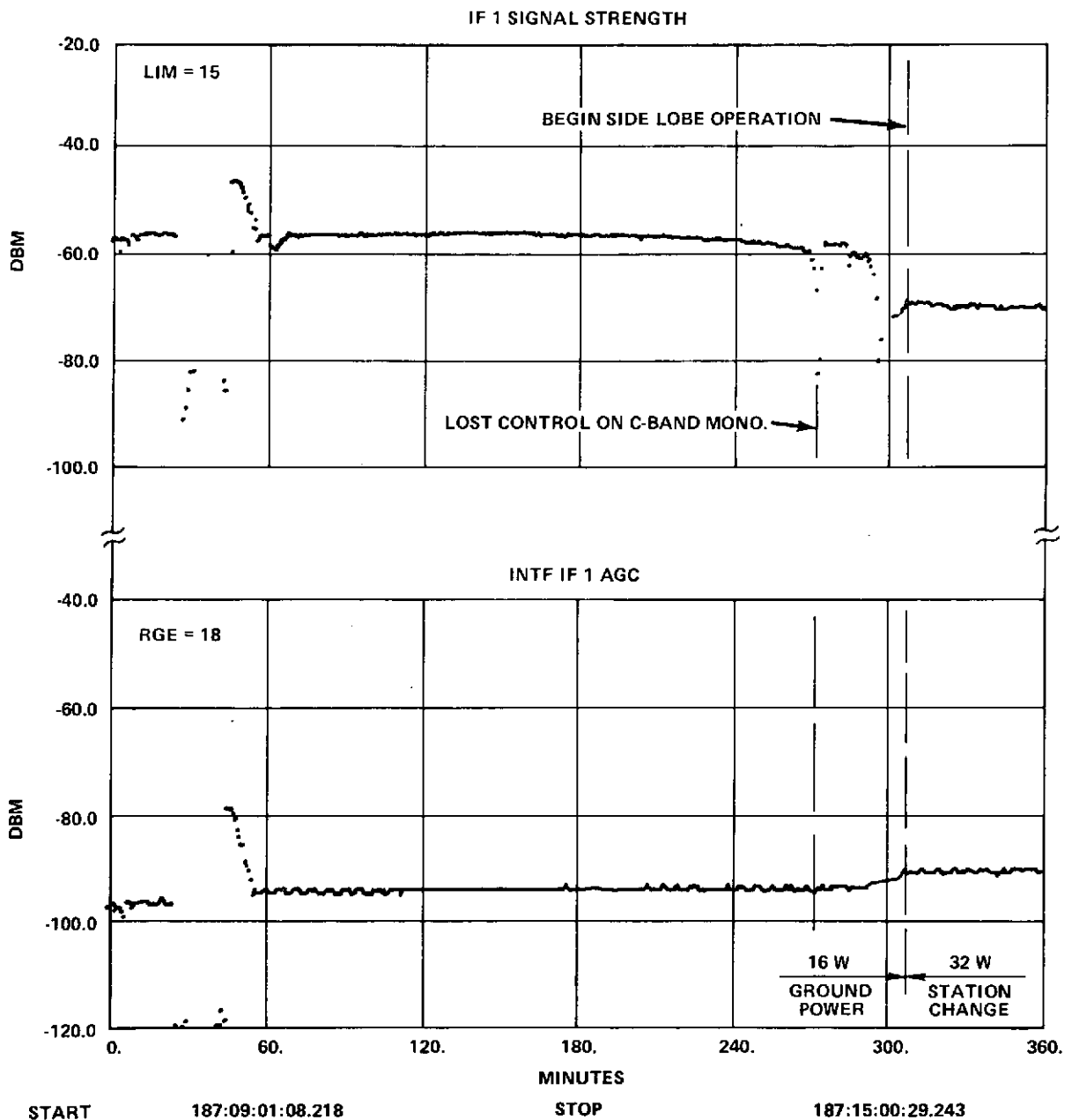
Figure 7-3 (Cont.). Monopulse and Interferometer
IF Signal Strength

Figure 7-3 (Cont.). Monopulse and Interferometer
IF Signal Strength

7-8
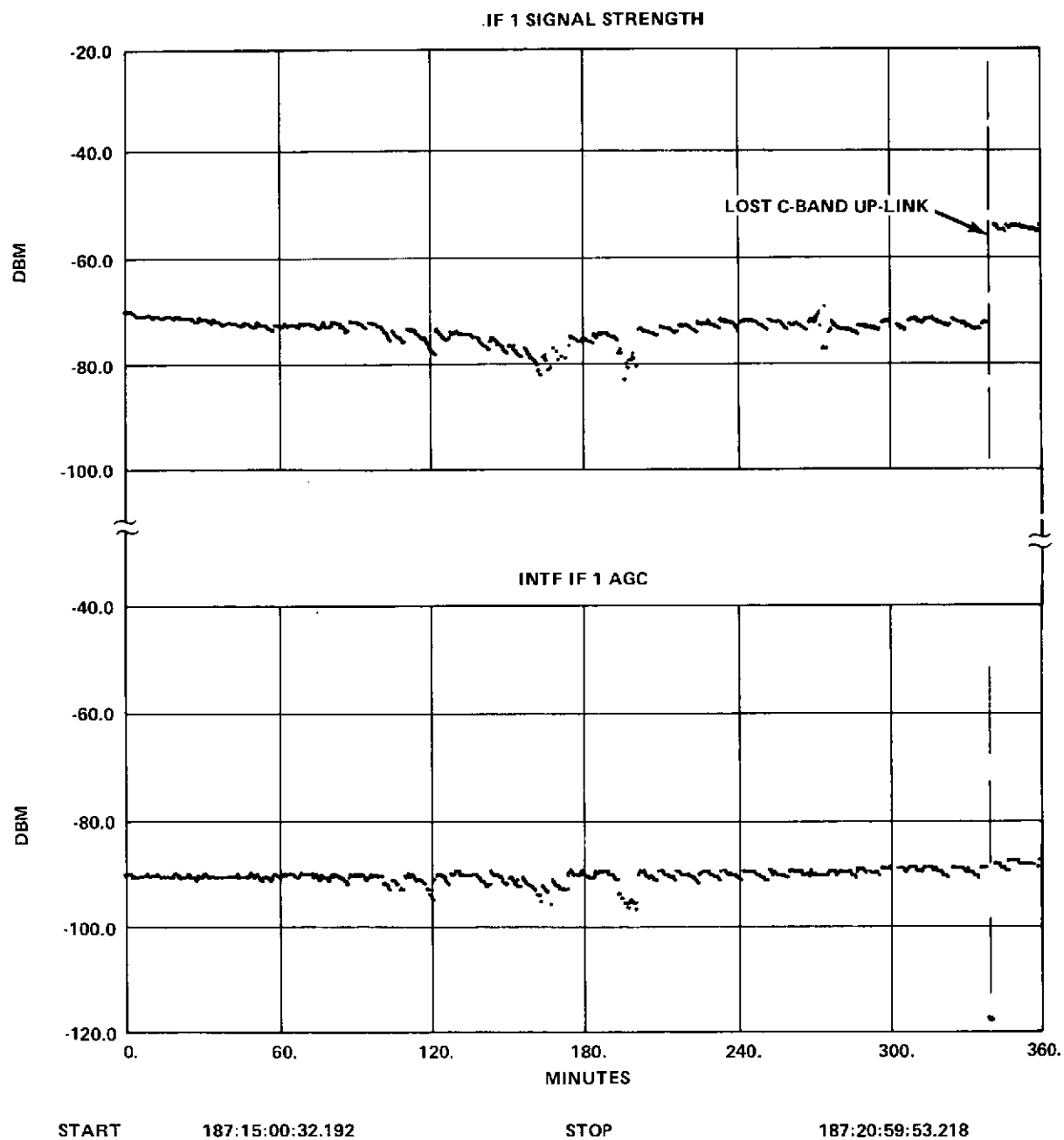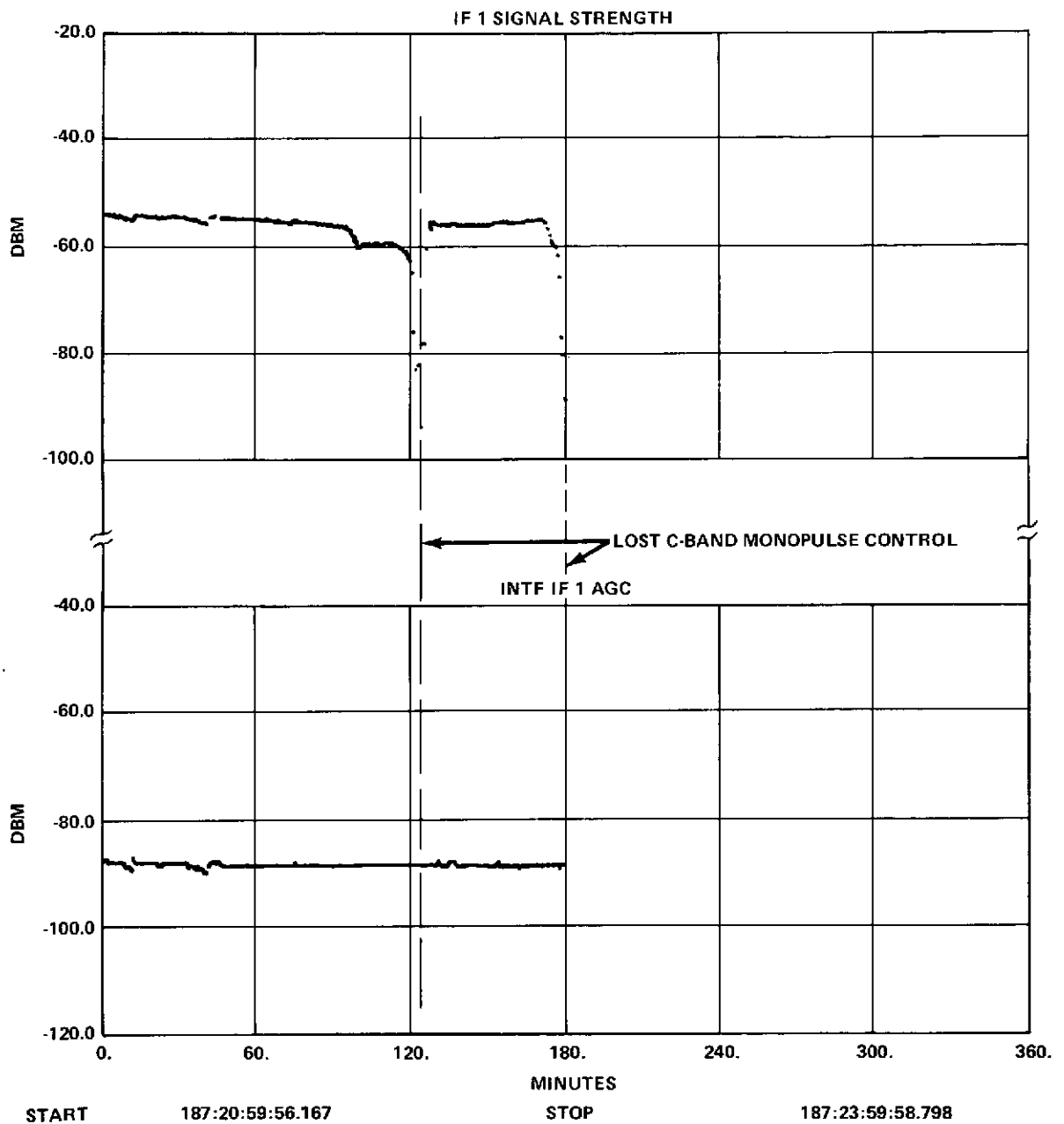
Figure 7-3 (Cont.).   Monopulse and Interferometer
IF Signal Strength

both telemetry channels. During the first five hours of monopulse control the interferometer roll signal went from -0.20° to -0.10°, and the pitch signal went from -0.05° to -0.10°.

Monopulse control was re-established at 187:10:07 with the AGC reading -53 dbm (Figure 7-2) and the interferometer roll and pitch errors (Figure 7-1) reading -0.20° and -0.02° respectively. At approximately 187:11:30 the roll wheel speed changed sign and the control system changed from the negative to the positive dead band. (Pitch wheel speed changed sign within a few minutes of re-establishment of monopulse control.) The change in monopulse error from approximately -0.03° to +0.03° was reflected in the interferometer roll error as a change of about 0.08°. It should be noted that the wheel control loop maintains the control error signal at the DOC deadband value of ±0.044° plus an amount to provide a sufficient drive signal to overcome the wheel run down torque. Since the wheel run down torque is always in the opposite direction from wheel-speed direction, the DOC will hold the sensor error at the positive dead band as long as the wheels are turning in a positive direction and vice versa. During the period from 11:48 to 13:30, the interferometer roll error signal changed from -0.06 to approximately +0.03 while the monopulse error remained steady. Similarly the interferometer pitch exhibited a change from -0.01° to +0.05° during the period from 11:12 to 12:40, again with no significant change in monopulse output. At 13:30 the monopulse lost control and the DOC was commanded to ESA and then to interferometer control. As may be seen from figures 7-2 and 7-3, no loss in interferometer AGC was recorded at this time.

C-band monopulse control was again established at 187:13:49; however, based on interferometer and earth sensor errors, (Figures 7-4 and 7-5), the monopulse appears to have settled on stable nulls approximately 1/2 degree off the ground station. Monopulse control was maintained for approximately seven hours with the monopulse AGC reading in the range of -66 dbm to -74 dbm. These signals strength levels confirm control on the antenna side lobe. At 14:10 the Rosman transmitter output power feeding the 85 foot dish was raised from 16 watts to 32 watts. This change was reflected in the interferometer AGC as a 3 db change and was later confirmed by a COMM IF 1 reading of -51 dbm when mainlobe operation was again attained. At approximately 19:30, the monopulse appeared to lose control, experiencing saturated telemetered outputs over a period of about one half minute, and then regained control at the same error values as before. As may be seen from figures 7-4 and 7-5, the interferometer and earth sensor pitch errors increased +0.9 degree, which indicates that control was transferred from the pitch negative side lobe to the pitch positive side lobe. The interferometer and monopulse AGC telemetry show no indication of ground transmitter loss to cause this temporary loss of control. Side lobe control terminated at 20:39 with loss of the C-band uplink.
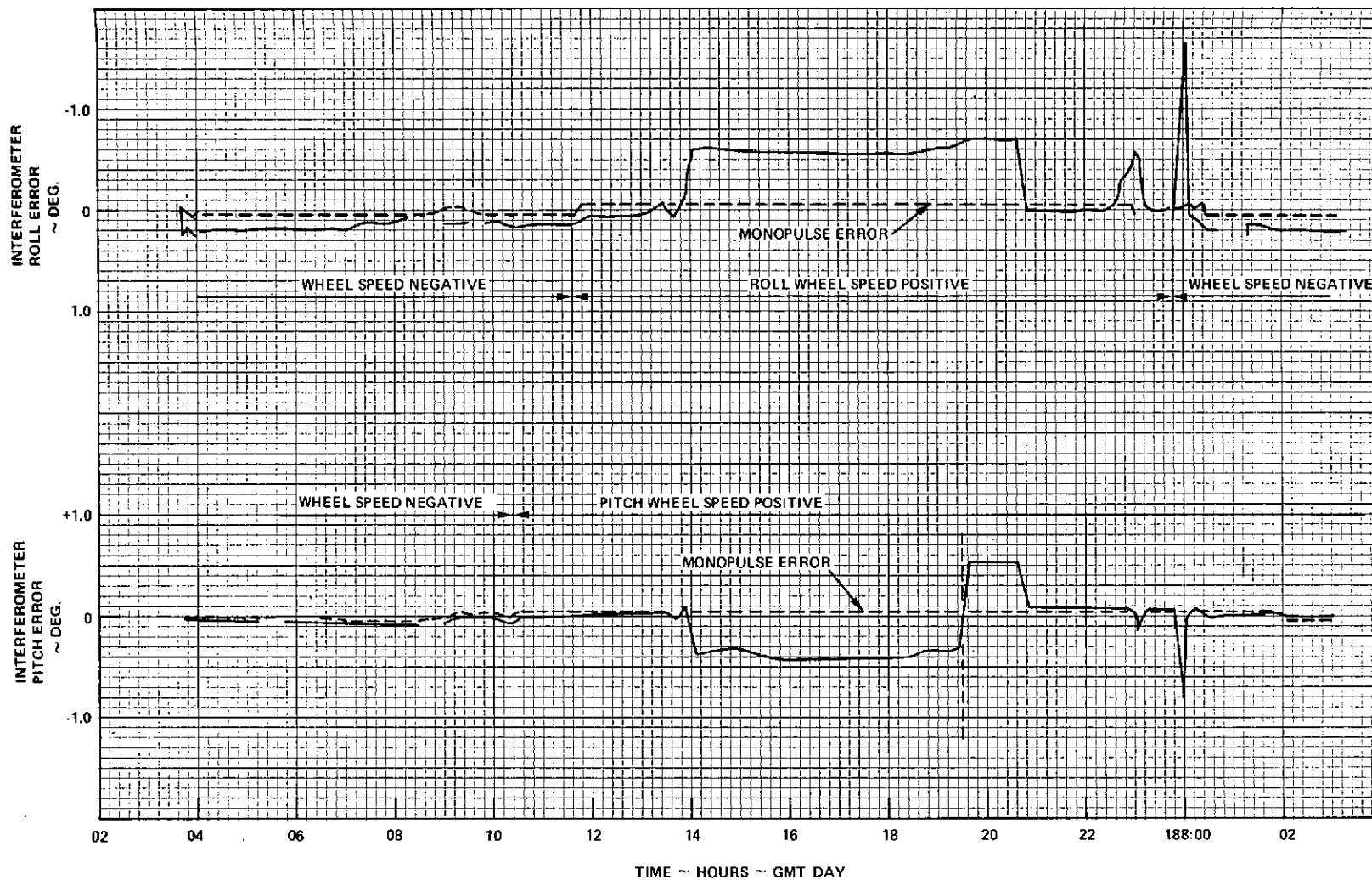
Figure 7-4. Day 187 – Interferometer Error

7-11
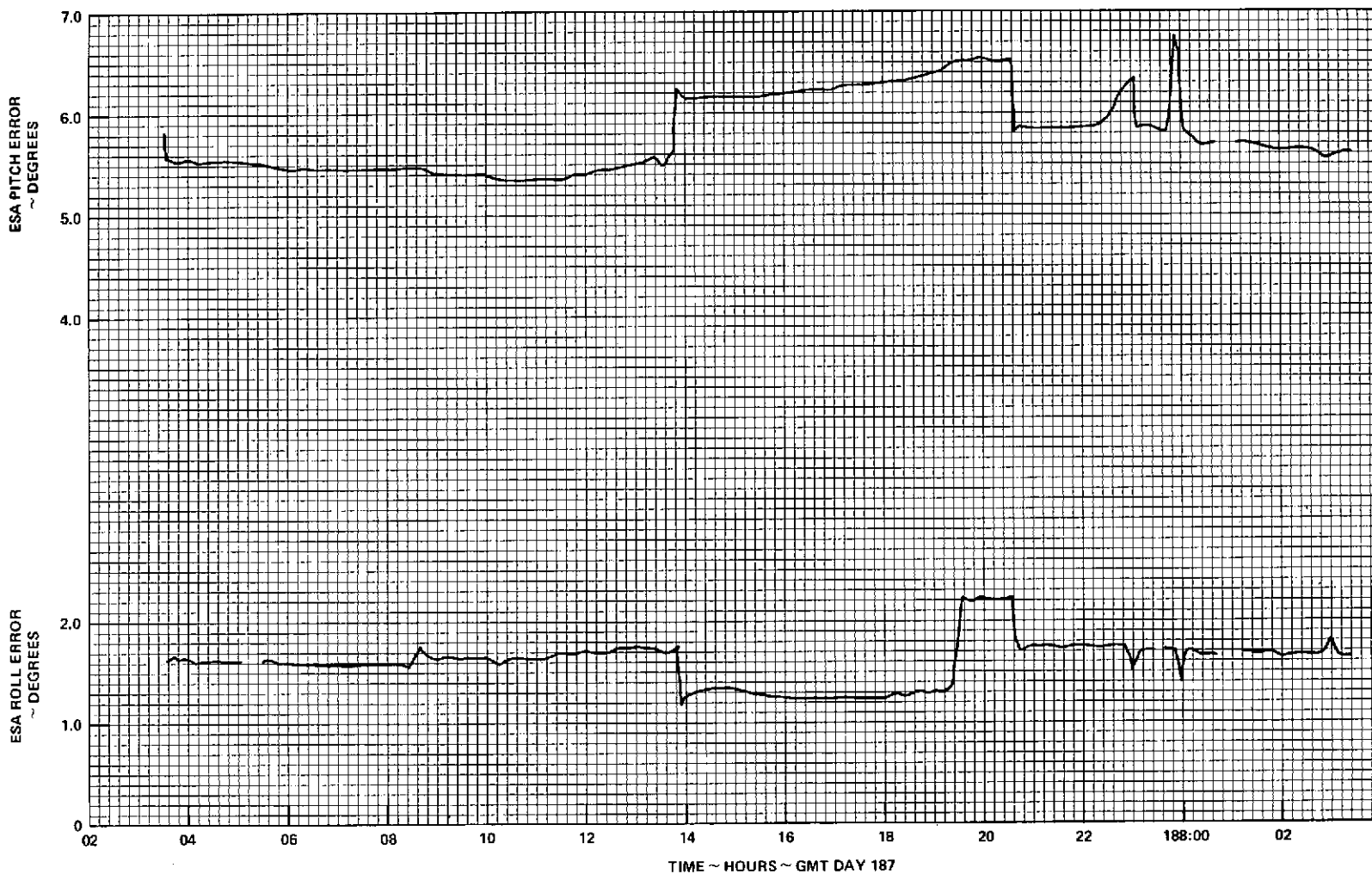
Figure 7-5. Day 187 – Spacecraft Attitude–Earth
Sensor Errors

C-band control was re-initiated directly from ESA-offset Point Ground at 20:47. The interferometer and earth sensor error signals indicate that control was attained on the monopulse main lobe which is confirmed by a monopulse AGC reading of -51 dbm (Figure 7-2). The control system operated on the positive DOC dead band (+0. 04°) during this period with the interferometer roll and pitch errors reading approximately -0. 07°, and +0. 05 degree respectively. At approximately 23:00, control was lost on the monopulse and was not successfully re-established until 188:00:22. The control loss was accompanied by a momentary loss of monopulse AGC but not interferometer AGC.

7. 3. 3 Results of Test

Comparison of monopulse and interferometer error signals shows monopulse roll misalignment to have been +0. 05 to +0. 15 degree during the early (04:00 to 12:00 hours) main lobe operation. Figure 7-6 presents a plot of monopulse misalignment relative to the interferometer as a function of time. During the same period, monopulse pitch appeared misaligned 0. 0 to -0. 05 degree. Side lobe operation precluded evaluation of a major portion of monopulse misalignment during the time when the roll wheel speeds were positive (positive dead band operation). During the one period where positive dead band data was available, the monopulse roll misalignment appeared to be +0. 06 degree and the pitch misalignment appeared to be -0. 02 degree. During the last portion of the test, the control system was operating on the negative dead band in both channels and monopulse misalignments appeared to be +0. 14 degree and -0. 02 degree in roll and pitch respectively. A smoothed estimate of the diurnal variation of monopulse misalignment is presented in Figure 7-6. This estimate shows an average misalignment of +0. 10 degree for the monopulse roll channel and +0. 01 degree for the pitch channel. The variation about these values is ±0.05 degree and ±0. 04 degree in the roll and pitch channels respectively and appears to be sinusoidal with an approximate period of one day. The actual pointing error of the monopulse beam is the misalignment plus the control dead band.

Two losses of control that cannot be attributed to loss of the ground transmitter signal occurred at 13:30 and 23:00 GMT (7:15 and 16:45 spacecraft local time). Both of these control losses were accompanied (11:50 to 14:00 GMT and 22:30 to 02:00 GMT) by changes in the apparent misalignment between the monopulse and interferometer as indicated by the interferometer roll error traces presented in Figure 7-1. These times encompass those periods when the thermal environment of the reflector goes through its greatest change. The mechanism by which thermal distortion of the reflector would cause loss of control and/or transfer to side lobes is not explained by the data.
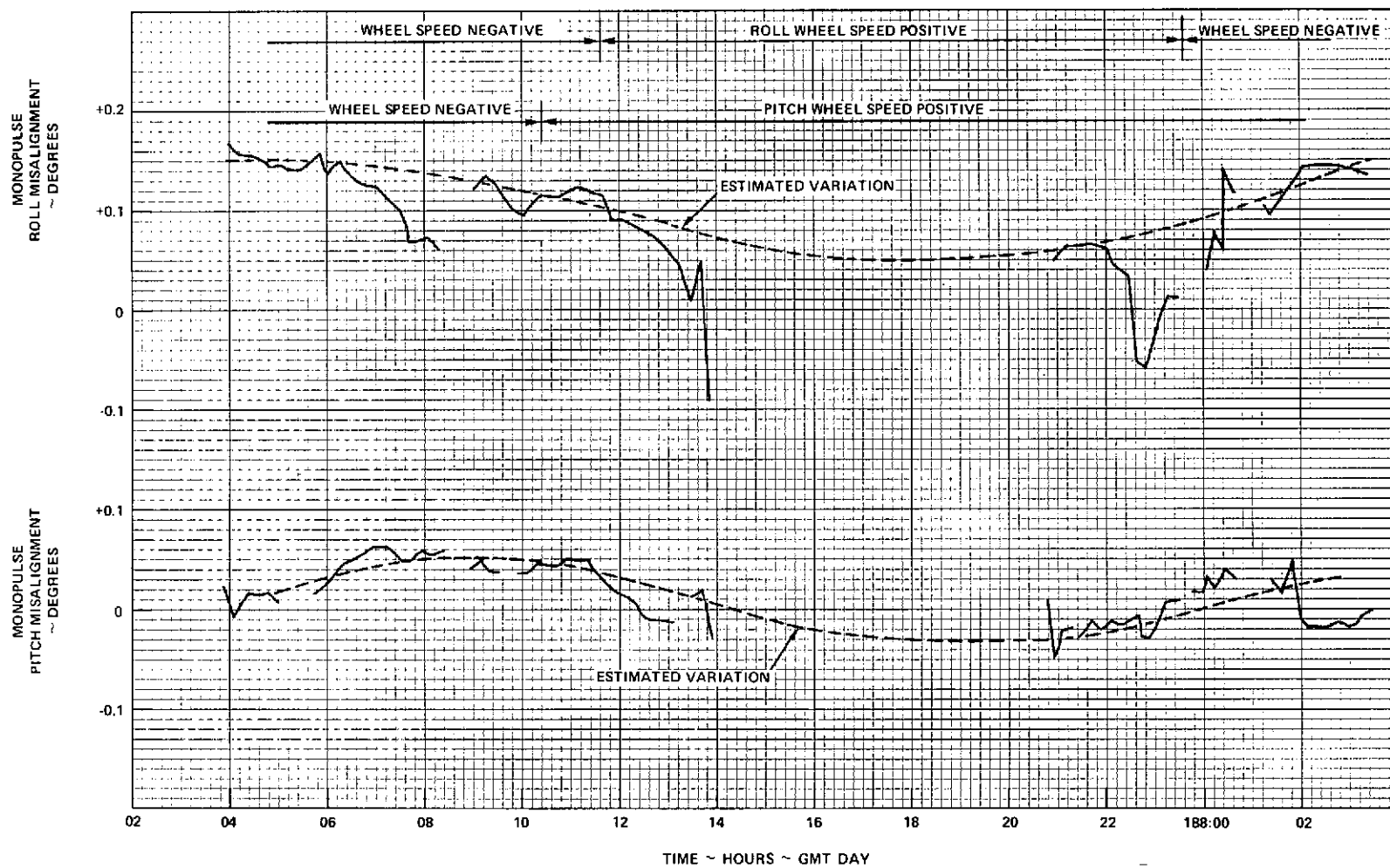
Figure 7-6. Day 187 -- Monopulse Misalignments

7.3.4 Conclusions and Recommendations

a. The day 187 C-band monopulse test was partially successful in that some misalignment data was obtained. A preliminary estimate of the diurnal variation of monopulse misalignment was obtained. Side-lobe operation, however, precluded obtaining complete data.

b. A number of losses of control were experienced while on monopulse control. A fully adequate explanation for these control losses is not evident from the telemetry data at this time.

c. An error in the ATTLMP monopulse calibration was discovered and has since been corrected.

It is recommended that the C-band monopulse misalignment test be run again with particular attention being paid to maintaining control on the monopulse main lobe. To facilitate analysis of the data it is suggested that the test planning be coordinated with the Information Processing Division of GSFC to provide appropriately scaled graphics plot of the telemetry data.

Should the control loss phenomenon be repeatable it is recommended that the test be repeated using S-band monopulse control so that a comparison of C-band and S-band may be made.

7.4 EARTH - MOON INTERFERENCE

7.4.1 Introduction

Prior to the launch of ATS-6, there was considerable discussion on possible effects of the Moon in the ESA field-of-view. There was conjecture as to whether or not the angle subtended by the Moon as viewed from ATS would be sufficiently large to have any detectable effect on ESA error processing. The question was also raised as to whether, under certain specific conditions, it would be possible to lose Earth Acquisition. A brief description of the physical observations to date confirming the Moon's influence on normal ESA operation, the technical rationale for interferences and some comments on impact to spacecraft operations are presented.

7.4.2 ESA Functional Description

The ESA is a two-axis (roll/pitch) scanning optical sensor capable of sensing infrared radiation from the Earth and its atmosphere. The ESA includes two identical heads mounted on the Earth Viewing Module (EVM). The heads are

mounted at right angles to each other such that the roll head scans north/south in the YZ plane and the pitch head scans east/west in the XZ plane (Figure 7-7). Each unit (or head) consists of a lens-filter-bolometer detector, scanning mirror, and an offset mirror. The electronics package completes the ESA. In the normal operating mode, the ESA scans through the major diameters of the Earth at a rate of 4 Hz. The scanned field-of-view (FOV) is ±13° and is automatically biased so that the Earth is always centered within the scans as long as both the roll and pitch errors are less than ±11.25°.
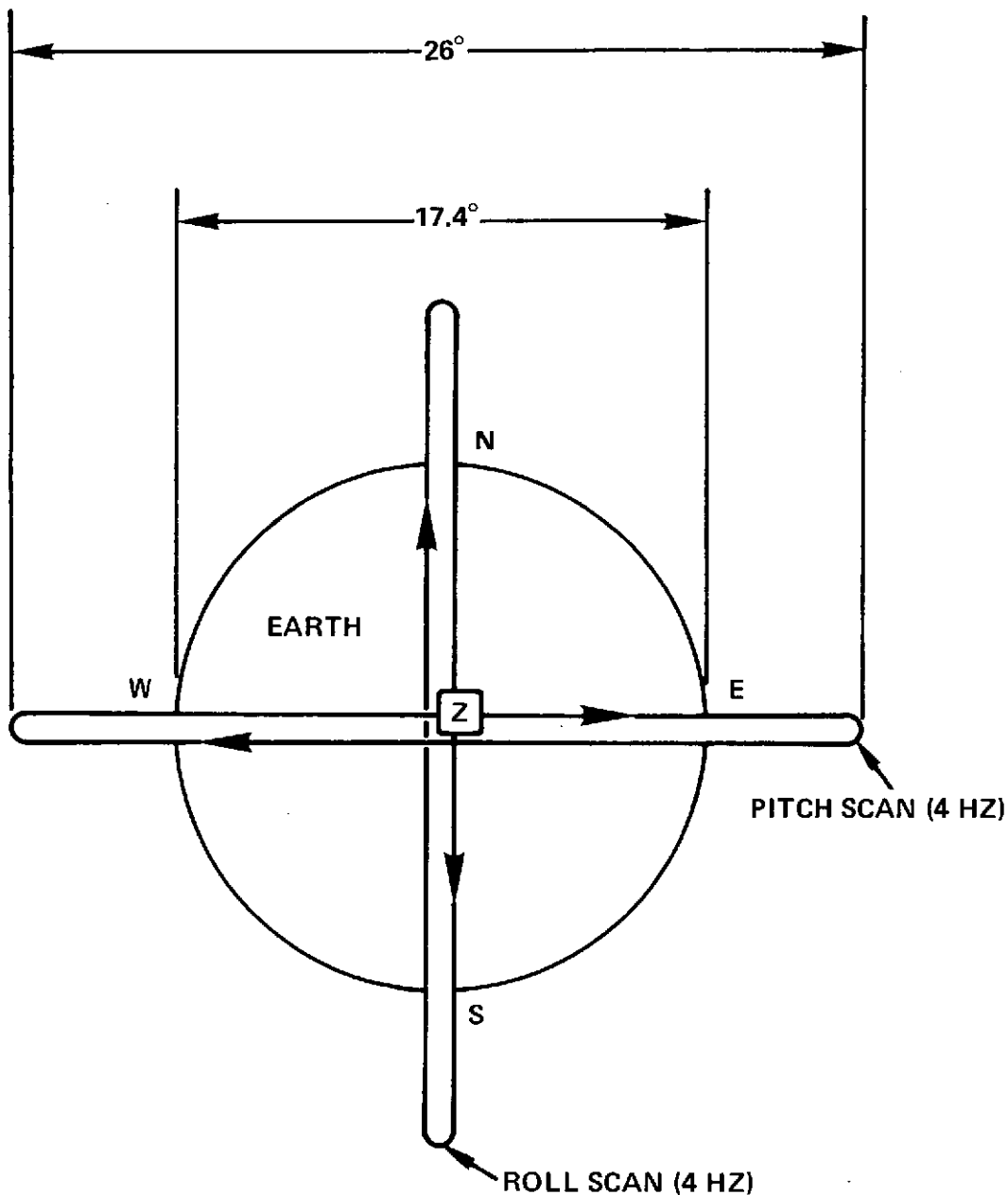
Figure 7-7. Earth Sensor Scan FOV

ESA error computation is achieved via an encoder physically attached to each scan mirror. The encoder determines the angular scan position and reference null crossing. When the radiance threshold criterion is met, the electronics accumulates encoder pulses by an up/down count, with counter direction determined by the sequence of events. Figure 7-8A illustrates the process of a typical off-local vertical case in pitch with the resulting error being proportional to the residual up/down counts at the completion of a scan cycle.

Consider now what occurs when the Moon passes through the ESA FOV. The instantaneous bolometer FOV is approximately 0.6° and the lunar disc as viewed from ATS is approximately 0.5°. When the Moon lies within the scan plane of either roll or pitch and its radiances exceeds the threshold, additional counting occurs thus making the Earth appear as though it were wider than it actually is (Figure 7-8B). In this case the attitude error will be derived from both bodies. With a full Moon entirely in the bolometer IFOV the apparent delta-width is approximately 1.1°. The ESA interprets this delta as an attitude error in the effected axis and the spacecraft will attempt to null the error. The magnitude of the resulting error may vary depending on several factors such as the Moon's phase, the location within the scan and the Earth/Moon radiance threshold sequence. Under certain conditions the perturbation to ESA error may even be greater than the apparent delta-width.

7.4.3 ATS-6 Lunar Effect

An example of the Moon's effect on the ESA occurred on ATS-6 at 152:15:10 GMT. The 9-photo sequence of Figure 7-9 shows the progression of the Moon through the ESA roll scan plane. The photos are of ESA roll radiance which is telemetered down via a special data link. Photo 7-9A shows a normal Earth Radiance trace for one complete scan cycle in roll. Subsequent radiance photos show the Moon sequentially entering, passing through and exiting the roll scan. In this instance the Lunar trajectory was perpendicular to the roll scan plane slicing through at an angle of approximately -12.4° in roll. From the radiance photos the apparent width of the Moon as viewed from the ESA was determined to be approximately 1.03° and the maximum deviation in ESA roll error recorded during the pass was about 1.5°. Since the ESA was in the control loop for the duration of the pass, the spacecraft reacted to null the error.

7.4.4 Loss of Acquisition

In addition to the previously described effect on error computation, under a specific set of circumstances the ESA acquisition logic can become confused by the Moon's presence in the scan with a resulting loss of Earth Acquisition. For this to occur, the Moon must be located exactly at the west turn-around point of the pitch scan or at the south turn-around point of the roll scan. These
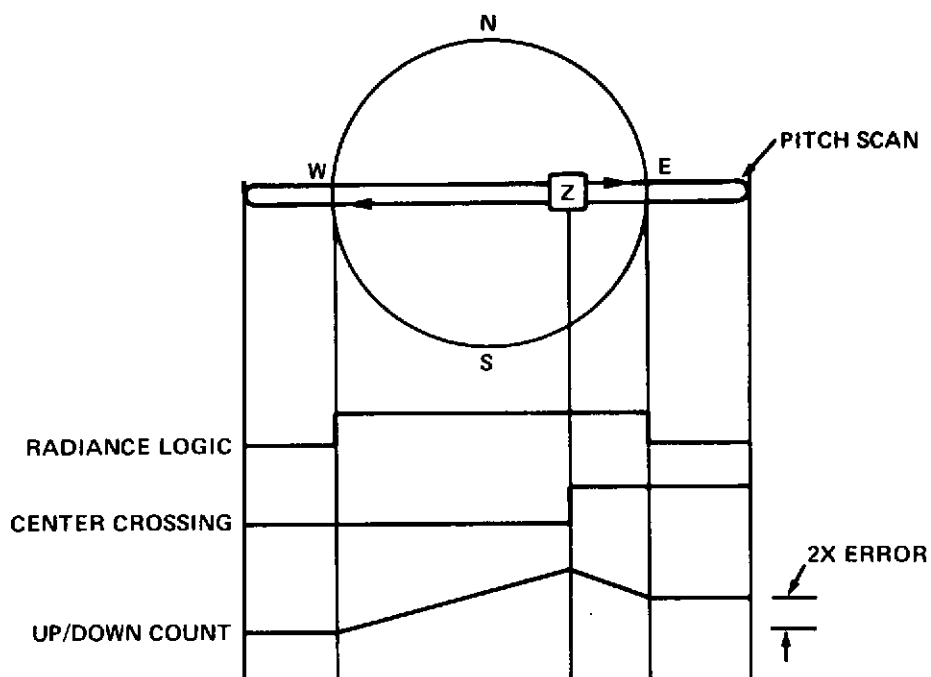
Figure 7-8A. ~ Normal ESA Error Computation
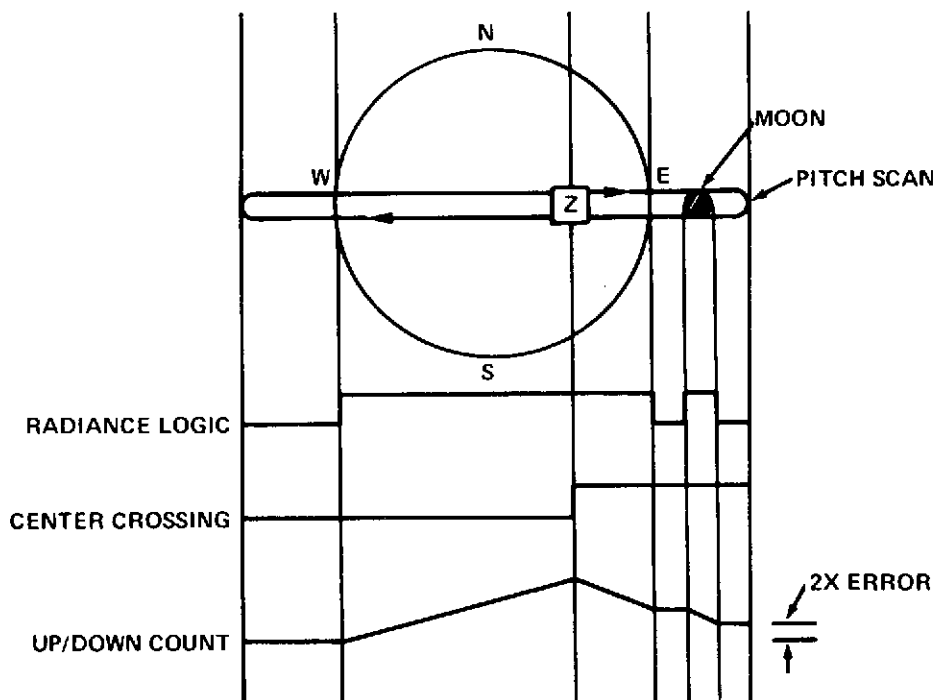
NOTE: FIGURES FUNCTIONALLY REPRESENT
ERROR COMPUTATION FOR ONE-HALF SCAN CYCLE

Figure 7-8B. ~ ESA Error Computation with Moon in Scan
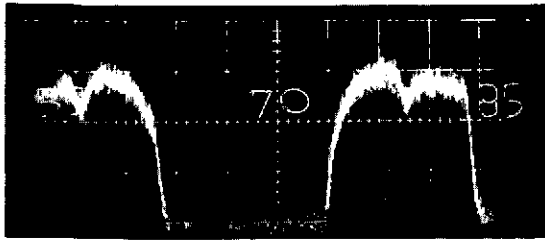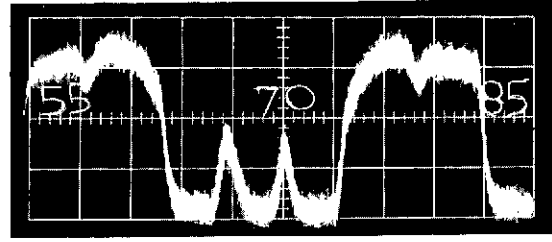
(a)   (b)
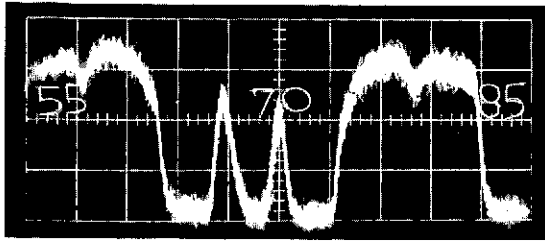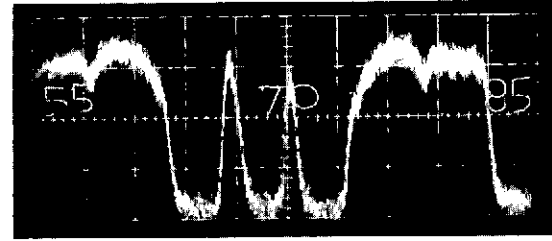
(c)   (d)
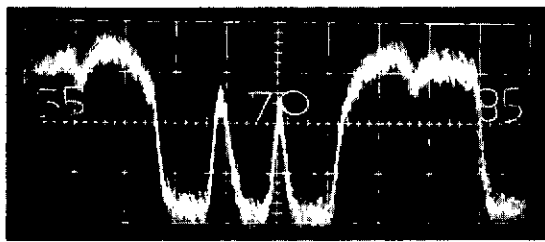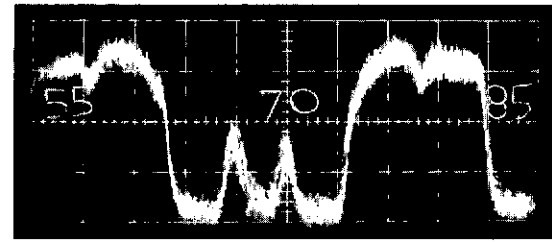
(e)   (f)
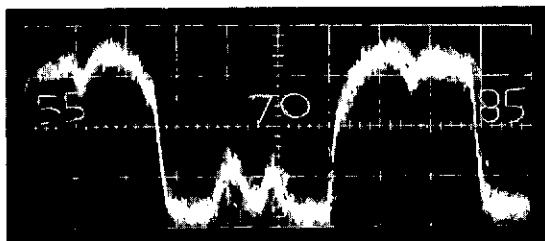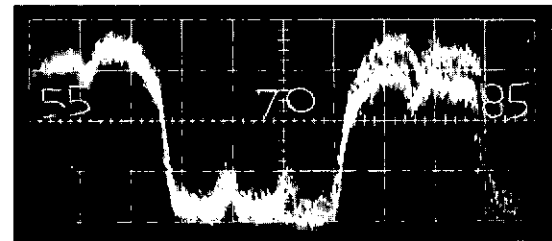
(g)   (h)
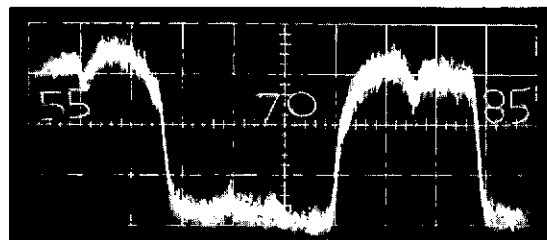
(i)

Figure 7-9. Progression of Moon Through ESA FOV

points lie approximately 13° south (roll) and west (pitch) of the center of the Earth. Furthermore, the Moon radiance must exceed the adaptively set Earth radiance threshold.

Loss of acquisition due to the Moon is a fallout of the mechanization of the ESA acquisition logic. In general, the generation of a single-axis acquisition signal required the scanned FOV to cross both edges of the Earth's disc with scan turn-around occurring in deep space. Figure 7-10 shows the scan cycle represented by four quadrants and their corresponding relationship to the scan mirror drive waveform. The single-axis acquisition signal is generated by controlling three latches. The first latch is set high if radiance above the adaptively set threshold is present when the transition is made from quadrant 2 to quadrant 3. This corresponds to having that particular scan turn-around on either the Earth or Moon. The second latch is set high if the radiance goes from a high state to a low state at any time during quadrants 3 and 4. The logic representing quadrant 2 always clears the first and second latches. The third latch is set only if the first latch is low, indicating no radiance at scan turn-around, and the second latch is high, indicating the scan has crossed the opposite horizon. The setting of the third latch provides the acquisition signal for that particular axis.

It is apparent from the preceding logic discussion that when and if the Moon enters one of the scans at the designated turn-around point, the first latch will be set high thereby precluding the third latch from being set which is required for an acquisition signal on that particular axis. To date, loss of Earth Acquisition due to the Moon has not been observed during in-orbit operation of ATS-6.

7.4.5 Interference Window

For a criterion to establish specific Moon interference times, refer to Figures 7-11 and 7-12. Figure 7-11 defines ZCOEL as the angle between the spacecraft local vertical and the spacecraft-Moon pointing vector. Figure 7-12 defines ZAZ as the clockwise angle measured from the -Y spacecraft axis to the Moon's projection in the spacecraft XY plane. (The +Z axis is assumed to be into the paper.) The Moon lies within the earth sensor roll scan when $8.5° \leqslant ZCOEL \leqslant 13°$ and $-1° \leqslant ZAZ \leqslant 1°$ or $-179° \geqslant ZAZ \geqslant 179°$. The moon lies within the earth sensor pitch scan when $8.5° \leqslant ZCOEL \leqslant 13°$, and $89° \leqslant ZAZ \leqslant 91°$ or $-89° \geqslant ZAZ \geqslant -91°$.

Very conservative calculations have placed the frequency of Lunar interferences at approximately 60 per year with duration time per interference ranging from 4 minutes to 22 minutes. These numbers include interferences on both the roll and pitch scans and presume that one interference occurs on each Moon transit through a potential interference region. Also, it is assumed that the ESA will respond the same to all Lunar phase angles, which is conservative, since the radiance from a new Moon would probably be below the ESA radiance threshold.
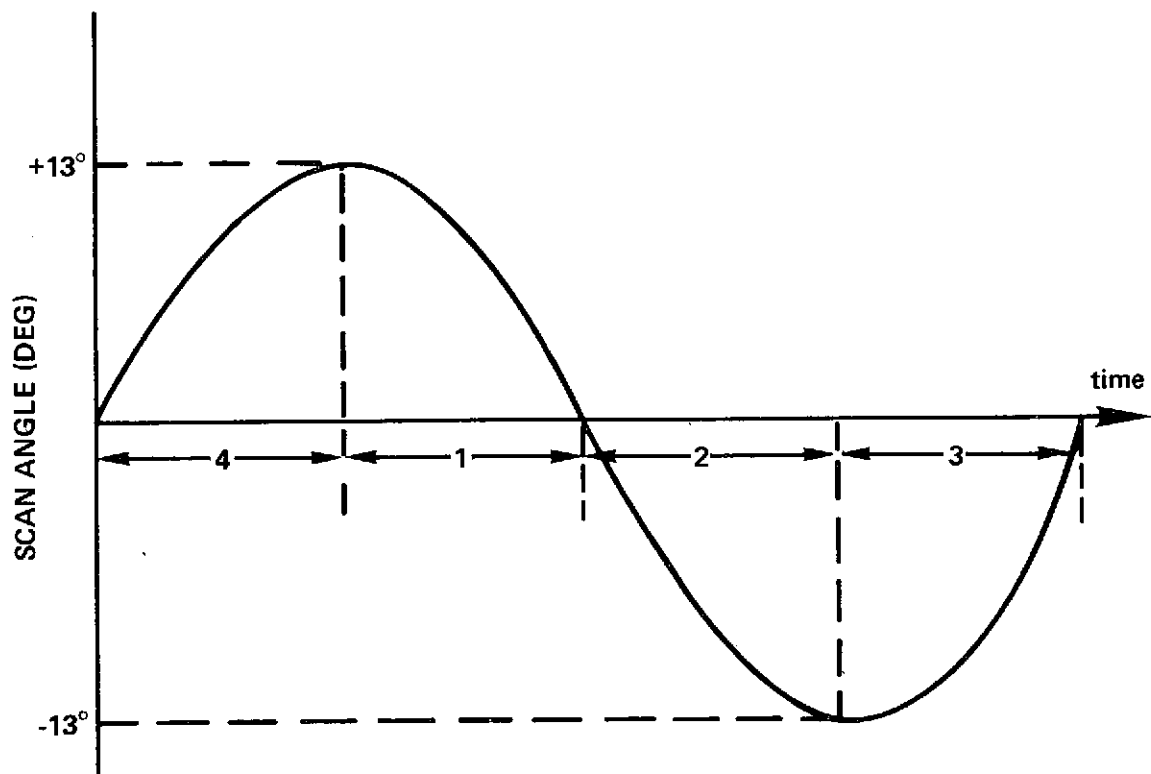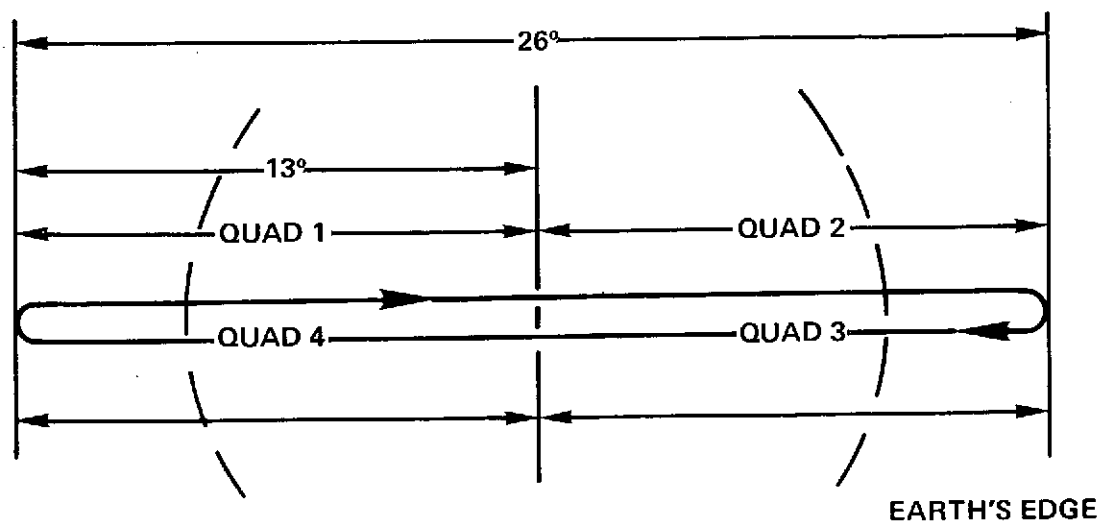
Figure 7-10.   Scan Geometry and Drive Waveform

-Y SK

+Z S/C (LOCAL VERTICAL)

MOON

ZCOEL

$\overline{M}$

+X S/C

(M=SPACECRAFT/MOON POINTING VECTOR)

Figure 7-11.   ZCOEL

Y S/C

(MOON'S PROJECTION S/C XY PLANE)

+Z S/C

ZAZ

+XS/C
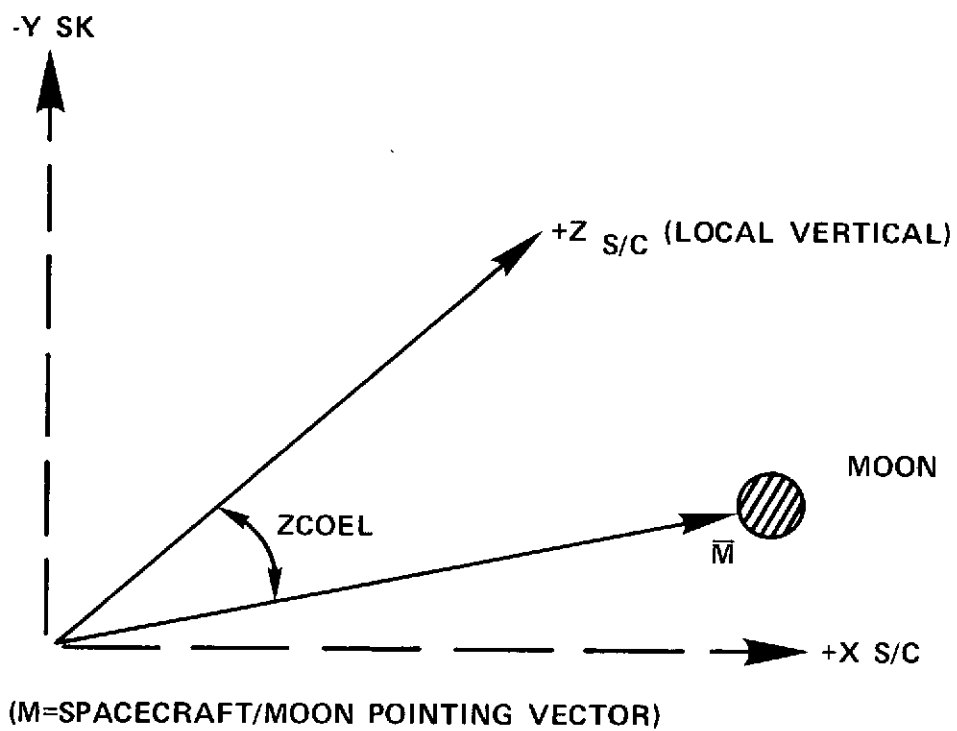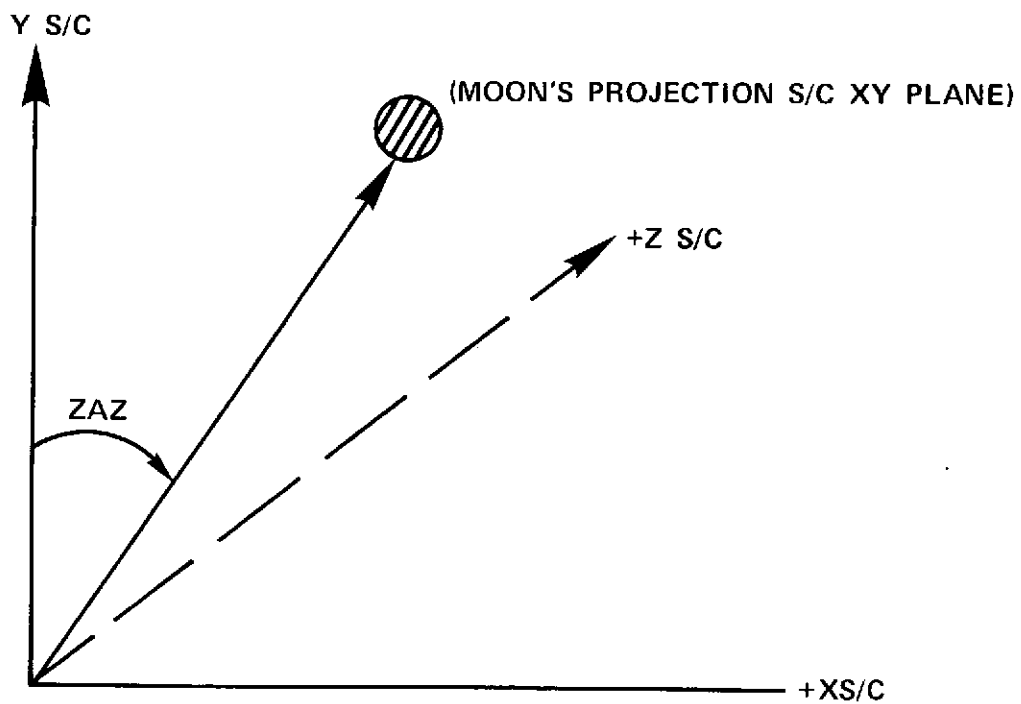
Figure 7-12.   ZAZ

7.4.6 Conclusions

While periodic Lunar interferences are annoying, to date they have presented no real problem to on-line spacecraft operations. Computer generated "predicts" formatted as shown in Table 7-1, have been available at ATSOCC to alert ACS console personnel to pending interferences times. The correlation between predict timer and actual recorded interference timer has been quite accurate. The only effects on operations thus far recorded have been minor perturbations in roll or pitch of spacecraft attitude lasting for the duration of the transit period. As stated earlier, loss of acquisition due to the Moon lying at one of the designated scan turn-arounds has not yet been observed. However, should loss of Earth Acquisition occur under these circumstances, it is not anticipated that it will cause a serious operational difficulty since the spacecraft will go into an immediate wheel-hold mode. The ESA "Roll Scan Offset-Positive or Negative" capability can also be used to avoid interferences in the roll scan plane. The only way to avoid interference in the pitch scan is to switch to a backup roll/pitch sensor (Interferometer or Monopulse) or purposely yaw from the orbit plane.

7.5 POLARIS SENSOR ASSEMBLY (PSA) TRACKING ANOMALIES

7.5.1 Introduction

Since its initial activation in orbit, the PSA has, on occasion, indicated incorrect yaw angle information. These errors which span the full PSA output range of ±3.5 degrees seem to be due to the tracking of false targets which often results in a loss-of-acquisition of Polaris by the PSA. Generally the resulting vehicle yaw attitude errors are of such short duration (less than 1-1/2 minutes) that they do not effect ACS experiment performance.

A review of the available data has suggested two causes: (1) sun reflections into the PSA image desecting tube (IDT) from various reflecting surfaces, and (2) sun reflections off particles resident in the field-of-view of the PSA. The sensitivity of the PSA to such stray light is illustrated by the example: if illuminated by the Sun at 0.001-inch diameter particle, with 10% reflectivity, placed 20 feet from the PSA has a brightness equivalent to that of Polaris.

7.5.2 System Description

7.5.2.1 PSA—The PSA is an electro-optical device that provides a yaw-axis error signal proportional to the subtended angle between the line-of-sight to the star and the pointing direction of the PSA.

Table 7-1

Anticipated Lunar Interference Times
from Launch Through June 13th

Date	GMT	ZCOEL°	ZAZ°	Moon Phase°
5/31	1445	8.93	-179.5	129
5/31	1450	9.01	+173.7	129
6/1	1530	13.02	-175.9	141
6/1	1535	13.02	179.4	141
6/9	2215	12.5	-176.5	235
6/9	2220	12.5	+178.5	235
6/9	2225	12.6	+173.6	235
6/10	2300	8.8	-176.77	247
6/10	2302	8.8	-179.6	247
6/10	2303	8.8	+178.98	247
6/10	2305	8.8	+176.15	247
6/12	2321	14.76	- 91.66	269
6/12	2326	13.67	- 91.82	269
6/12	2331	12.57	- 92	269
6/12	2336	11.48	- 92.21	269
6/12	2341	10.39	- 92.45	269
6/12	2351	8.2	- 93.10	269
6/13	0106	8.2	91.93	270
6/13	0111	9.29	91.56	270
6/13	0115	10.17	91.32	270
6/13	0120	11.26	91.06	270
6/13	0125	12.35	90.85	270
6/13	0130	13.45	90.66	270
6/13	0135	14.54	90.49	270

Images of any objects within the FOV are formed by the objective lens on IDT photocathode. The emitted photoelectrons are accelerated and imaged by the focus potentials into or through a conducting, grounded aperture plate which separates the focusing section from the dynode multiplier section of the IDT. The electron image of the FOV is scanned by the aperture plate by the application of a saw-tooth voltage to the yaw-angle deflection plate in the tube's image section. If a star is within the FOV, the scanning action modulates the resulting electron beam, which is amplified by the dynode multiplier section. Demodulation of this signal, after further amplification, provides a signal whose time-averaged amplitude and polarity is related to the mean star position offset from the center of the electron aperture. This signal is summed in an integrator, amplified, and fed back to the yaw angle deflection plates. This completes a control loop which nulls the mean star position on the electron aperture plate. The star yaw-angle offset is then directly proportional to the offset (tracking) voltage that maintains the null position. This voltage is provided to the Attitude Control Electronics as a yaw-angle error signal to be used for yaw stabilization of the spacecraft.

Prior to star acquisition the FOV which is the image of the electron aperture projected forward through the objective lens, is biased to the limiting yaw-angle (+4.0 ± 0.5 degrees) or acquisition bias position. If a star enters the FOV and exceeds the acquisition gate threshold, the bias signal is then removed from the deflection plates and the FOV is allowed to track the star. In the event of loss of acquisition, a flyback and sweep search of the entire yaw field (±4.5 degrees maximum) is made automatically in an attempt to reacquire. If the search is not successful, the FOV will return to the acquisition bias position.

Identification of Polaris is made on the basis of the modulated and amplified signal which is remodulated and summed to provide a signal with a narrow noise bandwidth related to the star illumination intensity. This signal provides the reference for the voltage supply which feeds the dynode multiplier structure. This completes an automatic gain control loop which provides a constant tube modulated output over a wide range of star intensities.

Star intensity information is obtained from the dynode voltage supply and is compared against low brightness limits (gates) for an identification decision. If the decision is affirmative, an acquisition signal is provided to the Attitude Control Electronics and the FOV will track as previously described. If no star meets the brightness criteria, the FOV will remain in the search position. Signals may be sent to the PSA which step the low gate to a lower value. Subsequent signals will set the low gate to a still lower value, then reset it to the original level. The acquisition of a star satisfying the brightness gates initiates logic which maintains track until such time as the FOV becomes dark enough to fall below the dropout level of the effective gate.

The roll angle deflection plates in the image dissector tube are used to provide five discretely-stepped roll angle offsets in the FOV to follow the variation in the roll angle of Polaris. Pulse commands sent to predetermined PSA input pins step the FOV.

A sun detector mounted to the baffle assembly is provided to activate the sun shutter should the spacecraft become oriented in such a way as to allow sunlight to directly enter the tracker optics. This shutter prevents the high intensity light from direct impingement on the photocathode.

7.5.2.2 Baffle Description—Figure 7-13 illustrates the two-stage FOV of the Polaris baffle. For input illumination at angles beyond the FOV, attenuation is achieved by multiple reflection and absorption within the outer baffles. The level of attenuation is controlled by the length-to-depth ratio of each baffling stage, while spectral and diffuse reflections off the baffle edges are limited by proper selection of their radii.

The extreme half-angle ray which illuminates the entire entrance aperture defines the primary field-of-view (PFOV); the secondary field-of-view (SFOV) allows direct illumination to the edge of the entrance aperture. The extreme ray is defined as the largest angle that a ray can illuminate the outermost plate of the inner baffle and is the worst case for illuminated light reflecting directly into the entrance aperture.

7.5.2.3 Location of PSA in ATS-6—Figure 7-14 shows the location of the PSA in the vehicle. It depicts reflective areas on the north solar array which are within the extreme ray angles of the baffle; i.e., requiring only one reflection in the baffle to reach the PSA's aperture. Also shown are reflective areas inside the array which see the aperture with two or more reflections in the baffle.

7.5.3 Data

The PSA 2 anomaly data given below is of five types:

    a. Typical anomaly characteristics
    b. Anomaly frequency distributions by day and hour
    c. Repetitiveness of anomalies
    d. Intensity data and temperature data
    e. Apparent tracking direction as a function of time

7.5.3.1 Typical Anomaly Characteristics—In Figure 7-15A the PSA angle diverges from a true Polaris track while the Star Intensity Signal (SIS) voltage rises; i.e., the intensity drops. Then the apparent intensity drops and the SIS voltage rises

Function	Yaw	Roll
Design Field-of-View	± 5°	± 14°
Primary FOV (PFOV)	± 6°	± 15° 15'
Secondary FOV (SFOV)	± 14° 15'	± 29° 21'
Extreme Ray	± 30°	± 39°
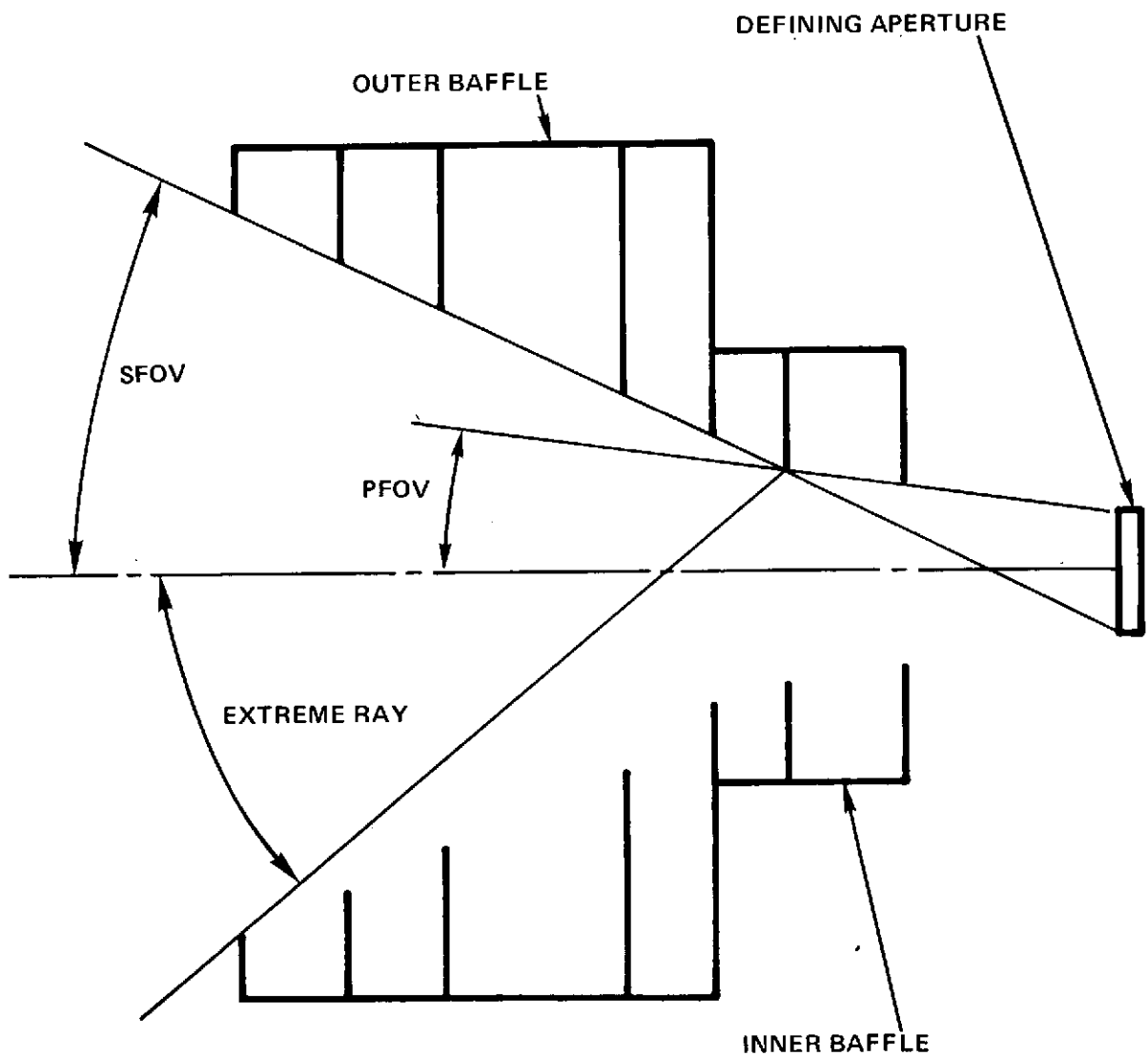
Figure 7-13. Two-Stage Field-of-View of the Polaris Baffle

PSA 2

	SENSITIVE ANGLE DEG	INSENSITIVE ANGLE DEG
1	10.6	30.5
2	12.7	35.3
3	15.6	41.4
4	10.6	43.9
5	0.88	44.4
6	0.93	41.8
7	33.0	45.5
8	26.1	45.5
9	0	33.2
10	0.59	37.94
11	0	43.04
12	0.7	38.1
13	10.6	44
14	0.59	42.5
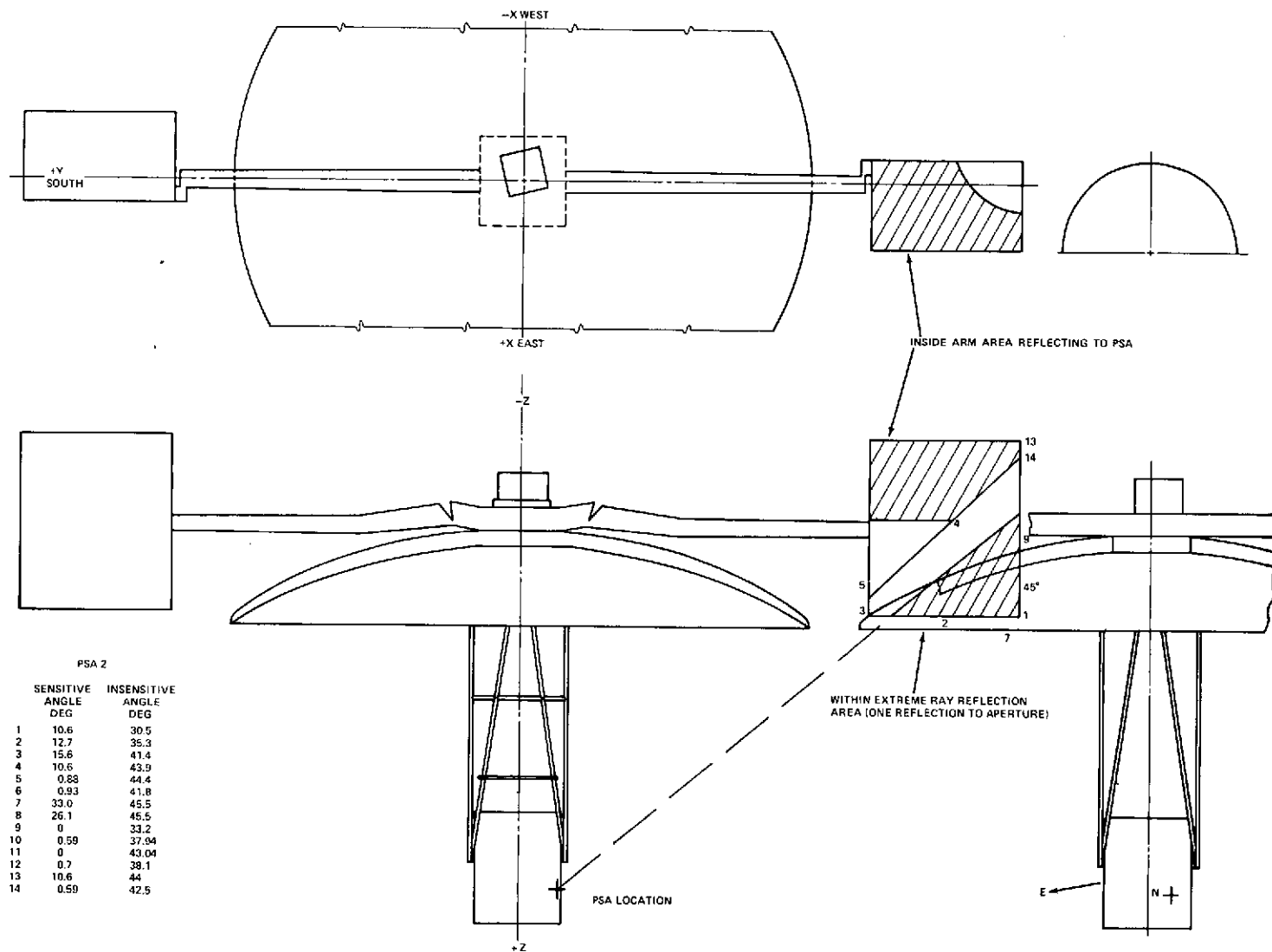
Figure 7-14. Sensor Field-of-View

to reach 4 volts. At that preset level, acquisition is lost and the PSA automacally executes a flyback and sweep to search for Polaris. Polaris is acquired and normal operation ensues. An explanation for this behavior is as follows: A bright light source appears at the + yaw edge of the FOV. The center of the scanned FOV (which determines the PSA output) moves to the centroid of the total incident light.

The apparent intensity drops because the PSA circuitry measures the fundamental component of the image dissector tube output at the scan frequency. This causes a drop in the intensity even though the total incident light increases. When the 4-volt acquisition threshold is reached, a flyback and sweep is initiated and the SIS voltage rises because no bright light is in the PSA FOV. Reacquisition of Polaris, at its initial intensity level, follows since the bright light source has disappeared.

Figure 7-15b depicts and anomaly similar to that just described with the following changes (a) tracking is from -Y to +Y, (b) the bright light passes through the FOV to increase the apparent intensity, (c) the initial rise in SIS voltage is insufficient to exceed the 4 volt flyback and sweep threshold, and (d) the bright light exited through the roll end of the scanned FOV (11 deg. in roll by 3 deg. in yaw) and when close to zero yaw angle so that no rise in SIS voltage is noticed when the light disappears. In contrast, figure 7-15C shows the bright light entering near the zero-yaw angle and exiting far from the zero-yaw angle. The corresponding changes in SIS voltage are noticeable.

In Figure 7-15D, the bright light is tracked across the PSA FOV after an initial flyback and sweep. The PSA keeps tracking that light through its full FOV of ±4.5° while its yaw output is limited to ±3.5°. When acquisition is lost, the resultant flyback and sweep ends in a reacquisition of Polaris. During the 70 seconds that the yaw signal was in error, a vehicle attitude error built up which resulted in a yaw attitude transient when proper PSA outputs were again established. This is observable in the yaw angle variation with time after Polaris reacquisition.

7.5.3.2 Anomaly Frequency Distributions—Figure 7-16 compares the number of PSA anomalies (hits) observed shortly after PSA activation and those observed three months later. The data is taken from the ACS console log at ATSOCC. Figure 7-17 compares the hourly distribution of tracking on an hourly basis during this period. The general character of the two curves is the same - a rough sinusoid with a 24-hour period and peaking at 5 AM and 9 AM local satellite time.

7.5.3.3 Repetitiveness of Anomalies—Most PSA anomalies are of short duration and their yaw angle vs time histories are without the uniqueness necessary to
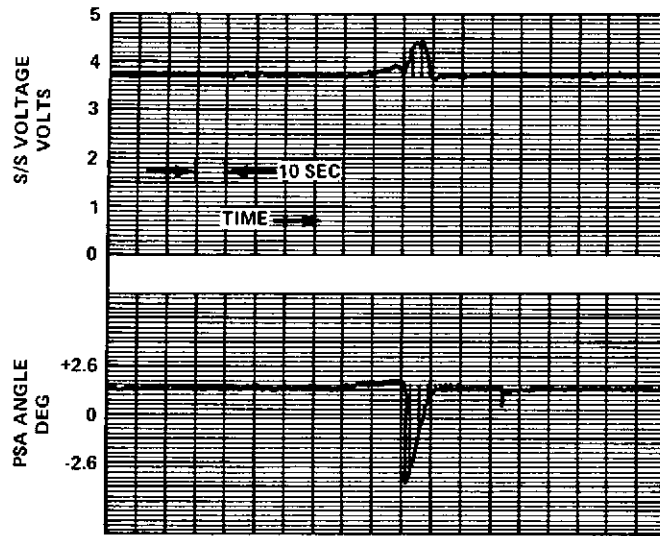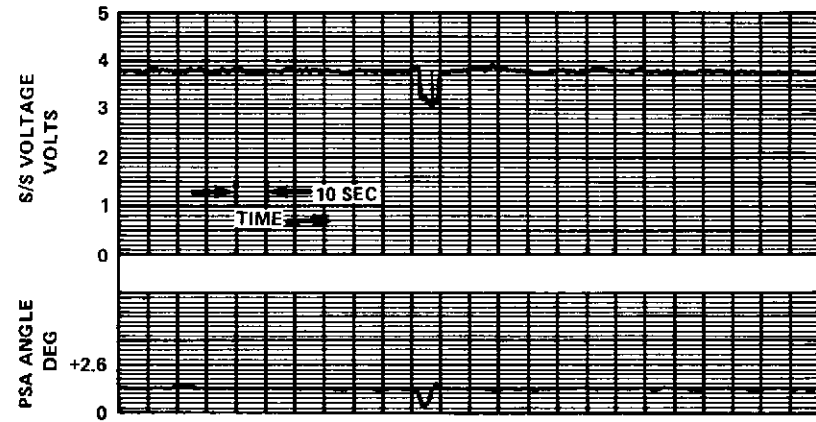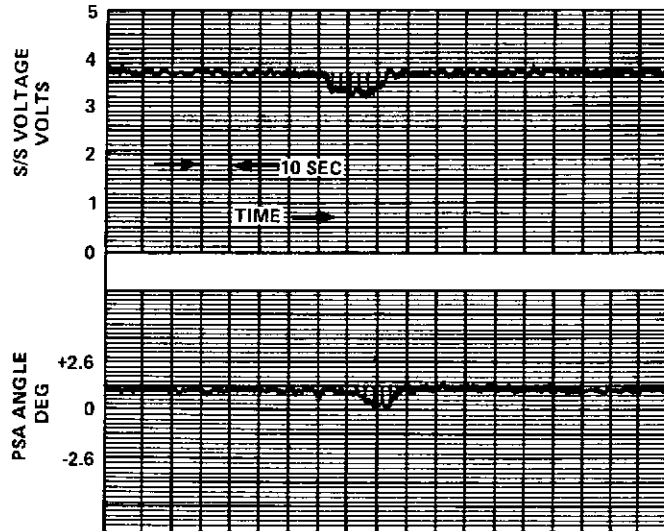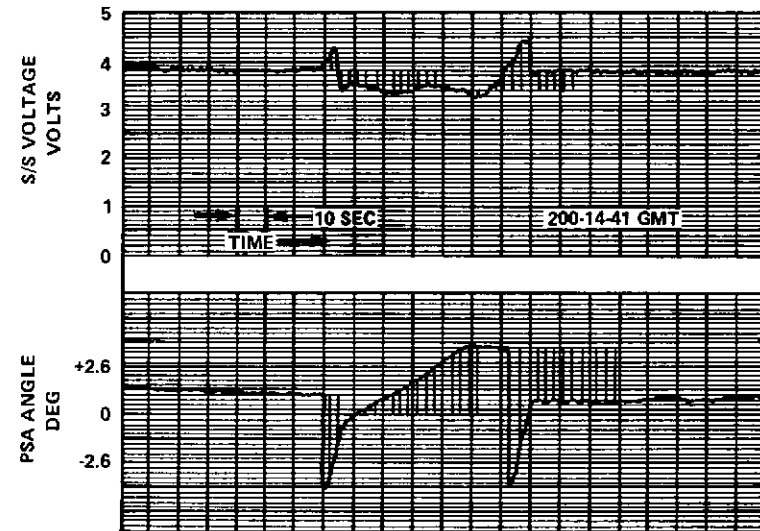
Figure 7-15. Typical PSA Anomalies
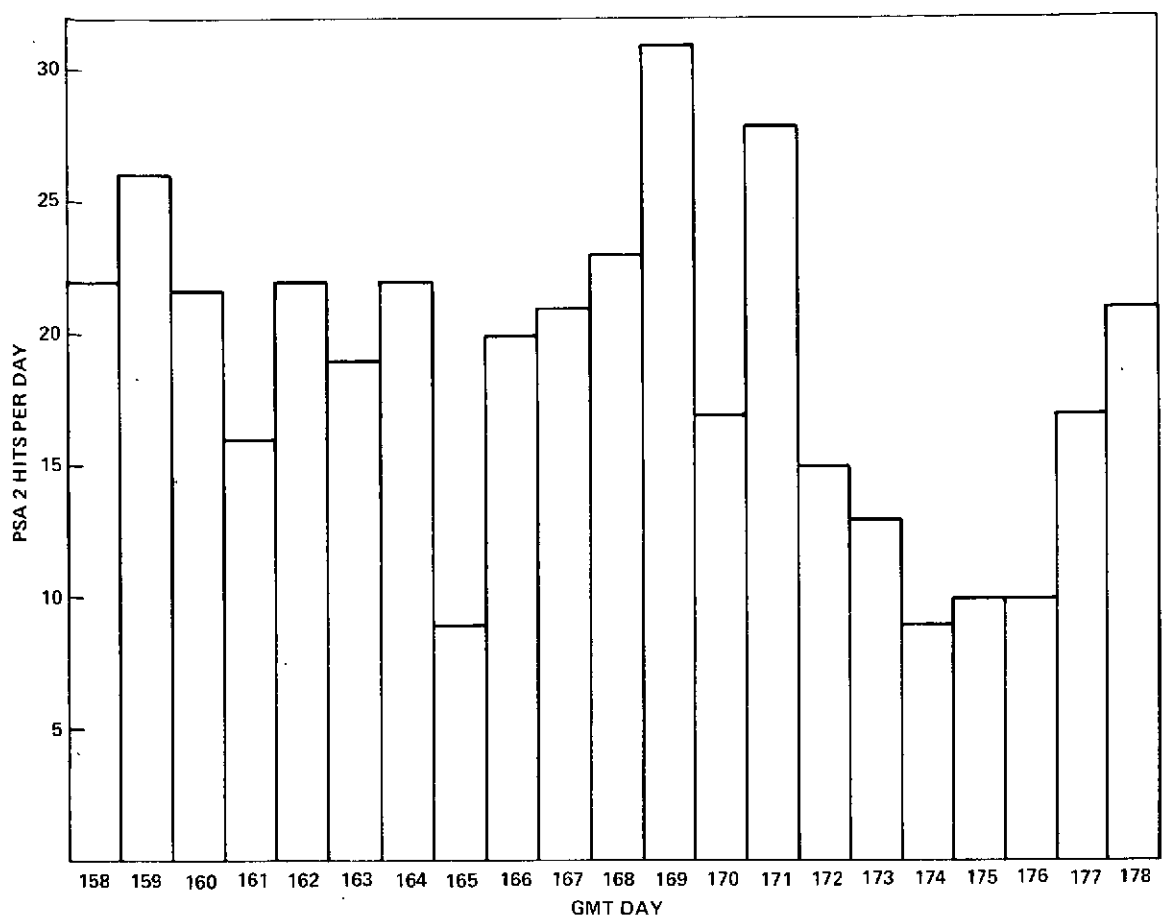
Figure 7-16.   (a) GMT Day
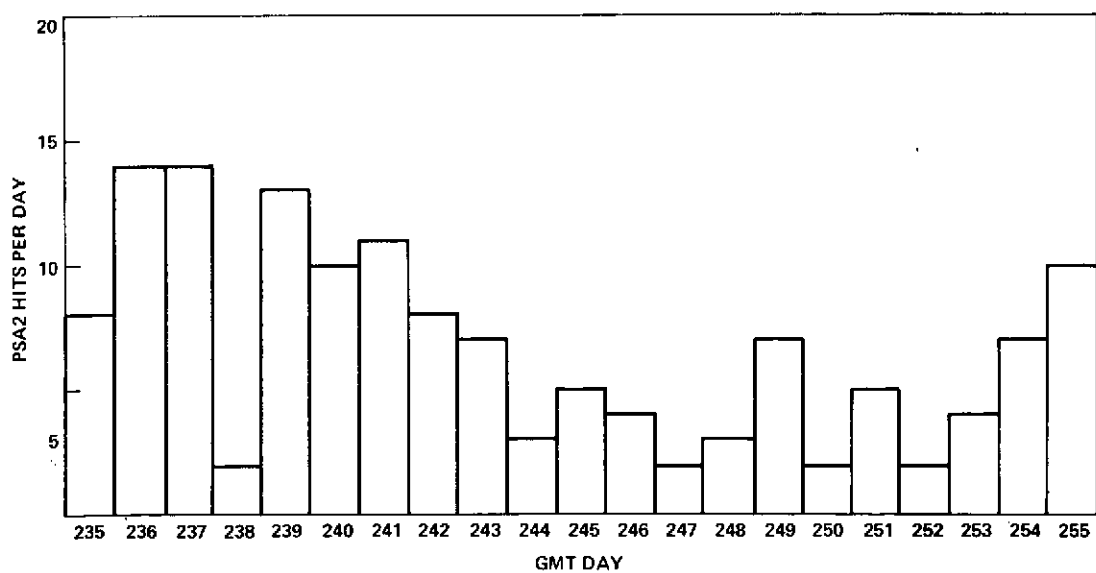
Figure 7-16.   (b) GMT Day
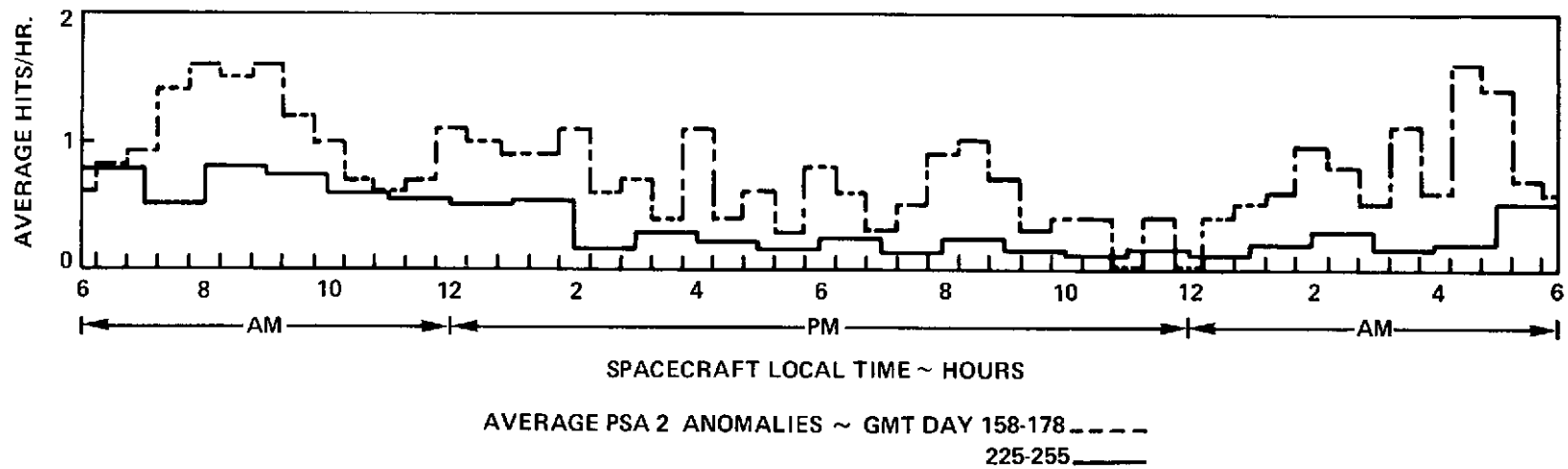
Figure 7-17.   Average PSA2 Anomalies ~ GMT Day

determine the existence of any repetitive quality. However, the anomaly often occurring at about 14:30 GMT is sufficiently long and distinctive to indicate repetitiveness. Figure 7-18 shows the PSA 2 output anomalies for days 253 and 256 at about 14:30. Figure 7-15D contains another member of the set for day 200.

Repetitiveness of anomalies with Sun orientation was examined for hours 14:00 to 15:00 GMT for days between 199 and 241. The position of the Sun path relative to the body is given by Sun azimuth (Sun ZAZ) and Sun elevation (Sun ZCOEL) coordinates as shown in figure 7-19 which contains the anomaly history for the days in question. There is a clear concentration of anomalies in specific areas of the ZAZ, ZCOEL plane. In particular in the circular area with radius 2.25 deg and centered on ZCOEL = 114 deg., ZAZ = 66.5 deg. there are twice as many hits as would be expected considering the total path length through that area and the average number of hits per unit path length over the full chart.

A similar set of data are shown in figure 7-20 for the period immediately after occult on days 248 through 258. Here, the data is presented in a SAZ, SEL coordinate frame. (Only discrete values of SAZ, SEL are computed because they depend upon DSS or ADSS data with resolutions of 0.5 and 1.0 degree, respectively. This inexactness of measurement accounts for the fact that for any specific SAZ, SEL pair there may be a hit one day and not on another.) Lines separating areas containing hits and areas with no hits were drawn. The result was a hamhock shaped area which is well defined on the upper and right sides but with an undefined lower left boundary. Tests were run on days 277 and 278 to confirm the theory that the area was hit-prone. On those days, shortly after occult, the vehicle was reoriented to achieve SAZ, SEL orientations within the hamhock area. The desired orientations were not achieved but the resultant anomalies at the actual orientations are consistant with the expected results; i.e., two hits were noted on day 277 near the previously undefined boundary and on day 278 no hits were observed near, and only one well away from the better defined boundary of the area.

7.5.3.4 Intensity Data—Figure 7-21 contains the telemetry recordings for day 203 for PSA 2 star intensity signal (SIS voltage), PSA 2 yaw angle readout, and PSA 2 temperature. It may be observed that the SIS voltage has a somewhat asymmetrical 24-hour wave component similar to the temperature wave but lagging it by about an hour. (No reason for temperature affecting SIS is known by the manufacturer.) The residual high frequency portion of the SIS voltage curve repeats every 12 hours. This is consistent with the fact that the rectangular scanned FOV makes two revolutions a day about the North Pole. Thus, stars in the neighborhood of the pole are periodically in the FOV of the tracker. The dips in the high-frequency component are identified as resulting from the high
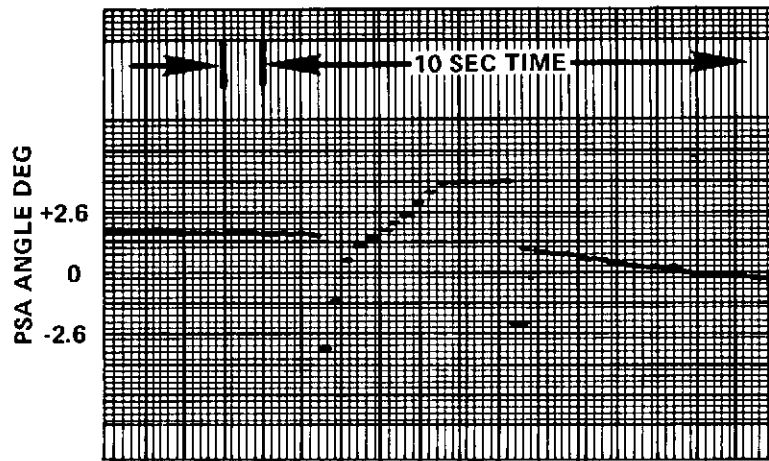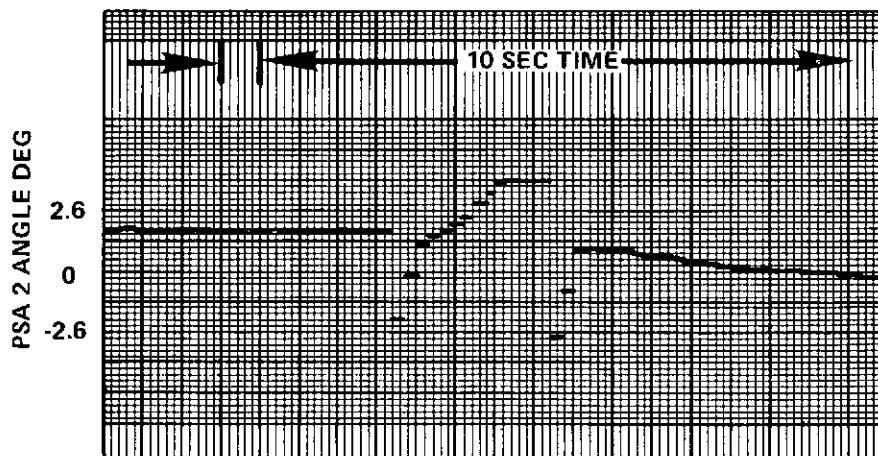
Figure 7-18. Similar Anomalies, Days 253 and 256
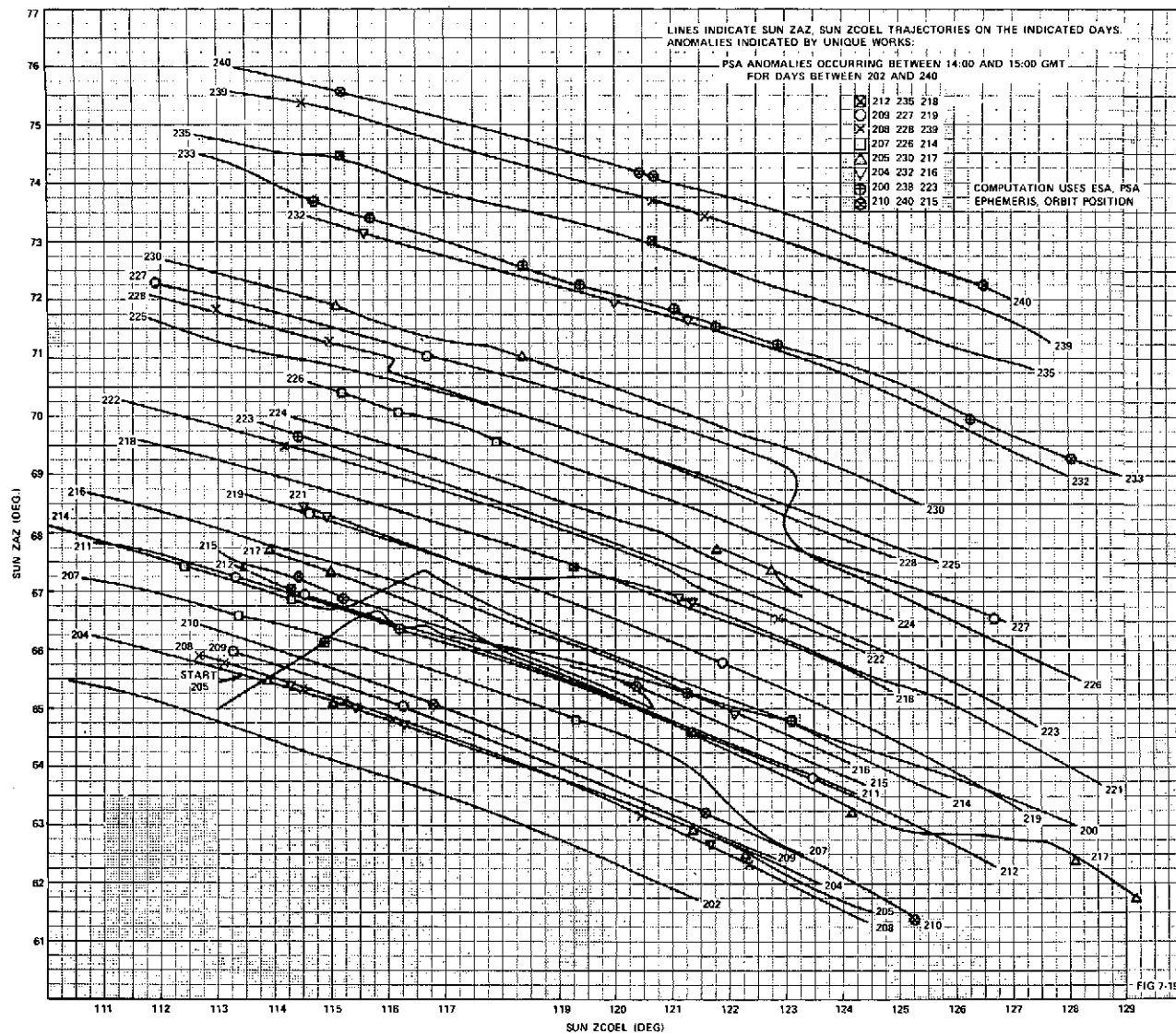
Figure 7-19. PSA 2 Anomaly History Between Days 202 and 240
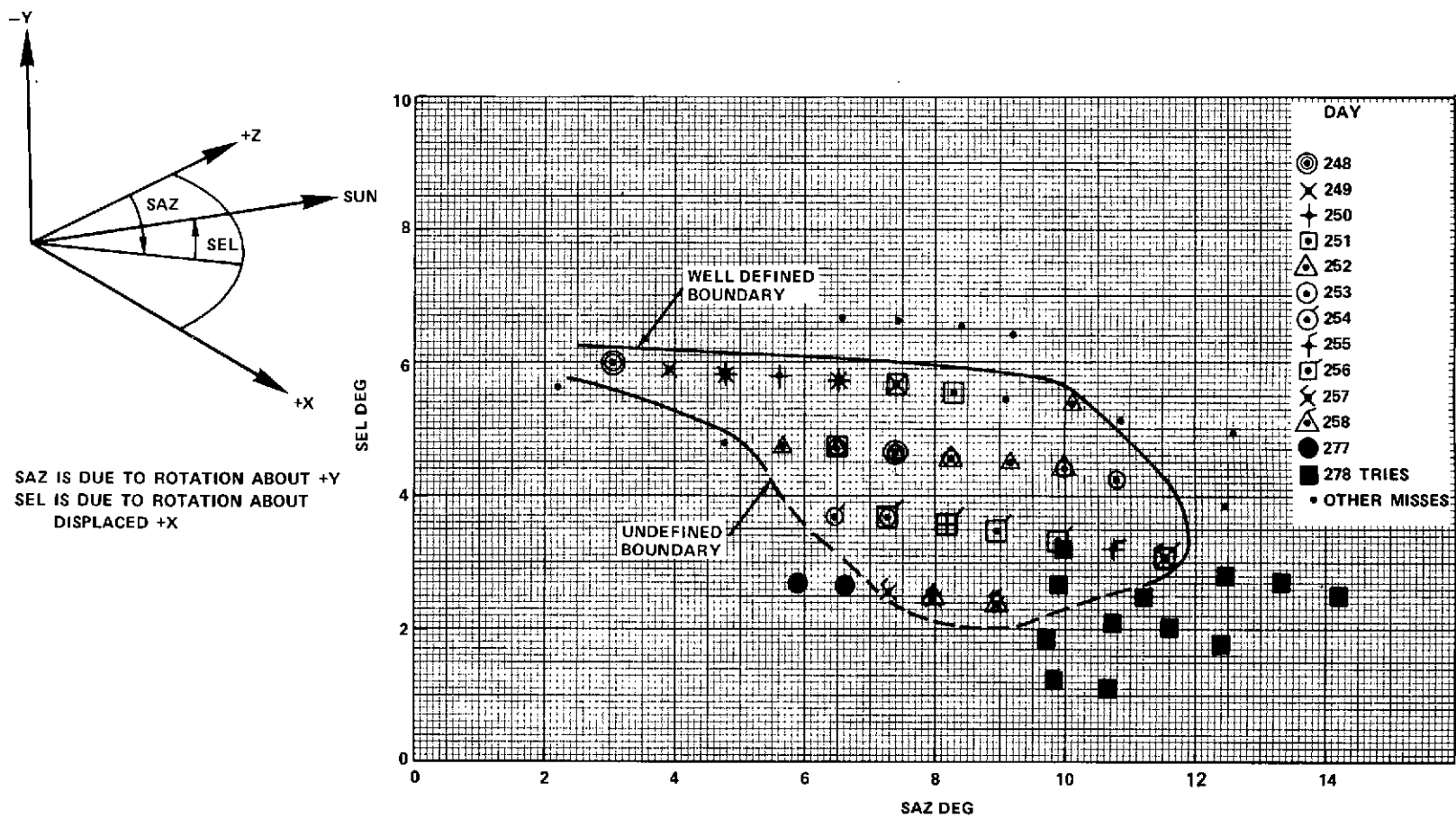
Figure 7-20. SAZ - SUN During PSA Anomalies After Occult

Figure 7-21. Intensity, PSA Angle, and
Temperature for Day 203

effective intensity due to the simultaneous presence of Polaris and other major stars in the center of the PSA's scanned FOV. The names of stars identified with specific dips are given on the SIS voltage recording.

A further verification of the association of SIS voltage variation with the star field is given by figure 7-22, wherein the effect of Earth travel about the Sun chauses changes in the relation between the star field and GMT. Approximately one degree change will occur each day. This effect is observed by the changing time at which the dips occur each day.

The data given in Figure 7-21 can be used to obtain a star intensity vs SIS voltage calibration. When star #6789 is aligned with Polaris in the PSA the total star intensity seen by the PSA is approximately 1.3 times the intensity of Polaris alone (1.3 × Polaris). With that alignment the SIS voltage is 3.72 volts. The resultant PSA in-orbit calibration is shown in figure 7-23.

During the PSA anomaly investigation the question arose as to the presence or nonpresence of a steady high intensity background at the PSA. Such a background might exist due to steady reflections from the solar array or reflector. Tests at approximately 9:30, 14:00, and 18:00 GMT on day 249 and 2:00 GMT on day 250 indicated intensity outputs of 0.05 to 0.06 × Polaris. When these intensity outputs are due to a flat background, rather than single stars in the FOV, the equivalent background intensity is approximately 1 × Polaris. Thus, high intensity background levels were not seen during the tested periods.

In Figure 7-22 the highest SIS voltages (about 390 counts = 3.9 volts) occur at about 14:30 GMT. Thus, at that time the introduction of a relatively small stray light can cause the SIS to exceed 4.0 volts and thereby trigger a flyback and sweep. This fact is probably of significance in causing the correlation between the SIS voltage 24-hour sinusoid and the hit rate per hour variation noted in Figure 7-17.

7.5.3.5 Apparent Tracking Direction—When PSA anomalies occur, it is usually possible to determine the direction of motion of the light being tracked. Practically all of the tracking indicates apparent motion of the source as being from minus yaw to plus yaw; i.e., if caused by reflections from a particle, the particle would be moving from the east toward the west face of the satellite. Reverse tracking (from plus yaw to minus yaw) usually occurs between 19:30 GMT and 23:30 GMT. Generally the reverse trackings occur one after the other with no intervening normal tracking.
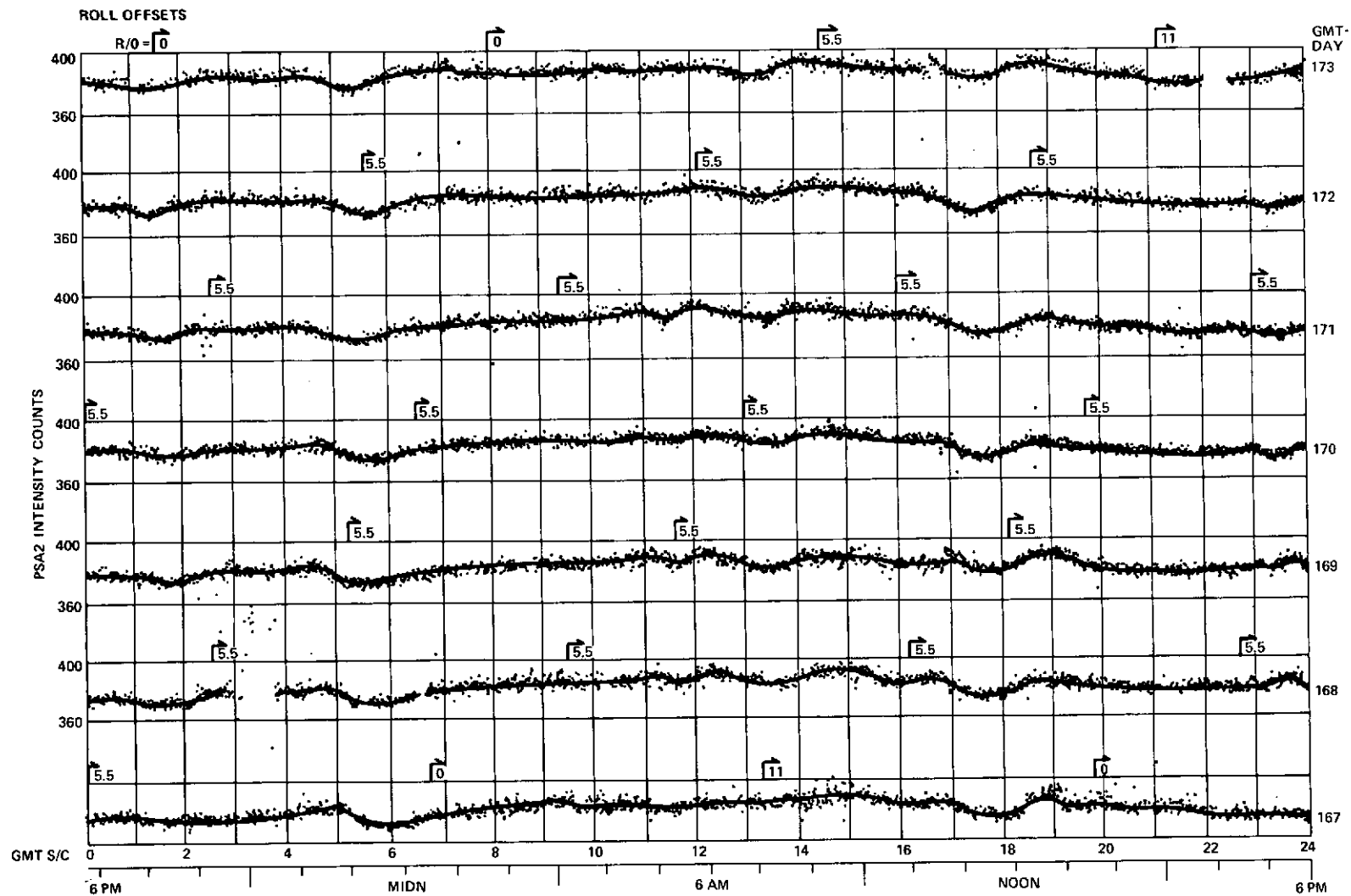
Figure 7-22. Variations in PSA2 Intensity Measurements
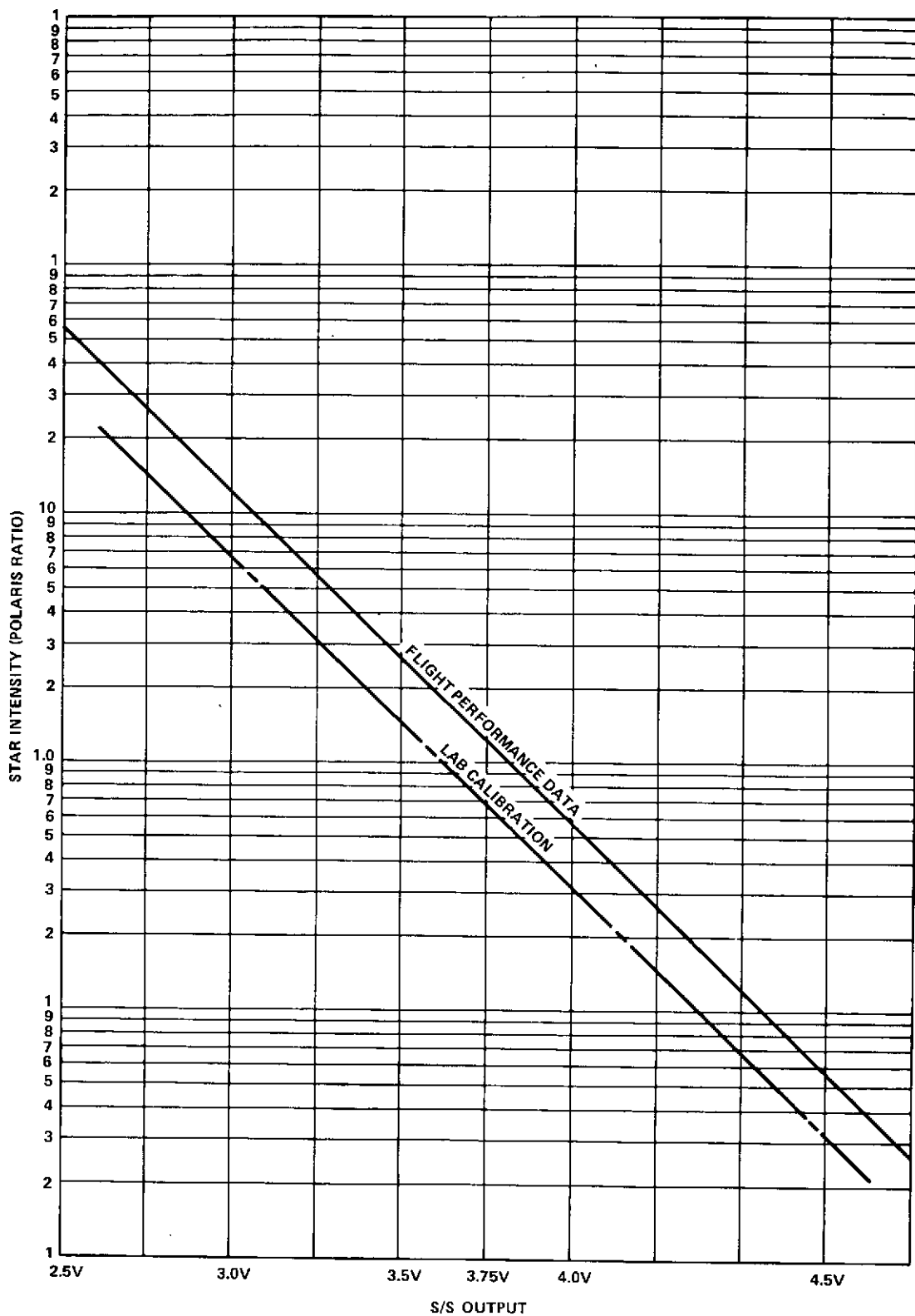
Figure 7-23. PSA #004 SIS Calibration for Single Star

7.5.4 Discussion

A review of the data indicates the following:

a. The daily SIS voltage variation is due to the star field in the neighborhood of the North Pole and the temperature of the PSA. The variation curve is equivalent to a hit susceptibility curve because near the peaks only small changes in incident light are needed to trigger flyback and sweeps.

   Based on this observation, a prediction can be made of large anomalies due to flyback and sweep: A quiet PSA hit period, due to flyback and sweeps, can be expected from day 282 ±2 weeks if the number of spall PSA anomalies is relatively constant. This result follows from three facts (1) The SIS variation due to the star field is relatively small at midnight GMT ±3 hours during the week starting on day 167; (2) 14:30 GMT is the time of maximum SIS voltage independent of star field; (3) At a rate of one degree per day, the star field corresponding to midnight GMT on day 170 will drift so that it will be seen by the PSA at 14:30 GMT in 112 days.

b. A large percentage, possibly 50%, of the anomalies noted early in the mission appear to be the result of reflections from particles. This conclusion follows from the sharp drop in total hits per day as time from launch has increased.

c. The data accumulated indicates that particle tracking is the reason for some of the anomalies. This is because solar pressure would drive particles from east-to-west during spacecraft morning and from west-to-east during spacecraft afternoon.

d. The repetitiveness data given above is strong evidence in favor of the theory that reflections from the ATS vehicle itself are the cause of PSA anomalies. Because such reflections are from surfaces outside the normal FOV of the PSA, it appears that the addition of a non-reflecting baffle should reduce hits if the baffle is oriented so as to shield the PSA from all ATS reflections. The baffle itself would be outside the FOV of the PSA. An attempt to reduce reflections by painting suspected reflecting areas will probably be ineffective because the intensities observed during some hits is as high as 50 × Polaris. Attenuations resulting from painting are unlikely to be as large as the factor of 50 required.

7.5.5 Conclusions

a.   The flyback-and-sweep threshold voltage of 4.0 volts in the PSA is too low. Raising the threshold SIS voltage to 4.5 volts in PSA serial no. 5 for the ATS-F' will eliminate some large changes in PSA output in response to small incident light perturbations.

b.   Most of the continuing PSA anomalies are the result of solar reflections from the north solar array and parabolic reflector. A baffle designed and constructed to shield the PSA aperture from light reflections from these areas will decrease the number of anomalies.

c.   Reflections from particles constituted a major cause of PSA hits early in the mission. As time proceeded the frequency of such reflections was sharply reduced.

d.   The occurrence of a large number of hits immediately after occult was not occult-related but was primarily the result of coincidence -- the Sun orientation at that time caused reflections into the PSA aperture.

e.   The correct PSA calibration curve is given in figure 7-23. Prelaunch calibrations understated star intensities by about 40%.

f.   There is no convincing evidence of abnormal PSA performance.

7.6   YIRU RATE BIAS COMPENSATION ANOMALY

During the initial in-orbit checkout of ATS-6, it was observed that the YIRU rate bias compensation function was not operating properly. The compensation value was changing from the commanded value to zero, and not responding to subsequent compensation change commands until the Rate Bias Reset/Rate Bias Enable command was issued. The time the compensation value would remain at the commanded value varied from less than a minute to several hours.

Figure 7-24 is a functional schematic showing the YIRU rate bias compensation electronics. K1 and K2 are nonlatch type relays. K3 is a latch type. The Rate Bias Reset/Rate Bias Enable command causes K2 to be energized long enough to reset the bias compensation to a value of 0.0 degree/hour, and to set K3. When K3 is set, the bias compensation is sent to the gyro for use, and the selected compensation value is sent to ground (via telemetry) for information purposes. The Rate Bias Disable/YIRU Heater Enable command causes K1 to be energized long enough to power-on the gyro heater, and to reset K3. When K3 is reset, the bias compensation to the gyro is disabled, and the telemetry reading for the bias compensation is zero.
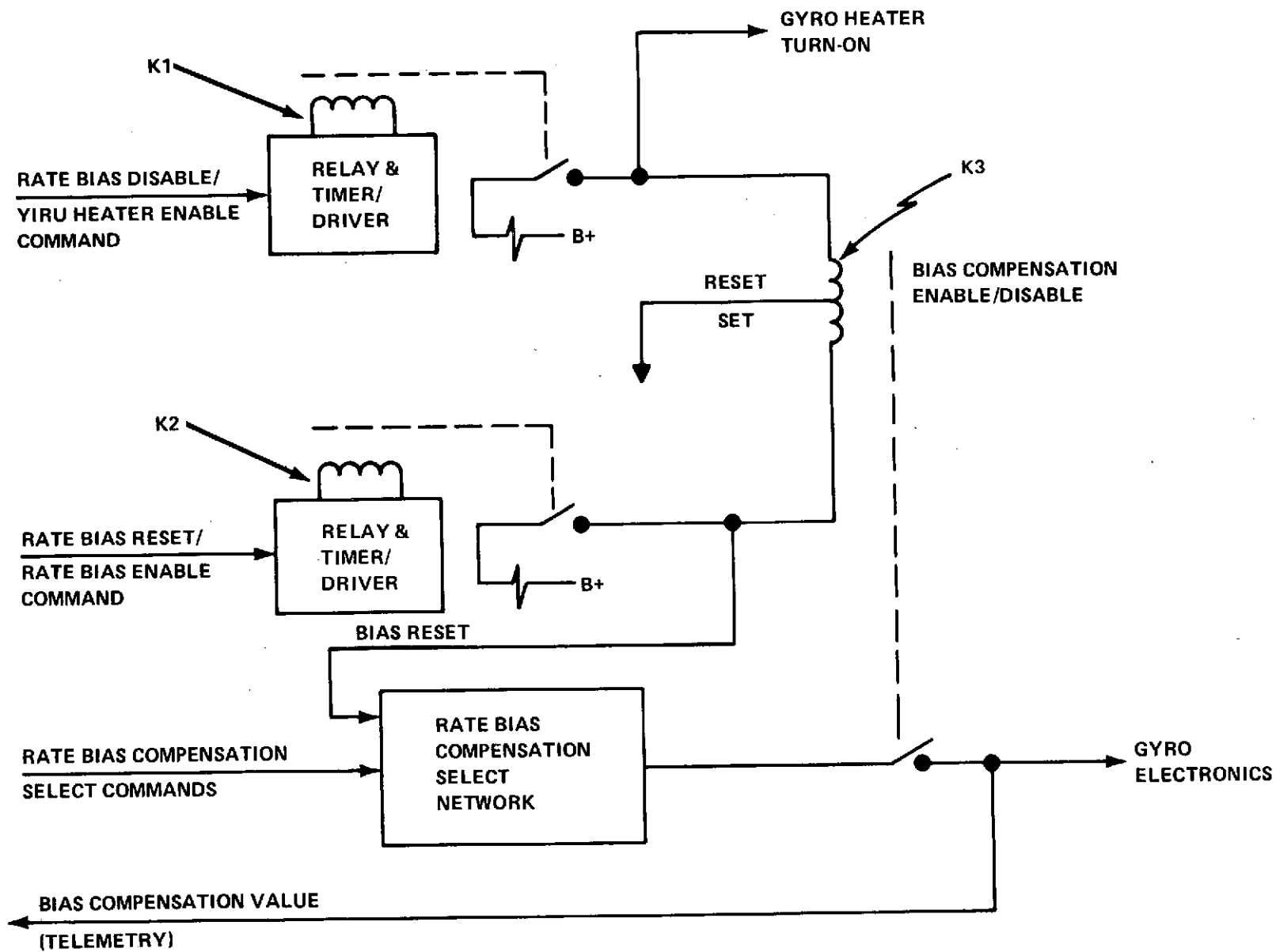
Figure 7-24. YIRU Rate Bias Compensation Schematic

It was suspected that K3 was being reset by K1 being inadvertently energized. Figure 7-25 is a schematic of a relay timer/driver circuit. The relay coil is energized when the SCR is fired. The nominal voltage to fire it is 0.8 volt. Three possibilities exist which could cause the SCR to fire inadvertently.

a.   High level noise on the command line

b.   The SCR has degraded and is being fired by low-level noise on the command line

c.   The input filter capacitor (C1) has failed open, allowing low level noise on the command line to fire the SCR.
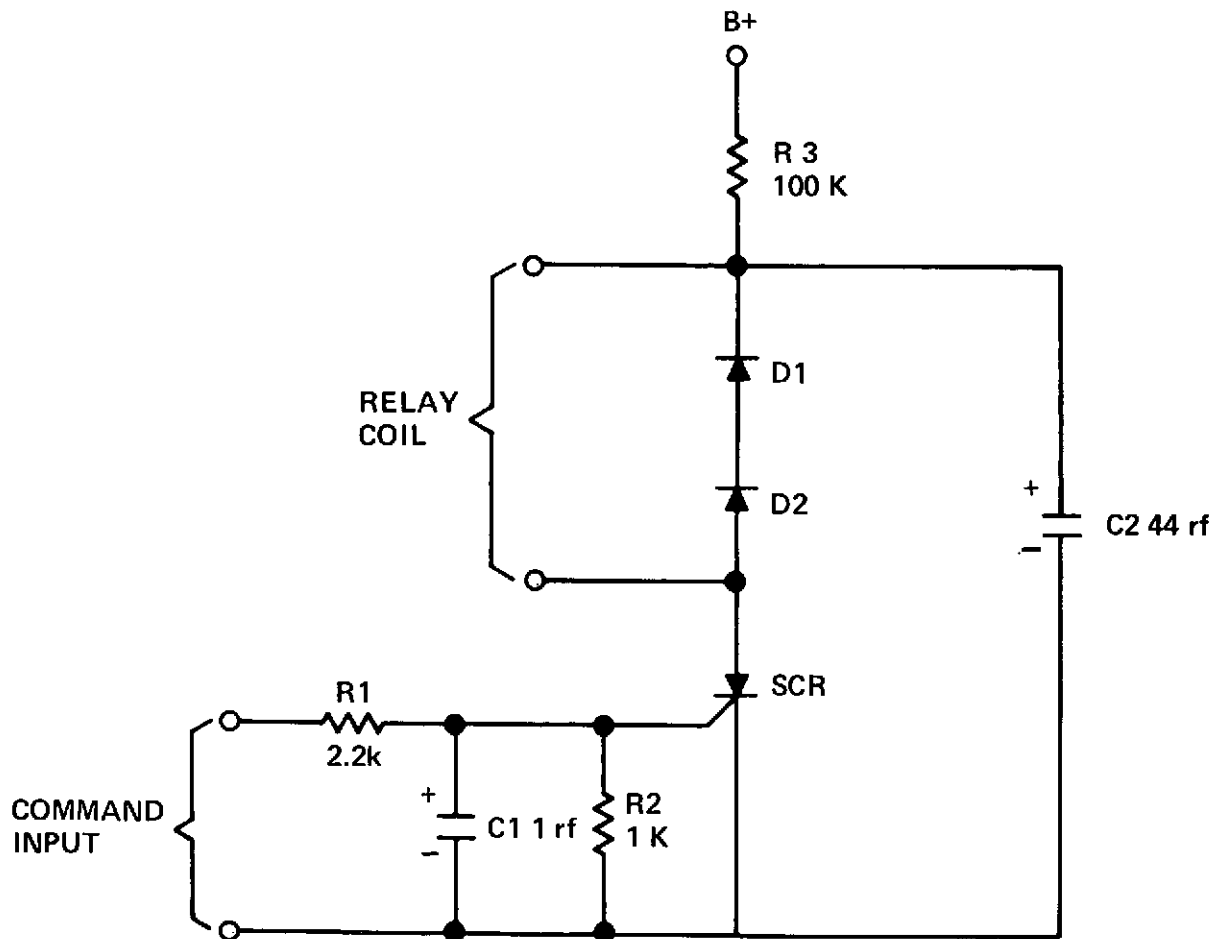
Figure 7-25.   Relay Timer/Driver Circuit

No test can be conducted to determine which of these conditions might exist. However, a test could be made to determine if the relay K1 was being energized. If the gyro heater power is turned off and the bias compensation enabled, then the gyro heater will turn on when the bias compensation changes to zero, if K1 is being energized.

A test to determine if this was happening was made on day 253. The gyro heater was turned off. The Rate Bias Enable command was sent and a select +0.8 degree per hour compensation was commanded. The bias compensation telemetry read +0.8 for approximately 50 seconds, and then went to zero. The gyro temperature began to rise indicating that the gyro heater had been enabled. A bias compensation of +0.8 was sent again. There was no change in the compensation telemetry value of zero, indicating that K3 had been reset, disabling the bias compensation. Commands were then sent to disable the gyro heater and enable the bias compensation. The test was repeated several times. The maximum time the compensation stayed in was 140 seconds. It has been noted that on other occasions the compensation stayed in for several hours.

The conclusions are that the most probable cause is a failure in the relay K1 timer/driver circuitry causing it to be sensitive to noise on the Rate Bias Disable/YIRU Heater Enable command line.

7.7 DOC COMMAND ANGLE ANOMALY

7.7.1 Introduction

Incorrect pitch and yaw command angles were generated by the DOC every 12 hours, lasting for approximately 3-3/4 minutes. This caused a pitch and yaw attitude transient of 3.3° and 1.2° respectively. The anomaly was traced to an overflow in the register for one of the elements of the inertial-to-local-vertical transformation matrix. DOC 1 was reprogrammed on day 179 and DOC 2 on day 163. The anomaly has not reoccurred. Additional details can be found in section 9.6.4 of the ATS-6 In-Orbit Checkout Report.

7.7.2 Yaw Axis Double Sided Limit Cycle

At launch, the DOC's had been preprogrammed to allow for ACS operation in fine deadband, (±0.04 degree, each axis) and wide deadband (±0.36 degree in roll and pitch, and ±0.33 degree in yaw). Fine deadband was to be used for all normal operations. Wide deadband was included to accommodate a possible noise figure degradation from the nominal. Selection of the deadband is via ground command. For either case, once the deadband is exceeded, loop gains, and therefore loop response, are the same.

The Polaris star tracker (PSA) output was noiser than anticipated resulting in the yaw axis having a double-sided limit cycle when the ACS was operating in fine deadband. This caused the yaw wheel to be driven in both directions and exercised the wheel and its driver electronics more than necessary. Since the fine deadband was being used during all normal operations, it was decided to increase the yaw-axis operational deadband slightly to reduce or eliminate the double-sided limit cycle, while still maintaining the specified pointing accuracy of ± 0.1 degree. Honeywell analysts selected a yaw-axis deadband of ± 0.0826 degree in yaw, and ± 0.04 degree in roll and pitch.

Three constants in the DOC FCP define the wide deadband in the roll, pitch and yaw axes for wide deadband operation in all modes employing the wheels except the Low Jitter Mode and for all sensors except the DSS in yaw. It was decided to change the three constants to give a wide deadband of ± 0.04 degree in roll and pitch, and ± 0.0826 degree in yaw, which is approximately double the yaw deadband for the fine deadband. It was not necessary to change the deadband for the Low Jitter Mode, since the loop has additional filtering that filters the tracker noise sufficiently to cause a single-sided limit cycle.

The changes were first made on the DOC breadboard at Honeywell. Test results showed that the desired results were obtained. On day 195, DOC 2 was reprogrammed to incorporate the changes. The increased yaw deadband resulted in a single-sided deadband. On day 214, the DOC 1 was reprogrammed. The change also resulted in a single-sided deadband for the yaw axis. The redefined wide deadband is now used during normal operations in lieu of fine deadband.

7.7.3 Interferometer Loss of Lock

When the signal received at the interferometer drops below its threshold, it loses lock and issues nonzero fixed counts to the DOC as well as continuing to maintain the validity bit to the DOC as valid. Consequently, the DOC is not able to recognize that the interferometer data is really invalid and continues to issue torquer commands. This results in loss of Earth acquisition unless appropriate ground action is taken quickly by switching to the earth sensor. To prevent this, the DOC FCP was reprogrammed to recognize that the interferometer had lost lock (fixed counts to the DOC), and that this was considered a critical fault. At a critical fault, the DOC stops issuing torquer commands, allowing the spacecraft to slowly drift, and sends telemetry to the ground indicating that a critical fault has occurred. This allows the ground operations personnel more time to react and take appropriate action to prevent loss of Earth acquisition.

The modifications were designed to accomplish the following:

a. A critical latchable fault will be set in any mode where the interferometer is in control if the roll count equals 1600_8 and the pitch count equals 1600_8 for a continuous period comprised of 14 interferometer read cycles (2.4 seconds on the average).

b. In the dual frequency mode (updates to DOC at 300 or 336 msec periods), the fourteen-in-a-row test is effectively reduced to a 6- or 7-in-a-row test.

c. In the case of interferometer loss-of-lock, the DOC will continue to read the interferometer, process data into attitude, compute and filter attitude error, derive rate, etc.

d. If invalid data is indicated by the interferometer, the loss-of-lock test is meaningless; however, an invalid data bit will continue to cause a critical latchable fault.

SECTION 8

SPACECRAFT PROPULSION SUBSYSTEM

SECTION 8

SPACECRAFT PROPULSION SUBSYSTEM

8.1 INTRODUCTION

Jet operation since launch has used SPS 1 Thrusters and propellant from the
SPS 1 tank. The SPS 2 feed manifold has remained evacuated from the EVM
and OCJ latching isolation valves to the thruster valves. Prime and backup line
heaters for both half-systems are operating in the Low-Automatic Mode and
SPS 1 and SPS 2 prime valve heaters (truss mounted thrusters) have been on.
SPS 1 cat bed heaters are activated just prior to jet firings.

The following paragraphs detail SPS activity beyond that reported in the ATS-6
In-Orbit Checkout Report (X-460-74-232).

In summary, the SPS 2 valve heater circuit failed on July 31, 1974. It was con-
cluded that this was a random failure in an undertermined Actuator Control
Electronics (ACE) driver circuit component. The backup heaters were activated
and they are maintaining valve temperatures as prior to the failure.

Two additional orbit correction burns have been completed, one involving a 180°
yaw maneuver. Wheel unloads continue every other day following a number of
manual unloads designed to lengthen the time between unloads.

Plots of the tank pressure-temperature hysteresis data indicate that the maxi-
mum uncertainty in tank pressure for the purpose of determining propellant
remaining is ±2 psi. This is equivalent to about ±$\frac{1}{2}$ lb of propellant at the
current blowdown state in tank 1, but the uncertainty will increase to about
±2 lb when the tanks are nearly empty.

Daily occult periods occur between September 4 and October 20, 1974. It has
been necessary to warm up the SPS 1 Truss Thruster valves using the backup
valve heaters before entering occult in order to limit the minimum valve tempera-
ture to 10°C.

An in-orbit test, activating various telemetry transmitters and antennas indi-
cates that the #14 thruster cat bed temperature remains sensitive to RF under
some conditions.

8.2 SPS 2 VALVE HEATER FAILURE

8.2.1 Description of Failure

During temperature checks on July 31 (GMT 212:12:40), it was noted that the four SPS 2 thruster valve temperatures were very low (#13, -16°C; #14, -4°C; #15, -22°C; #16, -20°C). Data for the previous day at the same time indicated values between 25°C and 40°C. Commanding the SPS 2 prime heaters on (again) produced no change in temperature. The SPS 2 backup heaters were then commanded on and valve temperatures rose to their normal values within three hours.

SPS valve temperatures, SPS power status, spacecraft load bus current and all spacecraft commands were evaluated for the 24 hour period covering the failure. Figure 8-1 is a plot of the temperature data from this period and shows the time of failure (211:19:38) and the subsequent temperature variations. The data are superimposed on curves for SPS 1 valves during a typical 24-hour orbit.

During this period no commands that could have effected the SPS had been executed and the spacecraft bus current showed no abnormalities.

The failure analysis focused on the nature and history of the heaters and on the design of driver circuits in the ACE.

8.2.2 Test History

The test history of the valve heaters was reviewed and no failures had occurred and no anomolous operation had been observed either at Rocket Research Corporation or at FL. Resistance, hipot and response-on-activation measurements had all been normal (Resistance = 294 to 304 ohms, spec. 296 ± 30; hipot = 35K to 80K Megohms, Spec. > 100 Megohms).

8.2.3 Malfunction Analysis

The prime and backup heater elements for each valve are potted together in a C shaped cylinder that is bonded to the valve body. The two lead wires from each heater element run from the heater to connector J-9 (SPS-1) or J-10 (SPS-2) on the ACE box. Inside the ACE, the eight leads from either a prime or backup set of four heaters (SPS 1 and 2) are wired in parallel on a terminal board and connected to a single driver circuit (Figure 8-2). The driver is a solid state switch with associated current limiting and latch circuits.
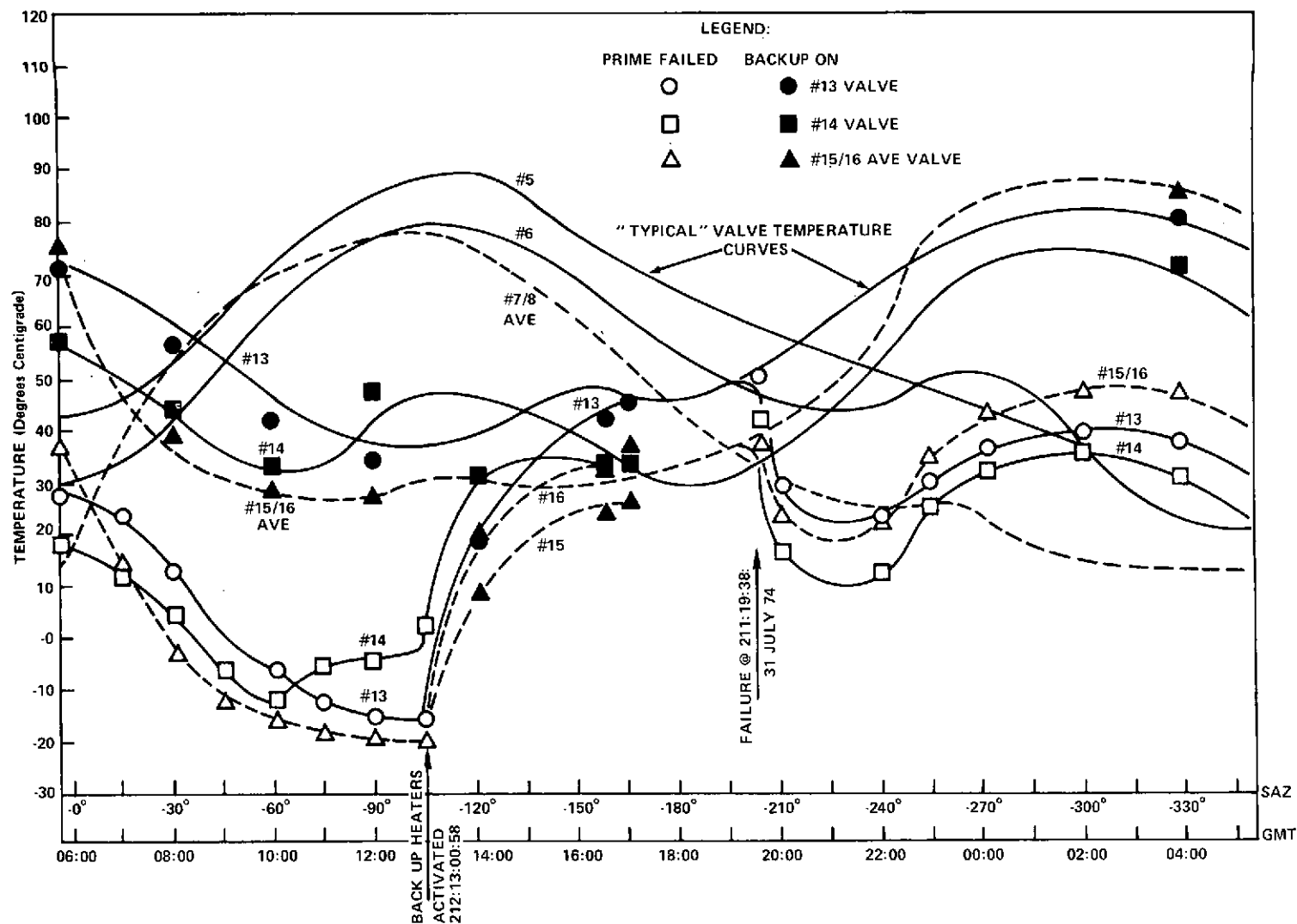
Figure 8-1. Valve Temperatures vs. GMT and SAZ
(During Valve Heater Failure)
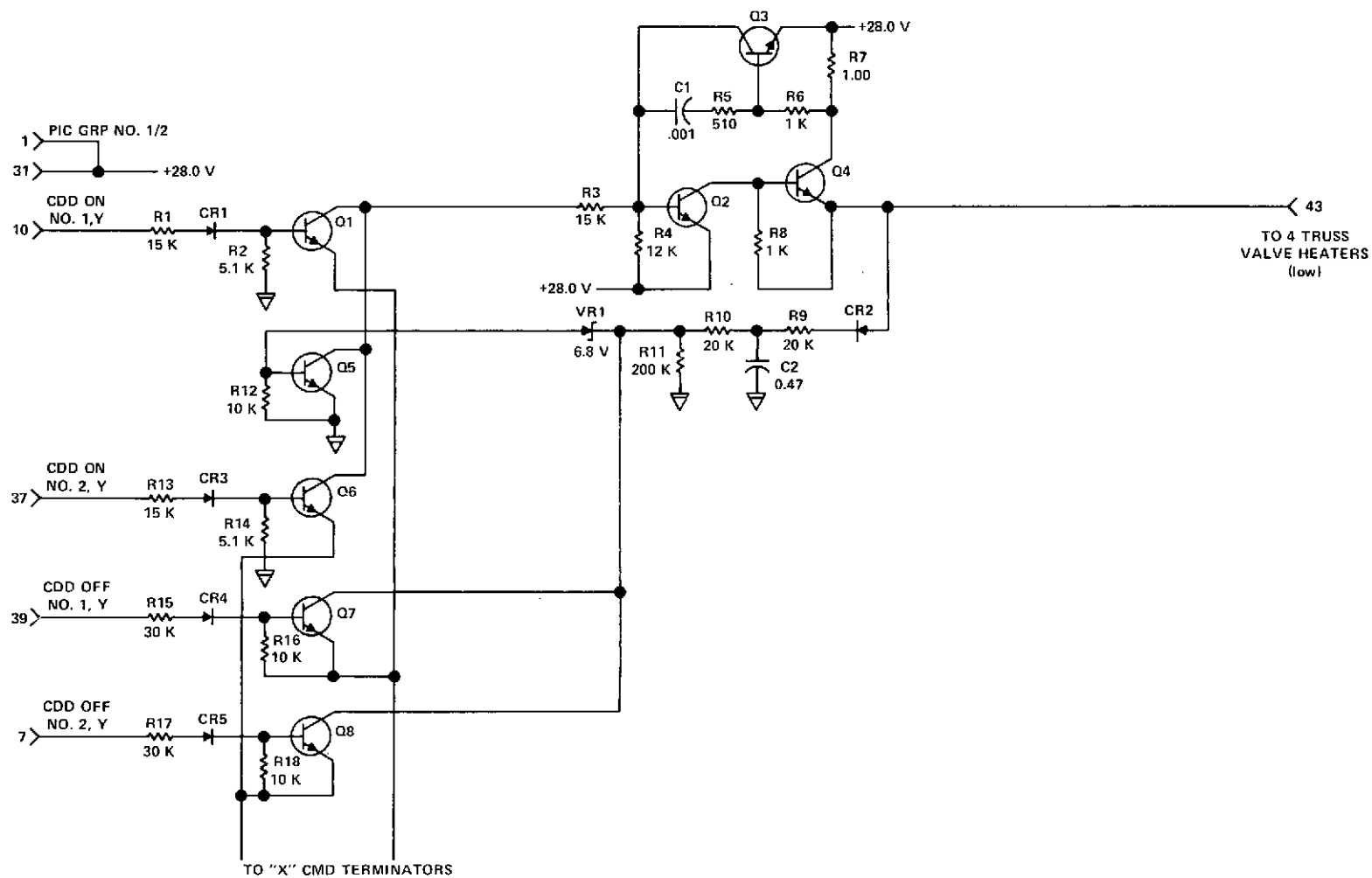
Figure 8-2. ACE Valve Heater Driver Circuit

The fact that an external open failure of any of the valve heaters would not prevent operation of the remaining heaters eliminates such a failure from consideration. An internal or external short would cause current limiting in the circuit and prevent heater operation. An internal open or circuit component failure would lead to the same result.

Current is limited by the circuit to 0.5 to 0.6 ampere and a short would result in a similar increase in the spacecraft bus current for the 250-ms heater command period. If no change in bus current occurred, an open failure would be implied. In addition, if the heater malfunction was the result of a failure of the latching function of the circuit, the normal current of approximately 0.3 ampere would be drawn during the command pulse. However, the probability of observing a 250-ms pulse with the DACU in the Normal Mode would be quite small (less than 0.10).

An attempt to detect changes in bus current during heater-on commands was inconclusive. DACU 1 was placed in dwell (S/C load bus current, Channel 65), with the current being monitored on a stripchart recorder and the ACS was configured for Low Jitter Mode to minimize fluctuations due to wheel currents. An examination of the data following SPS 2 heater commanding indicated that the variation in wheel currents probably would have masked any transients due to the heaters.

For the second test, the Communications Subsystem was configured to draw enough power to discharge the batteries. In this configuration changes in load current might be detected using the battery discharge current (Ch. 57) since it is about three times as sensitive as Ch. 65. In addition, the wheels were taken out of the control loop, eliminating their influence on load current. When the SPS 1 backup valve heaters were commanded on the normal current of 0.3 ampere was clearly evident on the stripchart recorder. The SPS 2 prime valve heaters were commanded on four times over a 25-minute period. No current transients were visible on the recorder, nor were any seen in the Ch. 57 digital printout.

A review of the circuit design by FI and Honeywell concluded that, while the driver circuit was specifically designed for the ATS program and had not been used on other programs, it is fully adequate for the application. This conclusion is reinforced by the fact that there were no malfunctions recorded during component and subsystem testing at Honeywell or in the ACE through FI integration and spacecraft level tests.

The probable cause is that the heater driver circuit is open due to a random failure of an unknown part.

8.2.4 Consequences of Failure

The temperature data shown in Figure 8-1 indicate that operation with the SPS 2 backup heaters is the same as with the prime heaters. Since propellant has not been bled into the SPS 2 manifold, it would be possible to operate with the backup heaters off, allowing the dry valves to go to temperatures below the freezing point of hydrazine.

The valve vendor, Parker Hannifin, has no low temperature cycle data on the valve. Rocket Research Corporation had subjected one dry valve to 25 cycles between -150°F and +100°F. Before-and-after leak and electrical checks indicate no change in performance. Freeze-Thaw tests at RRC during the ATS program subjected a valve filled with hydrazine to 10 cycles between -50°F and +150°F. The valve was operational and visual inspection showed no external damage; however, an additional nine cycles caused a circumferential valve body weld to crack allowing external leakage of hydrazine.

Discussions with Rocket Research indicate that neither they nor Parker Hannifin are concerned about dry valve temperature cycles between approximately -25°C and +50°C (as compared to +10°C to +90°C with the valve heaters on). The sensitive area where the poppet rests on the valve seat is under spring compression force and would tolerate any minor motions due to thermal expansion and for the 75°C to 80°C with very low thermal stress in the valve body. However, temperature cycling of a wet valve below the freezing point of hydrazine (2°C) could rupture the valve body and cause possible internal damage.

Current operation with the SPS 2 backup valve heaters on (with the prime heaters failed) leaves no backup. The bed heaters are normally off except for periods when jet operation is anticipated. It is estimated that one set of bed heaters operating without valve heaters would raise the valve temperatures by about 10°C which is not enough to bring them above the freezing point. If they could raise the temperature above the freezing point their use as a backup might justify the required 12 watts (8 × 1-1/2 watts per heater) since the valve heaters themselves consume 10 watts (4 × 2-1/2 watts per heater). The actual effect of the bed heaters on valve temperature would have to be determined experimentally. The following is a summary of predictions and orbital data.

VALVE TEMPERATURES

Bed Heaters	Valve Heaters	Actual In-Orbit	Predicted In-Orbit
ON	ON	25 to 96°C	5 to 88° C
OFF	ON	10 to 90°C	(not available)
ON	OFF	(not available)	(not available)
OFF	OFF	-25 to 50°C	-12 to 30°C

The spacecraft will continue to be operated with the SPS-2 backup valve heaters active.

8.3 ORBIT CORRECTION BURNS

East-west drift rate corrections #3 and #4 on 3 August and 14 September were made using SPS 1 Jet #7. Table 8-1 summarizes the pre- and post-maneuver orbital and spacecraft data.

Burn #3 was required to correct an eastward drift off station and would have normally used SPS 2 Jet #15. However, because of the SPS 2 prime valve heater failure, it was desirable to maintain the SPS 2 propellant manifolds dry. In order to perform the maneuver with the opposite jet (#7), the spacecraft was yawed 180°. Figure 8-3 illustrates the rate of this manuever and the fact that the initial turn had a variable rate. The yaw in both cases was initiated by commanding sixty 0.250 sec pulses with no delay (15 sec equivalent burn) to give a 0.037°/sec rate. During the first maneuver a total of 100 +y and 100 -y additional pulses were commanded in groups of 20 at various times to produce the rate changes shown. ACS automatic control was initiated as the maneuver was completed and the initial rate was removed by an opposing yaw jet.

Table 8-1 also documents changes in orbital elements and shows 0.14 lb of hydrazine used in each maneuver. Essentially the same burn time produced 19% more Δv during correction #4. The major portion of the difference in calculated Δv can be attributed to ranging errors.

8.4 WHEEL UNLOADING

The normal method of wheel unload has used the +R jet* to reduce roll wheel speed at a time when the roll-yaw cycle momentum exchange has reduced the yaw speed to near zero. This is done automatically by the ACS with the final roll wheel speed in the 300 to 400 rpm range. Two days of momentum buildup and exchange increase yaw and roll speeds to a point where they are approaching saturation speed of ±1500 rpm. The unload requires approximately twenty 0.2/10 (sec on/off) jet pulses.

Manual unloading of the roll wheel can reduce wheel speed to less than 300 rpm, resulting in longer times between unloads and fewer unload operations. A number of manual unloads were performed with Figure 8-4 representing an example of a

---

*Use of the longer moment arm roll jet results in fuel economy.

8-7

Table 8-1

Orbit Correction Maneuvers

GMT:	BURN #3 216:12:00:00 (3 Aug 74)			BURN #4 257:13:30:00 (14 Sept 74)		
Orbital Data	Premaneuver	Postmaneuver		Premaneuver	Postmaneuver	
	*	Predict.	Actual		Predict.	Actual
Semi Maj Axis, km	42161.3	42164.1	42163.9	42166.5	42169.2	42169.6
Eccentricity	.0002	.00016	.00012	.0004	.0004	.00039
Inclination, deg	1.588	1.588	1.590	1.507	1.507	1.510
RA Ascend. Node, deg	264.27	264.27	264.60	262.93	262.93	262.99
Drift Rate, deg/day	.0359 E	0.0	.0032 E	.0212 W	.0131 E	.0133 E
Sub Sat Long, deg	93.73	93.71	93.72	94.08	94.08	94.02
SPS/SC Data:						
SC Weight, lb.	2968.5		2968.4	2968.1		2968.0
Jet #7 Δt, sec.	—		265	—		260
ΔV, ft/sec	—		.307	—		.365
Wp, lb.	—		.14	—		.14
Thrust, lbf. (ave)	—		.116	—		.114
Tank 1 Press, psia	339.4		338.0	331.3		329.9
Tank 1 Temp, °C	27		27	24		24
Remaining Fuel,* (Tank 1)	—		51.76	—		51.4

*ASC Mode: Local Vertical Orbit Plane, East/west following 180° yaw maneuver.
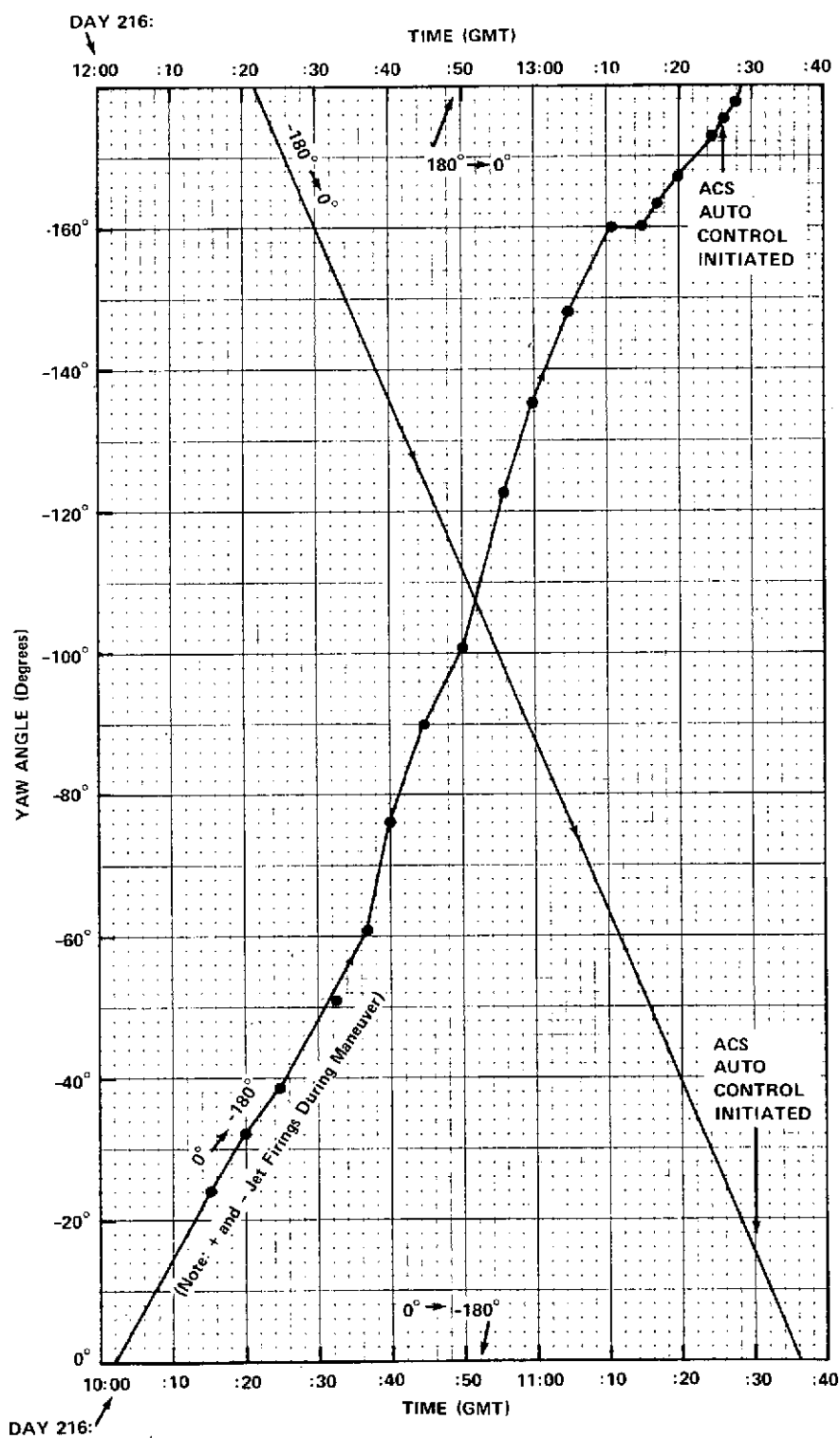
Figure 8-3. 180° Yaw Maneuver Prior to 3rd Orbit Correction
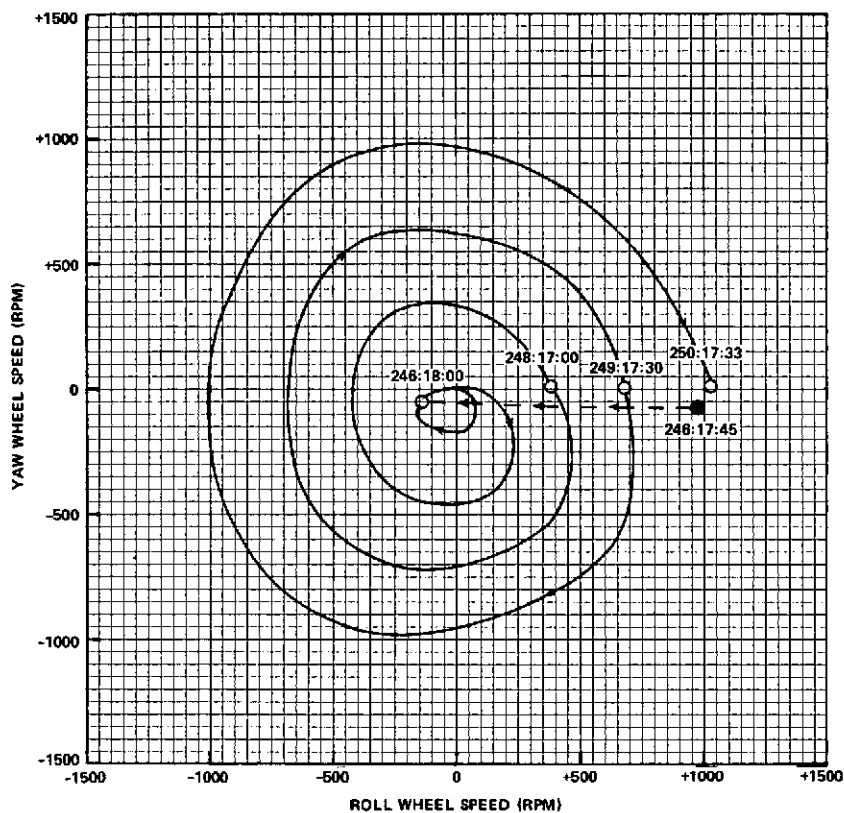
Figure 8-4. 4-Day Wheel Unload Cycle

four-day cycle (days 246 to 250). The total amount of jet impulse over a number of unloads is the same regardless of the length of the unload cycle. However, the unload impulse can be minimized by reducing the amount of cross coupling between yaw and roll during roll unload; i. e. , when yaw speed = 0.

It was concluded that the reduced number of unload operations did not justify the greater complexity associated with manual unloading. Normal operation will continue to be a two-day cycle using the automatic unload mode.

8.5   TANK PRESSURE/TEMPERATURE HYSTERESIS

A number of 24-hour tank pressure-temperature plots show a 4 psi/9°C variation for tank #1 and a 4 psi/7°C variation for tank #2. Figure 8-5 shows typical data.

The particular shape of the hysteresis cycles and the varying amounts of time spent at different P/T conditions does not allow easy interpolation in the selection of a tank pressure at a given temperature (20° for example). However, the worst case or maximum uncertainty in tank pressure is ±2 psi and is more likely ±1
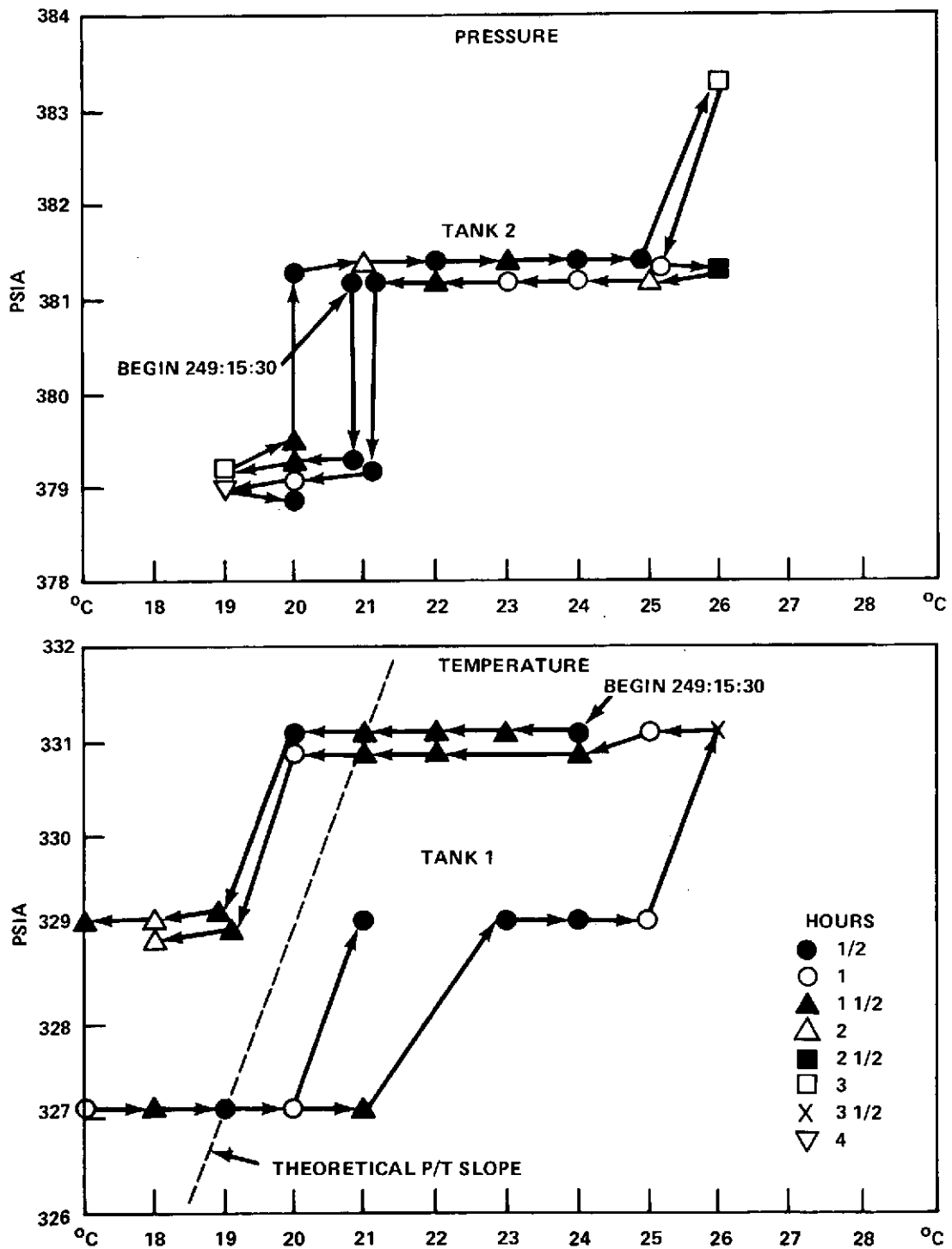
Figure 8-5. Tank Pressure/Temperature Hysteresis

psi. The larger uncertainty is equivalent to about $\pm\frac{1}{2}$ lb of hydrazine in Tank 1 at its current blowdown state. Because of the decreasing slope of the blowdown curves the uncertainty in propellant content increases to about ±2 lb when the tanks are near empty.

No attempt to improve tank pressure data is planned for operations in the near future.

8.6 OCCULT TEMPERATURE CYCLES

Figure 8.6 shows SPS 1 valve temperature data for Day 249 and 250 (4th day of shadow) with an occult period between 5:55:02 and 6:31:45 and an umbra condition between 5:59:41 and 6:27:06. The temperature of valves 7 and 8 had dropped to 8° and 9°C. Because of the exposure to sunlight during the daily cycle, SPS 2 valve temperatures are 20° to 60°C greater than those of SPS 1 at the time the spacecraft enters occult and they do not approach the freezing level during the shadow period.

Because of the need to conserve electrical power during occult, it was decided to warm the SPS 1 valves to the SPS 2 level using the backup heaters, turning them off just before entering shadow. Figure 8-7 illustrates the warm up, the case where the backup heaters are left on during occult and the case where they are turned off. The minimum temperature is 10°C (freezing point of hydrazine = 2°C). The warmup using the SPS 1 backup heaters is standard operation during the occult season.

8.7 IN-ORBIT CHECK OF RF INTERFERENCE WITH CAT BED TEMPERATURES

A test to determine the effect of telemetry RF on the SPS catalyst bed temperatures was conducted on 23 July 1974. Table 8-2 presents catalyst bed temperature data with the telemetry transmitters and antenna configured five different ways. The resolution of these temperatures is 4°C for an 8-bit system.

With no change in transmitter configuration (first two columns), five one count changes occurred in 5 minutes, some of which could have been actual temperature changes. Times between configurations were variable and all shifts were one count changes except when the A2 (137 MHz)/PFF combination was turned off, switching the temperature telemetry to A1 (136 MHz)/OMNI 2. In this case three significant shifts occurred, with thruster #14, which has always been sensitive to RF, showing a 16°C change.
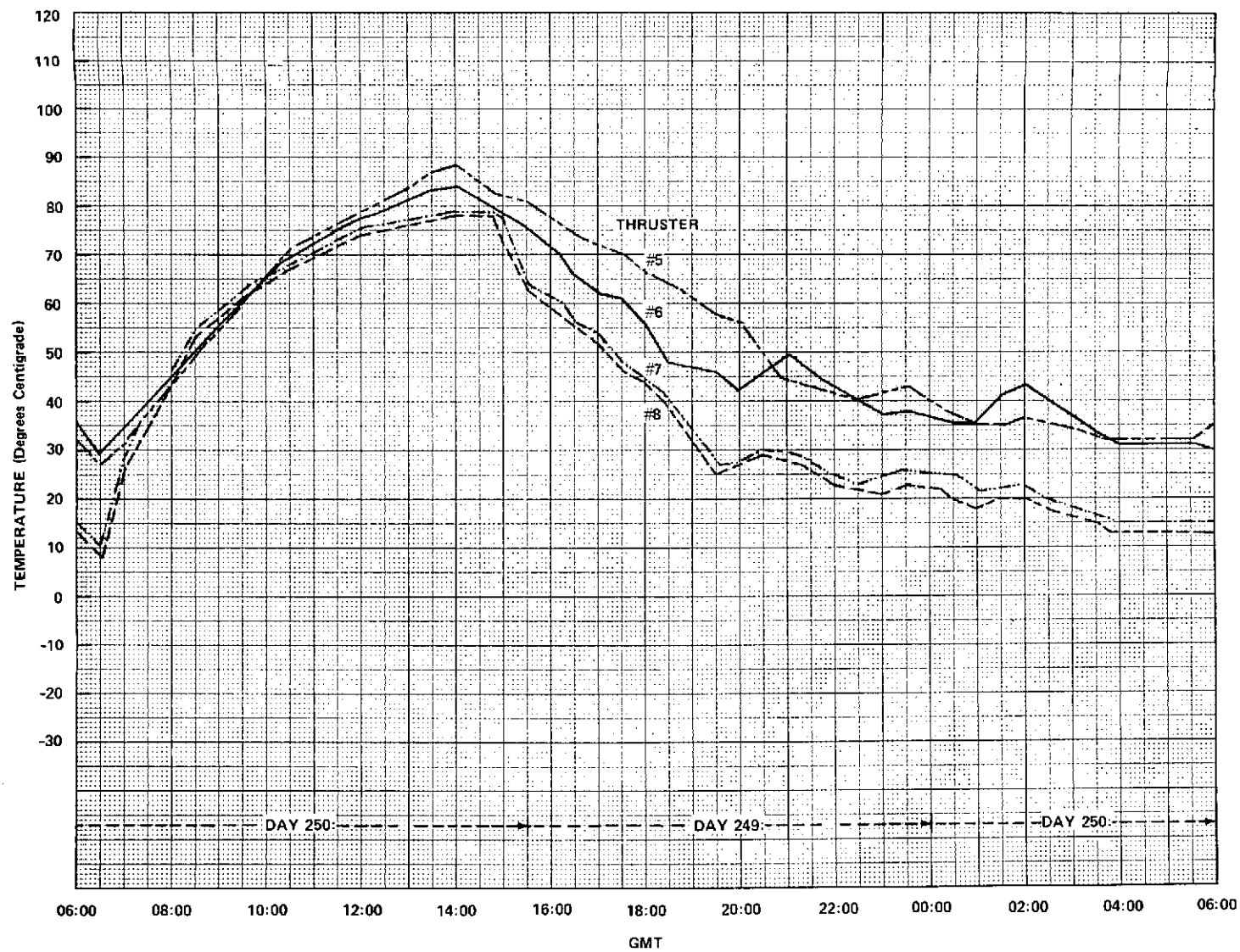
Figure 8-6. SPS Valve Temperatures vs. GMT During Occult
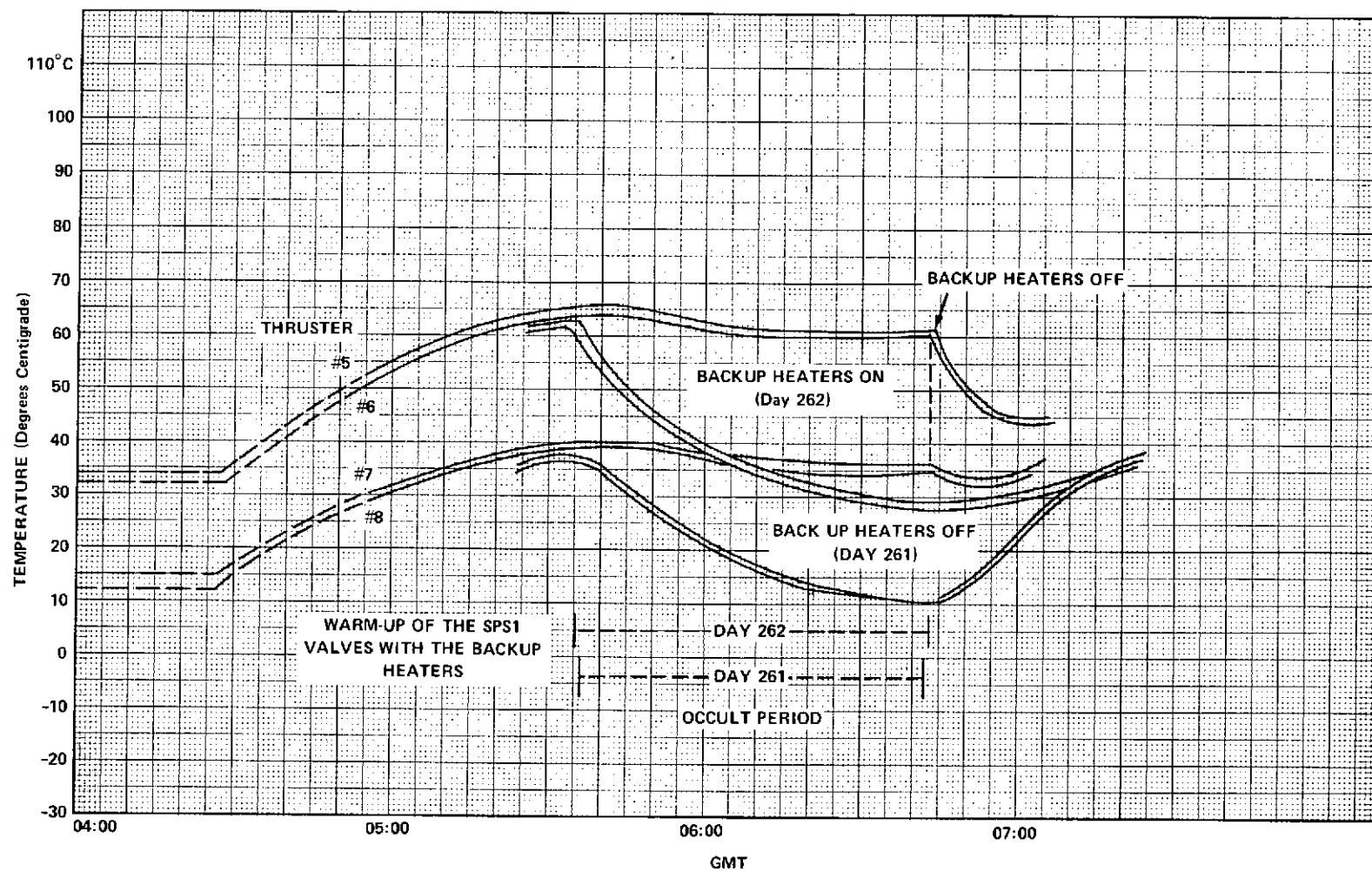
Figure 8-7. SPS 1 Valve Temperatures
(Prime Valve Heaters On)

Table 8-2

RF Effect on Catalyst Bed Temperatures

Telemetry Transmitter Condition								
					(Day 204)			
XMTR	Antenna	15:42:31	15:47:02	15:47:38	16:00:01	16:09:28	16:11:49	
136 A1	OMNI 2	ON	ON▲	OFF▲	ON	ON	ON	
137 A2	PFF	ON*	ON*	ON*	ON*▲	OFF	OFF	
136 A3	(None)	OFF	OFF	OFF	OFF	OFF	OFF	
136 A4	OMNI 1	OFF	OFF	OFF	OFF	OFF▲	ON	

Catalyst Bed Temperatures, °C

1	-R ⎤	47°C	43°	43°	43° ↓	39°	39°	
2	+R ⎟ EVM	15	15	15 ↑	19 ↓	15	15	"Typical Values"**
3	-P ⎟	63 ↑	67 ↓	63 ↓	59 ⬥	51	51	
4	+P ⎦	15	15	15	15	15	15	
SPS 1								
5	+Y ⎤	47	47	47	47 ↓	43	43	52°C
6	-Y ⎟ OCS	27	27	27	27	27	27	31
7	WP ⎟	51	51	51 ↓	47	47	47 ⎤	49
8	WB ⎦	47	47	47 ↑	51 ↓	47	47 ⎦	49
9	-R ⎤	39	39	39	39 ⬥	27	27	
10	+R ⎟ EVM	11	11	11	11 ↑	15 ↓	11	
11	-P ⎟	71	71 ↓	67 ↓	63	63 ↓	59	
12	+P ⎦	19 ↓	15	15 ↑	19	19	19	
SPS 2								
13	-Y ⎤	23 ↓	19 ↑	23	23	19	19	20
14	+Y ⎟ OCJ	11 ↑	15	15 ↑	19 ⬥	3	3	24
15	EP ⎟	-9	-9	-9 ↓	-5	-5	-5	-7
16	EB ⎦	11 ↑	15	15	15 ↓	11	11	13

Legend:
↓ ↑ = Normal Temperature Change
⬥⬥ = Rapid Temperature Change
▲ =

*Catalyst Bed Temperature Transmitter
**Refer to ATS-6 in Orbit Checkout Report (X-460-74-232) dated August 1974.

No quantitative conclusion can be drawn from the data. Qualitatively, it appears that switching in omni antennas has little influence on data being obtained via the prime focus feed. A major shift occurs when the telemetered temperatures are switched from the PFF to an omni and the PFF is turned off. Because of the drastically reduced RF field around the truss-mounted thrusters when using omni antennas, it is concluded that the last two columns are the more accurate temperature data.

SECTION 9

COMMUNICATION SUBSYSTEM

SECTION 9

COMMUNICATION SUBSYSTEM

9.1 INTRODUCTION

The Communication Subsystem (C/S) was checked out during the first 30 days of in-orbit operation. The C/S performance during this time was satisfactory in that the in-orbit performance met or exceeded requirements. Details of the C/S performance measurements may be found in the ATS-6 In-Orbit Checkout Report, GSFC document X-460-74-232.

Beginning in the first week of July 1974 when the spacecraft became operational, experiment checkout and data acquisition began in earnest. From this point on to the end of this quarter (31 August), the C/S primarily supported the communications experiments, except for investigative or special performance tests; i.e., antenna pattern measurements, G/T and EIRP measurements, etc. Therefore the main emphasis of performance analysis is in the area of C/S-experiment interface. Open items from the In-Orbit Checkout Report as well as anomalous performance is also discussed. Experiment results, however, are covered in later sections.

9.2 COMMUNICATIONS EXPERIMENTS

9.2.1 Complement of Experiments

Communications experiments as differentiated from the spacecraft experiments are defined as those experiments requiring C/S configuration or support. In this category are the following:

VHRR

PLACE

TRUST/SITE

C-Band RFI

TDRE/GEOS/SSE

MMW (Comm Mode)

SAPPSAC

HET

TV CAMERA

In addition to being configured for the above experiments, the C/S is used for non-experiment activities such as C-band ranging (spacecraft orbit determination), monopulsing, and interferometer HSDL operation.

9.2.2   Typical C/S-Experiment Configurations

Figures 9-1 through 9-7 shows typical C/S-experiment configurations for the various communications experiments. For the HET experiment, variations in the typical configuration consist mainly of switching HET transmitter beams to accommodate different locations and configuring on S-Band uplink to one of the HET transmitters for Alaska/IHS operations.

9.2.3   Experiment Operations

Communications experiment operational times, exclusive of any operational time logged during initial checkout of the spacecraft is summarized in Table 9-1. Supplementing this table is a matrix of C/S component operational times shown in Table 9-2. The intent of these two tables is to show the cumulative experiment/ C/S component operational times as an aid to future trend analysis. However, these tables are preliminary in nature as the data was extracted from ATSOCC log books. More accurate tabulation will be presented in future quarterly reports as flight history tapes and software become available.

9.3   COMMUNICATION SUBSYSTEM PERFORMANCE

C/S performance parameters consist primarily of the following:

> G/T and EIRP measurements
>
> Antenna pattern measurements
>
> Monopulse measurements
>
> Transponder signal characteristics
>
> Trend data

While these parameters were measured primarily during the first 30 days of operation, some of the measurements had to be repeated or were not obtained. In the case of antenna pattern measurements, some of the plots (S-band) shown in the ATS-6 In-Orbit Checkout Report were based on quick-look data and will be replaced as new plots become available.
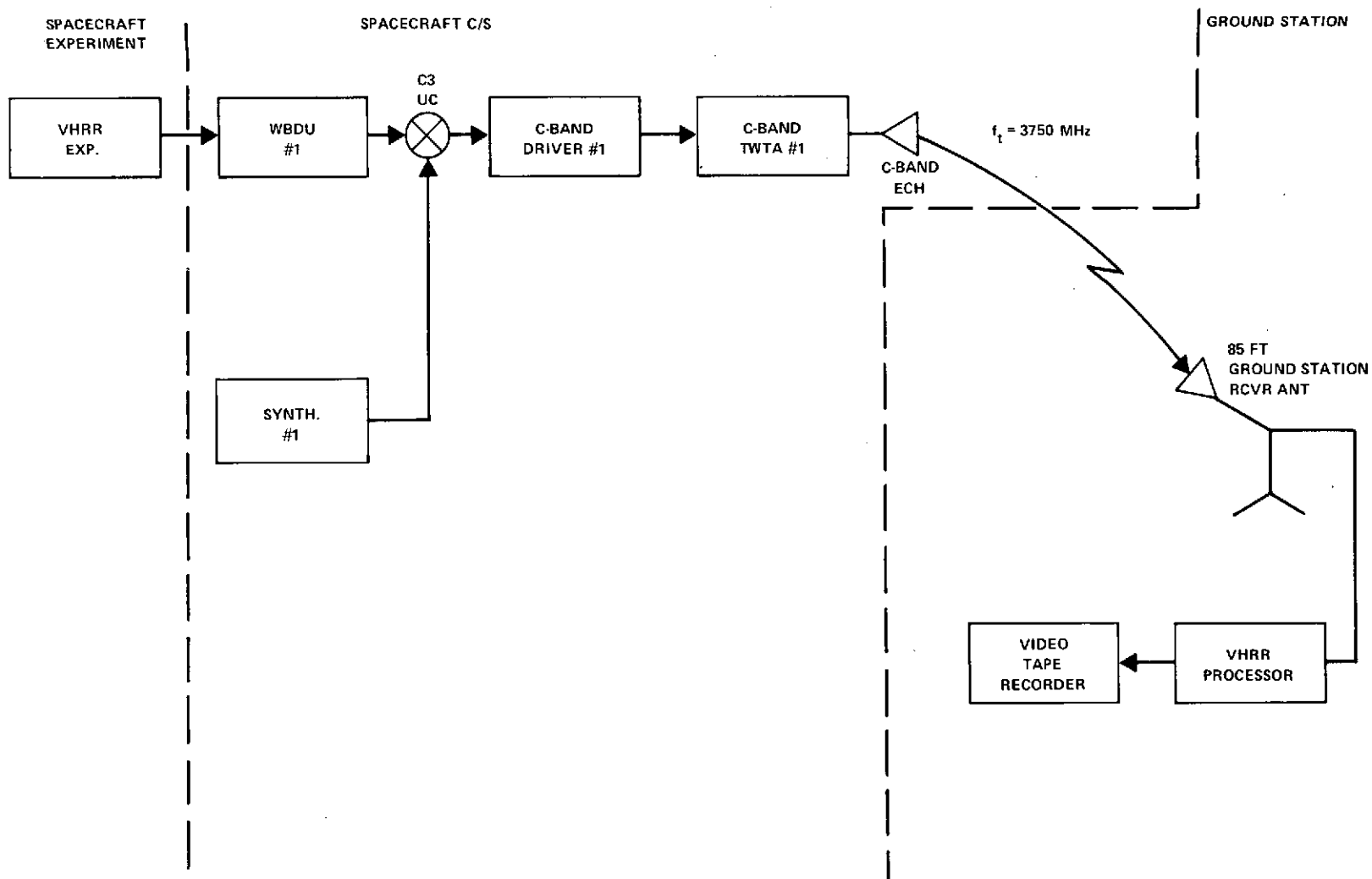
Figure 9-1 Typical VHRR Experiment Configuration
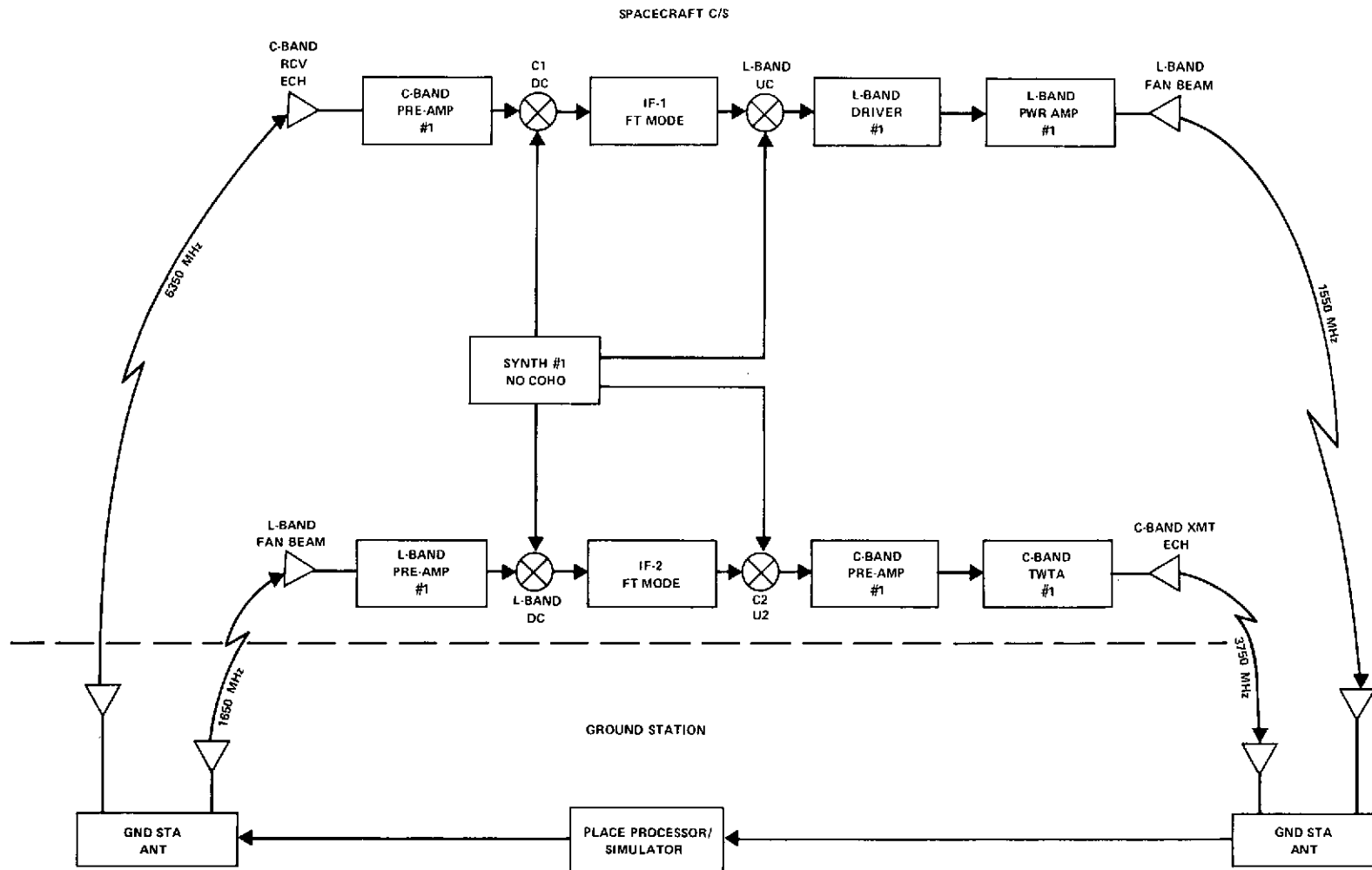
Figure 9-2 Typical PLACE Experiment Configuration
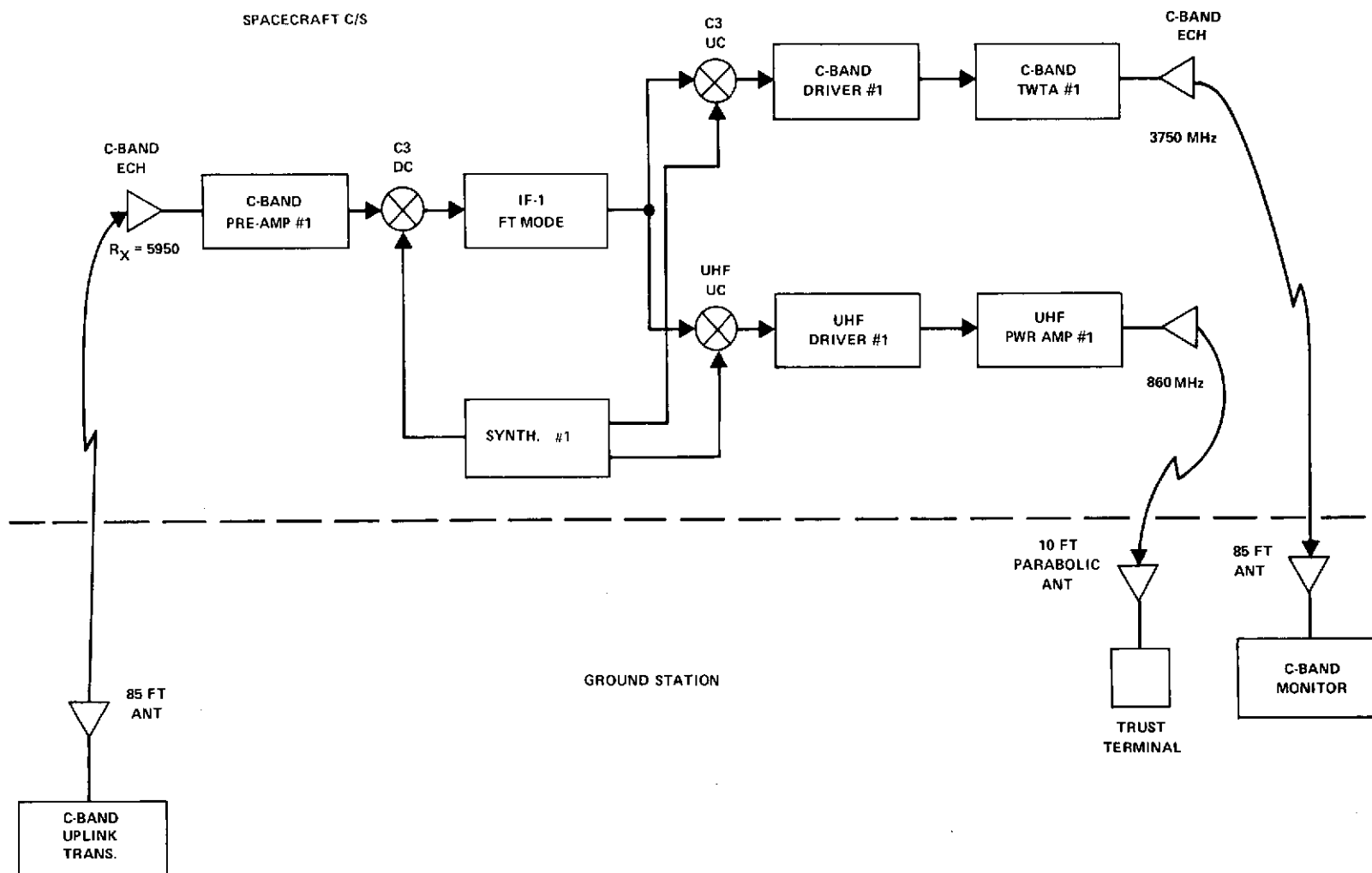
Figure 9-3 Typical TRUST Experiment Configuration

SPACECRAFT C/S

RFI
SIGNALS

C-BAND RCV
PFF

| C-BAND RFI TRANSPONDER | C-BAND DRIVER #1 | C-BAND TWTA #1 |

C-BAND XMIT
ECH

6GHz

3950 MHz

GROUND STATION

6 FT
ANT

85 FT
ANT

| CALIBRATION & TRACKING SIG. |

| DATA PROCESSOR | SCANNING SPECTRUM RECEIVER |
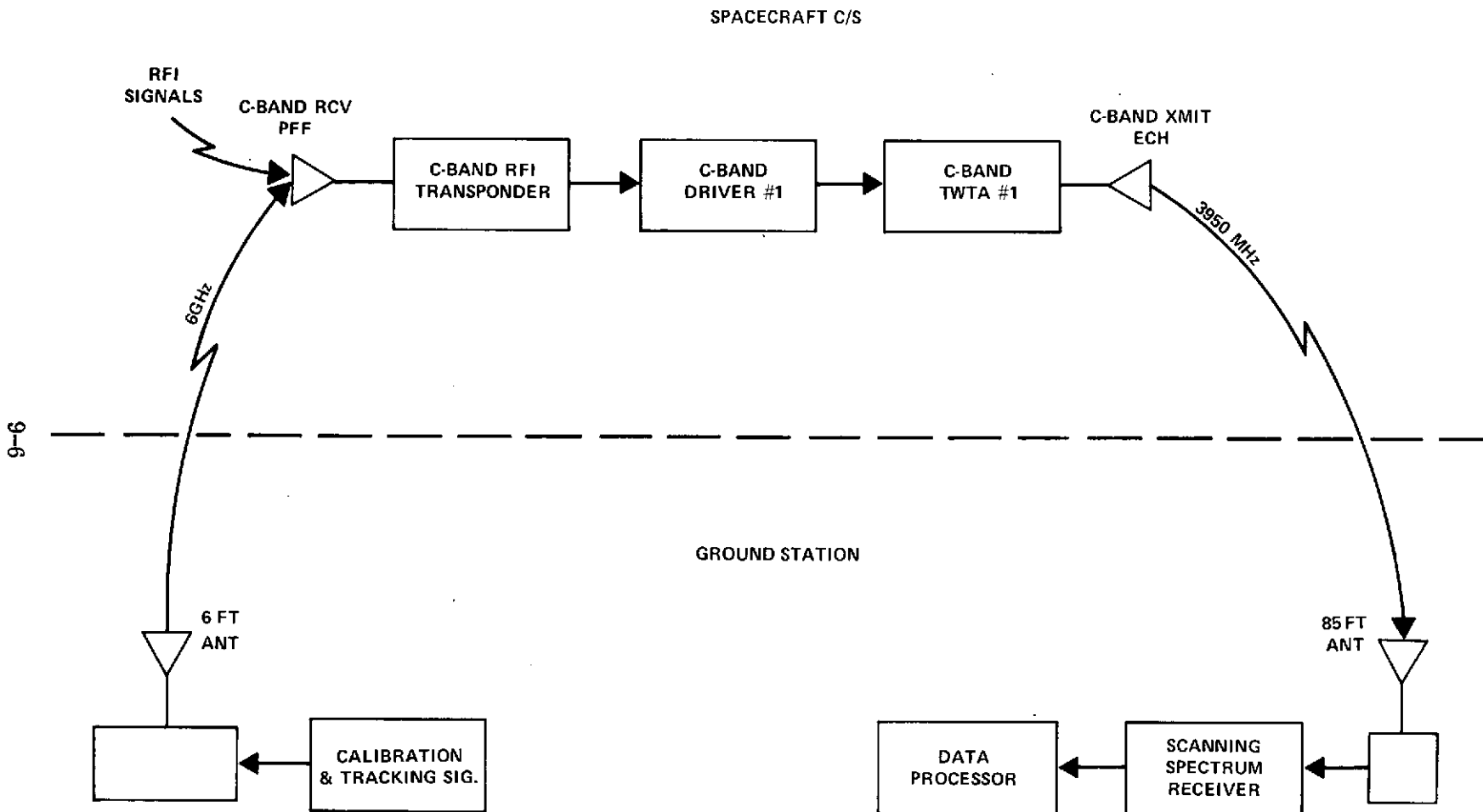
Figure 9-4 Typical RFI Experiment Configuration
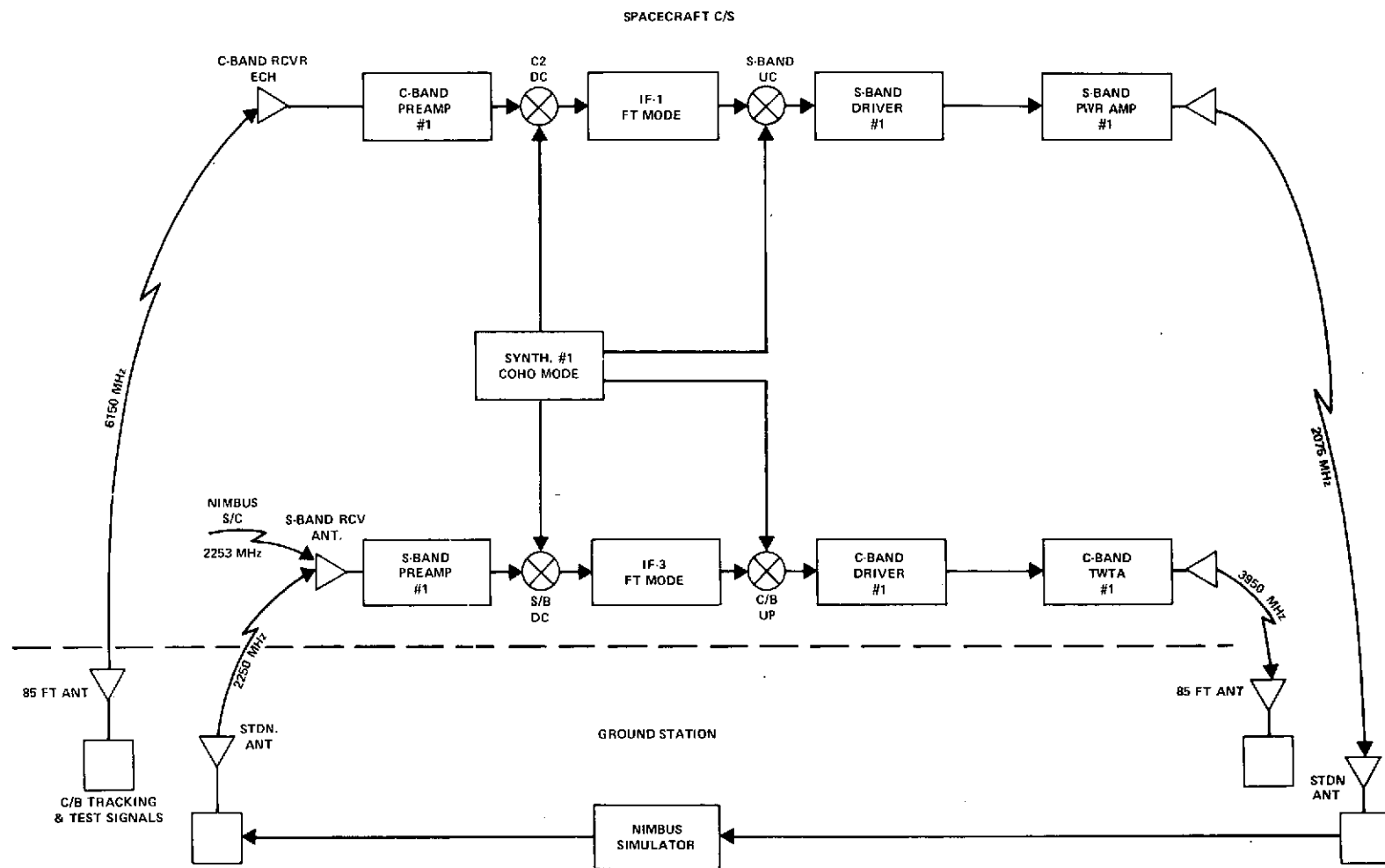
Figure 9-5 Typical TDRE/SSE Experiment Configuration
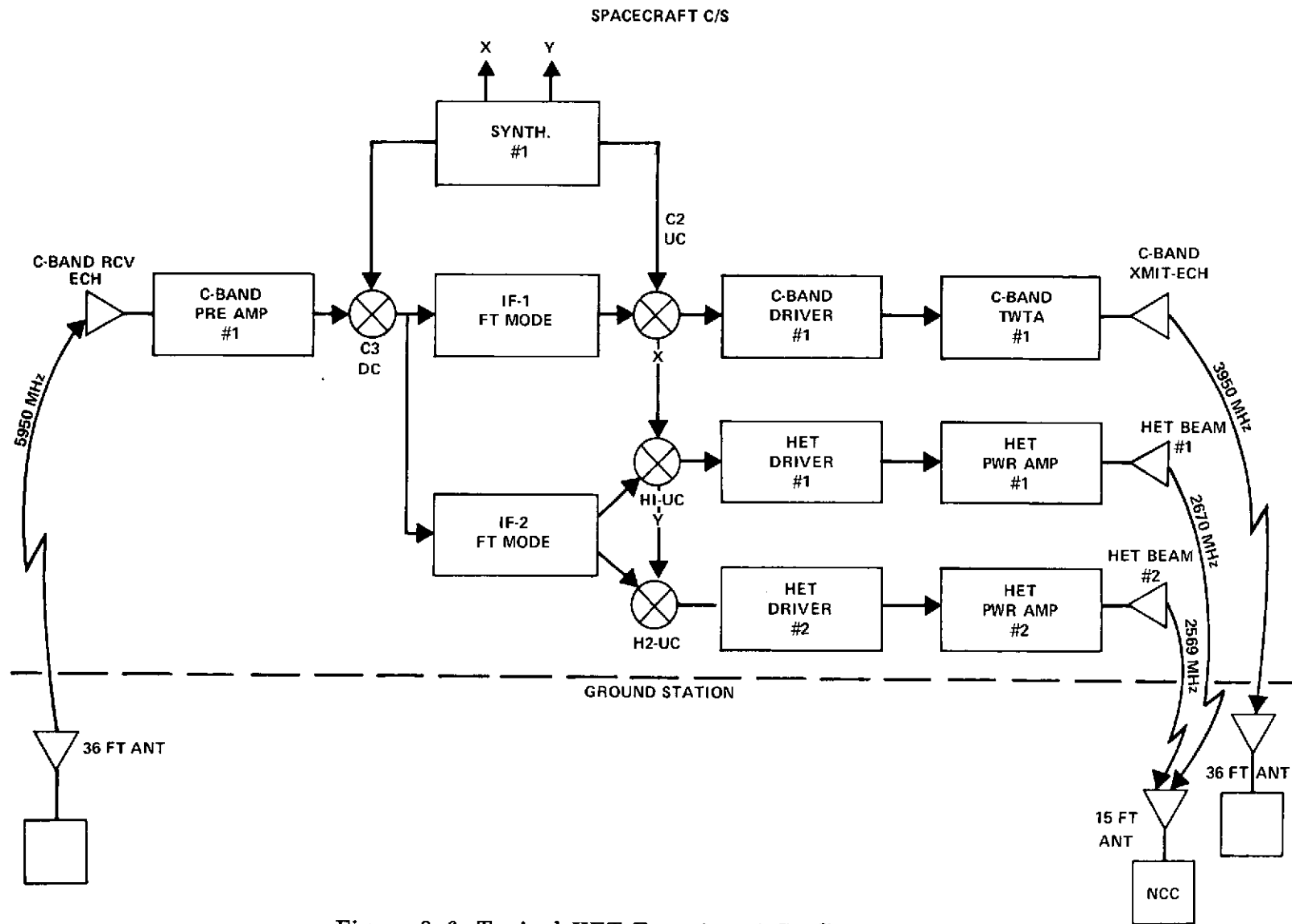
Figure 9-6 Typical HET Experiment Configuration

SPACECRAFT C/S

VHF
DC

VHF RCV ANT

VHF
MONOPULSE
RCVR

IF-2
FT MODE

MONOPULSE
UNIT

ROLL TM

PITCH TM

DACU #2

TLM
XMTR

VHF
153 MHz

SYNTH.
#1

C3
DC

INTERFEROMETER
HSDL

WBDU
#1

C-BAND
DRIVER #1

C-BAND
TWTA #1

C/B
XMIT ECH

ANT

GROUND STATION

85 FT
ANT

STDN ANT

GAC CMDS

SAPPSAC TERMINAL
PDP-11 COMP. COMPLEX
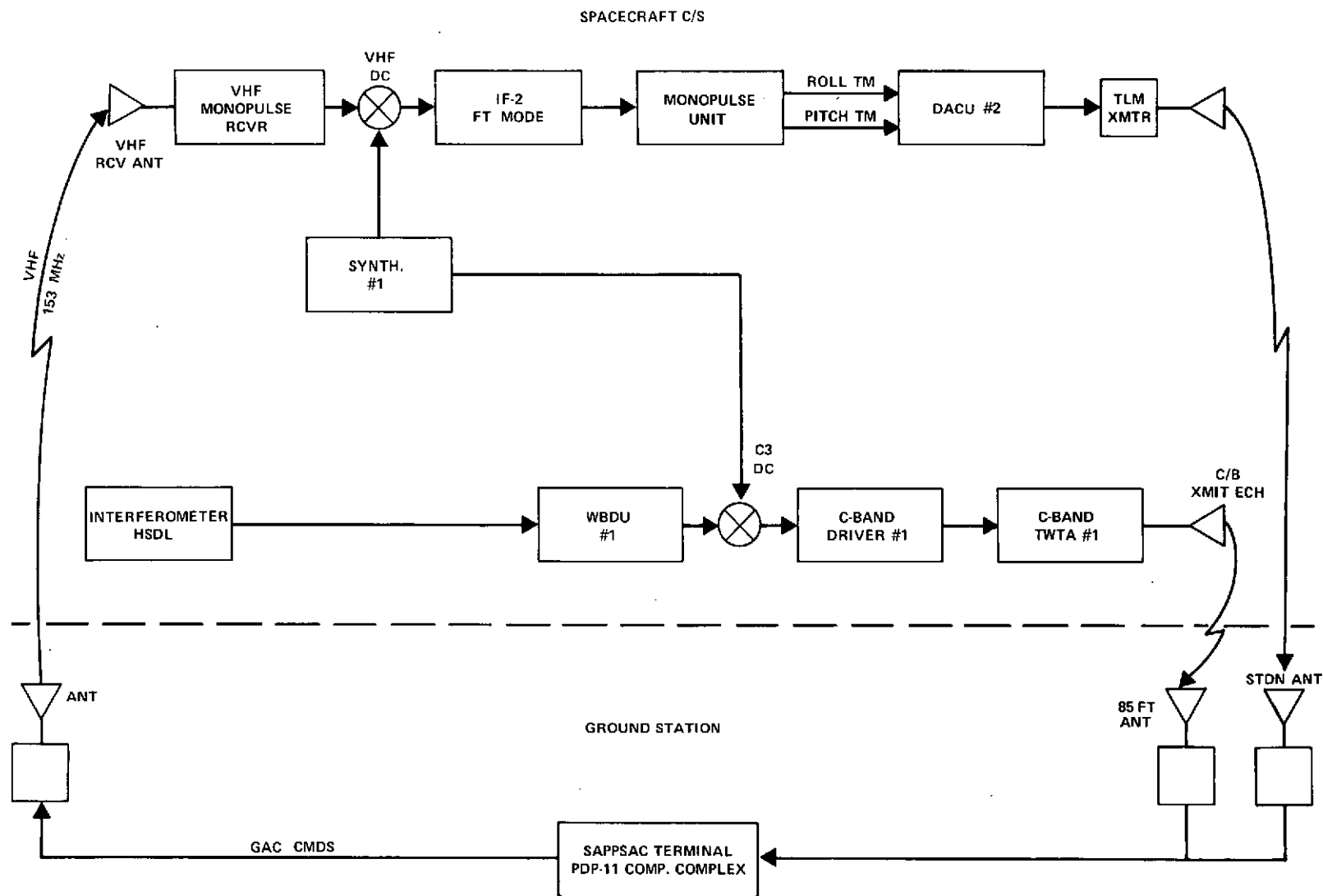
Figure 9-7. Typical SAPPSAC Experiment Configuration

Table 9-1

Experiment Operational Times
(16 July to 31 August)

Experiment	Scheduled Ops. Time	Actual Ops. Time	Remarks
VHRR	151.35 hrs	91.71 hrs	VHRR has problem starting at low temperature
PLACE	34.1	37.4	
TRUST/SITE	4.0	2.75	Incorrect test procedure resulted in one test being aborted.
C-Band RFI	10.0	13.75	RBE interference - RBE OFF when in RFI
TDRE	14.0	16.25	
MMW COMM	2.0	2.75	
GEOS/SSE	9.0	9.5	
SAPPSAC	8.0	9.5	SAPPSAC successfully demonstrated capability to control spacecraft using all possible sensor combinations
HET (VA, ARC, RME, RMW, IHS/ALED)	76.05	82.8	ARC/VA programming very good: RME, RMW, ALASKA/ IHS and GND. STA Checkout- Results good.

9.3.1 G/T and EIRP Performance Summary

Table 9-3 is a tabulated summary of G/T and EIRP parameter. This table is an update of Table 11-1 shown in the ATS-6 In-Orbit Checkout Report. The table shows that the in-orbit performance has met or exceeded requirements.

9.3.2 Antenna Patterns

Measuring in-orbit antenna patterns is a unique process for ATS-6. It is believed that this spacecraft is the first with the maneuverability and software-computer control capability necessary for antenna pattern measurements.

Table 9-2

Communications Subsystem Components
Operational Time Matrix
(16 July to 31 August)

Experiment	C-Band Rcvr	C-Band Mono Rcvr	S-Band Rcvr	S-Band Mono Rcvr	VHF Mono Rcvr	L-Band Rcvr	IF-1 Ass'y	IF-2 Ass'y	IF-3 Ass'y
MMW (COMM)	2.75						2.75	2.75	
Ranging									
VHRR									
TV Camera									
IHSDL									
HET	84.16		5.25				34.05	84.16	5.25
ITV/TRUST	2.75						2.75		
TDRE	16.25		16.25				16.25		16.25
PLACE	37.4					37.4	37.4	37.4	
C/B RFI									
GEOS/SSE	9.5		9.5						9.5
SAPPSAC	9.5				9.5		9.5	9.5	
Monopulse Ant. Patterns									
C-Band ECH Rcvr									
C-Band ECH Xmit									
C-Band PFF Rcvr									
S-Band On-Axis Rcvr									
S-Band On-Axis Xmit									
S-Band N5 Beam Xmit									
HET S1 Xmit									
HET S2 Xmit									
S-Band Cross									

Table 9-2 (Cont'd)

Communications Subsystem Components
Operational Time Matrix
(16 July to 31 August)

Experiment	C-Band Rcvr	C-Band Mono Rcvr	S-Band Rcvr	S-Band Mono Rcvr	VHF Mono Rcvr	L-Band Rcvr	IF-1 Ass'y	IF-2 Ass'y	IF-3 Ass'y
L-Band Fan Xmit									
L-Band Pencil									
UHF Xmit									
Miscellaneous									
Trouble Shoot.									
Total									

Experiment	Synth #1	WBDY #1	C-Band XMTR 1	HET XMTR 1	HET XMTR 2	S-Band XMTR 1	L-Band XMTR 1	UHF XMTR 1	DC/DC CONV 1
MMW (COMM)	2.75		2.75						2.75
Ranging									
VHRR	91.71	91.71	91.71						91.71
TV Camera									
IHSDL									
HET	84.16		34.05	84.16	80.16				84.16
ITV/TRUST	2.75		2.75					2.75	2.75
TDRE	16.25		16.25			16.25			16.25
PLACE	37.4		37.4				37.4		37.4
C-Band RFI			13.75						
GEOS/SSE	9.5		9.5			9.5			9.5
SAPPSAC	9.5	9.5	9.5						9.5
Monopulse									
Ant. Patterns									
C-Band ECH Rcvr									

Table 9-2 (Cont'd)

Communications Subsystem Components
Operational Time Matrix
(16 July to 31 August)

Experiment	Synth #1	WBDY #1	C-Band XMTR 1	HET XMTR 1	HET XMTR 2	S-Band XMTR 1	L-Band XMTR 1	UHF XMTR 1	DC/DC CONV 1
C-Band ECH Xmit									
C-Band PFF Rcvr									
S-Band On-Axis Rcvr									
S-Band On-Axis Xmit									
S-Band N5 Beam Xmit									
HET S1 Xmit									
HET S2 Xmit									
S-Band Cross									
L-Band Fan Xmit									
L-Band Pencil									
UHF Xmit									
Miscellaneous									
Trouble Shoot									
Total									

Table 9-3

Communication Subsystem Performance Comparison

Frequency (MHz)	Antenna	Required G/T (dB°K)		In-Orbit* G/T (db/°K) Approx. Peak
		Peak	FOV	
6350	ECH	-17.0	-20.0	-14.0
6350	PFF	13.5	10.5	16**
2250	On-Axis	9.5	---	10.4
1650	Fan	- 2.0	- 5.0	- 2.6
148/153				TBD
		EIRP (dBw)		(dBw)
3950	ECH	26.0	24.1	25.7
3950	PFF	48.2	43.5	48.3
2670	S-2	52.3	48.9	52.7
2570	S-1	52.3	48.7	52.7
2075	On-Axis	51	---	52.5
1550	Fan	45	42	42.1
860	PFF	51	48	52.6
136/137	PFF			TBD

*Calculated values based on in-orbit measurements.
**Actual measurement made on basis of relative PFF/ECH gain.

The general procedure for measuring antenna patterns requires that the space-craft be slewed over the Rosman ground station so that the RF illumination of the antenna pattern passes over the station. The RF signal strength is then measured both from the ground (receive) and from the spacecraft (transmit). The attitude maneuver planned in advance for the specific antenna pattern is executed from ATSOCC using the DOC in iterated angle slew and offset point modes to achieve the desired pattern contours, or cuts. The actual resultant attitude, specifically the line-of-sight to Rosman in spacecraft body phi-theta (antenna pattern) coordinates, is computed at ATSOCC in three second intervals and relayed to Rosman for input to the RFI Receiver/Analyzer system (PDP-11). The signal power measurements made, using the linear detector in the RFI

receiver/analyzer, are correlated with the attitude data to define the antenna patterns. Computations are required to convert the measured signal powers to antenna patterns, and these are performed, on-line, using the RFI receiver/analyzer. The measurement results are outputed from the RFI receiver/analyzer as a digital data tape which is used for off-line computer determination and analysis of the antenna patterns. The data consists of all of the identified power measurements, attitude, time of year, and selected telemetry parameters.

Obtaining the in-orbit antenna patterns required unique C/S configurations for the multifrequency transmit and receive antennas. Figures 9-8 through 9-12 show the general spacecraft configurations and ground station interfaces for obtaining the various patterns. Table 9-4 summarizes the status of the antenna patterns along with the outstanding measurements needed to satisfy the in-orbit checkout of the C/S performance. This table is an updated version of Table 11-4 shown in ATS-6 In-Orbit Checkout Report.

A comparative tabulation of the pertinent antenna parameters is shown in Tables 9-5 and 9-6. The in-orbit data was taken from the antenna patterns shown in Figures 9-13 through 9-41. No significant differences exist between in-orbit data and hard dish data taken at Philco-Ford.

9.3.3 Monopulse Tracking

Checkout of the three monopulse receivers (VHF, S-band and C-band) as open-loop and closed-loop pitch and roll sensors, was accomplished during the initial in-orbit checkout. Results of this monopulse tracking along with monopulse error curves for the three frequency bands is included in ATS-6 In-Orbit Checkout Report and will not be repeated in this report. However, monopulse testing conclusions and recommendations are repeated for continuity in reporting future monopulse test activities.

a. Monopulse Conclusions

C- and S-bands monopulse sensors worked very well. Actual error curves obtained during checkout compared favorably with theoretical error curves and the error slopes are quite acceptable as determined by their successful closed-loop operation with the Attitude Control Subsystem. The VHF error curves were somewhat disappointing in that their slopes were much lower than anticipated and never reached their saturated error voltages. The cause of this problem is reported in Section 9.5.2.
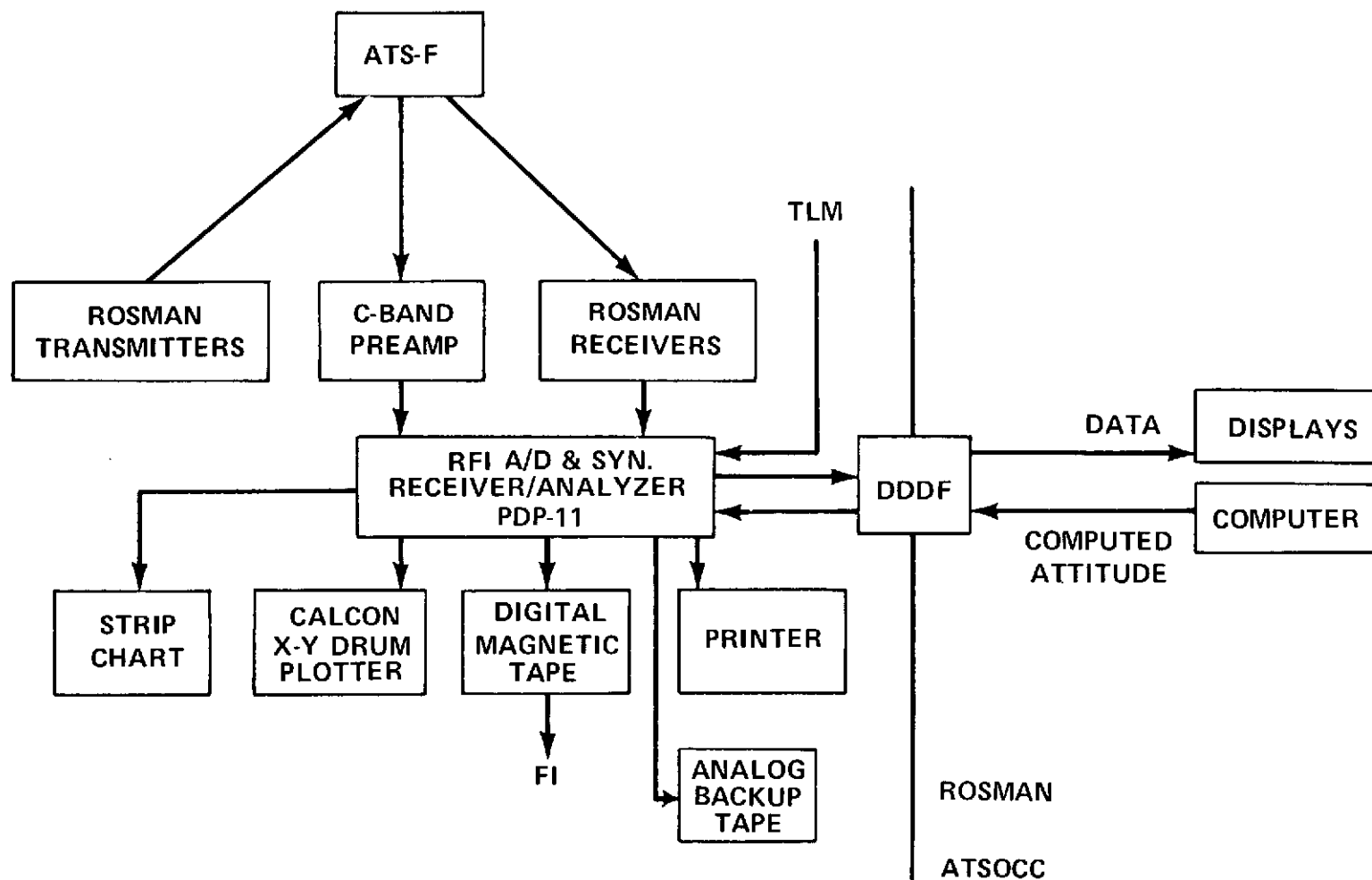
Figure 9-8. Ground Station Equipment Required for Antenna Pattern Measurement
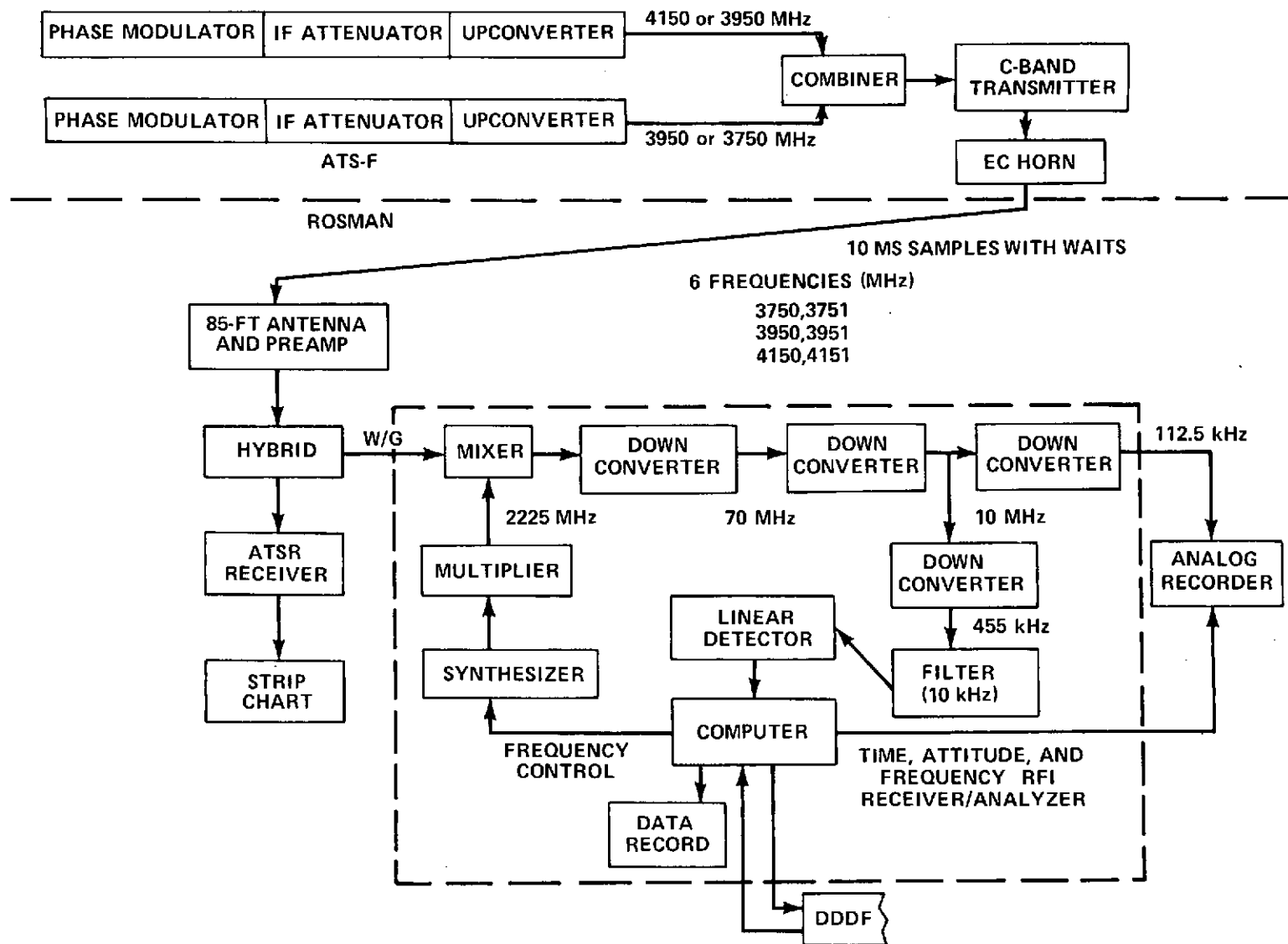
Figure 9-9. Equipment Configuration for Spacecraft C-band Transmit Antenna Pattern Measurements
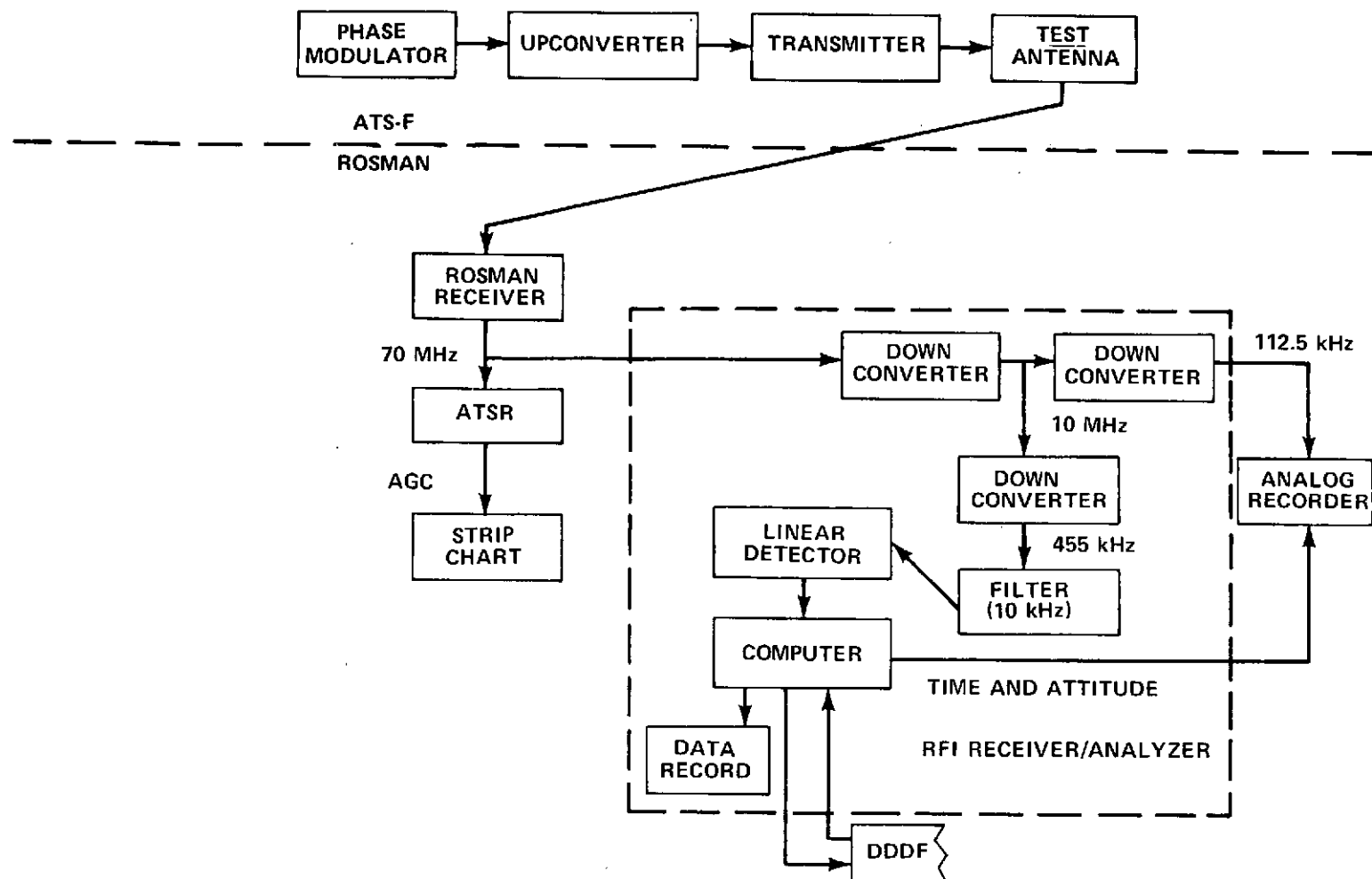
Figure 9-10. Equipment Configuration for Spacecraft Transmit
Antenna Pattern Measurements (UHF, S-band, and L-band)
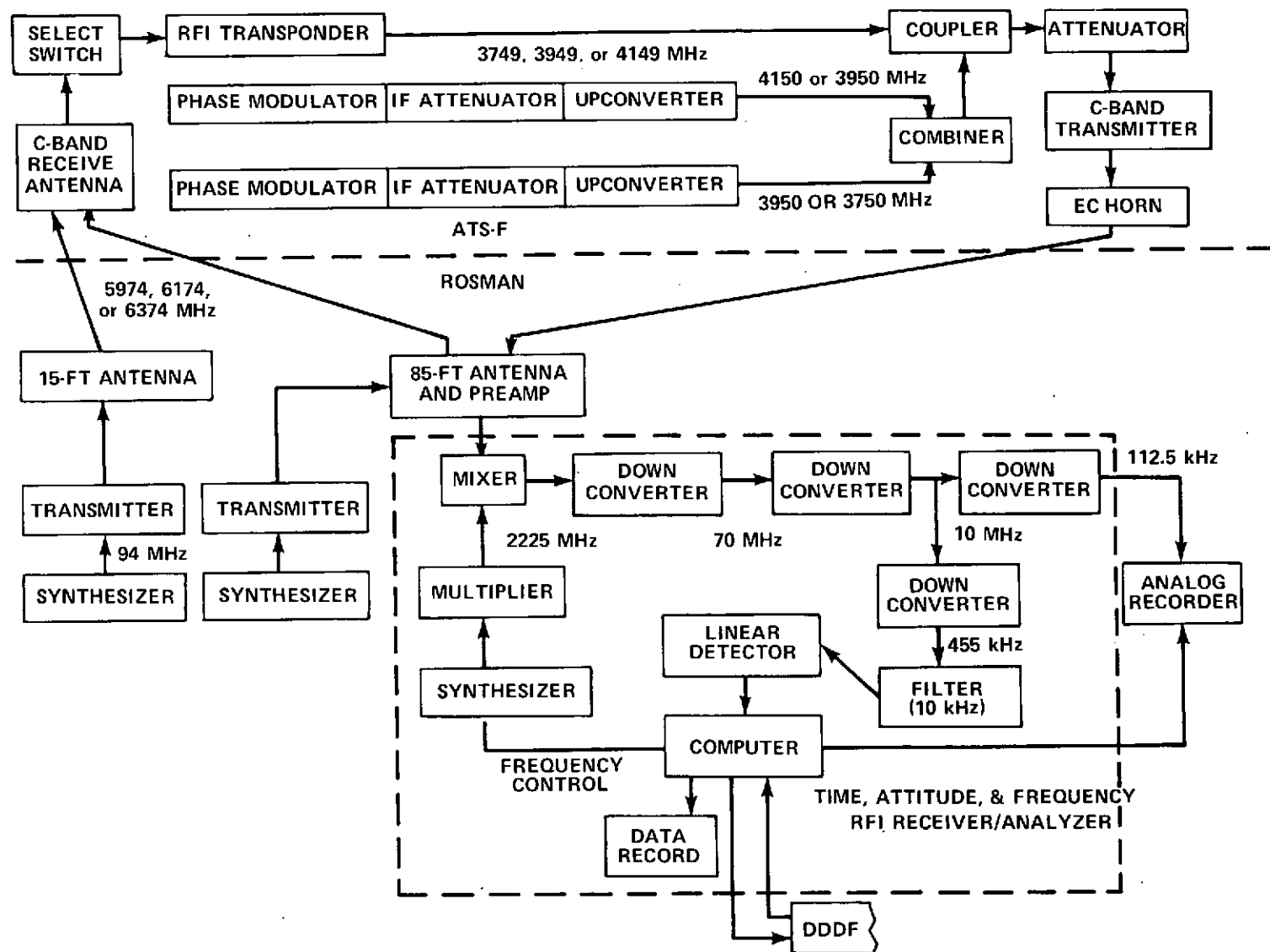
Figure 9-11. Equipment Configuration for C-band Receive Antenna Pattern Measurement
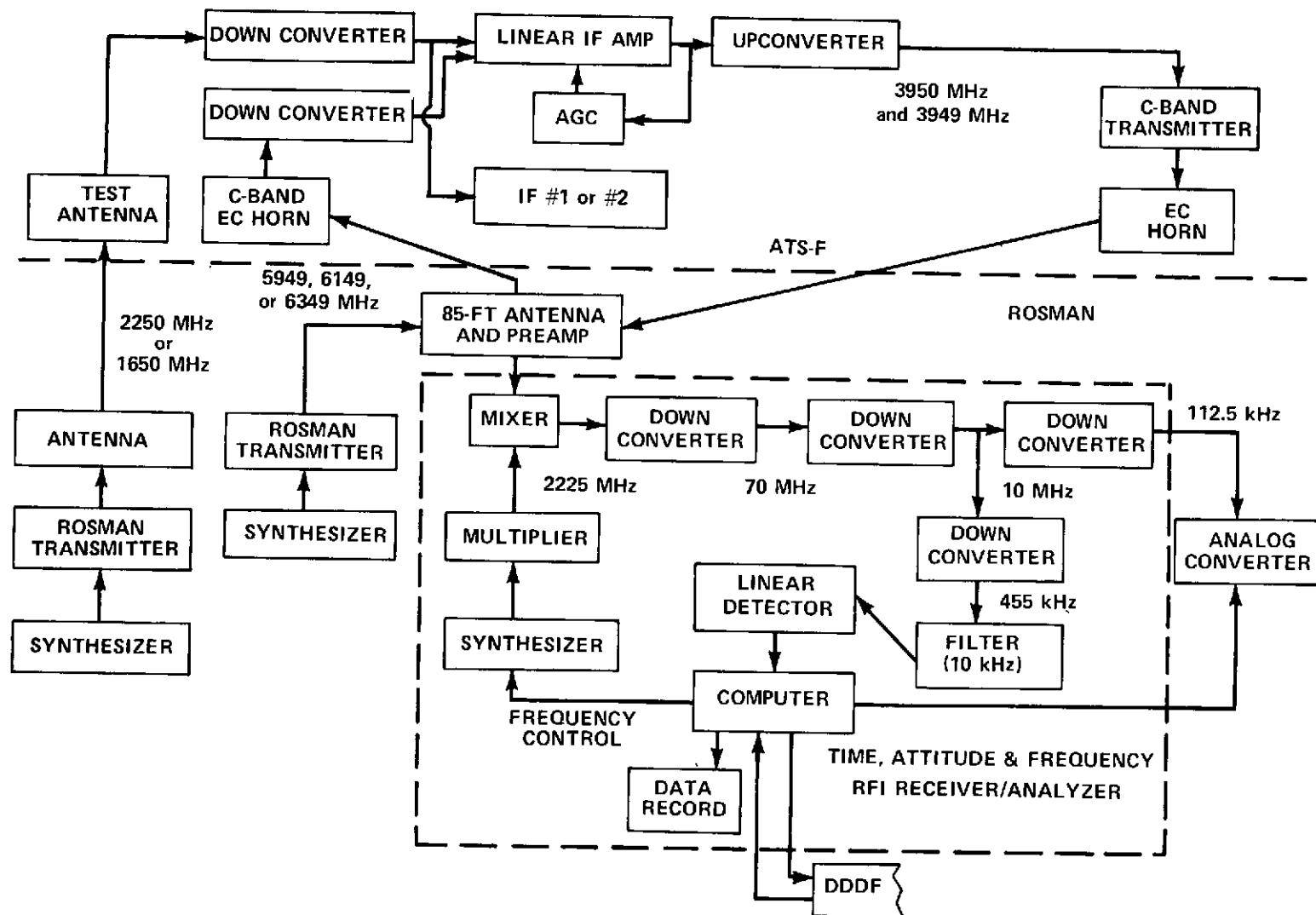
Figure 9-12. Equipment Configuration for Spacecraft Receive Antenna
Pattern Measurement (S-band, L-band & VHF)

Table 9–4

ATS–6 Antenna Pattern Summary Data

Pattern	West-to-East SL	HPBW	SL	NE-to-SW SL	HPBW	SL	South-to-North SL	HPBW	SL	NW-to-SE SL	HPBW	SL
S-Band, Xmit, On-Axis Run 6, 6/15/74	15.7 (13.4)	.93 .98	12.6 13.8	12.9	1.01	18.1	17.3 (14.9	.98 .97	13.3 15.4)	13.8	1.07	17.0
S-Band Cross 6/15/74 to 6/16/74				See Figures 11-25 through 11-28								
S-Band, Xmit N-S SCAN Run 7, 6/15/74	8.1	—	9.0	7.5	—	9.2	20.5	1.1 (.97)	6.6	6.5	—	20.1
HET Xmit, S-1 Element Run 9, 6/16/74	19.4	.64	20.5	12.7	—	16.7	19.0	*	12.2	7.9	—	16.2
S-2, Element Run 10 6/16/74	17.5	—	29.2	9.8	—	25.0	19.0	*	14.4	—	—	22.1
L-Band Xmit, Pencil Run 11, 6/16/74	11.6 (13.0	— 1.3	14.1 16.7)	11.5	—	30.7	18.8 (19.0	1.3 1.3	10.4 11.8)	11.5	—	22.4
L-Band Xmit, Fan Run 12, 6/16/74	1.4 dB DIP (4.0 dB DIP)						11.6 (11.1	1.0 1.0	2.8 3.4)			
UHF, Part 1, Run 4 Part 2, Run 5	22.5 (24.2	3.03 2.8	19.2 25.8)	(15.4	2.82 2.7	15.4 15.2)	21.7 (19.6	2.73 2.7	18.0 27.4)	14.4 (17.2	2.87 2.8	15.4 14.7)

LEGEND: Half power beam width (HPBW) in degrees side lobe gain (SL) in dB
*HPBW not available from in-orbit data. For comparison, acceptance test data (hard dish) shown in parenthesis.

Table 9-5

Communication Subsystem
In-Orbit Performance Compliance
(Receive Operations)

Receive Frequency (MHz)	30-Foot Antenna Near Peak Gain* (dB)	Field-of-View (FOV) (Deg)	Required Peak G/T (dB/°K)	In-Orbit Near Peak G/T* (dB/°K)
6350	48.4	0.4	13.5	16
6350	18.4 (ECH)	20	-17	-14
2250	40.6	1.0	9.5	10.4
1650	28.5	7.5 × 1.0	- 5.0 (FOV)	- 2.6 (FOV)

*Calculated values based on in-orbit measurements and given ground station characteristics

Table 9-6

Communication Subsystem
In-Orbit Performance Compliance
(Transmit Operations)

Transmit Frequency (MHz)	30-Foot Antenna Near Peak Gain* (dB)	Field-of-View (FOV) (Deg)	Required Peak EIRP (dBw)	In-Orbit Near Peak EIRP (dBw)
3950	40.1	0.6	48.2	48.7
3950	17.1 (ECH)	20 × 13	25.4	25.7
2075	40.0	1.0	51	52.5
2570	40.7	0.85	52.3	52.7
1550	26.8	7.5 × 1.0	42 (FOV)	42.1 (FOV)
860	33.3	2.8	51	52.6

*Calculated values based on in-orbit measurements and given ground station characteristics
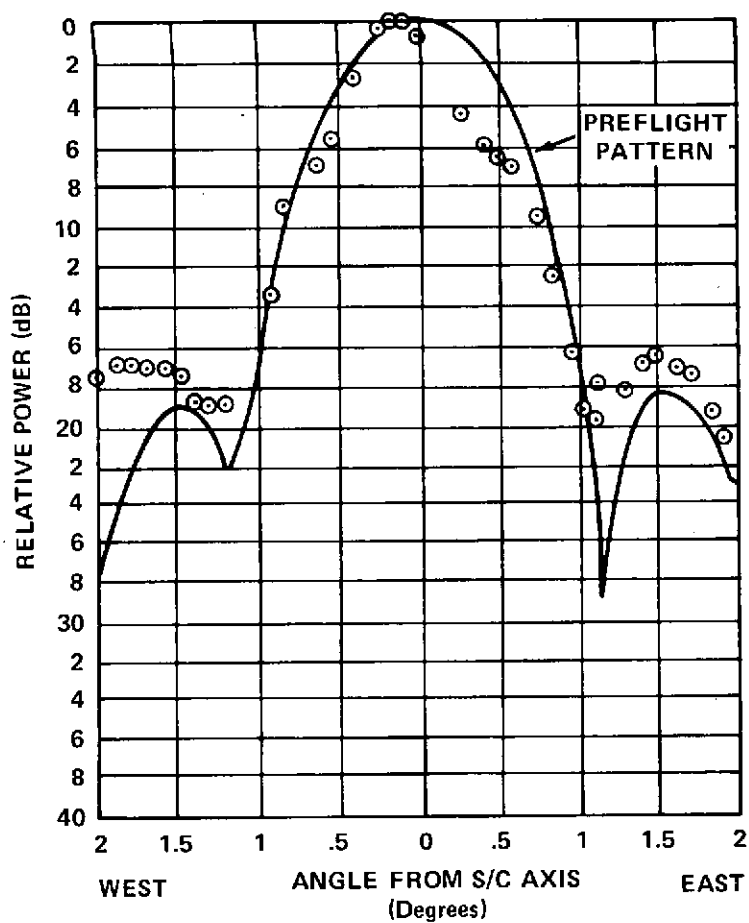
Figure 9-13. Antenna Pattern, S-Band Receive,
(On-Axis, West-East Cut)
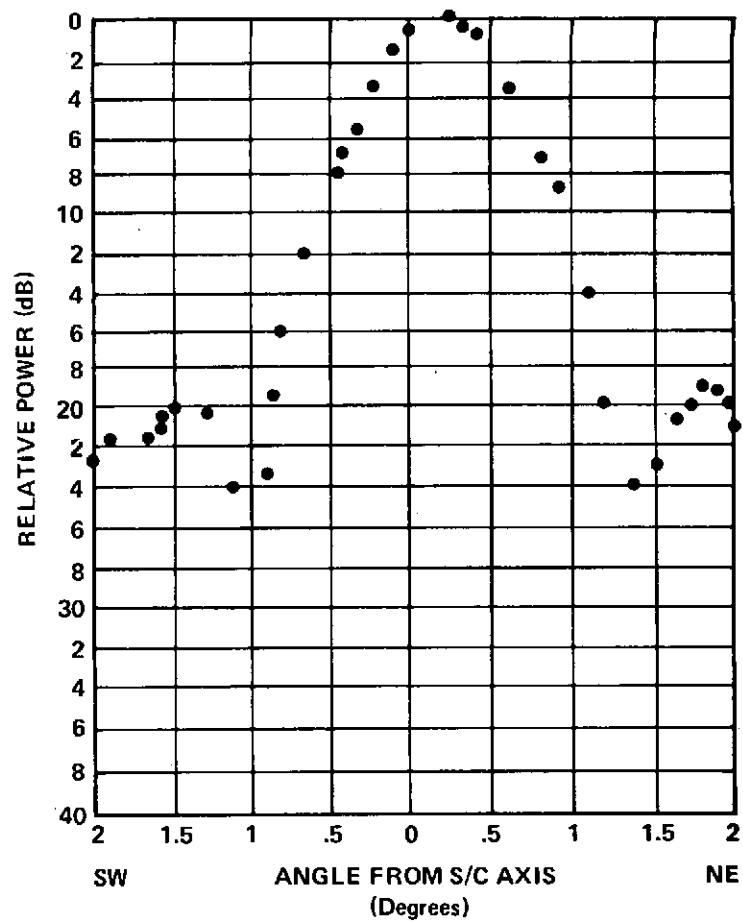
Figure 9-14. Antenna Pattern, S-Band Receive,
(On-Axis, Southwest-Northeast Cut)
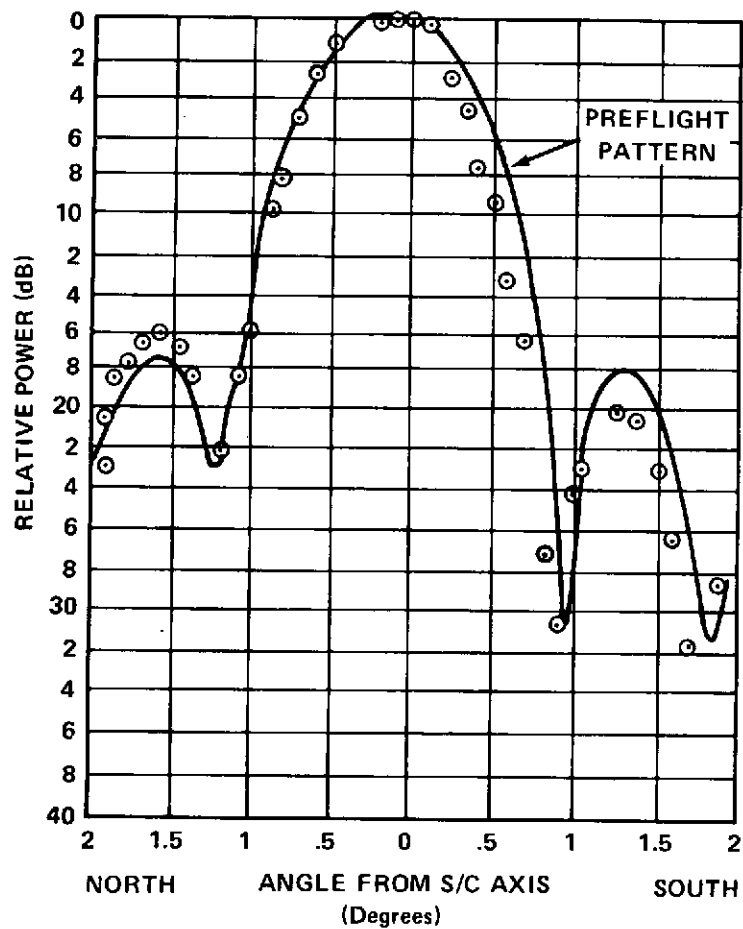
Figure 9-15. Antenna Pattern, S-Band Receive
(On-Axis, North-South Cut)
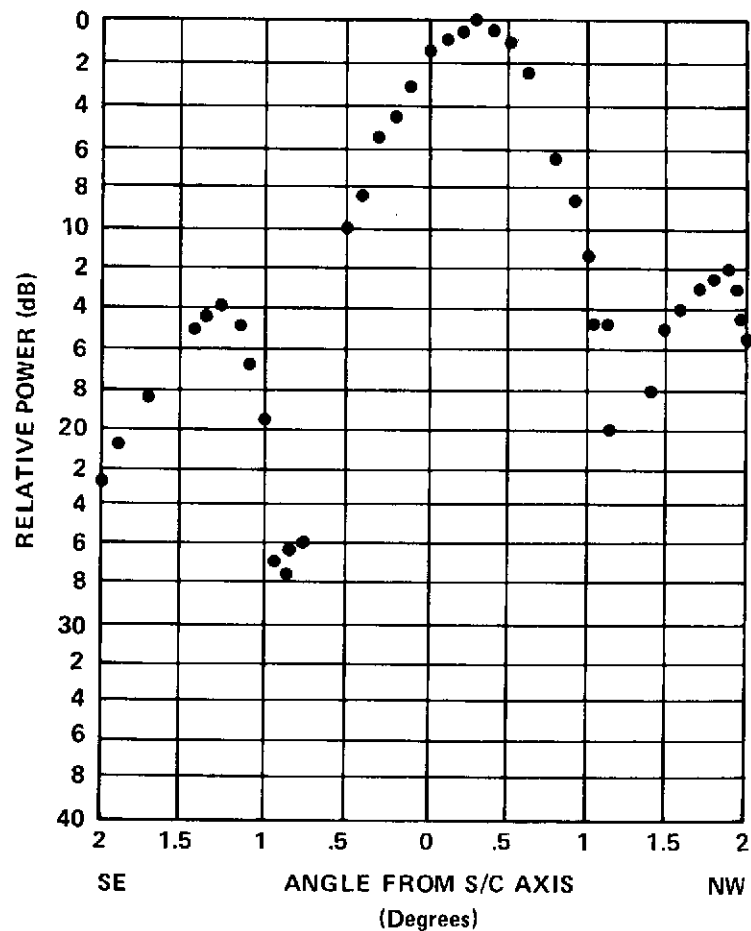
Figure 9-16. Antenna Pattern, S-Band Receive
(On-Axis, Northwest-Southeast Cut)
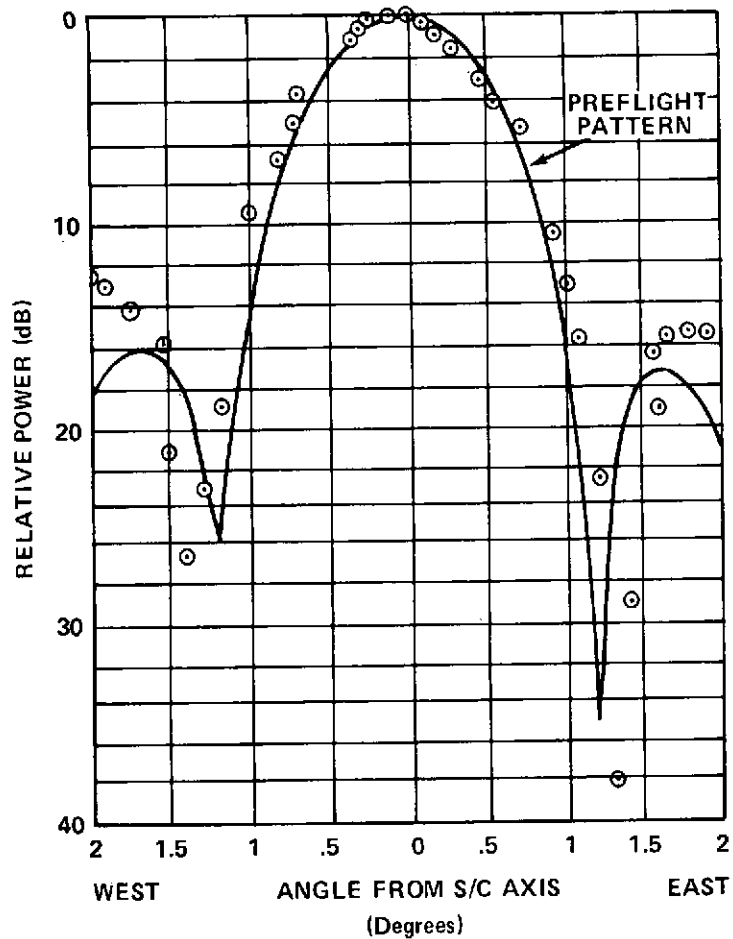
Figure 9-17. Antenna Pattern, S-Band Transmit (On-Axis, East-West Cut)

Figure 9-18. Antenna Pattern, S-Band Transmit (On-Axis, SW-NE Scan)
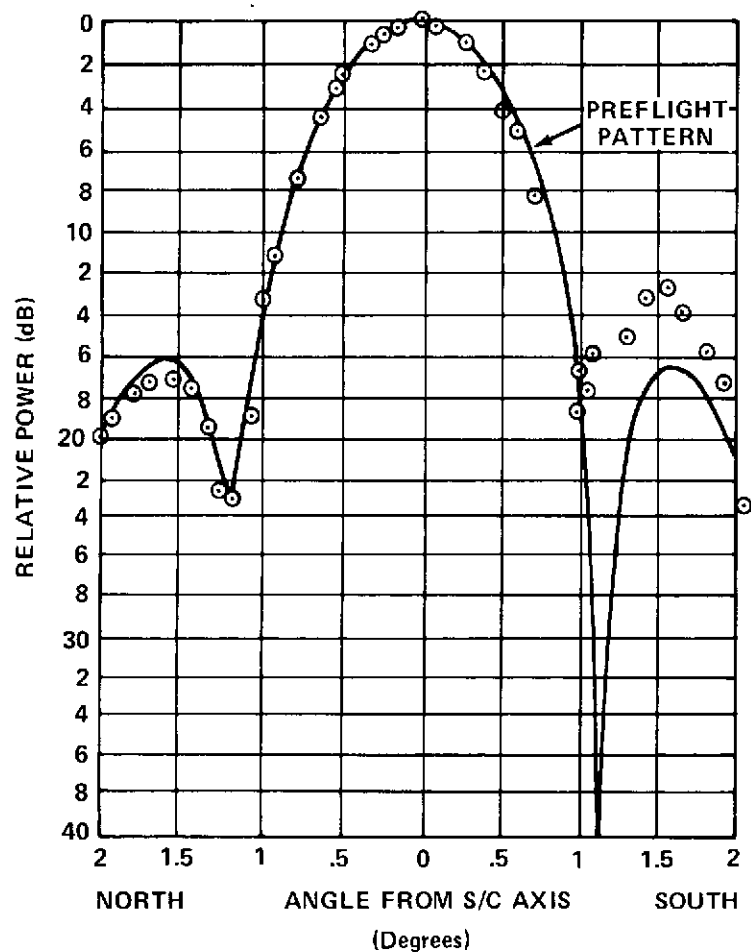
Figure 9-19. Antenna Pattern, S-Band Transmit
(On-Axis, North, South Cut)
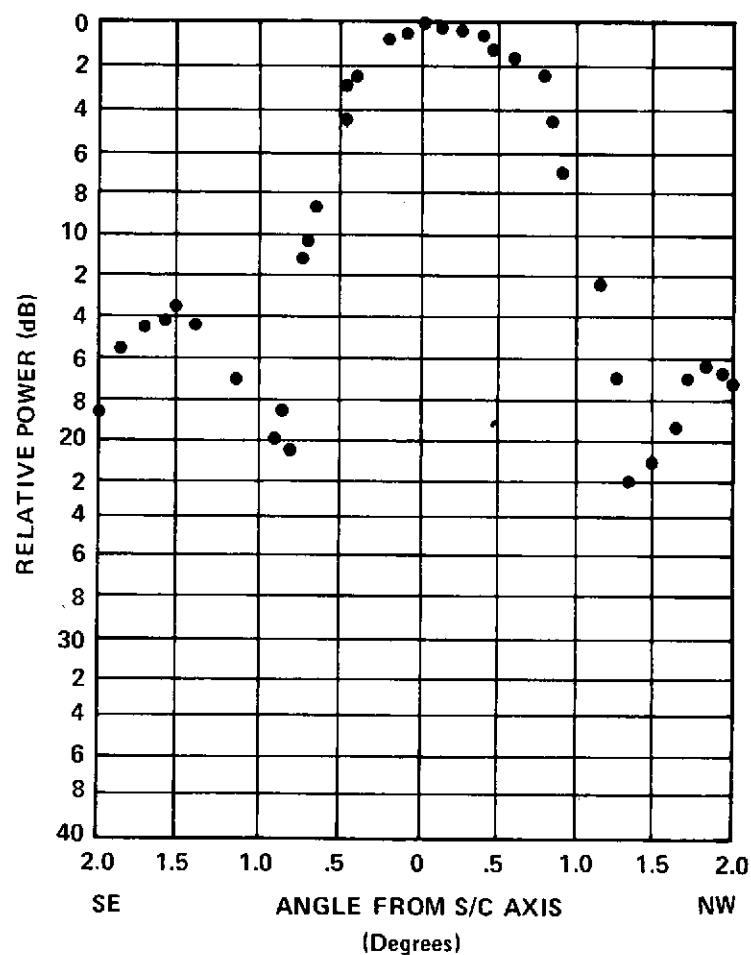
Figure 9-20. Antenna Pattern, S-Band Transmit
(On-Axis, Southeast-Northwest Cut)
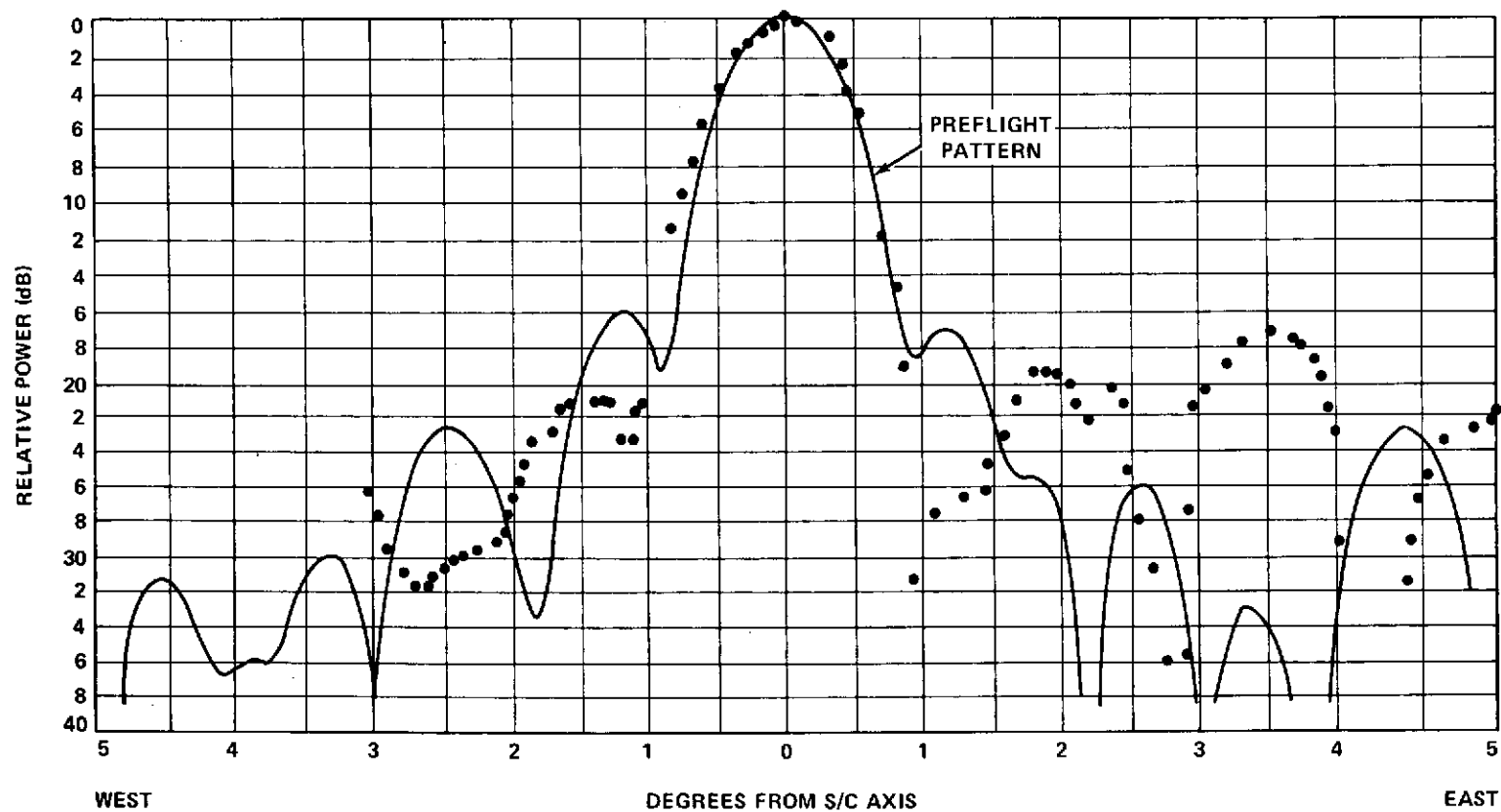
Figure 9-21. Antenna Pattern, HET S1 Transmit
(East-West Cut)
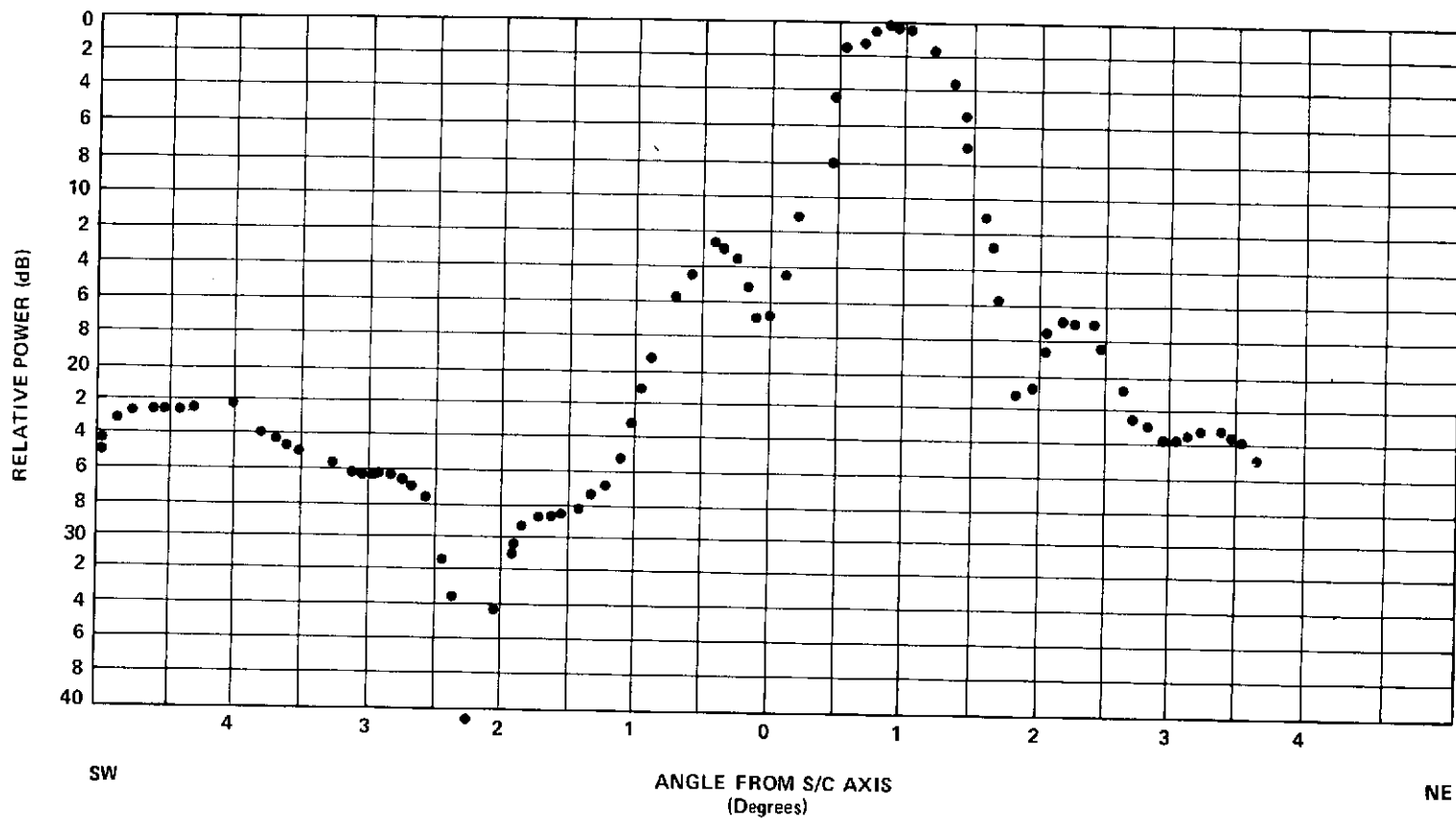
Figure 9-22. Antenna Pattern, HET S1 Transmit
(Southwest-Northeast Cut)
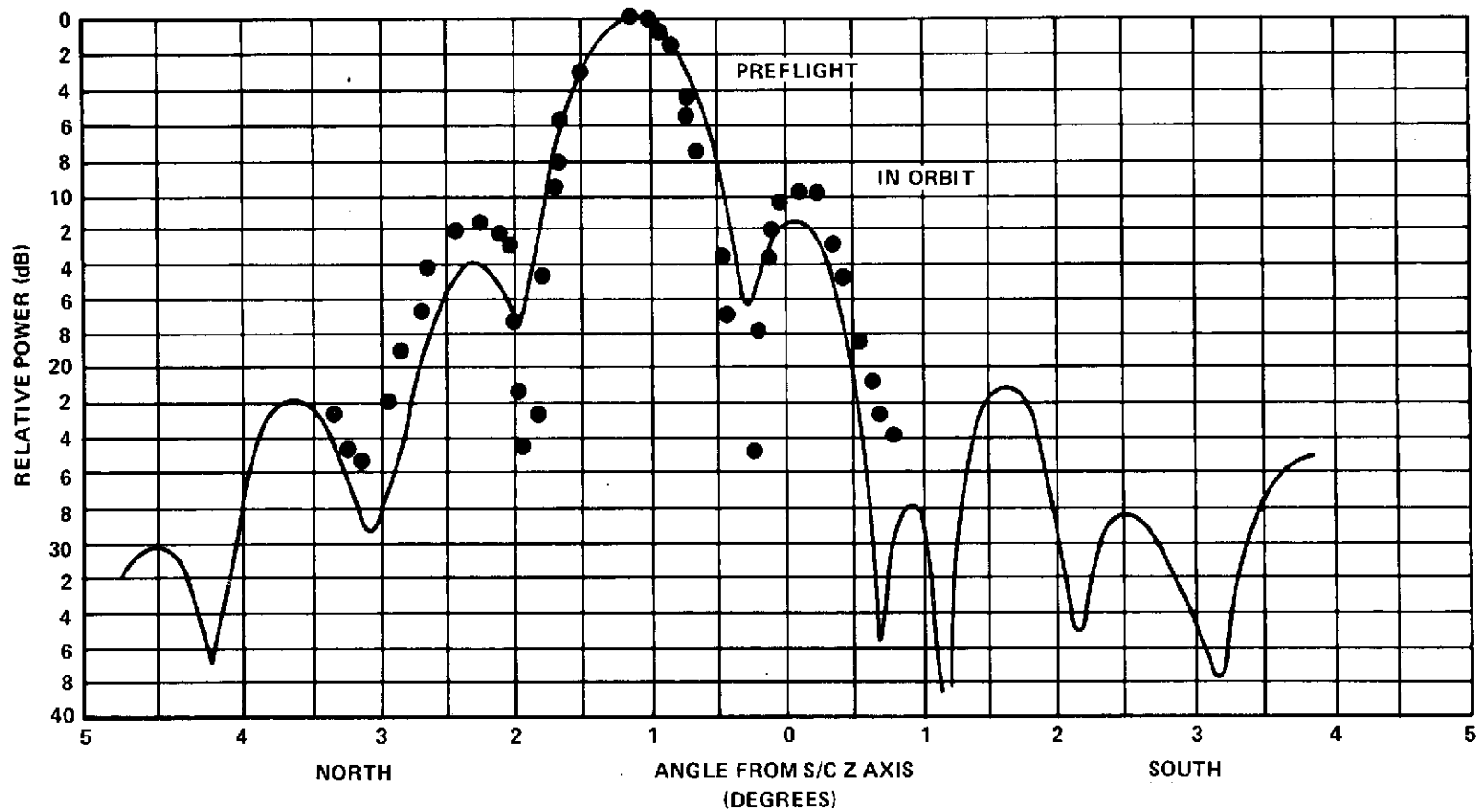
Figure 9-23. Antenna Pattern, HET S1 Transmit (North-South Cut)
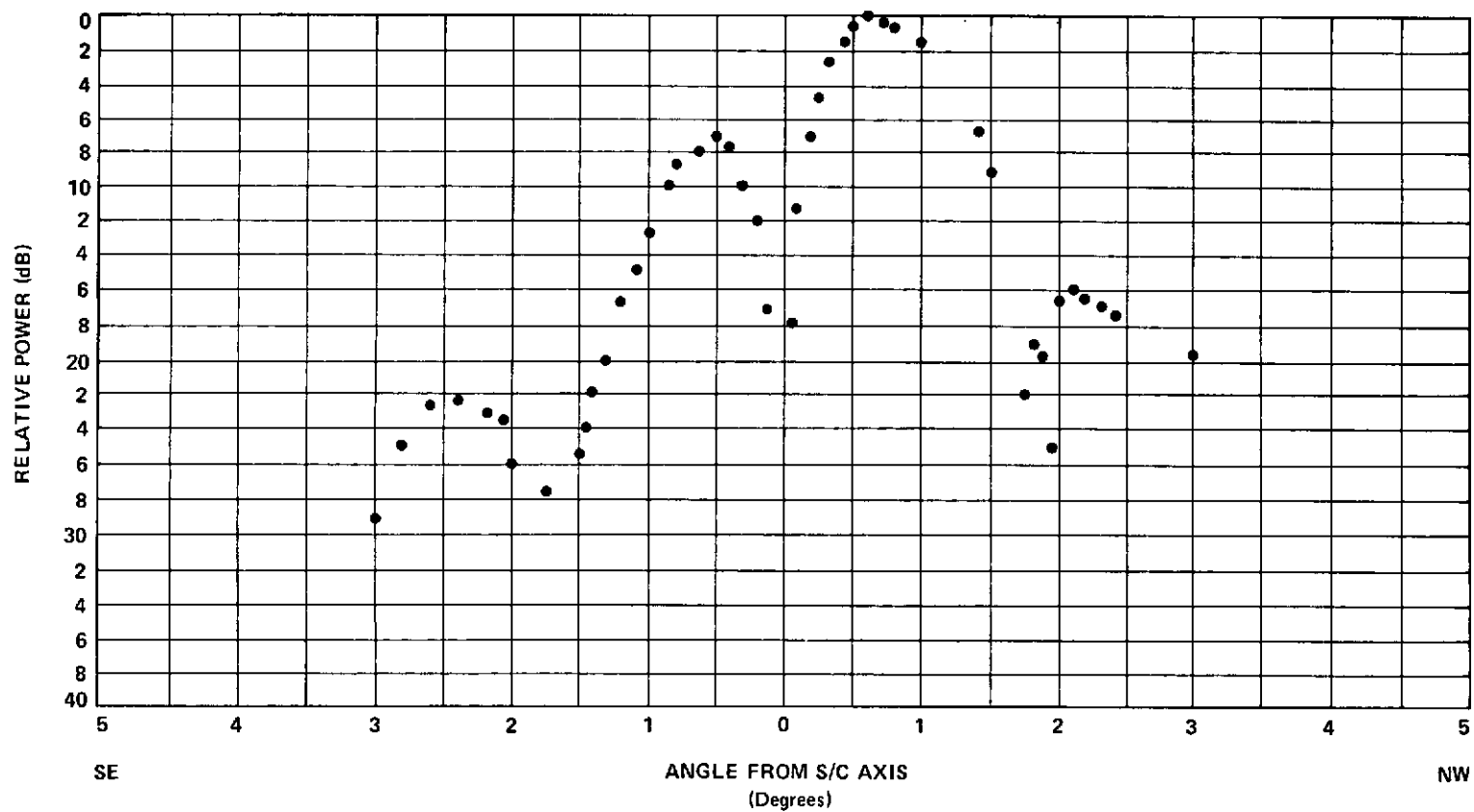
Figure 9-24. Antenna Pattern, HET S1 Transmit
(Southeast-Northwest Cut)
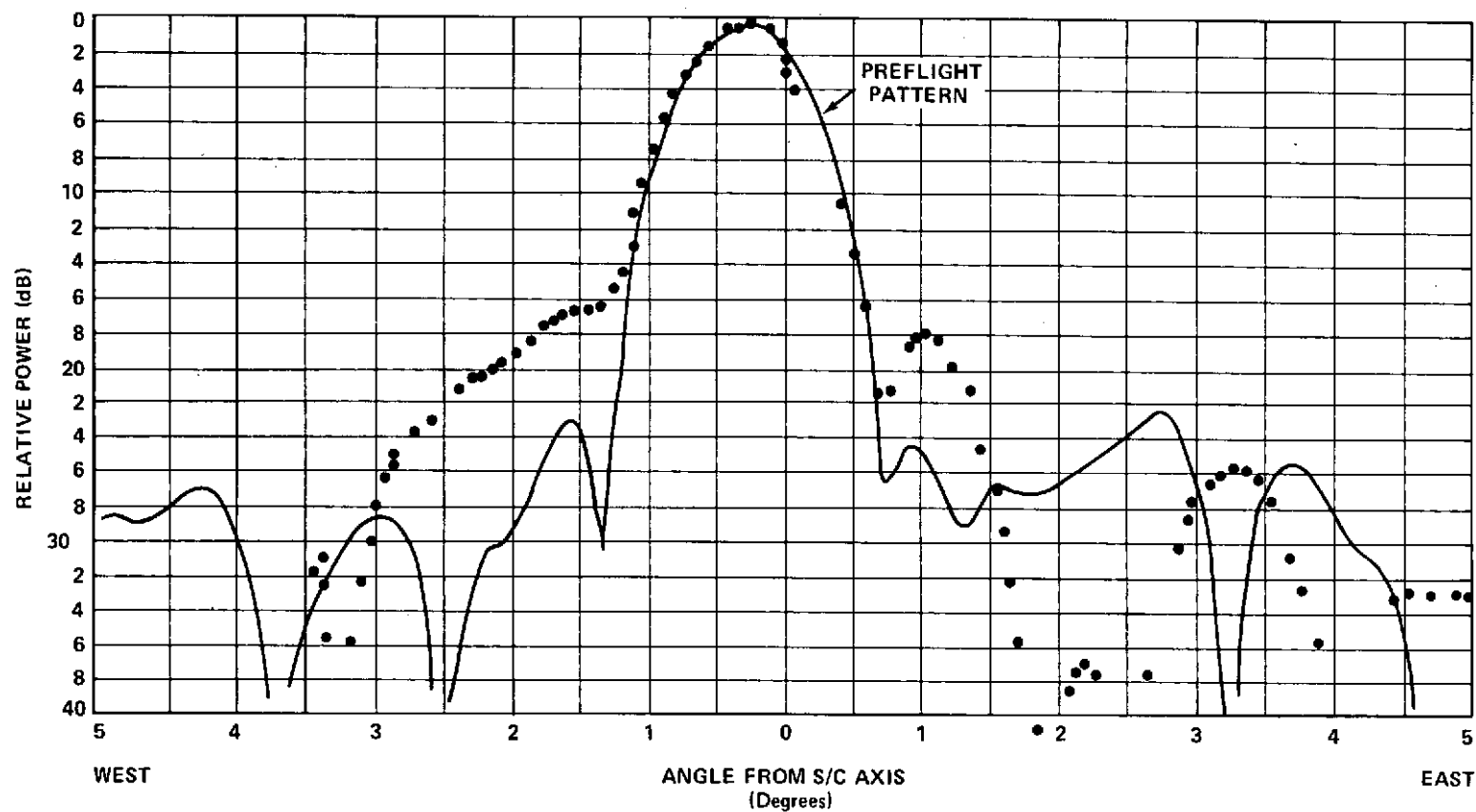
Figure 9-25. Antenna Pattern, HET S2 Transmit
(East-West Cut)
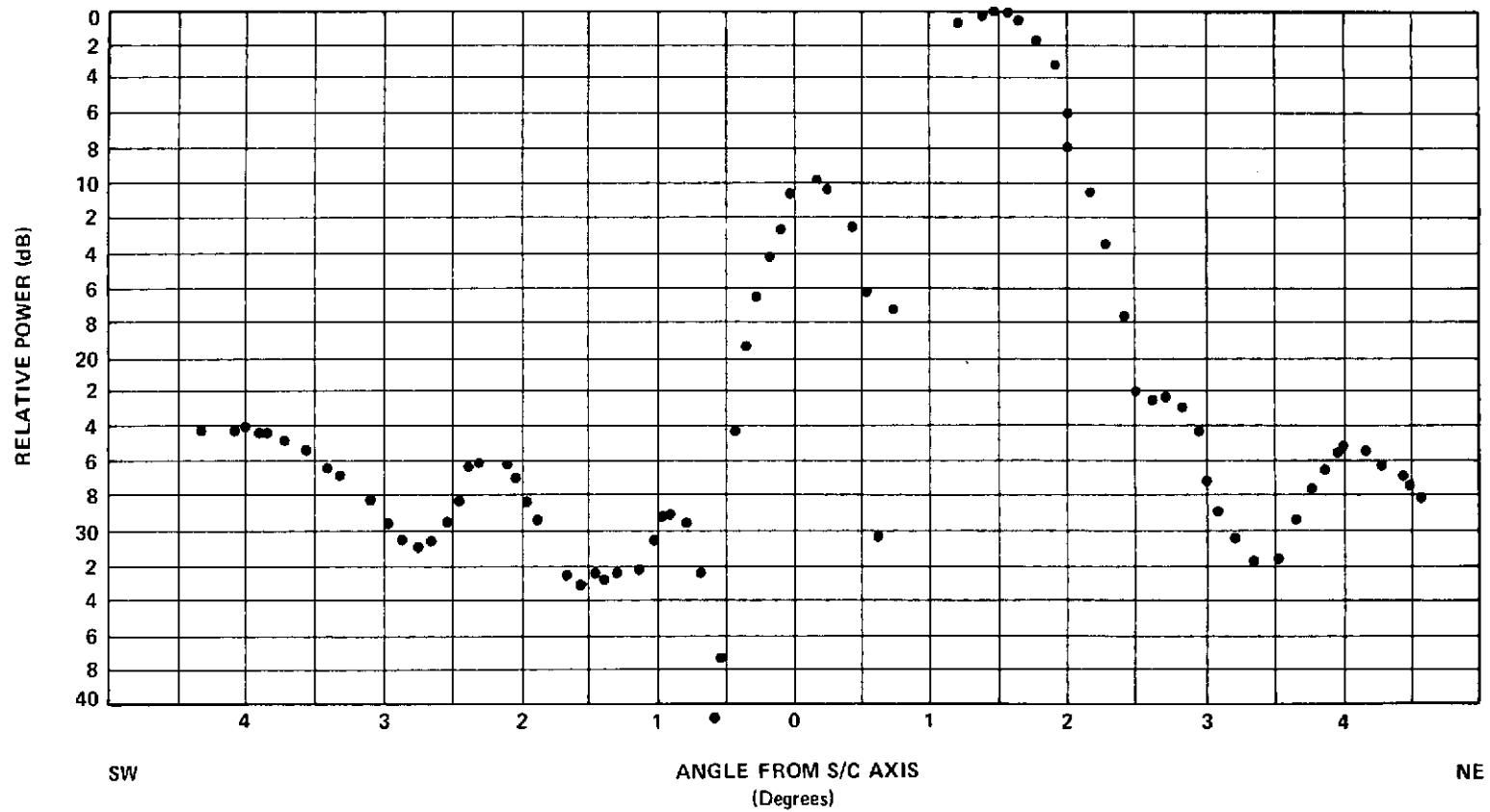
Figure 9-26. Antenna Pattern, HET S2 Transmit
(Southwest-Northeast Cut)
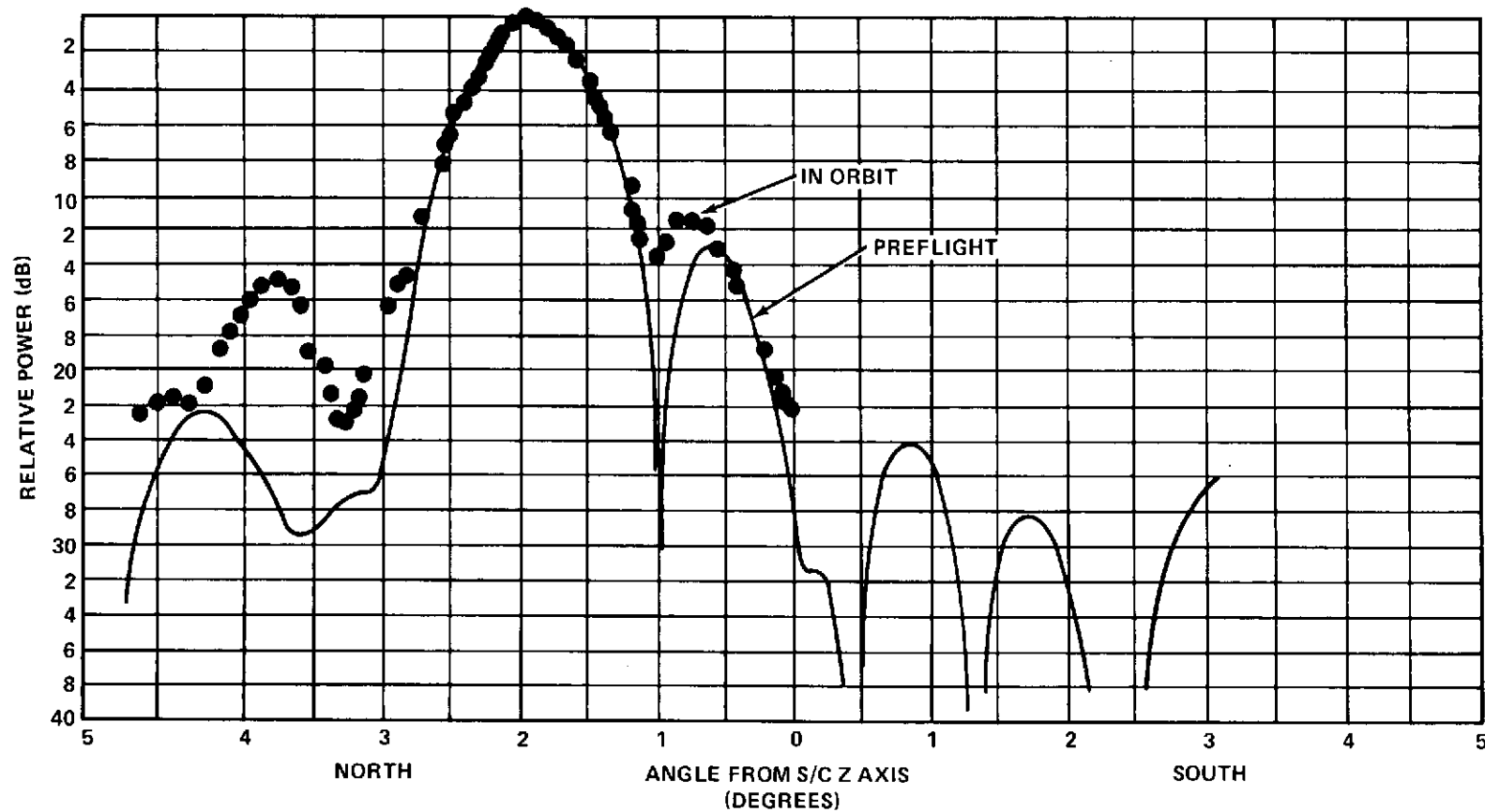
Figure 9-27. Antenna Pattern, HET S2 Transmit (North-South Cut)
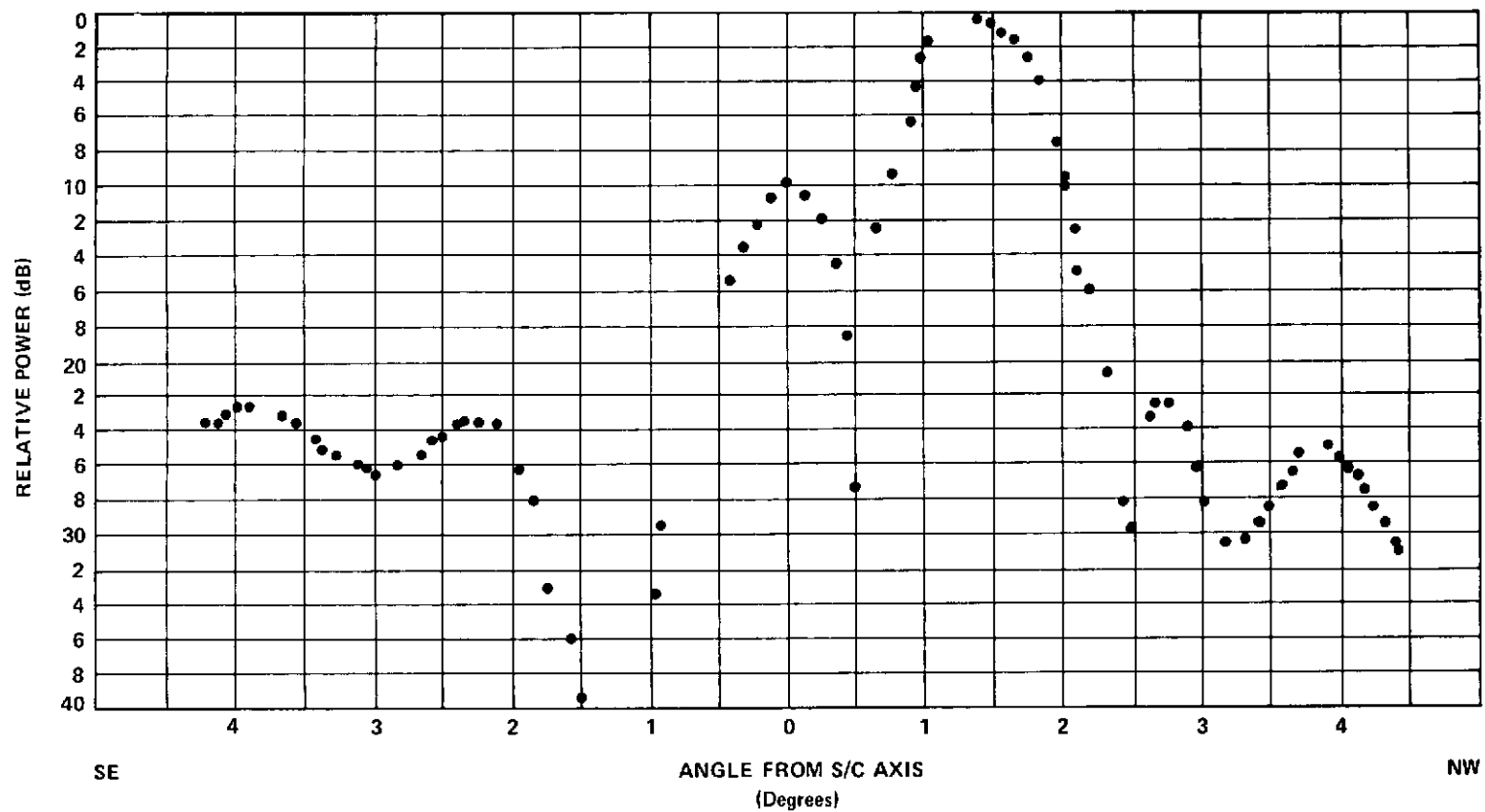
Figure 9-28. Antenna Pattern, HET S2 Transmit
(Southeast-Northwest Cut)
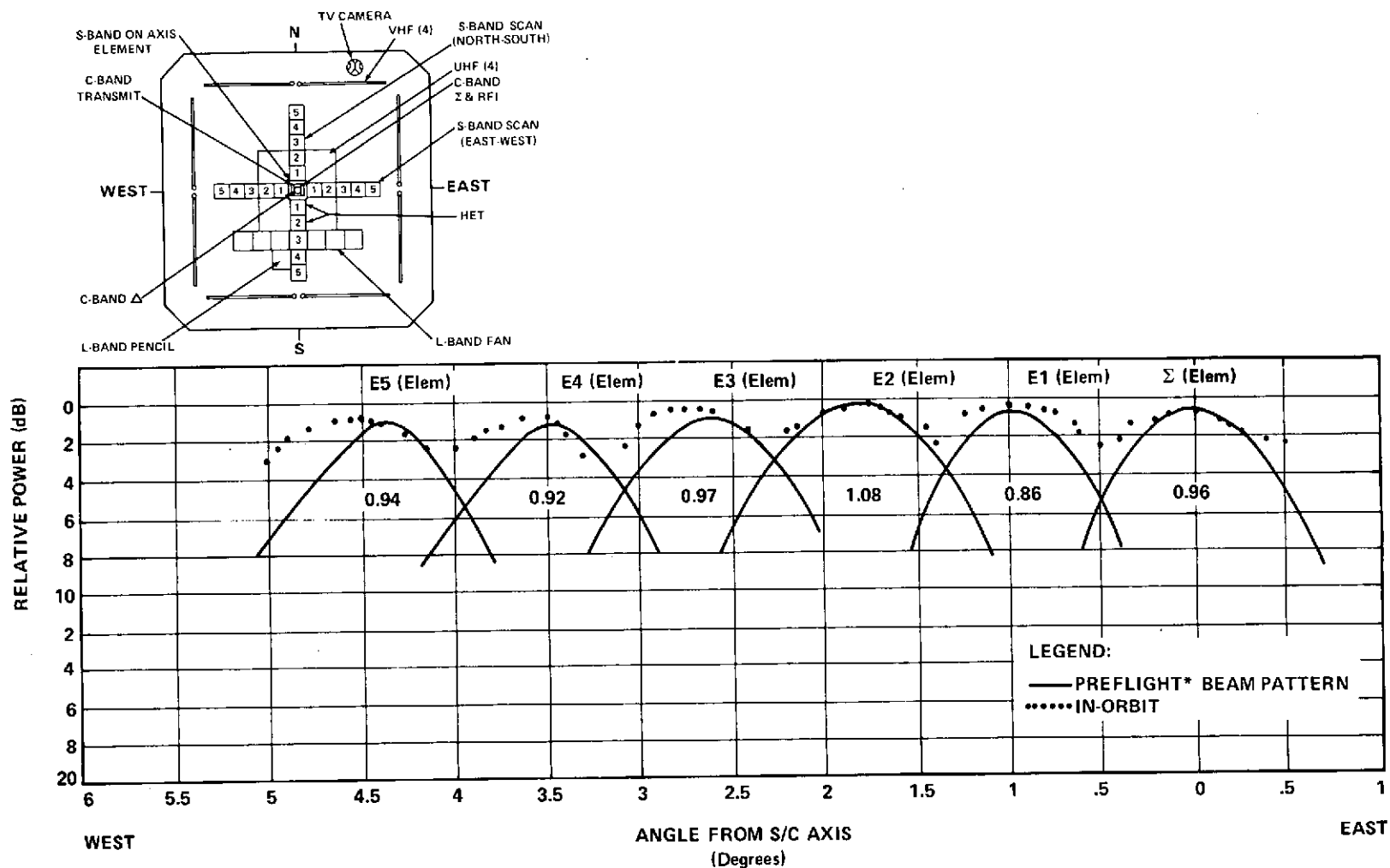
Figure 9-29. Antenna Pattern, S-Band Scan Cross Axis
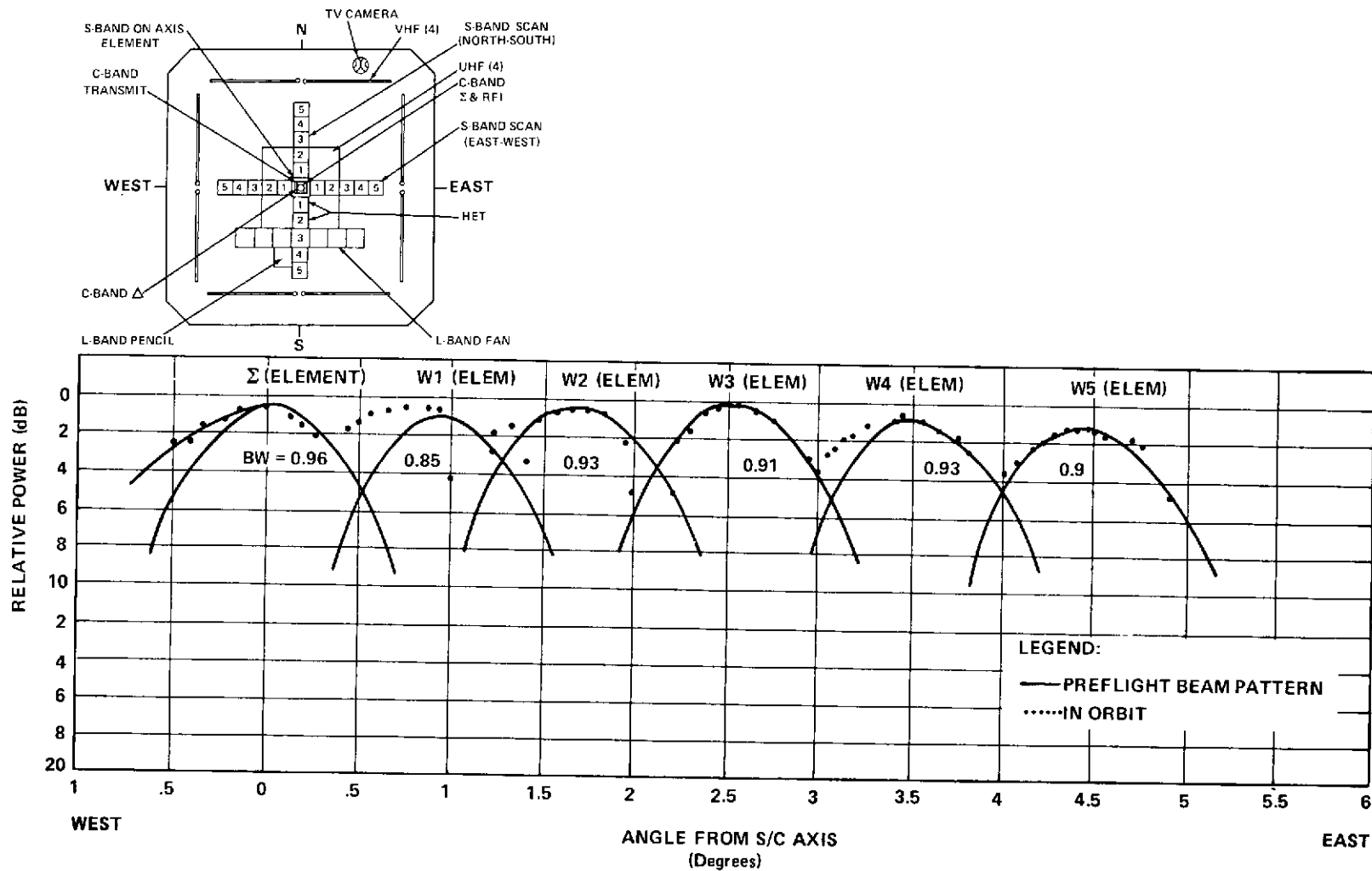
Figure 9-30. Antenna Pattern, S-Band Scan Cross Axis
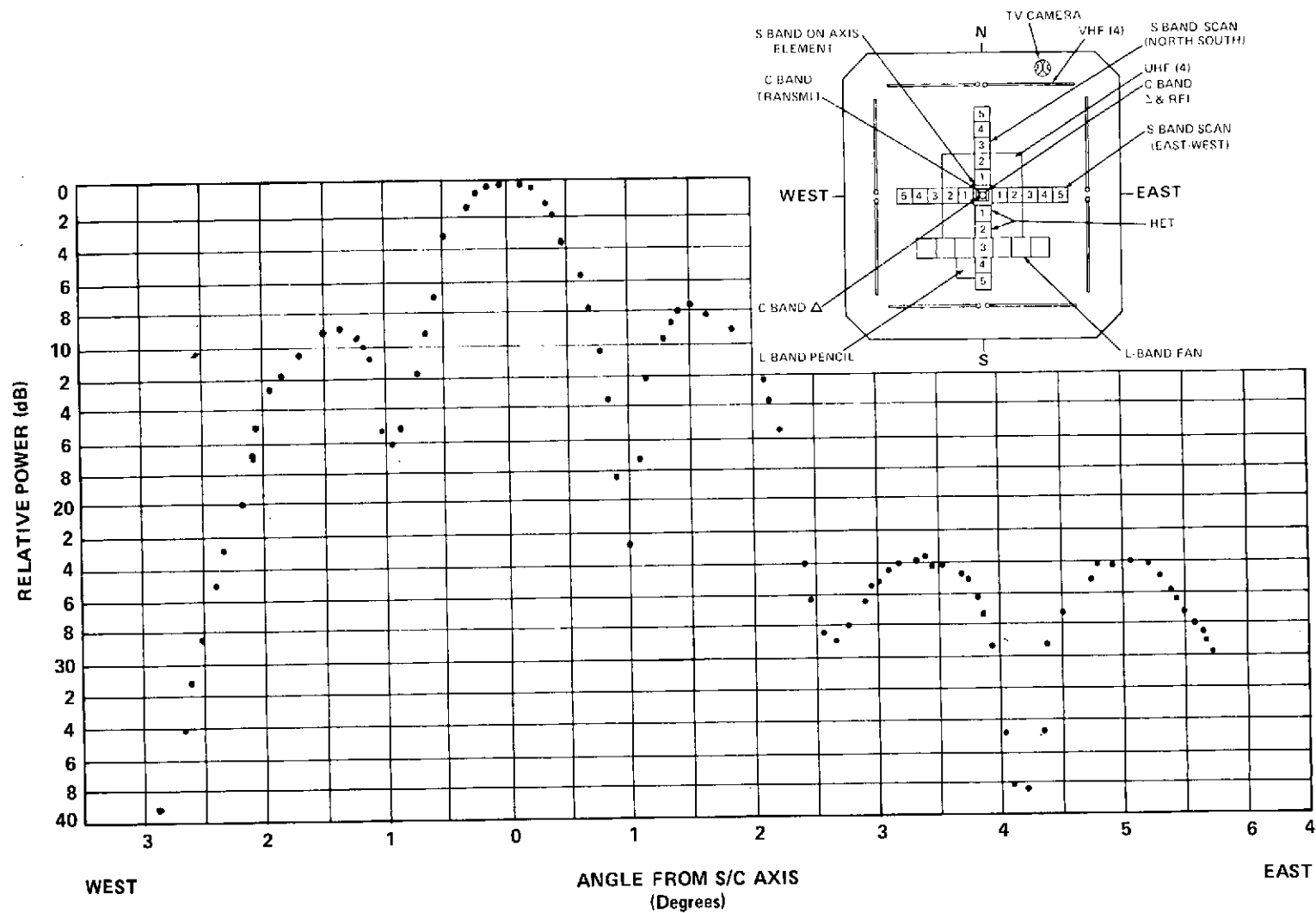
Figure 9-31.   Antenna Pattern, S-5 Element Transmit,
(East-West Cut)
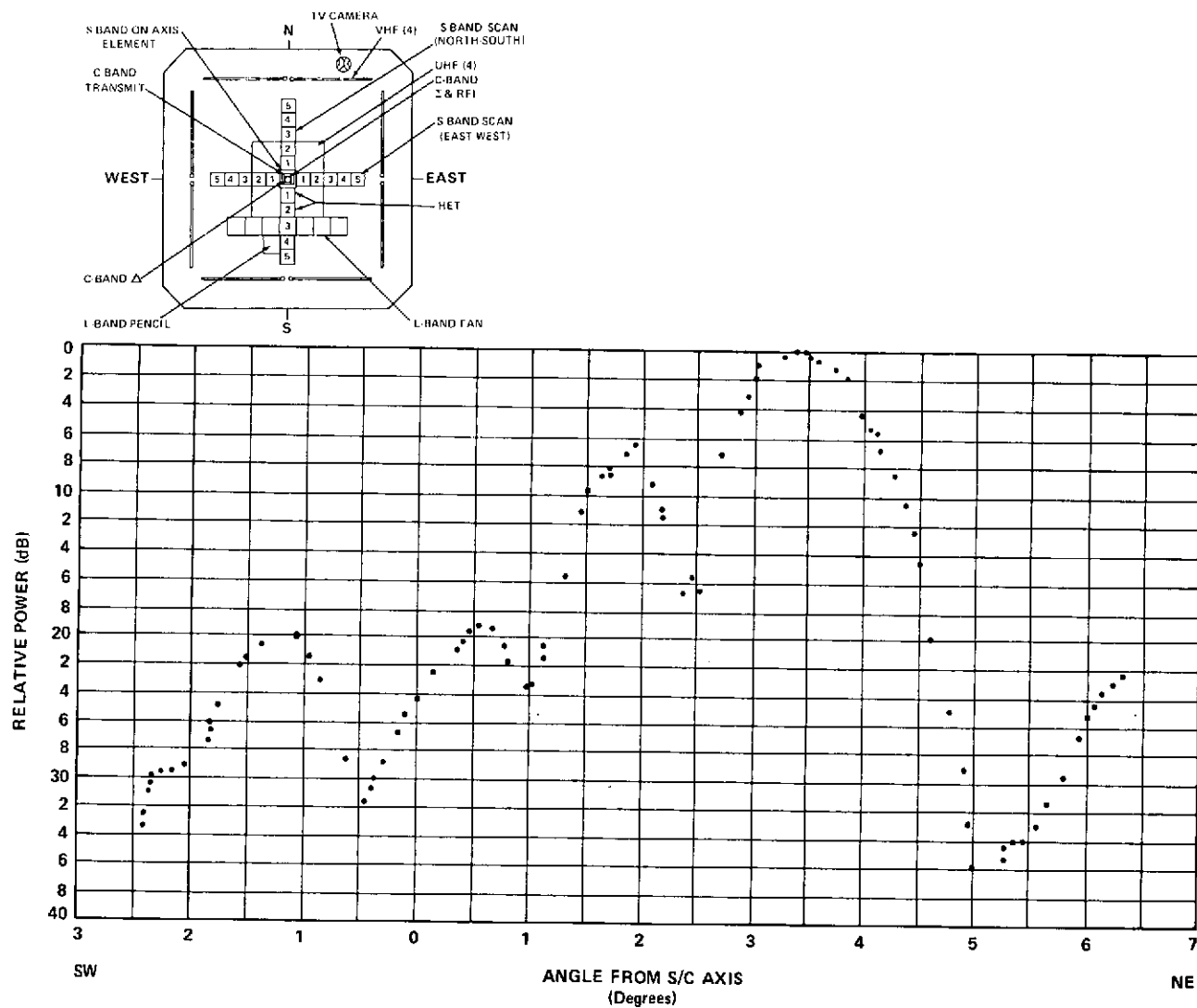
Figure 9-32. Antenna Pattern S-Band S-5 Element Transmit,
(Southwest-Northeast Cut)
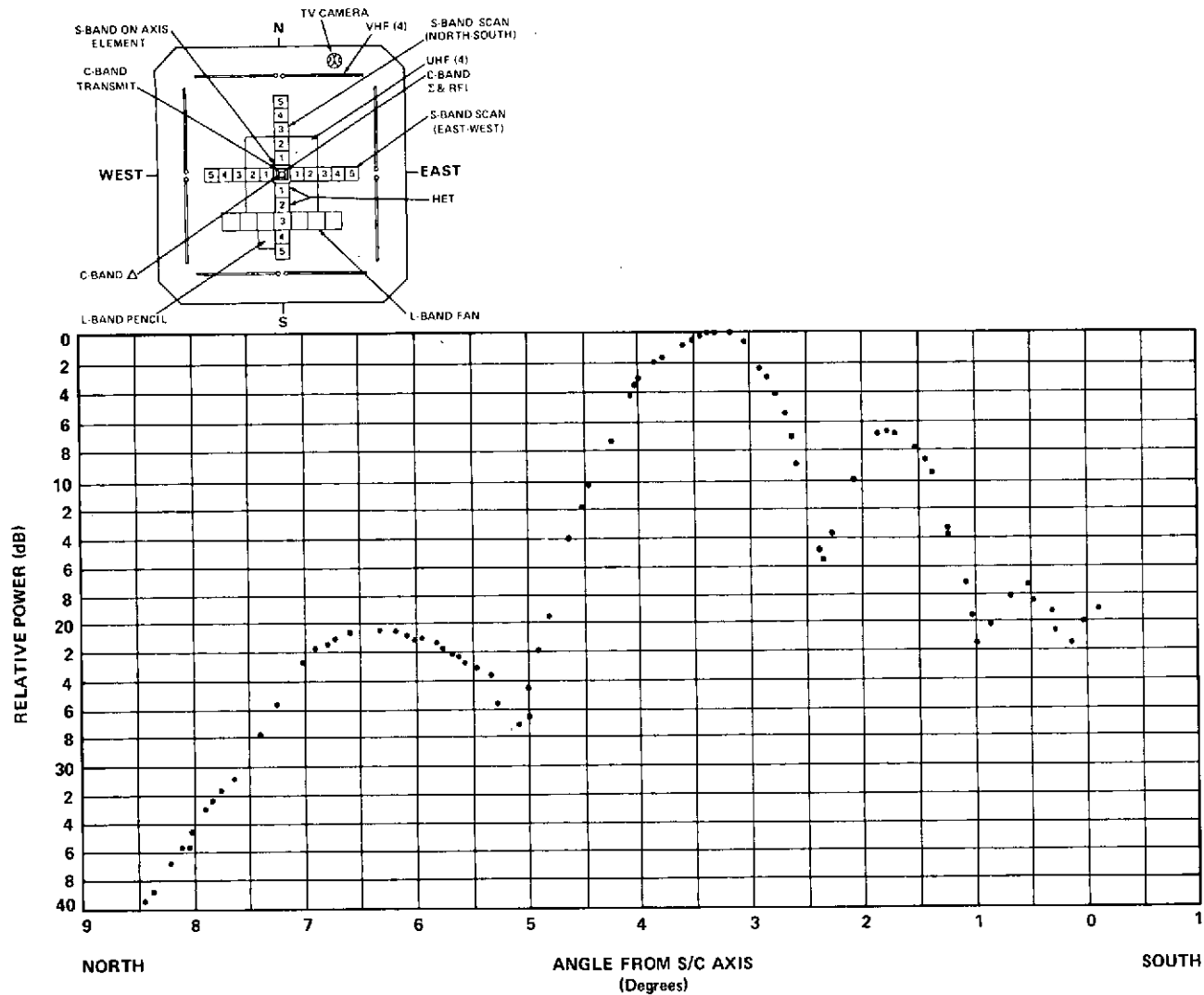
Figure 9-33. Antenna Pattern S-Band S-5 Element Transmit, (North-South Cut)
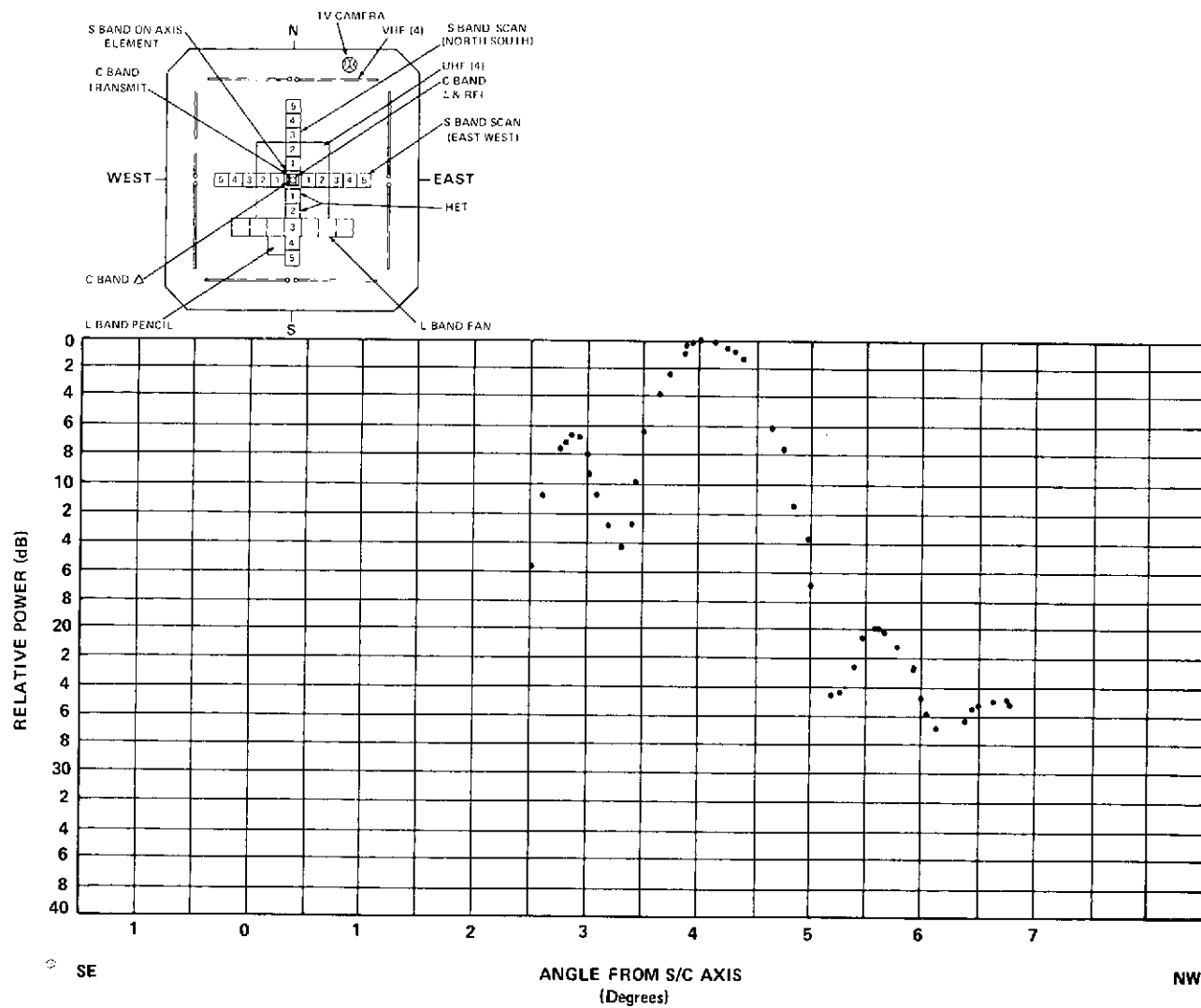
Figure 9-34.   Antenna Pattern, S-Band S-5 Element Transmit,
(Southeast-Northwest Cut)
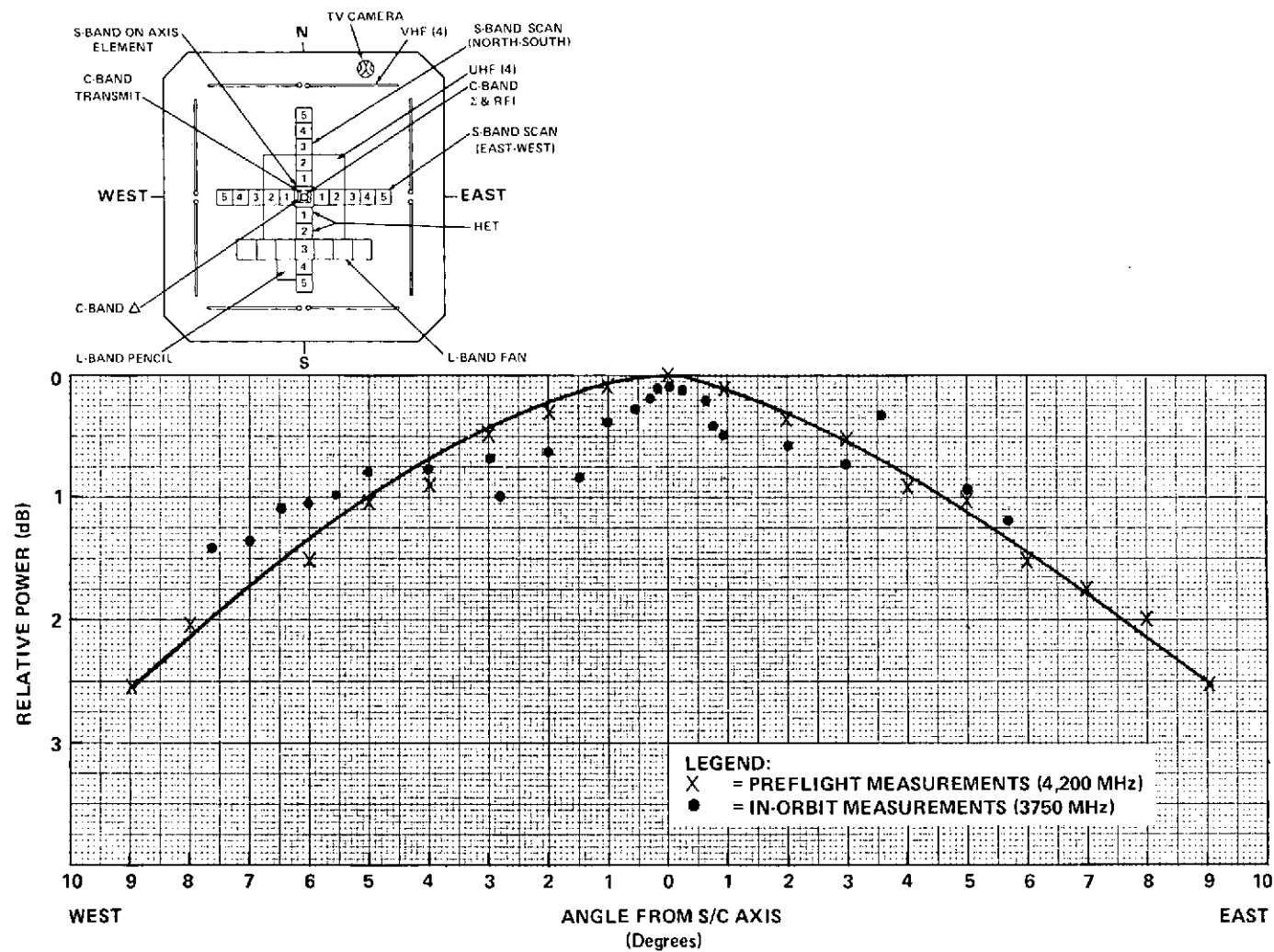
Figure 9-35 Antenna Pattern, C-Band Transmit (ECH), West-East Cut
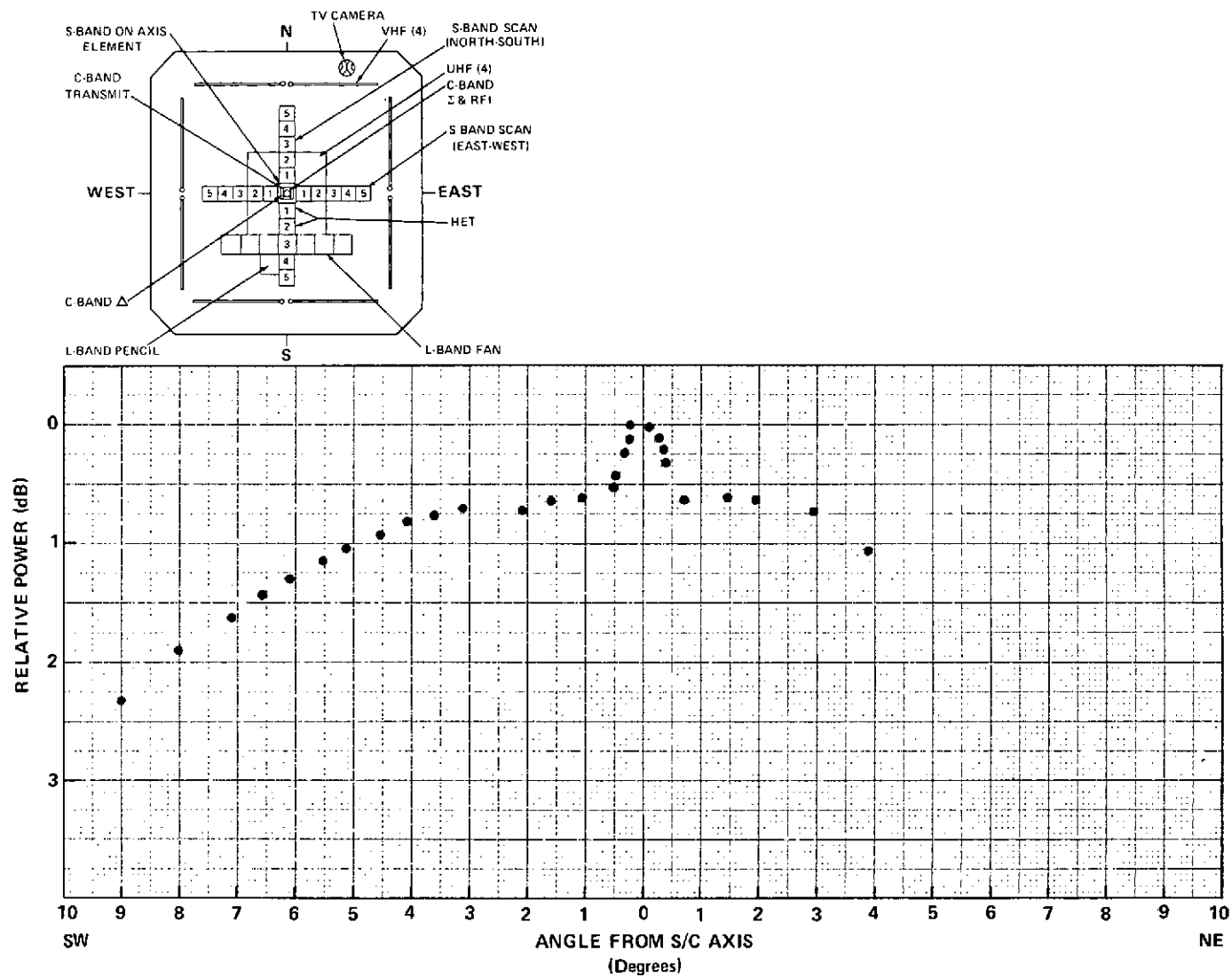
Figure 9-36. Antenna Pattern C-Band Transmit (ECH), Southwest — Northeast Cut
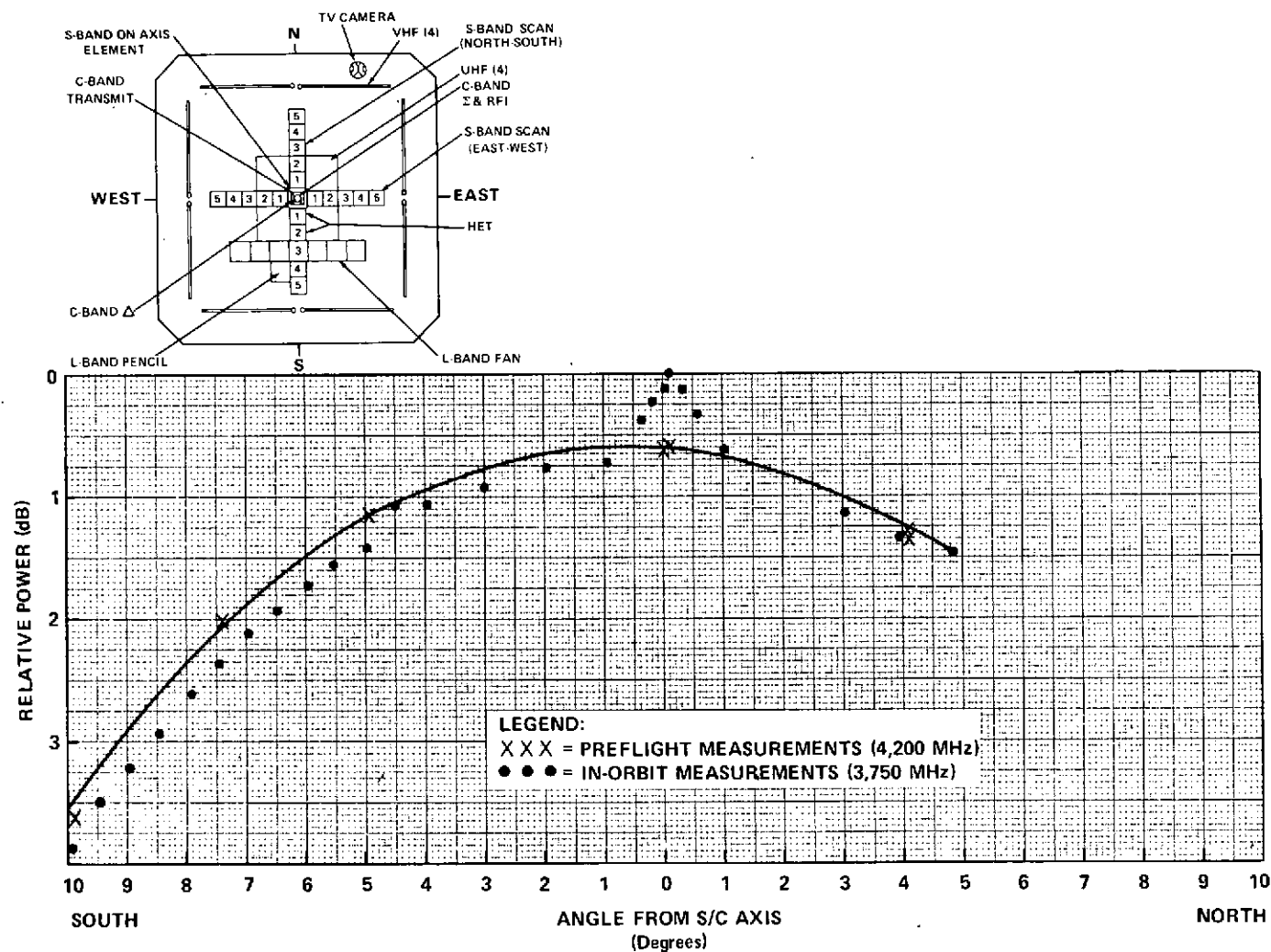
Figure 9-37 Antenna Pattern, C-Band Transmit (ECH), South-North Cut
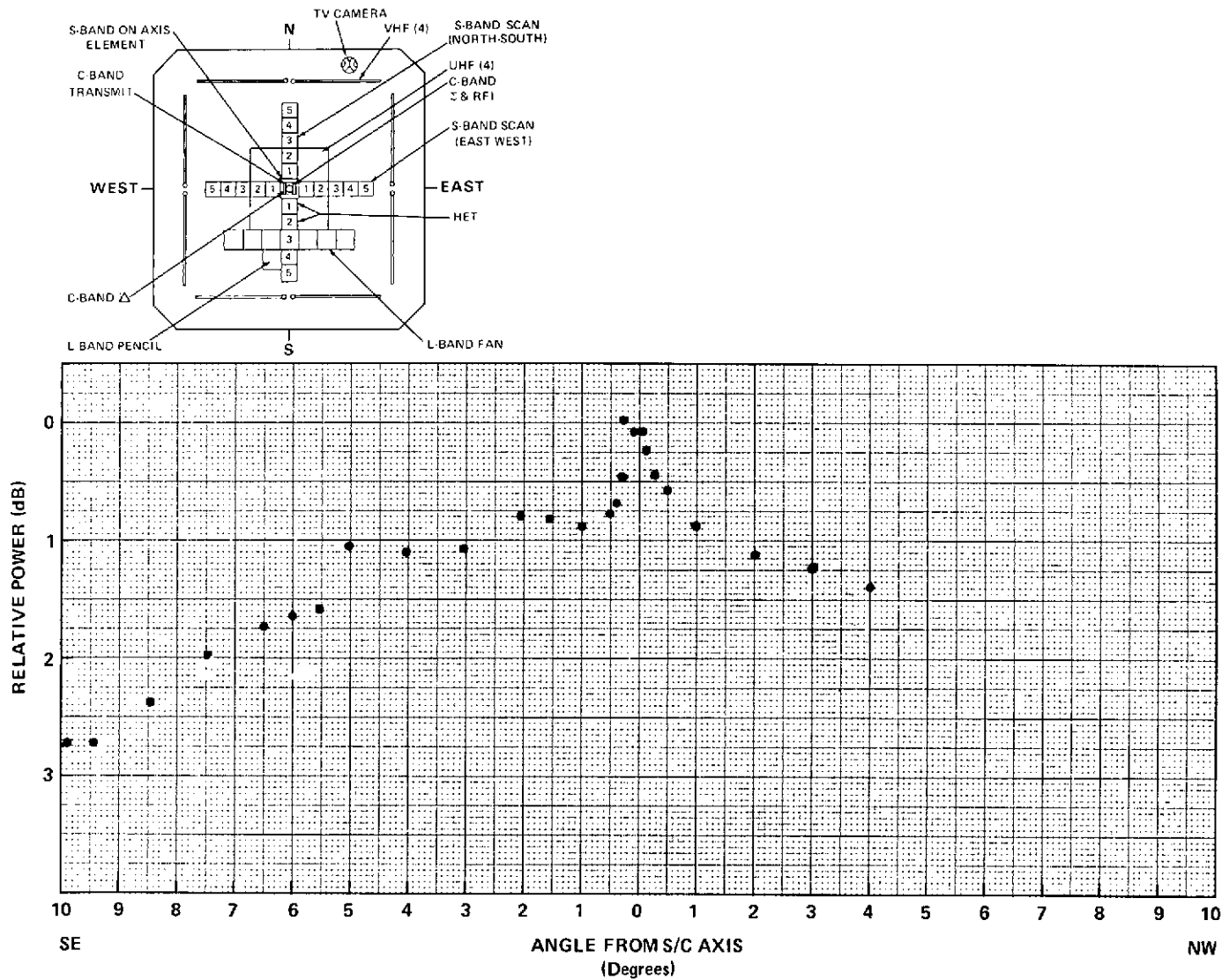
Figure 9-38 Antenna Pattern, C-Band Transmit (ECH), Southeast-Northwest Cut
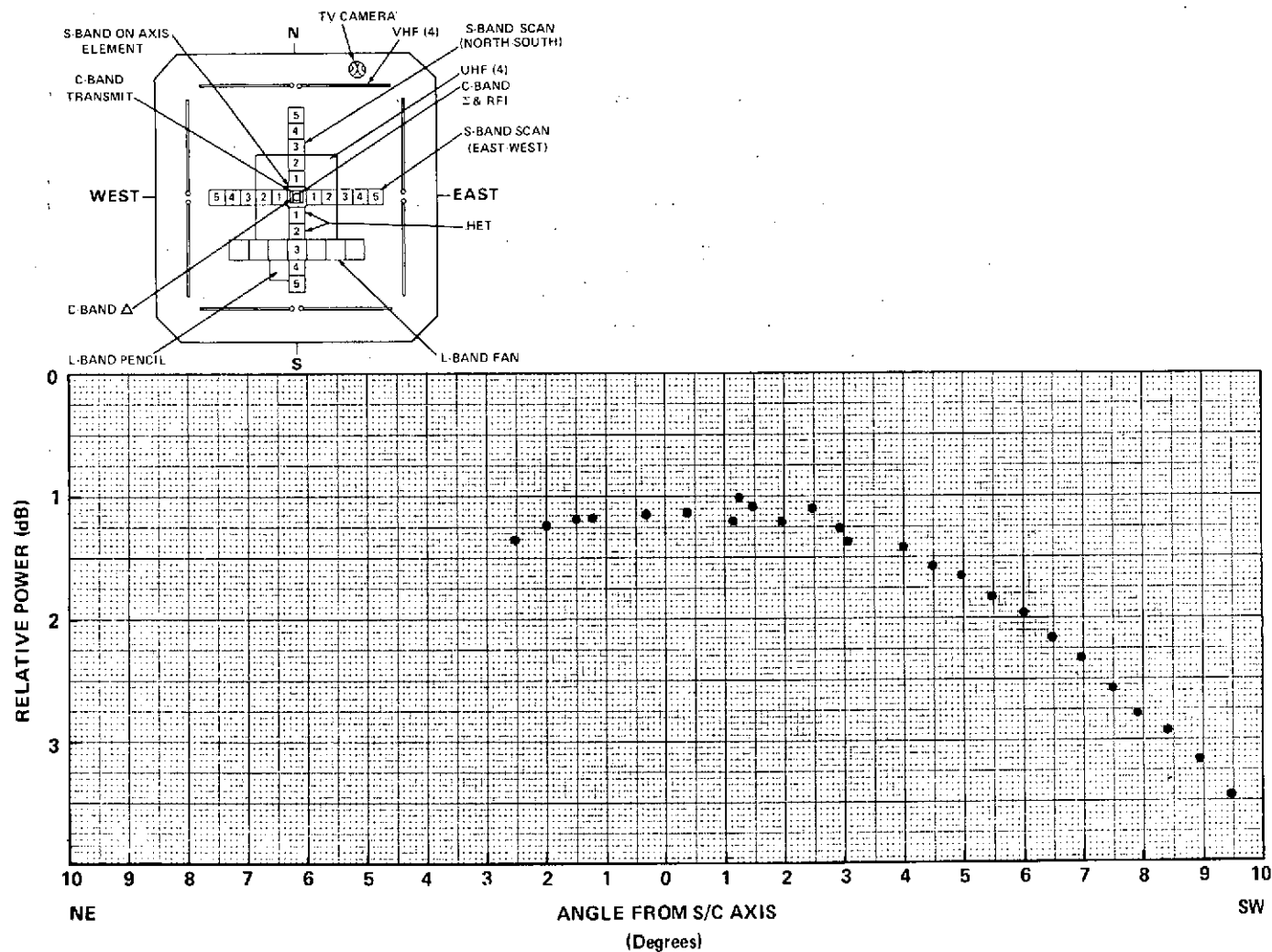
Figure 9-39. Antenna Pattern, C-Band Transmit (ECH), Northeast — Southwest Cut
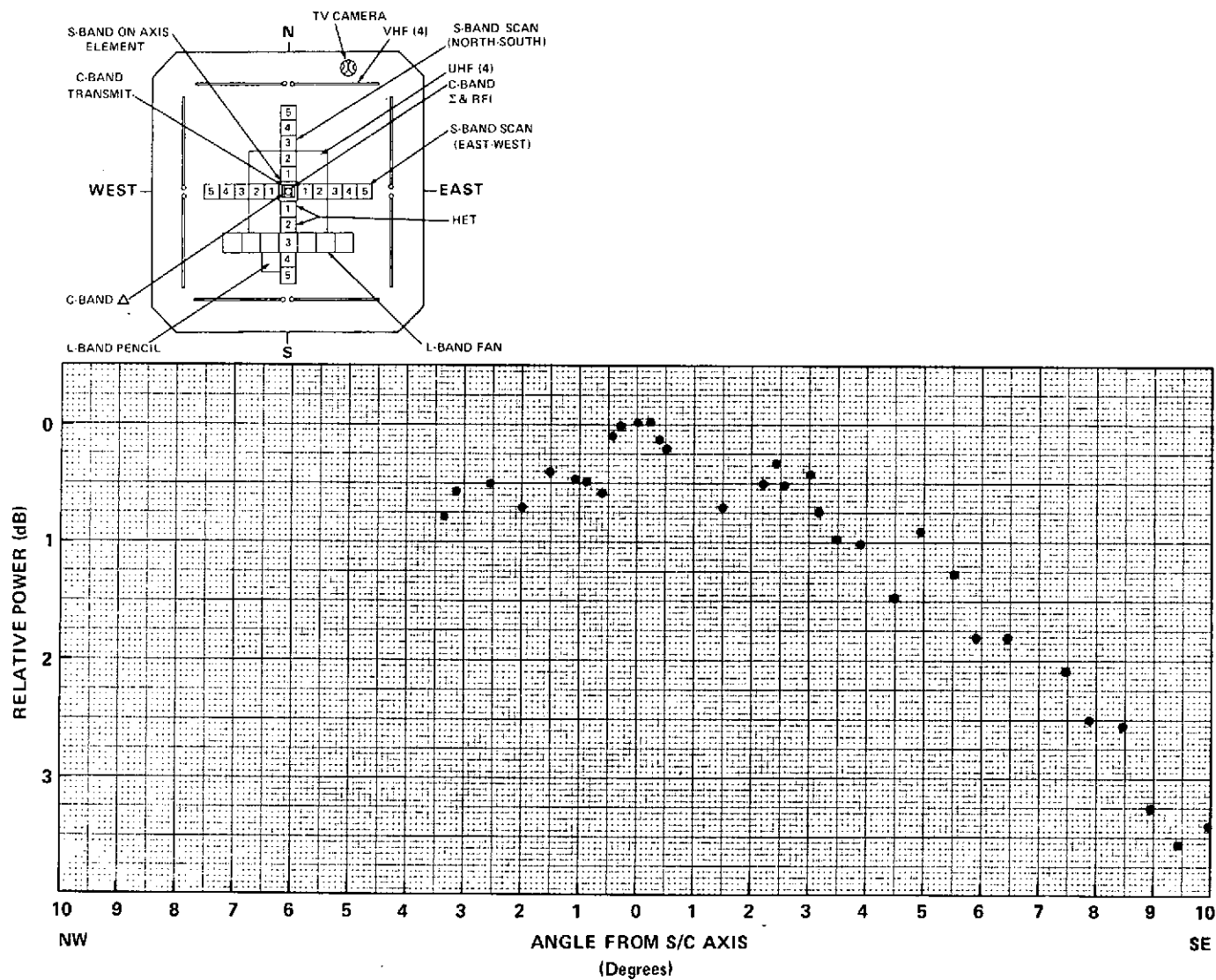
Figure 9-40. Antenna Pattern, C-Band Transmit (ECH), Northwest — Southeast Cut
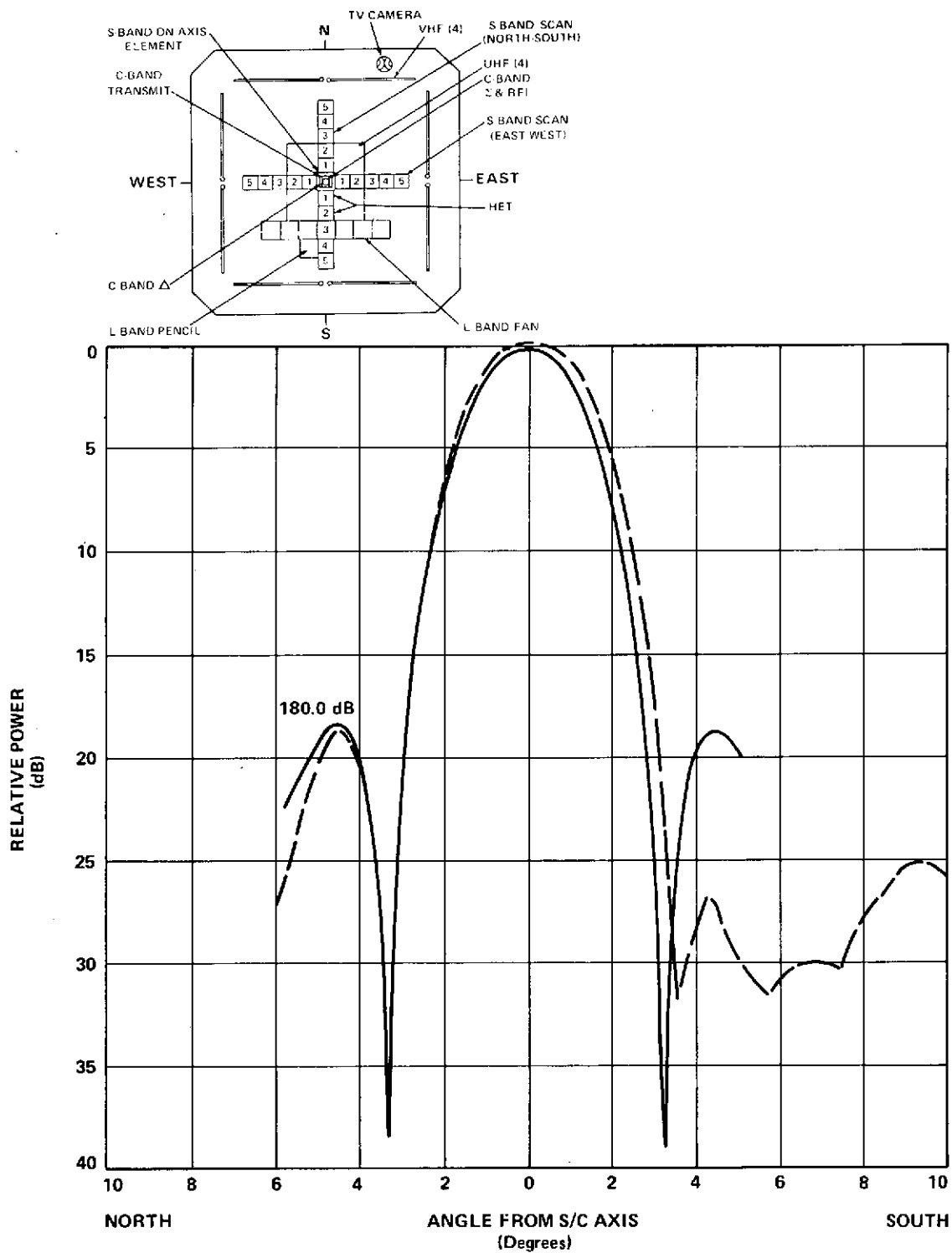
Figure 9-41. Antenna Pattern, UHF Transmit, North–South Cut

b. Monopulse Recommendations

Further monopulse testing should include:

    1. VHF monopulse testing with linear ground polarization, using linear east-west, linear north-south, and northeast to southwest.

    2. Reprogramming the DOC to increase the VHF monopulse gains and then determining the VHF acquisition and pointing capabilities.

c. Monopulse Testing

    1. On day 187 (6 July 1974), a 24-hour C-band monopulse test was performed to determine items (1) and (2) above. The results of this test are covered in the ACS section of this report. In summary, test results indicate that misalignments of (-0.03° to +0.05°) existed in the monopulse pitch channel. The roll channel exhibited an apparent misalignment from 0.05° to 0.15°. These misalignments are approximately sinusoidal within these limits over a 24 hour period. Four losses of monopulse control were experienced during the test; two losses are attributed to loss of ground station uplink signal while the other two losses may be attributed to the thermal environment of the reflector or C-band side-lobe operation.

    2. On day 243 (31 August 1974), another C-band monopulse test was scheduled. The purpose of this test was to obtain operational data relative to the thermal environment of the 30-ft. reflector and determine minimum C-band signal strength operation. The results of this test were inconclusive because of the difficulty of obtaining C-band capture; i.e. C-band monopulse axis is too far from the ESA and interferometer. Once C-band monopulse capture was obtained, the uplink signal strength was adjusted so that the spacecraft AGC varied between -67 dbm and -100 dbm in order to simulate side-lobe operation. The C-band monopulse, in station null mode, successfully controlled the spacecraft with a received AGC level of -97 dbm. Spacecraft control was lost at -100 dbm. This is well within the expected side-lobe signal strength when receiving a C-band signal from the 85-foot Rosman antenna.

    3. The diurnal effects on the 30-foot antenna and its subsequent effects upon C-band monopulsing still need to be determined. Future testing in this area is recommended. Additional C-band monopulse measurements using Rosman's 15-foot dish are also recommended to prevent possible saturation of the monopulse receivers.

9.3.4 Transponder Signal Characteristics

Spectrum analyzer photographs for the various down-link signals were obtained during the initial check-out period. These spectrum photographs showed excellent signal characteristics and as a result, no additional spectrum photos were obtained. In the future, spectrum photos will be obtained only if needed.

9.3.5 Transmitter Trend Data

The parameter of primary interest for trend analysis for the spacecraft transmitters is output power variation as a function of time. Figures 9-42 through 9-46 show output power variations monitored during operational periods from June through the end of August. The power variation figures shows a fairly constant level of performance for the conditions indicated. Power variations for the L-band transmitter are attributed to a change in drive (uplink signal) levels which varied during checkout and operations of the PLACE experiment.

Transmitter temperature variations are functions of operational time, ambient temperature, time of day, etc. Table 9-7 shows the range of temperatures which the transmitters experienced during operations. All temperature ranges were within expected and safe limits.

9.4 ANOMALOUS PERFORMANCE

During the first three months of in-orbit operation, several Flight Anomaly Reports (FAR) were written against the communications subsystem. A FAR was written for any apparently abnormal situation in order that off-line investigation would be conducted. After off-line analyses, many of the FAR's were determined to be false alarms and were closed out. In other cases the FAR's require some further action or disposition before they may be closed-out. As of 31 August 1974, 15 FAR's have been written against the C/S. The status and disposition of each of the FAR's is summarized in Table 9-8. Nine of the FAR's are considered spacecraft related anomalies while the remaining 6 FAR's are not; i.e., ground equipment, test procedure, or false alarm.

9.5 RESOLUTION OF EARLY ANOMALIES

9.5.1 C-Band "Glitches"

Power handling tests of the C-band transmitted output filter conducted at Philco-Ford, determined that the cause of the C-band glitches was slow outgassing of residual contaminants of Hysol A-18 epoxy. An accelerated life test of the filter established that it will not fail or change critical characteristics (VSWR, Insertion Loss, Bandpass) during the anticipated life of the spacecraft. As a
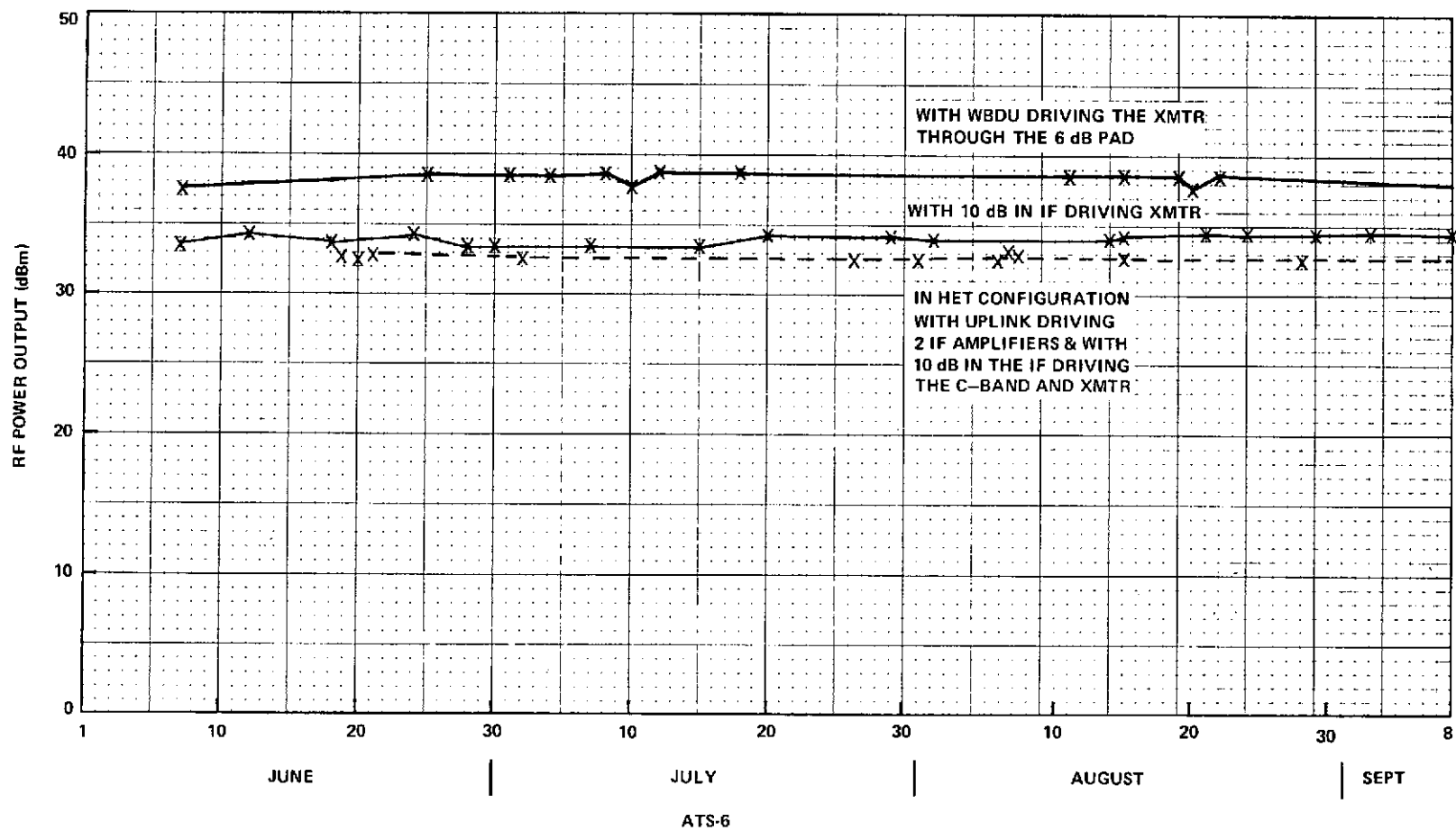
Figure 9-42. ATS-6 C-Band RF Output Power
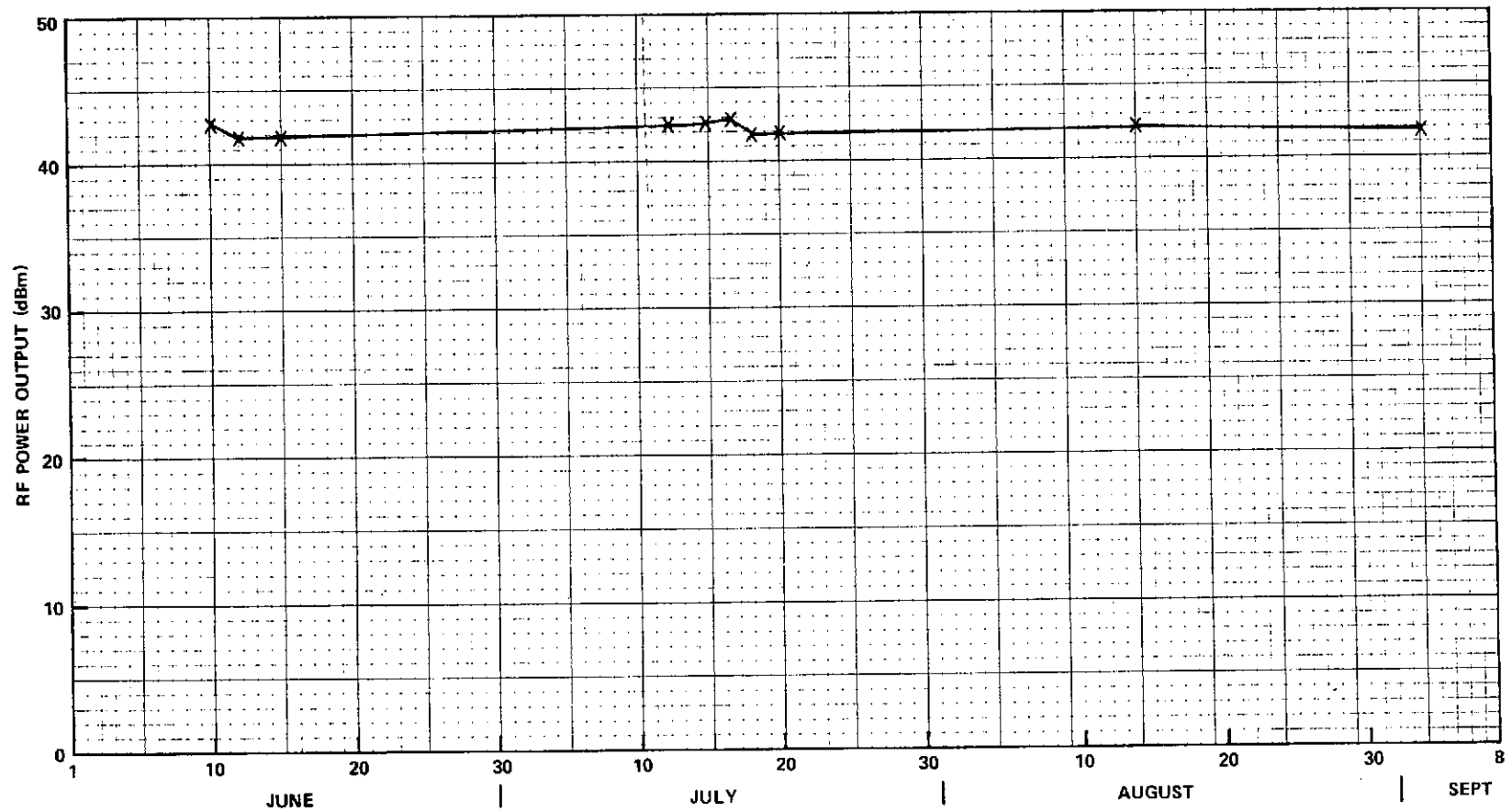
Figure 9-43. ATS-6 S-Band RF Output Power
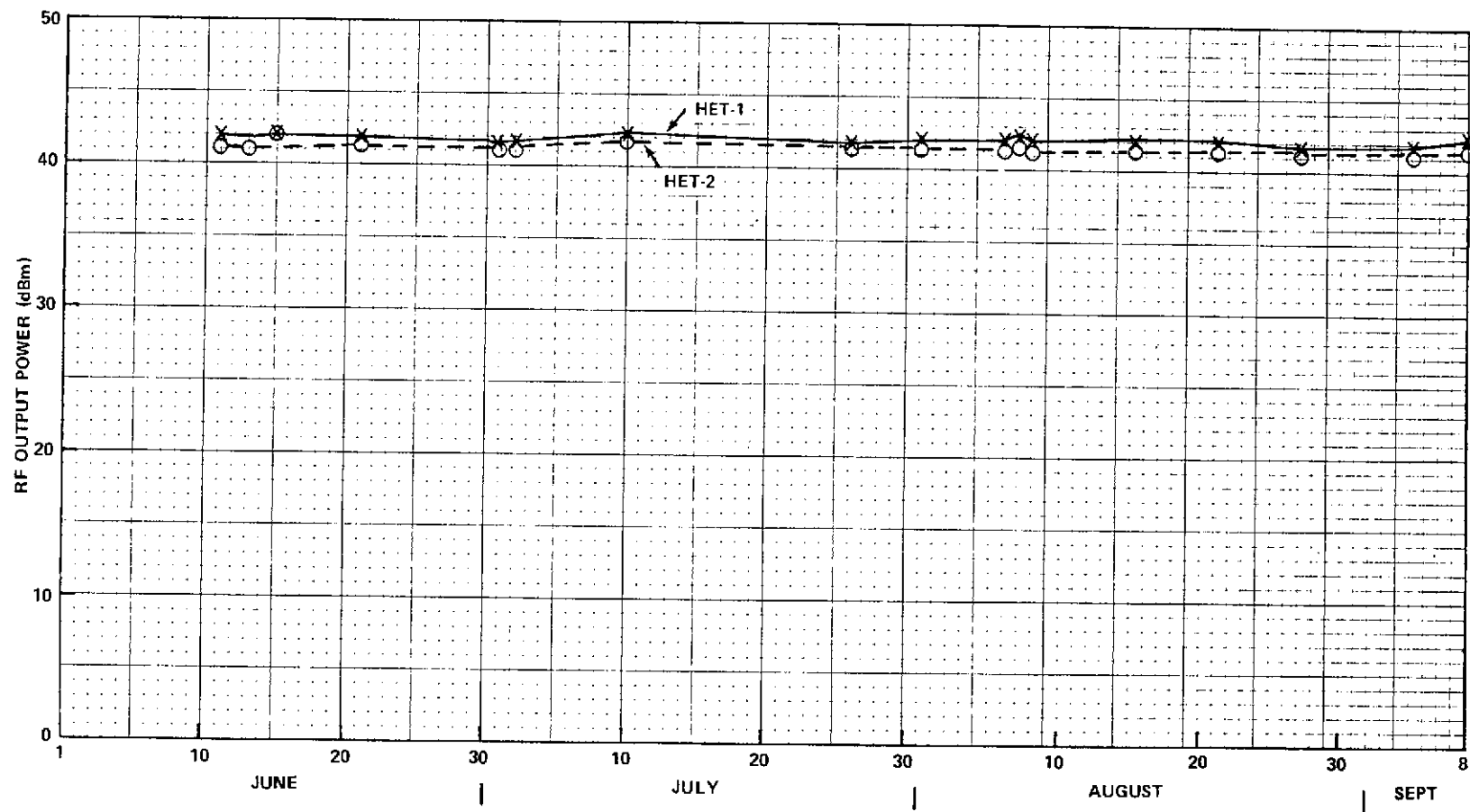
Figure 9-44 ATS-6 HET RF Output Power
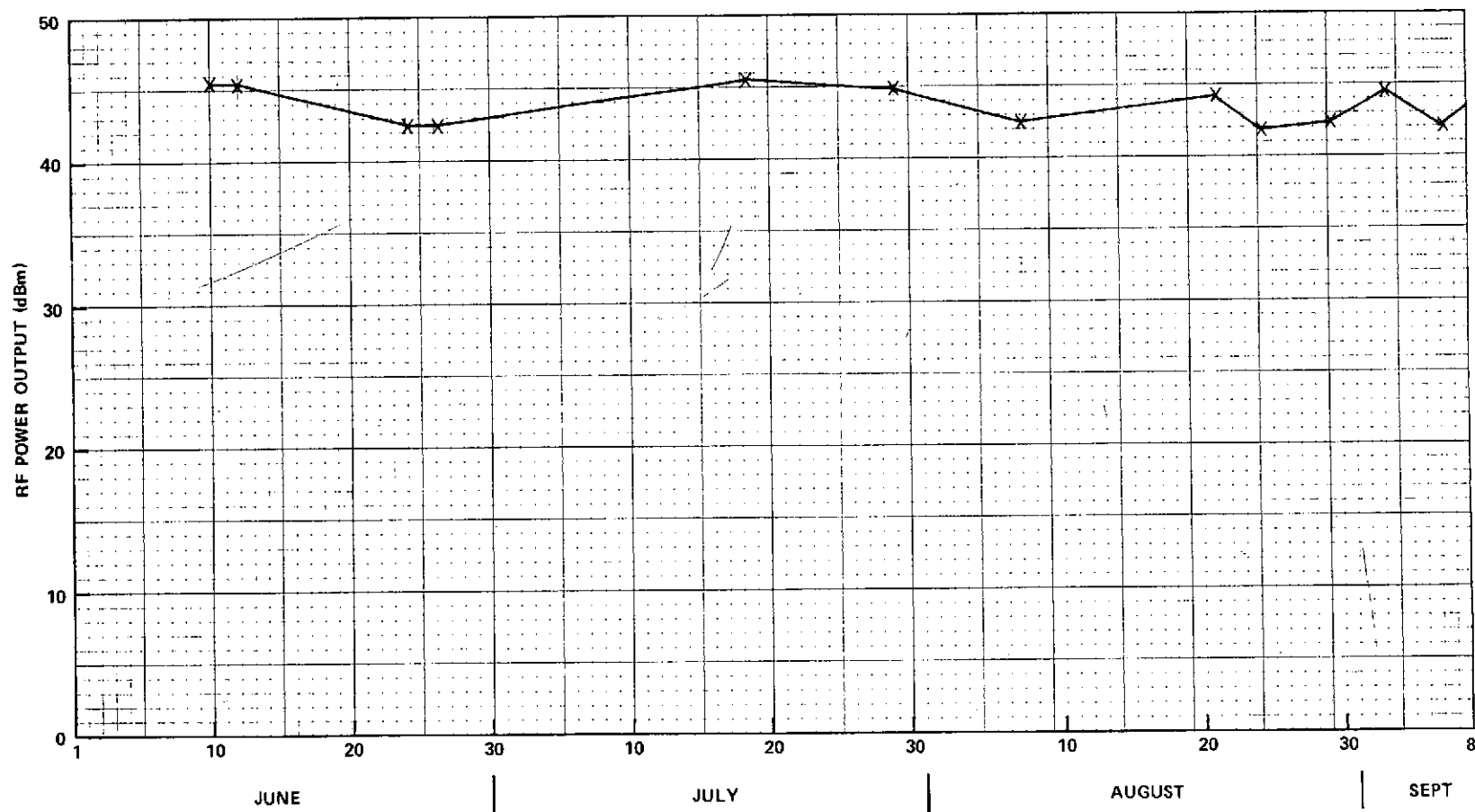
Figure 9-45. ATS-6 L-Band RF Output Power
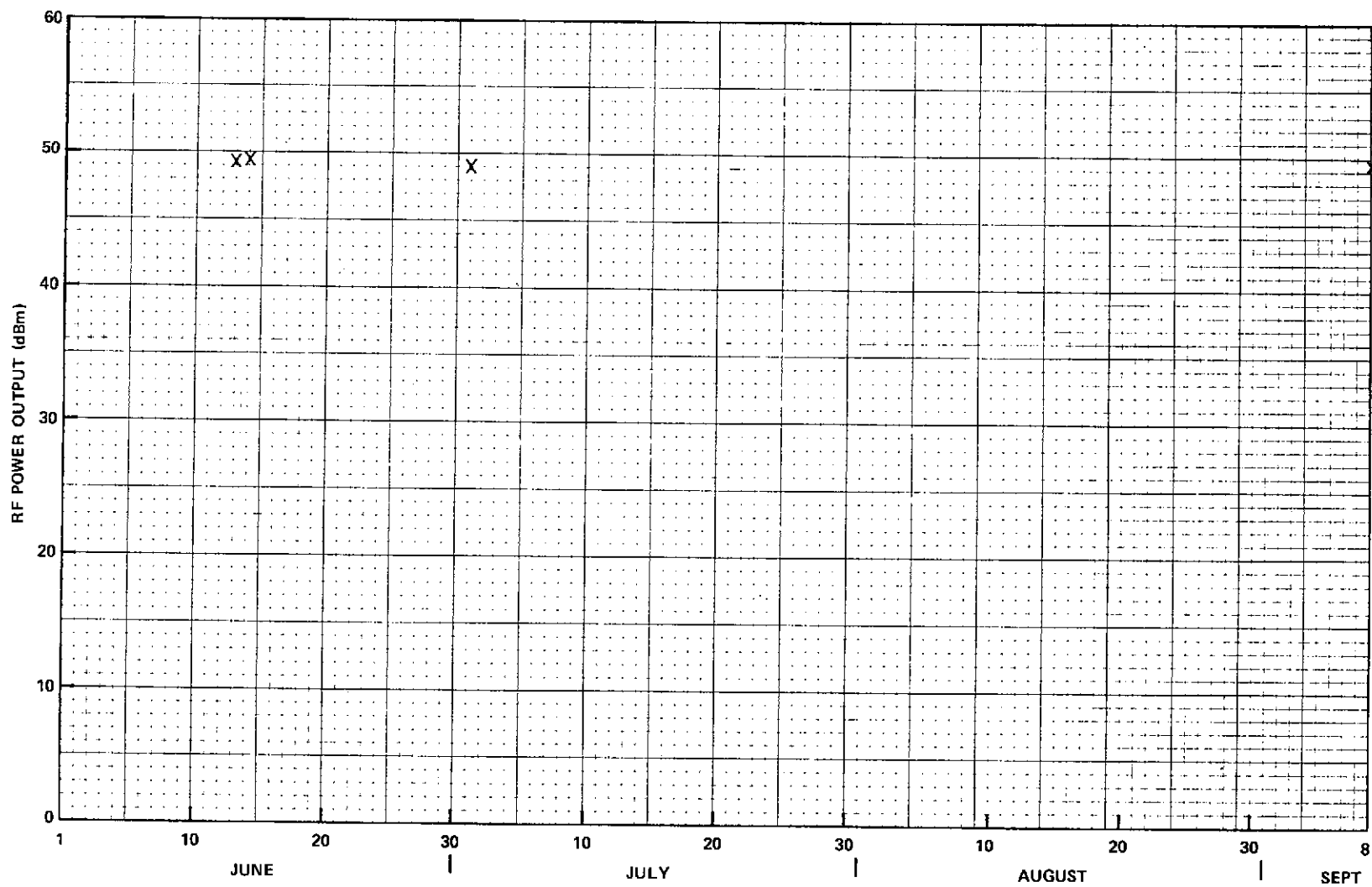
Figure 9-46. ATS-6 UHF RF Output Power

Table 9-7

Transmitter Temperatures

Transmitter	Min. Temp. °C	Max. Temp. °C
C-Band	23	39.1
HET-1	21.3	39.6
HET-2	27.7	42.0
S-Band	23.5	35.0
L-Band	28.6	38.0
UHF	24.1	39.4

Table 9-8

Communications Subsystem Flight Anomaly Reports

Anomaly Number	Description of Anomaly	Disposition Resolution	Date		Remarks
			Open	Closed	
301	C-Band Transmitter Power Glitch	Insert either 10 db in IF or 6 db RF Attn	6/3/74	8/15/74	Phenomena observed in T/V chamber at Philco. Problem is in C-band trans. output filter caused by residual epoxy contaminants. Operational constraint (See 9.5.1)
302	L-Band Noise Coupling during Place Exp.	Not considered flight anomaly since it occurred in test.	6/19/74	8/15/74	L-band trans. couples noise into RCVR when no drive signal present. Phenomena observed during ground test.
303	Synthesizer RFI	Turn synthesizer off when RFI exp. on	6/18/74	6/18/74	Synthesizer modulates C-band RFI downlink signal. Phenomenon observed during ground test.
304	Low AGC (C-Band Pol.)	See FAR 309	6/22/74	8/13/74	PFF/ECH coupling is a function of polarization.
305	L-Band Transmitter Power Glitch during Place Exp.	Not considered flight anomaly- GND Sta. ADJ.			Drop of 16-22 db in C-band uplink signal.
306	L-Band Transmitter Noise	See FAR 302	6/28/74	6/28/74	
307	C-Band TWTA FR Power & Helix Current Oscillations During First 30 Seconds of Operation.	Not flight anomaly.	6/30/74	8/15/74	Problem due to poor ATSOCC SCR instrumentation IDA SCR showed C-band parameters clean
308	RBE Interference to TDRE	RBE turned off during TDRE operations.	7/16/74	8/15/74	1 & 2 MHz spurs from RBE coupled on to C-band downlink turning off RBE removed spurs. Coupling mechanism under study.
309	C-Band ECH-PFF RCVR Coupling	Modify COMM standby config. to set C/B Pol. to Lin N-S	8/2/74	8/13/74	C-band polarization tests conducted when C-band pol. in Lin N-S setting.

Table 9-8 (Cont'd)
Communications Subsystem Flight Anomaly Reports

Anomaly Number	Description of Anomaly	Disposition Resolution	Date		Remarks
			Open	Closed	
310	L-Band/C-Band Crosstalk	Further tests planned GND equip. prob.	8/1/74		70 MHz spur noticed on C/B downlink
311	HET Video Crosstalk	Conf. HET-1/2 for Beam 1 pattern during Alaska/IHS ops. S/C misalignment set for Beam 1 location.	8/6/74	8/7/74	Video crosstalk observed when HET 1/2 xmtrs on Beam 2 pattern. Crosstalk disappears on Beam 1
312	HET Audio Crosstalk	Not S/C prob: HET GND eq. prob.	8/8/74	8/9/74	HET audio subcarriers (4) have had history of crosstalk problems. Use only 2 subcarriers to eliminate prob.
313	Synthesizer Freq. Drift	Synthesizer performing as expected.	8/16/74	8/17/74	Noticed 1 kHz/hr drift in Synth. freq. when meas. on L-band downlink (PLACE) to MHz IF subsequent drift meas. over 9 hr. period verified freq. of approx. 1 Kz. Freq. stability spec at 1550 MHz is ±15.5 KHz.
314	No UHF #2 Transmitter Power Output	Not S/C prob. incorrect ASP test proc.	8/16/74	8/16/74	ASP procedure configured UHF trans. #2 with Reg. Bus #1 needs Bus #2. Directive issued not to use redundant trans. unless given NASA permission.
315	PWR Dropout of C-Band Downlink During SAPPSAC C-Band RFI OPS.	Do not operate C-band RFI transponder when boresighting on a C/B trans. (C/B Interferometer cannot be used with RFI transponder.)	8/19/74	8/20/74	During SAPPSAC ops. C/B RFI transponder turned on: Spacecraft slewed to various locations including Rosman. When at Ros. spacecraft boresighted causing RFI transp. to saturate causing PWR dropout.
	HET Crosstalk, $H_{1,2} \rightarrow S$	7th order intermodulation.			

precautionary measure however, operational constraints limit C-band power output to the minimum necessary for each application.

9.5.2   VHF Monopulse Slope

Tests conducted at Philco-Ford have proven that the lower than expected VHF monopulse slope was caused by the difference in phase shift in the diplexer when used in space vacuum compared to measurements in a humid ground atmosphere.

Further experiments to determine the utility of VHF monopulse should include the use of stronger signal levels and reprogramming the DOC.

SECTION 10

APOLLO – SOYUZ TEST PROJECT
(ASTP)

SECTION 10

APOLLO – SOYUZ TEST PROJECT
(ASTP)

10.1 INTRODUCTION

The Apollo – Soyuz Test Project (ASTP) is a cooperative effort between NASA and the U.S.S.R. The ASTP consists of the development, scheduling, and test docking between a Soviet Soyuz spacecraft and an Apollo spacecraft in near-earth orbit. The ATS-6 spacecraft will be used to provide satellite communications support during the experiment. This support will consist of the real-time relay of telemetry, television, and voice communications from the Apollo command service module (CSM) to the hybrid terminal and voice communications and command from the hybrid terminal to the CSM. The basic relay configuration is shown in Figure 10-1.

It is planned to support the experiment from July 15, 1975, to July 25, 1975, when ATS-6 is located at 35°E longitude.

10.2 MODES OF OPERATION

10.2.1 ATS-6 to CSM Forward Link (Refer to Table 10-1)

The ATS-6 to CSM (forward link) will consist of a 2077.4-MHz S-band carrier, phase modulated by a composite signal of 30 kHz voice subcarrier and a 70-kHz up-data command subcarrier.

10.2.1.1 Voice (F1 Mode)—The 30-kHz subcarrier will be frequency modulated with uplink voice.

10.2.1.2 Voice and Up-Data Commands (F2 Mode)—The 30-kHz subcarrier will be frequency modulated with uplink voice. The 70-kHz subcarrier will be frequency modulated by a coherently related 1-kHz synchronous (sync) tone and a 2-kHz signal biphase modulated by 1000 bit per second digital command data.

10.2.1.3 Up-Data Command (F3 Mode)—The 70-kHz subcarrier will be frequency modulated by a coherently related 1-kHz sync tone and a 2-kHz signal biphase modulated by 1000 bit per second digital command data.

HIGH GAIN
ANTENNA

2077.4 MHZ   FORWARD LINK

2256.0 MHZ   REVERSE LINK

ATS-6

CSM

2272.5 MHZ FM
2287.5 MHZ PM

2106.4 MHZ

3756 MHZ
3956 MHZ
4156 MHZ
(SELECTABLE)

REVERSE LINK

C-BAND

FORWARD LINK

5952.4 MHZ
6152.4 MHZ
6352.4 MHZ
(SELECTABLE)

STDN

STDN

ATS-6
GROUND STATION
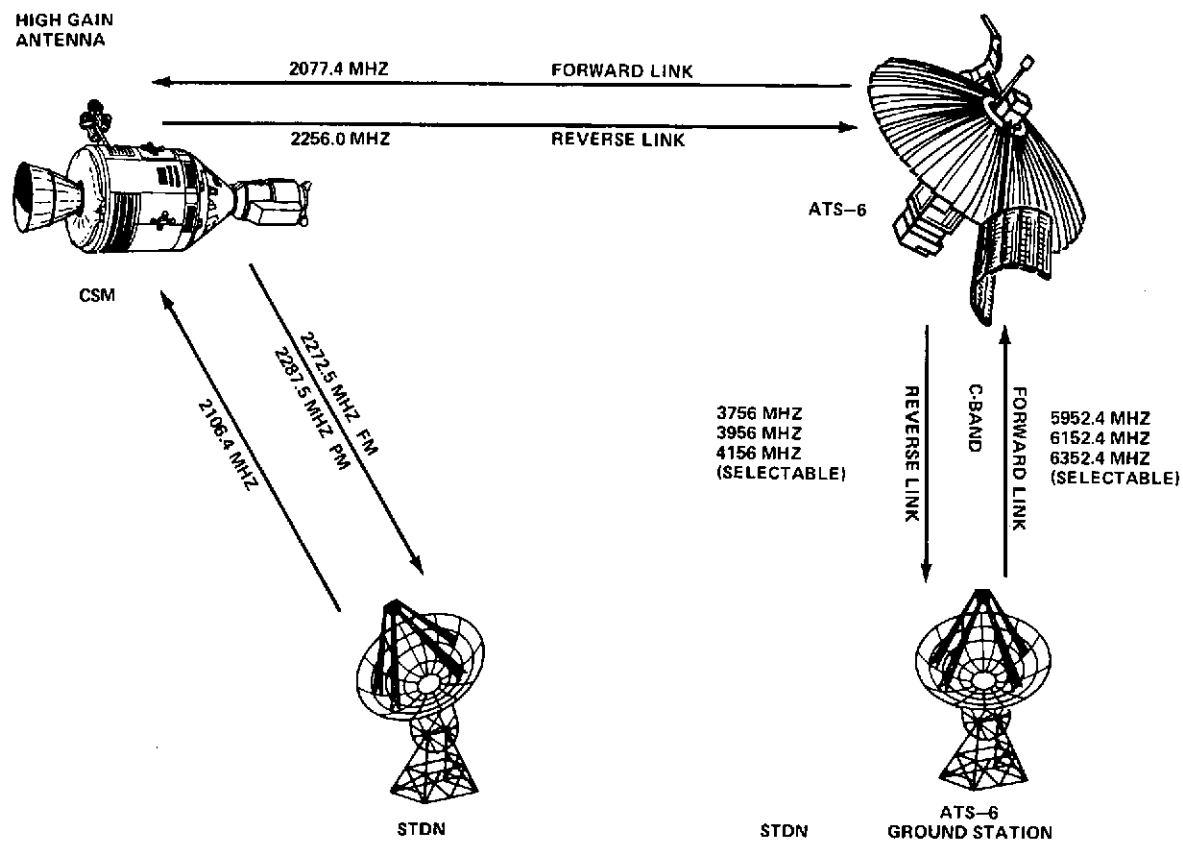
Figure 10-1. CSM/ATS-6/STDN Frequency Assignments

Table 10-1
ATS-6 to CSM (Forward Link) Transmission
Combinations Summary

Combination	Information	Modulation Technique	Subcarrier Frequency	Peak Carrier Deviation
F0	Carrier Only			
F1	Voice	FM/PM	30 KHz	1.1 rad. ± 10%
F2	Voice	FM/PM	30 KHz	1.1 rad. ± 10%
	Up-Data Commands	PSK/FM/PM	70 KHz	1.1 rad. ± 10%
F3	Up-Data Commands	PSK/FM/PM	70 KHz	1.1 rad. ± 10%

10.2.2 CMS to ATS-6 Reverse Link (Refer to Table 10-2)

The CSM to ATS-6 reverse link will consist of a 2256.0 MHz S-band carrier, either phase modulated (PM) or frequency modulated (FM) depending upon the selection of the CSM downlink mode.

10.2.2.1 PM Mode (R1)—In the (R1) PM mode, the reverse link S-band carrier frequency is coherently related to the received forward link S-band carrier frequency by a multiplication factor of 240/221 after forward link-lock is established, and is phase modulated by a multiplexed signal which is the composite of a 1.25-MHz frequency modulated real-time downlink voice subcarrier and a 1.024-MHz biphase modulated real-time pulse code modulation (PCM) telemetry subcarrier. The telemetry data being a high bit rate of 51.2 kbps.

10.2.2.2 PM Mode (R2)—In the PM mode, the reverse link S-band carrier frequency is coherently related to the received forward link S-band carrier frequency by a multiplication factor of 240/221 after forward link-lock is established, and is phase modulated by a multiplexed signal which is the composite of a 1.25-MHz frequency modulated real-time downlink voice subcarrier and a 1.024-MHz biphase modulated real-time PCM telemetry subcarrier. The telemetry data being a low bit rate of 1.6 kbps.

10.2.2.3 FM Mode (R3)—This real-time (R-T) television and R-T voice mode consists of the reverse link S-band carrier, frequency modulated by a television signal containing interleaved voice and central timing equipment (CTE) time.

10.2.2.4 FM Mode (R4)—This playback (PB) television and PB voice mode consists of the reverse link S-band carrier, frequency modulated by a television signal and interleaved voice and CTE time from the video tape recorder (VTR).

10-3

Combination	Information	Modulation Technique	Subcarrier Frequency	Peak Carrier Deviation
R1	Voice	FM/PM	1.25 MHz	0.7 rad.
	High Bit Rate Telemetry	PCM/PM/PM	1.024 MHz	0.94 rad.*
R2	Voice	FM/PM	1.25 MHz	1.2 rad.
	Low Bit Rate Telemetry	PCM/PM/PM	1.024 MHz	0.7 rad.
R3	Voice	PAM/FM (inter-leaved with TV)		
	Television	FM		8.0 MHz peak-to-peak**
R4	Playback Voice	PAM/FM (inter-leaved with TV)		
	Playback TV	FM		8.0 MHz peak-to-peak**
R5	Voice	FM/FM	95.0 KHz	187.5 KHz ±15%
	Science Data	PCM/FM/FM	125.0 KHz	275.0 KHz ±15%
	Playback Telemetry	PCM/PM/FM	1.024 MHz	1500.0 KHz ±15%
	Playback Voice	FM		250.0 KHz, +20%, -40%
	Playback Science Data	PCM/FM/FM	165.0 KHz	425.0 KHz ±15%
R6	Voice	FM/FM	95.0 KHz	187.5 KHz ±15%
	Science Data	FM/FM	125.0 KHz	275.0 KHz ±15%
	Telemetry	PCM/PM/FM	1.024 MHz	1500.0 KHz ±15%
	-----	-----***	165.0 KHz	425.0 KHz (unmodulated)

*Resultant carrier deviation when the 1.024-MHz subcarrier is modulated by 51.2-kbps telemetry data.
 Peak carrier deviation due to an unmodulated 1.024-MHz subcarrier is 1.2 radians.
**Minimum sync tip to saturated white for nominal input signal.
***Unmodulated subcarrier present.

10.2.2.5 FM Mode (R5)—This combination of R–T voice and science data, PB telemetry, voice and science data mode consists of the reverse link S–band carrier modulated by a composite signal of: a 95–KHz subcarrier frequency modulated by R–T voice; a 125–KHz subcarrier frequency modulated by R–T PCM science data; a 1.024–MHz subcarrier biphase modulated by PB PCM telemetry data; PB voice frequency modulating the reverse link S–band carrier direct and, a 165–MHz subcarrier frequency modulated by PCM PB science data.

10.2.2.6 FM Mode (R6)—This R–T voice, telemetry and science data mode consists of the reverse link S–band carrier, frequency modulated by a composite signal of 1.024–MHz subcarrier biphase modulated by R–T 51.2-kbps or 1.6-kbps PCM telemetry data, a 95–KHz subcarrier frequency modulated by R–T voice, a 125–KHz subcarrier frequency modulated by science data, and an unmodulated 165–KHz subcarrier.

10.2.3 Doppler Tracking

ATS-6 station keeping and position location is accomplished by the ATS Range and Range Rate System (ATSR) which operates at an uplink frequency of 5950, 6150 and 6350 MHz and downlinks at 3750, 3950 and 4150 MHz. ATS-6 will also provide a coherent two-way doppler relay capability when the CSM is configured to the PM mode. Ranging pseudo-random-noise (PRN) code turnaround capability is not provided on the CSM.

10.3   CSM MODIFICATIONS FOR ATS-6 OPERATIONS

The CSM telecommunications system has been modified for ATS-6 relay operations by the addition of an Apollo high gain S-band antenna (HGA) and associated communications relay equipment. These modifications provide an operational interface between the CSM and ATS-6 satellite. Figure 10-2 depicts the CSM communications relay equipment for communications between the CSM and the satellite tracking data network (STDN) using the ATS-6 system.

10.3.1 CSM to ATS-6 Communications Relay Equipment

The following equipments were added to the CSM communications system and makes up the CSM/ATS-6 communication subsystem:

a.   ATS-6 Premodulation Processor (PMP)

This unit is an Apollo type PMP and is identical to a second onboard PMP used in the CSM/STDN communication subsystem. Inputs such as audio, CTE, telemetry (TLM), data storage equipment (DSE), VTR and TV are parallelled to both PMP's. Input from the ATS-6 relay PM receiver is routed to the ATS-6 PMP only. Updata link (R-T commands) can be routed to either of the PMP's, but not both simultaneously. Inputs to the PMP are controlled by use of onboard switches and uplink commands.

b.   Unified S-Band Equipment (USBE)

The USBE consists of two PM transponders (one prime, the other backup), one FM transmitter, and associated switch gear for onboard control or for uplink command control. The ATS-6 USBE can be configured for one PM uplink and one PM downlink, one PM uplink and one FM downlink, or one FM downlink. The ATS-6 USBE is operationally independent of the STDN USBE, however, the two subsystems can be operated simultaneously in conjunction with their individual ground stations.
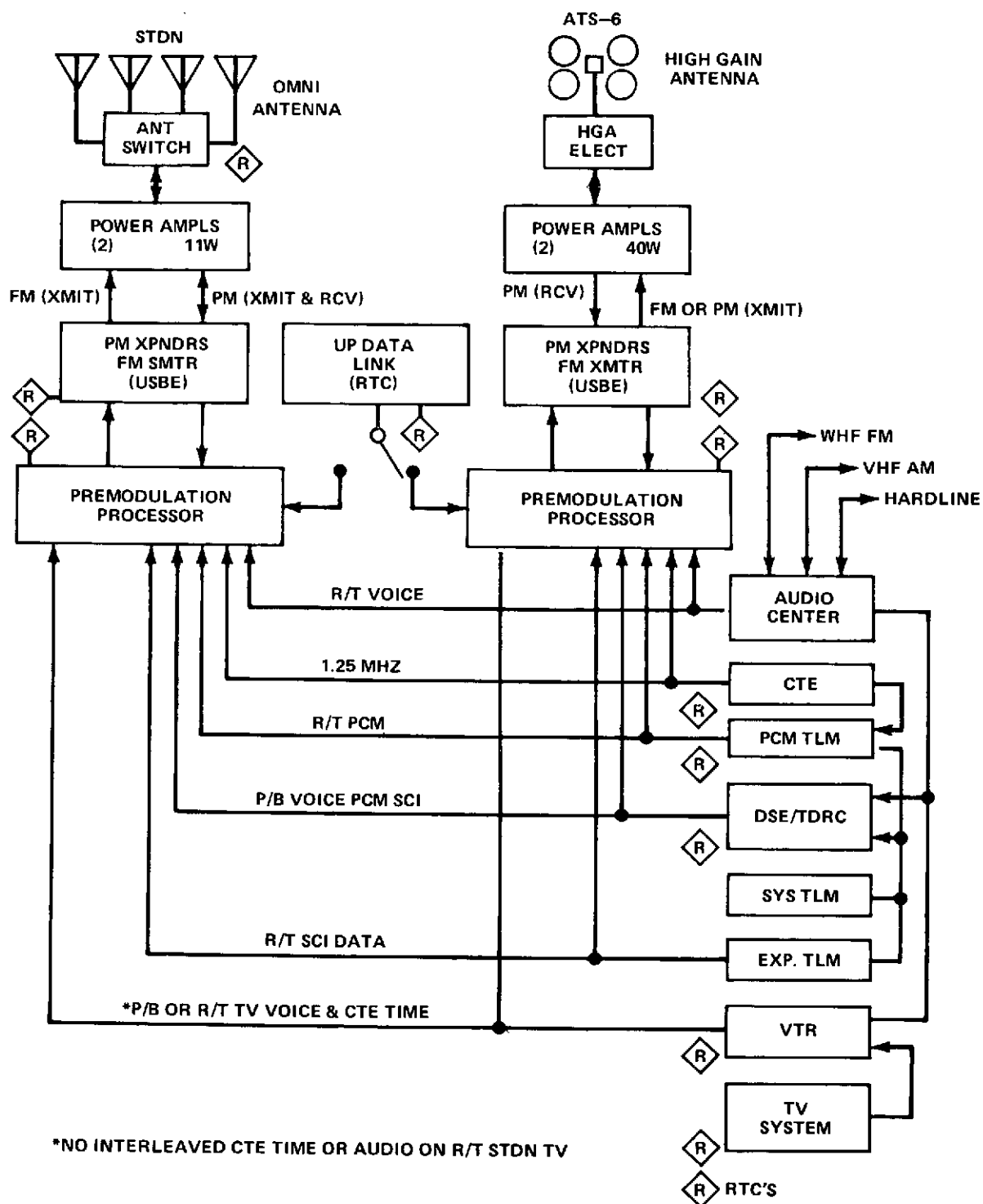
Figure 10-2. CSM to ATS-6 Communications Relay Equipment

c. CSM/ATS-6 Power Amplifiers

The CSM/ATS-6 relay subsystem will be furnished with two 40-watt
solid state, power amplifiers. These amplifiers can be used to transmit
either PM or FM to the ATS-6 satellite.

d. CSM/ATS-6 High Gain Antenna (HGA)

The CSM will have a modified Apollo type HGA mounted on the rear of
the service module. The associated electrical equipment is located in
the righthand equipment bay. The HGA can only be operated from onboard
and in either the manual slew mode, auto track mode, or reacquisition
(REACQ) mode. The HGA consists of four parabolic dishes, righthand
circular polarized. This provides for a narrow and a wide beam antenna
pattern. The wide beam pattern is approximately 40° at the 3 dB point.
The narrow beam is approximately 4° at the 3 dB point.

10.4 LINK CALCULATIONS

Tables 10-3 through 10-9 are the link calculations for the various modes of
operations.

10.5 TEST PROGRAM FOR PREPARATION OF EXPERIMENT SUPPORT

10.5.1 Test Descriptions

10.5.1.1 Johnson Space Center-ATS-6-Rosman Test (October 1974)

Configuration

The configuration for the first of the principle tests will be such that an engineering
prototype of the CSM (ATS-6 receivers, transmitters and high gain antenna) will
be situated at Johnson Space Center (JSC). These will be used to communicate
on both forward and reverse links at S-band to the ATS-6 satellite, pointed at JSC.

The satellite will be configured for S-band to C-band/C-band to S-band operation
and Rosman will use the ATS 85-ft antenna to-transmit and receive C-band signals
from ATS-6.

Rosman will be configured so that command and voice signals originate at the
Rosman I unified S-band (USB) complex and that telemetry, voice and video are
demodulated in the reverse link mode at the Rosman I USB complex.

Table 10-3
FM Link, Apollo to ATS-6 to ATS-6 97-Ft Ground Station,
Television Circuit Margin Summary (Modes R3 & R4)

APOLLO-TO-ATS-6

1.	Apollo power amplifier (PA) output (40 W min.)	+ 16 dBw	
2.	Insertion loss (PA to diplexer output)[1] (max.)	(-) 1.0 dB	
3.	Insertion loss (diplexer to HGA)[1] (max.)	(-) 1.3 dB	
4.	HGA pointing loss (max.)	(-) 0.2 dB	
5.	Apollo HGA gain (min.)	+ 25.7 dB	
6.	Apollo EIRP (min.)	+ 39.2 dBw	
7.	Space loss (R = 22000 n.m., f = 2256 MHz)	(-)191.8 dB	
8.	Polarization loss (1 dB RCP to 3 dB RCP) (max.)	(-) 0.3 dB	
9.	ATS-6 antenna pointing loss (included in gain)		
10.	ATS-6 antenna gain (3 dB FOV)	+ 36.3 dB	(39.3)*
11.	ATS-6 insertion loss[1] (included in gain)		
12.	Total received power	- 116.6 dBw	(-113.6)
13.	ATS-6 noise power	- 122.9 dBw	
	- Recr. IF NBW (40 MHz): 76.0 dB		
	- System temperature, T_s (940°K): 29.7 dB		
	- Boltzman constant (1.38 × 10^{-23}): -228.6 dBw		
14.	ATS-6 G/T: +6.6 dB, 3 dB FOV (9.6 on-axis)		
15.	ATS-6 IF signal-to-noise ratio (SNR) in 40 MHz	+ 6.3 dB	(9.3)
16.	IF SNR required in 40 MHz NBW	+ 7.5 dB	
17.	ATS-6 circuit margin (in 40 MHz)	- 1.2 dB	(+1.8)

ATS-6-TO-ATS-6 GROUND STATION

18.	ATS-6 transponder power output (12 W)	+ 10.8 dBw	
19.	Insertion loss[1]	(-) 1.3 dB	
20.	ATS-6 transmit antenna gain (13° × 20° FOV)[2]	+ 16.4 dB	
21.	ATS-6 antenna pointing loss (included in gain)		
22.	ATS-6 EIRP	+ 25.9 dBw	

[1] Insertion loss includes switches, cabling, VSWR mismatch losses, etc.

[2] For certain CSM orbits, the line-of-sight to the Madrid station could be such that the C-band horn antenna gain could be up to 6 dB lower than the value listed.

*Values given in parentheses are for ATS-6 antenna on-axis gain only and are applicable to the auto-track mode (but not the program-track mode).

Table 10-3 (Continued)

ATS-6-TO-ATS-6 GROUND STATION (Continued)		
23. Space loss (R = 22000 n. m. f = 3756 MHz)	(-)196. 2 dB	
24. Polarization loss (linear-to-linear)	(-) 0. 5 dB	
25. Receive antenna gain (97-ft dish) (3750 MHz) (min.)	+ 59. 4 dB	
26. Antenna pointing loss (included in gain)		
27. Insertion loss (included in gain)		
28. Total received power	- 111. 4 dBw	
- Signal only	- 112. 3 dBw	(-111. 9)
- Transmitted noise received in 40 MHz NBW	- 118. 6 dBw	(-121. 2)
- Transmitted noise received in 10 MHz NBW	- 124. 6 dBw	(-127. 2)
29. ATS-6 ground station IF noise power	- 140. 5 dBw	
- Recr. FM IF NBW (10 MHz): 70. 0 dB		
- System temperature, T_s (65°K): 18. 1 dB		
- Boltzmann's constant (1. 38 × 10^{-23}): -228. 6 dBw		
30. ATS-6 ground station G/T: 41. 3 dB at 3750 MHz		
31. Apparent IF signal-to-noise ratio (SNR) (in 10 MHz)	+ 29. 1 dB	
32. Transmitted SNR (in 10 MHz)	+ 12. 3 dB	(+15. 3)
33. ATS-6 SNR (relay) degradation	(-) 0 dB	
34. Actual IF SNR (in 10 MHz)	+ 12. 2 dB	(+15. 1)
35. ATS-6 ground station IF SNR required (in 10 MHz)	+ 12. 0 dB	
36. ATS-6 ground station IF circuit margin (in 10 MHz)	+ 0. 2 dB	(+3. 1)
37. ATS-6 ground station-to-STDN degradation	(-) 0 dB	
38. FM improvement[1]	+ 9. 1 dB	
39. Calculated TV postdetection SNR (rms/rms, equiv. sine wave)	+ 21. 3 dB	(24. 2)
40. Postdetection TV SNR required[2] (in 3. 1 MHz NBW)	+ 21. 0 dB	
41. Postdetection TV circuit margin	+ 0. 3 dB	(+3. 2)

[1] Based on a Δf = 4 MHz and a postdetection filter NBW of 3. 1 MHz.

[2] Based on a postdetection SNR of 30 db P-P/rms for Apollo-quality TV.

Table 10-4
FM Link, Apollo to ATS-6 to ATS-6 21-Ft Mobile Site,
Television Circuit Margin Summary

APOLLO-TO-ATS-6

1.	Apollo PA output (40 W min.)	+ 16.0 dBw
2.	Insertion loss (PA to diplexer output)[1] (max.)	(-) 1.0 dB
3.	Insertion loss (diplexer to HGA)[1] (max.)	(-) 1.3 dB
4.	HGA pointing loss (max.)	(-) 0.2 dB
5.	Apollo HGA gain (min.)	+ 25.7 dB
6.	Apollo EIRP (min.)	+ 39.2 dBw
7.	Space loss (R = 22000 n.m., f = 2256 MHz)	(-)191.8 dB
8.	Polarization loss (1 dB RCP to 3 dB RCP) (max.)	(-) 0.3 dB
9.	ATS-6 antenna pointing loss (included in gain)	
10.	ATS-6 antenna gain (3 dB FOV)	+ 36.3 dB (39.3)*
11.	ATS-6 insertion loss[1] (included in gain)	
12.	Total received power	- 116.6 dBw (-113.6)
13.	ATS-6 noise power	
	- Recr. IF NBW (40 MHz): 76.0 dB	
	- System temperature, T_s (940°K): 29.7 dB	
	- Boltzman constant (1.38 × 10^{-23}): -228.6 dBw	
14.	ATS-6 G/T: +6.6 dB, 3 dB FOV (9.6 on-axis)	
15.	ATS-6 IF SNR in 40 MHz	+ 6.3 dB (9.3)
16.	IF SNR required in 40 MHz NBW	+ 7.5 dB
17.	ATS-6 circuit margin (in 40 MHz)	- 1.2 dB (+1.8)

ATS-6-TO-MOBILE SITE

18.	ATS-6 transponder power output (12 W)	+ 10.8 dBw
19.	Insertion loss[1]	(-) 1.3 dB
20.	ATS-6 transmit antenna gain (13° × 20° FOV)[2]	+ 16.4 dB
21.	ATS-6 antenna pointing loss (included in gain)	
22.	ATS-6 EIRP	+ 25.9 dBw

[1] Insertion loss includes switches, cabling, VSWR mismatch losses, etc.

[2] For certain CSM orbits, the line-of-sight to the Madrid station could be such that the C-band horn antenna gain could be up to 6 dB lower than the value listed.

*Values given in parentheses are for ATS-6 antenna on-axis gain only and are applicable to the auto-track mode (but not the program-track mode).

Table 10-4 (Continued)

ATS-6-TO-MOBILE SITE (Continued)

23.	Space loss (R = 22000 n. m. f = 3756 MHz)	(-)196. 2 dB
24.	Polarization loss (linear-to-linear) (max.)	(-) 0. 5 dB
25.	Receive antenna gain (21-ft dish) (3750 MHz)	+ 44. 8 dB
26.	Antenna pointing loss (included in gain)	
27.	Insertion loss (included in gain)	
28.	Total received power	- 126. 0 dBw
29.	Mobile site IF noise power (21-ft dish)	- 138.6 dBw
	– Recr. FM IF NBW (10 MHz): 70. 0 dB	
	– System temperature, T_s (100°K): 20. 0 dB	
	– Boltzman constant (1. 38 × 10^{-23}): -228.6 dBw	
30.	Mobile site G/T: 24. 8 dB (min.)	
31.	Apparent IF SNR (in 10 MHz)	+ 12. 6 dB
32.	Transmitted SNR (in 10 MHz)	+ 12. 3 dB (15. 3)
33.	ATS-6 SNR (relay) degradation	(-) 0 dB
34.	Actual IF SNR (in 10 MHz)	+ 9. 0 dB (10. 4)
35.	Site IF SNR required (in 10 MHz)	+ 12. 0 dB
36.	Site IF circuit margin (in 10 MHz)	– 3. 0 dB (-1. 6)
37.	Mobile site-to-STDN degradation	(-) 0 dB
38.	FM improvement[1]	+ 9. 0 dB (9. 1)
39.	Calculated TV postdetection SNR (rms/rms, equiv. sine wave)	+ 18. 0 dB (19. 5)
40.	Postdetection TV SNR required [2] (in 3. 1 MHz NBW)	+ 21. 0 dB
41.	Postdetection TV circuit margin	– 3. 0 dB (-1. 5)

[1] Based on a Δf = 4 MHz and a postdetection filter NBW of 3. 1 MHz.

[2] Based on a postdetection SNR of 30 dB P-P/rms for Apollo-quality TV.

Table 10-5
FM Link, Apollo to ATS-6 to ATS-6 21-Ft Mobile Site,
Circuit Margin Summary for FM Voice, TLM, and Experiment Data
(Real-Time and Playback, ** Mode R5)

APOLLO-TO-ATS-6

1.	Apollo PA output (40 W min.)	+ 16. 0 dBw	
2.	Insertion loss (PA to diplexer output)[1] (max.)	(-) 1. 0 dB	
3.	Insertion loss (diplexer to HGA)[1] (max.)	(-) 1. 3 dB	
4.	HGA pointing loss (max.)	(-) 0. 2 dB	
5.	Apollo HGA gain (min.)	+ 25. 7 dB	
6.	Apollo EIRP (min.)	+ 39. 2 dBw	
7.	Space loss (R = 22000 n. m. , f = 2256 MHz)	(-)191. 8 dB	
8.	Polarization loss (1 dB RCP to 3 dB RCP) (max.)	(-) 0. 3 dB	
9.	ATS-6 antenna pointing loss (included in gain)		
10.	ATS-6 antenna gain (3 dB FOV)	+ 36. 3 dB	(39. 3)*
11.	ATS-6 insertion loss [1] (included in gain)		
12.	Total received power	- 116. 6 dBw	(-113. 6)
13.	ATS-6 noise power	- 122. 9 dBw	
	- Recr. IF NBW (40 MHz): 76. 0 dB		
	- System temperature, T_s (940°K): 29. 7 dB		
	- Boltzman constant (1. 38 × 10^{-23}): -228. 6 dBw		
14.	ATS-6 G/T: +6. 6 dB, 3 dB FOV (9. 6 on-axis)		
15.	ATS-6 IF SNR in 40 MHz	+ 6. 3 dB	(9. 3)
16.	IF SNR required in 40 MHz NBW	+ 1. 6 dB	
17.	ATS-6 circuit margin (in 40 MHz)	+ 4. 7 db	(+7. 7)

ATS-6-TO-MOBILE SITE

18.	ATS-6 transponder power output (12 W)	+ 10. 8 dBw	
19.	Insertion loss [1]	(-) 1. 3 dB	

[1] Insertion loss includes switches, cabling, VSWR mismatch losses, etc.

*Values given in parentheses are for ATS-6 antenna on-axis gain only, and are applicable to the auto-track mode (but not the program-track mode).

**Calculations are identical for the real-time-only FM voice and experiment data mode (Mode R6).

Table 10-5 (Continued)

	ATS-6-TO-MOBILE SITE (Continued)	
20.	ATS-6 transmit antenna gain (13° × 20° FOV)[2]	+ 16.4 dB
21.	ATS-6 antenna pointing loss (included in gain)	
22.	ATS-6 EIRP	+ 25.9 dBw
23.	Space loss (R = 22000 n.m., f = 3756 MHz)	(-)196.2 dB
24.	Polarization loss (linear-to-linear) (max.)	(-) 0.5 dB
25.	Receive antenna gain (21-ft dish) (3750 MHz)	+ 44.8 dB
26.	Antenna pointing loss (included in gain)	
27.	Insertion loss (included in gain)	
28.	Total received power	- 126.0 dBw
29.	Mobile site IF noise power (21-ft dish)	- 141.8 dBw
	- Recr. FM IF NBW (4.8 MHz): 66.8 dB	
	- System temperature, T_s (100°K): 20.0 dB	
	- Boltzman constant (1.38 × 10^{-23}): -228.6 dBw	
30.	Mobile site G/T: 24.8 dB (min.)	
31.	Apparent IF SNR (in 4.8 MHz)	+ 15.8 dB
32.	Transmitted SNR (in 4.8 MHz)	+ 15.4 dB (18.4)
33.	ATS-6 SNR (relay) degradation	(-) 0 dB
34.	Actual IF SNR (in 4.8 MHz)	+ 12.2 dB (13.6)
35.	Site IF SNR required	+ 8.0 dB
36.	Site IF circuit margin	+ 4.2 dB (5.6)

[1] Insertion loss includes switches, cabling, VSWR mismatch losses, etc.

[2] For certain CSM orbits, the line-of-sight to the Madrid station could be such that the C-band horn antenna gain could be up to 6 dB lower than the value.

**Calculations are identical for the real-time-only FM voice and experiment data mode (Mode R6).

Table 10-6
PM Link, Apollo to ATS-6 to ATS-6 21-Ft Mobile Site,
Voice & HBR Telemetry Circuit Margin Summary (Mode R1)

APOLLO-TO-ATS-6

1.	Apollo PA output (40 min.)	+ 16 dBw	
2.	Insertion loss (PA to diplexer output)[1] (max.)	(-) 1.0 dB	
3.	Insertion loss (diplexer to HGA)[1] (max.)	(-) 1.3 dB	
4.	HGA pointing loss (max.)	(-) 0.2 dB	
5.	Apollo HGA gain (min.)	+ 25.7 dB	
6.	Apollo EIRP (min.)	+ 39.2 dBw	
7.	Space loss (R = 22000 n.m. , f = 2256 MHz)	(-)191.8 dB	
8.	Polarization loss (1 dB RCP to 3 dB RCP) (max.)	(-) 0.3 dB	
9.	ATS-6 antenna pointing loss (included in gain)		
10.	ATS-6 antenna gain (3 dB FOV)	+ 36.3 dB	(39.3)*
11.	ATS-6 insertion loss[1] (included in gain)		
12.	Total received power	- 116.6 dBw	(-113.6)
13.	ATS-6 noise power	- 122.9 dBw	
	- Recr. IF NBW (40 MHz): 76.0 dB		
	- System temperature, T_s (940°K): 29.7 dB		
	- Boltzman constant (1.38 $\times 10^{-23}$): -228.6 dBw		
14.	ATS-6 G/T: +6.6 dB, 3 dB FOV (9.6 on-axis)		
15.	ATS-6 IF SNR in 40 MHz	+ 6.3 dB	(9.3)
16.	IF SNR required in 40 MHz NBW	+ 0 dB	
17.	ATS-6 circuit margin (in 40 MHz)	+ 6.3 dB	(+9.3)

ATS-6-TO-MOBILE SITE

18.	ATS-6 transmitter power output (12 W)	+ 10.8 dBw
19.	Insertion loss[1]	(-) 1.3 dB
20.	ATS-6 transmit antenna gain (13° × 20° FOV)	+ 16.4 dB
21.	ATS-6 antenna pointing loss (included in gain)	
22.	ATS-6 EIRP	+ 25.9 dBw

[1] Insertion loss includes switches, cabling, VSWR mismatch losses, etc.

*Values given in parentheses are for ATS-6 antenna on-axis gain only, and are
applicable to the auto-track mode (but not the program-track mode).

Table 10-6 (Continued)

ATS-6-TO-MOBILE SITE (Continued)

23.	Space loss (R = 22000 n. m. , f = 3756 MHz)	(-)196. 2 dB
24.	Polarization loss (linear-to-linear) (max.)	(-) 0. 5 dB
25.	Receive antenna gain (21-ft dish) (3750 MHz)	+ 44. 8 dB
26.	Antenna pointing loss (included in gain)	
27.	Insertion loss (included in gain)	
28.	Total received power	- 126. 0 dBw
29.	Mobile site IF noise power (21-ft dish)	- 141. 8 dBw
	- Recr. PM IF NBW (4. 8 MHz): 66. 8 dB	
	- System temperature, T_s (100°K): 20. 0 dB	
	- Boltzman constant (1. 38 $\times 10^{-23}$): -228. 6 dBw	
30.	Mobile site G/T: 24. 8 dB (min.)	
31.	Apparent IF SNR (in 4. 8 MHz)	+ 15. 8 dB
32.	Transmitted SNR (in 4. 8 MHz)	+ 15. 4 dB (18. 4)
33.	ATS-6 SNR (relay) degradation	(-) 0 dB
34.	Actual IF SNR (in 4. 8 MHz)	+ 12. 2 dB (13. 6)

HBR TELEMETRY (MODE 1: HBR TM & VOICE)

35.	Total received power (line 28)	- 126. 0 dBw
	- Signal only [1]	- 126. 9 dBw (126. 5)
	- Transmitted noise [1] received in 4. 8 MHz NBW	- 142. 4 dBw (-145. 0)
	- Transmitted noise received in 180 KHz NBW	- 156. 7 dBw (-159. 2)
36.	Telemetry modulation loss (β_{TM} = 0. 94, β_V = 0. 7)	5. 6 dB
37.	Telemetry subcarrier power	- 132. 5 dBw (-132. 1)
38.	Telemetry subcarrier predetection NBW (180 KHz)	52. 6 dB
39.	Mobile site noise (internal) in 180 KHz NBW	- 156. 0 dBw
40.	Total noise power in 180 KHz NBW	- 153. 3 dBw (-154. 3)

[1] The signal transmitted from ATS-6 consists of signal plus the noise in the
ATS-6 IF; the TRP received at the ground (line 28) has been separated into
the signal-only and noise-only components.

Table 10-6 (Continued)

HBR TELEMETRY (MODE 1: HBR TM & VOICE) (Continued)

41.	TM subcarrier predetection SNR	+ 20. 8 dB	(22. 6)
42.	TM subcarrier predetection SNR required (10^{-6} BER)	+ 8. 0 dB	
43.	Mobile-site-to-STDN degradation	(-) 0. 0 dB	
44.	HBR TM circuit margin (Mode 1)	+ 12. 8 dB	(14. 6)

PM VOICE (MODE 1: HBR TM & VOICE)

35.	Total received power (line 28)	- 126. 0 dBw	
	- Signal only [1]	- 126. 9 dBw	(-126. 5)
	- Transmitted noise [1] received in 4. 8 MHz NBW	- 142. 4 dBw	(-145. 0)
	- Transmitted noise received in 24 KHz NBW	- 165. 4 dBw	(-168. 0)
36.	Voice modulation loss (β_{TM} = 0. 94, β_V = 0. 7)	8. 7 dB	
37.	Voice subcarrier power	- 135. 6 dBw	(-135. 2)
38.	Voice subcarrier predetection NBW (24 KHz)	43. 8 dB	
39.	Mobile site noise (internal) in 24 KHz NBW	- 164. 8 dBw	
40.	Total noise power in 24 KHz NBW	- 162. 1 dBw	(-163. 1)
41.	Voice subcarrier predetection SNR	+ 26. 5 dB	(27. 9)
42.	Voice subcarrier predetection SNR required (90% WI)	+ 8. 0 dB	
43.	Mobile-site-to-STDN degradation	(-) 0. 0 dB	
44.	PM Voice circuit margin (Mode 1)	+ 18. 5 dB	(19. 9)

PM CARRIER (MODE 1: HBR TM & VOICE)

35.	Total received power (line 28)	- 126. 0 dBw	
	- Signal only [1]	- 126. 9 dBw	(-126. 5)
	- Transmitted noise [1] received in 4. 8 MHz NBW	- 142. 4 dBw	(-145. 0)
	- Transmitted noise received in 700 Hz NBW	- 180. 8 dBw	(-183. 3)
36.	Carrier modulation loss (β_{TM} = 0. 94, β_V = 0. 7)	3. 1 dB	

[1] The signal transmitted from ATS-6 consists of signal plus the noise in the ATS-6 IF; the TRP received at the ground (line 28) has been separated into the signal-only and noise-only components.

Table 10-6 (Continued)

PM CARRIER (MODE 1: HBR TM & VOICE) (Continued)

37.	Carrier power	− 130. 0 dBw (−129. 6)
38.	Carrier loop NBW (700 Hz)	28. 5 dBw
39.	Mobile site noise (internal) in 700 Hz NBW	− 180. 1 dBw
40.	Total noise power in 700 Hz NBW	− 177. 4 dBw (−178. 4)
41.	Carrier predetection SNR	+ 47. 4 dB (48. 9)
42.	Carrier predetection SNR required	+ 12. 0 dB
43.	Mobile-site-to-STDN degradation	(−) 0. 0 dB
44.	Carrier circuit margin (Mode 1)	+ 35. 4 dB (36. 9)

Table 10-7
PM Link, Apollo to ATS-6 to ATS-6 21-Ft Mobile Site,
Voice & LBR Telemetry Circuit Margin Summary (Mode R2)

APOLLO-TO-ATS-6

1.	Apollo PA output (40 W min.)	+ 16 dBw	
2.	Insertion loss (PA to diplexer output)[1] (max.)	(-) 1.0 dB	
3.	Insertion loss (diplexer to HGA)[1] (max.)	(-) 1.3 dB	
4.	HGA pointing loss (max.)	(-) 0.2 dB	
5.	Apollo HGA gain (min.)	+ 25.7 dB	
6.	Apollo EIRP (min.)	+ 39.2 dBw	
7.	Space loss (R = 22000 n.m., f = 2256 MHz)	(-)191.8 dB	
8.	Polarization loss (1 dB RCP to 3 dB RCP)	(-) 0.3 dB	
9.	ATS-6 antenna pointing loss (included in gain)		
10.	ATS-6 antenna gain (3 dB FOV)	+ 36.3 dB	(39.3)*
11.	ATS-6 insertion loss[1] (included in gain)		
12.	Total received power	- 116.6 dBw	(-113.6)
13.	ATS-6 noise power	- 122.9 dBw	

- Recr. IF NBW (40 MHz): 76.0 dB
- System temperature, T_s (940°K): 29.7 dB
- Boltzman constant (1.38 $\times 10^{-23}$): -228.6 dBw

14.	ATS-6 G/T: +6.6 dB, 3 dB FOV (9.6 on-axis)		
15.	ATS-6 IF signal-to-noise ratio (SNR) in 40 MHz	+ 6.3 dB	(9.3)
16.	IF SNR required in 40 MHz NBW	+ 0	
17.	ATS-6 circuit margin (in 40 MHz)	+ 6.3 dB	(9.3)

ATS-6-TO-MOBILE SITE

18.	ATS-6 transmitter power output (12 W)	+ 10.8 dBw
19.	Insertion loss[1]	(-) 1.3 dB
20.	ATS-6 transmit antenna gain (13° × 20° FOV)	+ 16.4 dB
21.	ATS-6 antenna pointing loss (included in gain)	
22.	ATS-6 EIRP	+ 25.9 dBw

[1] Insertion loss includes switches, cabling, VSWR mismatch losses, etc.

*Values given in parentheses are for ATS-6 antenna on-axis gain only, and
are applicable to the auto-track mode (but not the program-track mode).

Table 10-7 (Continued)

ATS-6-TO-MOBILE SITE (Continued)

23.	Space loss (R = 22000 n. m. , f = 3756 MHz)	(-)196. 2 dB
24.	Polarization loss (linear-to-linear) (max.)	(-) 0. 5 dB
25.	Receive antenna gain (21-ft dish) (3750 MHz)	+ 44. 8 dB
26.	Antenna pointing loss (included in gain)	
27.	Insertion loss (included in gain)	
28.	Total received power	- 126. 0 dBw
29.	Mobile site IF noise power (21-ft dish)	- 141. 8 dBw
	- Recr. PM IF NBW (4. 8 MHz): 66. 8 dB	
	- System temperature, T_s (100°K): 20. 0 dB	
	- Boltzman constant (1. 38 × 10^{-23}): -228. 6 dBw	
30.	Mobile site G/T: 24. 8 dB (min.)	
31.	Apparent IF SNR (in 4. 8 MHz)	+ 15. 8 dB
32.	Transmitted SNR (in 4. 8 MHz)	+ 15. 4 dB (18. 4)
33.	ATS-6 SNR (relay) degradation	(-) 0 dB
34.	Actual IF SNR (in 4. 8 MHz)	+ 12. 2 dB (13. 6)

LBR TELEMETRY (MODE 2: LBR TM & VOICE)

35.	Total received power (line 28)	- 126. 0 dBw
	- Signal only[1]	- 126. 9 dBw (-126. 5)
	- Transmitted noise[1] received in 4. 8 MHz NBW	- 142. 4 dBw (-145. 0)
	- Transmitted noise received in 7250 Hz NBW	- 170. 6 dBw (-173. 2)
36.	Telemetry modulation loss (β_{TM} = 0. 7, β_V = 1. 2)	10. 1 dB
37.	Telemetry subcarrier power	- 137. 0 dBw (-136. 6)
38.	Telemetry subcarrier predetection NBW (7250 Hz)	38. 6 dB
39.	Mobile site noise (internal) in 7250 Hz NBW	- 170. 0 dBw
40.	Total noise power in 7250 Hz NBW	- 167. 3 dBw (-168. 3)
41.	TM subcarrier predetection SNR	+ 30. 3 dB (31. 7)
42.	TM subcarrier predetection SNR required (10^{-6} BER)	+ 5. 9 dB

[1] The signal transmitted from ATS-6 consists of signal plus the noise in the ATS-6 IF; the TRP received at the ground (line 28) has been separated into the signal-only and noise-only components.

Table 10-7 (Continued)

LBR TELEMETRY (MODE 2: LBR TM & VOICE) (Continued)

43.	Mobile site-to-STDN degradation	(-) 0. 0 dB	
44.	LBR TM circuit margin (Mode 2)	+ 24. 4 dB	(25. 8)

PM VOICE (MODE 2: LBR TM & VOICE)

35.	Total received power (line 28)	− 126. 0 dBw	
	− Signal only[1]	− 126. 9 dBw	(−126. 5)
	− Transmitted noise[1] received in 4. 8 MHz NBW	− 142. 4 dBw	(−145. 0)
	− Transmitted noise received in 24 KHz NBW	− 165. 4 dBw	(−168. 0)
36.	Voice modulation loss ($\beta_{TM}= 0.7$, $\beta_V = 1.2$)	4. 1 dB	
37.	Voice subcarrier power	− 131. 0 dBw	(−130. 6)
38.	Voice subcarrier predetection NBW (24 KHz)	− 43. 8 dB	
39.	Mobile site noise (internal) in 24 KHz NBW	− 164. 8 dBw	
40.	Total noise power in 24 KHz NBW	− 162. 1 dBw	(−163. 1)
41.	Voice subcarrier predetection SNR	+ 31. 1 dB	(32. 5)
42.	Voice subcarrier predetection SNR required (90% WI)	+ 8. 0 dB	
43.	Mobile-site-to-STDN degradation	(-) 0. 0 dB	
44.	PM voice circuit margin (Mode 2)	+ 23. 1 dB	(24. 5)

PM CARRIER (MODE 2: LBR TM & VOICE)

35.	Total received power (line 28)	− 126. 0 dBw	
	− Signal only[1]	− 126. 9 dBw	(−126. 5)
	− Transmitted noise[1] received in 4. 8 MHz NBW	− 142. 4 dBw	(−145. 0)
	− Transmitted noise received in 700 Hz NBW	− 180. 8 dBw	(−183. 3)
36.	Carrier modulation loss ($\beta_{TM}= 0.7$, $\beta_V = 1.2$)	4. 6 dB	
37.	Carrier power	− 131. 5 dBw	(−131. 1)
38.	Carrier loop NBW (700 Hz)	28. 5 dB	
39.	Mobile site noise (internal) in 700 Hz NBW	− 180. 1 dBw	
40.	Total noise power in 700 Hz NBW	− 177. 4 dBw	(−178. 4)
41.	Carrier predetection SNR	+ 45. 9 dB	(47. 4)
42.	Carrier predetection SNR required	+ 12. 0 dB	
43.	Mobile-site-to-STDN degradation	(-) 0. 0 dB	
44.	Carrier circuit margin (Mode 2)	+ 33. 9 dB	(35. 4)

[1] The signal transmitted from ATS-6 consists of signal plus the noise in the ATS-6 IF; the TRP received at the ground (line 28) has been separated into the signal-only and noise-only components.

Table 10-8
ATS-6 21-Ft Mobile Site to ATS-6 to Apollo,
Upvoice Circuit Margin Summary (Mode F1)*

MOBILE SITE-TO-ATS-6

1.	Mobile site transmitter power output (2 kW)	+ 33.0 dBw
2.	Insertion loss[1] (max.)	(-) 2.0 dB
3.	Mobile site transmit antenna gain (21-ft dish) (min.)	+ 48.9 dB
4.	Mobile site antenna pointing loss (included in gain)	
5.	Mobile site EIRP (min.)	+ 79.9 dBw
6.	Space loss (R = 22000 n.m., f = 5952.4 MHz)	(-)200.2 dB
7.	Polarization loss (linear-to-linear) (max.)	(-) 0.5 dB
8.	ATS-6 antenna pointing loss (included in gain)	
9.	ATS-6 receive antenna gain (20° × 20° FOV)	+ 13.4 dB
10.	ATS-6 insertion loss[1]	(-) 0.6 dB
11.	Total received power	(-)107.9 dBw
12.	ATS-6 noise power	- 120.4 dBw
	- Recr. IF NBW (40 MHz): 76.0 dB	
	- System temperature, T_s (1650°K): 32.2 dB	
	- Boltzman constant (1.38 × 10^{-23}): -228.6 dBw	
13.	ATS-6 G/T: -19.4 dB	
14.	ATS-6 IF signal-to-noise ratio (SNR) in 40 MHz	+ 12.5 dB
15.	IF SNR required	+ 0.0 dB
16.	ATS-6 circuit margin (in 40 MHz)	+ 12.5 dB

ATS-6-TO-APOLLO

17.	ATS-6 transmitter power output (13.8 W)	+ 11.4 dBw
18.	Insertion loss[1] (included in antenna gain)	
19.	ATS-6 transmit antenna gain (3 dB FOV)	+ 36.7 dB
20.	ATS-6 antenna pointing loss (included in gain)	
21.	ATS-6 EIRP (3 dB FOV)	+ 48.1 dBw
22.	Space loss (R = 22000 n.m., f = 2077.4 MHz)	(-)191.0 dB
23.	Polarization loss (3 dB RCP to 2 dB RCP) (max.)	(-) 0.3 dB
24.	HGA receive gain (narrow beamwidth) (min.)	+ 23.0 dB
25.	HGA pointing loss (max.)	(-) 0.2 dB
26.	Insertion loss[1] (max.)	(-) 7.6 dB
27.	Total received power (at recr. input) (min.)	- 128.0 dBw

[1] Insertion loss includes switches, cabling, VSWR mismatch losses, etc.

*Mode F3, updata (only), circuit margin calculation is identical (mod index, bandwidths, etc., are all the same).

Table 10-8 (Continued)

ATS-6-TO-APOLLO (Continued)

28.	Apollo IF noise power (max.)		− 127.2 dBw
	− Recr. IF NBW (4.6 MHz):	66.6 dB	
	− System temperature, T_s (3020°K):	34.8 dB	
	− Boltzman constant (1.38 × 10^-23):	−228.6 dBw	
29.	Apollo G/T: −19.6 dB (min.)		
30.	Apparent IF SNR		− 0.8 dB
31.	Transmitted SNR (in 4.6 MHz)		+ 21.9 dB
32.	Actual IF SNR (in 4.6 MHz)		− 1.1 dB

VOICE (MODE 1: VOICE-ONLY)

35.	Total received power (line 27)	− 128.0 dBw
	− Signal only[1]	− 128.2 dBw
	− Transmitted noise[1] received in 4.6 MHz NBW	− 150.1 dBw
	− Transmitted noise received in 22 kHz NBW	− 173.3 dBw
36.	Voice modulation loss (β_V = 1.1)	3.5 dB
37.	Voice subcarrier power	− 131.7 dBw
38.	Voice subcarrier predetection NBW (22 KHz)	43.4 dB
39.	CSM noise (internal) in 22 kHz NBW	− 150.4 dBw
40.	Total noise power in 22 kHz NBW	− 150.4 dBw
41.	Voice subcarrier predetection SNR	+ 18.7 dB
42.	Voice subcarrier predetection SNR required (90% WI)	+ 10.0 dB
43.	Voice circuit margin (Mode 1)	+ 8.7 dB

CARRIER (MODE 1: VOICE-ONLY)

35.	Total received power (line 27)	− 128.0 dBw
	− Signal only[1]	− 128.2 dBw
	− Transmitted noise[1] received in 4.6 MHz NBW	− 150.1 dBw
	− Transmitted noise received in 800 Hz NBW	− 187.7 dBw
36.	Carrier modulation loss (β_V = 1.1)	2.9 dB
37.	Carrier power	− 131.1 dBw
38.	Carrier loop NBW (800 Hz)	29.0 dB
39.	CSM noise (internal) in 800 Hz NBW	− 164.8 dBw

[1] The signal transmitted from ATS-6 consists of signal plus the noise in the ATS-6; the TRP (line 27) has been separated into the signal-only and noise-only components.

Table 10-8 (Continued)

CARRIER (MODE 1: VOICE-ONLY) (Continued)

40.	Total noise power in 800 Hz NBW	– 164.8 dBw
41.	Carrier predetection SNR	+ 33.7 dB
42.	Carrier predetection SNR required	+ 12.0 dB
43.	Carrier circuit margin (Mode 1)	+ 21.7 dB

ACQUISITION SNR

35.	Total received power[1]	– 147.7 dBw
	– Signal only	– 147.9 dBw
	—Transmitted noise received in 4.6 MHz NBW	– 169.8 dBw
	– Transmitted noise received in 800 Hz NBW	– 207.4 dBw
36.	CSM noise (internal) in 800 Hz NBW	– 164.8 dBw
37.	Total noise power in 800 Hz NBW	– 164.8 dBw
38.	Carrier predetection SNR (unmodulated carrier)	+ 16.9 dBw
39.	Carrier predetection SNR required	+ 12.0 dB
40.	ACQUISITION circuit margin	+ 4.9 dB

[1] CSM HGA wide beamwidth, 3.1 dB gain, no pointing loss.

Table 10-9
ATS-6 21-Ft Mobile Site to ATS-6 to Apollo,
Upvoice & Updata Circuit Margin Summary (Mode F2)

MOBILE SITE-TO-ATS-6

1.	Mobile site transmitter power output (2 kW)	+ 33. 0 dBw
2.	Insertion loss [1] (max.)	(-) 2. 0 dB
3.	Mobile site transmit antenna gain (21-ft dish)	+ 48. 9 dB
4.	Mobile site antenna pointing loss (included in gain)	
5.	Mobile site EIRP (min.)	+ 79. 9 dBw
6.	Space loss (R = 22000 n. m. , f = 5952. 4 MHz)	(-)200. 2 dB
7.	Polarization loss (linear-to-linear) (max.)	(-) 0. 5 dB
8.	ATS-6 antenna pointing loss (included in gain)	
9.	ATS-6 receive antenna gain (20° × 20° FOV)	+ 13. 4 dB
10.	ATS-6 insertion loss[1]	(-) 0. 6 dB
11.	Total received power	(-)107. 9 dBw
12.	ATS-6 noise power	- 120. 4 dBw
	- Recr. IF NBW (40 MHz): 76. 0 dB	
	- System temperature, T_s (1650°K): 32. 2 dB	
	- Boltzman constant (1. 38 × 10^{-23}): -228. 6 dBw	
13.	ATS-6 G/T: -19. 4 dB	
14.	ATS-6 IF signal-to-noise ratio (SNR) in 40 MHz	+ 12. 5 dB
15.	IF SNR required	+ 0. 0 dB
16.	ATS-6 circuit margin (in 40 MHz)	+ 12. 5 dB

ATS-6-TO-APOLLO

17.	ATS-6 transmitter power output (13. 8 W)	+ 11. 4 dBw
18.	Insertion loss [1] (included in antenna gain)	
19.	ATS-6 transmit antenna gain (3 dB FOV)	+ 36. 7 dB
20.	ATS-6 antenna pointing loss (included in gain)	
21.	ATS-6 EIRP (3 dB FOV)	+ 48. 1 dBw
22.	Space loss (R = 22000 n. m. , f = 2077. 4 MHz)	(-)191. 0 dB
23.	Polarization loss (3 dB RCP to 2 dB RCP) (max.)	(-) 0. 3 dB
24.	HGA receive gain (narrow beamwidth) (min.)	+ 23. 0 dB
25.	HGA pointing loss (max.)	(-) 0. 2 dB
26.	Insertion loss [1] (max.)	(-) 7. 6 dB
27.	Total received power (at recr. input) (min.)	- 128. 0 dBw

[1] Insertion loss included switches, cabling, VSWR mismatch losses, etc.

Table 10-9 (Continued)

ATS-6-TO-APOLLO (Continued)

28.	Apollo IF noise power (max.)	$-$ 127. 2 dBw
	- Recr. IF NBW (4. 6 MHz): 66. 6 dB	
	- System temperature, T_s (3020°K): 34. 8 dB	
	- Boltzman constant (1. 38 $\times$ 10^{-23}): -228.6 dBw	
29.	Apollo G/T: -19.6 dB (min.)	
30.	Apparent IF SNR	$-$ 0. 8 dB
31.	Transmitted SNR (in 4.6 MHz)	$+$ 21. 9 dB
32.	Actual IF SNR (in 4. 6 MHz)	$-$ 1. 1 dB

VOICE (MODE 2: VOICE AND UPDATA)

35.	Total received power (line 27)	$-$ 128. 0 dBw
	- Signal only [1]	$-$ 128. 2 dBw
	- Transmitted noise [1] received in 4. 6 MHz NBW	$-$ 150. 1 dBw
	- Transmitted noise received in 22 KHz NBW	$-$ 173. 3 dBw
36.	Voice modulation loss (β_{UD}= 1. 1, β_V = 1. 1)	6. 4 dB
37.	Voice subcarrier power	$-$ 134. 6 dBw
38.	Voice subcarrier predetection NBW (22 KHz)	43. 4 dB
39.	CSM noise (internal) in 22 KHz NBW	$-$ 150. 4 dBw
40.	Total noise power in 22 KHz NBW	$-$ 150. 4 dBw
41.	Voice subcarrier predetection SNR	$+$ 15. 8 dB
42.	Voice subcarrier predetection SNR required (90% WI)	$+$ 10. 0 dB
43.	VOICE circuit margin (Mode 2)	$+$ 5. 8 dB

UPDATA (MODE 2: VOICE AND UPDATA)

35.	Total received power (line 27)	$-$ 128. 0 dBw
	- Signal only [1]	$-$ 128. 2 dBw
	- Transmitted noise [1] received in 4. 6 MHz NBW	$-$ 150. 1 dBw
	- Transmitted noise received in 22 KHz NBW	$-$ 173. 3 dBw
36.	Updata modulation loss (β_{UD}= 1. 1, β_V = 1. 1)	6. 4 dB
37.	Updata subcarrier power	$-$ 134. 6 dBw
38.	Updata subcarrier predetection NBW (22 KHz)	43. 4 dB
39.	CSM noise (internal) in 22 KHz NBW	$-$ 150. 4 dBw
40.	Total noise power in 22 KHz NBW	$-$ 150. 4 dBw
41.	Updata subcarrier predetection SNR	$+$ 15. 8 dB
42.	Updata subcarrier predetection SNR required	$+$ 10. 0 dB
43.	Updata circuit margin (Mode 2)	$+$ 5. 8 dB

[1] The signal transmitted from ATS-6 consists of signal plus the noise in the ATS-6 IF; the TRP (line 27) has been separated into the signal-only and noise-only components.

Table 10-9 (Continued)

CARRIER (MODE 2: VOICE AND UPDATA)		
35.	Total received power (line 27)	– 128. 0 dBw
	– Signal only [1]	– 128. 2 dBw
	– Transmitted noise [1] received in 4.6 MHz NBW	– 150. 1 dBw
	– Transmitted noise received in 800 Hz NBW	– 187. 7 dBw
36.	Carrier modulation loss ($\beta_{UD} = 1.1$, $\beta_V = 1.1$)	5. 7 dB
37.	Carrier power	– 133. 9 dBw
38.	Carrier loop NBW (800 Hz)	29. 0 dB
39.	CSM noise (internal) in 800 Hz NBW	– 164. 8 dBw
40.	Total noise power in 800 Hz NBW	– 164. 8 dBw
41.	Carrier predetection SNR	+ 30. 9 dB
42.	Carrier predetection SNR required	+ 12. 0 dB
43.	Carrier circuit margin (Mode 2)	+ 18. 9 dB

(NOTE: Acquisition circuit margin is calculated on the Mode F1 Sheets.)

[1] The signal transmitted from ATS-6 consists of signal plus the noise in the ATS-6 IF; the TRP (line 27) has been separated into the signal-only and noise-only components.

Common carrier lines are to be provided to transfer received demodulated signals from the Rosman I site back to JSC for evaluation.

The returned video signal will be color converted at JSC from field sequential TV to the National Television Standards Committee format.

Objectives

The objectives of this test and those performed in preparation for this test are:

1. To verify that the CSM modified high-gain antenna properly acquires and tracks the 2077.4-MHz signal transmitted by ATS-6, and to determine acquisition margin and verify the acquisition and reacquisition procedures.

2. To determine voice quality of the S-band forward link as a function of total received power and to determine the total received power level where the updata link equipment begins rejecting commands.

3. For the reverse link (S-band), to determine real-time and playback voice quality, telemetry data bit error rates, and television picture quality as a function of total received power.

4. To provide data necessary to compare measured performance with the performance predictions of the link calculations.

10.5.1.2 Kennedy Space Center-ATS-6-Rosman-Johnson Space Center Test (February 1975)

Configuration

There are two basic configurations required for this test. They may be called the ATS-relay configuration and the direct link configuration.

The first is a configuration that provides forward and reverse links at simulated signal levels expected during the mission between the CSM-111 at Kennedy Space Center (KSC) and Rosman where Rosman is connected by common carrier lines to the mission control center at Houston. The CSM is to be configured with actual pretested onboard hardware to be used in the mission; however, it will not use the actual high-gain antenna but the CSM ATS-6 transmitters and receivers will interface with a test antenna previously aligned to point at ATS-6 to simulate the high-gain antenna performance when tracking accurately.

Houston will be in the actual mission configuration with the video and audio distribution connected as planned for in the mission.

The Houston configuration will allow actual operational procedures in the MCC (Building 30) to be carried out with mission procedure documentation. Color conversion and picture quality enhancement will be under the control of Building 8 and distribution of picture sound and video will output from Building 1 as though to the networks.

The second configuration will simulate a direct-link site, as in Skylab missions, where the forward and reverse links at the USB frequencies are to a tracking station equipped for real-time video connection into JSC.

The CSM will communicate directly to the antenna at the Mila Tracking Station, Florida, site at USB frequencies with simulated signal levels expected during the mission and will be connected by common carrier back to JSC where by selection of appropriate lines in Building 47 will be interfaced into the JSC distribution and control configuration as for the ATS-6 relay configuration.

This direct-link configuration enables actual procedures of the planned mission operations to be exercised to their utmost. These will be used to control the test as much as possible and will essentially duplicate the Skylab procedures.

Objectives

The principle objectives of this test are:

- To demonstrate the performance of the CSM spacecraft with actual mission hardware in the ATS-6 relay configuration.

- To demonstrate the performance of the JSC configuration design as modified for the ASTP program.

- To show the effectiveness of operational procedures and to train personnel at JSC in the ASTP operational modes.

- To evaluate the differences between ATS-6 relay operation performance and direct-link performance on previous experience especially with regards to video TV and voice quality.

10.5.1.3 Johnson Space Center-ATS-6-Madrid-Buitrago Test (May/June 1975)

Configuration

This test exercises the actual mission facilities in Spain for ASTP relay through ATS-6. The CSM is simulated by prototype equipment at JSC including the prototype HGA. Forward-link modes are derived from signals from the USB complex at Madrid uplinked at C-band to ATS-6 via the hybrid terminal and down-linked to JSC at S-band. Reverse link modes are generated at JSC to ATS-6 and down-linked to the Buitrago site for modes R3 and R4 and to the hybrid terminal for other reverse modes.

The television reverse modes are relayed to JSC via Atlantic satellite and U.S. terrestrial common carrier, other reverse modes telemetry, data and voice are received via the hybrid terminal and their output is at the USB site and Madrid. These are then returned to JSC by Atlantic satellite and common carrier in a manner similar to that used in previous programs using direct-link communication from Skylab.

The TV voice from Buitrago is also sent to Madrid for distribution over general purpose air-ground voice monitoring in the ASTP network.

For this test to be effective both Houston and Madrid must be in line-of-sight of the ATS-6 satellite and at least 15 degrees above the horizon, thus the ATS-6 satellite must be located approximately between 55 and 40 degrees west. Since the drift of the satellite is 4 degrees per day this means there is a window of about 4 days for this test to be conducted effectively and scheduling of test readiness and drift program is very important.

The configuration at JSC will be the same as for the February test. JSC will be all-up with all personnel in attendance.

Objectives

The principle objectives of this test are:

- To show that the Buitrago-Madrid-Hybrid installation has effectively been implemented.

- To evaluate and compare performance of quality of TV and sound reception using the actual mission common carrier lines from Spain.

- To further exercise actual mission procedures at Houston and build on experience obtained in the February test.

10.5.2 Test Results

10.5.2.1 Johnson Space Center-ATS-6-Rosman Test (October, 1974)—The results of all tests except the antenna acquisition threshold measurements (without RF tracker signal filter), updata link message rejection rate measurements, and time code detector threshold measurements during video tape recorder playback show that positive circuit margins exist. The results of the antenna acquisition tests performed with an RF tracker filter installed indicate that the modification which is being incorporated in the CSM high gain antenna electronics box will increase the antenna acquisition threshold margin to a positive value greater than 7 dB. The failure of the updata link and timing channel to provide positive circuit margins is being investigated.

10.5.2.2 Forward Link Tests—Verification that the modified CSM high-gain antenna would properly acquire, track the ATS-6 2077.4-MHz carrier to bore-sight, and switch from wide to narrow beamwidth was accomplished. The measured wide to narrow beamwidth differential was 18.2 dB. These tests were performed at the nominal expected signal levels using the proposed initial acquisition procedures. CSM acquisition threshold (minimum total received power level in wide beamwidth where the antenna will switch to narrow 100% of trials) occurred at a received signal level of -114.5 dBm and was extended to -125.8 dBm with a 600-Hz low-pass filter installed in the CSM RF tracker signal line. The performance and interface specification defines the expected total received power level during acquisition as -117.9 dBm.

The forward-link voice at the CSM was graded to be quality 4 (fair voice—90% word intelligibility) for S-band total received power levels of -109 dBm and -106 dBm for modes F1 and F2, respectively. This agreed within 1.0 dB of the data collected for the ATS-6-Mojave-hybrid interface tests and the Electronic System Test Laboratory (ESTL) design verification tests (DVT). Thus, the data indicates positive circuit margins of 11 dB and 8 dB for modes F1 and F2 respectively. On the other hand, the updata link message rejection rate for mode F2 was approximately 14 dB worse than the results of the hybrid interface and DVT tests for one correct message rejected for one thousand correct messages transmitted. The measured circuit margin was a negative 6.7 dB; however, the results of the ATS-6-Mojave-hybrid tests and the DVT indicate the circuit margin should be a positive 7.5 dB. Further investigations of this anomaly are in progress.

10.5.2.3 Reverse Link Tests—The reverse link voice graded to be quality 4 (fair voice—90% word intelligibility) for S-band total received power levels at the ATS-6 satellite of -104 dBm, -89 dBm, -87 dBm for modes R1, R3, and R4, respectively. These results agreed within 0.5 dB, 1.0 dB, and 3.0 dB, respectively, of the results of the ESTL design verification tests. These total

received power levels represent positive circuits margins of 17.4 dB, 2.4 dB, and 0.4 dB, respectively, when compared to the worst case expected total received power level of -86.6 dBm defined in the performance and interface specification. For reverse link mode R5, real-time voice was graded to be quality 4 for an S-band total received power level of -92 dBm and playback voice was graded to be quality 4 for an S-band total received power level of -96 dBm. These results agreed within 1.5 dB and 0.5 dB, respectively, of the results of the ESTL design verification tests. Thus, the test results indicates positive circuit margins of 5.4 dB for real-time voice and 9.4 dB for playback voice.

The real-time 51.2-kbps telemetry data bit error rate of 10^{-6} occurred at an S-band total received power level of approximately -99 dBm at the ATS-6 satellite for mode R1. This total received power level was within 1.0 dB of the ESTL design verification tests results. The playback 51.2-kbps telemetry data bit error rate of 10^{-4} occurred at an S-band total received power level of -96 dBm for mode R5. This result was also within 1.0 dB of the data collected during the ESTL design verification tests. The playback 4.0-kbps telemetry data bit error rate of 10^{-4} occurred at an S-band total received power level of -95 dBm for mode R5. This total received power level was within 1.0 dB of the total received power required for a bit error rate of 10^{-4} during the ESTL design verification tests. The real-time 4.0-kbps telemetry data was not evaluated during the interface tests real-time. The results of the telemetry bit error rate tests indicate positive circuit margins of 12.4 dB for mode R1, 9.4 dB for mode R5 playback 51.2-kbps data, and 8.4 dB for mode R5 playback of 4-kbps data. The evaluation of the real-time data channel will be included in the final report.

The reverse-link television channel 3-dB bandwidth was measured to be 2.05 MHz and 1.8 MHz for modes R3 and R4, respectively. The quality of the color converted television pictures was graded to be a 5 (good quality; no clicks; stable synchronization) for an S-band total received power level of -85 dBm for modes R3 and R4. The quality of the color converted television pictures was graded to be a 4 (good quality; occasional clicks, slight synchronization instability) at an S-band total received power level of -87 dBm. The interleaved CSM CTE timing code on line 17 of each field at this power level was graded to be a 5 (days, hours, minutes, seconds stable; no errors in readout) for mode R4. For a picture quality grading of 4 (-87 dBm S-band total received power level) the mode R3 timing code had errors in the minutes and seconds readout and was unrecoverable for mode R4. Further investigations of this anomaly are in progress.

Doppler data was measured during the first four hours of testing and was omitted thereafter because of the time element. This data was collected to provide information on the ASTP Geodynamics Experiment MA-128 prior to the mission.

SECTION 11

SPACECRAFT CHARGE PHENOMENON

SECTION 11

SPACECRAFT CHARGE PHENOMENON

11.1 INTRODUCTION

Twice a year, about the vernal and autumnal equinoxes an equitorial synchronous satellite enters a period of approximately forty days when it passes through the Earth's shadow. These eclipses can last over one hour. It has been observed on other satellite programs[1] that, due to local magnetospheric conditions, a spacecraft can acquire a static charge in the kilovolt range during these eclipse periods. Due to the unique size, configuration, and complexity of the ATS-6, there was some question as to whether static charges of this magnitude might act in a manner detrimental to the spacecraft mission.

11.2 DESCRIPTION OF TESTS

A special In-Depth Analysis (IDA) group was assembled to monitor the ATS-6 spacecraft telemetry during the eclipses of September through October 1974. The purpose of this effort was:

   a. to observe and report any static charge accumulating on the spacecraft during eclipse.

   b. to observe and report any anomalous subsystem functions occurring during eclipse. The areas involved were: power, thermal, ACS, and spacecraft status.

   c. to observe and report post eclipse anomalies occurring in the Polaris Star Assembly (PSA) outputs.

Reference A reports the observation of static charge phenomena on the ATS-6 satellite. Spacecraft voltages of less than ten kilovolts were recorded and the charge phenomenon was observed less than fifty percent of the days that the spacecraft passed through the shadow of the Earth. A simplified explanation of the phenomenon causing this condition, as interpreted from Reference A, follows:

---

[1] Reference A: DeForest, S. E., "Spacecraft Charging at Synchronous Orbit", Journal of Geophysical Research, Vol. 77, p. 651, 1972.

Solar flare activity generates streams of particles (protons and electrons) which flow outward into space. Some of these particles are caught in the Earth's magnetic field and held at various altitudes. From Reference A, the net flux of particles arriving at the spacecraft may be expressed in the form:

$$J = J_p - J_e + J_{BS} + J_{sc} + J_{sp} + J_{PE}$$

where: J_p and J_e are the fluxes of the incoming protons and electrons, and J_{BS}, J_{sc}, J_{sp}, and J_{PE} are outward fluxes of electrons due to back scattering secondary emissions due to incoming electrons and protons, and photo electrons.

Under normal conditions, this equation balances sufficiently to result in a net spacecraft potential of a few volts positive. During an eclipse, photo electrons are not produced and the spacecraft assumes a negative charge. For a negative charge to exist, the electron flux, J_e, must be large enough to produce it. Substorms occurring in the magnetosphere result in a distortion which causes a disappearance of plasmasphere particles engulfing the spacecraft. It is postulated that at these times the major terms of the flux equation, J_e and J_p, are not strong enough to produce a significant spacecraft charge even when J_{PE} is zero.

The UCSD experiment contains three proton counters and two electron counters. These counters sweep an energy spectrum from -5 ev to +80 Kev in sixteen seconds. Between each sweep, the electronics is placed in a dwell mode where a predetermined energy band is sensed for eight seconds. The first four detectors are mounted in two rotatable heads, each containing an electron detector and a proton detector. The fifth detector, a proton detector, is inoperative. The two rotable heads are mounted orthoganally and scan a field-of-view of 225 degrees about the spacecraft x- and y-axes. For the eclipse effort, the east-west (y-axis) detectors (detectors 3 and 4) were fixed and the north-south (x-axis) detectors (detectors 1 and 2) were placed in the scan mode. Detector #1 is a proton detector, and detector #2 is an electron detector. When the spacecraft is charged it acts as a proton accelerator and electron decelerator and the energy spectra are shifted in opposite directions in proportion to the spacecraft charge.

In theory the shift in the electron and proton energy spectra could be used to determine the spacecraft charge; however, the resolution of the telemetry presentation precludes an accurate use of this technique. Since the spacecraft, when charged, acts as a proton accelerator, the proton spectrum is shifted by an amount equal to the spacecraft potential. In addition, protons at extremely low kinetric energies, essentially at rest, which are not normally observable are accelerated to an observable energy level. This results in a spike appearing

at an energy level which is numerically equal to the spacecraft charge voltage and an absence of flux below that level. This spike in the proton spectrum is sufficiently unique to identify the spacecraft potential value.

The UCSD experiment generates pulses for calibration purposes, which are arbitarily numbered 0 to 64 and are identified as "s" values. The conversion from "s" values to electron volts and thus spacecraft charge voltage is:

$$E_v = -21.0 + 16.1 \ (1.145)^s$$

Sixteen of these "s" pips (every fourth value) are used in the computer program that generates the IDIIOM display. Of these sixteen pips every fourth pip is set at zero, the rest being displayed on an ascending scale as shown in Figure 11-1.

By aligning the proton spike with the "s" value pips, the kinetic energy of the protons and, therefore, the charge voltage of the spacecraft may be estimated. Observation of the data revealed that the energy sweep was out of registration with the calibration pips. This registration error was accounted for in the reduction of the data. The scale of the presentation is such that data reduction is accurate to two or three "s" values. From the above calibration equation it may be seen that this means that proton energy readings may be off by as much as a factor of 1.5.

Figure 11-2 presents eclipse entry and exit times for autumn 1974 as a function of day number. As may be seen from the curve, spacecraft local midnight does not remain at the same GMT hour. This change is due to the difference in the mean sun (GMT) and the true sun.

Each night prior to entry into the eclipse the spacecraft was placed in local vertical control. On days 247, 248 and 249 yaw control was maintained using the Polaris star tracker. For the remainder of the eclipse period, yaw axis was controlled using the YIRU gyro. This was done in order to observe star tracker acquisition losses and anomalous tracking conditions, which occurred after the eclipses, without spacecraft motions which resulted from the tracker being in the control loop. The spacecraft was operated in a minimum load condition during the eclipses in order to assure maximum power system safety. Solar array tap voltages, shunt and bus currents and temperatures were monitored as were battery voltage, charge and discharge currents and temperatures. In order to monitor the command and telemetry status of the spacecraft, the telemetry frame count, the spacecraft time code generator, the command receiver, the AGC's and the command verify bit were recorded. Momentum wheel parameters, earth sensor output, PSA and YIRU outputs were monitored in the ACS area. The solar array tap voltages did not immediately drop to zero
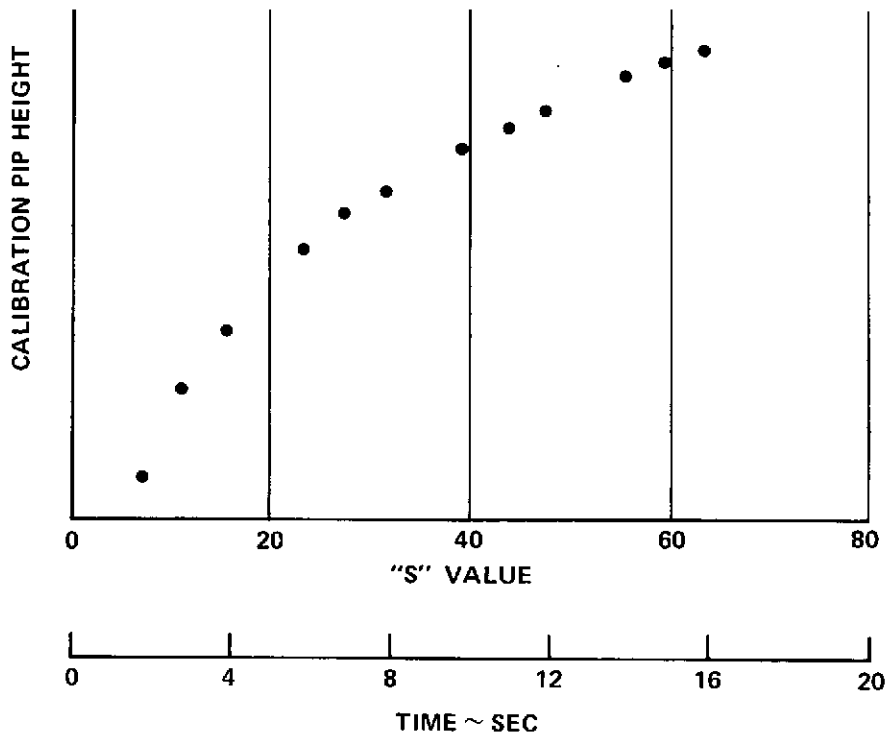
Figure 11-1. UCSD Calibration Scheme
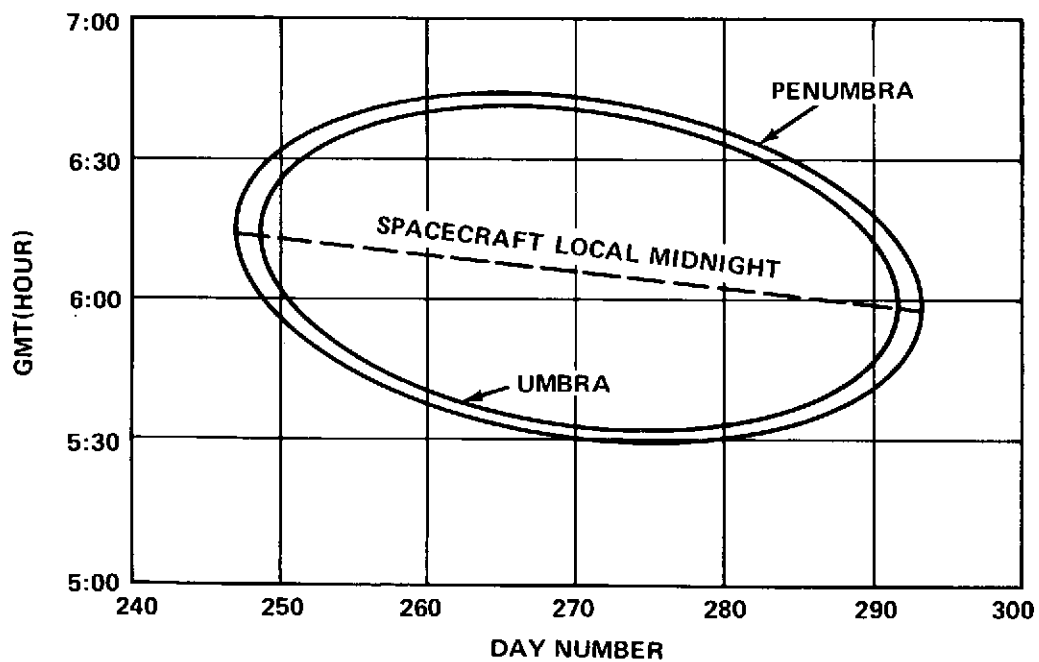
Figure 11-2. ATS-6 Eclipse Times – Autumn 1974

11-4

upon entry into the umbra, but were at 1.0 to 1.5 volts and decayed toward zero in several minutes. After spacecraft local midnight, the solar array tap voltages built up to about 1.5 volts prior to umbra exit. No explanation for this phenomenon has been developed. No other eclipse related anomalies were observed.

Few, if any, PSA hits were observed prior to entry into the earth's shadow, and none were observed during eclipse. A PSA hit is defined as any loss of PSA acquisition or a condition where the PSA yaw angle indicates that the PSA was tracking anything other than Polaris. During the half-hour period following the eclipse, PSA hits were observed on 29 days out of the 47 days of consideration. A plot of observed PSA hits as a function of day number is presented in Figure 11-3. Figure 11-4 presents spacecraft charge voltage as a function of day number. From Figures 11-3 and 11-4 there appears to be a correlation between spacecraft voltage and PSA hits. If such a correlation can be made, existence of a spacecraft charge resulted in a suppression of post-eclipse PSA hits. No explanation of why such a correlation should exist has been postulated. It may be noted that the envelope of PSA hits monotonically decreases over the eclipse period. Over the same period the declination of the sun progressed from the northern hemisphere to the southern hemisphere. Again no mechanism for this apparent correlation is postulated, the entire phenomenon of PSA being ill-defined at this time.

On twenty-five of the forty-seven days covering the eclipse period, spacecraft charge values of -10 volts or greater were observed. Of these, on twenty-one days, the spacecraft voltage was -1000 volts or greater. Figures 11-5 through 11-8 present time plots of spacecraft charge voltage time histories for some representative eclipse days.

Figure 11-9 presents a typical UCSD proton detector telemetry display for a pre-eclipse condition. A calibration error of approximately 4 "s" values may be seen where the spectrum drops off at the end of the sweep. Figure 11-10 shows the same display, during the eclipse, indicating a maximum spacecraft charge of approximately 7000 volts. During the latter days of the eclipse period, IDA personnel reported at times that either the rotatable heads of the UCSD experiment were not scanning or that the electronic sweep was not operating properly. Figure 11-11 shows a display frame of the data from day 292 where an abnormal electronic sweep was experienced with normal head scan. On day 293 (Figure 11-12) no scanning is indicated, accompanied by an abnormal electronic sweep. UCSD status telemetry for day 293 indicated that both functions should have presented normal displays as in Figures 11-9 and 11-10. The low energy spikes in the day 293 spectra were probably caused by ion engine operations performed on that day.

11-5
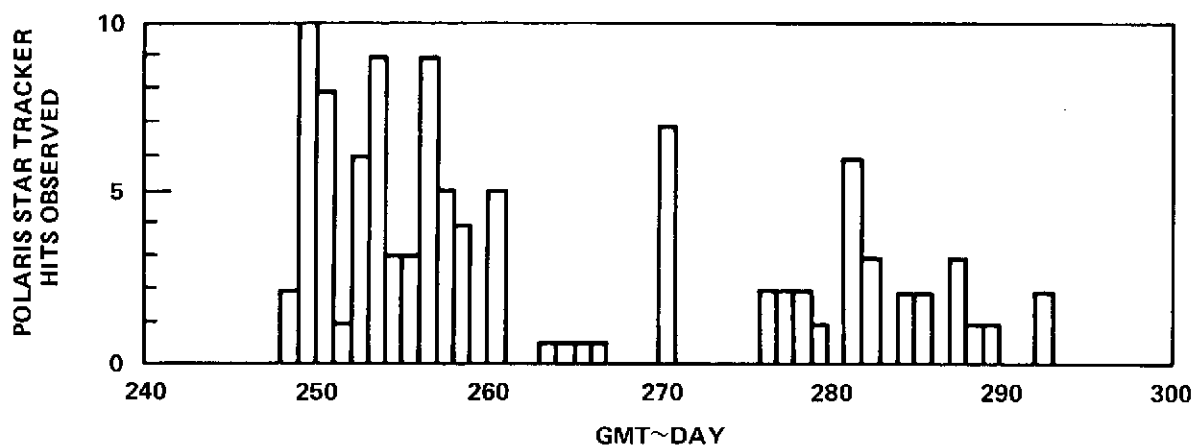
Figure 11-3. Observed PSA Hits After Eclipse
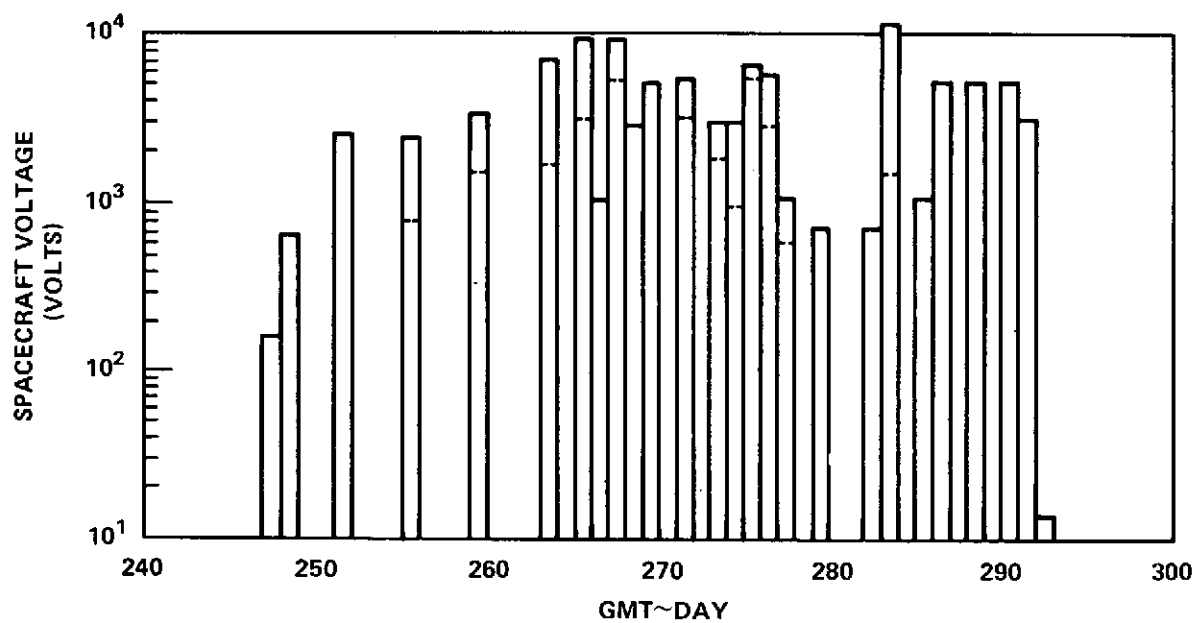
Figure 11-4. Spacecraft Charge Voltage
Observed During Eclipse
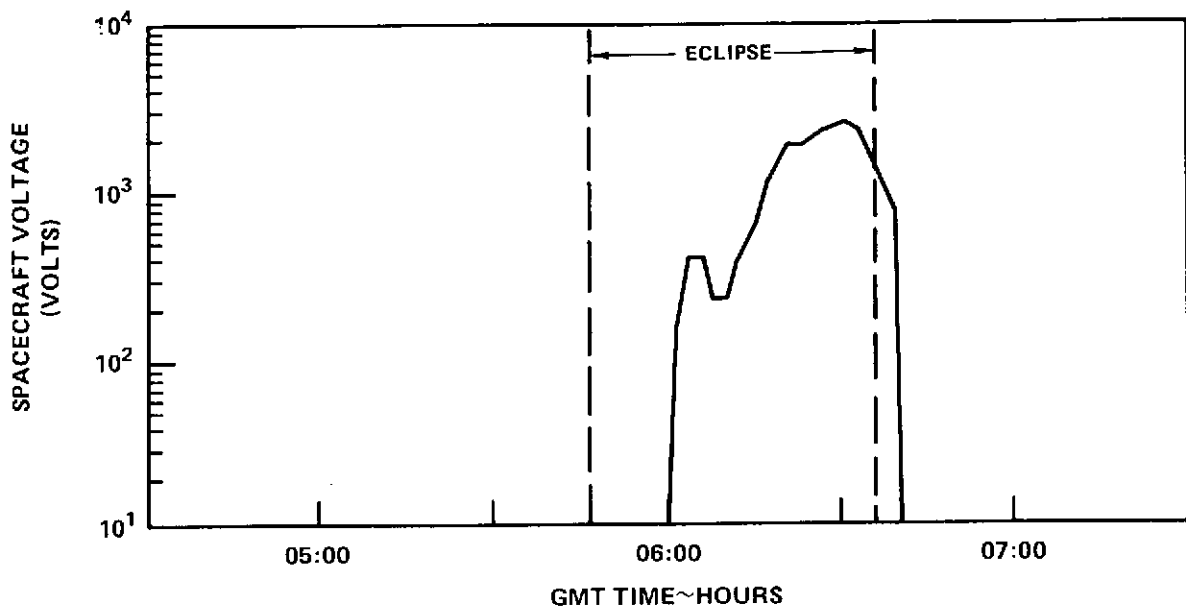
Figure 11-5. Spacecraft Charge Voltage ~ Day 255
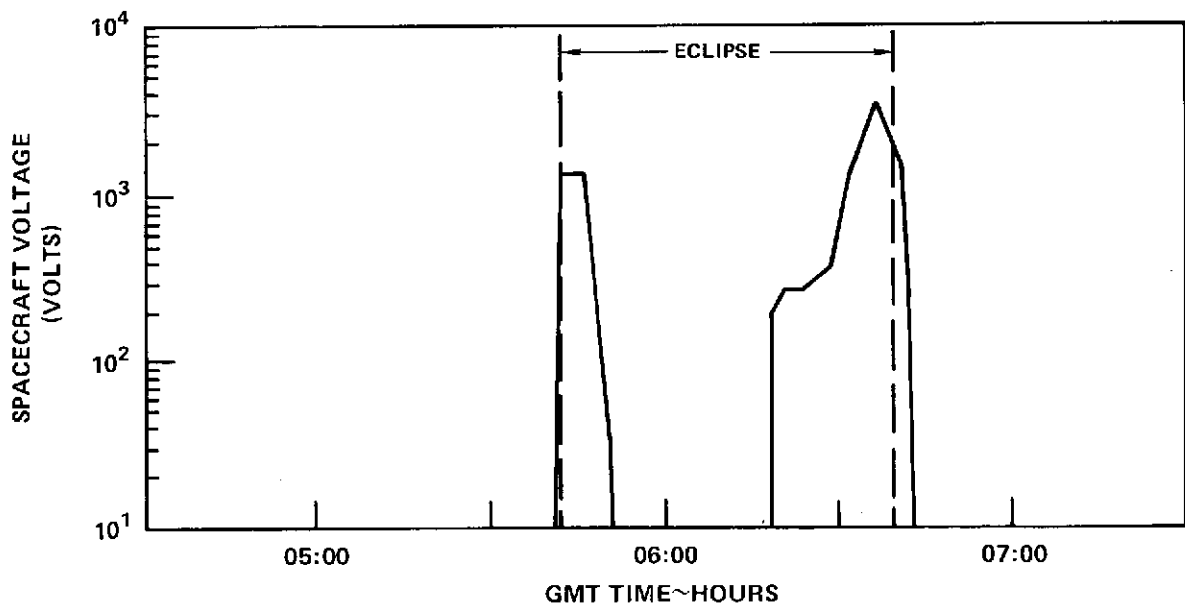
Figure 11-6. Spacecraft Charge Voltage ~ Day 259

11-7
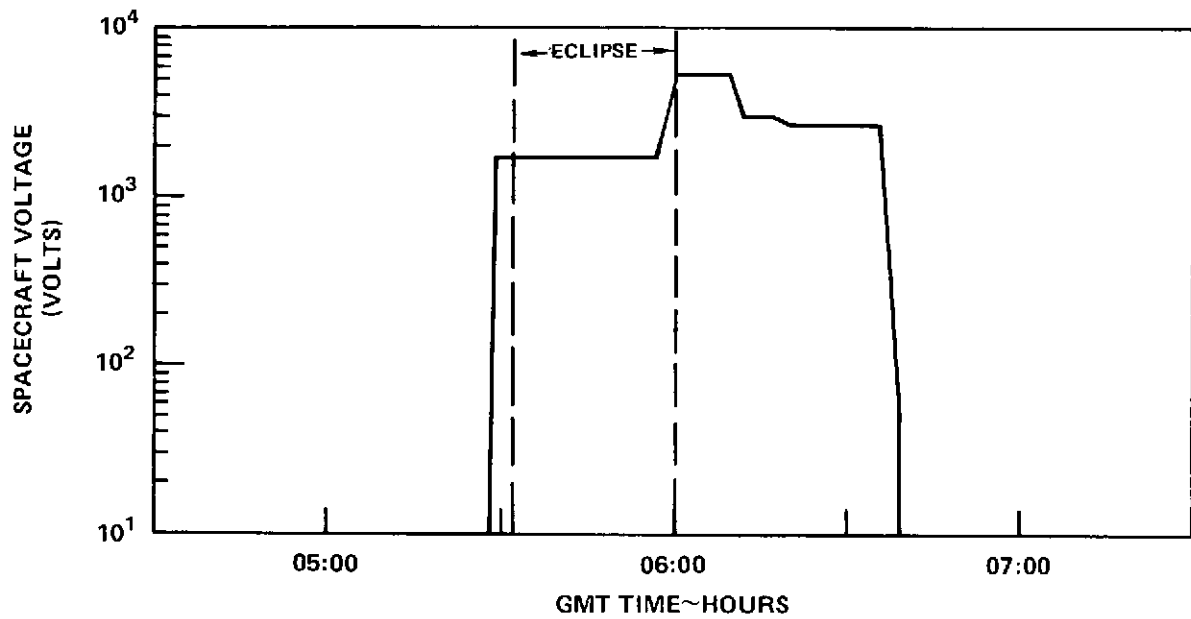
Figure 11-7. Spacecraft Charge Voltage ~ Day 276
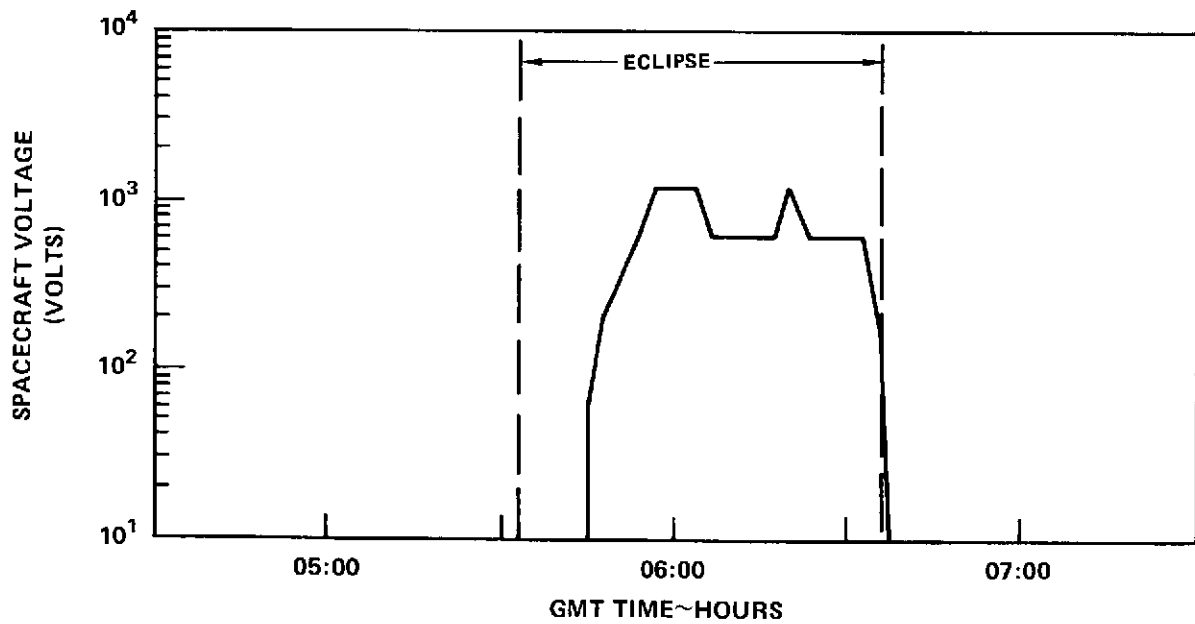
Figure 11-8. Spacecraft Charge Voltage ~ Day 277
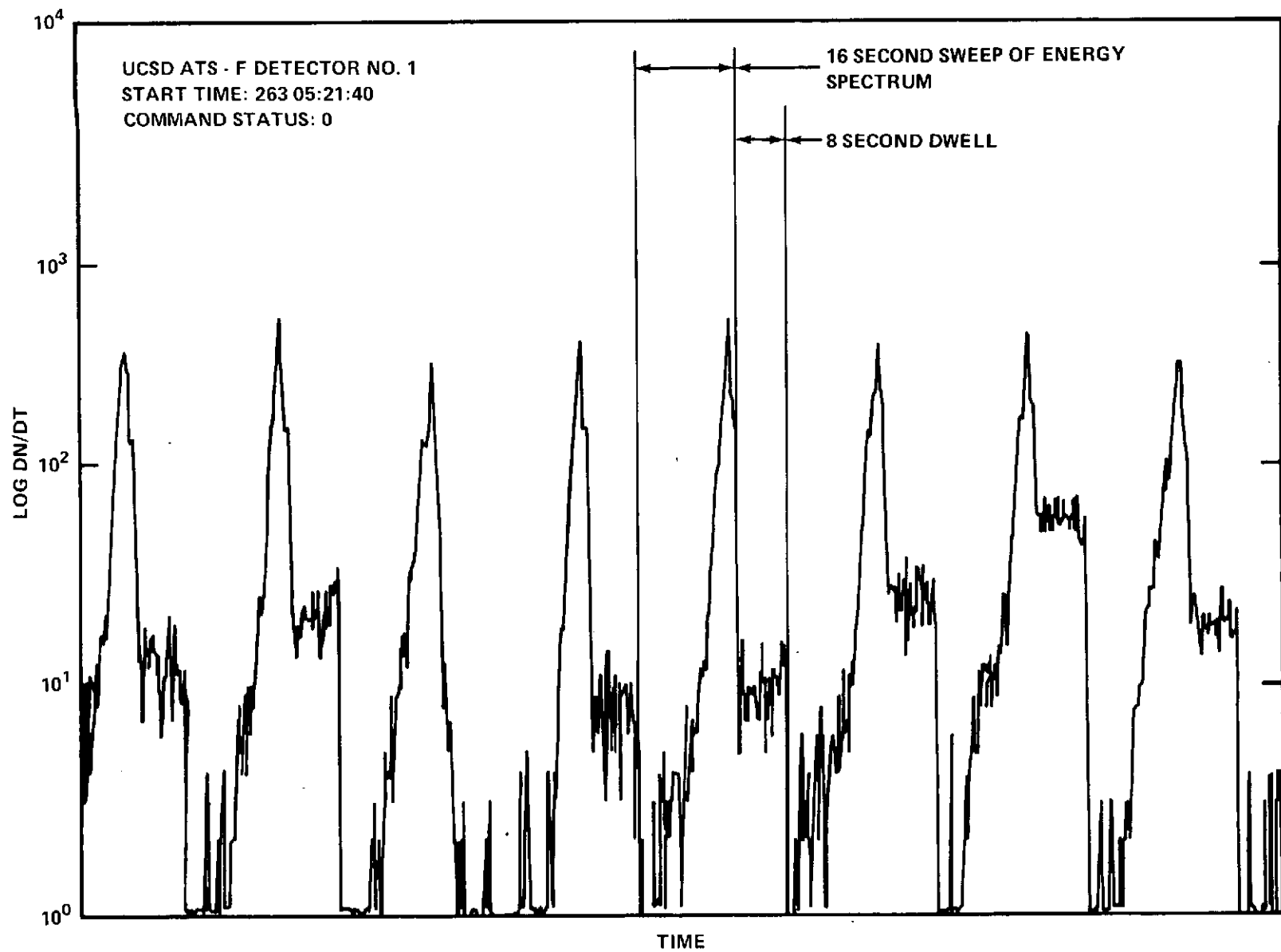
Figure 11-9. UCSD Proton Detector, Pre-Eclipse, No Charge
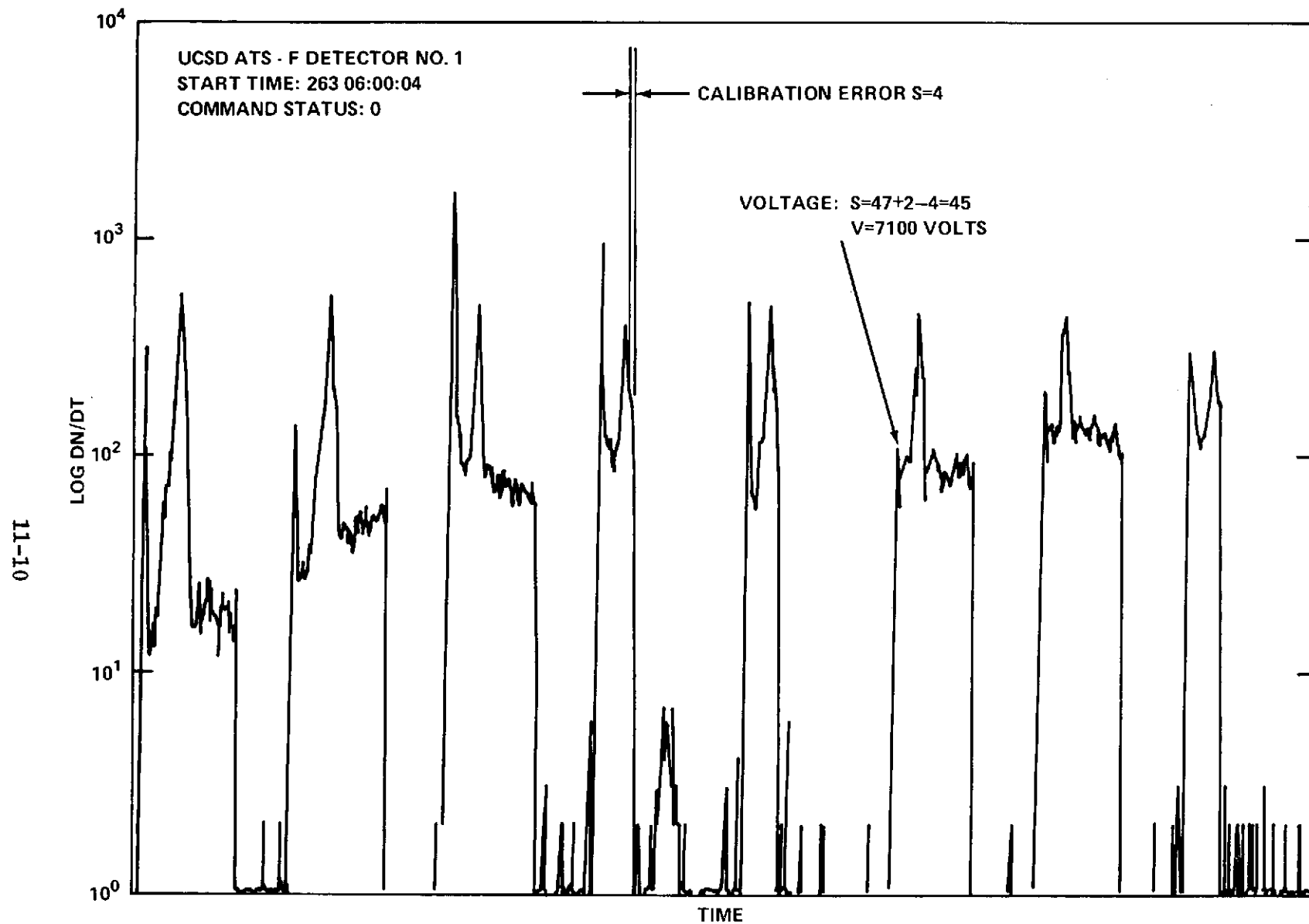
Figure 11-10. UCSD Proton Detector, Spacecraft Charge,
During Eclipse
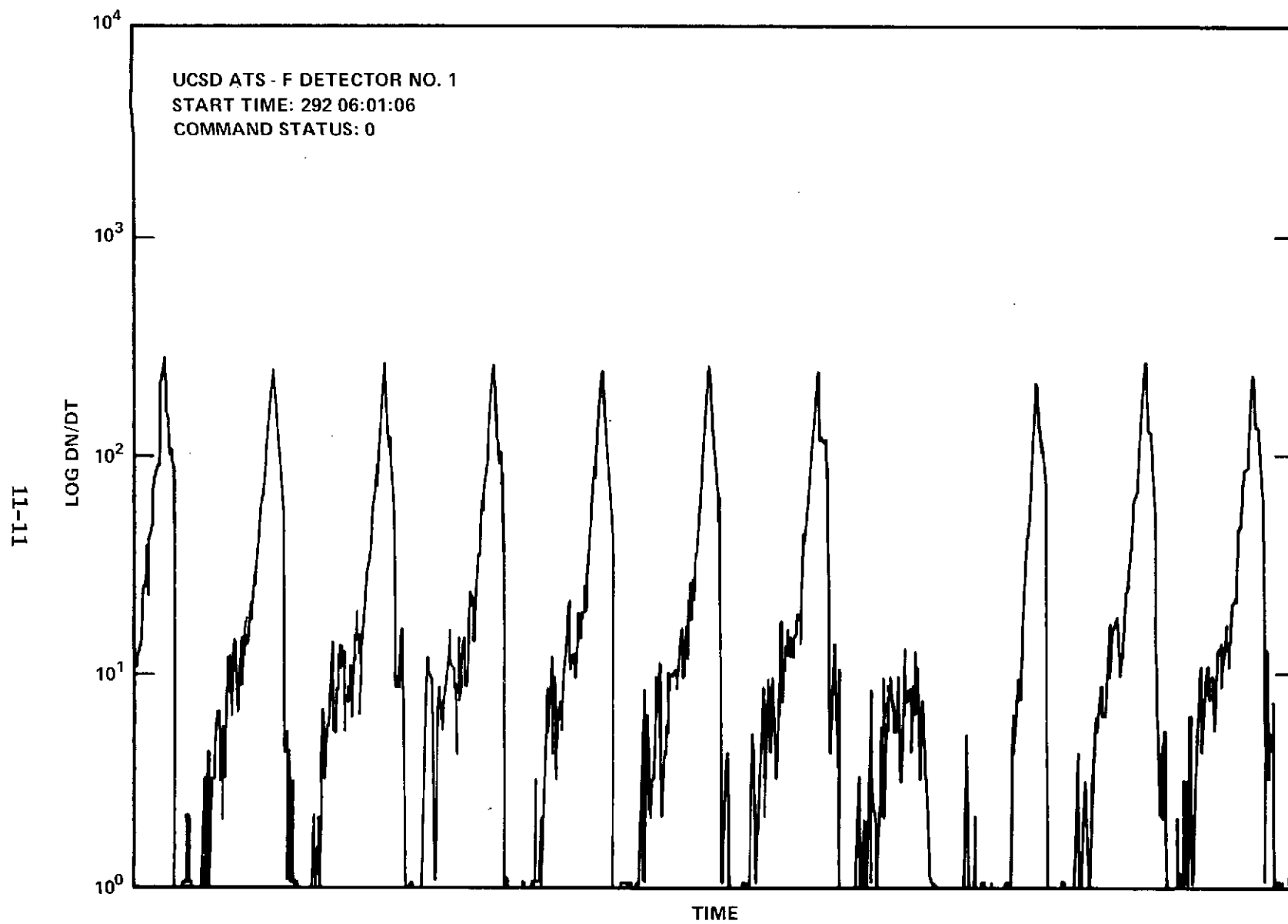
Figure 11-11. UCSD Proton Detector, Normal Scan, Abnormal Sweep
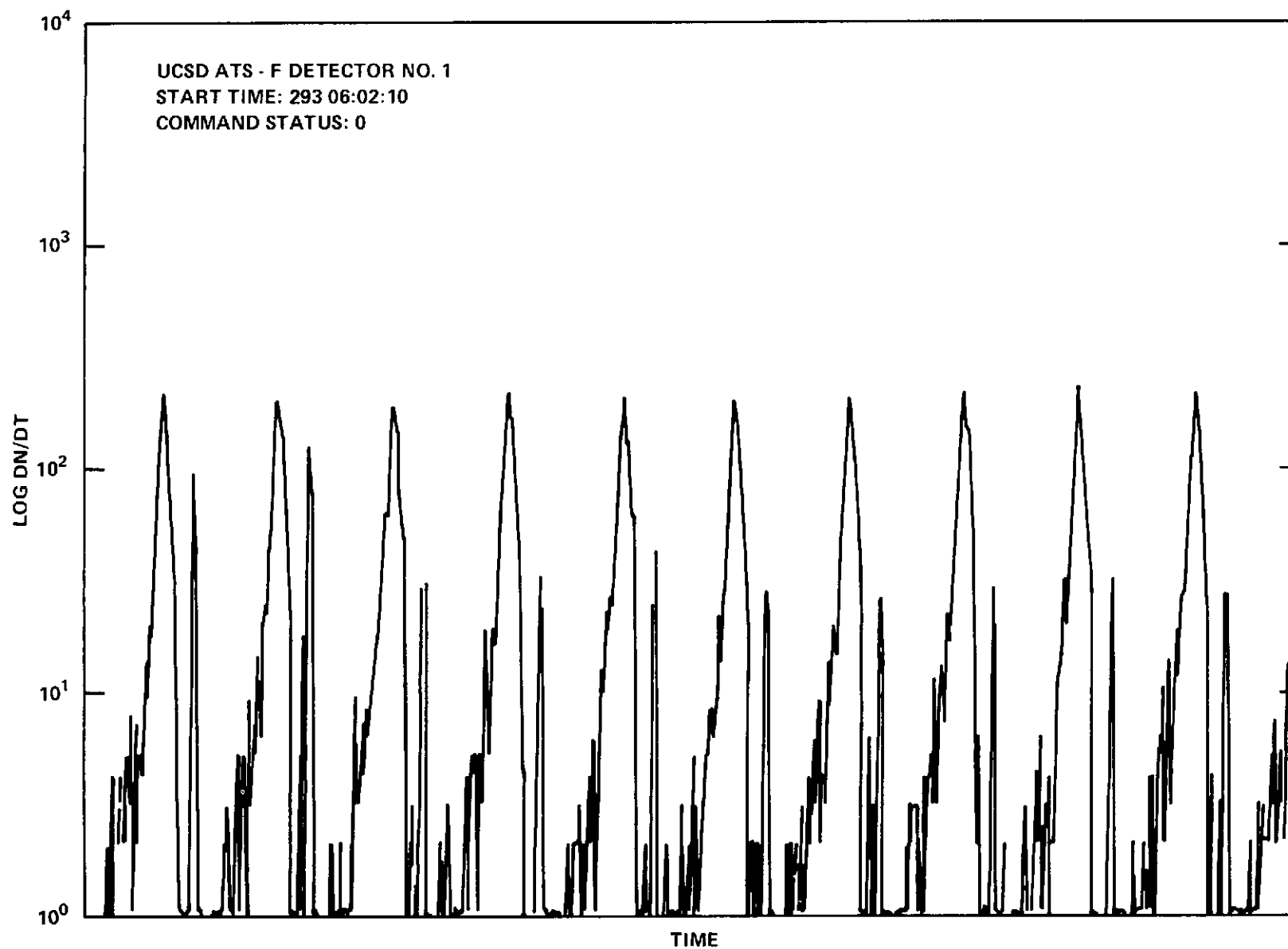
Figure 11-12. UCSD Proton Detector, No Scan,
Abnormal Sweep

11.3 CONCLUSION

The ATS-6 spacecraft operated successfully during the autumn 1974 eclipse period. Spacecraft charge voltages in the kilovolt range were experienced with no observable effect on spacecraft operations. Post eclipse PSA hits seem to be affected by spacecraft charge voltage and/or spacecraft-sun geometry. Anomalies were noted in the UCSD experiment operation as the eclipse period progressed.

SECTION 12

PROPAGATION EXPERIMENT

SECTION 12

PROPAGATION EXPERIMENT

12.1 INTRODUCTION

The redundant 13-GHz and 18-GHz transponders were found to be operating satisfactorily. The "A" unit has operated continuously during this reporting period.

The Andover, Maine, COMSAT receiving facility has operated with only minor problems, however the transmitting facility has experienced considerable equipment operational difficulty. The lack of attitude data on telemetry tapes required for data reduction has delayed analysis.

12.2 SCIENTIFIC OBJECTIVES

The purpose of the Propagation Experiment is to collect sufficient long-term data on propagation attenuation caused by precipitation for a large number of locations in the United States, to permit determination of minimum power margins needed in spacecraft communications systems operating at frequencies of 13-GHz and 18-GHz.

12.3 EXPERIMENT DESCRIPTION

Figure 12-1 is a block diagram of the propagation experiment transponder. The transponder is a single-frequency conversion repeater with separate inputs at 13.19 to 13.20 GHz and 17.79 to 17.80 GHz; its combined outputs are amplified and retransmitted at 4.150 GHz. Full redundancy is provided for each translation and for the combined output amplifiers.

12.4 EXPERIMENT PERFORMANCE EVALUATION

The propagation experiment was activated 2 weeks after launch. Both the A and B redundant transponders have checked out satisfactorily through the Andover, Maine, COMSAT receiving facility. The "A" units have been operating continuously during the last three months. During this time the gain has remained within 1 dB of nominal, well within the 3 dB specification limits.

The 4-GHz Andover, Maine, receiver and signal processor were acceptance tested in the last week of June and 24-hour per day operations began during the first week of July. One week of data was lost during power amplifier retrofit of the "big horn" for commercial backup service to the 97 foot INTELSAT antenna at the site.
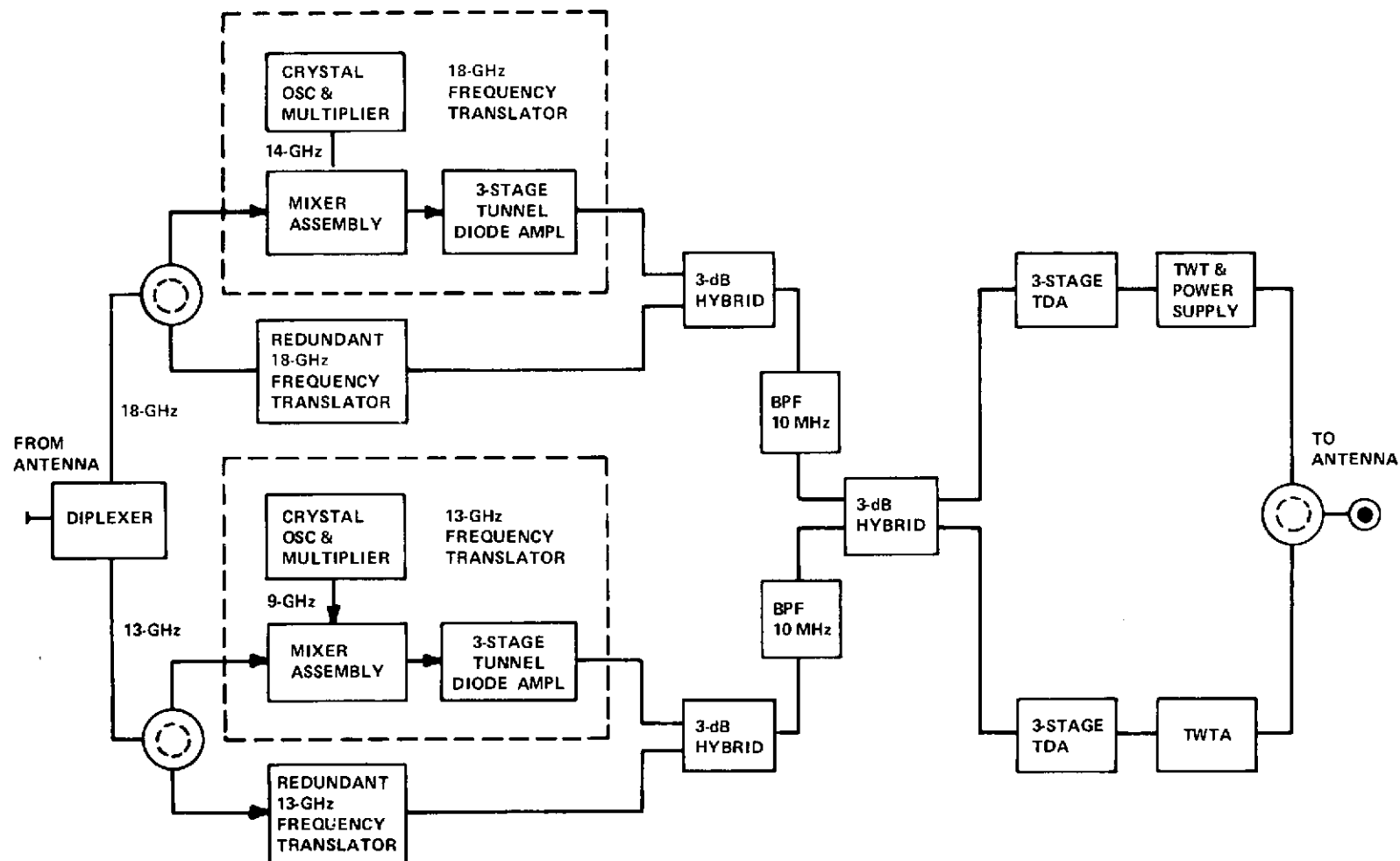
Figure 12-1. Block Diagram of the Propagation Experiment Transponder

The only major problem with the propagation experiment has been the reliability of the 18-GHz and 13-GHz ground transmitting sites. Both TWT and solid state oscillator sources have failed in the field, limiting the total number of operational signals from 19 to 28 out of a total of 40 carriers. The oscillator failure has caused more trouble than the TWT because of the number of failures and repair delays. The experiment is producing a significant amount of data on the 13 and 18 GHz rain attenuation, but the loss of 50 to 60% of the carriers during July has been disappointing.

About 150 hours of data from the Andover site with about 13 hours of calibration time and up to 6 hours of z-axis misalignment is being obtained each week. Repair time has flucuated from 0 to 7 hours per week and tape verification from 1 to 4 hours per week. At the present time, data reduction into useable plotted results has not been possible because of the lack of spacecraft attitude data on the telemetry tape.

Several 20-dB level fades have been recorded and noted on quick-look tables but meaningful results require the attitude TM tapes for complete computer processing. The first good TM tape was delivered to COMSAT on August 9, 1974 for July 4-6 data.

In the future the following actions are anticipated:

1. Routine: Repair transmitting sites and start producing attenuation and diversity plots (when TM data is available).

2. Special: Investigate oscillator source failures to determine if the manufacturer's present fix of shock mounting the units is adequate to prevent future failures. Look into more satisfactory electrical fix.

SECTION 13

MILLIMETER WAVE EXPERIMENT
(MMW)

SECTION 13

MILLIMETER WAVE EXPERIMENT
(MMW)

13.1   INTRODUCTION

Spacecraft operation employing the MMW Experiment was very active and successful until September 1. Since then, many requests for operation during storms in remote areas have not been honored due to requirements for HET and other experiment operations.

Measurements of the propagation characteristics in the 20-GHz and 30-GHz frequency bands were reported by the Principal Investigator at the conference of The United States National Committee of The International Union of Radio Science in Boulder, Colorado on October 18, 1974.

The spacecraft MMW equipment package has functioned well during this operating period except that the 20-GHz horn antenna TWT (H1) will not switch on. This loss will not impact any of the basic objectives of the experiment.

MMW color video tests conducted showed good picture quality at both 20 GHz and 30 GHz.

13.2   SCIENTIFIC OBJECTIVES

The millimeter wave experiment is designed to provide propagation data at 20 GHz and 30 GHz over a 1.44 GHz bandwidth.

The basic objective of the millimeter wave experiment is to provide information about propagation characteristics of the Earth's atmosphere, and the effect of weather on these characteristics, to efficiently use this portion of the electromagnetic spectrum for wideband communications and other scientific purposes. The MMW experiment will measure the propagation characteristics of the atmosphere between the ATS-6 spacecraft and the ground by transmitting 20-GHz and 30-GHz test signals from the spacecraft to the experimenter's ground equipment at the ROSMAN Ground Station.

13.3   EXPERIMENT DESCRIPTION

The millimeter wave experiment equipment consists of two transmitters, one radiating at 20 GHz and the other at 30 GHz. For two of the three operating

modes, all of the elements comprising the transmitters have redundant elements which may be switched in by command. For the third mode (communications) no redundancy is provided for some of the system elements. The equipment is divided into four major units: the RF multiplier, the 20/30-GHz modulator/power amplifier, the 20/30-GHz horn antenna assembly, and the 20/30-GHz parabolic antenna, all of which are located in the earth viewing module of the spacecraft. The equipment requires approximately 70 watts of power from the spacecraft bus.

13.4   EXPERIMENT PERFORMANCE EVALUATION

The ATS-6 millimeter wave experiment began operations on June 13, 1974, with a checkout of all spacecraft modes of operation. All systems operated well except for the 20-GHz horn antenna traveling wave tube, (20 GHz H1). Five attempts were made to energize the TWTA without success. Attempts to turn on 20 GHz H1 on July 12 were again unsuccessful. Tests will be repeated after further evaluation of the dwell mode data from the last test. Loss of 20 GHz H1 will not impact any of the basic objectives of the MMW experiment; however, the experiment has lost redundancy at 20 GHz.

The first successful MMW color video was transmitted through ATS-6 on July 12, 1974, with signal-to-noise ratios of 11.3 dB at 20 GHz, and 12.8 dB at 30 GHz.

Additional video tests at 20 GHz and 30 GHz at Rosman have shown that picture quality was improved with the 40-MHz IF filter in the spacecraft. Measurements with the 12-MHz filter showed loss of color and picture breakup.

The spacecraft systems have functioned smoothly and with nominal telemetry outputs through extensive data taking periods during July and early August.

The first rain-data measurements were obtained at Rosman on July 6, 8, 10, 13, 15, and 17. The receiver system, paramps, autotrack system, and PDP-11 software program all functioned properly. Problems still remain in some of the support equipment such as the 8-GHz radar, radiometer calibrations, and the program track software.

Intense fades up to 23 dB at 30 GHz and 11.5 dB at 20 GHz have been observed at Rosman through a number of storm events in early July and early August. Very little rain occurred during late July. The data quality looked good, and supporting radiometer and radar measurements performed as expected. Signal scintillations were observed at the GSFC and OSO sites on a number of occasions in both clear and rainy weather.

Long delays have been experienced with GSFC central processing because of computer system down time, delays in data transfer from Rosman, and software debugging problems. All efforts possible are being used to correct these areas.

The Rosman MMW station is the prime facility for this experiment and every effort is being extended to maintain the hardware in prime operating condition.

Since the beginning of spacecraft operations, participating stations at GSFC, Ohio State University, Virginia Polytechnic Institute, University of Texas, Bell Telephone Labs, COMSAT Labs and Westinghouse have worked with ATS-6.

During the upcoming weeks, stations at NRL, Battelle Institute, Westinghouse, and possibly USASCA, are expected to begin operations.

In summary, the data quality indicates that all major experiment objectives can be accomplished through the remaining months of spacecraft operations. A major problem will be the lack of satellite availability due to scheduling conflicts with HET and other experiments.

SECTION 14

ADVANCE THERMAL CONTROL

FLIGHT EXPERIMENT

(ATFE)

SECTION 14

ADVANCE THERMAL CONTROL FLIGHT EXPERIMENT
(ATFE)

14.1   INTRODUCTION

The Advanced Thermal Flight Experiment (ATFE) is designed to demonstrate
the thermal control capability of a thermal diode (one-way) heat pipe, a phase
change material (PCM) and a feedback-controlled, variable thermal storage
conductance heat pipe (FCHP). This experiment permits evaluation of these
components on an individual basis and as an integrated temperature control
system. The major performance goal of the ATFE is to maintain the tempera-
ture at the thermal diode/PCM interface at 29°C ± 3°C.

The ATFE has been in operation since its initial turn-on six-hours after
launch.

14.2   EXPERIMENT DESCRIPTION

A schematic of the ATFE is presented in Figure 14-1. In addition to the thermal
control components mentioned above the experiment contains a solar absorber
(1) and a space radiator (5). Supporting hardware not shown in Figure 14-1 con-
sists of a solid state electronics module, temperature sensors, foil heaters,
multi-layer thermal insulation blankets and a support structure. The electronics
module contains the controller for the feedback controlled heat pipe, signal
conditioning circuitry, and command relays.

The ATFE is mounted in the east wall of the Earth Viewing Module with only the
out-board surfaces of the solar absorber and radiator exposed to the external
environment.

Solar input is used as the primary heat source for the experiment. Because of
the geosynchronous orbit and three-axis stabilization, the solar flux incident
upon the east wall rises and sets with a sinusoidal variation over a 12-hour
period, followed by 12-hours of shadow. The solar cycle is essentially the same
as that experienced by a fixed point on the Earth's surface.

During the period of solar input, energy collected by the absorber is transported
by the diode to the PCM box. This energy is used to simulate power dissipation
during an electrical duty cycle, with the PCM package serving as a simulated
temperature controlled equipment shelf. Initially, the energy first melts the

Figure 14-1. Advanced Thermal Control Flight Experiment (ATFE)

1 SOLAR ABSORBER
2 GAS RESERVOIR
3 CONTROL HEATER
4 GAS/VAPOR INTERFACE
5 RADIATOR
6 FEEDBACK CONTROLLED
HEAT PIPE (FCHP)
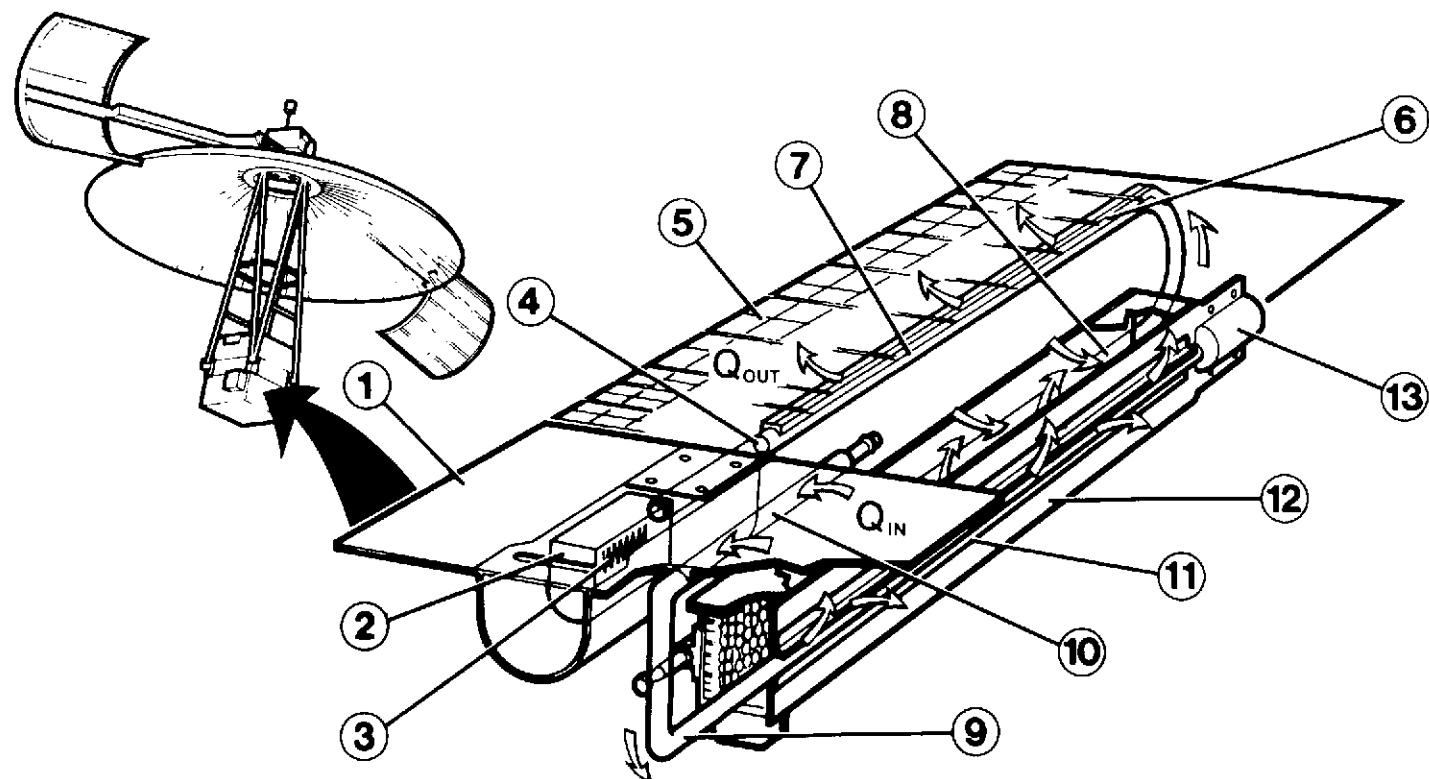
7 FCHP CONDENSER SECTION
8 FCHP EVAPORATOR SECTION
9 THERMAL DIODE HEAT PIPE
10 DIODE EVAPORATOR SECTION
11 DIODE CONDENSER SECTION
12 PHASE CHANGE MATERIAL (PCM) BOX
13 LIQUID RESERVOIR

PCM, which is octadecane with a melting point of 28°C. When melting has been completed, the energy then passes through the equipment shelf to the FCHP which transports it to the space radiator. During periods of operation when the PCM is melted, temperature control is provided by the regulated heat dissipation of the FCHP. As the shadow period is approached, the absorber and radiator begin to cool down below 28°C and the diode and FCHP shut down to minimize the parasitic losses from the PCM. Thermal energy released by the freezing of the octadecane is used to compensate for the heat loss during the transient shutdown period, and provides temperature stability over part of the shadow period. When all the octadecane has frozen, the temperature of the equipment shelf decreases at a rate consistent with the capacitance of the PCM box and its parasitic heat leaks. There is 0.8 lb of octadecane which provides temperature stability for about five hours of shadow after which the PCM box cools to approximately 0°C.

The major performance goal of the ATFE is to maintain the temperature at the thermal diode/PCM interface at 29°C ± 3°C. The temperature of the PCM box was allowed to decrease to 0°C in order to evaluate the effect of subcooling on the melting temperature of the octadecane. Temperature control is accomplished mainly by the action of the PCM and FCHP. The shutdown by the diode serves to minimize the amount of octadecane required for control during the shadow.

14.3   FLIGHT PERFORMANCE

The ATFE has operated almost continuously since launch. The following operational modes have been exercised during the first four months of orbit:

    a.   Normal
    b.   Passive
    c.   Auxiliary
    d.   Passive Auxiliary

A description of all ATFE modes is given in Table 14-1. The last two modes listed were not exercised because they require manual control of the back-up heater and are needed only if the FCHP's controller fails.

The performance of the ATFE to date can be summarized as follows:

    a.   The ATFE thermal control system and the individual components are all operative and performing as predicted with existing flight conditions.

    b.   All experiment objectives are being demonstrated. When operating in the normal mode, there is a daily loss of temperature control for

Table 14-1

ATFE Operational Modes

Mode	Description	Command Status
Normal	Normal operation of system, controller provides automatic regulation of FCHP	ATFE Experiment turn-ON (55436) ATFE FCHP Controller ON (55475) ATFE FCHP BU RSVR HTR OFF (55516) ATFE PCM BOX AUX HTR OFF (55536)
Auxiliary	Auxiliary heater on during 12-hr shadow and first and last 3 hrs of sun to provide additional exercise of FCHP or redundancy if thermal diode fails	ATFE Experiment Turn ON (55436) ATFE FCHP Controller ON (55475) ATFE FCHP BU RSVR HTR OFF (55516) ATFE PCM BOX AUX HTR ON (55535)
Passive	FCHP turned off, FCHP acts as a passive variable conductance heat pipe	ATFE Experiment Turn ON (55436) ATFE FCHP Controller OFF (55476) ATFE FCHP BU RSVR HTR OFF (55516) ATFE PCM BOX AUX HTR OFF (55536)
Passive-Auxiliary	FCHP controller off and auxiliary heater on as in Auxiliary Mode to exercise the FCHP in its passive mode	ATFE Experiment Turn ON (55436) ATFE FCHP Controller OFF (55476) ATFE FCHP BU RSVR HTR OFF (55516) ATFE PCM BOX AUX HTR ON (55535)
Backup	Manual control of the Backup Reservior Heater to provide redundancy in the event the FCHP Controller fails	ATFE Experiment Turn ON (55436) ATFE FCHP Controller OFF (55476) ATFE FCHP BU RSVR HTR ON/OFF* (55515/55516) ATFE PCM BOX AUX HTR OFF (55536)
Backup Auxiliary	Same as Auxiliary Mode except backup Reservoir Heater used if FCHP Controller fails	ATFE Experiment Turn ON (55436) ATFE FCHP Controller OFF (55476) ATFE FCHP BU RSVR HTR ON/OFF* (55515/55516) ATFE PCM BOX AUX HTR ON (55535)

*Turn on/off as required

4.5 hours around the period of maximum solar input. This represents a 5 to 10% degradation of experiment objectives. The loss of control is related to elevated radiator temperatures and is discussed below.

c. All command and telemetry functions are operative. The telemetry appears stable and indicates no EMI effects.

The one problem encountered to date is the loss of temperature control associated with the elevated radiator temperatures. There are two probable causes indicated by analysis of the flight data.

a. The temperature drop across the PCM box indicates that the net heat throughput could be as high as 27 watts during maximum solar input. This represents at least a seven watt increase over that experienced during ground tests. The increased power is more than the radiator was designed to carry and would result in elevated temperatures.

Electrical heaters attached to the underside of the absorber were used to simulate the solar input during thermal vacuum tests. It is possible that the concentrated distribution associated with the heaters did not adequately simulate the uniform solar flux. A detailed thermal analysis of the absorber is underway.

b. Degradation of the solar absorptivity (α) of the optical solar reflectors (OSR's) used as the radiator surface could also cause this result. If the possibility of increased thermal throughput from the absorber is neglected, analysis indicates that the absorptivity would have had to degrade from a nominal design value of 0.1 to 0.22 in flight. The absolute magnitude as well as the rate of degradation is difficult to explain when considering possible causes such as contamination due to outgassing.

Operation of the ATFE in the Auxiliary mode results in radiator temperatures in excess of 50°C. This mode was exercised for more than one month continuously, and contaminants should have been driven off the OSR's. However, to date, there has been no improvement in radiator performance. A thermal analysis is also being conducted to examine the various thermal inputs to the radiator to establish if there has been a degradation of the absorptivity.

14-5

SECTION 15

QUARTZ CRYSTAL MICROBALANCE

(QCM)

CONTAMINATION MONITOR

SECTION 15

QUARTZ CRYSTAL MICROBALANCE (QCM)
CONTAMINATION MONITOR

15.1 SCIENTIFIC OBJECTIVES

The primary objective of this experiment is to provide data regarding the presence of contaminants on the spacecraft. This is done by the use of a quartz crystal microbalance (QCM) which measures extremely small mass accretions. Sources of contamination on the spacecraft, in addition to general outgassing, include material ejected from the spacecraft propulsion subsystems and the Ion Engine experiment.

15.2 EXPERIMENT DESCRIPTION

The experiment flight hardware consists of two parts: a sensor assembly mounted externally on the north face of the Earth Viewing Module, and the electronic unit mounted internally on the same face. The sensor assembly contains the sensing and reference oscillating quartz crystals, heaters, and the electronic driving circuitry for the crystals. The electronics unit contains the signal processing, sensor temperature control, and command and telemetry circuitry.

The QCM uses a crystal whose resonant frequency will change with the amount of material deposition on its active surface. The change, in this case, is linear from 1500 Hz to 50 kHz. If, after 6 to 8 months, the frequency shift should exceed 50 kHz, a special degas heater will be turned on to effectively burn off the accumulated material and return it to approximately its original frequency.

15.3 EXPERIMENT PERFORMANCE EVALUATION

15.3.1 Performance Summary

Evaluation of prelaunch, launch, and early in-orbit performance indicates satisfactory operation. Preliminary data analysis indicates that the experiment objective of measuring molecular deposition/desorption has been met. The unit has been on continuously since five hours before launch. All commands function properly and the telemetry data accuracy of ±1 Hz has been met. A 24 hour bake-out of the crystals was performed resulting in the removal of 10 monolayers of molecular material. The orbital average temperature for the early orbits was about -20°C rather than the desired -70°C. On later orbits, this average has decreased to approximately -35°C reaching a minimum of -52°C for that orbit. The temperature is still decreasing; seemingly at a faster rate than the solar angle.

15.3.2 Prelaunch/Launch

The QCM was powered on at 150:08:16 while final checkout of the spacecraft was performed. There was no mass deposition during the period up to lift-off. The launch phase through the thermal maneuvering phase is shown in Figure 15-1. There are periods of no telemetry, but the indications are of the crystal out-gassing, perhaps reaching a minimum 16 minutes after lift-off. The subsequent rise of approximately 240 Hz can be attributed to mass deposition and equilibrium conditions being reached between the crystal and the surrounds. Alternately, the possibility of the reference crystal clenaing-up exists. The sensing crystal has a much higher pumping speed due to its view of space. The reference crystal would tend to lag due to its restricted enclosure.

The thermal maneuvering period is shown in Figure 15-2 with the crystals stabilized at -19°C during this time. The 200-Hz dips are caused by the Sun crossing the crystal face with a resulting thermal difference between the sense/reference crystal. The beat frequency remaining essentially constant at 1800 Hz can be attributed to equilibrium conditions or that the accreted material is polymerized and would never leave. Subsequent data is indicating that mass desorption is occurring; however, not enough time has elapsed to determine whether polymerization of the deposited material has occurred.

15.3.3 On-Orbit Performance

The on-orbit performance is shown in Figures 15-3 and 15-4 with the beat frequency plotted as a function of day-of-year and the crystal temperature being -22°C and -18°C. The mass accretion up to day 157 is shown to be about 20 Hz; corresponding to 9×10^{-8} gm/cm^2, an extremely small amount. Day 158 and part of day 159 was a 24 hour bake-out of the crystals with a high temperature of +50°C reached resulting in a loss of 100 Hz or 10 monolayers.

The long term performance, shown in Figure 15-4 indicates a period of equilibrium, followed by mass desorption from day 168 to day 172, and again a period of equilibrium.

15.4 CONCLUSIONS AND RECOMMENDATIONS

All functions of the QCM have performed satisfactorily during the check-out period. The data reduction and analysis is continuing in order to further define whether the small mass increases noted relate to spacecraft activity.

It is recommended that the QCM continue to operate, particularly through winter solstice, in an attempt to further define the thermal performance of the sensing unit.
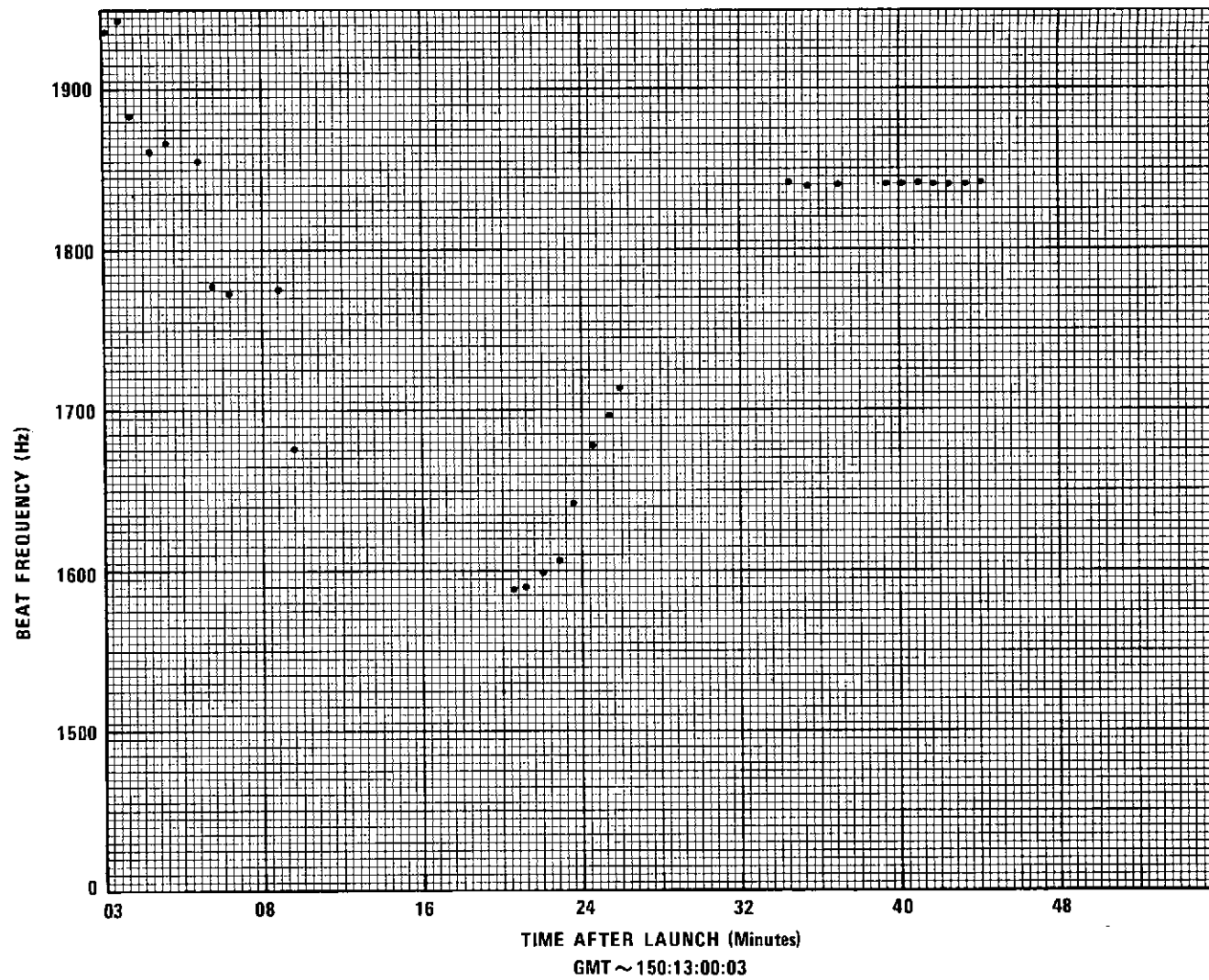
Figure 15-1. QCM Launch Data
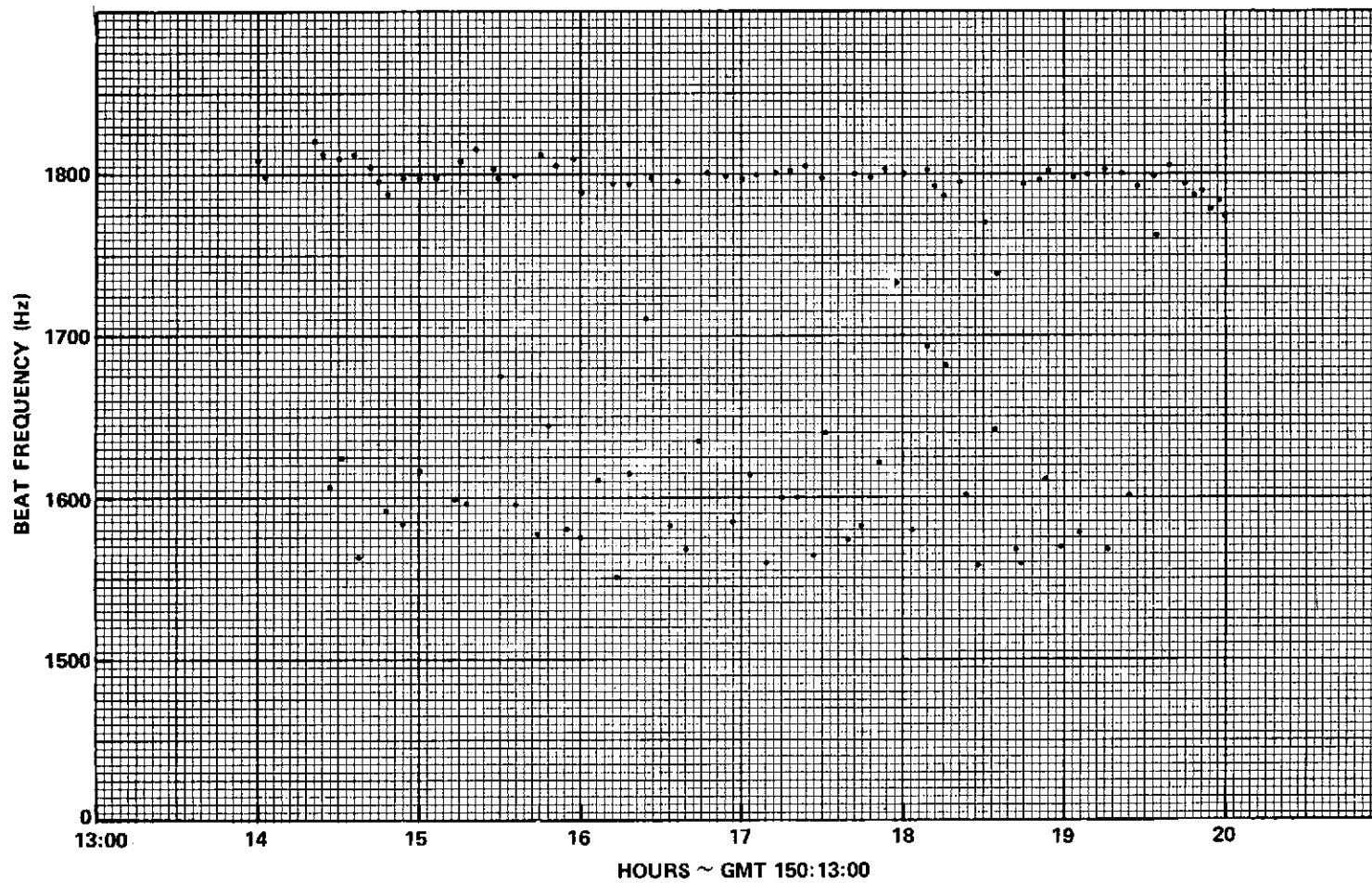
Figure 15-2. Thermal Maneuvering Phase
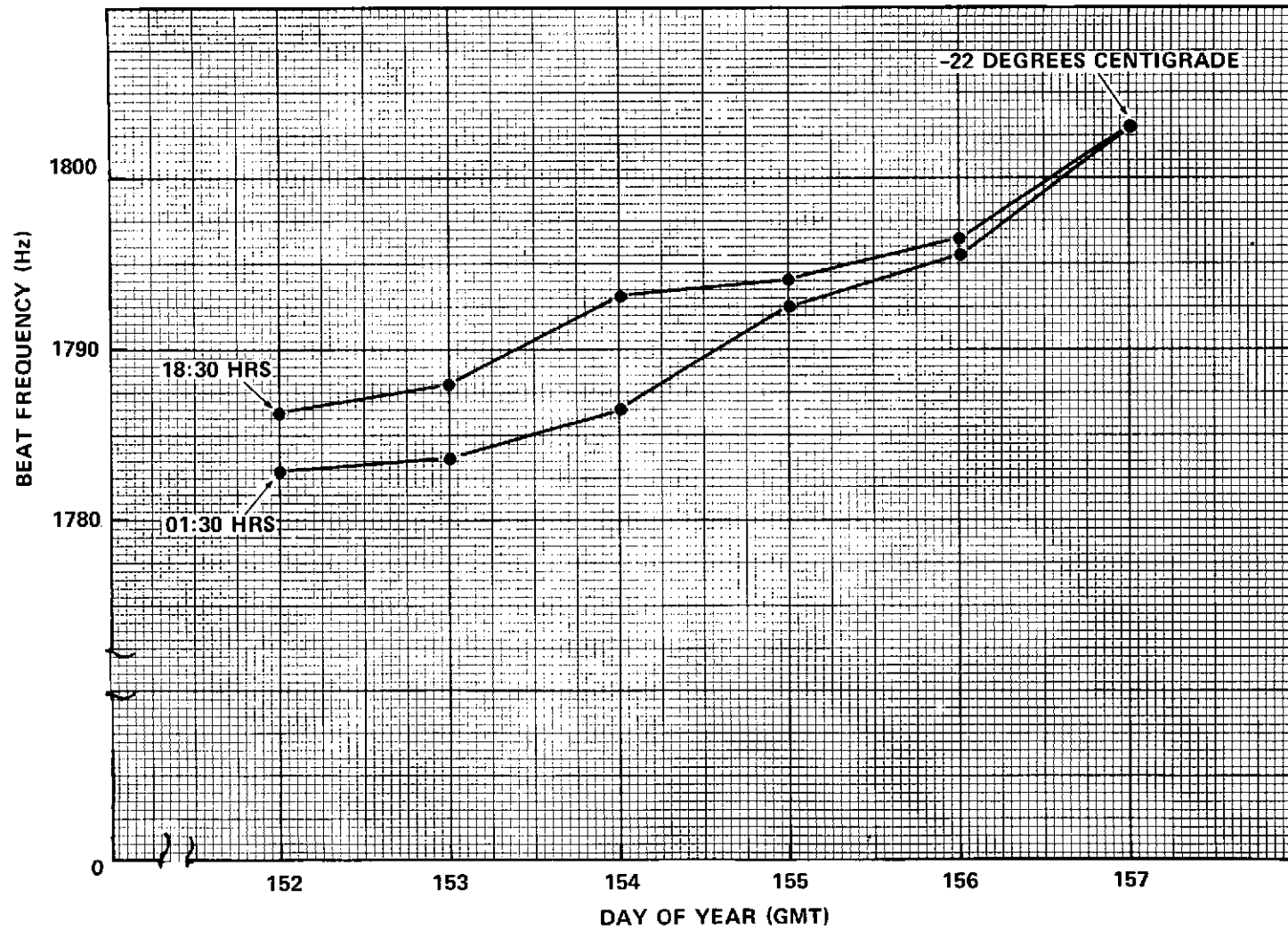
Figure 15-3. Beat Frequency vs. Day of Year
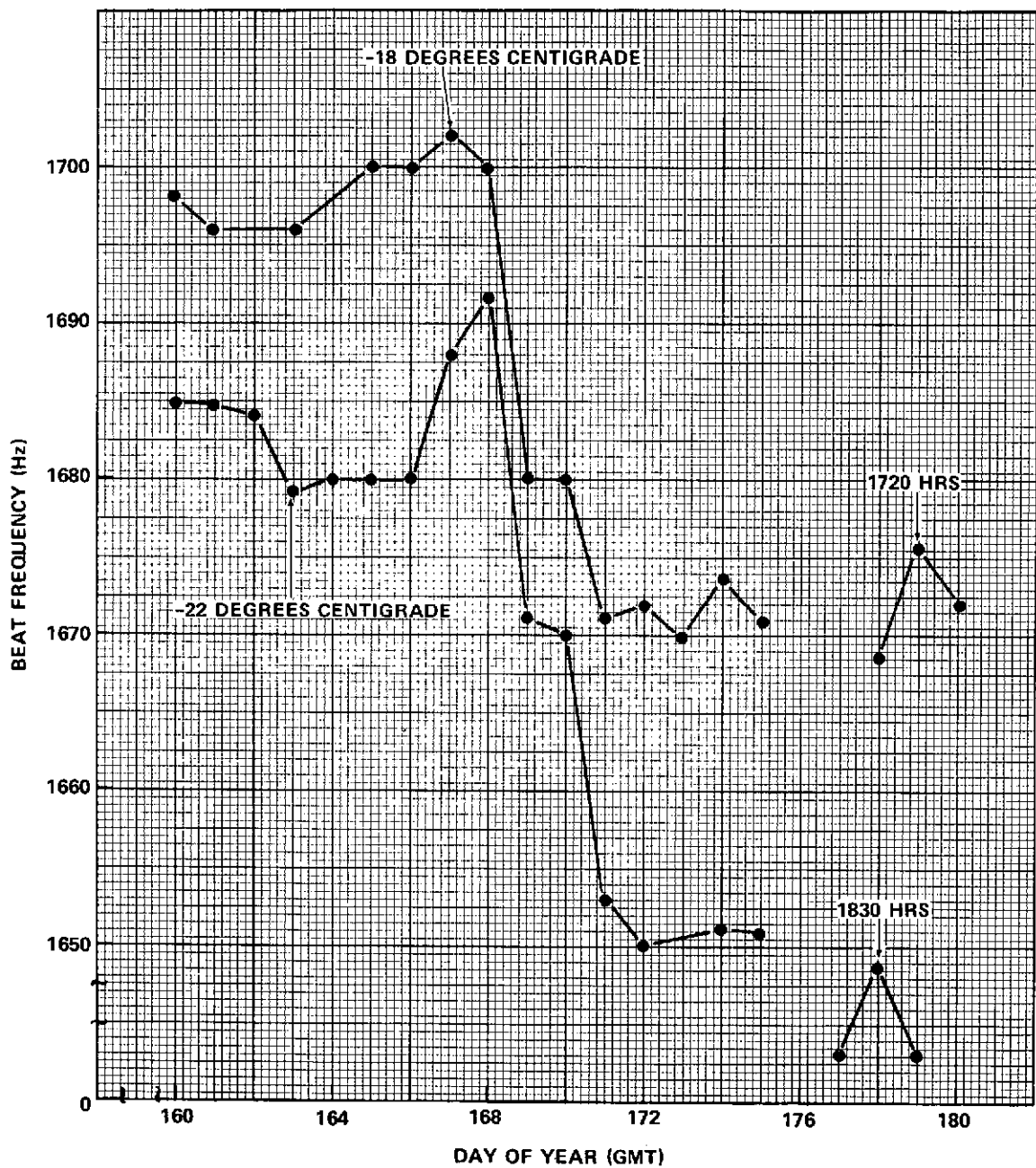
Figure 15-4.   QCM Long Term Performance

SECTION 16

GEOSYNCHRONOUS VERY HIGH RESOLUTION RADIOMETER

EXPERIMENT

(GVHRR)

SECTION 16

GEOSYNCHRONOUS VERY HIGH RESOLUTION RADIOMETER EXPERIMENT (GVHRR)

16.1 INTRODUCTION

On August 15, operation of the GVHRR experiment was terminated following failure of its chopper motor.

During the operational period, the scan servo performed satisfactorily with a pointing bias error of 1.5°N. E. Starting of the scan motor became unreliable after the first 30 days in orbit, and the minimum starting temperature became progressively higher each day.

Image data from the two visible and one IR channel were satisfactory.

The instrument was operated satisfactorily in single and automatic, full frame and sector scan, Rosman, and equatorial point modes.

Ground equipment for data reduction, transmission, and display operated well.

16.2 SCIENTIFIC OBJECTIVES

The objectives of the radiometer experiment are as follows:

a. The development of meteorological applications with registered visible and infrared measurements from a geosynchronous satellite.

b. Testing of a precision radiometer on a three-axis stabilized spacecraft.

The radiometer provides both day and night measurements for the determination of cloud motions, tropical storm life cycles, extratropical storm life cycles, mesoscale phenomena, and cloud climatology studies. In addition, the radiometer system supplies information used for earth albedo measurements, earth resources, and ocean temperature studies.

16.3 EXPERIMENT DESCRIPTION

The GVHRR instrument measuring 2 ft × 1.4 ft × 1 ft, with a 1 ft × 1 ft × 1.2 ft radiant cooler attached toward the end of one of its sides, weighs 96 pounds installed. Power consumption is 48 watts under normal operating conditions. The instrument operates in the 0.55 to 0.75μm and 10.5 to 12.5μm spectrum bands. An 8-inch Cassagranian telescope with a scan mirror in front of it provides the

visible and infrared channels with 5.5- and 11-km spatial resolution respectively. The instrument is installed in the northeast corner of the spacecraft Earth Viewing Module with the telescope/scan mirror optical opening looking out the earth viewing face and the radiant cooler looking out the north face. The electronics is concentrated in one box which is heat-sinked to the spacecraft.

The telescope housing containing the telescope, scan mirror, scan mirror servo motors, relay optics, chopper motor, black body reference, visible detectors, visible calibrator, and visible detector preamplifiers is thermally isolated from the spacecraft, and varies from +48°C to -6°C daily. The instrument has its own PCM digital encoder and multiplexer which supplies a 72 kb split-phase PCM serial bit stream containing image and housekeeping data to the spacecraft C-band modulator. A backup data transmission system for the image channels uses 32 kHz, 48 kHz, and 176 kHz FM VCO's combined and sent on command over the same line used by the digital data stream to the C-band modulator.

Visible and infrared radiant energy within the 20° by 20° field-of-view of the instrument is reflected 90° into the telescope by the scan mirror which provides full 20° × 20° scans in 25 minutes and 5° × 20° scans (sector scans) in 6.5 minutes. The scan mirror, upon completion of a full or sector scan, slews to look at a thermally monitored side of the optical housing to obtain in-flight warm point infrared calibration data. Space provides the zero level in-flight calibration data. Following completion of an image and calibration scan sequence, the scan mirror repeats the sequence until it is commanded to stop. Single scan sequences are also available by appropriate commands. Scene radiant energy is passed through the 8-inch diameter cassegranian telescope to the chopper wheel. When chopper teeth pass in front of the incoming beam, it is reflected 90° through the infrared relay optics to the HgCdTe cooled infrared detector. A radiant cooler passively maintains the infrared detector at 115°K. Automatic protection against accidental excessive sun input into the cooler is provided by a flexible door which closes over the inner portion of the cooler if the infrared detector temperature exceeds 210°K. Decontamination of the radiant cooler is provided by commanding the protective door closed and the cooler heaters on. When chopper wheel teeth are not in the way of the incoming beam, radiant energy passes between them, through the visible relay optics, to two identical silicon visible detectors mounted on the same chip. At the same time the infrared detector is able to see the 340°K reference blackbody. Conversely, the visible detectors may see the reference blackbody reflected on the back of the chopper wheel teeth when the teeth are in the way of the incoming beam. Signals from visible and infrared detectors are then ac amplified and demodulated synchronously, using clock signals derived from the chopper image signals.

Visible calibration is provided by injecting sunlight which passes through a diffuser plate on the bottom of the instrument, a light pipe and a solenoid operated mirror, into the normal beam position in front of the chopper wheel, while simultaneously blocking off the scene radiant energy. A summary of the GVHRR instrument specifications may be found in Table 16-1.

Table 16-1

ATS-6 Geosynchronous Very High Resolution Radiometer
Specifications Summary

1. Channels

IR	10.5-12.5 microns	
Visible	0.55-0.75 microns	

2. Resolution

IR	IFOV 0.3 mr	6 nm	11 KM		
Visible	IFOV 0.15 mr	3 nm	5.5 KM		

3. Dynamic Range

IR	0°-340°K
Visible	Albedo 1-100%

4. Noise Equivalent Temperature Difference of IR Channel

Scene Temperature	NEΔT
200°K	1.5°C
300°K	0.5°C

5. View (Whole Frame)

20° × 20°

6. Time for One Frame

24 minutes

7. Sector Scan

Nine overlapping 5° high sectors, 60% overlap (all 20° wide)

8. Time for 5° Sector Scan

6 minutes

9. Number of IR Samples Per Frame

2400 (50% overlapped) per line, 1200 lines

10. Number of Visible Samples Per Frame

2400 pairs per line, 1200 lines

Table 16-1 (Cont'd)

ATS-6 Geosynchronous Very High Resolution Radiometer
Specifications Summary

11. Digitization of Each Resolution Element
    9 bits plus odd parity

12. Aperture Size
    8 inches diameter

13. Scan Motion
    Reciprocating by line beginning in SW corner

14. Telescope
    Cassegrain

15. Chopper Wheel
    Operates at 3,000 rpm
    Passes Visible
    Reflects IR

16. IR In-Flight Calibration
    Hot - Temperature Monitored Telescope Housing
    Cold - Space

17. Visible In-Flight Calibration
    Bright - Solar Input
    Dark   - Space

18. Electronic Calibration
    6 Level, all channels

19. Detector Temperatures
    IR   115°K (Radiantly Cooled)
    Visible   300°K (Telescope Temperature)

20. Antifrost Protection (IR Detector)
    Cold Trap

21. Cooler Anti-Sun Protection
    Cooler mouth trap door

22. Primary Data Transmission
    Digital-split phase PCM

23. Digital Transmission Rate
    Approximately 72,000 bps

Table 16-1 (Cont'd)

ATS-6 Geosynchronous Very High Resolution Radiometer
Specifications Summary

24. Alternate Data Transmission	
Analog-Image information via three VCO's:	32 KHz
	48 KHz
	176 KHz
25. Power Requirement	
+28 volts, 60 watts	
26. Weight	
96 pounds	
27. Size	
Approximately 25" × 15" × 12" excluding cooler and sun shade	

At the ground stations two identical unique GVHRR PCM decommutation/computer
interface systems were provided by ITT, one each for the Rosman and Mojave
tracking stations. ITT also supplied the PDP-11 software which is used in
real-time to process received GVHRR data into 9T800 BPI digital tapes. Backup
analog tapes are also made and are retained at the ground station. A diagram
of the GVHRR data flow may be found in Figure 16-1. Over 600 digital tapes
were made from launch through the end of this reporting period.

Nonproduction IBM 360/91 and 360/75 interactive image processing routines
were adapted for use beginning immediately after launch for generating the data
and photographic images required for performance analysis and developing cali-
bration criteria for production calibration software. The first results began to
flow from this effort at the end of this reporting period. Figures 16-2 and 16-3
are samples of uncorrected visible and IR full Earth pictures.

16.4   EXPERIMENT PERFORMANCE EVALUATION

The instrument contract was awarded to ITT, Fort Wayne, Indiana, in January
1970. Thermal-structural, engineering and protoflight models were built. The
protoflight model flew. Two chamber control/bench check units and two ground
station systems were also fabricated and delivered. Delivery of the protoflight
unit was made to the spacecraft contractor's plant (Fairchild Industries) in
April 1973. The instrument was then integrated into the spacecraft and under-
went spacecraft level testing. During spacecraft systems thermal vacuum
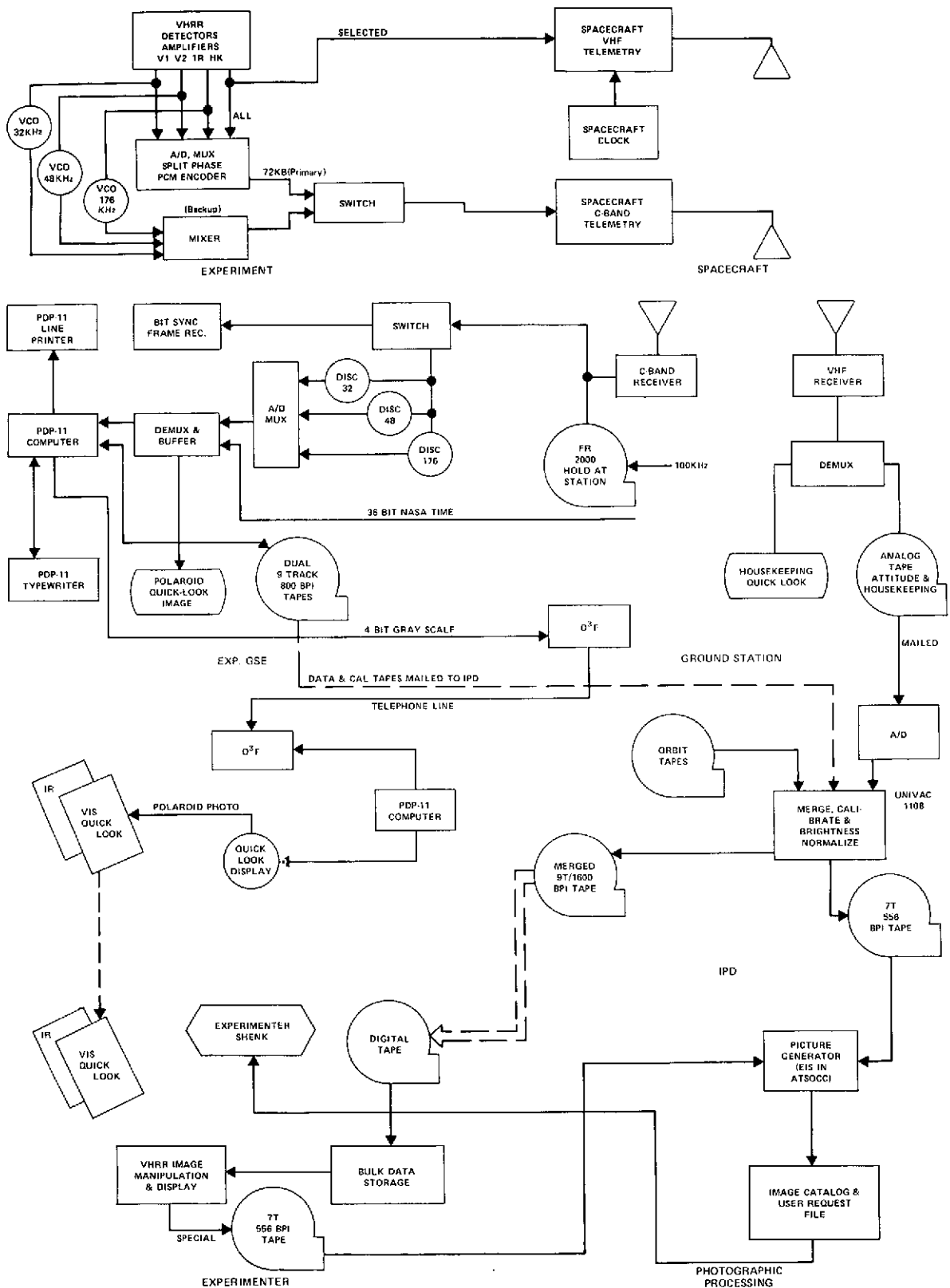
Figure 16-1. ATS-6 GVHRR Data Flow

ATS-6 GVHRR V1V2 R00367 195-1731Z Z493-2/Z494-1 9S C63 112074
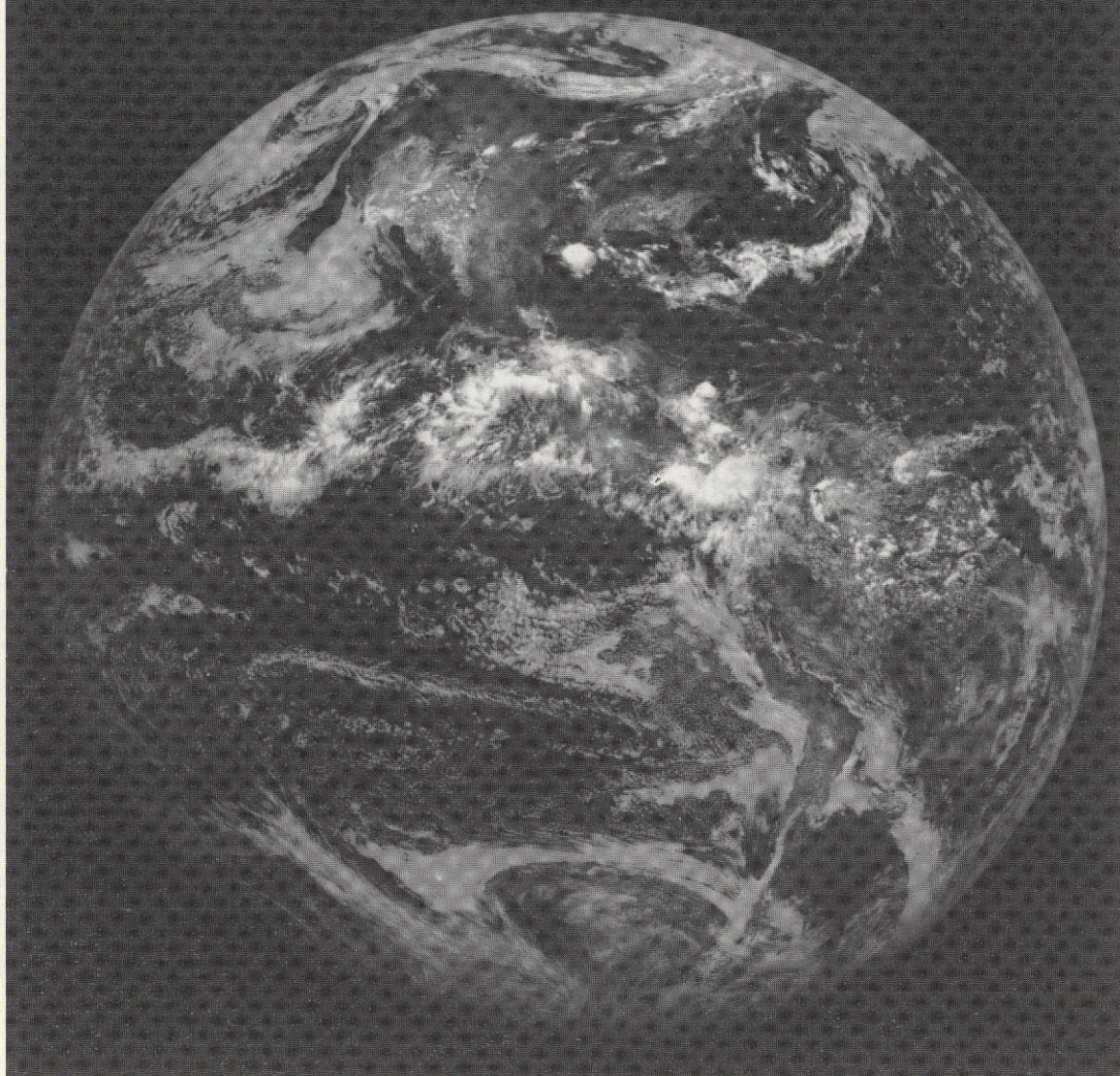
Figure 16-2. Uncorrected Visible Full Earth Picture

16-7

ATS-6 GVHRR IR 114.9K R00367 195-1731Z Z493/Z494-1 960 10224
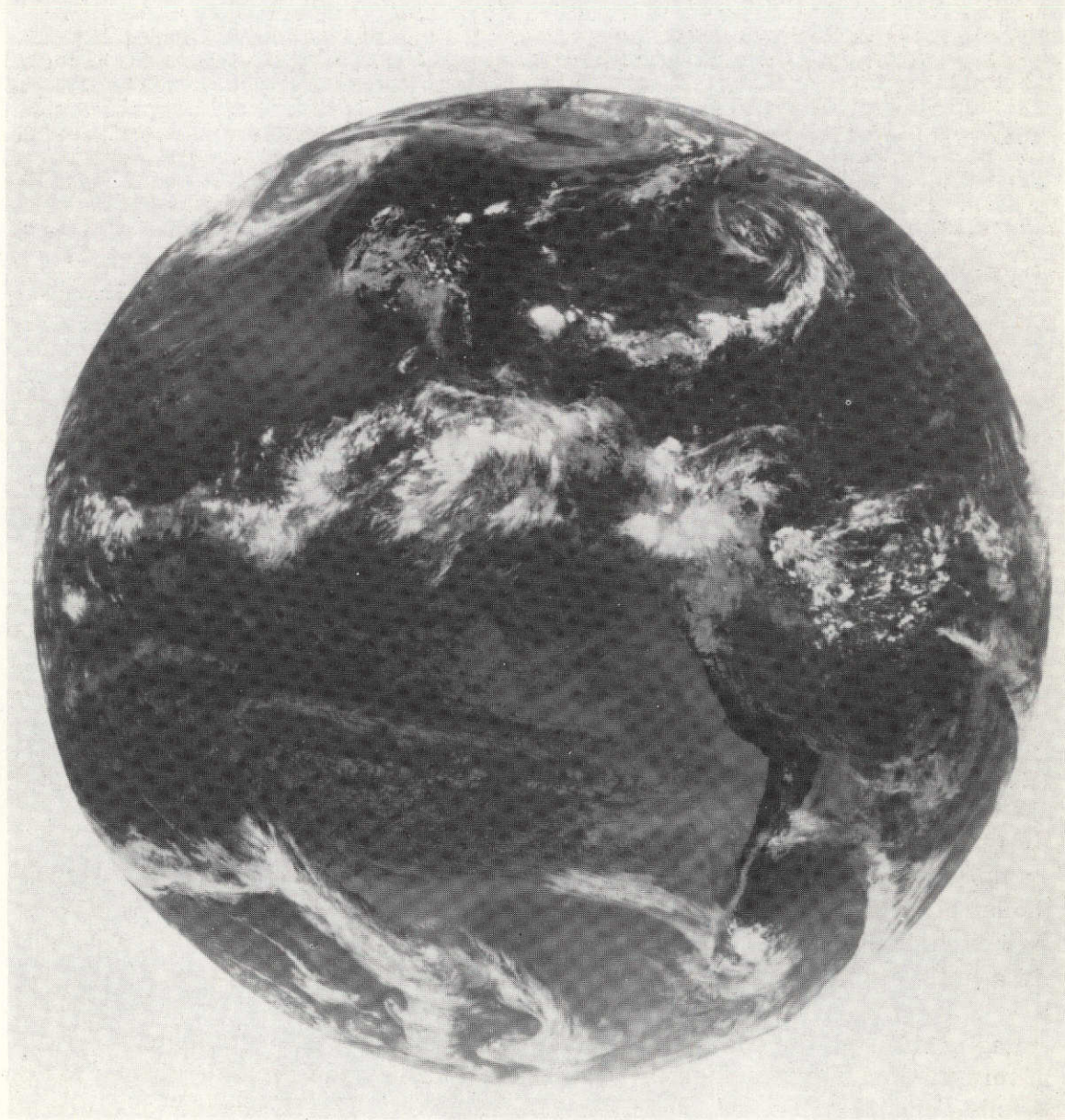
Figure 16-3. Uncorrected IR Full Earth Picture

16-8

testing, a problem was encountered with unreliable servo cold start below 0°C. Because of the serious impact on the spacecraft launch schedule, which removal of the instrument would have had, it was decided to proceed. Accordingly, no opportunity was available to troubleshoot the problem internally. A final IR calibration was conducted during spacecraft thermal vacuum testing. This calibration showed approximately a 20% shift in IR channel response from the calibration data taken over a year earlier when the instrument was calibrated prior to delivery from ITT. Also, the instrument radiant cooler and scan mirror reflective surfaces suffered severe contamination during spacecraft thermal-vacuum testing, necessitating cleaning several times before launch. Shortly before shipment of the spacecraft from Fairchild Industries for launch, one of the radiant cooler flexible door guides was damaged, rendering the door inoperative. The door guide was repaired and checked out on the launch pad.

Launch was May 30, 1974. The chopper motor was run and the radiant cooler cone door was closed through launch. A slight unexplained increase in total instrument current was noted after launch.

One day after launch the radiant cooler heaters were turned on. Two weeks after launch the radiant cooler cone door was commanded open and the cooler heaters were commanded off. The cooler cooled down to 115°K, the design temperature, and maintained the IR detector at that temperature as long as the sun elevation angle remained below the specified 23.5°. The scan servo performed satisfactorily except that pointing was apparently off about 1.5° to the northeast, requiring repointing of the spacecraft to the southwest to center the Earth in the instrument field-of-view. The scan system exhibited three known linecount skips which had the effect of temporarily mirror-imaging the data east for west.

Unreliable scan starts continued to occur as before launch, below approximately +2°C telescope housing temperature, for the first four weeks after launch. Then, in two periods separated by about one week, the unreliable servo cold start temperature climbed to +33°C. This increase was serious since the telescope housing maximum diurnal temperature was +48°C. The servo system was operated continuously for long periods of time and also turned on and off repeatedly in a futile effort to improve the unreliable servo turn-on problem.

Image data from the two visible and one IR channels were satisfactory. Preliminary analysis indicates that spatial resolutions and dynamic ranges for the visible channels are very nearly in-specification. The IR channel data are still being processed for analysis.

The chopper motor was satisfactorily run continuously except for several brief periods from before launch through the end of this reporting period.

Visible calibration was activated only for mechanical test and was not used at all operationally.

The Wideband Data Unit with the C/S successfully modulated high quality video signals both for the IR and visible spectrums on to the C-band downlink carrier. The addition of multiplexing the Interferometer High Speed Data Link (IHSDL) did not degrade the quality of the radiometer pictures.

The instrument was operated satisfactorily in single and automatic, full frame and sector scan, Rosman and equatorial point modes. Unique GVHRR ground equipment satisfactorily generated image data digital tapes which were subsequently mailed to GSFC for further processing. Quick-look images at ATSOCC were also provided via a 7.2 kb telephone modem from the Rosman tracking station. Satisfactory image photographs from uncorrected data have been made on a preliminary basis as work continues on production image data reduction software programs. Digital dumps and histograms of selected data are now also being generated on a nonproduction basis.

On day 227 (August 15, 1974), the GVHRR chopper motor failed. Since then no GVHRR pictures have been obtained.

16.5   FAILURE ANALYSIS

16.5.1 Chopper Motor History

During the test phase of S/N 2 chopper motor, two malfunction reports were written (MR D 04148 and MR D 01320) and listed below:

> MR D 04148 - Chopper motor would not start on second try (started once) at telescope temperature of -50°C. Warmed telescope to room temperature but chopper motor would not start. Removed instrument from chamber and fingered chopper; it felt slightly hung-up. Chopper operated properly after fingering.
>
> Attributed to the fact that the motor was at -50°C instead of the required -37°C. The chopper motor operated for approximately 700 hours after the failure prior to shipment.
>
> MD D 01320 - Block, board mounting was not properly adjusted and allowed one of the light sensor or light source boards to contact chopper wheel.
>
> After further study of the design, the light sensor and light source boards were eliminated from the system.

16.5.2 Preliminary Data Evaluation

Early data, at the time of failure, was interpreted to mean that the failure occurred in something less than forty-eight (48) seconds. This indicated a sudden hard stoppage. Subsequent review of better data tapes proved this to be incorrect. This latter review indicates the chopper motor slowdown/stop occurred over a period of some twelve (12) to fifteen (15) minutes.

Since the chopper motor bearings were lubricated at GSFC both the dry weight and lubricated weights as they left GSFC, are available. After shipment to Schaeffer Magnetics Inc. , some of the lubricant was blown off using an air brush and dry nitrogen. This was done because of the concern with the break-away torque value with too much lubricant.

Subsequent contacts with Schaeffer indicate that one of the bearings may have had as little as 1.7 milligrams of lubricant. This is one of the bearings used in chopper motor S/N 2, the failed unit. The accuracy of this data is being verified.

In view of the above, the Materials Group has impregnated an R-4 bearing with 1.7 milligrams of Krytox 143 AB. This bearing will be subject to a thermal vacuum environment; 60°C; 10^{-6} torr for five days. The bearing will then be reexamined.

Late Friday, September 27, 1974, an additional check with Schaeffer Magnetics revealed a different data point. At this time Schaeffer indicated the bearing lubricant weights was 11.7 milligrams and not 1.7 milligrams. The committee will endeavor to obtain actual weight records from Schaefer to verify the true lubricant weight.

16.5.3 Planned Actions

The engineering model, S/N 3 and S/N 4 chopper motors will be delivered to GSFC. In addition the engineering model drive electronics and the remaining flight printed circuit boards are to be delivered.

S/N 3 will be dismantled to measure both manufacturing tolerances and lubrication weight. S/N 3 will then be reassembled and tentatively will be tested with S/N 4 in a thermal vacuum environment over the flight temperature range. S/N 4 will definitely be tested.

A formal test plan and test procedure will be established.

Data is being evaluated to determine if the ATS-6 GVHRR began to draw higher current long before the time of failure. Plans are to take data from the launch pad activities period and at approximately 35 days into the mission. This will then be compared against the data at the time of failure.

Further attempts will be made to start the GVHRR. Two methods will be employed, one will be to send multiple rapid commands the other to power up the complete GVHRR and then command everything but the chopper motor to off. Both of these methods will be accomplished an odd number of times so that the last command is chopper motor on.

SECTION 17

ION ENGINE EXPERIMENT

SECTION 17

ION ENGINE EXPERIMENT

17.1 INTRODUCTION

Two major Ion Engine tests were conducted with the first test starting on day 199 and the second test starting two days later.

The first test, employing the south engine, lasted approximately 1.5 hours. Operation was entirely satisfactory, with telemetered parameters normal. Anomalies associated with spurious counts in the registers controlling X and Y deflections were noted but are not considered a serious problem. No compatibility problems with the communication subsystem were noted.

During the second test, lasting approximately 15 hours, the Ion engine High Voltage repeatedly cycled off after approximately 1 minute of operation. Additional tests were conducted on days 215, 226, 234, and 235, resulting in the same high voltage problem; however, spacecraft charge data was collected during these trials.

Circuit analysis and lab tests employing the flight spare thruster operating in a chamber at Fairchild produced no evidence which would explain the cause of the failure.

17.2 SCIENTIFIC OBJECTIVES

The primary objective of this experiment is to verify and obtain operational data on the use of an ion microthruster electric propulsion system for north-south stationkeeping orbital maneuvers. The ion engine, because of its inherent high specific impluse, is an ideal spacecraft propulsion device if feasible for this application.

17.3 EXPERIMENT DESCRIPTION

The Cesium bombardment ion thruster utilizes the magnetoelectrostatic plasma containment concept. A two-grid extraction system is employed to generate a high velocity ion beam and neutralizing electrons are produced by a plasma bridge neutralizer. Thrust vectoring is provided by the accelerator displacement method. Propellant is supplied by three capillary type reserviors operating at different potentials.

The experiment flight hardware consists of two identical cesium bombardment ion microthruster systems. The two systems are mounted in the Earth Viewing Module (EVM) and aligned so that their undeflected thrust vectors pass through the spacecraft center of mass, normal to the roll axis. The assumed angle between the thrust vector and the yaw axis requires that the thrust capability of each microthruster be 1.0 mlb. Each microthruster system weighs about 33 lbs and requires less than 150 watts of power.

17.4 EXPERIMENT PERFORMANCE EVALUATION

17.4.1 General

Initial operation of the ATS-6 Ion Engine Experiment was scheduled for mid-summer 1974 so that there would be ample time for characterization of the spacecraft and those experiments that might have some interaction with the Ion Engine Experiment. In addition, it was specified that the thrusters be thoroughly outgassed before operation. A month is entirely adequate for this purpose. The South engine was chosen for initial operation because of its minimum interaction; it is located on the side of the Earth Viewing Module away from the Polaris Star Tracker, the VHRR Cooler and the Quartz Crystal Microbalance.

The objective of the initial test was to demonstrate that the thruster was operating satisfactorily as indicated by telemetry and to demonstrate short-term compatibility with the spacecraft in general and with the communications system in particular. Approximately 1.5 hours was scheduled for this demonstration. A second test of approximately 6 hours duration was scheduled 48 hours later. Subsidiary planned activities included measurements of the spacecraft potential before, during, and after Ion Engine operation by the EME and generation of a small impulse along the orbit trajectory by pitching the spacecraft by approximately 5 degrees.

Initial operation of the South Ion Engine was entirely satisfactory, but subsequent attempts to operate the engine were unsuccessful. This report describes the initial test, subsequent attempts at operation, diagnostic operations, and ground test simulations carried out in support of the operation.

17.4.2 Initial Test

17.4.2.1 Test Plan—Initial operation of the South Ion Engine was scheduled for the evening of July 17, 1974. The test plan is shown in Table 17-1. It is derived from procedures followed during the initial operation of the ion engines during laboratory tests. Evening operation was scheduled so that the effect of ion engine operation on spacecraft potential near spacecraft midnight could be observed;

Table 17-1

Test Plan for Ion Engine 2
(Initial Test, Day 199)

Time (min)	Function	Command
0	Preheat	Ion Engine 2 LIC On Ion Engine 2 Master Converter On
120	Start Neutralizer	Neutralizer Vaporizer On Neutralizer Adjust, Step 10
140 (approx)	Neutralizer operating in spot mode; start thruster	High Voltage On Cathode Vaporizer On Anode Vaporizer On
160 (approx)	Thruster operating stably at 0.75 mlb; increase to 1 mlb	Anode Vaporizer
210	Shut down thruster; bake out	Anode Vaporizer Off Cathode Vaporizer Off Neutralizer Vaporizer Off
240	Shut down test	Ion Engine 2 LIC Off

it is during the hours near midnight when potential excursions in the several hundred volt range are occasionally seen.

17.4.2.2 Test Operation—The command log for this operation is shown in Table 17-2; strip chart recording of telemetry is shown in Figure 17-1. Thruster preheat started at 00:29:56 with Load Interface Circuit On and Master Converter On. The Neutralizer On command at 01:10:14 was due to an operator error; it was not part of the test plan and was corrected 12 minutes later. After 2 hours and 25 minutes of preheat, the thruster startup sequence was started at 02:54:53 with Neutralizer On and setting the Neutralizer Reference at Step 9. (The plan called for Step 10.) At 03:09:40 neutralizer operation made the transition from plume mode to spot mode as evidenced by the drop in neutralizer probe potential. This was at the low end of the expected range of time for achieving spot mode operation (20 to 50 minutes). With the neutralizer in operation, no further delay in starting the thruster was required, so at 03:14:12 the high voltage, cathode vaporizer and anode vaporizer were commanded on. Telemetry showed that the cathode vaporizer and anode vaporizer were cycling on and off as they

Table 17-2

Command Log for Ion Engine 2
(1st Test, Day 199)

Time	Command
00:29:56	LIC On
00:35:02	MC On
01:05:01	10 Neutr. Adj.
01:09:45	
01:10:14	Neutr. On
01:22:14	Neutr. Off
02:54:53	Neutr. On
03:08:09	9 Neutr. Adj.
03:11:35	
03:14:12	HV On
03:14:41	K Vap On
03:15:34	A Vap On
03:16:48	Neutr. Off
03:19:27	MC On
03:20:23	HV On
03:20:53	K Vap On
03:21:22	A Vap On
03:24:19	Neutr On
03:24:58	10 Neutr. Adj.
03:36:10	
03:44:46	AV On
04:00:36	12 Y Defl.
04:04:35	
04:05:22	Neutr. Adj.
04:13:37	8 Y Defl.
04:16:11	
04:17:45	11 X Defl.
04:21:32	
04:24:23	15 Y Defl.
04:29:39	
04:32:41	A Vap. Off
04:33:38	K Vap. Off
04:34:42	Neutr. Off

Figure 17-1. Initial Test Telemetry (Strip Chart Recording)

would in the case of high voltage sparking. This continued for 85 seconds, at which time the arc counter issued a Master Converter Off command, shutting down the system. The Neutralizer Off command issued at 03:16:48 was thus superfluous.

At 03:19:27, Ion Engine 2 was restarted with the series of commands required for 3/4 millipound operation. After the initial period of high voltage sparking which led to system shutdown, the thruster sparked only occasionally. At 03:31:00 the neutralizer went into spot mode and shortly thereafter, at 03:31:50, the thruster discharge was initiated and ion beam generation began. The vaporizer control loops all operated normally and within 6 minutes had stabilized operation at 3/4 millipound. At 03:44:46 a second Anode Vaporizer On command was given, calling for 1 millipound operation, and operation quickly stabilized at the new level. The accelerator drain current rose gradually to a peak of 4 ma, then fell again to a normal operating level of 1 ma. At about 03:48:00, near the accelerator current peak, four spurious Y+ deflection steps were taken by the CLPC, presumably caused by thruster sparking.

At 04:03:10, the neutralizer propellant flow rate was no longer sufficient to sustain spot mode and the transition to plume mode was made. The neutralizer interlock turned off the high voltage and the thruster vaporizers. At 04:05:22 one additional Neutralizer Adjust command was issued, putting the refernece at step 11. By 04:12:00, thruster operation has again stabilized.

At 04:00:36 a series of 12 Y-deflection commands was given to advance the deflection register from 4 to 16 which is the same as zero. For some reason not understood, the net result was a deflection of 8 steps. An additional 8 steps issued at 04:13:37 brought back to zero.

At 04:03:20, X-deflection telemetry indicated that X-deflection had jumped to Step 4. Eleven X-deflection commands, issued at 04:17:45, returned X-deflection to zero. It is not understood why this had the effects of 12 commands.

At 04:24:23, 15 Y-deflection commands were given, producing full deflection in the -Y direction. Additional spurious commands left the system at +6 steps, where it remained for the remainder of the test.

At 04:32:41 the anode, cathode and neutralizer vaporizer were commanded off, starting system shutdown. By 04:35:00 the thruster arc had extinguished and operation was terminated. The Master Converter remained on for approximately two hours, providing an extended bakeout of the system after operation.

In general, operation of the thruster in this initial test was excellent; all telemetered parameters were normal and thruster operation was typical of that seen in initial operational cycles.

17.4.2.3 Anomalies—Anomalies observed during the test were all associated with spurious counts in the registers controlling X and Y deflection.

On three occasions, extra counts appeared in the Y deflection register, and on two occasions extra counts appeared in the X deflection register. These counts have been seen before in operational testing and, while certainly undesirable, do not represent a serious problem to the experiment.

17.4.2.4 Correclation with Other Spacecraft Measurements and Parameters Environmental Measurements Experimental—During the time that the Ion Engine Experiment was being operated, the EME package was on and output data was being monitored. Particular attention was paid to the low energy particle spectra from the Auroral Particles Experiment. Interpretation of the energy spectra led to the conclusion that before and after the ion engine operation, the spacecraft potential was approximately 10 volts positive with respect to the ambient plasma, but while the ion engine was in operation, the spacecraft potential was approximately 10 volts negative. This was as predicted and is consistent with laboratory test results where the thruster floating potential is typically 5 to 10 volts negative with respect to the interior surface of the vacuum test chamber.

Since the possibility of radio frequency interference (RFI) from the Ion Engine Experiment has long been recognized, the communications subsystem was configured to monitor for such disturbance during the operation of the experiment. Three receivers were connected to the three I.F. amplifiers and the AGC's of these amplifiers were monitored via telemetry. The center frequency and bandwidth of these receivers were as follows:

Band	Center Frequency	Sensitivity (G/T, FOV)	Bandwidth
VHF	153 MHz	$\geq$ - 25 dB/$^\circ$K	6 MHz
S	2250 MHz	$\geq$ 6.0 dB/$^\circ$K	40 MHz
C	6150 MHz	$\geq$ 9.1 bB/$^\circ$K	40 MHz

In addition, the VHF receiver was up-converted to the 3950 MHz C-Band transmitter and its spectrum monitored at the Rosman Data Acquistion Facility on a spectrum analyzer. At no time during the operation of the Ion Engine experiment were there any indications signals as measured on the IF amplifier AGC telemetry or observed on the Rosman spectrum analyzer. Furthermore, no interference was observed with the spacecraft VHF command and telemetry sybsystem during the operation of the experiment.

The integrated torque produced by positive Y deflection between 03:48 and 04:16 was 0.07 ft-lbf-sec applied in the negative direction about the roll axis. The change in roll momentum wheel speed during this time was about 18 RPM corresponding to an angular impulse of 0.12 ft-lbf-sec. Since the angular impulse is near the limit of resolution for the momentum wheel, the principal conclusion to be reached is that the change in momentum was of the proper sign.

17.4.2.5 Summary—Initial operation of Ion Engine 2 was completely successful. All test objectives were met: the engine started normally and operated smoothly throughout the test period, compatibility of the ion engine with the satellite communication systems was demonstrated, and the prediction of the spacecraft potential during ion engine operation was verified.

17.4.3 Second Test Period

17.4.3.1 Test Plan—The second operation of the South Ion Engine (No. 2) was scheduled for the evening of July 19 (Day 201). The test plan is shown in Table 17-3; it is based on schedules followed in repetitive cycling of thrusters during qualification and acceptance testing. The six-hour test period provides for operation around spacecraft midnight as well as allowing ample time for a thorough checkout of ion engine system operation.

17.4.3.2 Test Operation—The command log for the first 5 hours of this operation is shown in Table 17-4. Thruster preheat started at 02:27:16 with LIC On and Master Converter On commands. After a 40 minutes preheat period, the Neutralizer Vaporizer was commanded on and the reference was set at step 11. Vaporizer heater current telemetry was 3.90 volt, about 5% less than normal. During the next ten minutes it decreased an additional 0.1 volt.

During the preheat period the boundary anode current rose to a peak of 0.250 A before decreasing to < 0.010 A; the plasma anode current rose to 0.650 A, then decreased to < 0.030 A. These values are appreciably higher than are observed in repetitive operations; typically, no appreciable boundary or plasma anode current is seen until the discharge is initiated.

At 03:28:25, high voltage was commanded on, followed by the cathode vaporizer and anode vaporizer at 03:28:51 and 03:31:42. Telemetry indicated zero cathode and anode vaporizer currents. When the anode vaporizer command was executed, enabling high voltage in the absence of the neutralizer spot mode, oscillating I+ and I- telemetry signals were seen. I- typically varied between 1.5 volts and 0 on alternate telemetry updates, while I+ varied between 0.1 volt and 0. After 60 seconds, the Master Converter was turned off by the system arc counter. The 60-second time indicates that the overloading of the high voltage supplies was continuous rather than intermittent.

Table 17-3

Test Plan for Ion Engine 2
(Second Test, Day 201)

Time (min.)	Function	Command
0	Preheat	LIC On Master Converter On
40	Start Neutralizer	Neutralizer Vaporizer On Neutralizer Adjust, Step 10
60	Start Thruster	High Voltage On Cathode Vaporizer On Anode Vaporizer On
80	Full Thrust	Anode Vaporizer On
280	Shutdown Thruster	Anode Vaporizer Off Cathode Vaporizer Off Neutralizer Off
310	Shutdown Test	LIC Off

At 03:37:30 the master converter was commanded on agin, followed by High Voltage On at 03:53:26 and anode vaporizer On at 03:54:22. No attempt was being made to start the thruster; this was done in investigation of the completely unexpected high voltage cycling. Again voltage overloading was seen with no indication of anode vaporizer current and fluctuating indications of I+ and I- as before. After 70 seconds was shut down by the arc counter.

This basic procedure was repeated seven times during the next 3-1/2 hours. The results were very consistent; in each case the master converter was turned off by the arc counter approximately 70 seconds after high voltage was applied.

In the eighth attempt, the neutralizer was operated in spot mode; this permits high voltage to be turned on without turning on the anode vaporizer. Neutralizer vaporizer TM indicator was 3.35 volts. Basic behavior was the same; the system shut down 65 seconds later, but the I- telemetry indication was less oscillatory. The ninth attempt was very similar to the eight, except that the cthode and anode vaporizers were also on. Figure 17-2 shows strip chart records for the first and nonth attempts. This phase ended at 07:35 (3:35 am, Saturday).

Table 17-4

Command Log, Day 201

Time	Command	Comment
02:27:16	IE 2 LIC On	
02:44:14	MC On	1 –40 min preheat
03:21:50	Neutr. On	
03:22:16	11 Neutr. Adj.	
03:27:41		
03:28:75	HV On	
03:28:51	KV On	
03:31:42	A V On	
03:40:04	MC On	2 (Really must have been 03:37:30)
03:53:26	HV On	
03:54:22	A V On	
04:03:19	MC On	3
04:18:36	HV On	
04:18:59	A V On	
04:21:30	MC On	4
04:37:02	HV On	
04:37:31	A V On	
04:40:22	MC On	5
04:43:49	HV On	
04:44:09	A V On	
05:17:02	IE 2 LIC Off	Measure input current
05:19:36	IE 2 LIC On	
05:24:13	MC On	6
05:24:51	HV On	
05:25:21	A V On	
05:27:22	MC On	7
05:44:52	HV On	
05:45:15	A V On	
05:49:23	MC On	8
05:50:54	Neutr. On	
05:51:15	6 Neut. Adj.	
05:53:22		
06:20:24	Neutr. Off	
06:30:49	Neutr. On	

Table 17-4 (Cont'd)

Command Log, Day 201

Time	Command	Comment
06:31:21 06:33:02	6 Neutr. Adj.	8 (cont'd)
06:53:14	HV On	
07:01:20	MC On	9
07:05:55	Neutr. On	
07:31:28	KV On	
07:31:46	AV On	
07:32:36	HV On	
07:34:53	MC On	10

The system was then left with the Master Converter on for approximately 11 hours to let the power being applied to the thruster, vaporize the excess cesium presumed to be causing the faulty operation. At 18:31 the LIC was turned off by the 6 hour clock. The tenth attempt started at 19:02 with LIC On and Master Converter On. A high voltage check was made at 19:02 by commanding high voltage On and Anode Vaporizer On. High voltage appeared to be staying on with only occasional overloads as indicated by the anode vaporizer current telemetry. After about 80 seconds, anode vaporizer telemetry was commanded off followed by the Neutralizer On at 19:31. Neutralizer vaporizer telemetry started at 3.45 V and decreased gradually to 3.35 volts over the next 30 minutes. High voltage, anode and cathode vaporizers were commanded on about 19:58. The net result was the same; the system cycled off in 90 seconds. There was a significant difference in the telemetry indications during the 90 seconds, however. No I+ or I- indications were seen, but both anode vaporizer and cathode vaporizer current TM alternated between 0 and full on indication, indicating that the high voltage was spending an appreciable fraction of the time in the on condition.

This test was repeated. In the 13th and 14th attempts, the vaproizer telemetry indications were much smaller, never reaching the full on indication. This suggested some deterioration in thruster condition. Figure 17-2 shows the strip chart records for the 10th thru 14th attempts.

After the 16th attempt, at 21:30 the system was left with master converter On and full deflection commanded in both X and Y to maximize thruster power input.
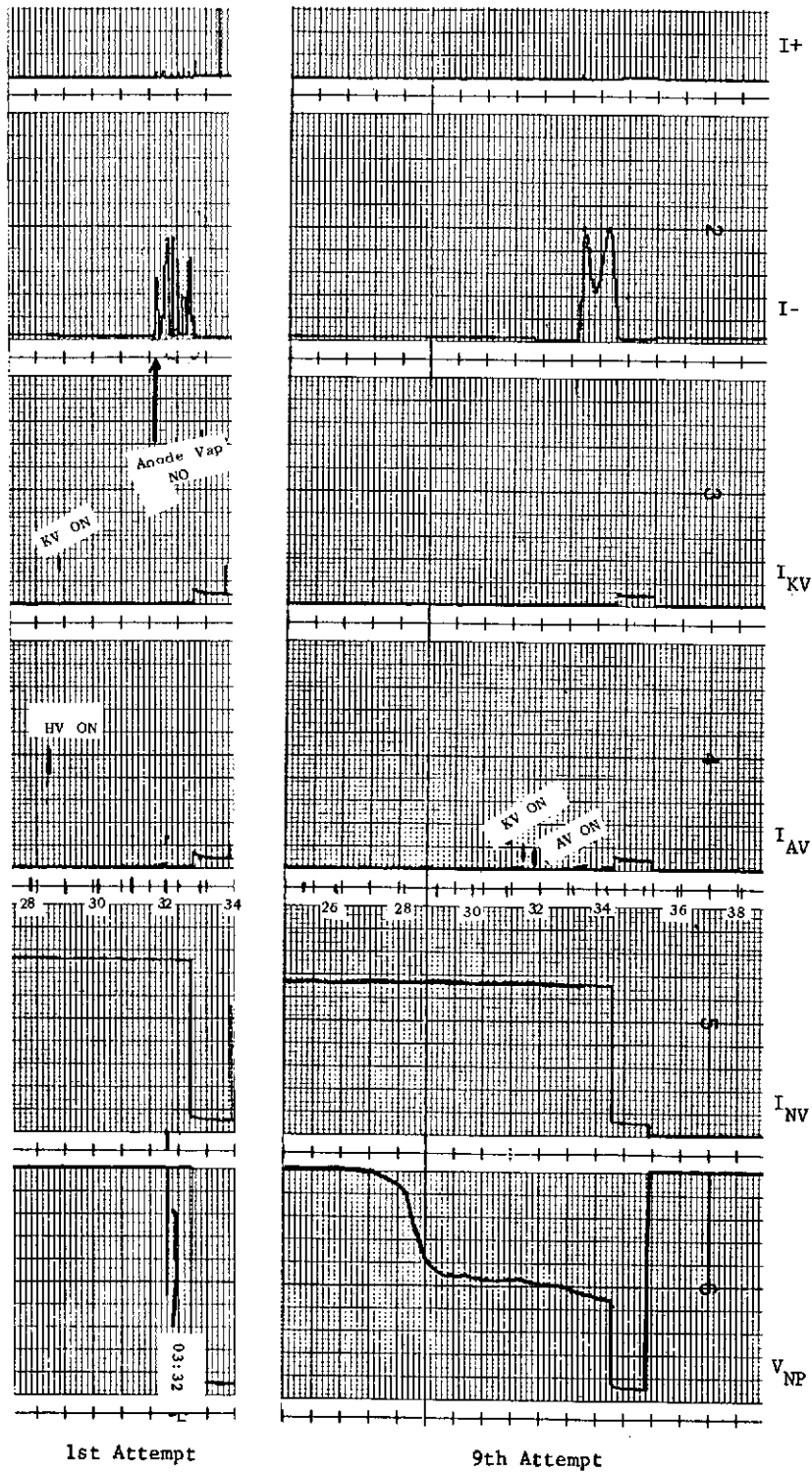
Figure 17-2. First and Ninth Attempts

Figure 17-3

10th - 14th Attempt
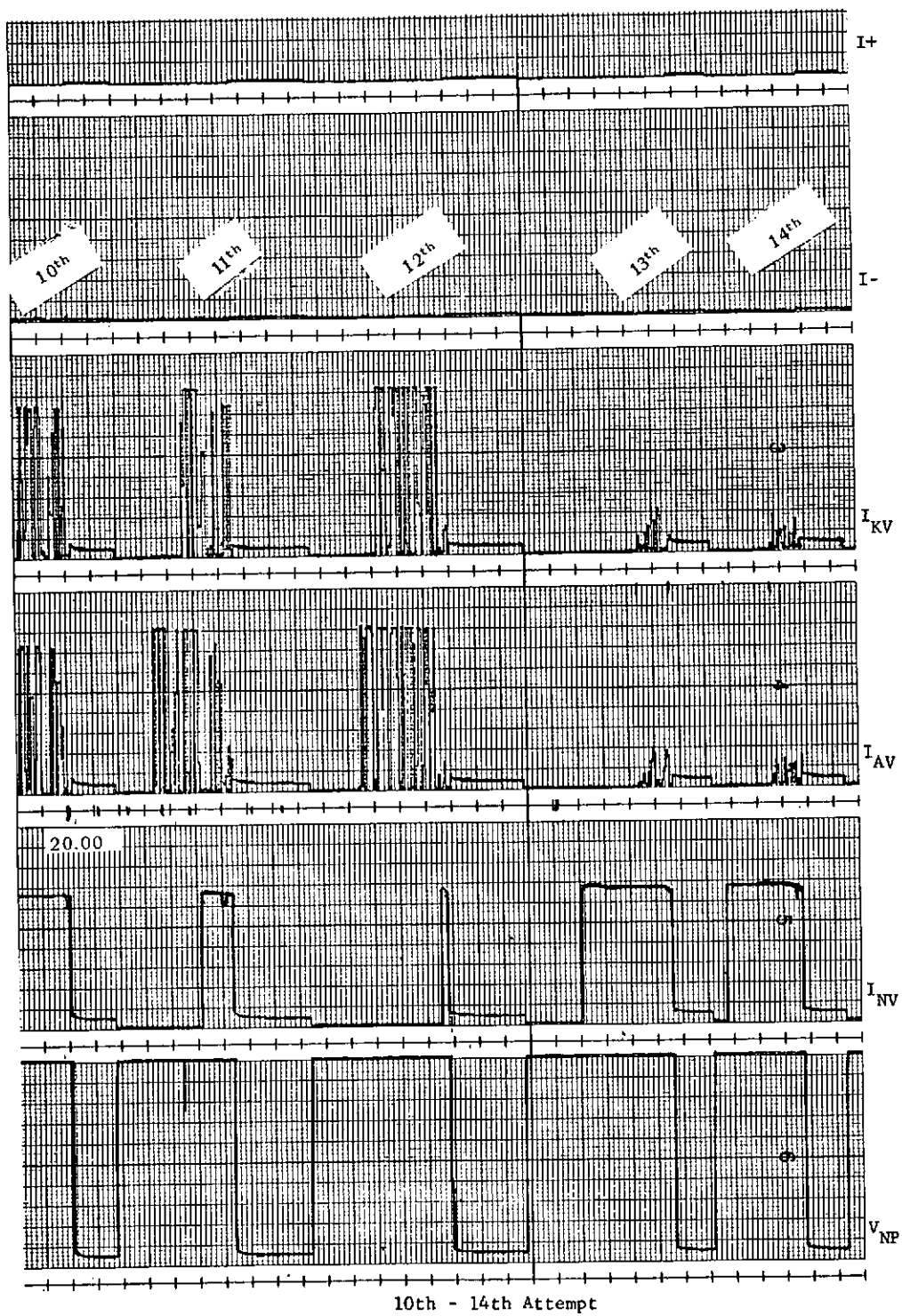
On approximately 01:00 of day 202 exploration of thruster behavior continued and once again it was discovered that changes had taken place. The length of time high voltage would stay on was gradually increasing, under conditions where either the Neutralizer Vaporizer or the thruster vaporizers were off. On-times of 360 seconds were repeatedly observed. However, if this condition were not met, the system would cycle off within 60 seconds. These experiments were repeated until approximately 04:40, at which time the thruster was left with master converter On for 80 minutes. The master converter and LIC were turned off at 06:00.

At 17.29 Sunday, 11.5 hours later, a test was conducted with the thruster in the cold condition. The master converter was turned on, followed by high voltage On, and Anode Vaporizers On. After observing the high voltage stay on for approximately 180 seconds with only 3 interrupts in the smooth telemetry record, the Neutralizer Vaporizer was commanded on, causing the system to cycle off in 50 seconds.

The next few hours were devoted to accumulation of I+, I- and anode vaporizer current with the TM system operation in the dwell mode to provide additional bandwidth. This phase of the operation was completed at 22:00, day 202 (6:00 pm Sunday).

17.4.3.3 Summary—The ion engine was unable to operate during this period of approximately 15 hours because of repetitive overloading of the high voltage power supply. Early in the period it was not possible to maintain high voltage on the engine under any circumstances. As the period progressed, the characteristics changed so that high voltage would stay on if either the neutralizer or thruster vaporizers were turned off. Another observation was that the neutralizer vaporizer full-on telemetry indication was approximately 3.45 volts instead of the normal 4.1 volts seen during the first operation. Deflection telemetry was also lower than normal.

None of these observations were consistent with experience gained during development and test of the ion engine and could not be immediately explained, even tentatively, by the staff responsible for the development and test effort.

17.4.4 Neutralizer Operation for Spacecraft Potential Control

Since control of the spacecraft potential relative to the ambient plasma at geosynchronous altitude is an item of interest to both the program office and the experimenters, a test was made during the second operation period to determine how operation of the Ion Engine 2 plasma neutralizer would effect spacecraft potential. The predicted result of the experiment was that the neutralizer would cause the spacecraft to go to a potential 5 to 10 volts below ambient.

During a period when the EME experiment package was operating, the neutralizer was started by commanding LIC On, master converter On and neutralizer On. In approximately 15 minutes, the neutralizer began spot mode operation, although the neutralizer probe potential did not drop into the closed-loop control range.

Before the experiment started the spacecraft was reported as having a positive 5 to 10 volt potential. With the neutralizer operating, the predicted result of negative 5 to 10 volts was confirmed. When the neutralizer was turned off, the spacecraft returned to its original positive potential. The utility of this experiment is that it demonstrates a relatively simple way of preventing the large and possibly harmful potential variations observed on geosynchronous satellites, particularly near eclipse and during magnetic storms.

17.4.5 Subsequent Operations

An additional test was conducted starting at 14:00 on day 215. Since the last test, the system has been left with LIC On and master converter On for as much time as was available to continue the "baking out" process. Approximately 100 hours has been accumulated since day 202.

The neutralizer vaporizer current telemetry indication was somewhat higher than it had been: 3.9 volts versus a low of 3.45 volts during the test and a normal value of 4.1 volts. Otherwise, the condition of the thruster had apparently degraded. High voltage could not be kept on for extended periods under any combination of vaporizers on or off, but repeatedly cycled off in approximately 80 seconds. Some dependence on vaporizer configuration remained however; with neutralizer vaporizer off, the thruster vaporizer current telemetry spent an appreciable fraction of the time in the full-on condition, while with neutralizer vaporizer on, the indication seldom, if ever, reached full-on indication.

Basically the same behavior was seen in 25 attempts over a three hour period. As the test progressed, the severity of the high voltage overloading appeared to increase: the vaporizer current TM indications were smaller and time to automatic shutdown by the arc counter decreased.

A number of subsequent attempts at operation were made over the next few weeks. Details were not sufficiently different from earlier tests to warrant separate discussion, but one significant point did emerge. It was found that tests which followed extended periods of Master Converter On generally indicated more severe high voltage overload conditions that those tests which followed LIC On only. This is contrary to expectations since it is normally found that power applied to a contaminated thruster hastens the cleanup process. Present results indicate that the addition of cathode and anode feed ring heater power increases rather than decreases the contamination.

17.4.6 Supporting Ground Test Operations

17.4.6.1 System Tests—A consideration of possible causes of the Ion Engine 2 malfunction on the second and subsequent operations exposed the fact that the first operation had been unusual in that the thrusting time was only an hour, much less than the 6 hours operation typical of the development, qualification, acceptance and life test operations conducted to date. Since the thruster system does not come into thermal equilibrium for several hours, it was suggested that the one hour operation could have left the engine in a contaminated condition.

No precise mechanism for this was available, nor was it readily apparent why the contaminated condition, if formed, should be so persistent. Nevertheless, it seemed worthwhile to simulate the operation in the laboratory and make an experimental evaluation of the hypothesis.

A simulated spacecraft surface was fabricated which just fit into a three foot diameter liquid nitrogen flooded liner. The surface of this simulated spacecraft was covered with thermal insulation provided by Fairchild, and the flight spare thruster was mounted on the spacecraft surface using the spare mounting shim also provided by Fairchild. Thermal grease of the type used on the spacecraft was used between the mounting surface and the shim and between the shim and the thruster mounting plate. The simulated spacecraft surface temperature was controlled at 24°C which was the measured spacecraft internal surface temperature during operation of the south ion engine on ATS-6. After installation of thermocouples on the accelerator grid, vaporizers, and mounting plate, the thruster was bolted to the spacecraft and placed in the 3-foot diameter by 9-foot long vacuum chamber. The simulated spacecraft arrangement is shown in Figure 17-4. After the chamber was evacuated, the linear was flooded and a cold soak period begun. After all temperatures had stabilized, the thruster preheater was turned on and all temperatures allowed to stabilize. The master converter was then turned on and again the temperatures were stabilized. This was repeated after the deflection circuitry was turned on to maximum power in both X and Y axes. A table of the measured temperatures is included as Table 17-5. At the completion of the thermal test the thruster was removed from the chamber and the thermocouples removed.

The thruster was then replaced in the chamber and operated in a manner as close to that as experienced by the ATS-6 thruster as possible. The thruster started normally, was operated for an hour and shut down. Liquid nitrogen cooling of the chamber liner was continued and the simulated spacecraft was maintained at 24°C. Twenty-four hours later the thruster was again operated in simulation of the ATS-6 test. Thruster operation was completely normal, indicating that the nonstandard first operation cycle on ATS-6 should have had no deleterious effect.
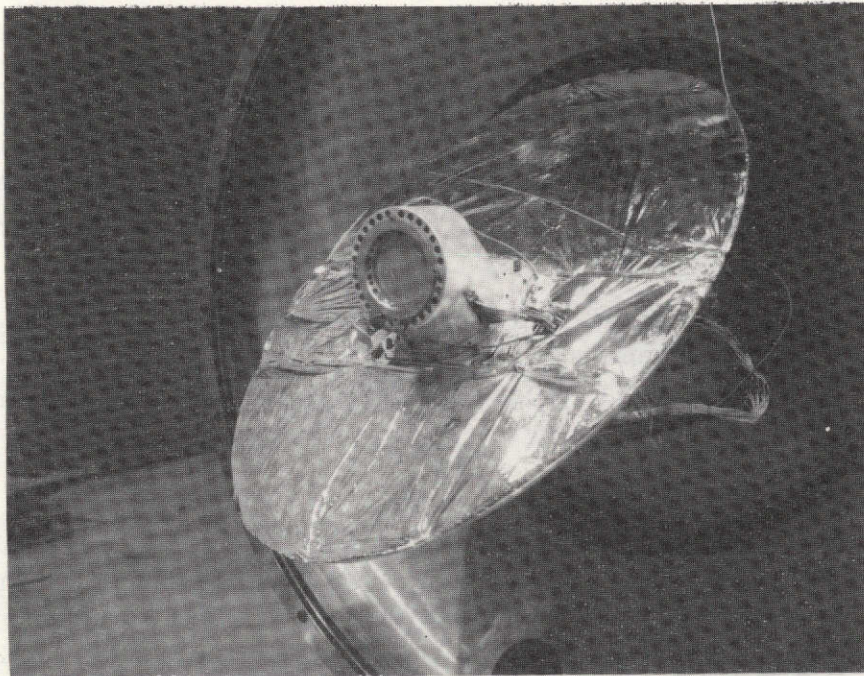
Figure 17-4. Flight Spare Thruster on Simulated Spacecraft

17.4.6.2 Power Conditioning Unit Investigations—An investigation was under-taken to see what could be learned about the power conditioning unit that would aid in interpreting three features of the data received from Ion Engine 2;

a. The reduction at certain times of the Neutralizer Vaporizer Current telemetry indication from a normal 4.1 volts to as low as 3.45 volts.

b. The unfamiliar interlocking mode which permitted the high voltage to stay on only if either the neutralizer or the thruster vaporizers were off.

c. The variability in telemetry returns from I+, I−, and Cathode and Anode Vaporizer Current during high voltage cycling. (Early in the second operation, and I− return was seen, with no response from the vaporizer channels. Later, fluctuating vaporizer signals were seen with no response from I+ and I−.)

Reduction in neutralizer vaporizer current could have several causes:

a. Partial failure of the neutralizer vaporizer magamp. This cannot be ruled out, but is considered very unlikely.

b. Leaky capacitor across control winding (C236). This is a possibility but it would have to be very leaky since this is a fairly low impedance circuit; if it is leaky it should be thermally unstable and prone to failure.

c. Low output from master converter causing reduced drive current to the neutralizer vaporizer magamp. This possibility is discussed further.

d. Partial short from magamp drive transistor to some low-voltage point. This lead runs from the mother board (A7 module) to the lower chassis and passes many other wires. However, a partial short of the correct valve is difficult to imagine, especially one as stable as the I_{NV} TM indicates.

There is the possibility that the I_{NV} is the correct value and that the I_{NV} telemetry is simply inaccurate. This could be caused by a partial short in the I telemetry circuit transformer (T216), by a leaky current filter capacitor (C235), by a leaky rectifier (CR281, 282, 241 or 242), or by a faulty telemetry operational amplifier. It could also be caused by a leaky capacitor or other component in the telemetry circuit after the operational amplifier. This has been ruled out by examining the data from the alternate telemetry encoder on the spacecraft.

The neutralizer vaporizer can be reduced by shunting either the V_{NK} leads or the V_{KH} leads. Ground test performance data is summarized in Table 17-6. The deflection telemetry also shows a small reduction. The mutual loading effect is coincident with an increase in master converter operating frequency, obviously caused by the switching transistors coming out of saturation.

Table 17-5

S/N 01 Temperatures, ATS-6 Simulation

Function	Accel	A_{VAP}	K_{VAP}	N_{VAP}	Liner
Cold Soak	– 18°C	+ 6°C	+ 15°C	+ 8°C	-155°C
Preheater	+ 33°C	+37°C	+ 48°C	+38°C	-163°C
Master Converter	+ 55°C	+87°C	+116°C	+79°C	-148°C
Full Deflection	+103°C	+92°C	+125°C	+85°C	-144°C

The amount of telemetry voltage reduction was, in most cases, less than that observed with S/N 101. This could be at least partly due to variations in switching transistor characteristics (beta).

Table 17-6

Ground Test Malfunction Performance Data

	H. V. ON Neut. ON I_{AV} ON No Short	H. V. OFF Neut. ON No Short	H. V. OFF Neut. ON V_{NK} Shorted	H. V. OFF Neut. OFF V_{NK} Shorted	H. V. ON Neut. ON I_{AV} ON V_{KH} Shorted
I_{NV} TM	4.00 V	4.00 V	3.70 V		3.55 V
X_{DEFL} TM (Step +15)	4.60 V	4.60 V	4.52 V		≈ 4.5 V
I_{IN}	2.9 A	2.3 A	2.0 A		
Freq.	11 kHz	11 kHz	22 kHz	22 kHz	42 kHz

It was suggested that the HV overload circuit might not allow recovery from a transient when the HV converter was operating at such high frequencies. An investigation showed that it worked normally.

Interaction between the HV converter and vaporizers could also have several causes:

    a. Plume mode interlock. This is the interaction path which comes to mind first. Transients on the neutralizer probe, or from the comparator circuit in the A7 module, could affect the high voltage overload circuit if they reached it; however, there is a 100μF filter capacitor connected on the mother board next to the HVOL module (A13), intended to prevent sensitivity to probe voltage transients. Furthermore, unless the system is not in simmer mode, a transistor effectively shunts the plume mode interlock signal to ground. One can visualize interaction between probe transients and high-voltage converter operation (but not between the neutralizer vaporizer and high-voltage operation) if both the capacitor and the shunt transistor were open; however, the transistor is known to be good since the plume mode interlock has been

demonstrated to be defeated in simmer mode, as required. Furthermore, the behavior of the system on ATS-6 does not depend or whether or not the system is in simmer mode.

b. High voltage command register. The command register circuit is in the A2 module which is physically very close to the A13 module which contains the HVOL circuit, which in turn controls the state of the high voltage converter. Therefore, the only way so far imagined for the command register to affect the converter in a way like that exhibited is for it to receive rapid, randomly-spaced HV ON and HV OFF commands from the spacecraft command decoder. This was considered unlikely, especially since it would have to happen only when the I_{NV} and I_{AV} or I_{KV} had been commanded on. It was was ruled out when the alternate spacecraft command decoder was used and the same anomalous behavior appeared.

c. Spark counter. The spark counter has clearly been the means by which the system has been shut down as a result of the system's behavior. However, no means has been visualized for the spark counter to respond to anything other than the cycling of the HVOL circuit, short of outright failure resulting from the +10 volt and/or -10 volt supplies vanishing. The spark counter is contained in the A13 module along with the HVOL circuit but is electrically isolated enough that it cannot conceivably cause high voltage cycling.

d. I+/I- sensing circuits. The failure of certain components within, or associated with, the HVOL circuit, could cause increased sensitivity to actual I+ or I- transients, and also to transients induced in the sensing leads by nearby circuits or wires. An examination was made of the wire routing, and although it seemed unlikely, there could be some coupling between the neutralizer vaporizer lead and the I+ or I- sensing lead. (Tests were performed later on the breadboard and were not successful in achieving any interaction with the neutralizer vaporizer. Even removing the filter capacitor from the I- sensing resistor, shorting the threshold-providing zener diode in the H.V.O.L. input circuit, and lacing the I_{NV} lead together with the I- sensing lead for 3-1/2 inches, produced no interaction.)

The I+ and I- sensing leads, and the neutralizer vaporizer magamp drive lead, are the only ones among those likely to cause any interaction which run from the mother board to the lower chassis. If the magamp drive winding filter capacitor (C236) was open, the transients on the drive lead would be larger. However, it was demonstrated that

they are largest when the neutralizer vaporizer is commanded off, not on. This is due to the low impedance of the drive transistor's emitter when in the on state.

Circuit analysis and laboratory tests, so far, have produced no evidence which would allow identification of the interaction path.

Telemetry returns during high-voltage cycling were investigated experimentally by connecting a variable length spark gap between V+ and V- on the breadboard power conditioning unit. Listed below are the observations for various gap settings.

Wide gap (0.008") (soft short)	Cathode and anode vaporizer TM cycles from zero to full. No I+ or I- indication.
Medium gap (0.006")	Cathode and anode vaporizer TM cycles from zero to partial on. No I+ or I- indication.
Medium gap (0.004")	No cathode or anode vaporizer indication. No I+ or I- indication.
Short gap (0.002") (hard short)	No cathode or anode vaporizer indication. I+ or I- TM produces an indication.
Zero gap (crowbar)	Same indications as hard short.

This produces a possible rationale for the various telemetry indications seen during attempts to start the thruster and may even be used to give some indication of the degree of contamination of the thruster.

17.5 CONCLUSIONS

The initial test of Ion Engine 2 was completely successful; the engine operated as specified during a short, approximately one hour, run. Subsequent tests, conducted over the next two months, were unsuccessful in achieving engine operation due to what appears to be repetitive overloading of the high voltage power supplies. It was postulated that the overloading was caused by an excess of cesium propellant in the thruster, a phenomenon which has been observed in development tests, so the usual procedure, application of power to heat

the thruster and evaporate the excess cesium, was tried. This procedure was unsuccessful. In fact, there are indications that application of maximum power by operating the thruster cathodes and anode feed ring heater leads to more severe overloading of the high voltage supplies than does application of preheater power alone.

It was also postulated that the very short initial test run, shorter than any laboratory test of record, had left the thruster in a contaminated condition. This was explored by simulating the initial test and subsequent test attempts in laboratory operation. The flight spare thruster system used in the simulation operated satisfactorily both times, indicating that the problem was not an operational one.

The fact that operating procedures do not seem to be at fault and that the thruster does not respond to corrective measures ordinarily found effective in laboratory testing suggests that the problem is one of two things: (1) a difference between terrestrial and orbital operation, perhaps involving the migration of cesium propellant under zero-g conditions, or (2) a physical defect in the thruster such as a leak in the propellant system between the propellant reserviors and the thruster. Analysis of these possibilities is continuing; no conclusion has been drawn to date.

Attempts to operate the thruster will continue in the hope that either operation will improve or further understanding of the problem will be gained.

SECTION 18

ENVIRONMENTAL MEASUREMENTS EXPERIMENTS (EME)

SECTION 18

ENVIRONMENTAL MEASUREMENTS EXPERIMENTS
(EME)

18.1 INTRODUCTION

Seven of eight experiments are performing well having met or exceeded their design goals. The exception is the University of New Hampshire (UNH) Low Energy Proton Electron Experiment, which when first turned on June 18, for 1.5 hours caused a permanent malfunction in the 64 level subcomutator word #189. All of the EME experiments use this word for housekeeping data, and are therefore affected to some degree.

A second attempt to turn on the UNH experiment on August 1, 1974 for a 42-minute period, resulted in a similar irregular performance. It is not planned to turn on the UNH experiment again. Anomaly investigations using the prototype unit will continue.

Temperature measurements for most of the experiments were reported to be higher than the pre-flight predictions.

In addition to the UNH anomaly discussed above the following experiments reported minor anomalies:

    Aerospace – Omnidirection Spectrometer
    UCLA – Magnetometer
    UMINN – Particle Acceleration
    HUGHES – Solar Cell Radiation Damage Experiment is experiencing erratic
data from one of its signal processors. Half of the data sample size is expected to be lost as a result of this anomaly.

The experimenters report that their data reduction capabilities are improving and that the rate at which data tapes are being received is increasing.

18.2 EXPERIMENT DESCRIPTION

The Environmental Measurements Experiment (EME) package is a group of eight experiments carried on board the ATS-6 that are designed to study the spacecraft environment at synchronous altitude and to gain information on electromagnetic-ionospheric interactions. Six of the experiments are designed to obtain data on charged particles of several different types and over wide energy ranges. A seventh experiment is to provide magnetic field data, to be used in conjunction with the charged particle measurements to determine the

dynamic processes which take place in the synchronous orbit environment. The eighth experiment is a continuation of previous ATS engineering studies into solar cell degradation.

The energy ranges covered by the charged particles are shown in Figure 18-1 ATS-6/EME Particle Spectrum.
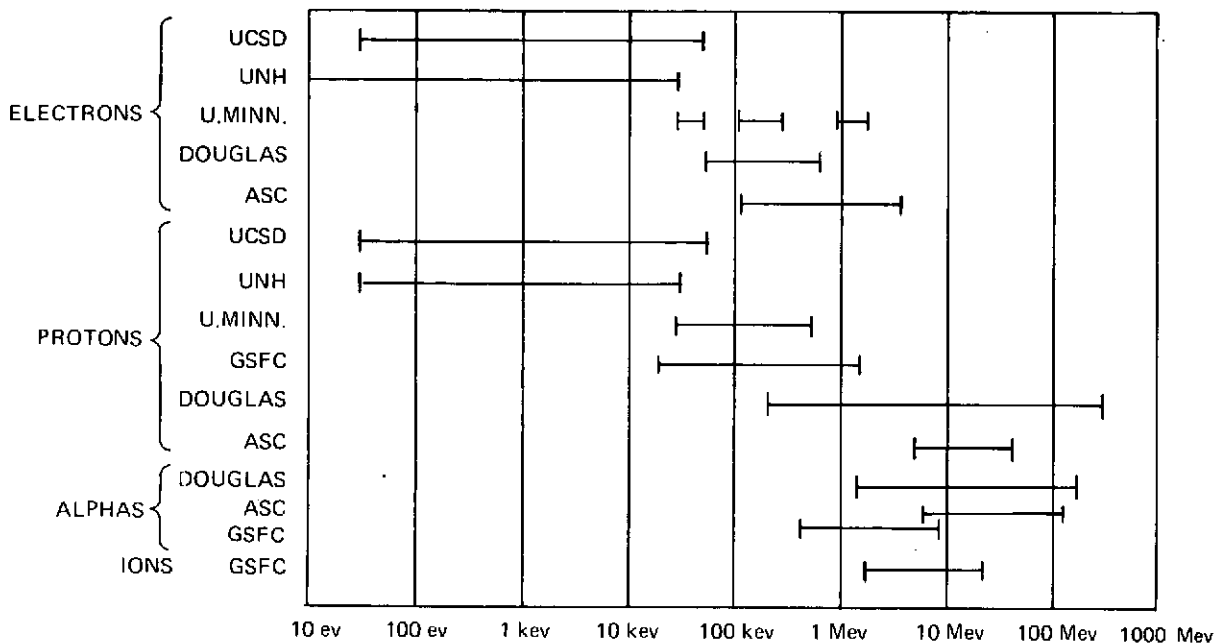
Figure 18-1. ATS-6/EME Particle Spectrum

Pertinent information regarding each of the eight EME experiments is shown in. Table 18-1.

Table 18-1

Environmental Measurements Experiments

Experimenter	Experiment	Purpose	Wgt. (lb)	Avg. Power (watts)	Size X-Y-Z (in.)
Dr. R. Arnoldy Univ. of New Hampshire	Low-Energy Proton-Electron	Make swept and pitched angle measurements of low energy electrons and protons in the magnetosphere.	7.0	5.0	9×6×6
Dr. T. Fritz GSFC/NOAA	Low-Energy Proton	Study low energy protons and heavier ions	6.1	1.0	7×9×4
Mr. A. Masley McDonnell/ Douglas Aircraft Corp. (MDAC)	Solar Cosmic Ray	Study solar cosmic rays, entry and propagation within magnetosphere, make detailed measurements of trapped electrons.	15.3	2.8	8×8×6
Dr. C. McIlwain Univ. of Calif. at San Diego (UCSD)	Auroral Particles	Study the distribution of low energy electrons and protons.	12.2	6.0	6×9×6
Dr. J. Winckler Univ. of Minnesota	Electron-Proton Spectrometer	Investigate the origin of the Van Allen trapped radiation.	6.6	4.0	6×6×5
Dr. P. Coleman Univ. of Calif. at Los Angeles	Magnetometer	Study the magnetic field at synchronous distances.	8.3	4.5	8×8×6
Mr. W. Dunkerly Hughes	Solar Cell Radiation	Measure life characteristics and performance degradation of solar cells in space.	7.8	8.0	5-1/4× 9-1/2× 3
Dr. G. Paulikas Aerospace Corp. (ASC)	Omnidirectional Spectrometer	Measure omnidirectional fluxes and spectra of electrons and protons.	2.7	0.63	4×4×6
		Total	66.0	31.93	25×25×15

18.3 ELECTRO-MECHANICAL INTERFACE

The EME experiment package is located on a structure at the base of the 30-foot parabolic reflector on the outboard side of the reflector hub. Included in the EME package is support equipment consisting of a command decoder that accepts data word commands from two spacecraft command addresses producing 78 EME commands and a telemetry encoder that accepts the experiment's data and formats it into an 1800 bit/sec sequence complete with synch words and clock. The power subsystem operates from a single spacecraft LIC to provide additional regulation and distribution to the individual EME experiments. The EME structure includes an active thermal control system.

Figure 18-2 shows the EME and how the scientific experiments are integrated with it.

18.4 EXPERIMENT OPERATIONS

18.4.1 Initial Operational Chronology

Date	Approximate Time (EDT)	Event
May 30, 1974	0900	Lift off
	2100	EME on, UCLA on, HAC on
	2200	Spacecraft Yaw Maneuver
May 31, 1974	2000	First automatic operation of HAC solar cell experiment
June 3, 1974		UCLA continuously in calibration mode. Recycled experiment power and normal operation was restored.
June 10, 1974	1410	NASA/NOAA experiment on. Operation normal.
June 14, 1974		UMINN, ASC, MDAC on. One UMINN medium energy channel inoperative, ASC E2 channel intermittent, MDAC OK, operation normal.
June 15, 1974		UCSD on. All UCSD mode commands exercised. Rotating detector assembly temperature excursions wider than expected.
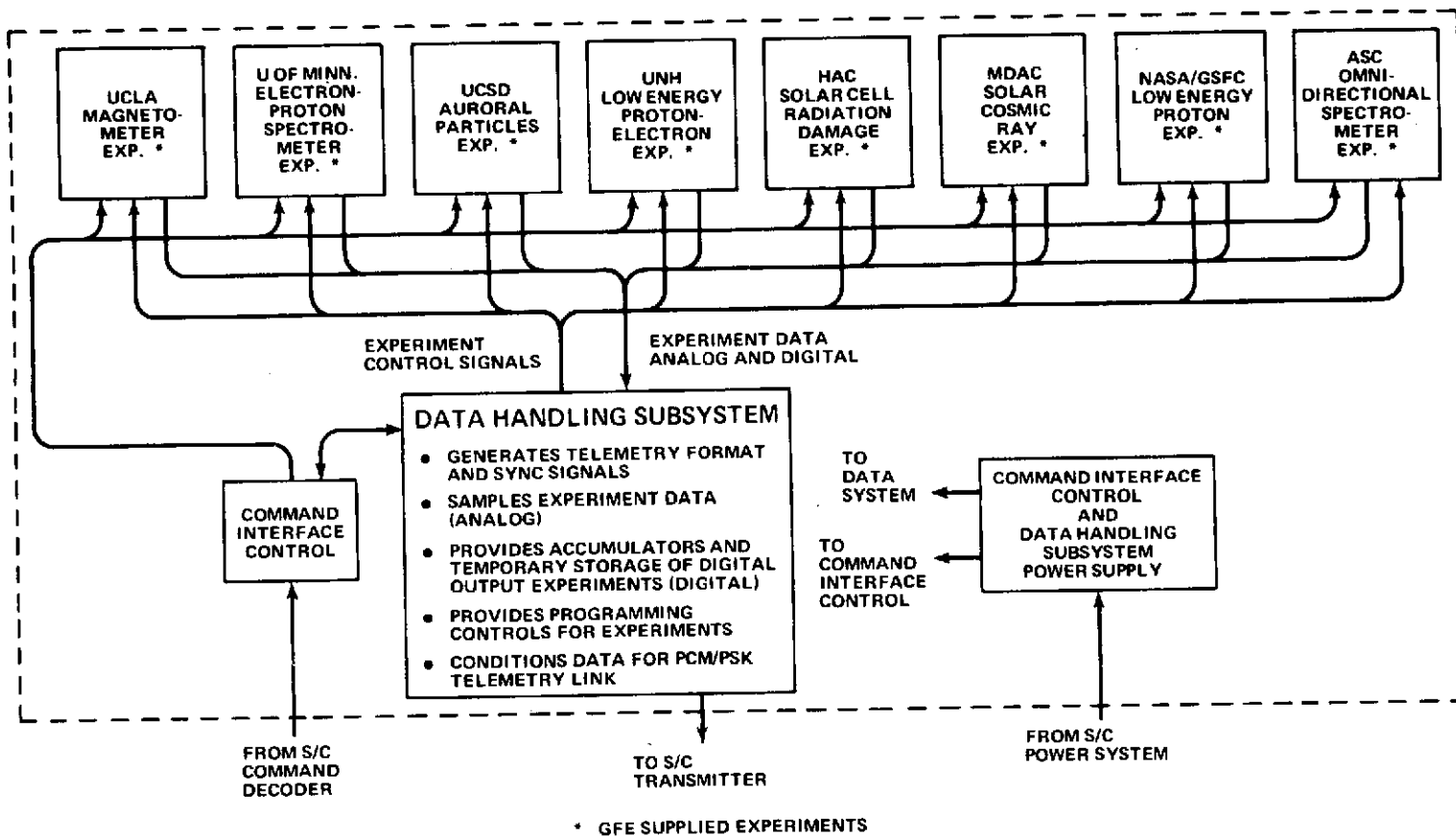
Figure 18-2. ATS-6 Environmental Measurements Experiment

Date	Approximate Time (EDT)	Event
June 18, 1974	1300	UNH ON. Several anomalies relating to basic EME performance were noted. UNH was turned OFF after approximately 1.5 hours of operation until cause of the anomalies could be isolated.
Through June 30, 1974		All EME experiments ON except UNH. Average Power dissipation 31 watts.

18.4.2 Thermal Performance vs. Design Goals

The UCLA experiment magnetometer sensor is warmer than preflight analysis (see Figure 18-3). The approximate 0°C to 21°C range is, however, a very comfortable temperature range for the sensor operation. In mid-June, the unit is at or near its hottest time of the year. Maximum temperature levels should lower as equinox is approached when the solar load on the north face, which is painted black, becomes less.

The University of Minnesota experiment sensor in situ temperatures are shown in Figure 18-4. The temperatures obtained during prototype steady state tests were 50°C at equinox and -3.5°C at solstice. The high temperature was determined to be caused by specular reflections from the EME cover. A diffuse coating was applied in order to reduce these reflections at equinox. It appears that the coating may reduce equinox temperature levels, but increase temperatures during summer solstice. The sensors will run cooler during the winter months.

The EME deck temperatures are about 4°C higher than was expected. Figure 18-5 shows the flight mean deck temperature plotted with the predicted mean deck temperature. Examination of the flight data indicates that there is a larger gradient across the deck than was expected indicating that the north radiators are absorbing more solar energy or radiation from the spacecraft than anticipated. Prototype test showed 27°C average deck temperature which corresponds quite well with the 28°C average deck temperature from flight data, but the increased gradient causes higher local temperatures along the north side of the package.

UCSD sensor temperatures are substantially higher than expected. Latest preflight calculations predicted -15°C to +55°C. Figure 18-6 shows the flight data test results for the two sensors. The temperatures of these sensors are very sensitive to their orientation, and it was found that the high temperatures were occurring while the apertures were viewing the sun. It has been hypothesized
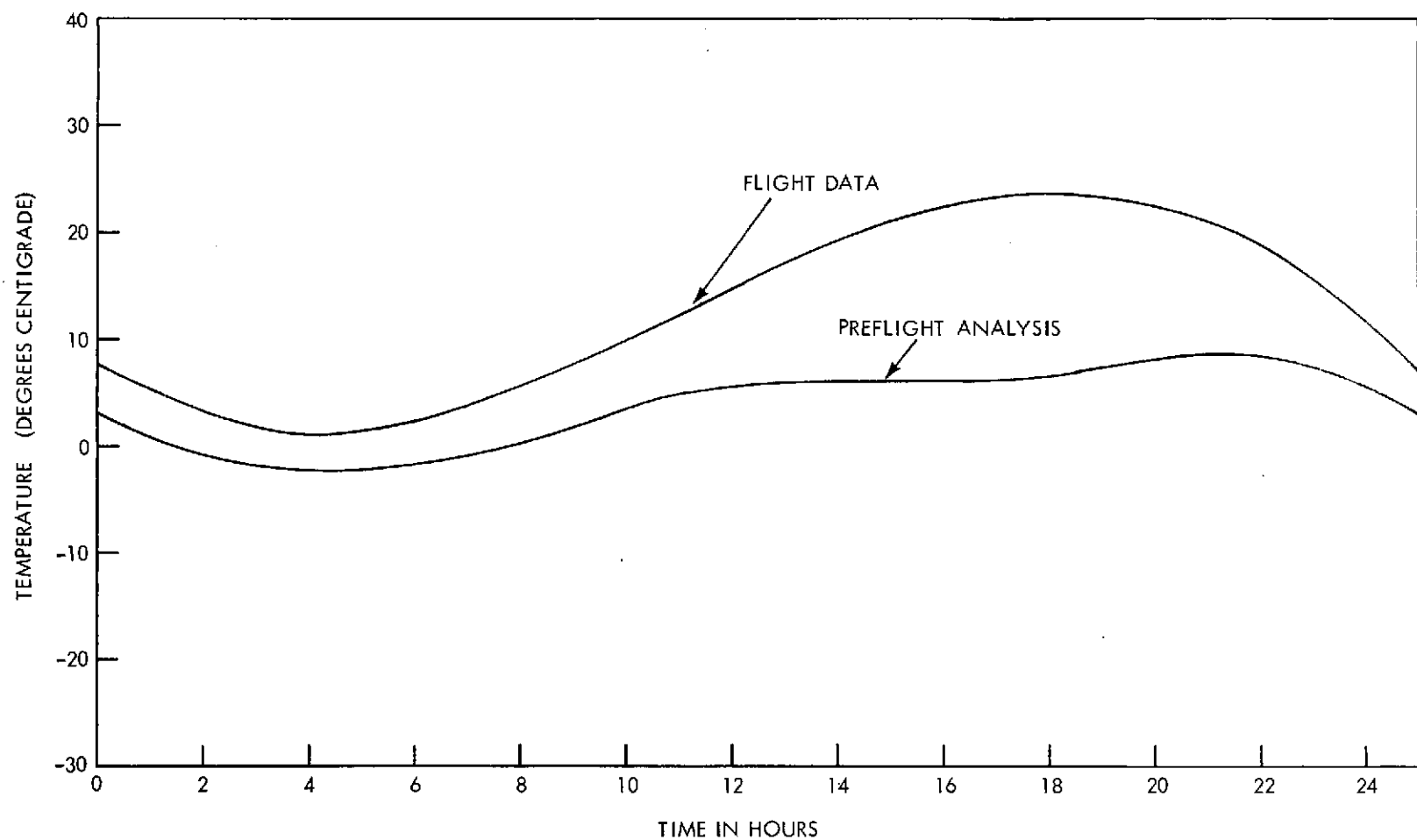
Figure 18-3. Magnetometer Sensor Temperature
(Flight Data from 6/17/74)
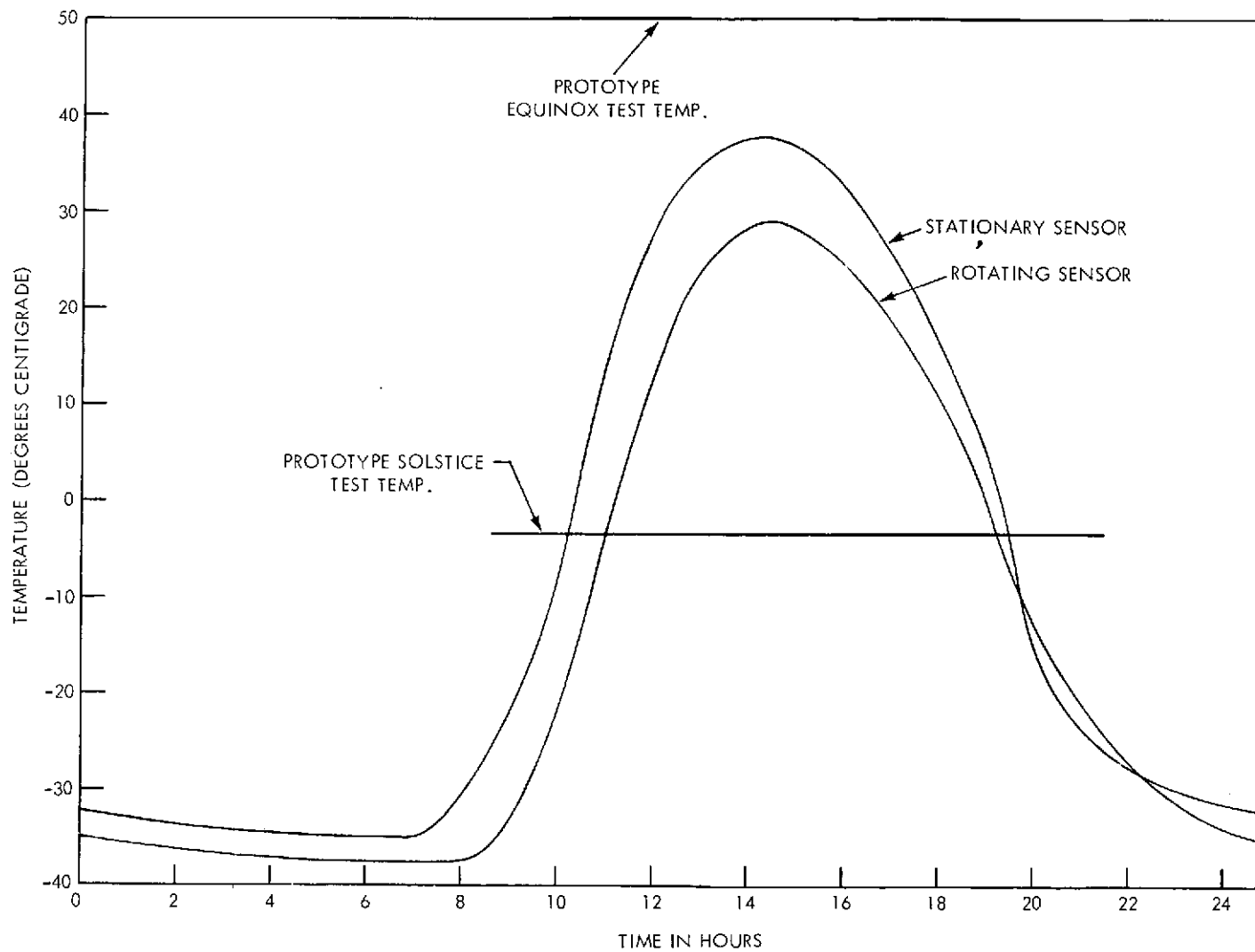
Figure 18-4. Minnesota Sensor Temperatures
(Flight Data from 6/17/74)
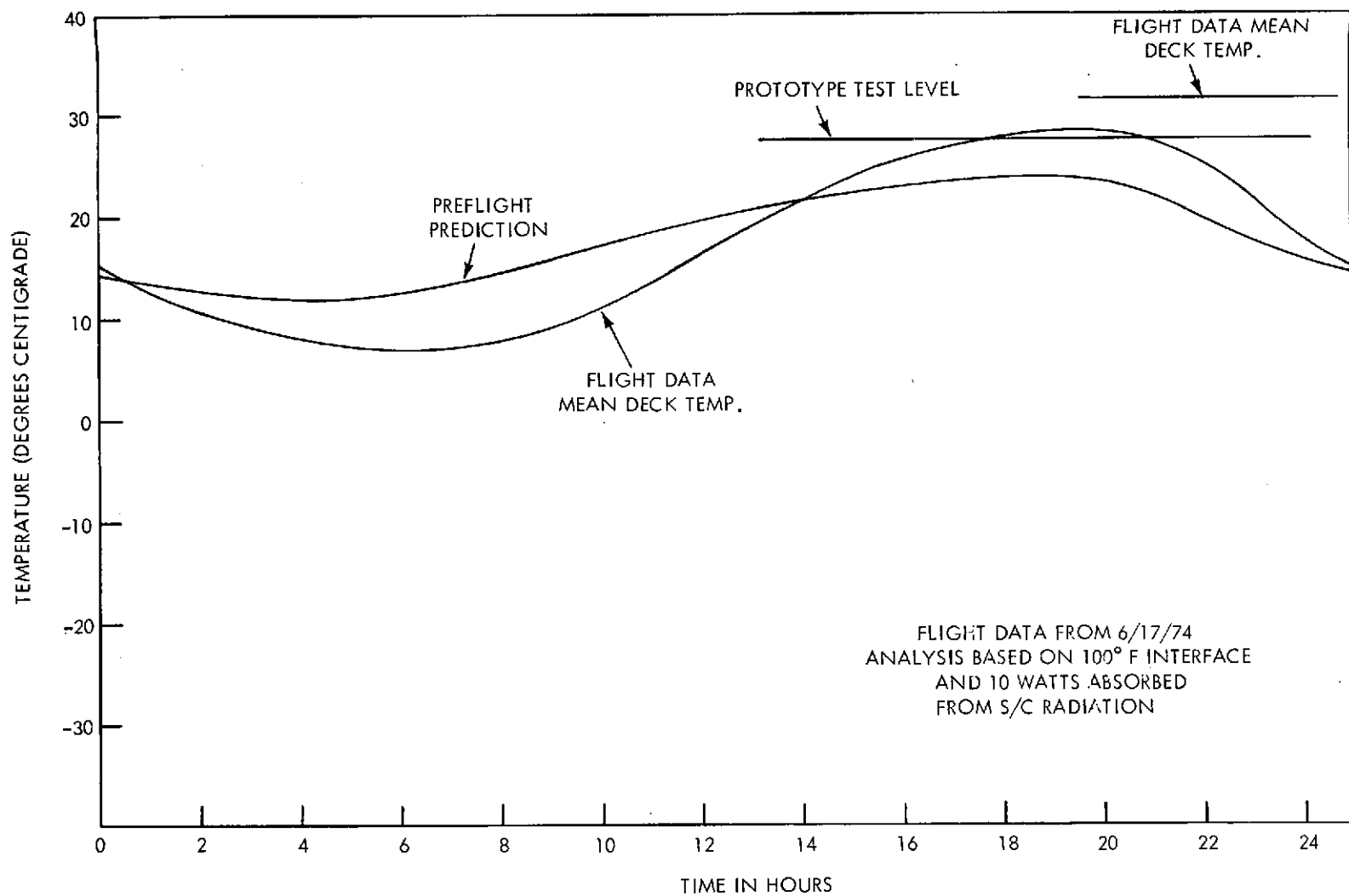
Figure 18-5. EME Average Deck Temperature
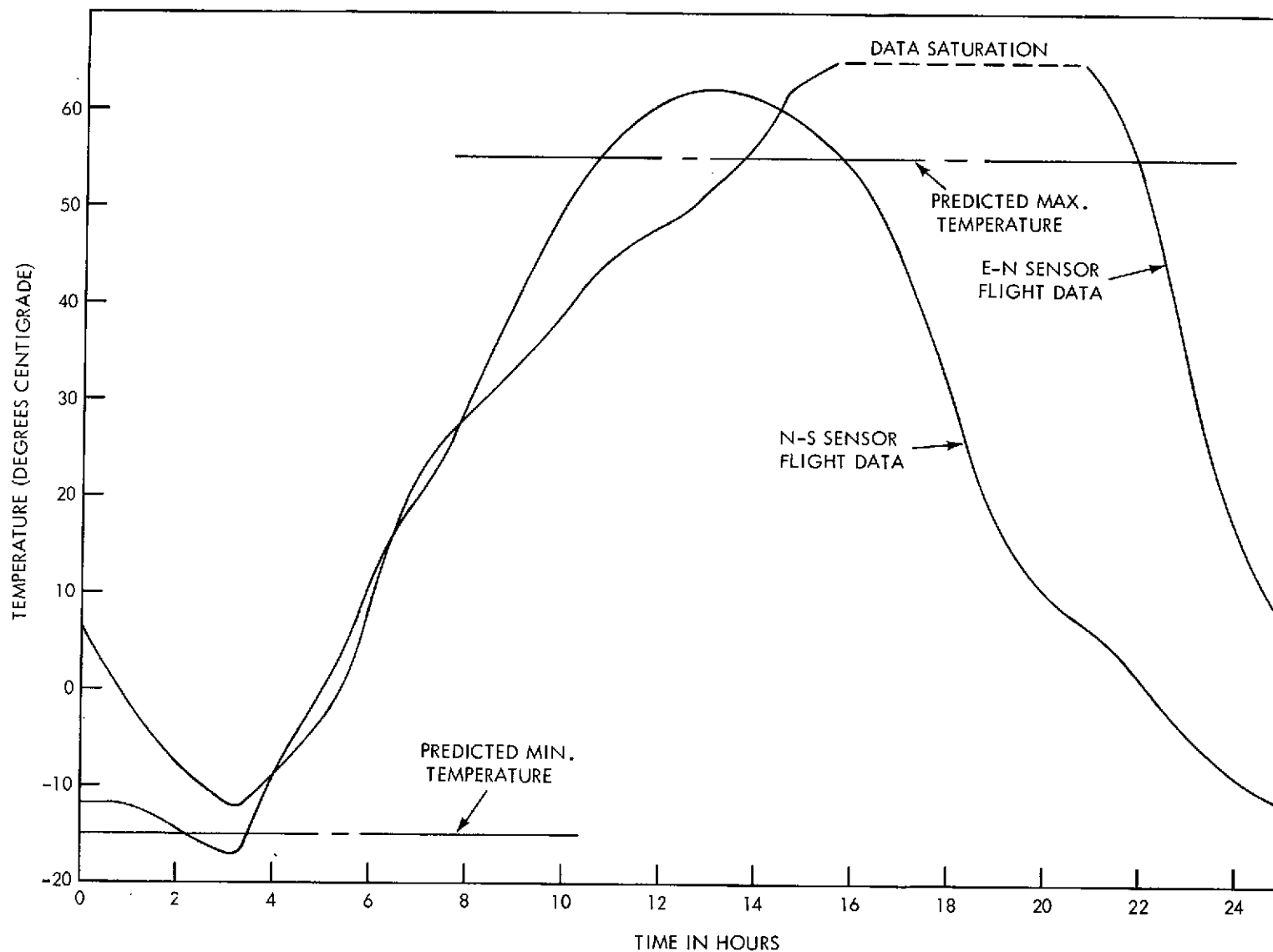
Figure 18-6. UCSD Sensor Head Temperatures

that the silver paint on the gold-plated surface of the sensors has turned black in UV illumination. This would explain the higher-than-predicted temperatures.

GSFC cold plate temperatures (Figure 18-7) are higher than expected. It appears from the data, that the cold plate is following the deck temperature. This would indicate either that the cold plate is not insulated from the deck as was expected, the radiator is not emitting the heat that was intended, or the sensors are absorbing more heat than calculated. Unfortunately, this unit was not available during the prototype EME thermal balance tests, therefore, no reference data is available.

18.4.3 Performance Anomalies

a. UCLA occasionally goes into the in-flight calibration mode and remains there until the experiment power is recycled or the timed calibration cycle (8 seconds) occurs automatically once a day. This anomaly is recognizable in the data and although it is a nuisance, the calibration offset can be subtracted from the data.

b. ASC electron data in the E2 channel is intermittent as a function of temperature of the detector.

c. ASC E1 data has a count offset of approximately 4000 counts for 3 hours after the automatic operation of the HAC solar cell experiment. This is related to the solar cell lockout signal generated in the encoder.

d. UMINN channel UM10 is inoperative.

e. On June 18, 1974, during the approximately 90 minutes that the UNH experiment was on, four anomalies occurred which affected the EME clock, digital registers, and analog channels of the EME telemetry encoder and command system. The UNH experiment was deenergized and these anomalies have not recurred. The only permanent damage noted in the data was the loss of telemetry word 189 which contains primarily experiment housekeeping data. Investigations are in progress as to the cause and how the interaction relates to the UNH experiment being energized.

18.5 SUMMARY OF INDIVIDUAL EXPERIMENT PERFORMANCE

18.5.1 Low-Energy Proton-Electron Experiment (UNH)

The low-energy proton-electron experiment measures electrons and protons whose energy is from 0 eV to 22 keV at two differential pitch angles. More specific objectives are:
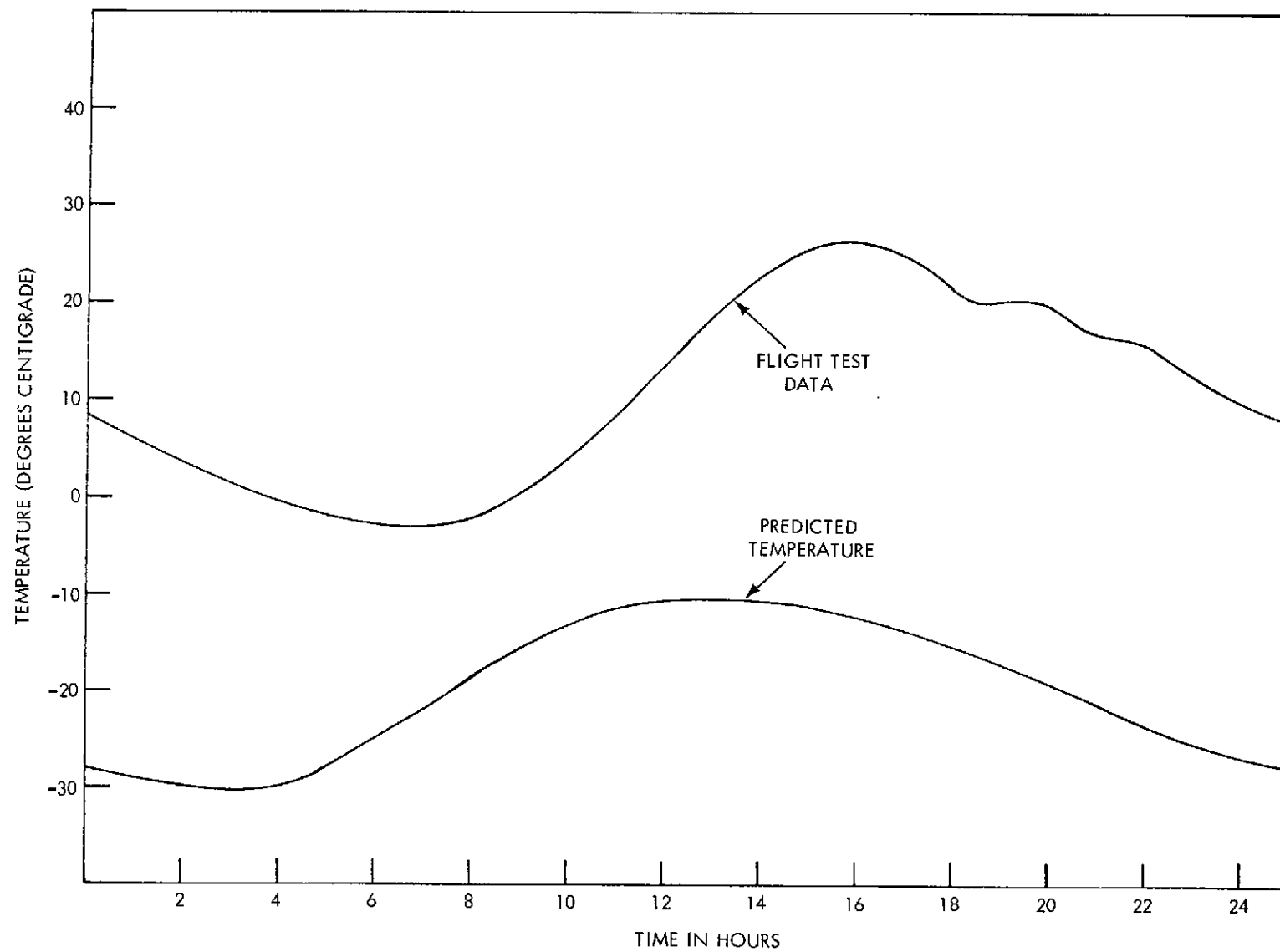
Figure 18-7. GSFC Experiment Cold Plate Radiator

a. High-resolution electron measurements for those particles that mirror near the equatorial plane.

b. A two-point sampling of the pitch angle distribution for electrons and protons every second.

c. A study of dependence of observations on local time.

d. A study of intensity time fluctuations of low-energy electrons and protons when an enhanced solar wind might push the subsolar magnetospheric boundary into the geostationary orbit.

e. Correlation of the ATS data with ground, balloon, and rocket studies.

The UNH experiment was first turned on June 18. All experiment science data appeared normal. After about one hour of operation a jump in the EME clock was observed and the experiment was turned off. No change in the science data was observed that would indicate a high voltage arc or corona. Insufficient operational time prevented evaluating potential science contributions from the experiment, although all experimental functions and calibrations appeared to operate as designed.

Following the first turn-on of the UNH experiment, a permanent malfunction was observed in the EME 64-level subcomutation word #189. This word is used by all EME experiments for housekeeping data. Other experimenters are reporting varying degrees of failure in this respect.

Considerable analysis was done to determine if additional damage would ensue if the UNH experiment was turned on again. It was decided to make a second attempt, and on August 1, the experiment was turned on for approximately 40 minutes, resulting in similar irregular performance. As previously, the EME clock jumped and new changes were noted in the odd and even channel responses of word #189.

Boeing Aerospace Company was contracted to investigate this problem using their computerized sneak circuit program. They recommended that without additional prototype testing and evaluation a risk would be involved in re-energizing the UNH experiment.

It is not planned to turn on the UNH experiment in the future. Anomaly investigations using the prototype unit located at the University of New Hampshire, is continuing.

18.5.2 Low-Energy Protons Experiment (GSFC/NOAA)

The low-energy proton experiment originated as an in-house experiment of the NASA Goddard Space Flight Center and was later transferred to National Oceanic and Atmospheric Administration (NOAA). It is the purpose of the experiment to answer questions such as:

a. Where in local time are the protons injected into the magnetosphere?

b. How closely in time is the injection of protons associated with auroral substorms?

Energy ranges covered are:

Protons	20 keV to 2.1 MeV
Alpha	0.6 MeV to 4.0 MeV
Light Ion	2.1 MeV to 12.2 MeV
Medium Ion	9.5 MeV to 22.7 MeV
Heavy Ion	$\geq$ 20 MeV

The NOAA experiment was first turned on June 10, 1974 at approximately 1600 GMT. A check-out of the experiment operation confirmed that everything was operating in a nominal manner. The experiment remained on until June 15 when the remaining EME experiments were activated. Over the weekend of June 15-16, the possible effects of the other experiment turn-ons on the NOAA experiment were evaluated. None were observed. On Tuesday, June 18, the UNH experiment was activated for the first time and while this experiment was on, a failure occurred at $\sim$1830 which has effected the subsequent operation of the NOAA experiment. This is described in detail below. The experiments were apparently turned off at $\sim$2155 and after reactivation of the NOAA experiment no further anomalies occurred in the first 30 days of operation.

The performance of the experiment in terms of its design goals is essentially perfect. Figure 18-8 is a spectrum which shows the agreement of the response of the B telescope in the NOAA experiment with the UCSD and UMINN experiments. A more informative spectrum is Figure 18-9 which involves the response of both the A and H telescopes. The fact that all channels agree so well indicates the satisfactory operation of the following difficult-to-check items.

1. The A telescope channels ($\triangle$ E) have a geometric factor which is of 2 to 3 times smaller than the separate H telescope channels ($\triangle$ H) and the agreement in the response indicates the accuracy of these two numbers.
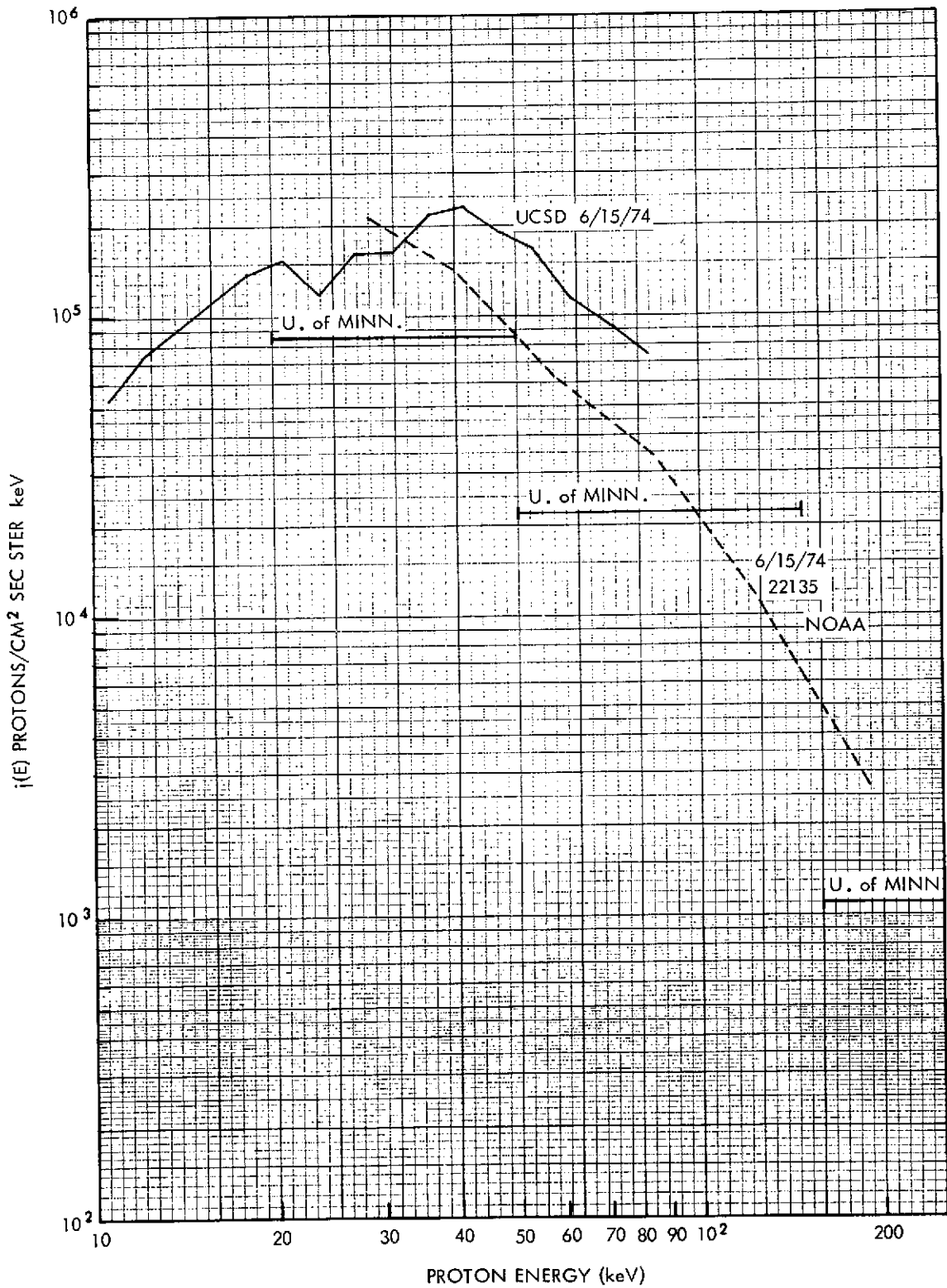
Figure 18-8. Spectrum Agreement (NOAA Experiment B Telescope
Response, U. of Minn. and UCSD Experiment)
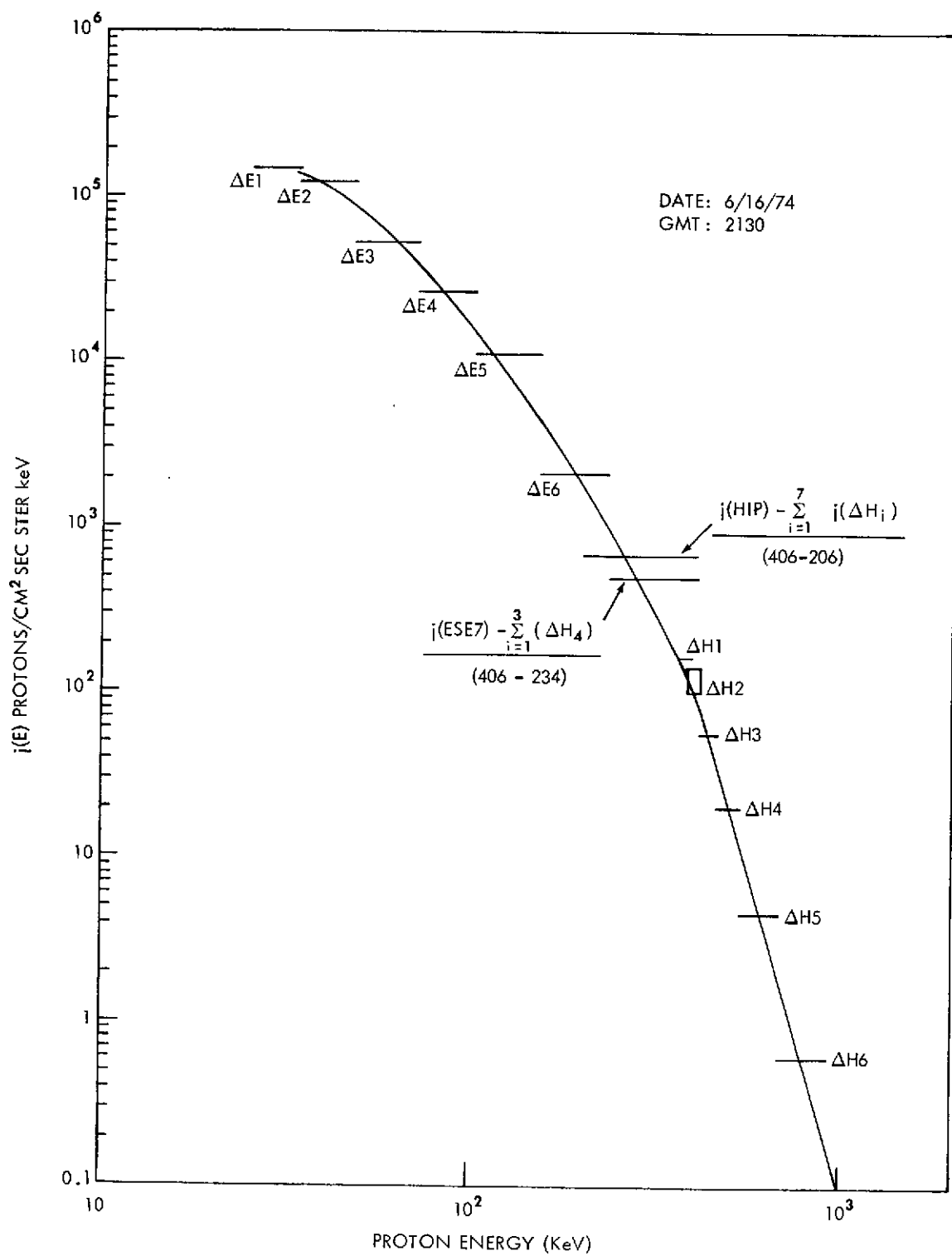
Figure 18-9. NOAA Low-Energy Proton Experiment
(A and H Telescopes)

2. The ΔE channels operate on a principal of anticoincidences whereas the ΔH channels use a coincidence technique between the two elements of the respective telescopes. The agreement of these responses indicates the proper electronic operation of these techniques, particularly the coincidence H telescope operation.

3. The smooth joining of the spectral curve across the gap between the ΔE and ΔH channels indicates a very good agreement to the preflight proton accelerator beam calibrations. This confirms the survival of an extremely thin (900 Å) aluminum foil used for light protection in the H telescope.

4. The proper fitting of the response of the HIP and $E > E7$ channels on the curve indicate a number of things:

   a. The proper operation of a complex circuit involving a fourteen bit accumulator and a digital-to-analog converter is verified.

   b. The response of the circuit in (a) above is outputted through EME telemetry word 14. The nominal operation of the EME 9 ±1 bit analog-to-digital converter is also inferred.

   c. The HIP response which is a level response on the thin (H) telescope incorporates a delay-line clipped pulse of $\sim200 \times 10^{-9}$ sec. The absence of any electron pile-up effects in the HIP response indicate the proper operation of this fast circuitry.

There have been no anomalies in the operation of the NOAA instrument that resulted from a failure within the experiment. The only anomaly in the first 30 days of operation occurred during the initial turn-on of the UNH experiment. This anomaly affected only the information outputted through EME telemetry word 189. The NOAA experiment uses the subcom positions in frame 3 through frame 9 on this word for a combination of housekeeping information and heavy ion rate information data. As a result of the anomaly:

1. Information on frame 3 is unrecoverable. This position was further subcommutated within the NOAA experiment and was used to output the only two temperature measurements made within the experiment. In addition the most significant bit (output greater than or less than 2.5 volts) was used as an identification bit for the internal NOAA subcommutator.

2. Information on frame 9 is unrecoverable. This position was used to monitor two operational voltages in the experiment.

3. The retrieval of information on frame 5 and frame 7 is possible but has been made difficult. These two positions are each subcommutated with two sets each of heavy ion $(z \geq 2)$ rate information. The rate information is recoverable by visual inspection of the data but is not easily amenable to processing with computer techniques as planned.

4. Information on frames 4, 6, and 8 was initially effected but recovered during the experiment-off period following 2155 GMT on June 18 and remained nominal during the rest of the first 30 days of operation.

The quality of the data being received and the high level of operational performance of the instrument indicate that all of the scientific objectives of the NOAA experiment should be achieved. In addition to proton temporal and spectral information being returned by the instrument, the measurements of fluxes of geomagnetically trapped energetic $(z \geq 2)$ heavy ions for the first time at the geostationary orbit is proving to be a powerful tool in understanding the magnetospheric substorm and particle acceleration processes.

Plans are presently in operation to acquire data from the NASA Explorer 45 satellite in a special operational mode that will concentrate on the behavior of the heavy ion populations during upcoming magnetic storms in conjunction with the ATS-6 data set. In the future when ATS-6 is moved to 35° E it is hoped that special operational considerations can be given to the coordination of the EME data with the ESRO geostationary satellite GEOS scheduled to be launched in September 1976.

18.5.3 Solar Cosmic Ray Experiment (McDonnel Douglas)

The general objective of this experiment is to conduct a basic study of solar cosmic rays, their entry and propagation within the magnetosphere, and to measure detailed parameters of trapped electrons, both as functions of local time in orbit. Each measurement is performed at two different pitch angles. The measurements will be made with sufficient detail, energy resolution, dynamic intensity range, and time resolution to allow several studies during the period following maximum solar cosmic ray activity. Some of the specific objectives are to:

a. Investigate the mechanism by which low-energy solar cosmic rays gain entry and propagate within the magnetosphere.

b. Investigate the mechanism responsible for cutoff variations during geomagnetic activity.

c. Use the data as a test to evaluate and to improve a recently developed magnetospheric model which includes the tilt of the dipole axis to the solar wind.

d. Compare the time history and development of solar cosmic ray events at $L = 6.6Re$ to the Douglas observatories in the Northern and Southern Polar regions.

e. Study the behavior of trapped electrons as a function of local time and geomagnetic activity in the ATS orbit.

f. Directly compare spectral and intensity changes between two families of particles which traverse vastly different regions of the magnetosphere in order to investigate acceleration and propagation processes during geomagnetic activity and during quiet periods.

Energy ranges are, for alpha particles 2 MeV to 250 MeV, for protons 0.2 MeV to 230 MeV and for electrons 50 keV to 1 Mev.

For the proton-alpha particle telescopes, all 50 digital data channels are responding as originally designed to the local radiation levels. The small solar cosmic ray event which began on 5 July reached sufficient intensity to activate all the p and alpha channels above their background levels verifying the proper function of all logic modes of the telescopes. The data is free of any anomalies which can be attributed to the experiment. In the 5 July data some probable data transmission errors were seen giving occasional very large numbers in a few of the channels. Figure 18-10 shows a plot of the normal and parallel 300 keV proton channels for 15-16 June. Figure 18-11 is a spectrum of normal and parallel protons during the early part of the solar event showing channels P1 to P10 above background.

All eight channels of the electron spectrometer are providing excellent high time resolution data. The short sample time of (.1 sec) and large entrance aperture give very fine time resolution with excellent statistics for electrons over the entire 50 keV – 1 MeV energy range. The high time resolution coupled with a very interesting orbital location (10° off the magnetic equator) is providing data with features not seen by earlier experiments.

Some examples of data are given below:

Figure 18-12 shows a highly disturbed time period with numerous magnetic field inflation events and a number of substorm electron injections.
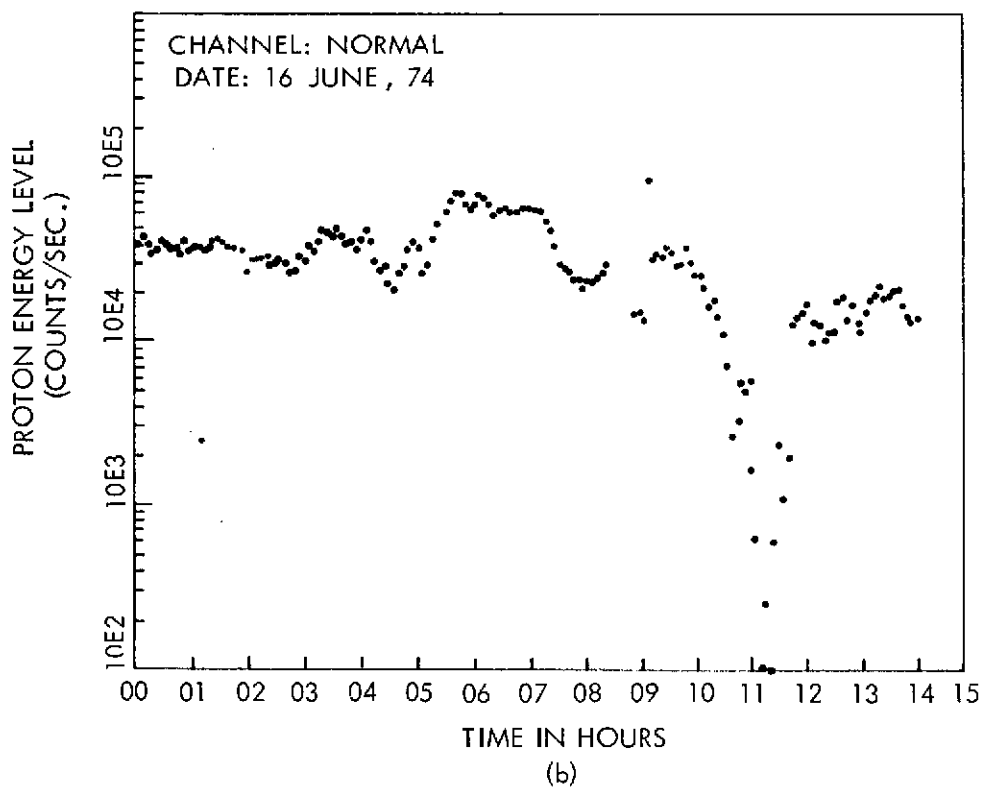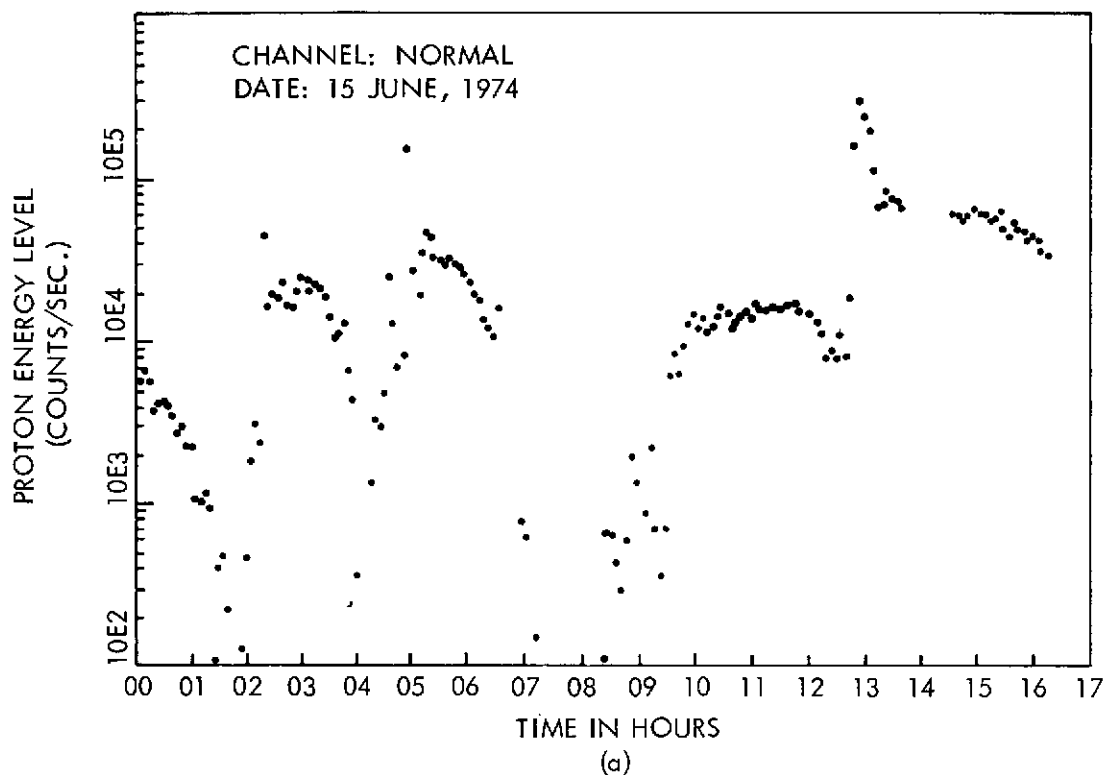
Figure 18-10. 300 keV Normal Proton Channels
(Days 166 and 167)
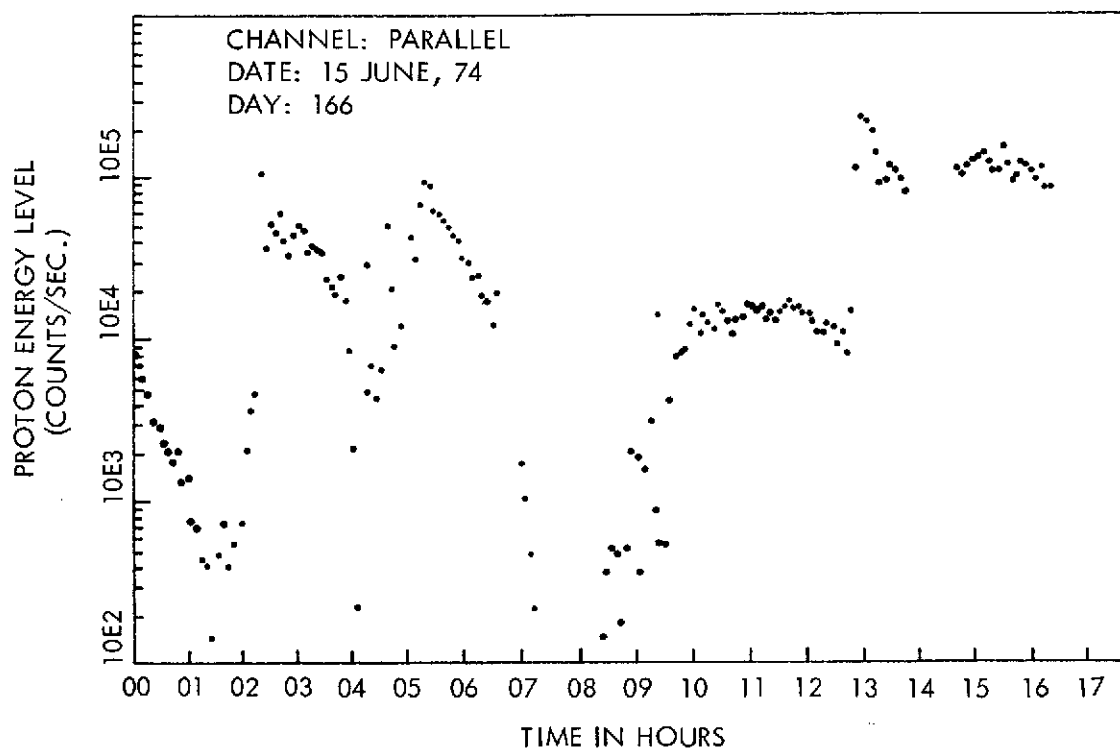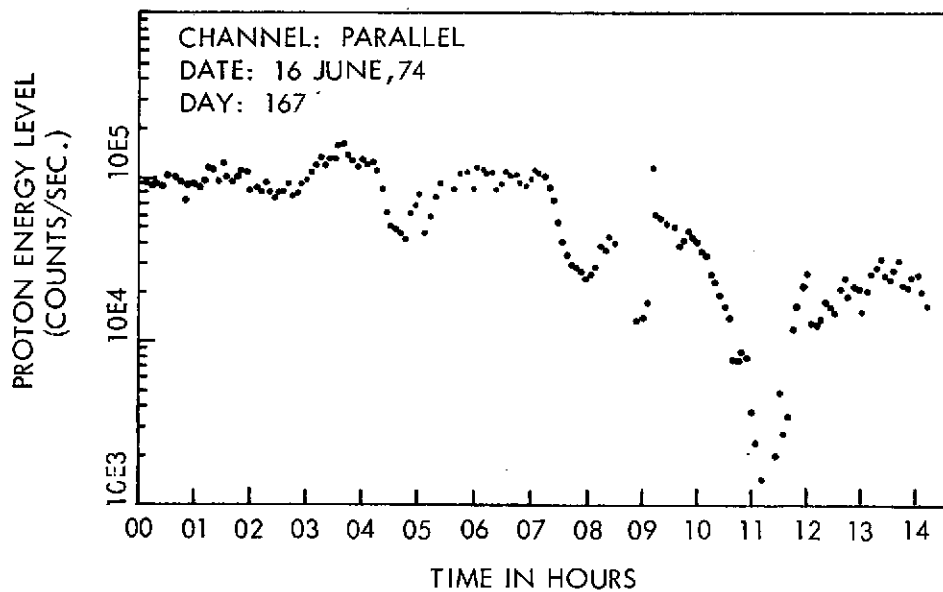
Figure 18-10 (Cont'd). 300 keV Parallel Proton Channels
(Days 166 and 167)
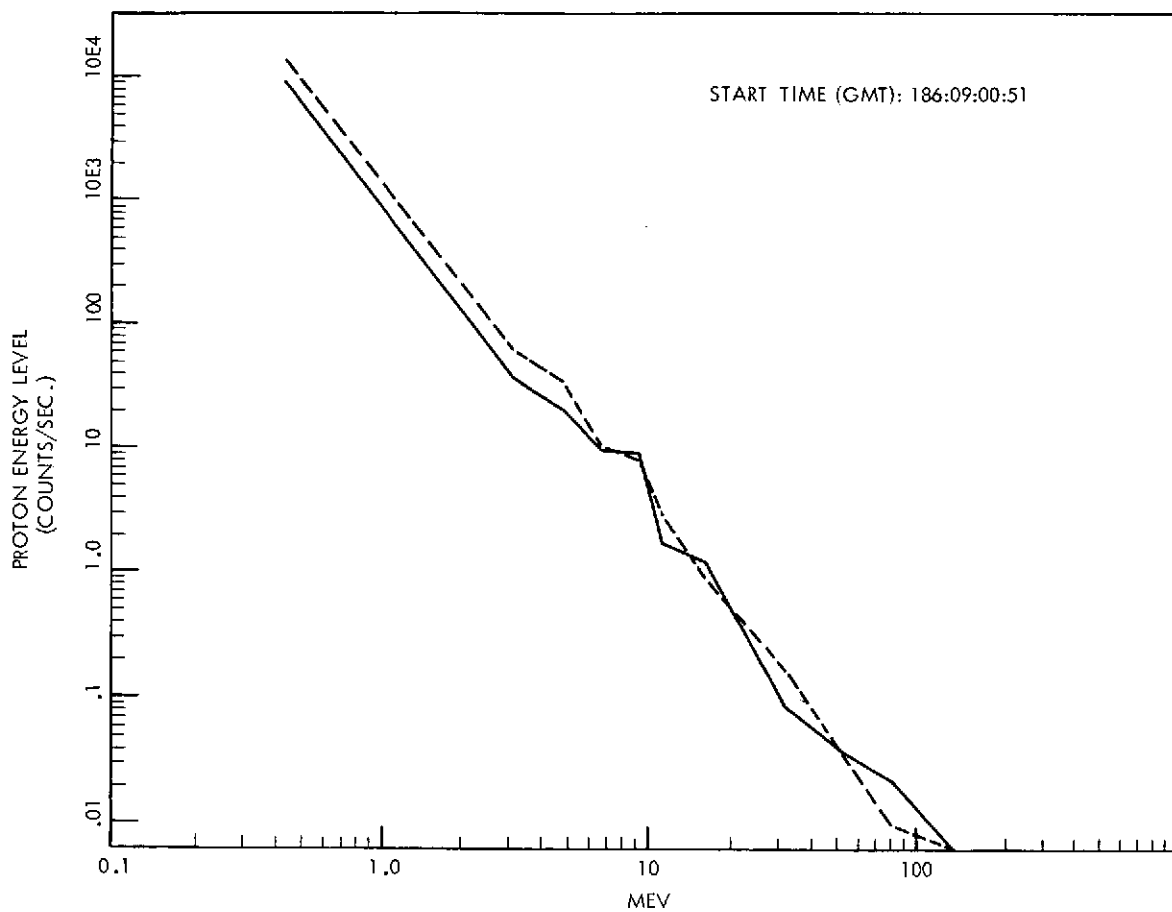
Figure 18-11. MDAC Proton Spectra
(Normal and Parallel Channels)
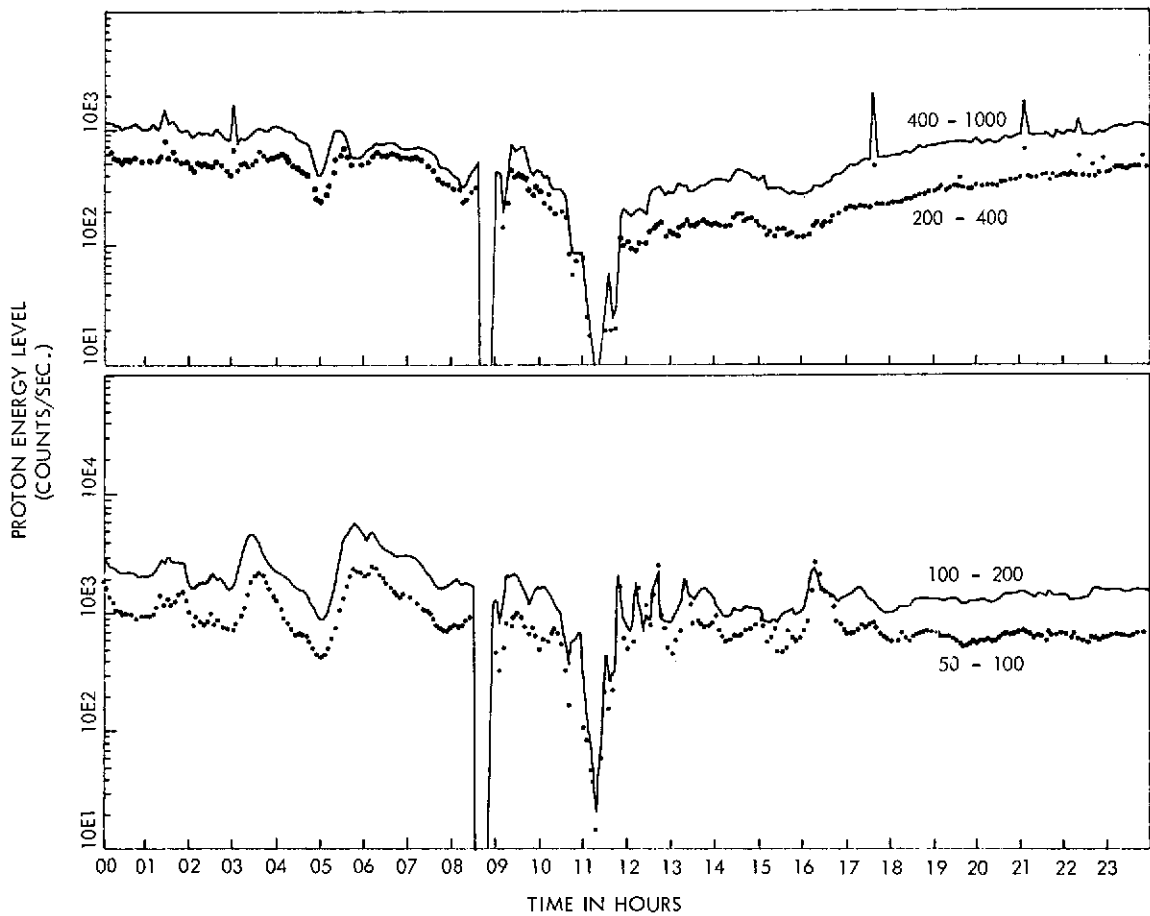
Figure 18-12. MDAC's Spectrometer 24-Hour Profile
(Start Time (GMT) 166/18:26:35)

Figure 18-13 shows an isolated substorm injection event observed just past dawn. Dispersion effects and drift velocity delays which are a function of energy are clearly visible. Such high resolution injection events can be used to determine the exact location and extent of the injection region.

In Figure 18-14 the two low energy channels show an example of the wave structure that is frequently observed by the experiment. The wave amplitude and phase are energy dependent. Since the experiment has a resolution of 0.1 sec, it will be possible to look for bounce time resonances for electrons having energies greater than 50 keV.

To date, the spectrometer continues to function normally except that two of the lowest threshold channels become somewhat noisy at the extremes of the daily temperature cycle.

As of 16 August, 6 EME data tapes and 10 Quick-Look (Q/L) tapes have been received, giving 14 separate days of data after experiment turn-on. In addition, several days of data have been received in the form of microfilm plots from the GSFC data reduction facility.

The status of software at the present is as follows: a tape cracking routine for data tapes is in working order and has been used to provide dumps of several EME and Q/L tapes. The plot package is in final stages of preparation and will be operational in a few weeks.

Due to the UNH/EME problem, the functions of half of this experiment's analog parameters have been lost. This represents an annoying but not serious problem since most analog words were monitoring engineering parameters of the detectors and not scientific data. Since the Q/L data from day 213 has not yet been received, no comment can be made regarding effects of the second UNH turn-on on this experiment. It is hoped that the experimenters will soon be receiving the EME status TWX's as an aid in determining operational status of the experiments, as well as the physical status of the EME.

18.5.4 Auroral Particles Experiment (UCSD)

The scientific objectives of the experiment are as follows:

a. Map the distribution of low energy (1 eV to 80 keV) electrons and protons on a constant line of force so that correlation studies between these particle fluxes and the visible aurora can be conducted to determine the nature of the accelerating mechanism in the magnetosphere.
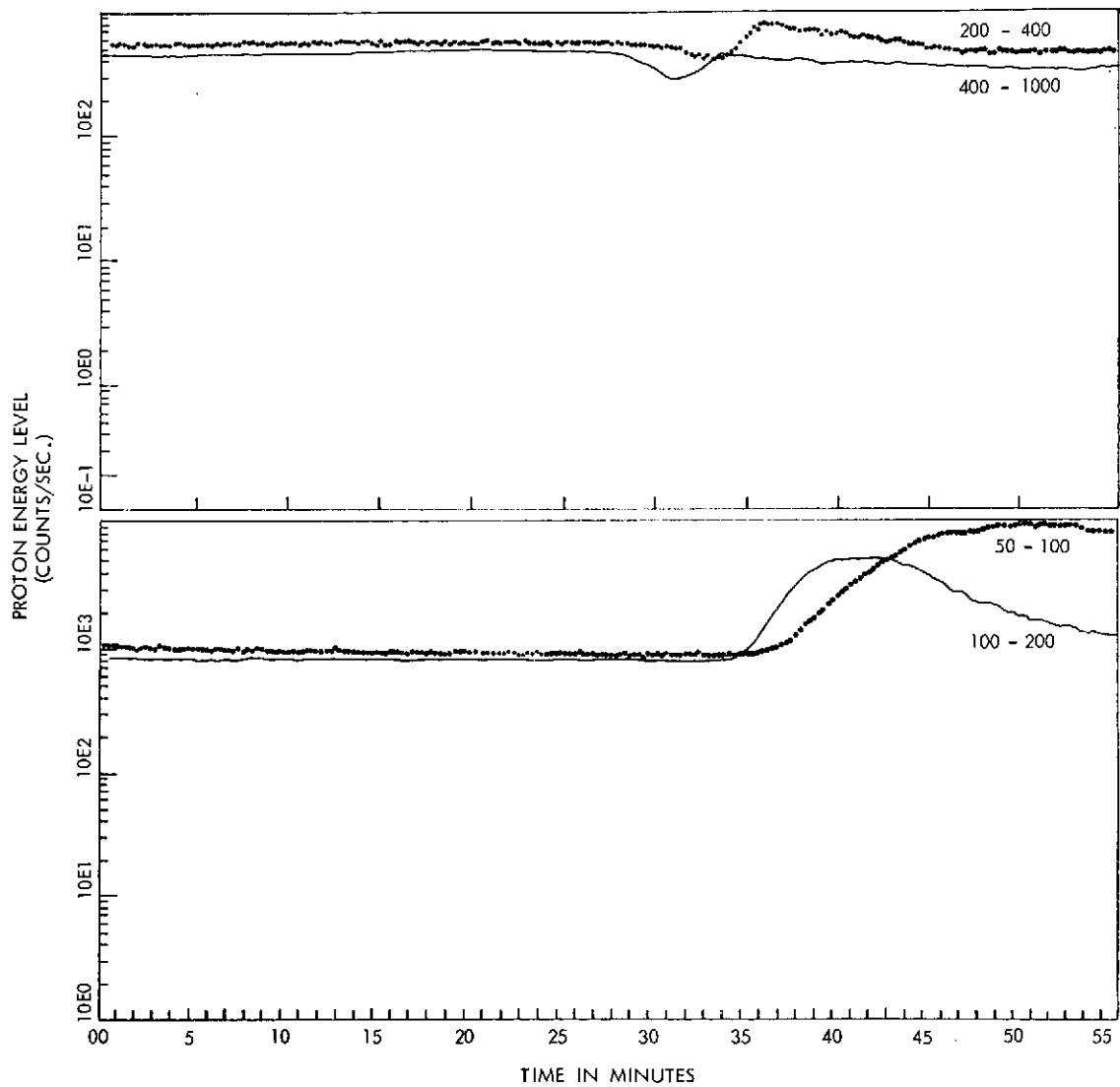
Figure 18-13. MDAC Spectrometer 1 Hour Profile
(Start Time (GMT) 169/13:00:14)
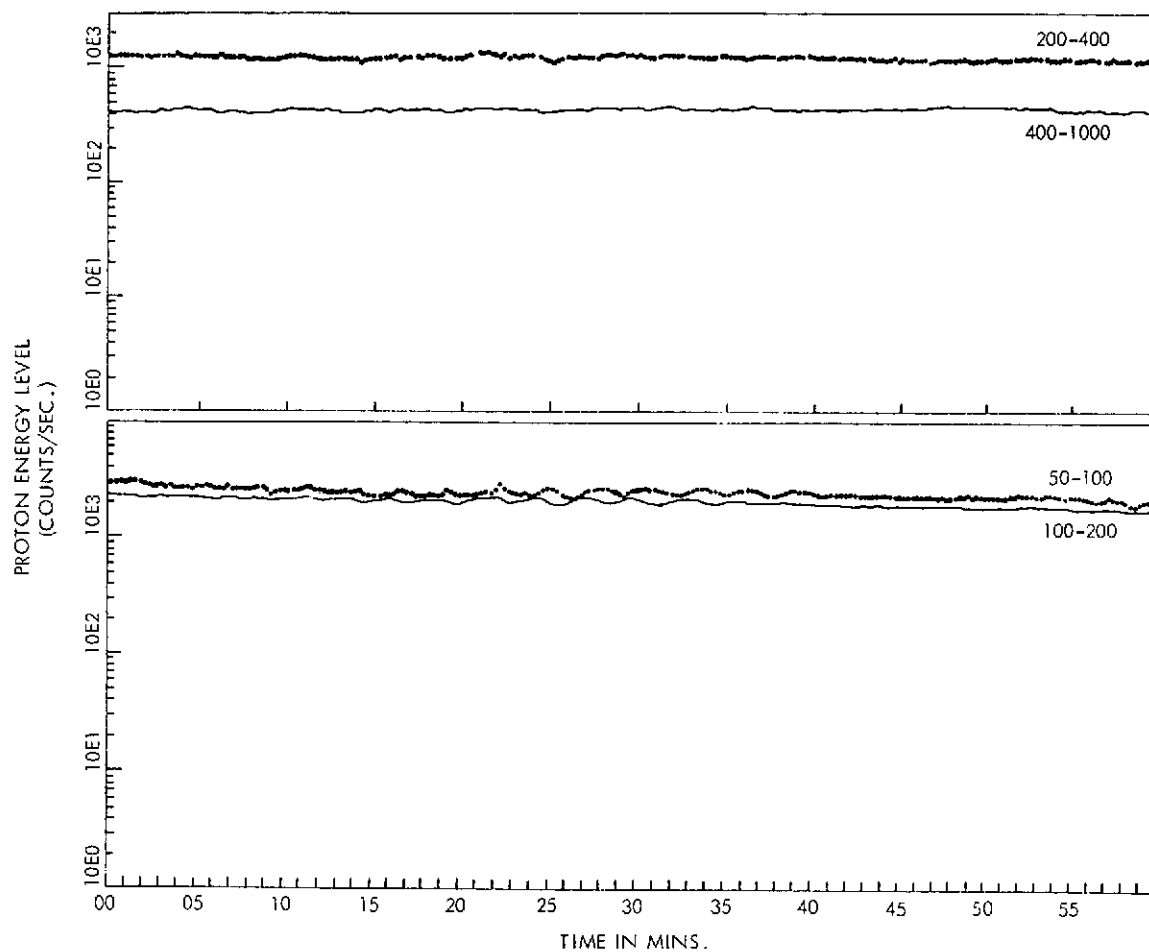
Figure 18-14. MDAC Spectrometer 1 Hour Profile
(Start Time (GMT) 166/14:35:38)

b. Study variations in particle fluxes as a function of pitch angle.

c. Study variations in particle fluxes as a function of azimuthal angle.

d. Study the slow temporal variations in particle fluxes holding the rotating detector assemblies at fixed angles (much like ATS-5).

e. Study the fast temporal variation in particle fluxes at specific energies.

f. Perform a detailed study of low energy (< 50 eV) particle fluxes.

g. Compare ATS-F data with that from other spacecraft.

h. Study the spacecraft charging phenomena.

i. Make detailed studies of the energy balance between particles and fields at their location and relate it to the magnetosphere as a whole.

During the first thirty days the instrument performance met or exceeded design goals in the following anomalies observed:

a. Fixed Detector Noisy [<2% of total time]

b. Sync Loss Rotating Det [<1% of cycles]

c. Spiraltron Gain Degradation Electron Channel East/west RDA

d. Word 189 performance parameters inoperative.

18.5.5 Particle Acceleration Measurements Experiment
        (UMINN Electron-Proton Spectrometer)

The objective of the University of Minnesota experiment is to investigate the origin of the Van Allen trapped radiation. Measurements of the intensity and time variations of protons and electrons in the vicinity of the synchronous orbit, and detailed analysis of these variations in their relationships to polar and magnetic storms and other perturbations of the magnetosphere will further the knowledge of magnetospheric dynamics of acceleration and modulation processes in several ways:

a. Establish, in a more direct manner, the existence or nonexistence at the geostationary orbit of certain rapidly varying electron fluxes commonly observed in precipitated fluxes.

b. Study the role the protons of these energies play in the dynamics that produce large fluxes of energetic electrons.

c. Study the pitch angle distribution characteristics of protons and electrons during the various modulated activities, such as the quasi-periodic pulsation activity.

d. Study more precisely the dynamic variables that may be affected in transit from the equator to the auroral zone.

Energy ranges are for protons 20 keV to 500 keV and for electrons 20 to 40 keV, 100 to 200 keV, and 1 to 1.5 MeV.

The University of Minnesota electron-proton spectrometer experiment was designed to measure the intensity and time variations of electrons and protons at synchronous orbit. The spectrometer consists of two identical particle detection systems. One system is fixed with a look direction toward EME east and the other system is a scanning system with 13 look directions spaced in 15° steps from EME north to south through west. The directional capabilities of the scanning system together with the measured magnetic field at the satellite by the onboard magnetometer will allow the pitch angle distribution characteristics of electrons and protons to be studied. Each detector system measures the directional flux, as averaged over an acceptance solid angle consisting of a cone of approximately 5° half-angle, in each of three electron and three proton energy ranges. The detector labeling and their designed nominal energy ranges are given in Table 18-2. The lowest energy channels E11, P11, E12 and P12 have a sampling rate of 8/second and the higher energy channels sample at a rate of 1/second. The scanning system steps to a new scan position once every 8 seconds. The scan position at 45° from EME north is used for background measurement and the scan position at 150° from EME north is used for calibration. The in-flight calibration source is a double radioisotope source consisting of strontium (Sr-90) and promethium (PM-147).

The Minnesota experiment was initially turned on for tests at 1125 GMT on June 14, 1974 and by 1250 GMT it was operating in the final experiment configuration. Except during brief periods when it was turned off, the experiment (with the exception of detector E22) has been operating reliably and collecting good data. A quick check of the scanning system's operation is provided by the in-flight calibration source data. Included in Figure 18-15 are calibration source counts/sec from each of the six scanning system detectors obtained at 1815 GMT (≈ ATS-6 local noon) from seven days between June 15 and August 13. These count rates are within the statistical range of those obtained on preflight calibration runs and indicate the detectors are correctly measuring the calibration source count rates.

Table 18-2
Electron-Proton Spectrometer Energy Channels*

Particles	Scanning System	Fixed System	Energy Range (kev)**
Electrons	E11 E21 E31	E12 E22 E22	30-50 150-200 > 500
Protons	P11 P21 P31	P12 P22 P32	30-70 70-170 170-500

**Nominal values for prototype and flight models.
*Explanation of Subscript System:

The E or P designates electron or proton channel respectively. The first subscript (1, 2, or 3) following one of these letters designates the energy channel. The second subscript (1 or 2) designates the scanning or fixed magnet-detector system, respectively. The three electron channels are labeled to correspond with three different Ortec surface barrier detectors and all three proton channels are associated with one Ortec surface barrier detector. Thus, for example, the E21 energy channel is the 150 to 200 keV electron channel corresponding to the electron detector #2 (E2) in the scanning magnet-detector system.
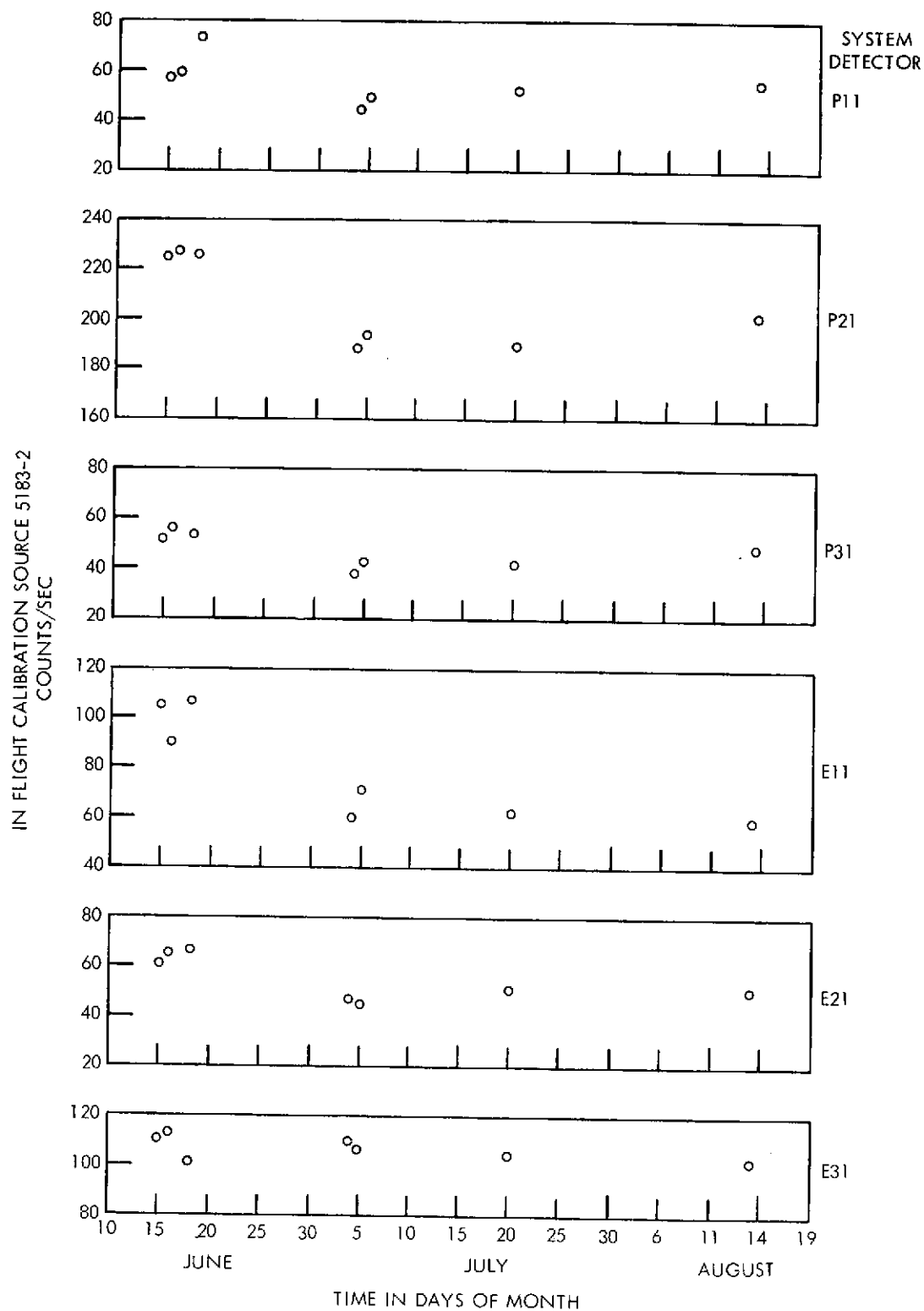
Figure 18-15. Calibration Counts vs Time

Goddard Q/L data tapes have been received for June 15, 17, 18, 26, 27, 29 and July 4, 5, 12, 18, 20 and processed data tapes for June 16, 17 and July 4, 5, 6, 21, 23. Preliminary study of selected portions of this data indicate that the experiment is operating as designed. Electrons and protons are distinguished from each other and the measured fluxes of each are consistent with expected synchronous orbit nominal values. Comparisons of the performance of the fixed and scanning detectors indicate, that as designed, the two systems are giving comparable count rates in corresponding channels. The scanning mechanism is operating as designed. The detectors are responding well to time variations in the particle populations and are counting over the full ranges of intensity changes.

As noted previously, one problem with the experiment is that the electron detector E22 from the fixed system is not counting and is apparently dead. This is not a serious loss since the corresponding detector E21 on the scanning system is working well. The other 11 detectors are continuing to operate well. A problem does exist with the thermal shielding on the spacecraft. Measured temperatures by the University of Minnesota sensors indicate a diurnal variation of from -35°C near local midnight to +35°C near local noon. The detectors operate most efficiently at about -5°C. The colder temperatures near midnight pose no problems; however, there is concern that the exposure of the detector heads to the high temperatures on the sunlight side of the Earth may lead to their premature deterioration. The background counts, particularly in the low energy channels, are also larger on the sunlight side due to increased detector noise at the higher temperatures. Another problem related to the in-flight calibration is that during active magnetic times the count rates from the calibration source are generally larger. This is apparently due to an increased flux of penetrating radiation and/or increased scattering from the calibration post into the detectors associated with an enhanced radiation belt particle population. Thus, care must be taken in interpreting the calibration data obtained during the more active periods.

To illustrate the type of data collected, the response of the detectors and the comparison of the fixed and scanning systems, Figures 18-16 and 18-17 are plots of some preliminary data from June 18, 1974. On these figures, 32-sec average counts/sec are plotted from selected detectors every 6 minutes. The period of time plotted is interesting in that substorm activity occurred during 0400-0630 GMT and 0900-1030 GMT as is indicated by the H-component magnetogram trace from College, Alaska (also shown).

In conclusion, the electron-proton spectrometer has reliably collected particle data of high quality from synchronous orbit consistent with the objectives of its design. Thus far, instrument performance has been satisfactory, and the data obtained should be very useful in helping to further understand the physics of the magnetospheric processes governing the outer zone trapped radiation.
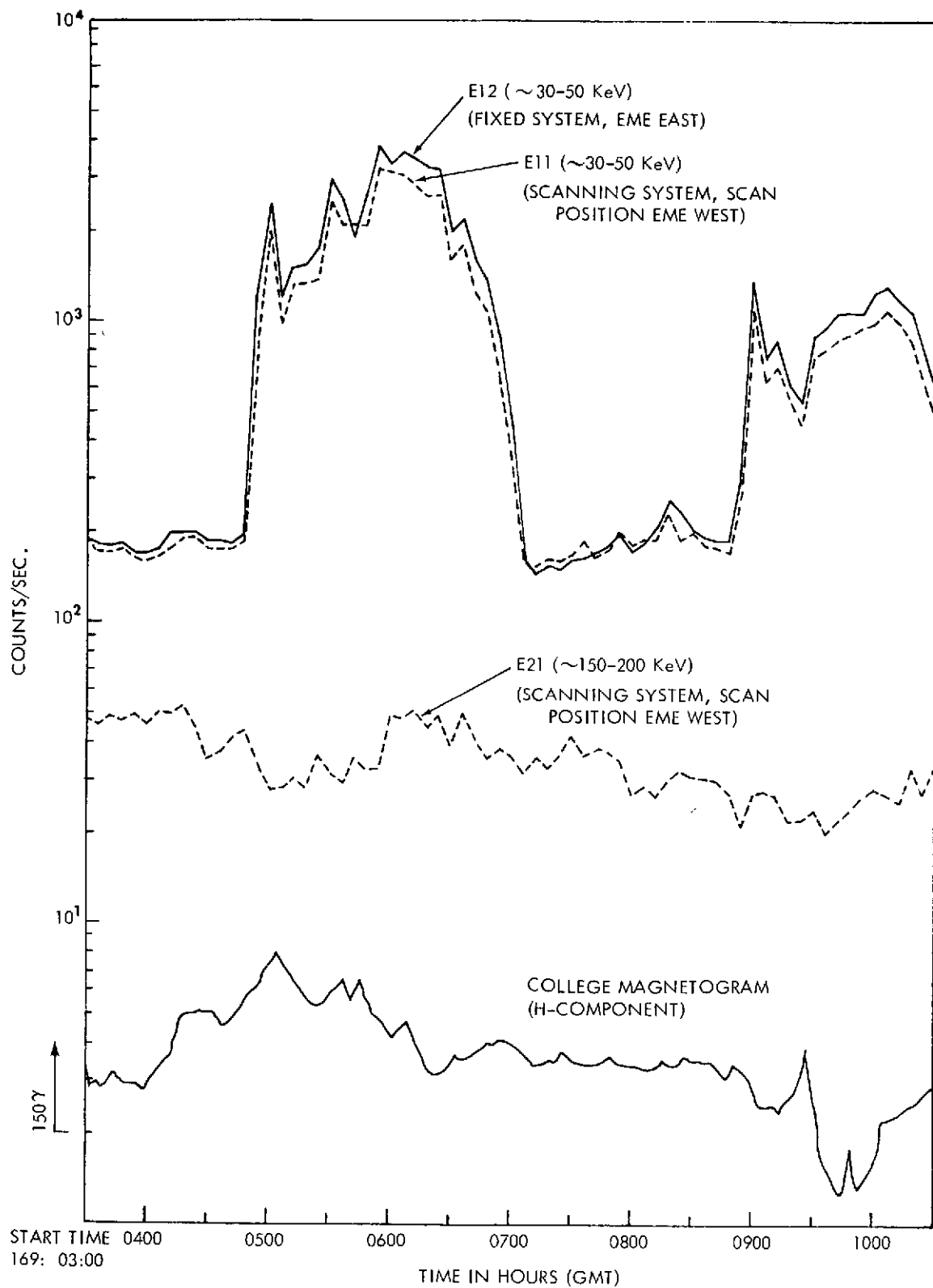
Figure 18-16. Preliminary Electron Data Plots

18-32
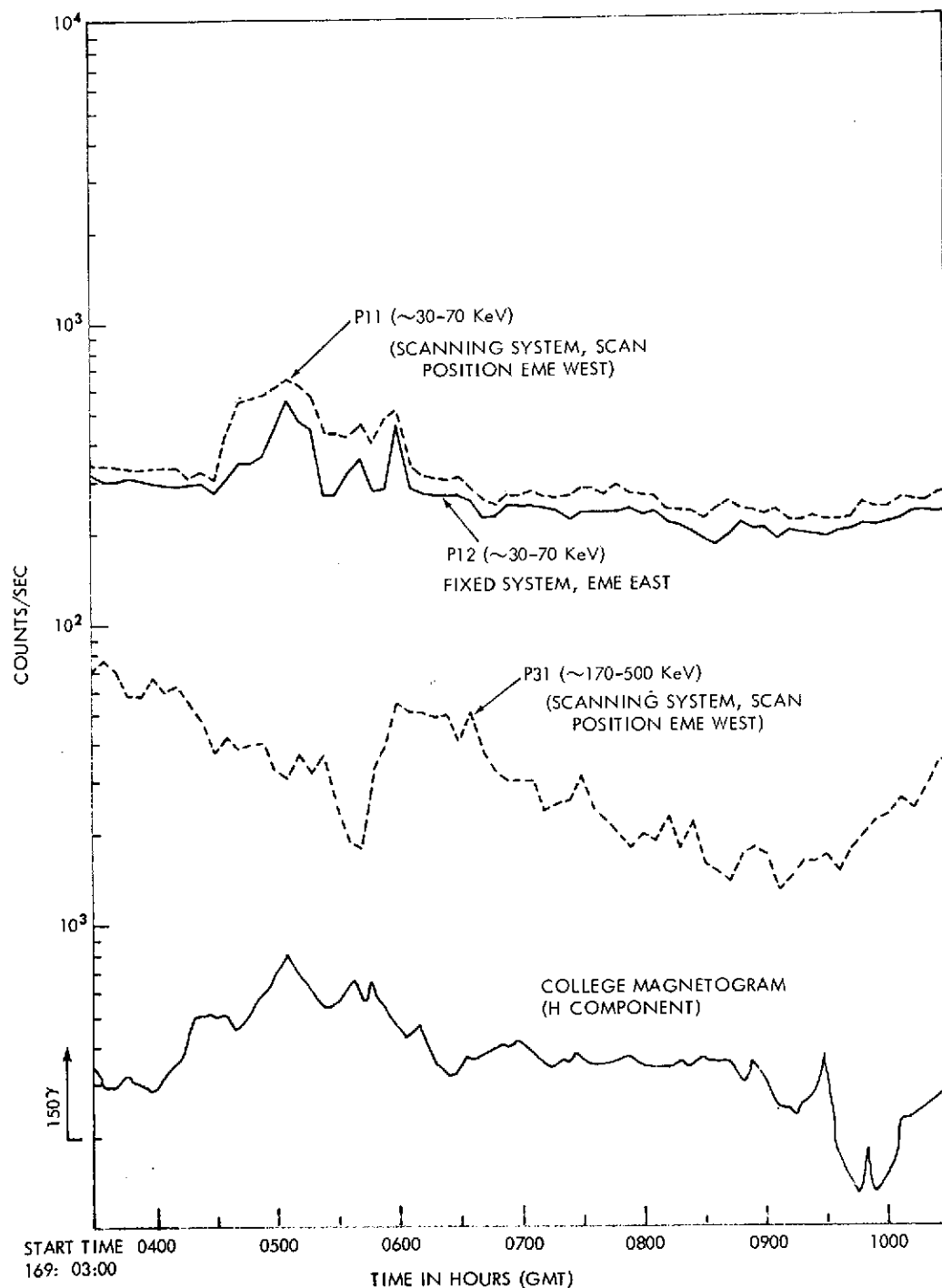
Figure 18-17. Preliminary Proton Data Plots
(University of Minnesota)

The experiment should be left in continuous operation as it has been.

18.5.6 Magnetometer Experiment (UCLA)

The primary objective of the UCLA experiment is the study of the magnetic field at synchronous distances along the three orthogonal axes of the spacecraft. The specific goals are as follows:

a. Study the properties of various magnetohydrodynamic phenomena in the magnetosphere, the magnetospheric tail, and the magnetosheath.

b. Study the interaction of the solar wind with the magnetosphere and the magnetospheric tail.

c. Study the properties of the magnetospheric boundary or magnetopause.

d. Study the properties of the magnetosheath.

The ATS 6 magnetometer has performed in conformance with the design goals. Two anomalies have been observed. First, the magnetometer sometimes goes into the first step of the calibrate sequence at unscheduled times. This is attributable to noise spikes on the spacecraft command line. Once the magnetometer has begun the sequence, further commands are required to complete it. Thus, the magnetometer frequently remains in the calibrate mode from the time of the first noise pulse until the end of the next normal calibration sequence. Since the calibration field is known, this anomaly does not affect the information on the ambient field.

Second, the data from the Z-axis are slightly noisier than those from the other two axes. As yet, the source of this noise has not been identified.

At present, no reports are available on which to base a precise operational chronology for the magnetometer.

Daily plots and a BCD tape of sequence averages are now being supplied to the other ATS-6 investigators.

A preliminary survey of the data available so far indicates that the properties of the magnetic field at the position of ATS-6 are significantly different from those of the field at the position of ATS-1. Much of this difference can be accounted for in terms of the different positions of these two spacecraft relative to the plasma sheet, especially when the spacecraft are at local midnight. It has also been observed that Pc 3 fluctuations may be clearly resolved (periods in the range of about 30 seconds) and that these fluctuations occur frequently.

18.5.7 Solar Cell Radiation Damage Experiment (HUGHES)

The objective of this experiment is directed primarily toward isolating the pre-dominant degradation mechanism(s) associated with current production solar cells and eliminating anomalous data through increased data points and instru-mentation accuracy. A total of 80 solar cells are individually monitored on the flight experiment with a total of 12 current-voltage points and temperature data for each solar cell transmitted to ground on a real-time basis. Five solar cells of 16 types have been included to provide a statistically meaningful sample size. A solar aspect sensor on the EME insures that the sun is normal to the test cells at the time of the measurements.

The SCRDE was commanded on manually at 0230 GMT on the first day after launch. Since then, it has been turned on once a day for periods of approximately 3 minutes. When the experiment is on, data are transmitted providing voltage and corresponding current values for 12 resistive loads on each of 80 solar cells under study. A complete run through 80 cells requires approximately 19 seconds so the 3 minute daily operational period permits an adequate sampling of cell data.

Data have been reduced for the first month in orbit, but the processing is incom-plete. Further information regarding spacecraft attitude control data is required and will soon be provided by GSFC. Such data are necessary to determine the angle of solar incidence and the corresponding solar irradiation incident upon the solar cells under test. The actual solar irradiation levels are used to correct the cell performance values to a preestablished set of standard conditions. By this means, the performance of the cells in space can be accurately compared with the performance of the cells before launch.

Although absolute performance values are presently unavailable, the cells, rela-tive to one another, are behaving as expected. This is true for the 40 cells being processed by Signal Processor Unit No. 1 (the experiment has two SPU's, each processing signals from 40 cells). Erratic data from the current channel are being obtained from SPU 2. It is tentatively concluded that an operational amplifier in SPU 2 is malfunctioning.

If this initial judgment is correct, data from 40 cells will be lost. There is no repetitive pattern; e.g., a constant off-set, to allow a correction for the anomaly. However, the cells under study have been distributed in such a manner that in-formation from all 16 cell configurations is being obtained. With SPU 2 out, the sample size suffers; down from 5 cells per configuration to 2 or 3 cells per configuration.

For future operations, the frequency of experiment activation will be reduced to once a week and eventually to once a month. The particulate radiation damage under observation has its most severe impact initially, the damage slope then decreasing exponentially with time. Once the daily data sampling establishes a performance degradation curve, the frequency of sampling can be reduced as planned.

18.5.8 Omnidirectional Spectrometer Experiment (Aerospace)

The purpose of this experiment is to measure the omnidirectional fluxes and spectra of electrons and protons. Four detectors count protons from 2 MeV to 60 MeV. They also count, respectively, electrons of energies greater than 150 keV, 700 keV, 1.4 MeV, and greater than 3 MeV.

The experiment was powered on 14 June 1974. Verification of the outputs was accomplished on 14 and 15 June. It has been on, except for brief off periods, associated with tests of other experiments onboard the EME.

Performance of the experiment has met all design goals with the exception of the anomalies described later.

a. All electron channels are operating as expected and yielding high quality data.

b. All proton channels are operating and yielding high quality data.

c. All alpha particle channels are operating and yielding high quality data.

d. All performance parameters gave the expected readings prior to the malfunction apparently induced by the turn on of the UNH experiment.

The following anomalies have been noted:

a. At low temperatures the count rates in the E2 channel go abruptly to zero. This occurs at internal experiment temperatures below about 0°C. It is postulated that an open occurs either in the detector or the preamp output which interrupts the flow of the signal. The cause of this open may be the very high thermal gradient between the outside of the bubble containing the 1×1 mm detector and the interior of our experiment. There is some evidence that the internal temperature may be as much as 30°C higher than the bubble temperature, a condition which was not anticipated. The anomaly disappears if the system warms up and is not observed on most days.

b. Systems Anomalies

1. The housekeeping data was destroyed, apparently by the turning on of the UNH experiment. No valid housekeeping data were obtained after Day 169.

2. The encoding process appears to be effected by the HAC solar cell experiment. The E1 channel displays an anomaly (Figure 18-18) which is interpreted as being the removal of the 1 bit after the most significant 1 bit. It appears likely that this anomaly occurs in the log compression circuitry. There is at present, evidence that only the 4096 or 2048 bits are effected. This occurs during the HAC Lockout following operation of the solar cell experiment.

The following items represent preliminary findings in the data examined to date:

a. There is an impression that the energetic electron population at the synchronous altitude is more dynamic than that observed in the 1966-1969 time period on ATS-1. That is, there seem to be frequent total disappearances of the electron flux, a condition which occurred relatively rarely on ATS-1. This effect may be a result of an actual change in magnetospheric topology or it may be merely a geometric effect due to the somewhat higher magnetic latitude at which ATS-6 is located compared to ATS-1.

b. Changes have been observed in the solar proton fluxes associated with magnetic activity. It is believed that these changes are indicative of the development of quasi-trapped fluxes of solar protons as the spacecraft moves from open to closed field lines.

c. Several solar proton enhancements associated with sudden commencements have been observed. Analysis of these data will provide experimental measurement of charged particle lifetimes and diffusion coefficients.

d. A suprisingly high flux of > 4 MeV electrons has been observed. This data, when compiled, may be of importance to spacecraft system designers.

The ability to obtain data at the GSFC facility in near real time has been extremely valuable. Future requirements for rapid access to ATS-6 data are anticipated and it is urged that provision be made to retain the display and hard copy capabilities now existing for ATS-6.
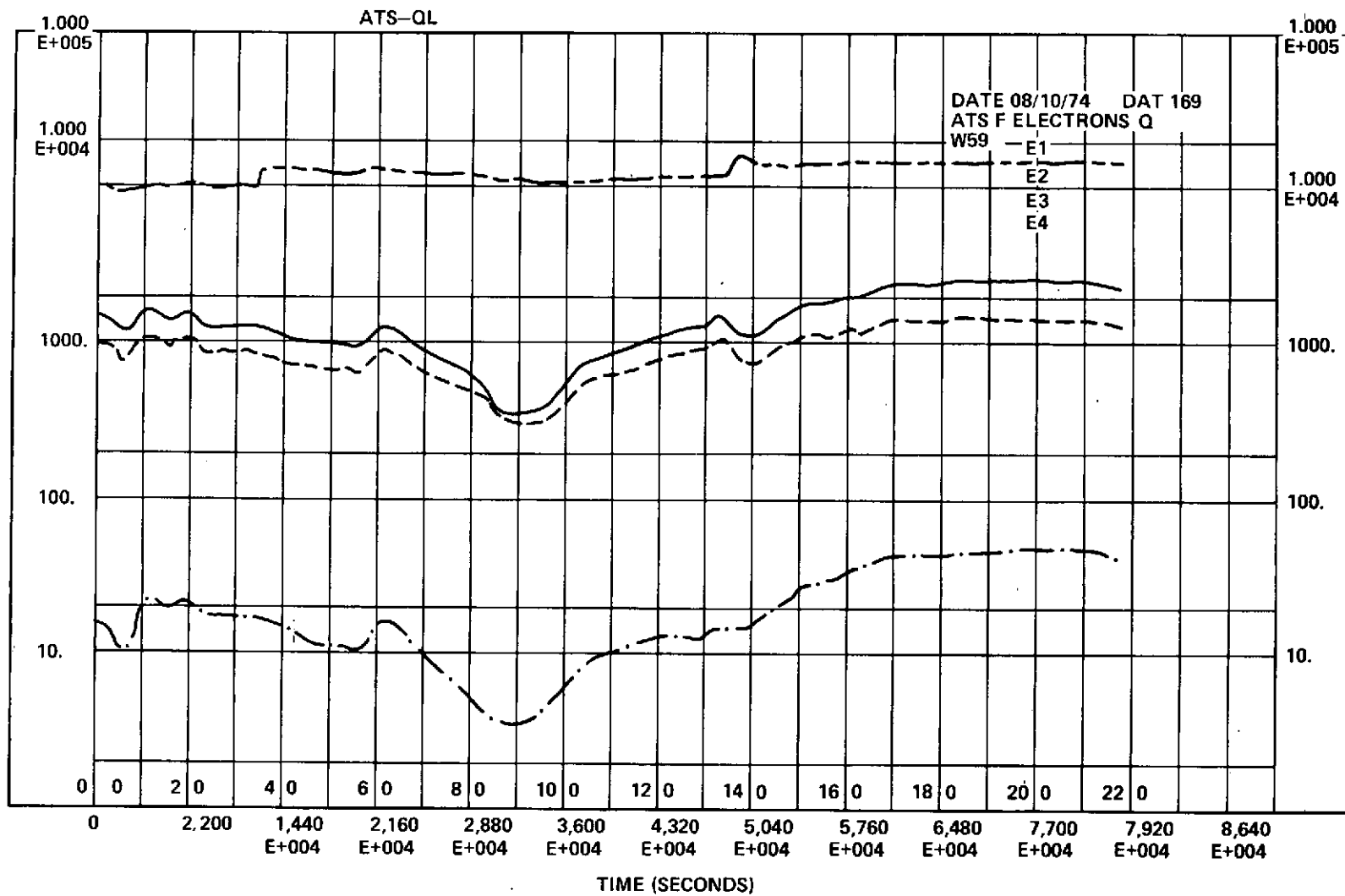
Figure 18-18. Anomaly Displays, Channel E1

SECTION 19

TRACKING AND DATA RELAY EXPERIMENT
(T&DRE)

SECTION 19

TRACKING AND DATA RELAY EXPERIMENT (T&DRE)

19.1 INTRODUCTION

There are two tracking and data relay experiments, one involving equipment installed on the Nimbus-F Spacecraft and the other on GEOS-C. Their purpose is to evaluate tracking of and data transmission from low orbit spacecraft through a geosynchronous spacecraft. The ATS-6 is the geosynchronous spacecraft supporting these experiments.

Communication between the ground and ATS-6 is at C-band and between ATS-6 and the Nimbus F and GEOS-C satellites at S-band. The ATS-6 provides coherent frequency conversion necessary for the precision tracking of the two spacecraft. The Nimbus-F ranging transponder is of the crystal type where the return ranging signals modulate a subcarrier. This arrangement allows data to be multiplexed below the subcarrier on the return link. The GEOS-C includes a phase-lock-loop (PLL) transponder that turns around the ranging signals directly. When data is transmitted by the GEOS-C, range measurements cannot be made; however, range rate measurements can be maed on the coherent carrier and used for orbit determination. Thus the two experiments evaluate two variations on the basic relay tracking scheme.

The T&DRE equipment on the Nimbus-F spacecraft includes a gimballed antenna that provides about 15 dB gain and S-band transmitter power of nominally 2, 4 and 8 watts.

The GEOS-C experiment equipment includes an antenna with switched elements that provide a maximum gain of 5 dB at a transmitter power of 5 watts.

The ATS-6 spacecraft will track the low-orbit spacecraft either by program track through the Digital Onboard Controller which generates pointing angles from ephemeris data, or by monopulse tracking of the received S-band signal.

The basic relay configuration is shown in Figure 19-1.

19.2 TEST PROGRAM

A test program is underway to evaluate all experiment modes prior to the launch of the Nimbus-F and GEOS-C spacecrafts. For this, GEOS and Nimbus transponders, together with sufficient equipment to simulate spacecraft functions, are located at GSFC. In addition, Nimbus transponder simulators are located at Rosman, Mojave, and Santiago and a GEOS transponder is located at Rosman.

ATS-6
SPACECRAFT

S-BAND LINKS

C-BAND LINKS

LOW ORBIT
SPACECRAFT

85' ANTENNA

ATS
GROUND
STATION
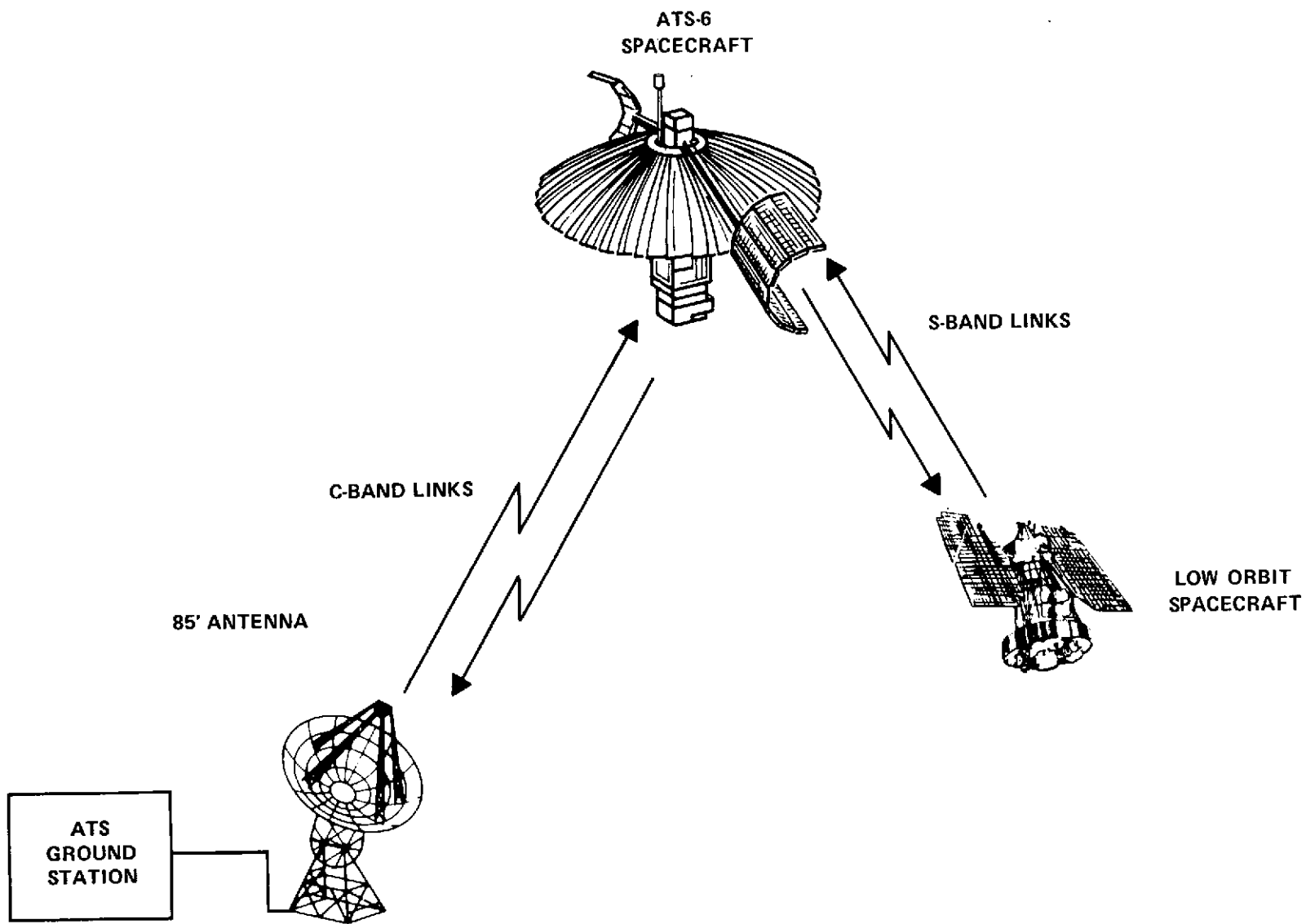
Figure 19-1. Basic Relay Configuration

This allows relay tests with the ATS-6 spacecraft at distances close to the actual distances when the tracked spacecraft are in low orbit.

The tests can be divided into three phases:

1. Experiment functional checkout
2. Evaluation of all operating modes
3. Operational simulation

Phase 1 has been completed since virtually all functions have been exercised. Phase 2 is in progress and in general good data has been obtained for all modes at various times. The performance has been variable and more testing is required to determine the cause of the variability and make changes in equipment and procedures where possible to obtain more consistent results.

19.3 NIMBUS-F T&DRE

19.3.1 Operating Modes

The basic Nimbus-F T&DRE relay test configuration is shown in Figure 19-2. Command and telemetry for the ATS-6 spacecraft is transmitted over the normal VHF links. The ATS ground station generates a C-band beacon signal which the ATS-6 synthesizer uses for coherent translation of the forward and return link signals. The ground station also generates ranging signals through the ATSR equipment modified to operate in the crystal and PLL transponder mode. The ranging signals are transmitted at C-band, translated to S-band in the ATS-6 spacecraft and received by the Nimbus-F transponder at GSFC. The Nimbus-F transponder retransmits the ranging signal on a 2.4 MHz subcarrier which is relayed to the ground station. The ground station makes range measurements on the range tones and range rate measurements on the return carrier and the 2.4 MHz subcarrier in combination. The ground station produces a punched tape which is transmitted via teletype to the Operations Support and Computing Division (OSCD) for analysis at GSFC.

Data, for evaluation of the data relay function, is transmitted by the Nimbus-F transponder at GSFC, relayed through the ATS-6 spacecraft and received at the ground station. The prime evaluation data is the digital evaluation mode (DEM) which is a pseudo-random digital sequence which can be transmitted at any of four bit rates. The ground station has the capability of providing a quick-look error check of the DEM data and also records the data for evaluation by the Information Processing Division (IPD). The Nimbus-F transponder also transmits Nimbus-F VIP and THIR data. The VIP Nimbus telemetry data is the Nimbus-F PCM telemetry at a bit rate of 4 kbps. The THIR (Temperature-Humidity Infrared Radiometer) data is experiment data on a subcarrier at

ATS-6 SPACECRAFT

ATS-6 VHF
CMD & TM LINKS

RELAY
C-BAND
LINKS

RELAY
S-BAND
LINKS

85' ANTENNA

ATS-6 COMMANDS

ATSOCC

ATS-6 TM

**ATS GS
ROSMAN II**

R & RC DATA

OSCD

DEM DATA TAPES

QUAD HELIX
ANTENNA

GSFC

NIMBUS-F TRANSPONDER

- RETURNS RANGING
  SIGNALS ON 2.4 MHZ
  SUBCARRIER
- TRANSMITS DEM,
  VIP & THIR DATA
- RESPONDS TO RELAY
  COMMANDS

IPD

T & DRE
CMDS

VIP &
THIR
DATA

T & DRE
COMMANDS

**NIMBUS
OSC**

VIP & THIR DATA

ROSMAN I

Figure 19-2. Basic Nimbus-F T&DRE Relay Test Configuration

approximately 43 kHz. The ground station receives the VIP and THIR data and transmits the data to Rosman I where it is recorded and also transmitted to Nimbus Meteorological Data Handling System (MDHS) for evaluation.

The Nimbus T&DRE also evaluates relay commanding. Experiment noncritical functions can be controlled through the relay link. The commands are generated by the Nimbus MDHS transmitted to Rosman I where they are transferred to the ground station for transmission through the relay link.

The various relay operating modes described above can be performed separately and in certain combinations. The possible relay modes are as follows:

    a. R&RR only
    b. DEM
    c. DEM and R&RR
    d. VIP
    e. VIP and R&RR
    f. THIR
    g. VIP and THIR

In addition to the relay modes described above, the Nimbus T&DRE includes other modes to improve the tracking accuracy. The ATS-6 spacecraft can be tracked directly in a coherent ranging mode using the experiment ranging system. Also, Nimbus simulators have been installed at Rosman, Mojave and Santiago so that the ATS-6 spacecraft can be effectively tracked with respect to those stations in a trilateration or sequential ranging mode. (See Figure 19-3). These Nimbus simulators have the capability of transmitting data and receiving commands so that they can be used for data and command tests as well as for ranging.

19.3.2 Test Results

A summary of the Nimbus-F T&DRE tests that have been performed with a gross indication of results is shown in Table 19-1.

19.3.2.1 Received Signal Strength — An engineering model Nimbus-F T&DRE antenna has been used at NTTF. This antenna is mounted on a tripod and the pointing angle is peaked on the ATS-6 S-band signal. The received signal level at the Nimbus-F T&DRE transponder has been measured as -98 and -99 dBm for the various tests using the internal signal strength telemetry. This is about 2 dB higher than predicted based on ATS-6 prelaunch EIRP information.
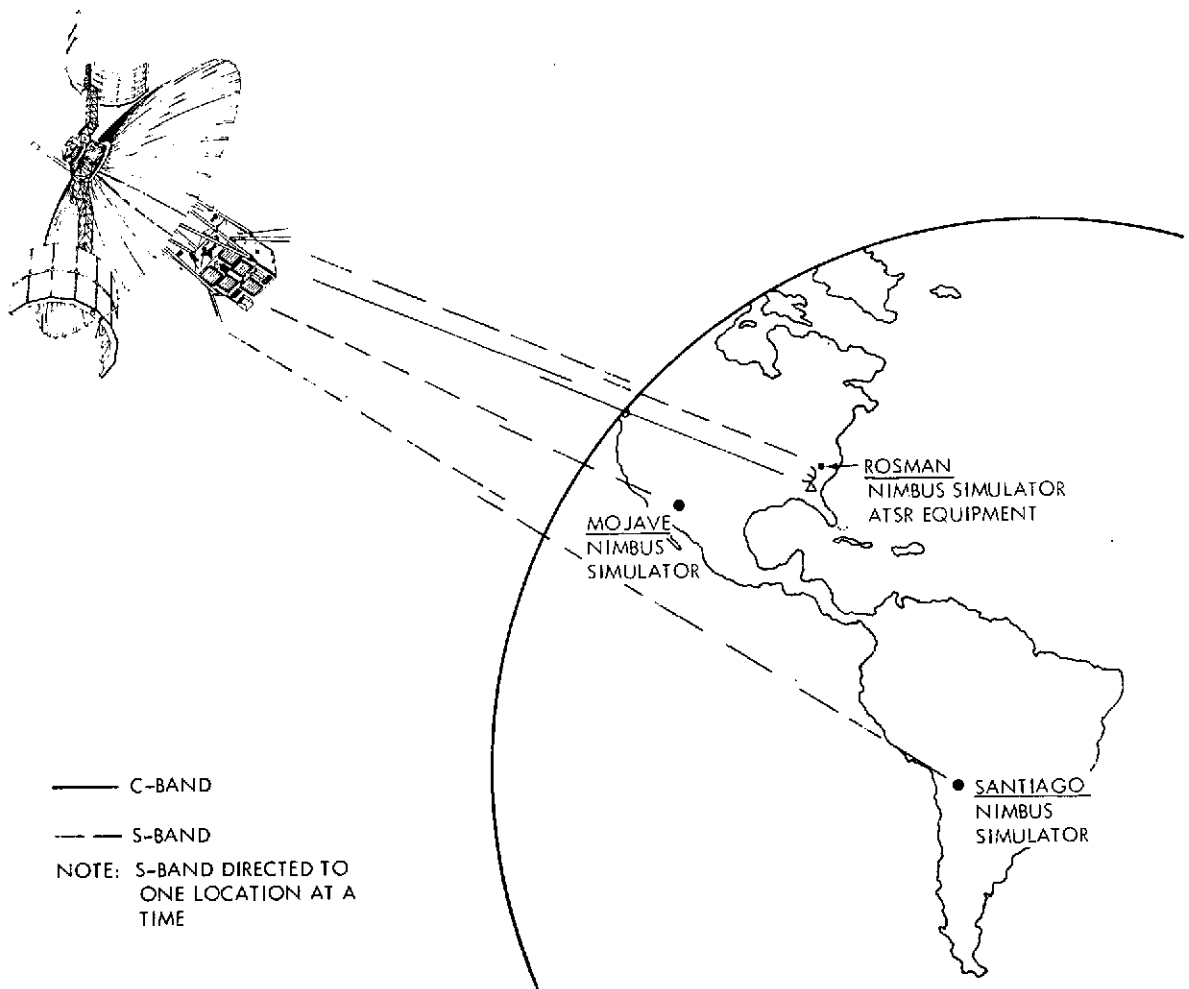
Figure 19-3. ATS-6 Nimbus-F T&DRE Trilateration Configuration

Table 19-1
T&DRE Test Summary

			June 12	July 11	July 17	July 19	July 25	Aug. 16	Aug. 27	Sept 1&2	Sept. 4	Oct. 2nd
R&RR	Coherent	Rosman					1	*		1		1
		Mojave										
		Hybrid								1		
	Trilateration	Rosman/Rosman					1			1		
		/Mojave					1			1		
		/Santiago					1					
		Hybrid/Rosman										
		/Mojave								1		
		/Santiago										
	Relay	Rosman/NTTF		1				*	*			1
		Hybrid/NTTF										
Data	Rosman	Dem	dB/vs predicted	*	?		1				*	1
		Dem/R&RR									*	*
		VIP			*		1					
		VIP/R&RR					1					
		THIR			?		1					1
		VIP/THIR			*/?		1/1		*/*			1/*
	Hybrid	DEM										
		Dem/R&RR										
		VIP										
		VIP/R&RR										
		THIR										
		VIP/THIR										
Command	Rosman	DTS			?	*		1	*			
		Wideband		?	?	1		1	*			
	Hybrid	Tape								?		
Monopulse				0				1	1	1		
Electroscan							1					

LEGEND: 1 Satisfactory Results
         * Degraded Performance or Error Point
         ? Data not Analyzed
         0 Unable to Perform Function

The return S-band signal level received at the ATS-6 spacecraft from the Nimbus T&DRE equipment is measured indirectly by spectrum analyzer measurements at ground station C-band downconverter output. With the Nimbus T&DRE transponder in the 8-watt mode, a signal-to-noise ratio between 17 and 20 dB is obtained in a 10-kHz bandwidth. Calculations indicate this value should be 21 dB but the difference is within the accuracy of the spectrum analyzer measurement. Direct measurement using the spacecraft AGC of the received signal level is not possible since the signal-to-noise ratio is -14 to -20 dB depending on the Nimbus-F T&DRE power level.

The test conditions, using the antenna peaked at GSFC, provide probably better than nominal signal strength conditions. At maximum range where there is greater space loss (loss due to limitations of antenna gimbal angle and through the atmosphere propagation losses), the signal will be attenuated approximately 5 dB from the test level. Further tests will introduce an attenuation to simulate conditions out to the maximum range.

19.3.2.2 Tracking Data — The design capability for the tracking modes has been verified by the tests. Range noise generally less than 3 meters has been achieved. Range-rate noise is generally less than 0.5 mm/sec have been achieved at 10 seconds integration period and generally less than 4 mm/sec at 1 second integration period.

One of the earlier tracking data tests was a trilateration operation involving Rosman, Mojave and Santiago ground station. The Rosman ground station made coherent ranging measurements on ATS-6 and relay measurements on Nimbus T&DRE simulators at the three ground stations. Good results were obtained. Orbital computations were performed on the data and orbital elements and ranging residuals are shown in Tables 19-2 and 19-3. The period of data acquisition was short, less than 4 hours; however, the results show that good data can be obtained in the trilateration mode.

Table 19-2
ATS-6 Orbit Determination
using Trilateration Data
(19 July 1974)

Semimajor Axis	a — 42149581 Meters
Eccentricity	e — .000233
Inclination	i — 1.6233 Deg
Ascending Node	Ω — 265.201 Deg
Arg. or Perigee	ω — 127.453 Deg
Mean Anomaly	M — 199.903 Deg

Table 19-3
Ranging Data Residuals
(19th-20th July 1974)

Station	Pass	Residual RMS (meters)	No. of Points
Rosman	1	52	32
Rosman	2	18	120
Rosman	3	43	32
Rosman	4	6	120
Rosman	5	72	32
Rosman	6	27	120
Santiago	1	8	32
Santiago·	2	2	120
Mojave	1	30	32
Mojave	2	10	120
Rosman*	7	24	120
Rosman*	8	32	16
Rosman*	9	25	32
Rosman*	10	11	120

*Direct measurements on ATS-6 in the
coherent mode.

From September 1st through 3rd, experiment range and range-rate measure-
ments were combined with a 24-hour routine ATS ranging period. During the
24-hour period trilateration type measurements using Nimbus-F T&DRE
ground transponders, were made with Rosman and Mojave stations participating.
The Hybrid terminal at Mojave, which will be used at Madrid during Western
hemisphere operations, was exercised for the first time. After the 24-hour
ranging period, relay range and range-rate measurements were made to GEOS-C
transponders at Rosman and GSFC. The Hybrid terminal appears to have per-
formed well at the first attempt. The range and range-rate noise for the relay
measurements is shown in Table 19-4. Range and range-rate noise for direct
coherent measurements on ATS-6 is shown in Table 19-5 for a number of the
measurements made. Orbital computations for this test period are in process.

Some difficulties have been encountered in performing ranging measurements
particularly for two of the Rosman/GSFC relay tests. The problems were in
setting synthesizers at the ATS ground station and locking to the ranging tones.
These problems are being overcome by more careful procedures and by per-
forming more checks. The range and range-rate readouts are checked at each
measurement to verify that the readings are close to predicted values.

Table 19-4
ATSR Relay Measurement Noise
(1-3 September 1974)

Transmitting Station	Receiving Station	Transponder Type	Start Time (DDD/HHMM)	Sample Rate (sec)	Ranging Noise (meters)	Range-Rate Noise (mm/sec)
Rosman	Mojave	Nimbus	244/1715	1	2.022	3.1
Hybrid	Mojave	Nimbus	244/1925	1	1.401	2.5
Hybrid	Mojave	Nimbus	.244/1930	1	1.473	3.1
Rosman	Mojave	Nimbus	244/2032	1	1.881	3.3
Rosman	Mojave	Nimbus	244/2035	1	1.542	2.9
Hybrid	Mojave	Nimbus	245/0421	1	1.536	3.0
Rosman	Mojave	Nimbus	245/0817	1	1.488	2.8
Hybrid	Mojave	Nimbus	245/0823	1	0.891	8.5
Rosman	Mojave	Nimbus	245/1204	1	1.632	3.8
Hybrid	Mojave	Nimbus	245/1211	1	1.452	33.2
Rosman	Rosman	GEOS-C	245/1908	10	1.518	0.5
Rosman	NTTF	GEOS-C	245/1941	10	No Rng.	0.5
Rosman	NTTF	GEOS-C	245/1956	10	No Rng.	0.6
Rosman	NTTF	GEOS-C	245/2019	10	–	0.5
Rosman	Rosman	GEOS-C	245/2123	10	2.685	0.4
Rosman	NTTF	GEOS-C	245/2153	10	12.240	0.6
Rosman	NTTF	GEOS-C	245/2202	10	3.480	0.4
Rosman	Rosman	GEOS-C	246/0740	1	1.890	3.1
Rosman	Rosman	GEOS-C	246/0748	10	2.388	0.4
Rosman	Rosman	GEOS-C	246/1249	10	2.145	0.4

Table 19-5
ATSR Coherent Measurement Noise
(1-3 September 1974)

Xmitting Station	Signal Type	Start Time (DDD/HHMM)	Sample Rate	Rng. Noise (meters)	RRate Noise (mm/sec)	Frequency
Rosman	Coherent	244/1610	1 sec	2.079	3.1	Nimbus
Rosman	Coherent	244/2000	1 sec	2.259	3.4	Nimbus
Rosman	Coherent	244/2003	1 sec	1.818	3.0	Nimbus
Rosman	Coherent	244/2023	1 sec	1.698	4.6	Nimbus
Rosman	Coherent	245/0010	1 sec	1.950	2.8	Nimbus
Rosman	Coherent	245/0445	1 sec	1.812	3.6	Nimbus
Rosman	Coherent	245/0804	1 sec	1.923	3.4	Nimbus
Rosman	Coherent	245/1152	1 sec	1.554	3.7	Nimbus
Rosman	Coherent	245/1840	10 sec	1.359	0.3	GEOS-C
Rosman	Coherent	245/2215	10 sec	6.930	0.4	GEOS-C
Rosman	Coherent	246/0646	10 sec	0.942	0.3	GEOS-C
Rosman	Coherent	246/0801	1 sec	1.875	4.4	GEOS-C
Hybrid	Coherent	244/1910	1 sec	0.032	1.0	Nimbus
Hybrid	Coherent	244/1942	1 sec	-	11.6	Nimbus
Hybrid	Coherent	245/0027	1 sec	0.927	44.8	Nimbus
Hybrid	Coherent	245/0832	1 sec	1.593	3.4	Nimbus
Hybrid	Coherent	245/1219	1 sec	3.780	3.1	Nimbus
Hybrid	Coherent	245/1606	10 sec	-	0.1	Nimbus
Hybrid	Coherent	245/1621	10 sec	1.362	0.3	Nimbus
Hybrid	Coherent	245/1702	10 sec	0.0	0.0	Nimbus

19.3.2.3 Data Relay – The Digital Evaluation Mode (DEM) data has been relayed from GSFC on four occasions and DEM with R&RR on two occasions. In two instances the DEM only could not be properly evaluated due to failure of the code correlator used at the ATS ground station for evaluations of the DEM data. The test results are shown in Figure 19-4. These results show that data can be transmitted with quality close to that predicted.

Figure 19-5 shows the DEM performance when transmitted in combination with R&RR. The performance deviates from the predicted performance at lower bit rates. This was traced to a problem in the code correlator which provided insufficient attenuation of the 2.4 MHz ranging subcarrier.

VIP and THIR data has been of variable quality as in the case of DEM data. Four tests have been performed involving VIP and THIR. The data was successfully transmitted on two occasions and VIP quality was good either alone or with THIR. THIR data was somewhat degraded in the combined mode and this is thought to be due to interference of THIR data by VIP data due to distortion is the relay system. For the other tests VIP and THIR data was not of expected quality due to operational problems. Additional testing is planned to resolve these problems.

19.3.2.4 Commanding – The Nimbus T&DRE can be commanded via the relay link by commands generated by Nimbus MDHS. These commands are transmitted to the ATS ground station through the DTS or wideband link. Consistent results have not been obtained from the command tests. The problems appear to be associated with the quality of ground transmission. Difficulty in commanding is usually accompanied by distortion of the command waveform and possible incorrect phasing of the clock amplitude modulation with the command tones. Of the three tests performed, the wideband link has performed satisfactorily on two occasions and the DTS once.

On the occasions when commanding has been successful, discrete commands have been executed and full antenna programmer loads have been transmitted. The antenna programmer memory loads have been checked for accuracy by running the antenna programmer at a faster than normal rate and observing the digital output on a display.

The command frequency modulator at the ground station was not operational for all tests. On one occasion the range tone modulator in the ATSR equipment was used to transmit commands successfully. An integrator was incorporated to convert the phase modulation characteristics of the ATSR equipment to the required frequency modulation characteristic.
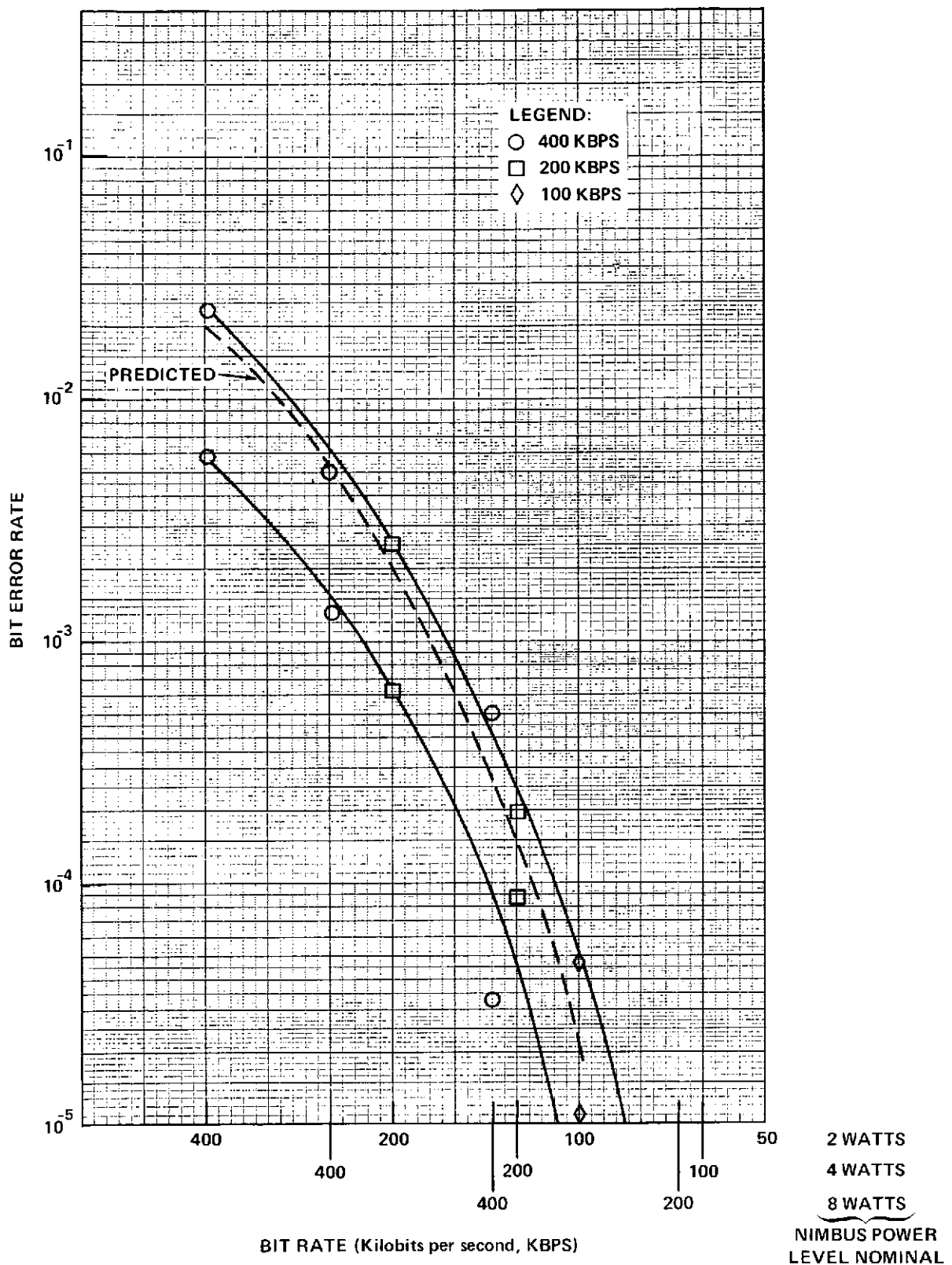
Figure 19-4. Digital Evaluation Mode (DEM) Bit Error Rate
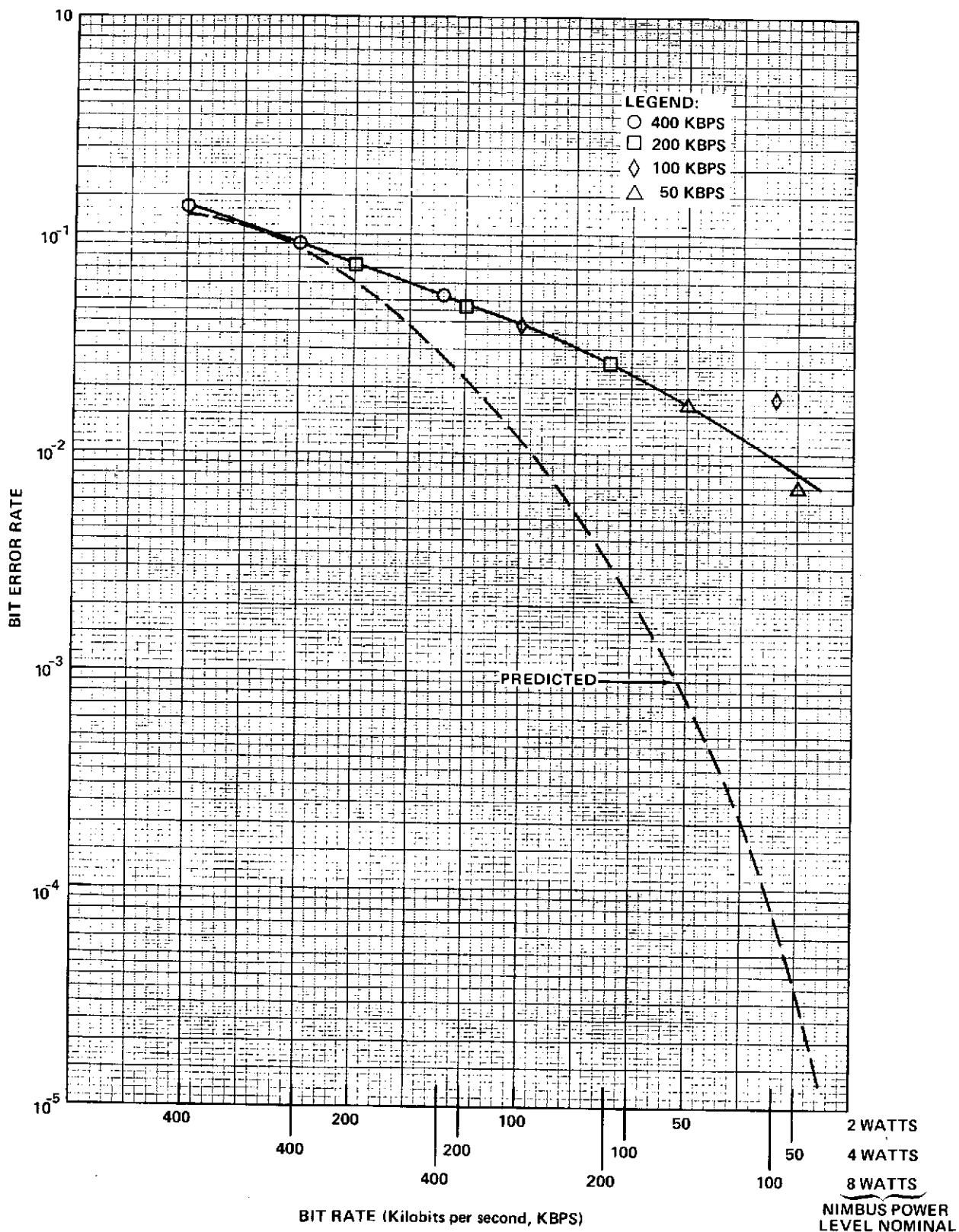
Figure 19-5. Digital Evaluation Mode (DEM) Bit Error Rate

19.3.2.5 Monopulse Tracking – Two monopulse tests have been performed. In one case merely an indication of proper operation was obtained within the test period. In the second, more extensive results were obtained and will be described.

The Nimbus T&DRE transponder was operated at GSFC in the 2-watt mode. The ATS-6 spacecraft was first pointed towards GSFC by offset pointing using the earth sensor reference. The monopulse receiver was checked for near-zero error in this condition. The ATS-6 spacecraft was then switched to the monopulse tracking mode. The spacecraft remained at the same pointing angle. The ground S-band transmitter located at GSFC was then turned off and the spacecraft pointing allowed to drift up to 0.7° away from GSFC. The transmitter was turned on again and the spacecraft returned to GSFC pointing. The first half of Figure 19-6 shows the response of the ATS-6 in capturing the S-band signal from GSFC. The results indicate a classic response starting with an offset of about 0.5° from the final settled pointing angle. Range tones were added during the settling period and apparently did not interfere with the monopulse operation.

The threshold of the monopulse was investigated. The signal level was gradually reduced until the spacecraft pointing started to drift and then was increased until the spacecraft corrected. A dual variable coupler was used to adjust the signal level into and out of the Nimbus-F transponder and the received signal strength at the transponder was used as the reference. At -109 dBm the spacecraft drifted off pointing and at -107 dBm started to correct. These results indicate that monopulse can be used over the predicted signal range.

19.3.2.6 Electroscan – The ATS-6 electroscan capability was used in support of the Nimbus F T&DRE during the trilateration operation where the ATS-6 is pointed at three stations in sequence. In this situation the electroscan can reduce the amount of spacecraft slewing required.

Electroscan was used during the test of July 19th. Initially the ATS-6 was bore-sighted on Rosman and antenna feed E5 was used to electroscan the S-band beams to Mojave. The spacecraft was then slewed to a point between Rosman and Santiago, specifically 77°W long. and 1°N lat. From this point the beam was directed through feed N5 to Santiago and through feed S5 to Rosman.

Small slews were performed about the Rosman and Santiago stations to determine whether the signal strength would be improved. An improvement of about 6 dB in signal strength was indicated within 0.5 degree. This shows that to obtain the best signal-to-noise ratio a minor slew should be performed at each location in conjunction with the electroscan.
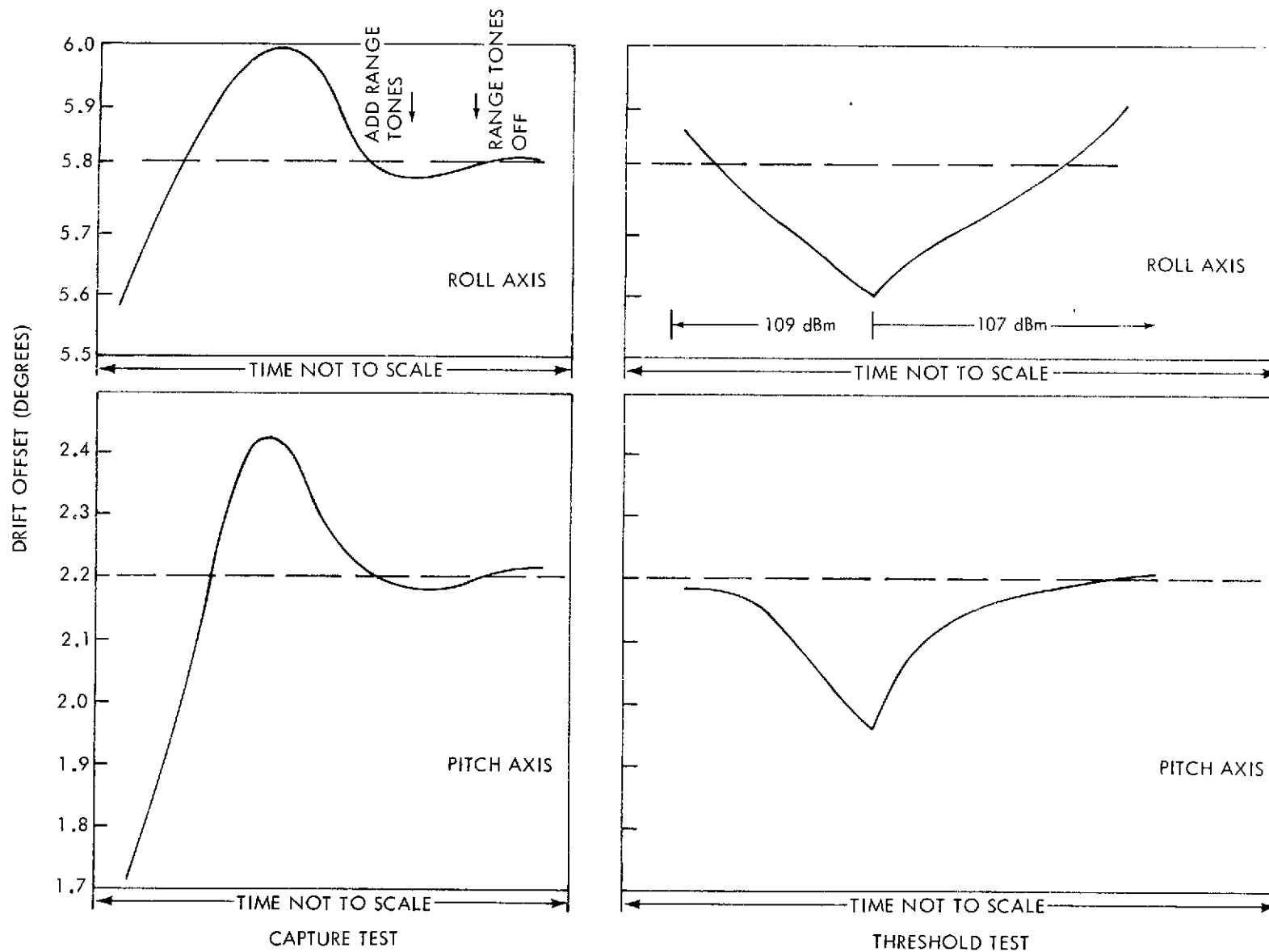
Figure 19-6. Monopulse Test-ES Readout

19.4 GEOS-C T&DRE

19.4.1 Operating Modes

The GEOS-C T&DRE test configuration is shown in Figure 19-7. Command and telemetry for the ATS-6 spacecraft are transmitted over the normal VHF links. The ground station generates a C-band beacon signal which the ATS-6 synthesizer uses for coherent translation of the forward and return links. The ground station also generates ranging signals through the ATSR equipment modified to operate in the crystal and PLL transponder modes. The ranging signals are transmitted at C-band, translated to S-band in the ATS-6 spacecraft and received by the GEOS-C transponder at GSFC. The GEOS-C transponder is of the phase-lock-loop type and retransmits the ranging tones on the return carrier. The reference oscillator is locked in phase to the received carrier and provides the reference for the transmitted S-band carrier so that the received and transmitted carrier signals are coherent. The ATS-6 spacecraft converts the received S-band signal to C-band and retransmits the signal to the ground station where range measurements are made on the range tones and range rate measurements on the received carrier.

GEOS-C data is transmitted through the GEOS-C transponder at 1.562 kbps or 15.62 kbps. The prime data mode is 1.562 kbps and 15.62 kbps will only be used if shown to be feasible through tests. The data is relayed to the ground station where it is recorded for later analysis. Data can be transmitted in a noncoherent mode with the GEOS-C free running oscillator or in a coherent mode where the oscillator is locked to the forward carrier. In the coherent mode range-rate measurements can be made on the return carrier with data present. Ranging tones cannot be transmitted with data by the GEOS-C transponder so that combined data and ranging operations are not possible.

A summary of GEOS T&DRE tests is given in Table 19-6 with a gross indication of results.

19.4.2 Test Results

19.4.2.1 Received Signal Strength – The engineering model T&DRE Nimbus antenna was used at GSFC for the initial GEOS-C T&DRE tests. It has a gain about 10 dB higher than the GEOS-C antenna. A variable coupler was used at the antenna to reduce the signal level in both the forward and return links. Tests were run down to the predicted worst case signal level of -115 dBm as measured through the GEOS-C received signal strength telemetry. A later test used the GEOS-C antenna. With this antenna the received signal strength was -109 dBm. versus predicted received signal strength for the tste configuration of -110 dBm.

ATS-6
SPACECRAFT

ATS-6 VHF
CMD & TM LINKS

RELAY
C-BAND
LINKS

RELAY
S-BAND
LINKS

ATS-6
COMMANDS

ATSOCC

ATS-6 TM

ATS
GROUND
STATION
ROSMAN II

GSFC

GEOS-C TRANSPONDER

- RETURNS RANGING
  SIGNALS ON RF
  CARRIER
- TRANSMITS TELEMETRY
  DATA AT 1.562 UBPS
  OR 15.62 UBPS.
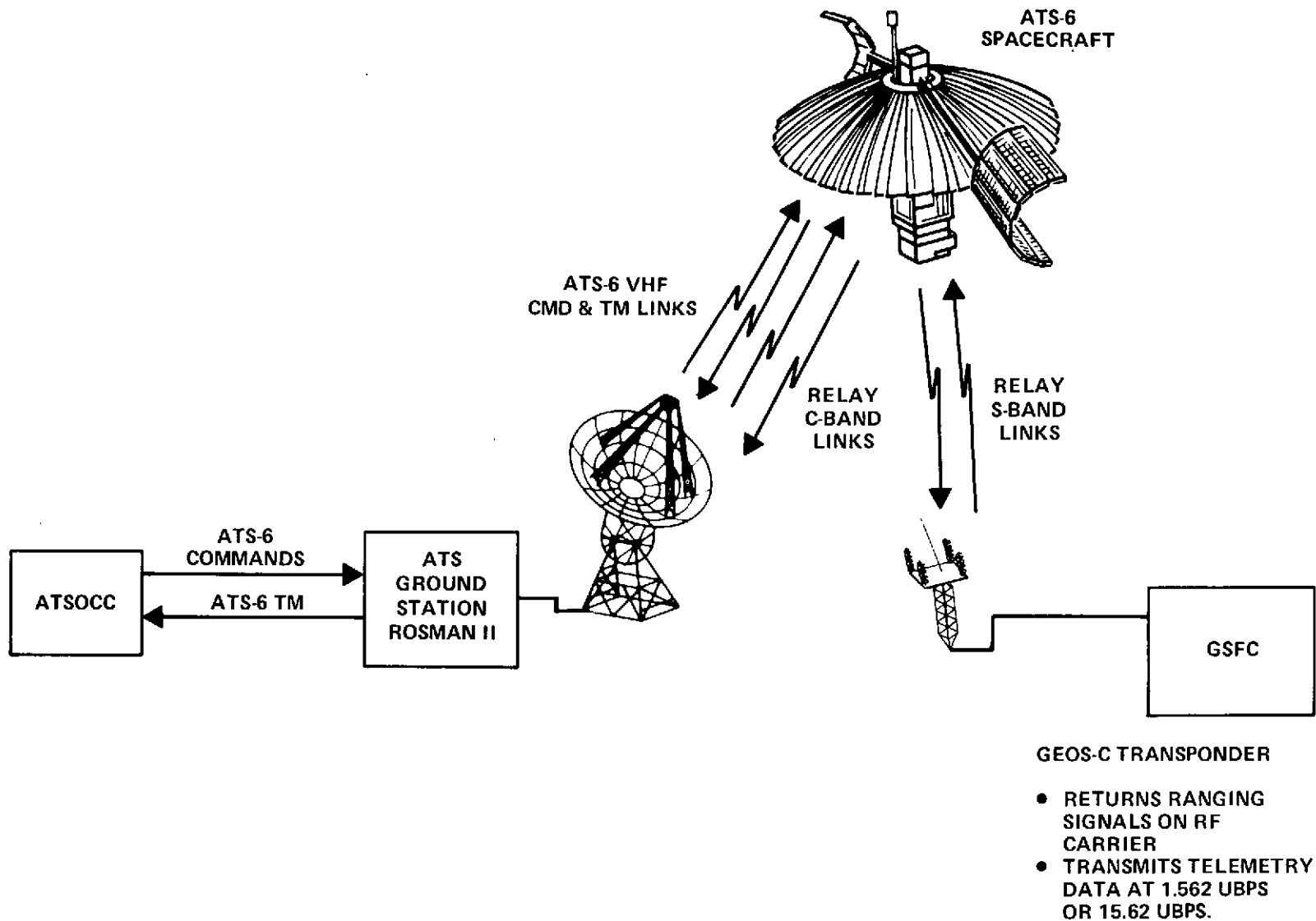
Figure 19-7. GEOS-C T&DRE Test Configuration

Table 19-6
GEOS T&DRE Test Summary

Date			Aug. 13	Aug. 14	Sept. 2	Sept. 20
R&RR	Coherent	Rosman	1	1	1	1
		Hybrid				
	Relay	Rosman/NTTF	*	1	1	1
		/Rosman			1	1
		Hybrid/NTTF				
		/Rosman				
Data	1.562 kbps	NTTF/Rosman		?	?	1
		Rosman/Rosman				*
		NTTF/Hybrid				
		Rosman/Hybrid				
	15.62 kbps	NTTF/Rosman		?	0	
		Rosman/Rosman				
		NTTF/Hybrid				
		Rosman/Hybrid				
Monopulse						1

Legend: 1 Satisfactory Results
* * Degraded Performance or Error Points*
0 Unable to Perform Function
? Data not Analyzed.

The S-band received signal strength at the ATS-6 spacecraft was measured indirectly by measurement of signal-to-noise with a spectrum analyzer at the ATS ground station C-band downconverter output. The carrier-to-noise ratio was measured as 12 dB in a 1-kHz bandwidth versus a predicted value of 15 dB. The error is within the accuracy of the spectrum analyzer carrier-to-noise measurement

19.4.2.2 Tracking Data — The tests results show that the system meets the design capability. Range noise generally less than 2 meters has been achieved. Range-rate noise has been generally less than 0.6 mm/sec and for the 10 second integration period and generally less than 2 meters for 1-second integration.

GEOS-C relay ranging measurements were made between Rosman and GSFC, and Rosman and the S&L Band Building at Rosman subsequent to a 24-hour routine ATS ranging operation. The results are shown with the Nimbus-F results in Table 19-4. Coherent measurements directly to the ATS-6 spacecraft are shown in Table 19-5.

In general few problems have been experienced in making ranging measurements with the GEOS-C equipment. On occasion the ATS ground station has had difficulty locking to range tones when the received signal level at the GEOS-C transponder is at the predicted worst case level of -115 dBm. This indicates that the system is near threshold at this signal level.

19.4.2.3 Data Relay — Data tests have been performed by transmitting recorded GEOS-C data through the return links. Bit synchronization has been achieved on recorded 1.562 kbps data at the ATS ground station; however, the ground receiver degrades the data. Tests have not been successful at 15.62 kbps. Further evaluation has not been possible at the ATS ground station since the PCM DHE is not programmed to handle the GEOS-C data.

19.4.2.4 Monopulse — One monopulse test has been successfully performed with the GEOS-C T&DRE equipment at GSFC using the GEOS-C antenna. The ATS-6 spacecraft was pointed towards GSFC in the offset pointing mode using the earth sensors. Monopulse tracking was initiated to hold the spacecraft on GSFC using the GEOS-C S-band signal. The spacecraft maintained the pointing angle with carrier only and with data modulation on the carrier. The received signal level at the GEOS-C transponder was -109 dBm. Tests at the GEOS RF threshold (-115 dbm into the GEOS transponder) showed that the ATS-6 spacecraft could not monopulse track at this signal level.

SECTION 20

HEALTH EDUCATIONAL TELEVISION EXPERIMENT
(HET)

SECTION 20

HEALTH EDUCATIONAL TELEVISION EXPERIMENT (HET)
AND
RADIO ASTRONOMERS REPORT

20.1 INTRODUCTION

The HET flight evaluation tests were started June 11, 1974. All equipment functioned well with audio and video signal quality very good.

HET antenna polarization at ground stations was found to be reversed for reception. Corrections were made using field modification kits.

During HET operation, while using the spacecraft video transmit frequency channel B (2667.5 MHz), radio astronomy observers using the 140-foot telescope of the National Radio Astronomy Observatory in Green Bank, West Virginia, observed signal spillover into their band (2690 MHz to 2700 MHz) measuring 13 dB above the CCIR level of -247 dB w/m² Hz.

20.2 SCIENTIFIC OBJECTIVES

The HET objective is to evaluate the performance of satellite relay at S-band of educational programming and health care delivery to learning centers, hospitals, clinics, and community television distribution systems.

20.3 EXPERIMENT DESCRIPTION

The HET experiment hardware, which is part of the communications subsystem, provides its own redundant local oscillators and upconverters for generating two RF carriers at 2569.2 and 2670 MHz. Each transmitter may be operated independently of the other and either may be switched to the S-1 or the S-2 HET feed of the PFF or both may be fed simultaneously to either feed through the cross-switching matrix and duplexer arrangement. However, one transmitter cannot feed two elements at the same time.

20.4 EXPERIMENT PERFORMANCE EVALUATION

The HET transmitters were turned on June 11, 1974. Beginning June 13, the HET Flight Evaluation Plan (Table 20-1) was used to checkout the HET system. In addition to the evaluation plan, tests have been conducted during the period covered by this report, to (1) determine beam offsets, (2) verify beam pointing, (3) test performance of ground terminals, (4) maximize total system performance (improve audio performance and eliminate TV hum bars) and (5) evaluate video

Table 20-1
HET Flight Evaluation Plan

Seq #	Operation	ACS Mode	COMM Mode
HET 1	Transmit C-band uplink with HET video/voice signals from Rosman. Receive C-band downlink video monitor signal	Offset point to Rosman	C-band up/downlink via ECH
HET 2	Transmit C-band uplink with HET video/voice signals from Rosman. Receive C-band and S-band HET1 (2569.2 MHz) via S1 feed	Offset point to center S1 feed on Rosman	C-band up/downlink via ECH S-band HET1 downlink via S1 feed
HET 3	Transmit C-band uplink with HET video/voice signals from Rosman. Receive C-band and S-band HET2 (2670.0 MHz) via S1 feed	Offset point to center S1 feed on Rosman	C-band up/downlink via ECH S-band HET2 downlink via S1 feed
HET 4	Transmit C-band uplink with HET video/voice signals from Rosman. Receive C-band and S-band HET1 (2569.2 MHz) and HET2 (2670.0 MHz) both via S1 feed	Offset point to center S1 feed on Rosman	C-band up/downlink via ECH S-band HET1 and HET2 downlink via S1 feed
HET 5	Transmit S-band (2250 MHZ) uplink with HET video/voice signals from Rosman. Receive C-band and S-band HET1. (2569.2 MHz) via S1 feed	Offset point to center S1 feed on Rosman	C-band downlink via ECH S-band HET 1 up/downlink via S1 feed
HET 6	Transmit C-band uplink with HET video/voice signals from Rosman. Receive C-band and S-band HET1 (2569.2 MHz) and HET2 (2670.0 MHz) both via S2 feed	Offset point to center S2 feed on Rosman	C-band up/downlink via ECH S-band HET1 and HET2 downlink via S2 feed
HET 7	Transmit C-band uplink with HET video/voice signals from Rosman. Receive C-band downlink video monitor signal	Offset point to Rosman	C-band uplink via ECH. Downlink via PFP with RF and IF attenuators

crosstalk. At the present time the quantitative data has not been reduced, but everything appears to be functioning in accordance with the ground test results.

During July, the Appalachian Education Satellite Project (AESP) has been conducting graduate level, college credit seminars; the Veterans Administration has been conducting their experiment; and the Federation of the Rocky Mountain States has been conducting the Materials Distribution System (MDS). The Federation and Alaska are continuing testing and checkout of the earth stations.

The quality of the video and audio signals received at Goddard and reported from the field is generally superlative. All of the technical facilities tested and determined operational during this period are as predicted by prelaunch tests and calculations. The response to the total system and the courseware has been good. Many operational bugs have been worked out of the current operating system.

20.4.1 Polarization Problem on HET Terminals

On June 13, the HET Flight Evaluation Plan was used to check out the HET system. Participating ground stations were Rosman and Goddard. Time was short due to the number of misalignment data blocks that had to be sent. The ASP tapes could not be used, primarily due to the C-band "glitches." Sequences #1, 2, 3, 5, and 8 were completed. Sequence #8 used a VA pointing (so GSFC could participate) and an ARC spacecraft configuration so the radio astronomy community could make signal level measurements. During all the tests but #8, good data were taken. Neither Rosman or GSFC, who had nominal signals in the other tests, received adequate signals.

Additional time was provided to complete the flight evaluation plan and to determine the reason why test 8 failed. On June 18, tests #4, #6, #8, and #7 were conducted and the data looked good. On June 20, spacecraft pointing and beam offsets were determined as well as data taken to determine EIRP. The spacecraft was moved to a RME pointing and no valid data were collected. Examining the common elements of the tests that failed, it appeared to depend on one type antenna used. The prime contractor for the HET terminal investigated the polarization of the system and the polarization of the feed. Rosman has a linearly polarized system; GSFC has LCP but can change the hybrid connection for RCP; and Denver has a helical feed which is potted and whose sense could not be determined. The response was unsatisfactory, so action was taken to get a prototype antenna (like GSFC) installed in Denver. Attempts were made to reduce the data collected to determine the fault. As new test plans for that night's exercise were being generated, it was determined that cross-polarization existed at 116 stations. Field modification kits were manufactured.

The top priority was the ARC and VA sites; 26 total. The installation contractor was notified and plans were made to have eight sites retrofitted by June 25. On the morning of June 25, the eight sites participated in a successful system checkout.

At present, all 26 sites have been modified as well as sites in Alaska and the Rockies. All sites will be completed prior to their originally scheduled operational dates.

A problem arises in the definition of circular polarization. It is easily seen that there is no reversal of the vectors off the reflector; however, what does occur is a change of reference. A copy of the definition, Report 321, is shown as Figure 20-1. The reference is behind the antenna looking at a receding wave. What is needed for an LCP system is an RCP feed. Fortunately, the error was determined early and with the cooperation of all concerned, the problem was corrected without impact to the experiment.

20.4.2 Radio Astronomer's Report[1]

20.4.2.1 Introduction—The NASA ATS-6 satellite was launched in early June 1974. This satellite is to be used to transmit educational television programs to remote areas. The satellite will be moved to India after one year and will then transmit programs to India for a year. At that time if the satellite is still functioning it will be brought back to transmit to Appalachia. Its main transmission frequency is adjacent to the protected radio astronomy band at 11 cm (2690 to 2700 MHz). A schedule of tests was arranged with several radio observatories to determine the extent and nature of the interference with radio observing at 11 cm. Problems developed with the satellite, particularly with regard to the positioning of the antenna beam, so that the first two of the three nights of tests were not in accordance with the original schedule. As a result when the data were being taken on the first two nights we were not always sure what transmitting mode the satellite was in or where it was pointing. Because of the large intensity of the signal and its very large dynamic range between the peak at 2667.5 MHz and the radio astronomy band, it was difficult to obtain a very accurate calibration of the intensity of the signal and its spectral characteristics. The signal spillover into the radio astronomy band was approximately 13 dB above the CCIR level of -247 dB W/m^2 Hz = 20 Janskys = 2×10^{-25} W/m^2 Hz. The 140-foot telescope

[1] Reformatted but otherwise unedited from "Observations of the ATS-6 Satellite With the 140-Foot Telescope of the National Radio Astronomy Observatory" by David Buhl and Alan Parrish, National Radio Astronomy Observatory, Green Bank, West Virginia and Frank J. Kerr, University of Maryland, College Park, Maryland.

SECTION CIV B: VOCABULARY

RECOMMENDATIONS AND REPORTS

Recommendations

There are no Recommendations in this section.

———————

Reports

REPORT 321*

TERMS AND DEFINITIONS

Right-hand (clockwise) or left-hand (anti-clockwise) elliptically
or circularly polarized (electro-magnetic) waves

(Resolution 21-1)

(1963)

It has become clear that the definitions found in the main existing publications (British Standards Institution, B.S. 204, 1960: Nos. 51 009 and 51 010; – Institution of Radio Engineers 1950; – International Electrotechnical Commission, Draft 1/60 (Secretariat) 281: Nos. 60.20.030 and 60.20.035) on the direction of rotation of the electric field vector in waves elliptically or circularly polarized, might be easily misunderstood, with serious practical consequences, especially at a time when space communications are being developed.

Doc. 108 (U.K.), Geneva, 1963, points out the causes of ambiguity and offers solutions. The following definitions have been drafted to avoid any danger of ambiguity in future.

1.   Right-hand (clockwise) polarized wave

An elliptically or circularly-polarized wave, in which the electric field-intensity vector, observed in any *fixed plane*, normal to the direction of propagation, whilst looking in (i.e. not against) the direction of propagation, rotates *with time* in a *right-hand* or clockwise direction.

Note. – For circularly-polarized plane waves, the ends of the electric vectors drawn from any points along a straight line normal to the plane of the wave front, form, *at any instant*, a *left-hand* helix.

2.   Left-hand (anti-clockwise) polarized wave

An elliptically or circularly-polarized wave, in which the electric field-intensity vector, observed in any *fixed plane*, normal to the direction of propagation, whilst looking in (i.e. not against) the direction of propagation, rotates *with time* in a *left-hand* or anti-clockwise direction.

Note. – For circularly-polarized plane waves, the ends of the electric vectors drawn from any points along a straight line normal to the plane of the wave front, form, *at any instant*, a *right-hand* helix.

————————

*This Report was adopted unanimously.

Figure 20-1. Report Number 321 Terms and Definitions.

of the National Radio Astronomy Observatory in Green Bank, West Virginia was used for the observations reported here.

On June 18, 20 and 21, 1974, from 0^h to 6^h UT, we made measurements of the ATS-6 satellite which transmits a 30 MHz wide signal with a main carrier frequency of 2667.5 MHz. Our main object was to determine the level of interference in the protected Radio Astronomy Band from 2690 MHz to 2700 MHz. We also wished to determine the spectrum and strength of the signal transmitted by the satellite. We used an 11-cm parametric amplifier receiver which had a system temperature of 300 K and a 384 channel autocorrelator operated in the parallel mode. This gave us two 10 MHz wide spectral receivers which were arranged to cover 2680 to 2690 MHz and 2690 to 2700 MHz. Total power observing was done to obtain a clear spectrum of the satellite. Calibration was done with a noise tube which gave a 71.4 K cal. When the telescope was pointed directly at the satellite there were problems with overloading in the receiver. The strong signal caused the system temperature derived from the calibration signal to be increased substantially. This has been noted on the spectra where the system temperature diverged from 300 K. To calibrate the intensity of the signal transmitted by the satellite, we measured the antenna temperature adjacent to the radio astronomy band and then used the spectrum to determine the signal intensity at the peak. A Hewlett-Packard spectrum analyzer was used to display the spectrum and calibrate the signal intensity since it has a wider bandwidth and greater dynamic range than the autocorrelator. The pictures in this report were photographed from the display screen of the spectrum analyzer.

20.4.2.2 Observations On and Near the Satellite—In Figure 20-2 we show the spectrum of the satellite signal for various orientations of the satellite and telescope. Picture 5 was taken with the telescope pointed 9° N of the satellite where the signal has been suppressed by a null in the 140-foot antenna pattern. This position was used to obtain the reference spectra which were subtracted from the spectra taken at other positions. It was found that the initial reference which was taken before the satellite transmission began was not good for the length of the observing period so that reference spectra were taken frequently. When the telescope was pointing at the satellite there is clearly some depression of the baseline, particularly when it was pointing at Appalachia (Picture 1).

Figure 20-3 shows spectra taken with the modulation off and on. With the carrier only the system temperature is not disturbed and the main effect is a tilt in the passband from 2690 to 2700 MHz and a gradually rising pedestral toward 2680 MHz, which is probably modulation noise on the satellite carrier. When the modulation is switched on the spectrum becomes very spiky and the system temperature increases drastically. The spectrum from 2680 to 2683 MHz always exhibits the same pattern indicating modulation sidebands from the satellite.
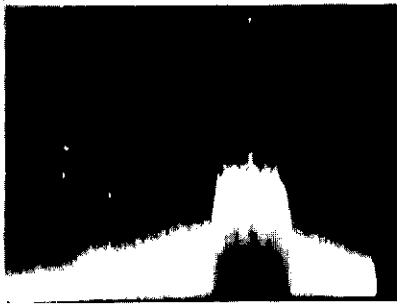
Pict. 0 Modulation off, Telescope on Satellite

Pict. 1 Satellite pointing at Appalachia, Telescope on Satellite

Pict. 2 Satellite pointing at Appalachia, Telescope 10' N of Satellite

Pict. 3 Satellite pointing at Rocky Mountains, Telescope on Satellite

Pict. 4 Satellite pointing at Rocky Mountains, Telescope 10' N of Satellite
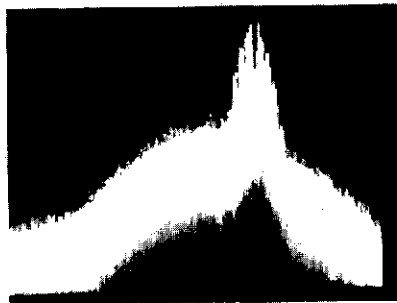

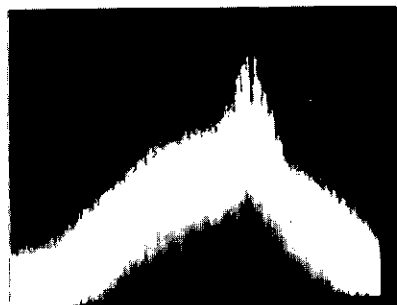Pict. 5 Satellite pointing at Rocky Mountains, Telescope 9° N of Satellite (Null Position)

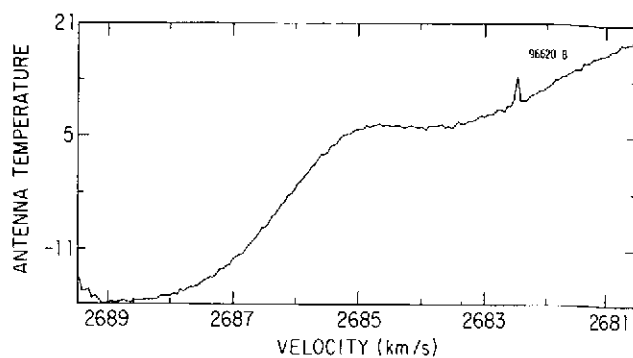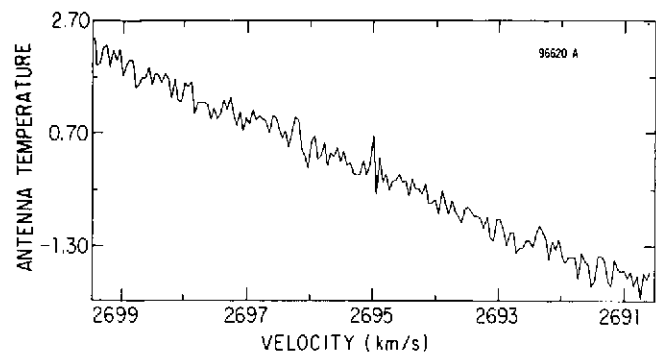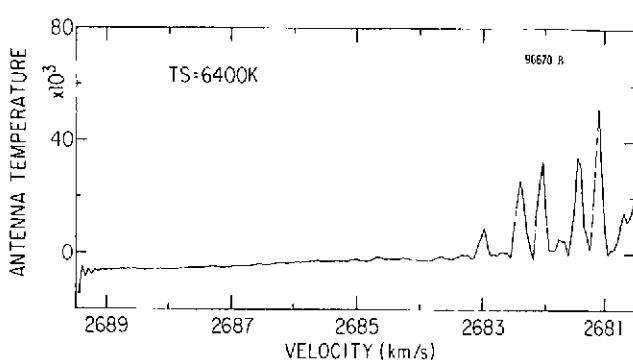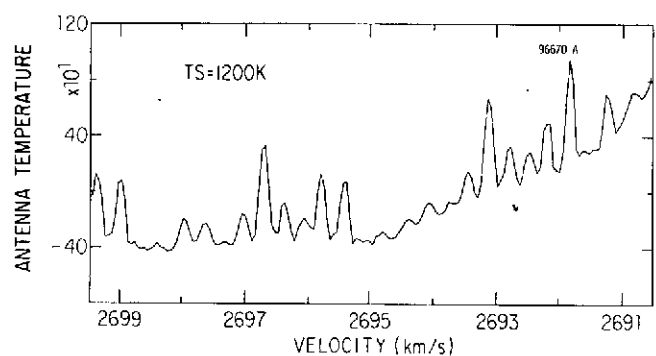Pict. 6 Satellite pointing at Chile, Telescope on Satellite

Center of Picture is 2695 MHz (150 MHz)
Vertical Scale 10 db/cm
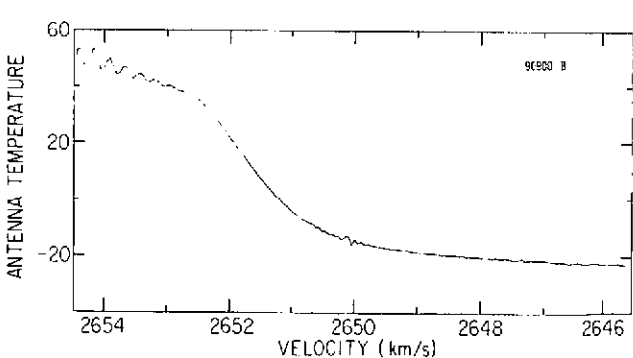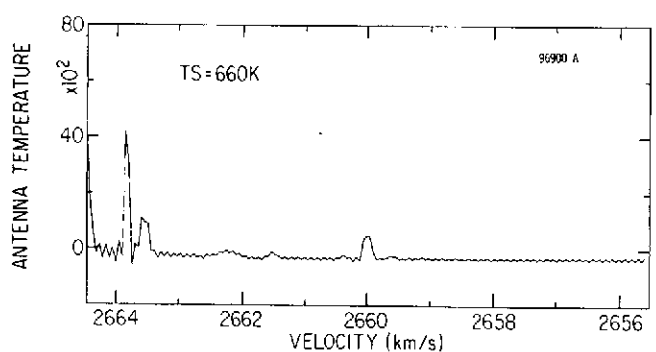Horizontal Scale 20 MHz/cm   1 cm
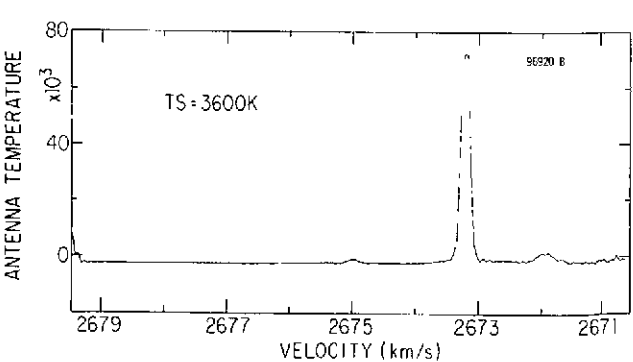Pict. 0 Atten. Extra 10 db

Figure 20-2
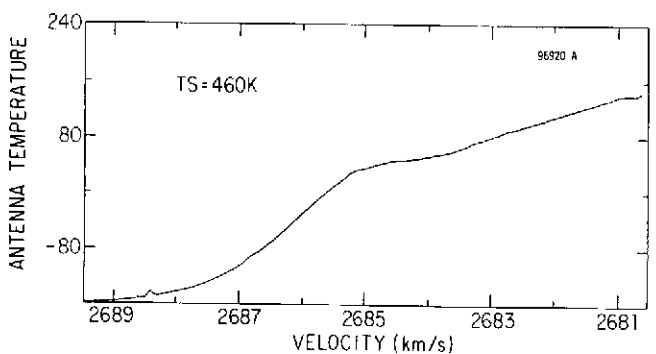
Figure 20-3.   Spectra With and Without Modulation, June 20, 1974

The spiky signals in the 2690 to 2700 MHz band are a combination of saturation in the receiver and modulation signals from the satellite spilling over into the Radio Astronomy Band. When the telescope is moved 10' N of the satellite (Figure 20-2), the paramp bandpass straightens out considerably (compare pictures 1 and 2). The corresponding spectrum (Figure 20-4) shows a decrease of ~2 with the telescope moved 5' N of the satellite. With the telescope 10' N the spectra are reduced ~10 in the strength in the 2680 to 2690 MHz band, while the signals in the 2690 to 2700 MHz band are not detectable (limit ~50 below the level with the telescope pointing at the satellite). The sharp line in the center of the 2690 to 2700 MHz passband is probably due to local oscillator signals from the interferometer and 300-foot telescopes which were also operating at 11 cm.

Positioning of the satellite toward the Rocky Mountains or Chile (Figure 20-5) reduced the signals in the 2680 to 2683 MHz range as well as reducing the slope across the band. The 2690 to 2700 band seems to have a slope when the satellite was pointed toward the Rocky Mountains similar to the slope observed when the satellite was pointed toward Appalachia and the telescope was pointed 10' N of the satellite (Figure 20-4). Movement of the telescope to positions further away from the satellite (Figure 20-6) showed no observable signals in either the 2680 to 2690 MHz band or the 2690 to 2700 MHz band. Integration time was 5^m, which was sufficiently long to investigate interference over the CCIR limit. We also attempted an observation of the H134α–recombination line in M17 while the satellite was transmitting. The line is ~2.5 K, which is 10 Janskys (10^{-25} W/m^2 Hz or –250 dB W/m^2 Hz) assuming 1 K = 4 Jy for the 140-foot telescope. At this point M17 was about 40° away from the satellite, and observations at that position were not noticeably interfered with in a 5^m integration. Time did not permit a longer integration on a weak source, where a noticeable effect could be expected, by calculating from the measured flux density.

20.4.2.3 Power Spectrum of the Satellite—The power spectral density as a function of frequency of the signal radiated from the ATS–6 satellite was measured on 20-21 June 1974. The results are shown in Figure 20-7. The level is approximately 13 dB stronger than that designated by the CCIR as a harmful interference level at the 2690 MHz edge of the radio astronomy band.

At 2690 MHz, the satellite spectral level is equivalent to that of a continuous source with a flux of the order of 500 Janskys if the satellite antenna is pointed at the "Appalachia" position.

The spectrum shown is a composite of measurements made with a HP 8554 spectrum analyzer for frequencies up to 2685 MHz and those made with the NRAO Model II autocorrelation spectrometer in the range above 2680 MHz. The use of the correlator to measure the low-level signal at the edge of the spectrum was required to obtain an overall dynamic range of 55 dB.
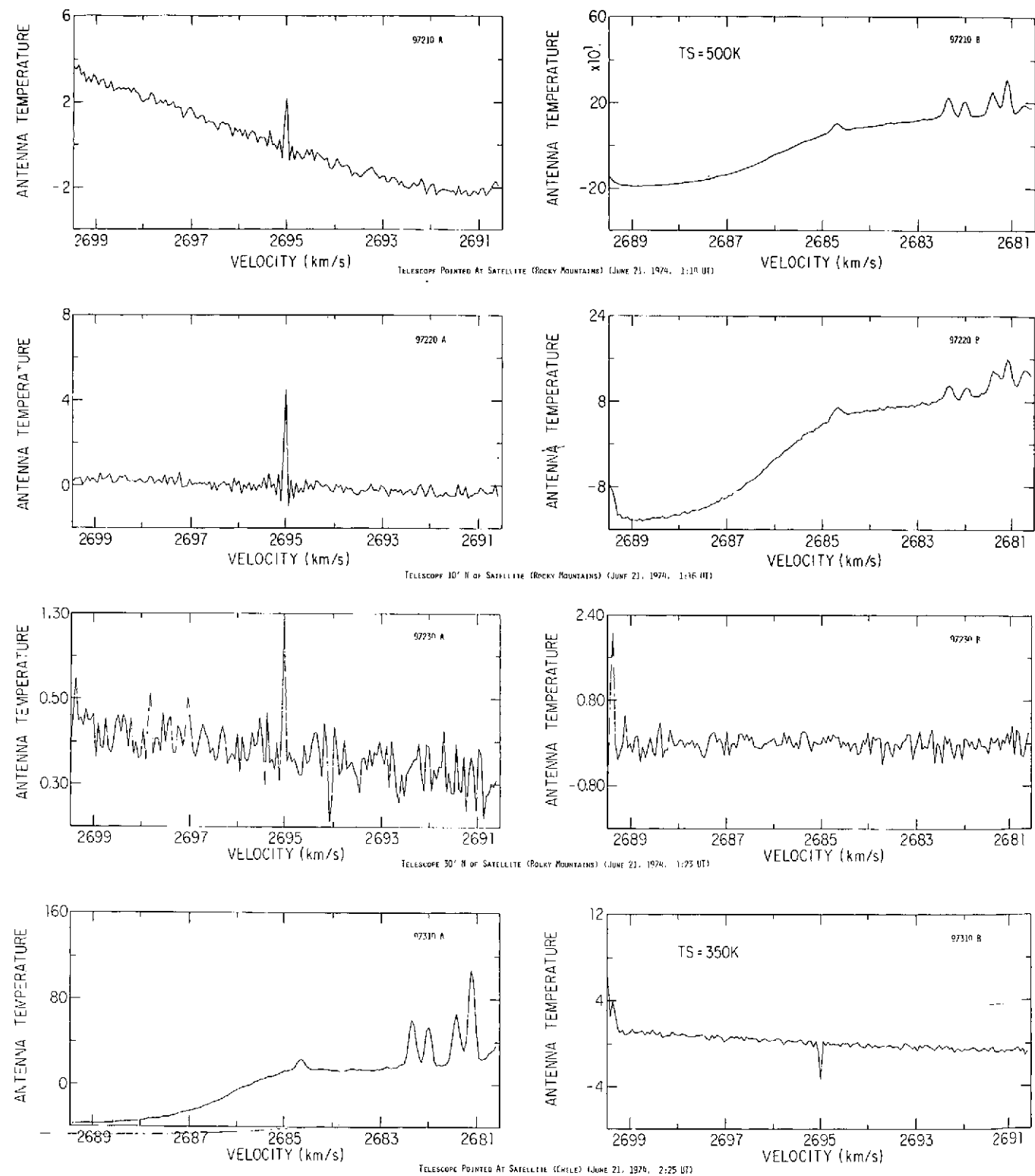
Figure 20-4. Spectra, June 21, 1974

Figure 20-5. Spectra, June 21, 1974
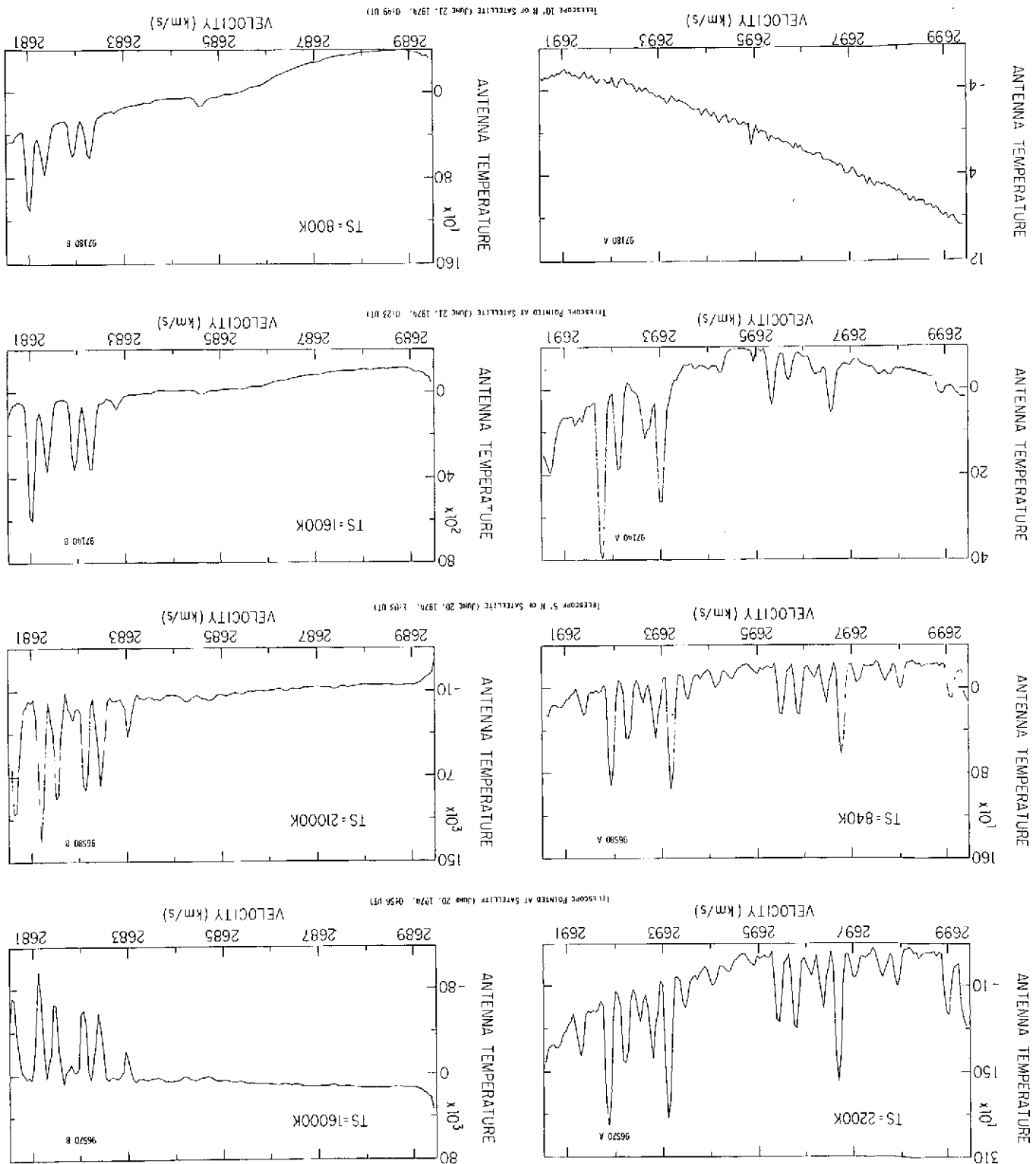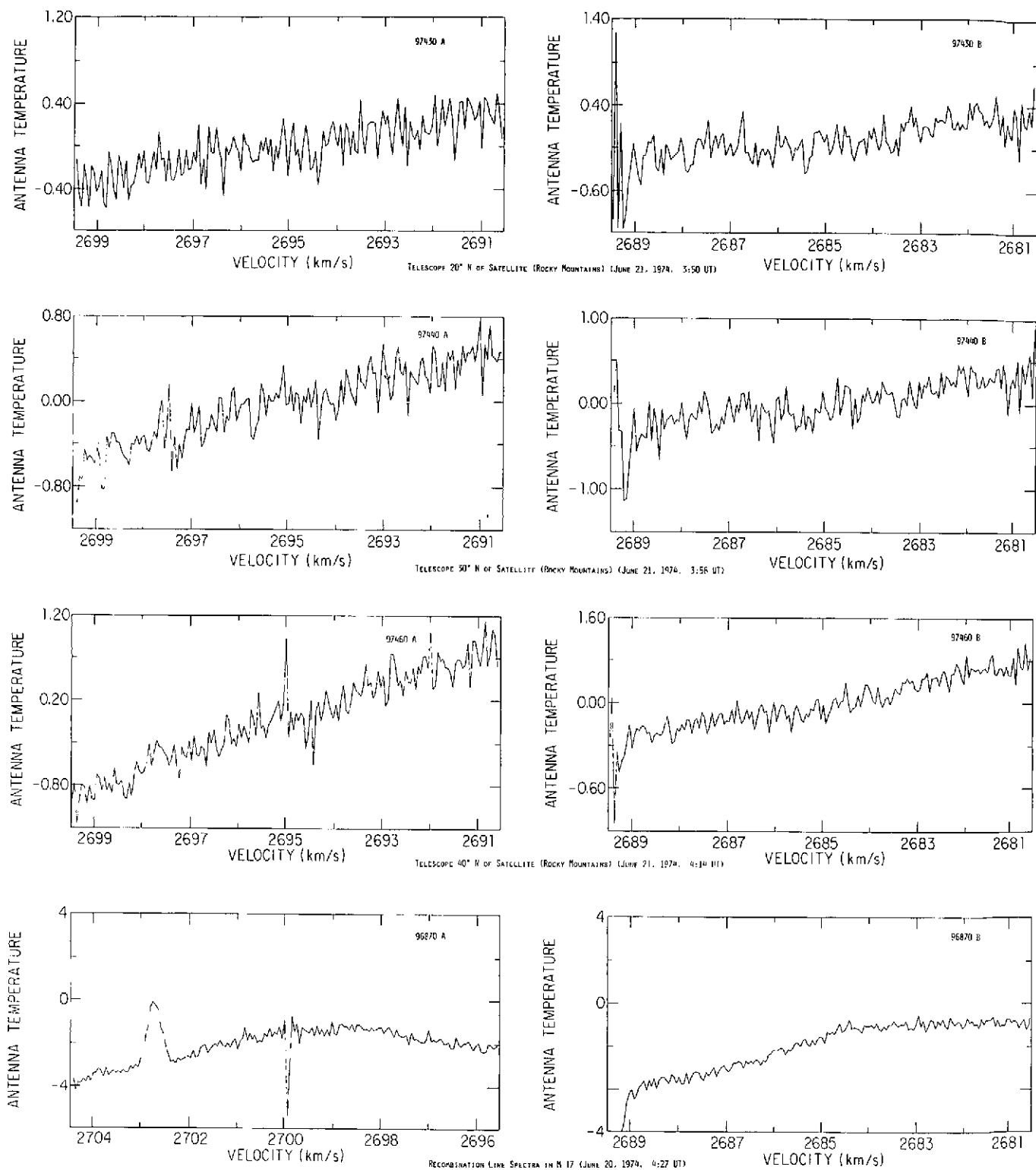
Figure 20-6. Spectra, June 20 and June 21, 1974
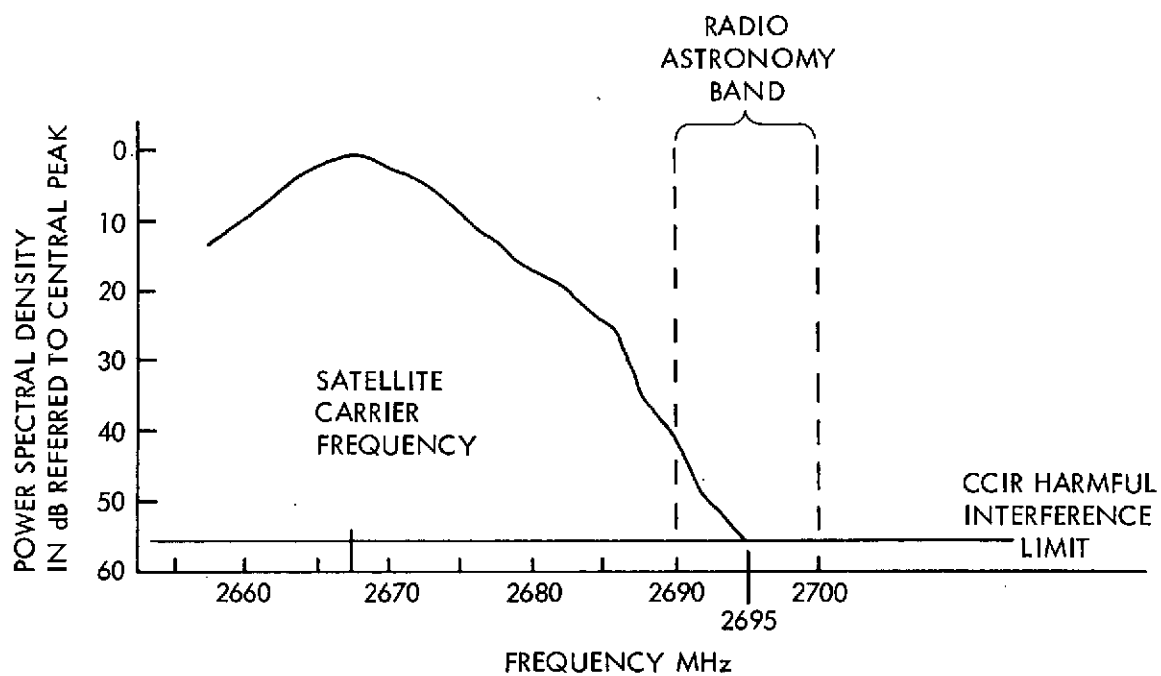
Figure 20-7. Spectrum of ATS-6 Satellite as Determined from Spectrum
Analyser and Autocorrelator Measurements

To avoid overloading amplifier stages in the receiver, the signal level was reduced by switching the paramp pump off or by pointing the telescope away from the satellite. The receiver linearity was tested by varying, by means of a precision variable attenuator, a carrier that was injected into the receiver front end by means of a directional coupler in the antenna circuit. Levels were adjusted to insure that the intensity of this carrier could exceed that of the satellite by at least 10 dB before receiver nonlinearity was observed.

The same carrier injection circuit was used to demonstrate that the measurements with the autocorrelator were unaffected by aliasing of the high spectral level outside the radio astronomy band. The carrier was set at a level exceeding that of the satellite at 2667 MHz by 10 dB. Observations were made with this additional intense carrier set at several frequencies between 2660 and 2680 MHz. No features attributable to the test signal were found in the autocorrelator data for the radio astronomy band.

S. Weinreb has pointed out that, while a receiver may appear linear to simple tests such as that described above, low levels of odd order distortion products may cause spurious signals to be generated in the receiver from intense signals lying outside the band of interest. The direct measurement of the low-level distortion parameters of the receiver used have not been made; however, the apparent intensities of false signals generated by this mechanism will go as some high power of the applied signal. This check was made by varying the applied signal level by changing the antenna beam position relative to that of the satellite, and no features exhibiting the power law characteristic were found in the data. Therefore, the data in Figure 20-7 are accurate to ±3 dB and are not the result of any spurious effect.

20.4.2.4 Discussion—During our observations of the ATS-6 satellite, we measured signals of approximately 100 K (400 Janskys = 234 dB W/m^2 Hz) in the radio astronomy band from 2690 to 2700 MHz. This is about 13 dB stronger than the CCIR limit for signals in this band. The signals were obtained while pointing the telescope directly at and slightly off the satellite. Under these conditions there is some overloading in the receiver which will have some effect on the resulting spectra. The satellite produces signals in the adjacent 2680 to 2690 MHz band which are approximately 10^5 K (4×10^5 Janskys = -204 dB W/m^2 Hz). The spectral measurements indicate that the signal is 30 MHz wide and has a peak intensity of 10^{-18} to 10^{-20} W/m^2 Hz centered at 2667.5 MHz.

20.4.3 GSFC Comment on Radio Astronomer's Report—The preceding material (Section 20.4.2) has been reformatted to be compatible with the body of this report. It is otherwise unchanged from "Observations of the ATS-6 Satellite With The 140-Foot Telescope of the National Radio Astronomy Observatory"

by David Buhl and Alan Parrish of the National Radio Astronomy Observatory, Green Bank, West Virginia and Frank J. Kerr of The University of Maryland, College Park, Maryland.

Since this paper implies interference with the Radio Astronomy Band from ATS-6 in excess of prescribed limits, it is appropriate to list GSFC comments on the Radio Astronomer's Report.

First: The CCIR limit cited in four places in Section 20.4.2 refers to CCIR Paper 224-2, "Radio Astronomy Characteristics and Factors Affecting Frequency Sharing With Other Services," Volume IX, Part 2, Proceedings of the XII Plenary Assembly of the International Radio Consultation Committee, New Delhi, 1970. The levels of rf interference cited in the CCIR report are neither CCIR recommendations nor ITU regulations.

Second: The test procedure is open to question. During the test periods, energy dispersal was not used. Normally, energy dispersal of 800 KHz peak-to-peak deviation would be used. This would reduce all spectral components by 23 dB or to a level of -257 dB W/m^2/Hz.

This subject, and especially the test procedure and receiving equipment used, is currently being studied by cognizant GSFC personnel.

20.5 HET APPLICATIONS

During this reporting period, the HET experiment has been extensively employed for classroom training of both pupils and teachers, and medical lectures and consultations. Geographic areas covered have been the Western United States, the Appalachian states and Alaska. The photographs described in the following sections illustrate the equipment in use at various sites and scenes of actual classroom sessions.

20.5.1 Western United States—Figure 20-8 is a typical intensive terminal site with 10-ft parabolic antenna for S-band reception and a helical VHF antenna used for audio talk-balk through ATS-1 or ATS-3. Figure 20-9 is a scene showing a teacher training career development course in Winnemucca, Arizona. Figures 20-10 and 20-11 are examples of classroom use of HET in Colorado and Arizona.

20.5.2 Appalachian States—Figure 20-12 is a photograph of a televised discussion being held in a studio at the University of Kentucky at Lexington. Such programs are recorded and transmitted live through ATS-6 to rural areas in the Appalachian region of the United States.
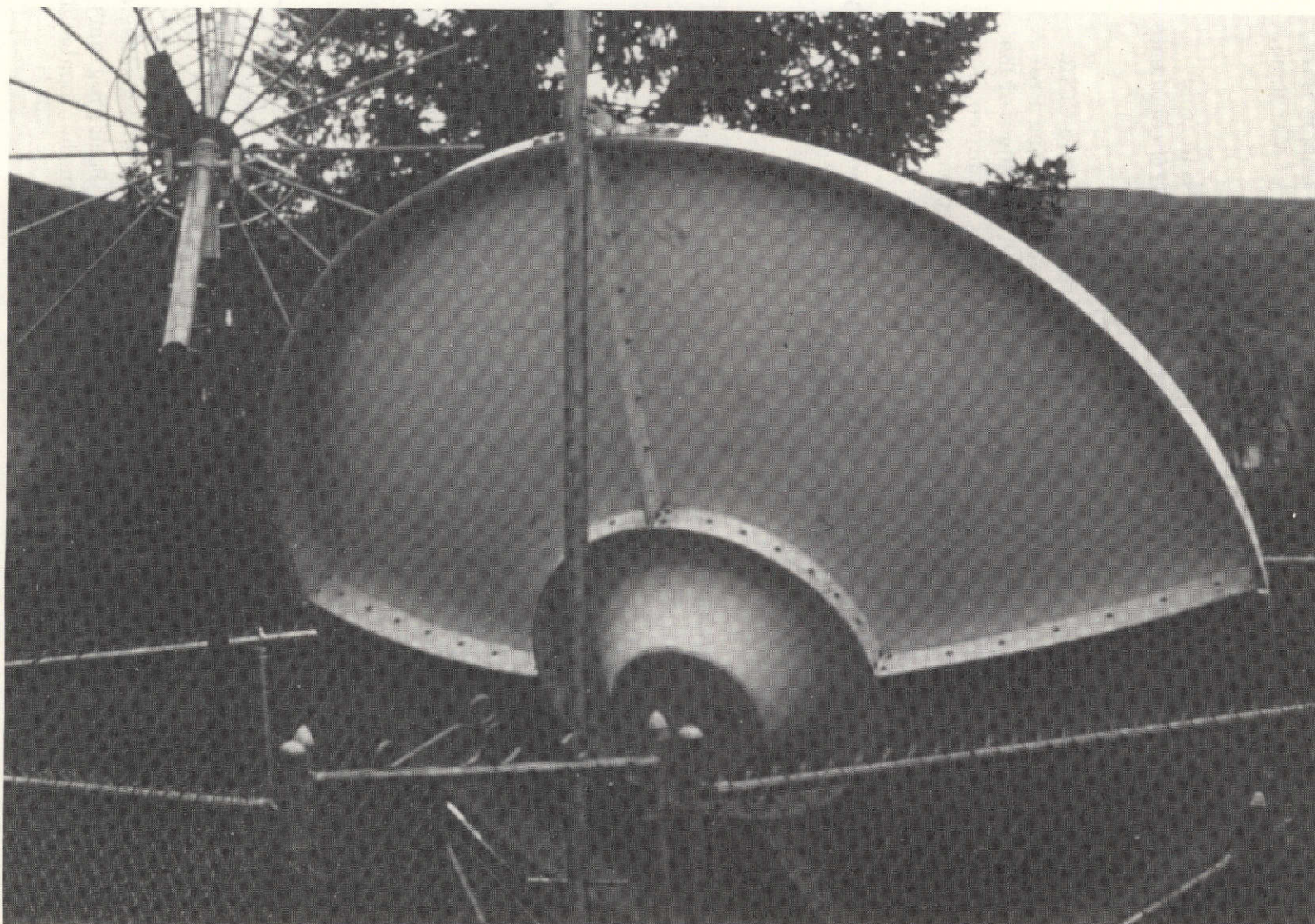
Figure 20-8. Typical Intensive Terminal Site

Figure 20-9. Teacher Training at Winnemucca, Arizona

Figure 20-10. Primary Classroom in Craig, Colorado
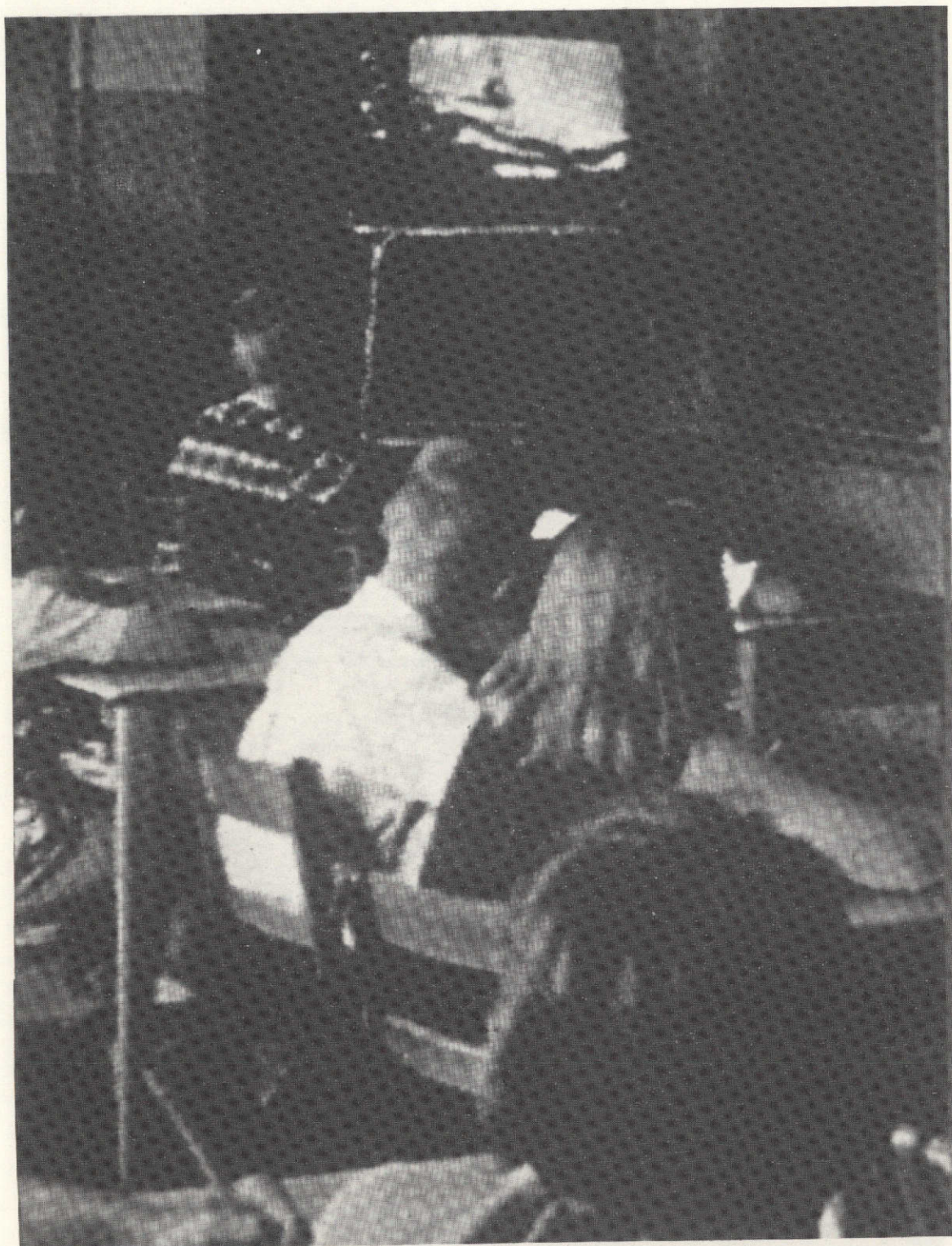
Figure 20-11. Classroom Science Lecture in Gila Bend, Arizona

Figure 20-12. Television Studio at the University of Kentucky at Lexington

An in-service teacher training lecture at the Cumberland Vocational Technical Center, Cumberland, Maryland, is shown in Figure 20-13. As part of a 3-credit graduate-level course offered by the University of Kentucky in conjunction with the Appalachian Regional Commission, educational television is broadcast from Lexington to the classroom.

20.5.3 Alaska—Video transmissions from remote medical clinics in Alaska are relayed through ATS-6 to Anchorage General Hospital to facilitate diagnoses. The S-band antenna in Figure 20-14 is on the roof of the Anchorage General Hospital. Figure 20-15 shows two S-band antennas at the Fort Yukon, Alaska Medical Clinic. The very low elevation angle from Alaska to ATS-6 is evident in this photograph. A remote Indian health service clinic at Galena, Alaska is shown in Figure 20-16. This clinic has S-band two-way simplex video through ATS-6 and VHF audio and medical data through ATS-1. Figure 20-17 is a photograph of the examination room at Fort Yukon, Alaska. Equipment shown provides audio and video capabilities for the facility.

Figure 20-13. In service Teacher Training Lecture at Cumberland, Maryland

Figure 20-14. S-band Antenna at Anchorage General Hospital
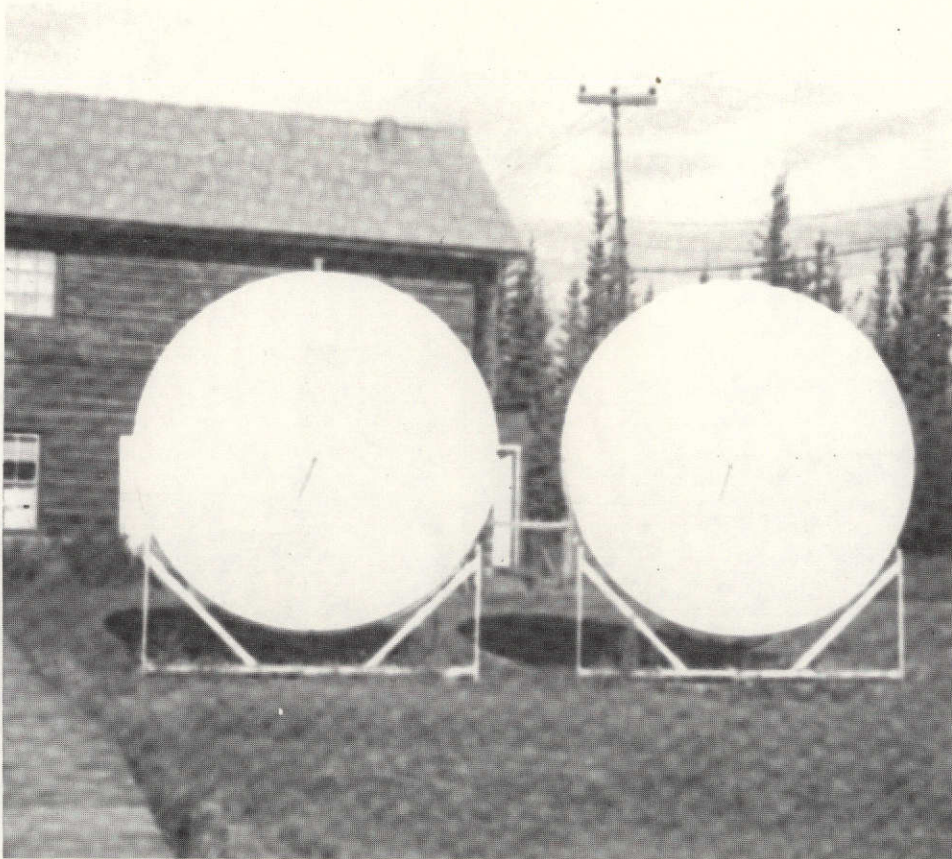
Figure 20-15. S-band Antenna at Fort Yukon, Alaska
medical clinic

Figure 20-16. Indian Health Service Clinic at Galena, Alaska
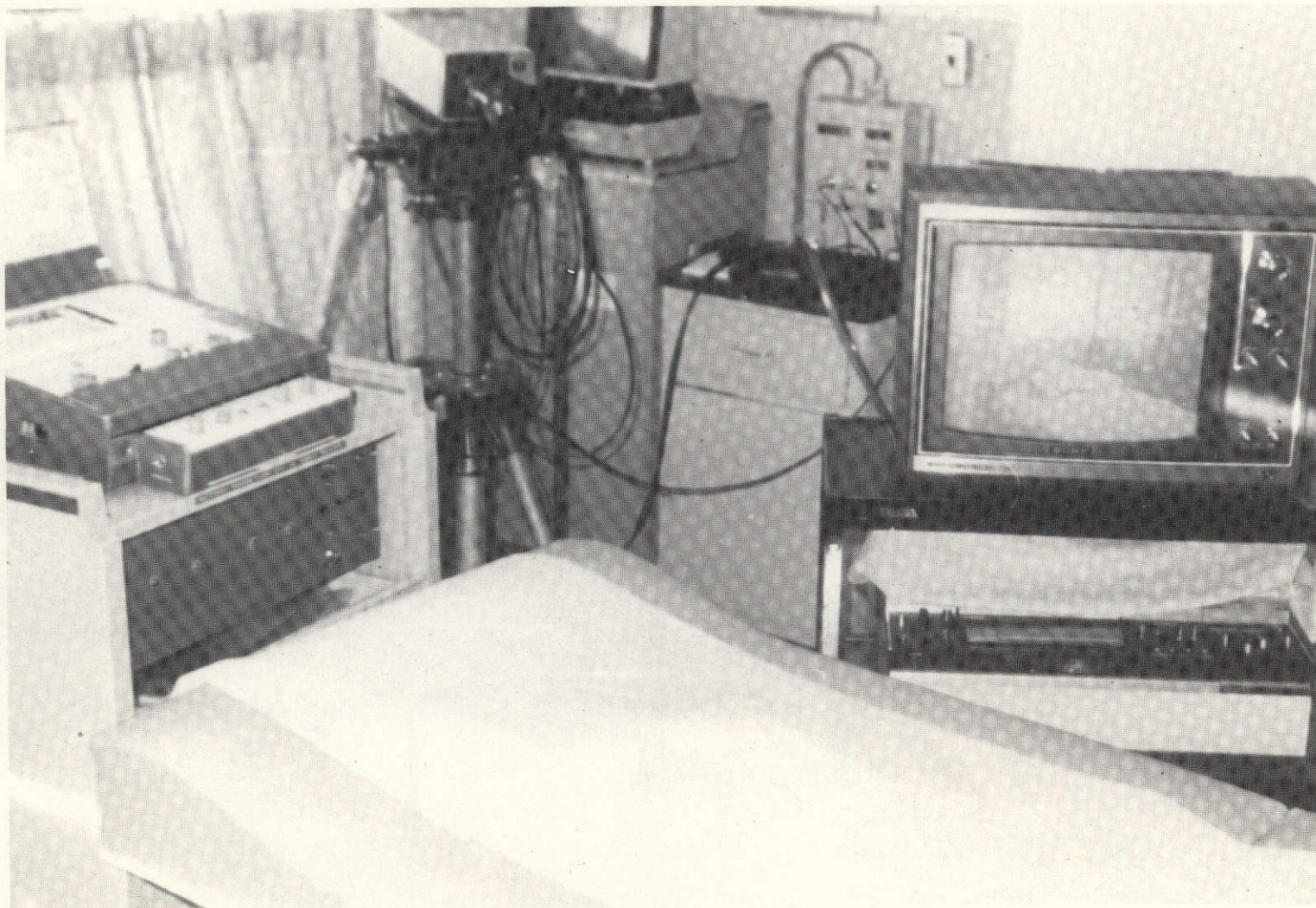
Figure 20-17. Examination Room at Fort Yukon, Alaska

SECTION 21

C-BAND RADIO FREQUENCY INTERFERENCE (RFIME) MEASUREMENT

EXPERIMENT

SECTION 21

C-BAND RADIO FREQUENCY INTERFERENCE MEASUREMENT EXPERIMENT

(RFIME)

21.1 INTRODUCTION

RFIME spacecraft activity has been reported for 22 days during this reporting
period. Eight of 13 measurement modes have been exercised, of which four
modes have been used repeatedly to acquire C-band RFI data from 30 geographic
areas in the continental United States, Alaska, and Hawaii.

Computer software failures, and lack of measured in-orbit antenna patterns
for the ATS-6 PFF at C-band, have thus far precluded establishing precise
geographic location of RFI sources.

21.2 SCIENTIFIC OBJECTIVES

The principle objective of the Radio Frequency Interference Measurement Experi-
ment (RFIME) is to demonstrate the feasibility of using a high gain, accurately
pointed spacecraft antenna, and a wideband, computerized spectrum analyzer
receiver system to precisely measure and define the electromagnetic environment
of the synchronous orbit. To accomplish this objective, the RFIME equipment
measures and identifies earth based radio frequency transmitter sources radiating
in the 5925- to 6425-MHz band when their radiation levels exceed 10 dBW EIRP.

The information gained from this experiment will provide for more effective use
and regulation of radio transmissions. It will thus aid the development and im-
plementation of advanced spacecraft communications systems. In addition, the
following information will be obtained:

    a. The flux density of 6 GHz interference power at the satellite
    b. Practical gain-to-noise ratio limits for the satellite
    c. Geographical and frequency distribution of terrestrial RF noise sources
    d. Data for establishing mathematical models for predicting RF interference

21.3 EXPERIMENT DESCRIPTION

For this experiment, the ATS-6 9-meter parabloic antenna will be used to collect
microwave RF signals in the 5925- to 6425-MHz frequency bands that reach the
synchronous orbit altitude from Earth. These signals will be transmitted to a
wideband RFI transponder (500 MHz) on board the spacecraft, automatically

converted to a 4-GHz signal, and relayed to the ATS ground station at Rosman, North Carolina.

The experiment measurement system configured as shown in Figure 21-1 uses a computer controlled, special purpose spectrum analyzer receiving system and data processor located at the Rosman ATS ground station.

ATS-6 will scan the entire United States to identify hot spots of RFI. Then a narrowband analytical system will be used to determine the frequency, power level, and the geographic location of each area of interference. By positioning the 9-meter antenna such that its shadow covers the hot spot from three different angles, triangulation techniques can be used to pinpoint locations within an area of 16 km (10 miles radius).

Data outputs include the carrier frequency distribution, rf power density levels, and geographic locations of the Earth transmissions. Short-term (daily) and long-term (monthly) observations will be analyzed relative to establishing spectrum sharing criteria among synchronous satellite telecommunication systems and terrestrial point-to-point microwave relay systems in the 6-GHz common carrier frequency band. Measured data are compared with predictions based on a mathematical model, and significant discrepancies are flagged to provide iterative updating of the model.
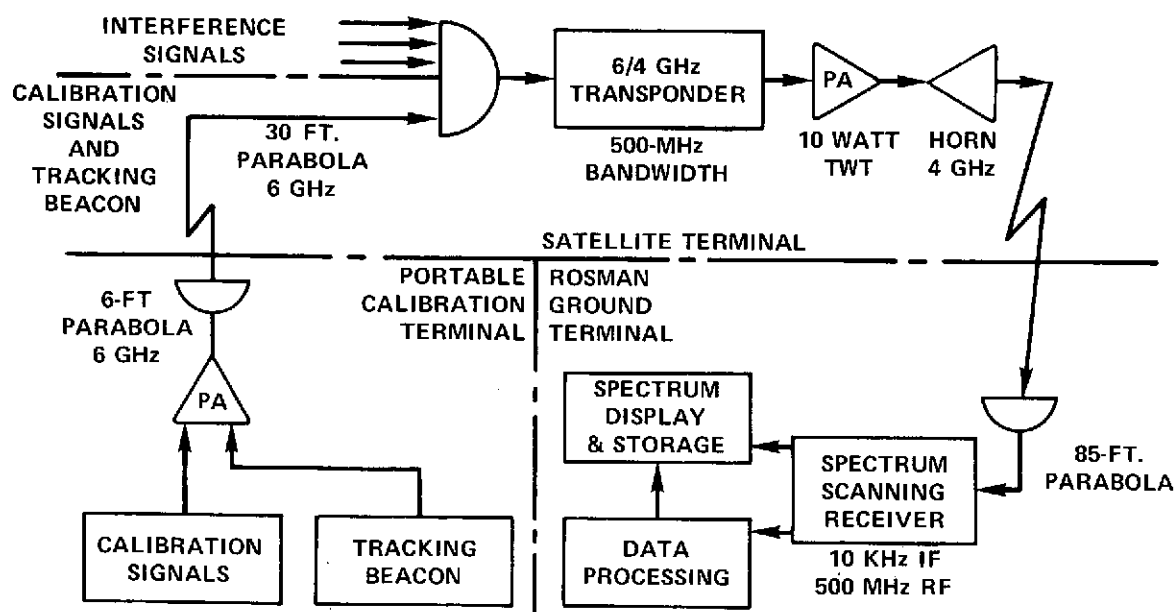
Figure 21-1. C-Band RFI Experiment Configuration

21.4 EXPERIMENT PERFORMANCE EVALUATION

As of September 1, 1974, eight of 13 measurement modes have been executed on the RFIME. Four modes have been used repeatedly to acquire RFI data from 30 geographic areas in the continental United States (CONUS), Alaska, and Hawaii. The names of cities centrally located in the areas surveyed are listed in Table 21-1. Preliminary analysis of this data shows potential RFI sources numbering approximately 100 to 200 in each area with EIRP levels of 10 dBW to 30 dBW. These levels represent the integrated rf power measured in a 10-kHz frequency slot for each source, and the carrier frequencies are randomly distributed across the 500-MHz bandwidth of measurement, i. e., 5925 to 6425 MHz. Histographs in Figures 21-2 through 21-6 illustrate typical distribution of RFI sources as a function of EIRP levels and geographic locations.

Table 21-1

RFIME Survey Areas
(July to August 1974)

Area No.	Location City	Latitude	Longtitude
1	Andover, ME		
2	New York City		
3	Ithica, NY		
4	Detroit, MI		
5	Columbus, OH		
6	Chicago, IL		
7	Kansas City, KA		
8	Pierre, SD		
9	Denver, CO		
10	Pocatello, ID		
11	Spokane, WA		
12	WAMI Pointing		
13	Pacific Ocean	38°N	135°W
14	San Francisco, CA		
15	Mojave		
16	San Diego, CA		
17	Phoenix, AR		
18	Alamogordo, NM		
19	Monterrey, Mexico		
20	Houston, TX		
21	Dallas, TX		
22	New Orleans, LA		

Table 21-1 (Cont'd)

RFIME Survey Areas
(July to August 1974)

Area No.	Location City	Latitude	Longtitude
23	Huntsville, AL		
24	Atlanta, GA		
25	Orlando, FL		
26	Miami, FL		
27	Rosman, NC		
28	Atlantic Ocean (quiet spot N of Bermuda)		
29	Honolulu, Hawaii		
30	Fairbanks, Alaska		

21.5 ANOMALIES AND FUTURE PLANS

Computer software failures, and lack of measured in-orbit antenna patterns for the ATS-6 PFF at C-band, have precluded establishing precise geographic location of RFI sources. Based on a knowledge of the location of the majority of earth transmitters in the RFIME band, the electromagnetic environment at the synchronous environment should be anisotropic. However, comparison of data taken with ATS-6 pointed at New York City and at a point 500 miles west of San Francisco where there are no known sources, indicates there is no significant difference in number of RFI sources and EIRP (see Fig. 21-5). Pending the correction of computer software errors, and implementation of the portable calibration terminal, antenna patterns of the PFF at C-band will be measured and additional RFI data runs will be made.
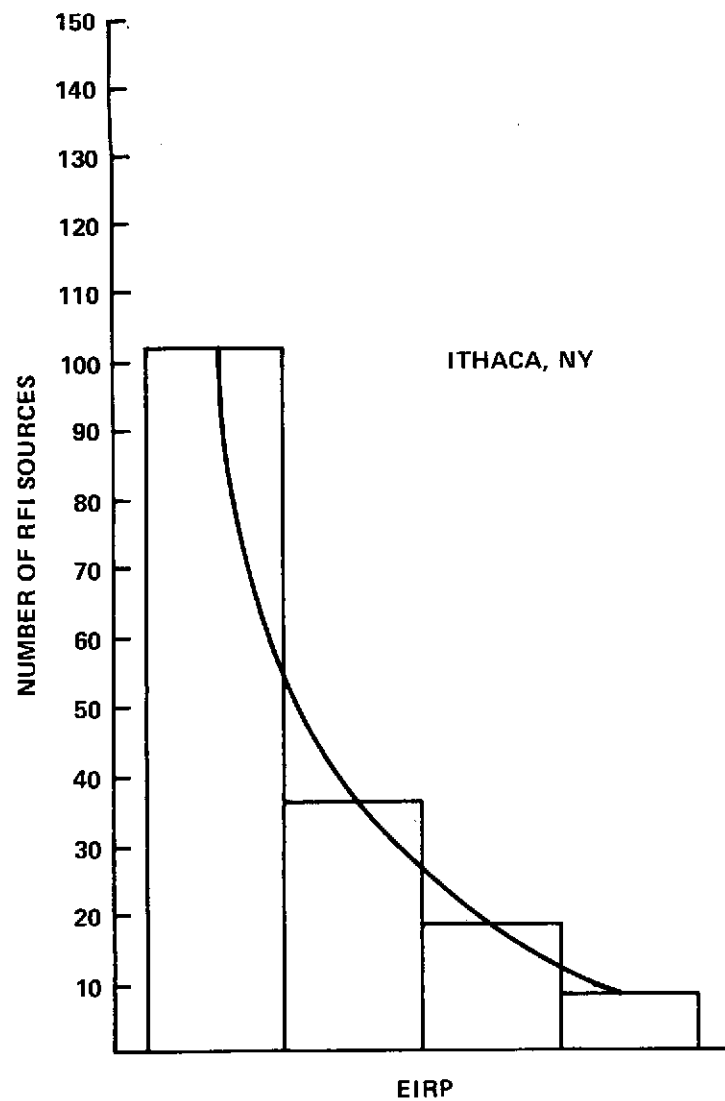
Figure 21-2. C-Band RFI Survey,
July to August 1974
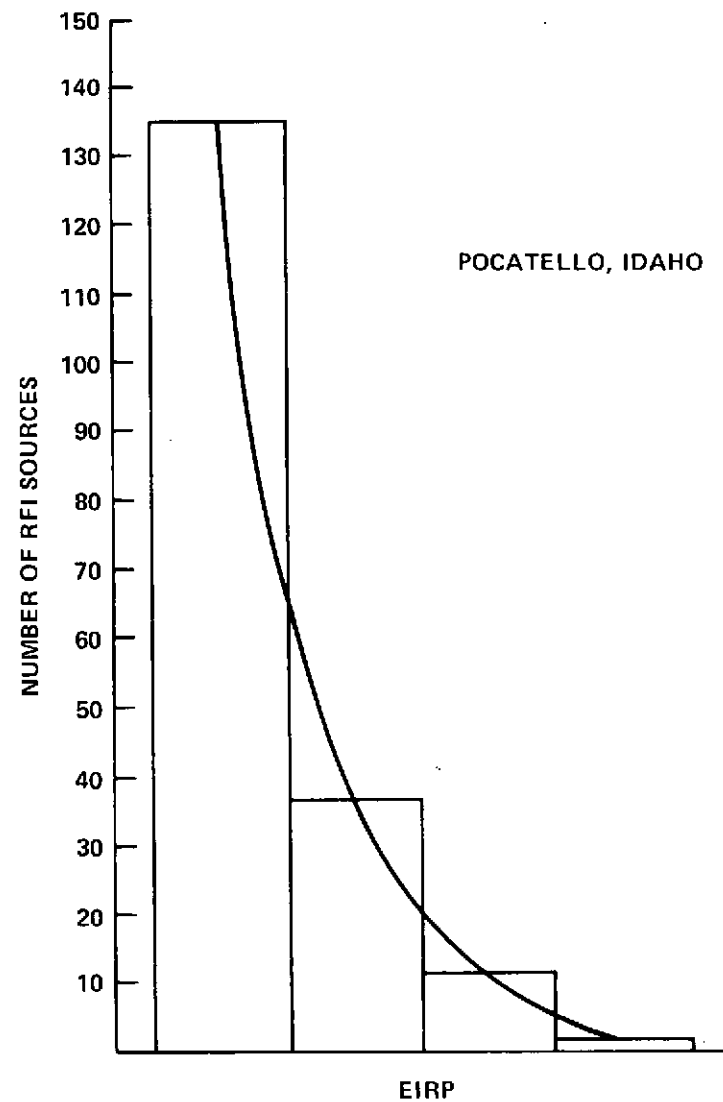
Figure 21-3. C-Band RFI Survey,
July to August 1974

21-5
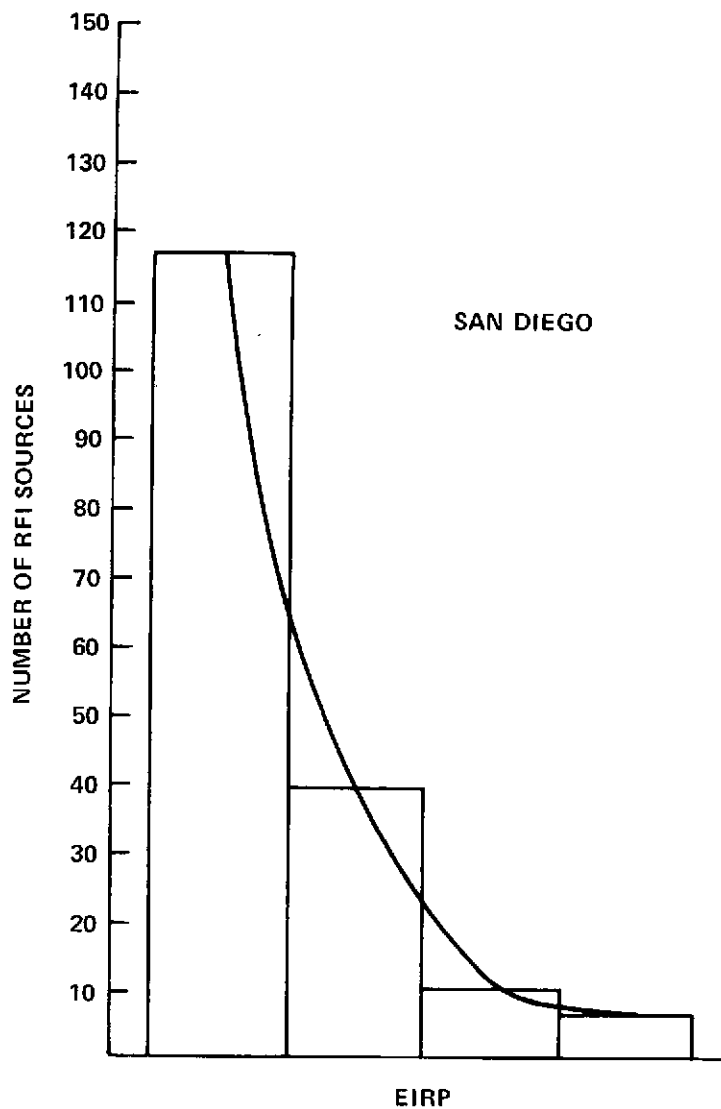
Figure 21-4. C-Band RFI Survey,
July to August 1974
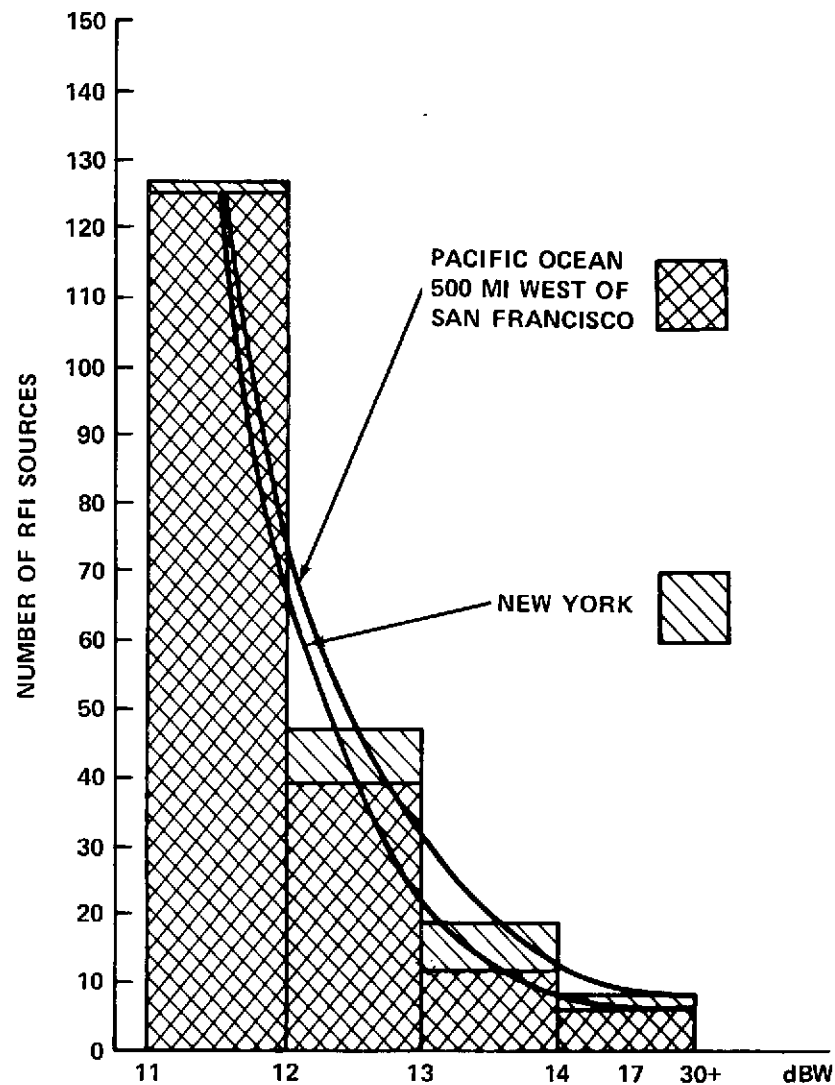
Figure 21-5. C-Band RFI Survey,
July to August 1974
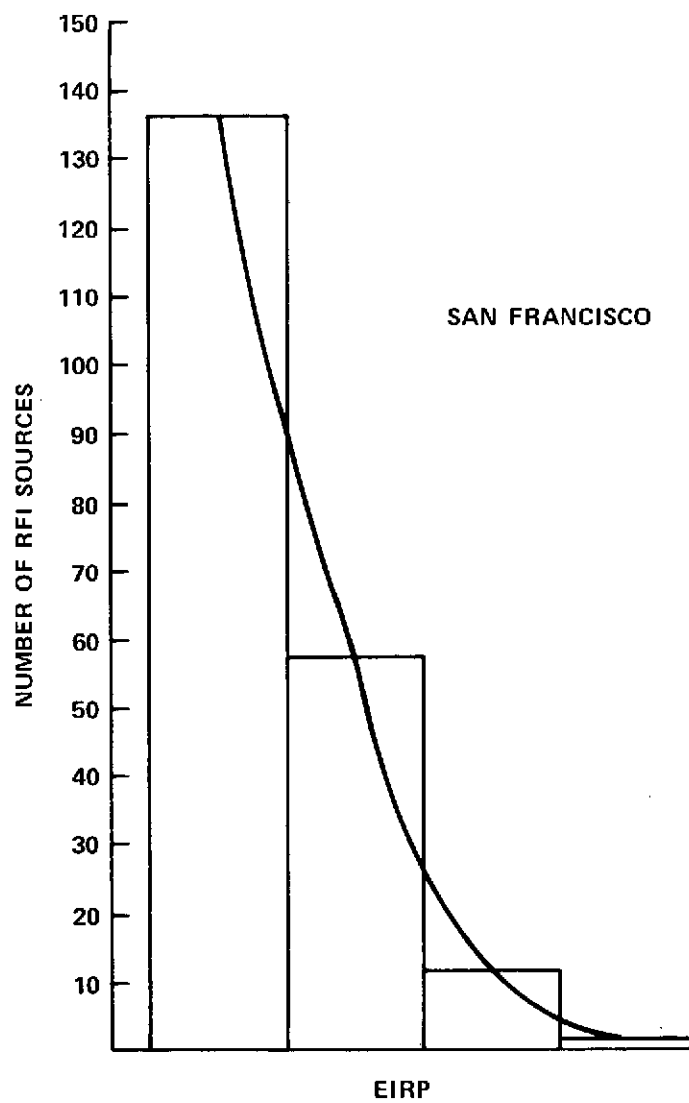
Figure 21-6. C-Band RFI Survey, July to August 1974

SECTION 22

SATELLITE INSTRUCTIONAL TELEVISION EXPERIMENT (SITE)

AND

TELEVISION RELAY USING SMALL TERMINALS (TRUST)

SECTION 22

SATELLITE INSTRUCTIONAL TELEVISION EXPERIMENT (SITE) AND TELEVISION RELAY USING SMALL TERMINALS (TRUST)

22.1 INTRODUCTION

The received power and ground station antenna gain measurements for TRUST and SITE type installations, as observed at GSFC, have been further refined by more accurate calibration techniques and the use of a revised computer program to account for the actual position of the spacecraft in longitude and latitude.

The test data for the SITE and TRUST antenna indicates gains of 23.4 dB and 26.5 dB respectively.

The SITE antenna and input configuration consists of a single helix, and the SITE head-end, which downconverts 860 MHz to 70 MHz. An overall conversion gain of approximately 35 dB is realized.

The TRUST antenna and input configuration consists of an antenna system employing two bifilar helices, and the TRUST front-end, which downconverts 860 MHz to 70 MHz. An overall conversion gain of approximately 30 dB is realized.

The received carrier level power at 860 MHz was -103.6 dBm for a linearly polarized isotropic antenna when GSFC was at beam center.

22.2 SCIENTIFIC OBJECTIVES

The SITE objective is to assess the potential value of satellite technology in establishing effective mass communication and instruction in developing countries. SITE operates at UHF.

The TRUST objective is to advance the state-of-the-art in space communications at UHF by demonstrating CCIR quality wideband television transmission from ATS-6 to inexpensive ground stations.

22.3 EXPERIMENT DESCRIPTION

The UHF downlink at 860 MHz is used for both direct reception by low cost augmented TV receivers and by higher sensitivity Earth stations for rebroadcast at VHF frequencies to conventional TV receivers.

The more sensitive TRUST ground terminal employs a front-end with a noise figure of 4 dB compared to the SITE front-end noise figure of less than 6.5 dB.

Operation at the UHF frequencies has been restricted to less than three hours during this reporting period. In general, due to potential interference to TV translators operation must be scheduled during the early morning hours when the translators are not operating.

22.4 EXPERIMENT PERFORMANCE EVALUATION

22.4.1 UHF Carrier Level Measurements

Three receiving systems were employed for measurement of the UHF (860 MHz) carrier power level received at GSFC:

1.   A standard gain horn, amplifier and spectrum analyzer was used as a reference receiver, since the gain of the horn and hence the overall ground terminal gain to the analyzer is accurately known

2.   The TRUST antenna system and front-end

3.   The SITE antenna system and head-end

Figure 22-1 shows the test configuration and some features of each system. The TRUST antenna system employes two bifilar helices which are electrically offset by 90°. A quadrature hybrid combines the signals on each helix and phaseshifts one by 90° so that the signals are summed in phase. This reduces ellipticity.

The TRUST front-end downconverts the 860 MHz to 70 MHz and provides an overall conversion gain of approximately 30 dB.

The SITE antenna system consists of a single helix, and the SITE head-end downconverts 860 MHz to 70 MHz and provides an overall conversion gain of approximately 35 dB.

The spectrum analyzer was used as the level indicator for all three receiving systems. The high resolution IF section used during these measurements was operated in the 2 dB/division display mode so that the difference between the smallest CRT divisions represented 0.4 dB.
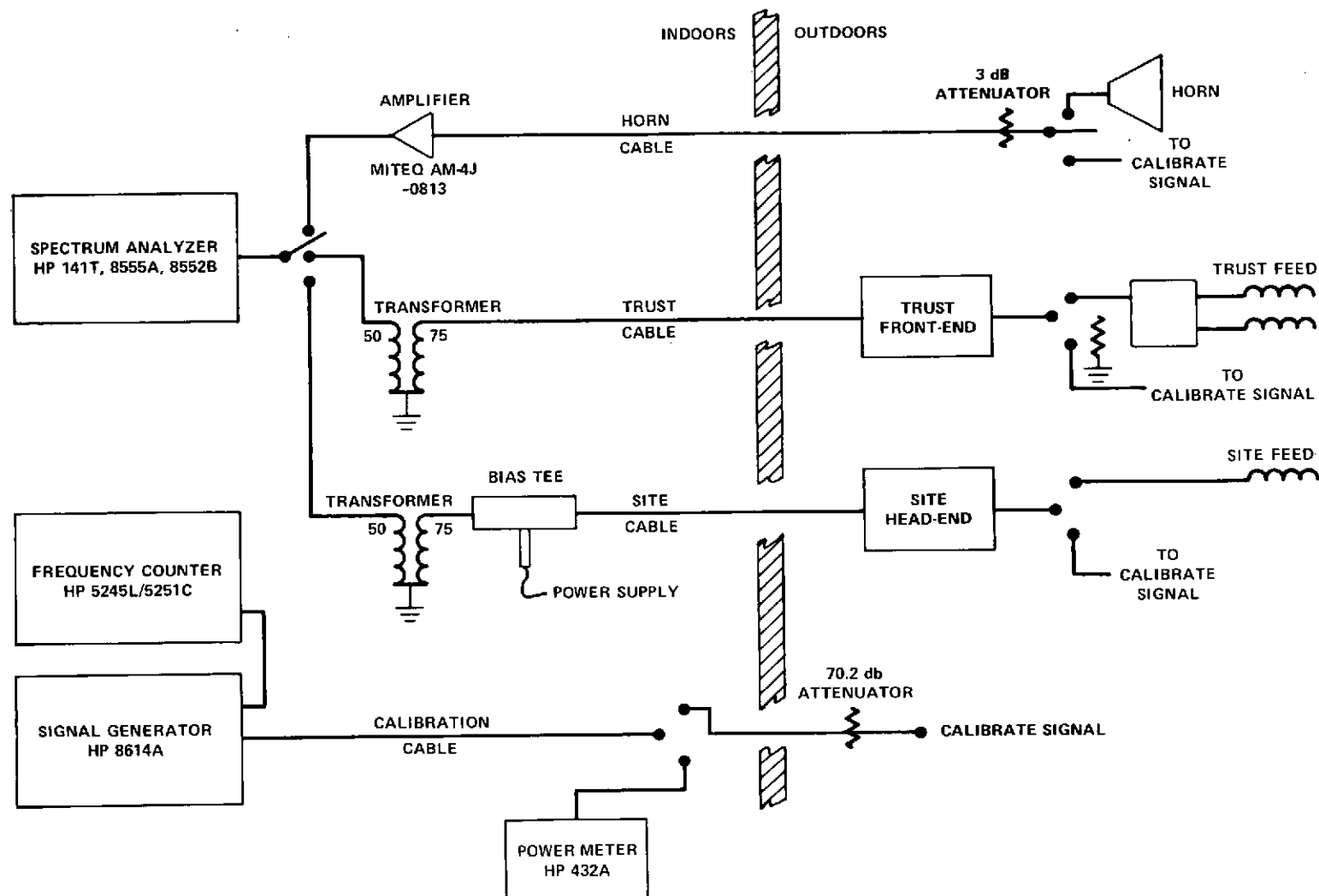
Figure 22-1. Test Configuration for UHF Carrier Level Measurements from ATS-6

The net gain of each receiving system was calibrated before or after the carrier level measurements. The frequency of the signal generator, HP8614A, was adjusted to 860 ±0.1 MHz by viewing the display of the frequency counter, HP5245L/5254C. The end of the calibration cable was connected to the power meter, HP432A, the power meter was rezeroed, and then the signal generator power level was adjusted until the power meter indicated a level of -10.0 dBm. The cable was then disconnected from the power meter and connected to a 70.2 dB attenuator (two attenuators in series, a 20.0 dB and a 50.2 dB attenuator). An accurate calibration signal of -80.2 dBm at 860 MHz was thus established. This calibration signal was then inserted into the three receiving systems at the antenna outputs, as shown in the attached test configuration diagram, and the subsequent power level at the spectrum analyser recorded. This procedure eliminates the need for absolute accuracy at the analyser, since the reference power level is established at the power meter. The difference between the calibration signal and its corresponding spectrum analyser level yields the net gain of each receiving system from the antenna output to the analyser input and accounts for losses from cables, transformers, attenuators, etc. The net gain for each system on each test day is shown on the attached data sheet. Day to day variation of net gain may be due to power supply variations or temperature variations.

The horn, TRUST, and SITE antenna output levels were computed for each test day by subtracting the net gains derived from the calibration sequence from the spectrum analyser levels obtained from the satellite carrier transmission. The TRUST antenna gain for each test day was subsequently computed by taking the difference in the antenna output level between the antenna and the horn and adding 15.4 dB, the gain of the horn, to that difference.

As can be seen from Table 22-1, the TRUST antenna gain, computed as described above, averaged 26.5 dB over the three test days, with a maximum deviation from this average of only 0.6 dB.

During these tests the TRUST helices were wound to receive a right circular polarized wave. Since the polarization should have been left circular, the TRUST bifilar helices and quadrature coupler constituted a linearly polarized feed.

The SITE antenna input level for each test day was computed by adding 3 dB to the antenna input level established by the horn (because the horn is linearly polarized, the SITE helix is circularly polarized and the incoming signal is circularly polarized). The SITE antenna gain for each test day was then computed by taking the difference between this antenna input level and the antenna output level. The SITE antenna system underwent various changes between the test

Table 22-1

UHF Carrier Level Data
(at GSFC, from ATS-6)

Function	Date											
	7-1-74			7-2-74			7-3-74			7-5-74		
	Horn	TRUST	SITE	Horn	TRUST	SITE	Horn	TRUST	SITE	Horn	TRUST	SITE
Spectrum analyser level (-dBm)	57.6	54.5	65.0	58.4	55.2	–	61.0	–	67.4	60.4	56.9	55.8
ACT gain from antenna output to analyser (from cal) (+dBm)	32.6	24.7	27.0	31.0	23.7	–	31.0	–	25.6	31.6	23.5	25.2
Antenna output (-dBm)	90.2	79.2	92.0	89.4	78.9	–	92.0	–	93.0	92.0	80.4	81.0
Antenna gain (+dB)	15.4	26.4	10.6	15.4	25.9	–	15.4	–	11.4	15.4	27.0	23.4
Antenna input (-dBm)	105.6	105.6	102.6	104.8	104.8	–	107.4	–	104.4	107.4	107.4	104.4

days. On July 1, 1974, it was determined that the winding sense of helix was incorrect and was causing the low antenna gain of only 10.6 dB. By July 3, 1974, a new helix had been wound, with the correct left circular polarization, but still yielded an antenna gain of only 11.4 dB. Closer inspection of the feed then revealed that the helix to coaxial cable electrical connection was marginal, and measurements on the feed showed a VSWR of 5:1. A better connection was made and resulted in an improved VSWR of 1.8:1. On July 5, 1974, the satellite/ground terminal measurements showed the SITE antenna system gain to be 23.4 dB, which was in the range of expected values.

Table 22-2 is a revised analysis of the carrier power as received by the standard gain horn. A preliminary version of this data was based on a simplifying assumption, namely that ATS-6 was positioned at 94°W Longitude with zero inclination.

To account for the actual position of ATS-6 (Latitude and Longitude) the computer program has been rewritten. The results indicate that the previously calculated received power levels were about 0.6 dB lower than they should have been. Table 22-3 is a corrected summary of the results. Table 22-4 is a print-out of the calculation for off-axis loss to both Rosman and GSFC. These results are used in the revised summary.

Table 22-2

Analysis of The Carrier Power as Received by
The Standard Gain Horn

Function	Carrier Level
EIRP	+ 82.1 dBm
Path Loss to GSFC	-182.7 dB
Relative Gain of Linearly Polarized Isotropic Antenna	- 3.0 dB
Received Power	-103.6 dBm

Table 22-3

Summary of Recalculated Received Power Levels

Function	Date	Loss
Calculated Off-Axis Loss (dB)	7-1-74	− 1.5
	7-2-74	− 2.4
	7-3-74	− 3.5
	7-5-74	− 2.3
Calculated Received Isotropic Power (dBm)	7-1-74	−105.1
	7-2-74	−106.0
	7-3-74	−107.1
	7-5-74	−105.9
Measured Received Isotropic Power (dBm)	7-1-74	−105.6
	7-2-74	−104.8
	7-3-74	−107.4
	7-5-74	−107.4
Difference Between Measured and Calculated Isotropic Power (dB)	7-1-74	− 0.5
	7-2-74	+ 1.2
	7-3-74	− 0.3
	7-5-74	− 1.5

It should be noted that the normalized antenna gain around the boresight is assumed to be given by;

$$\frac{G(\theta)}{G(o)} = \epsilon^{-2.772\left(\frac{\theta}{\theta_3}\right)^2}$$

where θ = angle off boresight

θ_3 = 3 dB beamwidth: taken as 2.8° at 860 MHz

The validity of this approximation will be evaluated against measured ATS-6 UHF antenna patterns.

As yet unresolved are the relatively large differences between measured and calculated received power for July 2 and July 5, 1974 (Table 22-3). They could be the result of a number of items ranging from calibration error to measurement error. There was no pre- or post-calibration of the amplifier gain on July 2, 1974. The received carrier level for July 2, 1974, is based on the precalibrate data from July 3, 1974. A closer agreement to the expected level would result if the July 1, 1974 post-calibration data were used. However, at this point, to do so would amount to juggling the calibration data to fit the data. This is unwarrented.

Table 22-4

Off-Axis Loss to Rosman and GSFC

DATE: 7-1-74

B.C. LAT, LONG; 31.5700   77.8700   S/C LAT, LONG; 1.6740   95.2300
ROLL = 4.944   PITCH = 2.470

GSFC
ROLL = 5.9184   PITCH = 2.3936   DIST = 0.9931   G = -1.5145 DB

ROSMAN
ROLL = 5.4456   PITCH = 1.7270   DIST = 0.9420   G = -1.3627 DB

NEXT DATA SET

B.C. LAT, LONG; 31.6300   77.8000   S/C LAT, LONG; 1.6610   95.2300
ROLL = 4.954   PITCH = 2.475   -1.5

GSFC
ROLL = 5.9199   PITCH = 2.3936   DIST = 0.9857   G = -1.4919 DB

ROSMAN
ROLL = 5.4473   PITCH = 1.7270   DIST = 0.9441   G = -1.3688 DB

NEXT DATA SET
                    DATE: 7-2-74

B.C. LAT, LONG; 29.9100   76.9900   S/C LAT, LONG; 1.6680   95.1800
ROLL = 4.6933   PITCH = 2.6837

GSFC
ROLL = 5.9193   PITCH = 2.3866   DIST = 1.2614   G = -2.4434 DB

ROSMAN
ROLL = 5.4465   PITCH = 1.7195   DIST = 1.2235   G = -2.2986 DB

NEXT DATA SET

B.C. LAT, LONG; 29.9600   77.6500   S/C LAT, LONG; 1.5470   95.1800
ROLL = 4.7192   PITCH = 2.5890   -2.4

GSFC
ROLL = 5.9334   PITCH = 2.3861   DIST = 1.2311   G = -2.3271 DB

ROSMAN
ROLL = 5.4623   PITCH = 1.7192   DIST = 1.1440   G = -2.0096 DB

Table 22-4 (Cont'd)

Off-Axis Loss to Rosman and GSFC

DATE: 7-3-74

B. C. LAT, LONG; 28.4800   76.5700   S/C LAT, LONG; 1.6570   95.1100
ROLL = 4.4843   PITCH = 2.7762

GSFC
ROLL = 5.9208   PITCH = 2.3772   DIST = 1.4909   G = -3.4131 DB

ROSMAN
ROLL = 5.4481   PITCH = 1.7094   DIST = 1.4377   G = -3.1738 DB

NEXT DATA SET

B. C. LAT, LONG; 28.3900   76.1900   S/C LAT, LONG; 1.6780   95.1200
ROLL = 4.4669   PITCH = 2.8342   -3.5

GSFC
ROLL = 5.9183   PITCH = 2.3784   DIST = 1.5213   G = -3.5538 DB

ROSMAN
ROLL = 5.4454   PITCH = 1.7108   DIST = 1.4898   G = -3.4081 DB

NEXT DATA SET
DATE: 7-5-74

B. C. LAT, LONG; 30.0800   77.0400   S/C LAT, LONG; 1.6670   95.0100
ROLL = 4.7188   PITCH = 2.6477

GSFC
ROLL = 5.9200   PITCH = 2.3656   DIST = 1.2339   G = -2.3379 DB

ROSMAN
ROLL = 5.4471   PITCH = 1.6963   DIST = 1.1981   G = -2.2042 DB

NEXT DATA SET

B. C. LAT, LONG; 30.1400   77.0400   S/C LAT, LONG; 1.6680   95.0100
ROLL = 4.7273   PITCH = 2.6458   -2.3

GSFC
ROLL = 5.9199   PITCH = 2.3656   DIST = 1.2251   G = -2.3045 DB

ROSMAN
ROLL = 5.4469   PITCH = 1.6964   DIST = 1.1914   G = -2.1795 DB

SECTION 23

POSITION LOCATION AND AIRCRAFT
COMMUNICATION EXPERIMENT
(PLACE)

SECTION 23

POSITION LOCATION AND AIRCRAFT
COMMUNICATION EXPERIMENT
(PLACE)

23.1 INTRODUCTION

Spacecraft operation with PLACE ground and shipboard equipment occurred on 22 different days of this reporting period. The spacecraft PLACE-associated equipment performed well and should adequately support the planned experiments.

Special tests related to signal power sharing (PLACE and MARAD), S&R, Voice, Data Channel C/No in both forward and return links, and data channel bit error rate, have furnished data which indicates that the required C/No system performance is achievable.

The tests were involved with the following:

    a. Primary ground station at Rosman
    b. NASA ground station at Mojave (receive mode)
    c. MARAD station at Kings Point
    d. MARAD ship terminal at Moorestown
    e. TCS Cambridge-USCG ship terminal
    f. MARAD-COMSAT modem (voice and data)
    g. ESRO-EPIRB buoy receiving equipment located at Rosman
    h. ROSMAN/MOJAVE ranging, voice and data.

23.2 SCIENTIFIC OBJECTIVES

The objective of the Position Location and Aircraft Communication Experiment is to demonstrate a communication link between ground stations and a large number of aircraft and to define the location of these aircraft.

The feasibility and benefits of satellite communications to airplanes and ships has been demonstrated in the past by the use of the ATS-1 and -5 satellites. This experiment is an extension of prior experiments and its major objective is to provide data from which requirements can be derived for operational systems to be established later in this decade. The experiment is international in scope with participation with the following agencies:

    a. NASA/Goddard Space Flight Center
    b. Department of Commerce/Maritime Administration (MARAD)

c. Department of Transportation (DOT)
   - Federal Aviation Administration (FAA)
   - U.S. Coast Guard (USCG)
   - Transportation Systems Center (RSC)
d. European Space Research Organization (ESRO)
e. Canadian Department of Communications and Ministry of Transport

23.3 EXPERIMENT DESCRIPTION

The experiment performed at the L-band frequencies (1.5- to 1.7-GHz) allocated for aeronautical and maritime use by the World Administrative Radio Conference.

Performance tests will be conducted on several communications and position-location techniques using the ATS-6 and ATS-5 spacecraft with airborne planes and ships at sea. Other tests will include ground-based simulation and engineering exercises.

From its position at 94 degrees west longitude over the Galapagos Islands, ATS-6 will provide two-way communications between mobile units and ground stations located in a 1081 kilometer (672 mile) wide area extending from the east coast of the U.S. two thirds of the way across the mid-Atlantic Ocean.

Tests conducted between the ground stations and the aircraft and ships underway are designed to determine the effects of ionospheric, noise, and multipath disturbances as well as the geographic location of the tracked units on both L-band communications and position location techniques. Tests will encompass:

   a. Communications link performance;
   b. Multiaccess performance;
   c. Power and frequence control techniques; and
   d. Quality and ranging precision for the various techniques under test.

Position location tests require altimeter readings from aircraft and accurate range measurements from each of the two ATS spacecraft and the aircraft or ship being tracked.

Precise spacecraft location is obtained by a trilateration technique in which accurate measurements of the distance from three ground stations to each spacecraft are used. These measurements will be made from the three NASA tracking stations at Rosman, Mojave, and Santiago. ATS-5 trilateration stations will be located in Schenectady, New York, Hawaii, and Buenos Aires, Argentina.

The ATS ground station at the Rosman site will serve as the primary L-band experiment support facility for communicating with the ATS-6 and the ATS-5 spacecraft. A terminal at the National Maritime Research Center, Kings Point, New York, also will serve to communicate with ATS-6.

Other ground facilities planned for monitoring ATS-F L-band transmissions include the FAA's National Aviation Flight Experiments Center at Atlantic City, N. J.; the Transportation Systems Center's facility at Westford, Mass.; and the Canadian Communications Research Centre's facility in Ottawa, Canada.

Four jet aircraft and six ships will be provided for this experiment by the United States, ESRO, and Canada. All these units will be equipped with special L-band communications and ranging equipment. An ESRO-provided ship also will be equipped to test an L-band emergency buoy designed to provide search and rescue teams with a distressed ship's final position, information vital to locating survivors. The six ships are as follows:

    USCG: Sherman and Gallatin
    ESRO: Skeinsfjord and Otto Hahn
    MARAD: American Ace and Lash Atlantico

As many as 100 mobile terminals can communicate with a ground terminal through the ATS-F spacecraft in a completely coherent system. The links are established by first phase locking the ATS-F communications transponder to a C-band signal from the ground station. The C-band signal is processed through the receiver and IF amplifier. It is then coherently upconverted to L-band at 1550 MHz and transmitted to the aircraft transponder. Information from the aircraft is transmitted in the form of a single sideband modulated signal in 10 kHz channels in the L-band from 1650-MHz to 1652-MHz. ATS-F receives the spectrum from 1650-MHz to 1652-MHz and, after preamplification, downconverts it to baseband in the IF amplifier. This baseband signal is used to phase modulate a carrier (coherent to the C-band signal) which is then upconverted to C-band and is processed through the transmitter. The ground station receives the carriers and recovers the aircraft signal.

The special multiple-access capability provides for simultaneous operation of C-band to L-band, and L-band to C-band. To achieve this, the communications subsystem provides a receiver linearity that prevents the multiple carriers from producing significant intermodulation components. When the multiple carriers are received, they are translated to baseband frequencies and then phase modulated onto a single carrier by the use of selectable baseband filters. The phase modulation index is held by automatic gain control at 0.85 radian rms, independent of the number of carriers.

23.4 EXPERIMENT PERFORMANCE EVALUATION

23.4.1 Spacecraft and Experiment Checkout

L-band experiment system checkout began on July 17 with the first allocation of spacecraft (S/C) time to the experiment. Prior to this date, ATSOCC had tested the S/C L-band system and taken data for L-band antenna patterns while conducting spacecraft checkout. During the period June 17 to July 31, 1974, approximately 57 hours of S/C time was provided for the L-band experiment system checkout. This time has been used to check out the spacecraft operating characteristics, the various ground station systems and the mobile unit terminals which comprise the Integrated L-band experiment. The sections that follow summarize the week-by-week activities of these checkout operations.

23.4.1.1 Chronology of L-Band Experiment Systems Checkout — The basic plan for the L-band experiment system checkout was to exercise the systems of the participating ground stations starting with the experiment primary station at Rosman, North Carolina. Table 23-1 is the proposed operations checkout test schedule of May 10, 1974, and the update of July 22, 1974. The next stop was the checkout of the MARAD station at Kings Point, New York. With both these stations checked out, it was then necessary to establish the S/C Power Sharing Procedure, followed by the checkout of the NASA ground stations at Mojave, and Santiago and the mobiles both aircraft and ships units. Upon completion of these ground station checkouts, initial operations tests of the ATS-6 L-band trilateration and two-satellite ranging systems are to be conducted. During this checkout period, experiment participants also asked for time to conduct specific tests to meet individual system requirements to insure readiness for the integrated L-band experiment which commences in September, 1974.

23.4.1.2 Week of June 17 — Rosman Ground Station equipment problems caused some difficulties during the first few days of checkout. These problems were worked out and by the end of the first week operations had smoothed out. During these tests, a nominal C/No was measured and the PLACE avionics and ground equipments had locked-up on the ranging signal indicating that the systems were functioning within system tolerances. These early equipment problems prevented operations in the S/C Coherent Mode, and also prevented L-band checkout of the Remodulation Mode. This will be conducted at a later date.

Radio frequency interference (RFI) measurements were conducted on board the Maritime Vessel "American Alliance" during the period June 17-20, 1974. These tests were conducted to identify potential interference problems for the operational L-band shipboard terminals to be used in this experiment. Preliminary

Table 23-1

L-band Preintegrated Experiment Operations Transmission Requirements

Test Group	Proposed	No. of Hours	S/C Mode	No. of Hours	L-Band Pierce Pt.	S/C Configuration FWD Link C × L				Return Link A × C				M.O. Synth. Mode
						BW	Freq. Up	Freq. Down	Attn.	BW	Freq. Up	Freq. Down	Attn.	
A	June	15-10m	Ft.	7-40	ROS	40 MHz	6150	1550	Out	40 MHz	1650	3950	In	NONCOH
			Ft.	1-20	ROS	12 MHz	6350	1550	Out	40 MHz	1650	3950	In	NONCOH
			Remod	6-10	ROS	12 MHz	6350	1550	Out	40 MHz	1650	3950	In	COH
B	July	6	Ft.	6	Kings Pt.	40 MHz	6350	1550	Out	40 MHz	1650	3950	In	NONCOH
C	July	8	Ft.	8	ROS	40 MHz	6350	1550	Out	40 MHz	1650	3950	In	NONCOH
D	July	9	Ft.	9	35N 100W	40 MHz	6350	1550	Out	40 MHz	1650	3950	In	NONCOH
E	July	5	Ft.	5	ROS	40 MHz	6350	1550	Out	40 MHz	1650	3950	In	NONCOH
F	July	9	Ft.	9	ROS	40 MHz	6350	1550	Out	40 MHz	1650	3950	In	NONCOH
G	July/Aug	16	Ft.	7-40	ROS	40 MHz	6350	1550	Out	40 MHz	1650	3950	In	NONCOH
				8-20	TBD	40 MHz	6350	1550	Out	40 MHz	1650	3950	In	NONCOH
H	Aug	23-20m	Ft.	5	ACY	40 MHz	6350	1550	Out	40 MHz	1650	3950	In	NONCOH
				18-20	TBD	40 MHz	6350	1550	Out	40 MHz	1650	3950	In	NONCOH
I	Aug/Sept	8-30	Ft.	8-30	TBD	40 MHz	6350	1550	Out	40 MHz	1650	3950	In	NONCOH
			Ft.		TBD	40 MHz	6350	1550	Out	40 MHz	1650	3950	In	COH
	Back-Up Modes		Ft.		TBD	12 MHz	6350	1550	Out	40 MHz	1650	3950	In	COH
			Ft.		TBD	12MHz	6350	1550	Out	40 MHz	1650	3950	In	NONCOH

Table 23-1 (Continued)
L-band Preintegrated Experiment Operations Transmission Requirements

Experiment Test Group	Test Description and Time Blocks

A	**Rosman Place Mode Readiness Tests**
	
	 1. Ft Mode BW
	     a. 1 hour − 50 minutes 40 MHz
	     b. 1 hour − 20 minutes 12 MHz
	     c. 3 hours − 00 minutes 40 MHz
	     d. 2 hours − 50 minutes 40 MHz
	
	 2. Remodulation Mode
	     a. 1 hour − 40 minutes
	     b. 4 hours − 30 minutes

B	**Kings Point L-Band Readiness Test** Rosman to monitor C & L Channels 1. 3 two (2) hour time block
C	**Rosman/Kings Point L-Band Power Sharing Tests** 1. 4 two (2) hour time blocks Establish working procedure between stations
D	**Rosman-Mojave Place Readiness Test** Kings Point may operate in power share mode 1. 1 hour − 50 minutes 2. 4 hours − 20 minutes 3. 2 hours − 50 minutes
E	**Rosman-Santiago Place Readiness Tests** Kings Point may power share 1. 3 hours 2. 2 hours

Table 23-1 (Continued)
L-band Preintegrated Experiment Operations Transmission Requirements

Experiment Test Group	Test Description and Time Blocks
F	**Rosman-Place Avionics Unit (A/C)** (Seattle or NAFEC) Kings Point may power share 1. 1 hour − 50 minutes 2. 4 hours − 20 minutes 3. 2 hours − 50 minutes

G	**Place ATS-F Trilat**
	
	1. Rosman-Mojave-Santiago
	
	    a. 3 hours − 50 minutes
	    b. 3 hours − 50 minutes
	
	2. Rosman-Mojave-Santiago-A/C Unit
	
	    a. 4 hours − 10 minutes
	    b. 4 hours − 10 minutes
	
	Note: Kings Point may power share during Trilat Tests

H	**Place Two (2) Sat Ranging Tests**
	
	1. Rosman-Mojave-Santiago-A/C Unit
	
	Note: Kings Point may <u>not</u> power share during this test
	
	    a. 5 hours
	
	2. Rosman-Mojave-Santiago-A/C Unit
	
	    a. Five (5) 3-40 minute tests
	
	Note: Kings Point <u>may</u> power share on these tests.

I	**Place L-Band System Tests − TBD** 1. 2 hours 2. 2 hours − 30 minutes 3. 2 hours 4. 2 hours Note: Kings Point power sharing − TBD

information from these tests indicates that RFI can be eliminated or reduced to acceptable levels with proper positioning of L-band equipment and antennas on the ship and the use of suitable filtering. A summary of these results follows. Results of these tests will be published separately.

An EMI shipboard survey was conducted on the American Alliance container ship of the United States Lines during the period June 16-20, 1974. The ship was equipped with both S-band (10 cm. wavelength) and X-band (3 cm wavelength) radars.

The 4-foot diameter, paraboloid antenna, duplexer, low-noise preamp amplifier and downconverter of a prototype L-band terminal were used in the series of EMI measurements to investigate interference to the ship's 10-cm. wavelength (S-band) and 3-cm wavelength (X-band) radars, as well as potential interference to the L-band shipboard terminal. Measurements were made of conducted emissions on the ship's power lines which were compared with similar measurements made on land-based power lines.

Field intensity measurements were made at a candidate location for installation of the L-band shipboard terminal on the ship's flying bridge and on the radar mast, as well as in the equipment room where part of the L-band terminal will be installed near the radar cabinets. An evaluation was made of band-pass and low-pass microwave filters installed in the L-band terminal to alleviate potential interference.

Using a radiometer, antenna sky-noise temperature measurements were also made using the L-band shipboard terminal antenna. Measurements were made at sea and at the Port Elizabeth, Philadelphia and Savannah harbors. Antenna-noise temperatures measured ranged from 30°K to 150°K, at 1.6 GHz, depending upon elevation angle, these values being within theoretical expectations.

Other findings include:

  a. The powerline conducted emission EMI environment is more severe than that encountered in typical land-based operations. Peak interference measurements in the 150 kHz to 32 MHz range were typically 15 to 50 decibels higher.

  b. Case radiation from the S-band and X-band radars was on the order of 1.0 V/m/MHz at a distance of 1 meter (m). This indicates that the L-band terminal equipment mounted near the radar cabinet should be well shielded.

c. Interference of the L-band terminal to the S-band and X-band radars was not encountered.

d. Radar interference to the L-band terminal will be influenced by the relative location of the antennas. On the American Alliance, the antenna separation was on the order of 8 m for the L-band to S-band antennas and 10 m for the L-band and X-band antennas. However, the selectivity of the L-band terminal duplexer is very effective in mitigating direct radar interference.

23.4.1.3 Week of June 24 – The MARAD station at Kings Point commenced check-out on the 24th with mixed results. They had operational difficulties radiating to the spacecraft transponder. The problem was related to antenna pointing and was resolved. A MARAD ship terminal located at Moorestown, New Jersey, monitoring the tests was able to pick up the signals with adequate signal-to-noise ratios.

First attempts at power sharing between Rosman and Kings Point were conducted. By the end of this week the Power Sharing Operation Procedures were established.

23.4.1.4 Week of July 1, 1974 – Power sharing procedures were exercised while Kings Point and the Ship terminals checked out different modems. Power suppression testing was conducted to determine the optimum power sharing parameters for L-band operations with Rosman and Kings Point.

The Mojave Ground Station was exercised in the receive mode. C/No measurements were taken at all stations with nominal results.

A spacecraft anomaly in the L-band system was observed and reported to the project. This anomaly, Desensitization of the L-band receiver, is described in section 23.4.2.

TSC Cambridge was brought up for an operational test of their USCG ship terminals, however, results were inconclusive. MARAD found on retest of its COMSAT modem that the receiver mode was inoperative.

With the exception of the EPIRB buoy receiving equipment, ESRO Equipment for the Rosman Station has been installed and checked out. System operations was performed on ATS-6 in C to L mode, simultaneously with VHRR Experiment operations. This test proved the concept of working with VHRRE to be operationally feasible.

The spacecraft L-band receiver quieting performance was tested by varying the ground equipment C-band uplink frequency. Data obtained showed an apparent

12 db less quieting at the MARAD frequency of 6359-MHz vs the PLACE frequency of 6350-MHz.

Signal level shifts were observed during the experiment checkout while using auto tracking on the VHF signal. It was recommended to ATSOCC that auto tracking using the C-band signal (beacon) be provided to stablize the signal levels.

23.4.1.5 Week of July 8, 1974 – No L-band operations were conducted.

23.4.1.6 Week of July 15, 1974 – As a result of our earlier testing recommendations were made and agreed to by the ATS-6 Project to conduct a series of tests to characterize the spacecraft operating performance in the G-to L-band and L-to C-band links. The main points of these tests are to evaluate (1) the desensitization of the L-band receiver, (2) frequency dependency of spacecraft transponders, and (3) the mutual experiment-to-experiment interface.

Rosman L-band integration continued with the receipt of the DOT/TSC racks and cables.

Data taken during the last three weeks has been used to prepare Section 23.5. The Measured Transfer Characteristics of the ATS-6 Satellite in the L/C and C/L Crosstrap Modes.

23.4.1.7 Week of July 22, 1974 – Testing this week concentrated on the following areas:

    a. Kings Point/Ship Terminal evaluations of the COMSAT voice and data modems.

    b. Rosman/Mojave ranging, voice and data qualification.

    c. Spacecraft spectrum characteristics.

Evaluation of the data received proceeds slowly because of manpower limitations. It is now evident that the prelaunch power sharing will have to be reevaluated. One factor affecting this could be the possible frequency-dependent quieting response of the S/C L-band receiver.

23.4.1.8 Week of July 29, 1974 – S/C time continued to be allocated to the checkout of the COMSAT Modem by Kings Point on the MARAD link. Additional S/C time would still be required to complete the testing.

Rosman Ground Station was beset with L-band equipment problems notably in the PLACE aircraft modem. Indications were that not as much time as needed was being spent on PLACE equipment troubleshooting and equipment maintenance. The difficulty was caused by the fact that at Rosman, the one man per shift responsible for the L-band experiment also had responsibility for the VHRR experiment. Since VHRR tests had been scheduled extensively, corrective maintenance of L-band ground equipment had not been adequate.

The Santiago PLACE Avionics unit failed on site prior to launch of ATS-6. The unit was returned to the United States for repairs and then checkout at Rosman.

23.4.1.9 Summary of System Operations Checkout — The ATS-6 satellite generally performed very well and should adequately support the planned L-band experiments. EIRP was somewhat higher than expected.

The PLACE equipment generally performed well during the operational tests and should adequately meet L-band experiment requirements.

23.4.2 Anomalies Affecting L-Band Operations

23.4.2.1 Desensitization of L-Band Receiver — It has been discovered that noise power from the L-band transmitter apparently is desensitizing the L-band receiver whenever there is little or no signal in the forward link (C × L). The effect is minimized, if not eliminated, when the C-band signal received at the S/C is equal to or better than 84 dBm. However, a frequency dependence has been noted. The problem is under investigation.

23.4.3 C-Band ARC

A signal fluctuation has been observed on the C-band downlink which is apparently caused by arcing in the C-band output filter. The effect is considerably reduced by operating with a 10 dB attenuator in the S/C IF output. This causes approximately 6 dB less signal strength in the downlink (the overall C/N_0 ratio is essentially unaffected, since the determining links are the L-band up- and downlinks). The presence of the 10 dB pad is not expected to affect L-band experiment operations.

23.4.4 ATS-5 L-Band Transponder Receiver

The ATS-5 L-band transponder receiver failed in test. A strong possibility exists that the receiver will be successfully turned on during subsequent operations. However, without this receiver operating, the GE trilateration tests with ATS-5 using stations at Schnectady, Hawaii, and Buenos Aires, cannot be conducted. Ranging through ATS-5 using C × L mode is unaffected; therefore, the two satellite ranging experiments may still be conducted.

23.5 PRELIMINARY DATA EVALUATION

23.5.1 Test Data

The test data has not yet been reduced; however, preliminary measurements of C/No in the forward and return links show that the required system performance is achievable. Those tests which have been performed include the following:

a. Signal power sharing (PLACE and MARAD)

b. S&R, voice, data channel C/No in both forward and return links

c. Data channel bit-error rate.

The results from the above tests all indicate that satisfactory system performance may be expected.

23.5.2 Antenna Patterns

Antenna pattern measurements have been made from the S/C transmit pencil and fan beam antenna patterns. The data was obtained at Rosman and recorded on magnetic tape and is being processed. In addition, Canada recorded the transmit pattern using orthogonal linear feeds in order to determine the polarization ellipticity. The data was recorded at Ottawa and is approximately 75% processed.

Additional tests will be scheduled as required.

23.5.3 Measured Transfer Characteristics of the ATS-6 Satellite in the L/C and C/L Crosstrap Modes

23.5.3.1 Introduction – A series of experiments were initiated using the NASA/Rosman and MARAD/Kings Point, New York ground stations to characterize the L- to C- and C- to L- links of the ATS-6 satellite in the configuration to be used for the Integrated L-band experiment. The tests reported here were run on July 1, 3, and 19, 1974. In addition to the tests, a set of calculations were performed which were used to evaluate the resulting measurements. These sections describe both the measurements and the calculations.

23.5.3.2 Forward Link – Due to the potential difficulties associated with ATS-6 power sharing for the Rosman and Kings Point signals, a measurement of the ATS-6 power sharing characteristics was made. The satellite was configured

in the L- to C-band and C- to L-band, noncoherent cross-strap mode with the fan beam pointed toward Kings Point. The S/C was configured as follows:

Forward link: C-band (ECH) × L-band (Fan), IF No. 1 WBFT
Return link: L-band (Fan) × C-band (ECH), IF No. 2 WBFT, 10 dB attenuation in.

The ground stations used the following antennas with the indicated CW signals for these tests:

	Uplink Frequency	Transmit Antenna	L-Band Down-link Frequency	Receive Antenna
Rosman	6350 MHz	85-ft dish	1550 MHz	15-ft dish
Kings Point	6359 MHz	10-meter dish	1559 MHz	4-ft dish

Both ground stations transmitted C-band carrier signals to the satellite. The power levels were varied and the resulting L-band downlink signals were monitored at Rosman and at Kings Point.

Table 23-2 presents a calculated link budget for the resulting carrier-to-noise (C/N_0) density at Rosman as a function of the nominal Rosman and Kings Point EIRP's. The suppression of the weaker Kings Point signal by the satellite was obtained from the laboratory measurements referenced in the table. The satellite transmit pointing loss to Rosman shown in the table (17.3 dB) occurred since the satellite antenna was directed toward Kings Point. This pointing loss was determined by comparing the received C/N_0 at both Kings Point and Rosman and by knowing the antenna G/T at both locations.

$$(C/N_0)_{Ros} = EIRP + (G/T)_{Ros} - (SL)_{Ros} - (PL)_{Ros}$$

$$(C/N_0)_{KP} = EIRP + (G/T)_{KP} - (SL)_{KP} - (PL)_{KP}$$

Where

C/N_0 is the carrier-to-noise density in dB-Hz

Ros indicates Rosman

KP indicates Kings Point

EIRP is the satellite EIRP on the antenna fan beam axis in dBW

G/T is the ground antenna system performance in dB/°K

S/L is the space loss from the satellite to the appropriate ground station in dB

PL is the reduction in satellite antenna gain or pointing loss to the selected location.

Table 23-2

ATS-6 Forward Link Calculation Showing the Predicted Nominal L-Band
Received C/N_0 at Rosman vs the Kings Point and Rosman C-Band EIRP

Operational Functions	PLACE Signal from Rosman	MARAD Signal from Kings Point
Transmit Power (watts)	40	100
Transmit Antenna Coupling Loss (dB)	1.0	.8
Transmit Antenna Gain (dB)	61.5[1]	53.8[2]
Transmit EIRP (dBw)	76.5	73.0
Transmit Antenna Pointing Loss (dB)	1.0	1.0
Polarization Loss (dB)	0.5	0.5
Atmospheric Attenuation Loss (dB)	0.1	0.1
Transmit Free Space Loss (dB)	199.9	200.1
Satellite Antenna Gain ECH (dB)	17.4	17.4
Receive Signal Level (dBm)	-77.6	-81.3
Receive G/T (dB/°K)	-15.0	-15.0
Receive Noise Power (dBm)[3]	-90.0	-90.0
Total Power Received (dBM)[4]	-75.9	-75.9
Receive C/N_0 (dB/Hz)	88.6	84.9
Power Sharing Signal Suppression (dB)[5]	1.9	9.6
L-Band EIRP	45.3	37.6
Transmit Pointing Loss (dB)[6]	17.3	17.3
Transmit Free Space Loss to Rosman (dB)	187.9	187.9
Rosman Receiver Antenna Gain (15') (dB)	35.0	35.0
Receive Antenna Pointing Loss (dB)	1.0	1.0
Receive Total Signal Power (dBm)	-95.9	-103.6
Receive G/T (15') (dB/°K)	11.0	11.0
Rosman C/N_0	78.7	71.0

Notes:

  1. 85-ft. dish at 6350-MHz.
  2. 10-meter dish at 6359-MHz.
  3. Assumes a 40-MHz noise bandwidth.
  4. Assumes a linear summation of the two signal powers and the
     received noise power.
  5. This is based on the suppression measured by Fairchild in the
     laboratory for ATS-6. Reference "Measured ATS-F C/L-Band
     Transponder Power Sharing Characteristic" by Ralph Taylor and
     Fred Kissel, NASA/Westinghouse Internal Memo, April 4, 1974.
  6. The fan beam was pointed at Kings Point for this test. The
     pointing loss was obtained from evaluating $(G/T)_{Ros} - (G/T)_{KP}$
     $+ (C/N_0)_{KP} - (C/N_0)_{Ros}$ where $(G/T)_{Ros} = 11.0$ dB/°K, $(G/T)_{KP} = -5.0$
     dB and the average $(C/N_0)_{KP} - (C/N_0)_{Ros} = 1.3$ dB.

For this test it is assumed:

$$(SL)_{Ros} = (SL)_{KP}$$
$$(PL)_{KP} = 0.$$

Thus,

$$(PL)_{Ros} = (C/N_0)_{KP} - (C/N_0)_{Ros} + (G/T)_{Ros} - (G/T)_{KP}$$

The numerical values used to obtain satellite pointing loss to Rosman are shown in Table 23-2.

Figure 23-1 shows the effect of fixing the power at Kings Point to 100 watts (73 dBW) and varying the power level at Rosman from approximately 10 watts to 200 watts (70 dBW to 83 dBW). The predicted value derived from Table 23-2 for the Rosman PLACE C/N_0 is 78.7 dB-Hz, which is 3.2 dB above the actual measured signal of 75.5 dB-Hz. Similarly, the calculated MARAD C/N_0 is 71.0 dB-Hz which is 4.0 dB above the actual measured signal of 67.0 dB. Note that the difference between the actual PLACE and MARAD signal received is about 8.5 dB which generally agrees with the 7.7 dB difference predicted from the laboratory measurements shown in Table 23-2. Thus, the calculated value of received C/N_0 appears to contain approximately a 3 dB error which probably occurs in the computation of the satellite L-band downlink pointing loss. The results of a second test which varied the Kings Point power while the C-band power at Rosman was held at 40 watts (67.5 dBW) is shown in Figure 23-2.

A few preliminary results are inferred from the curves and calculations:

a. The forward-link power calculations are about 3 to 4 dB stronger than the actual measurements taken.

b. The relative power between PLACE and MARAD indicates approximate agreement with the previous laboratory measurements.

c. The measured degradation for the PLACE signal strength due to the MARAD signal at the nominal C-band power levels (40 watts at Rosman and 100 watts at Kings Point) appears to be about 1 dB. The degradation derived from the laboratory measurements is 1.9 dB.

d. The change in PLACE and MARAD signals with Rosman EIRP and Kings Point EIRP has been measured and presents no difficulty to control the power sharing function since both curves are smooth and appear more or less monotonic when the effect of measurement noise is considered.
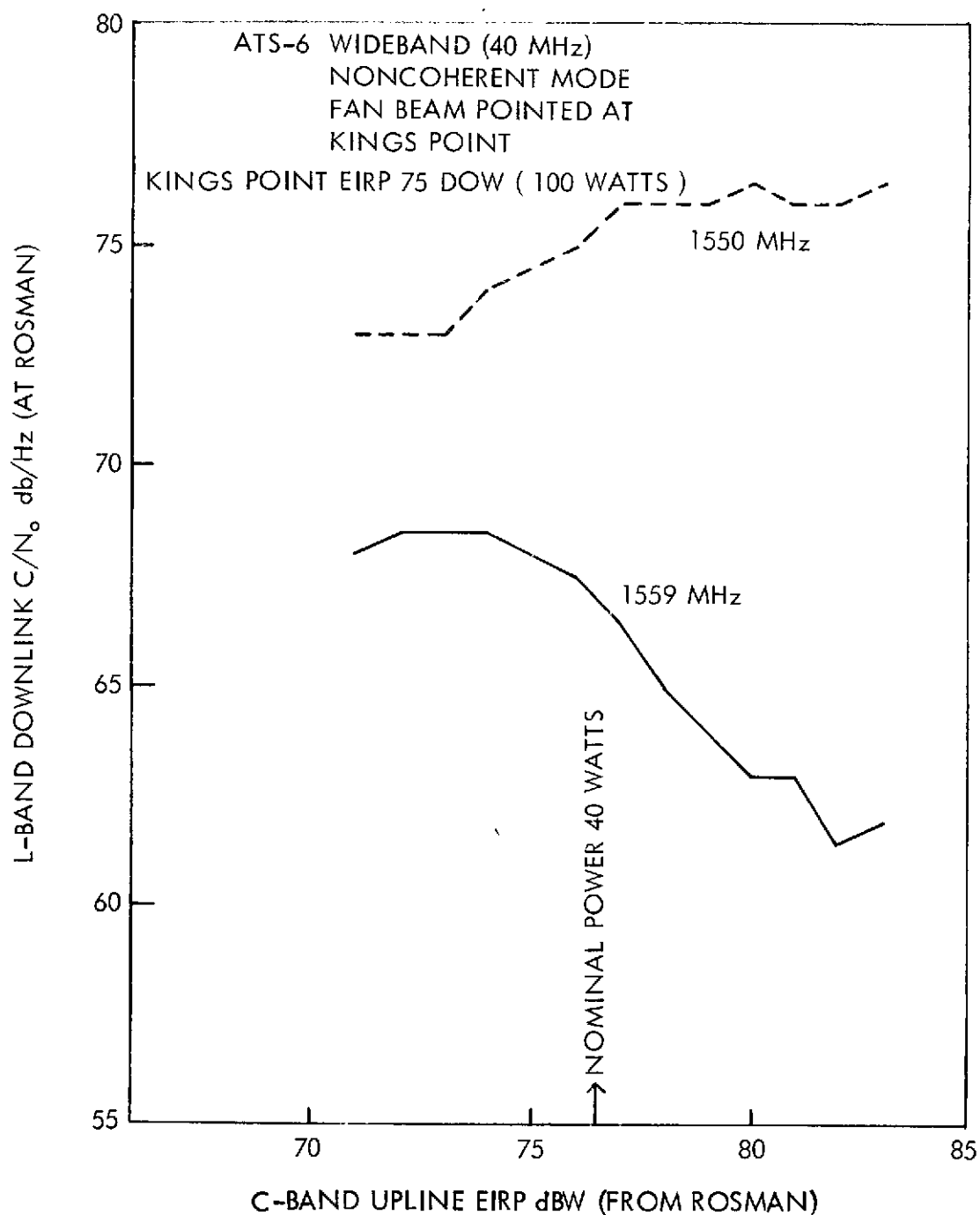
Figure 23-1. Forward Link Power Sharing (Data taken 7/1/74)

The figure is a graph. The y-axis is labeled "L-BAND DOWNLINK C/N$_0$ db/Hz (AT ROSMAN)" ranging from 55 to 80. The x-axis is labeled "C-BAND UPLINE EIRP dBW (FROM ROSMAN)" ranging from 70 to 85.

Annotations within the graph:
ATS-6 WIDEBAND (40 MHz)
NONCOHERENT MODE
FAN BEAM POINTED AT
KINGS POINT
KINGS POINT EIRP 75 DOW (100 WATTS)

1550 MHz (dashed curve)
1559 MHz (solid curve)
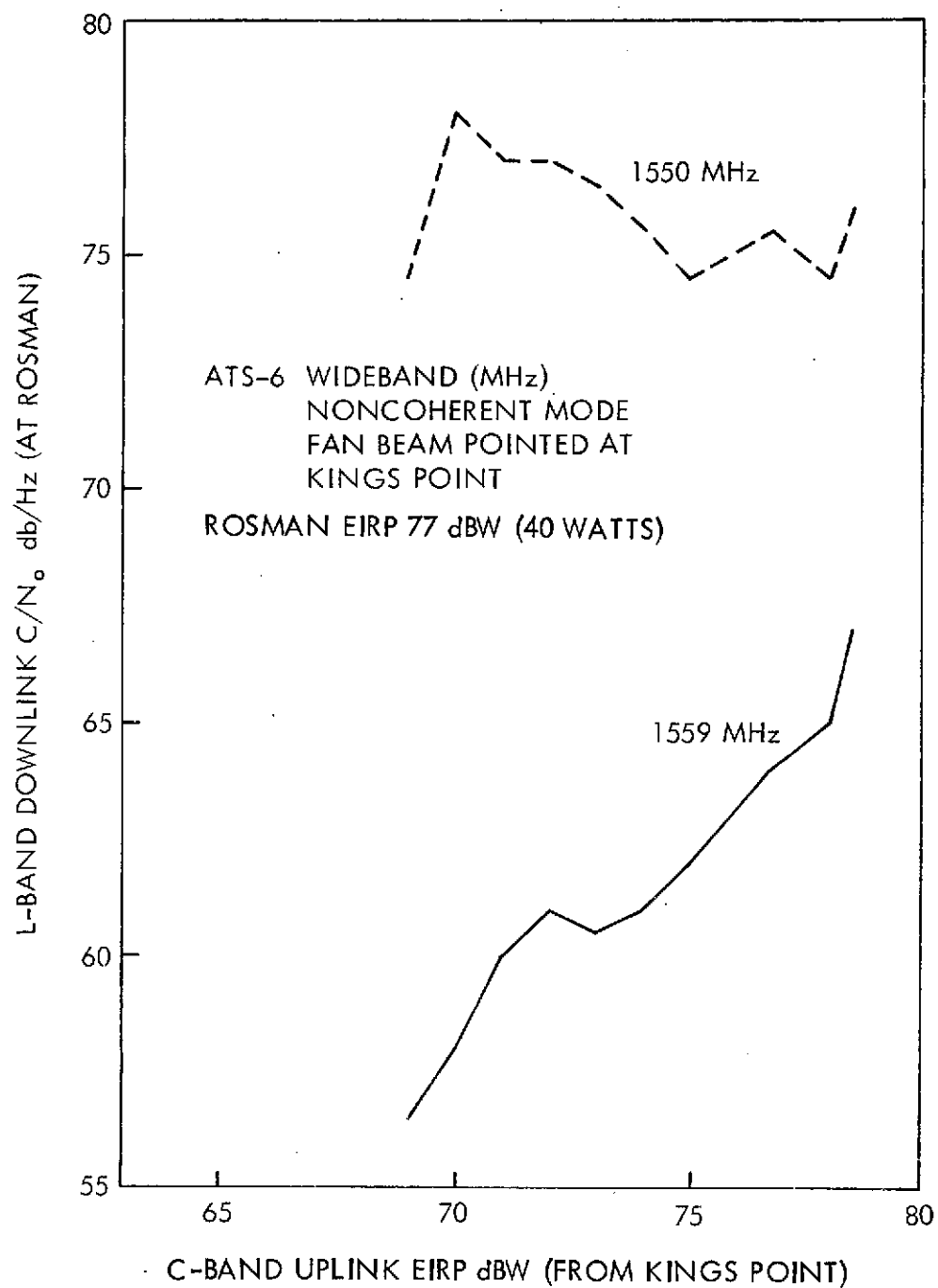NOMINAL POWER 40 WATTS

Figure 23-2. Forward Link Power Sharing (Data taken 7/3/74)

e. The calculated received C-band power levels at the satellite ECH antenna terminals is -90 dBm for noise alone, -77.6 dBm for the PLACE signal alone, -81.3 dBm for the Kings Point signal alone and -75.9 dBm for the two signals and the noise appearing simultaneously.

23.5.3.3 Return Link — Early tests on ATS-6 revealed difficulty in establishing communications in the return link (L- to C-band). This difficulty has been tentatively associated with wideband noise from the L-band transmitter used in the forward link (C- to L-band) being coupled into the L-band receiver causing saturation and desensitization. Fortunately, the presence of sufficient C-band signal power in the forward direction from Rosman appears to reduce the transmitted L-band noise and to eliminate the saturation problem.

The test was designed to show how the presence of any remaining coupled noise degraded the performance of the satellite return link. During this test the L-band fan beam was directed toward Rosman and the satellite was configured in the L to C and C to L cross-strap mode. Rosman and Kings Point both transmitted their nominal C-band uplink signals to the satellite at 40 watts and 100 watts respectively. Rosman then proceeded to transmit at L-band and receive the resulting C-band signal. Both the MARAD signal (1659 MHz) and the PLACE signal (1650 MHz) were sent at different times for the expected range of user terminal EIRP's through the satellite and back to Rosman at C-band where a determination of the received C/N_0 was made. These measurements were made with the satellite L-band transmitter turned on and with the transmitter turned off so that a measurement could be made with and without the additional coupled noise.

A calculation showing the expected C/N_0 as a function of return link EIRP is shown in Table 23-3. The actual measurements are shown in Figure 23-3 and these show the effect of cross-coupling between the L-band transmitter and L-band receiver on the satellite. The received Rosman C/N_0 at C-band is shown to degrade about 2 to 3 dB for the MARAD signal (1659 MHz) and about 1.5 dB for the PLACE signal (1650 MHz) when the L-band transmitter used for the forward link is switched on and with the ground stations operating at their nominal C-band power levels. The calculated link budget derived in Table 23-3 shows good agreement with the measured C/N_0 at 1559 MHz when the L-band transmitter is turned on. It should be noted that while PLACE and MARAD signals are degraded by L-band transmitter noise, the degraded signal levels agree with the theoretical calculation which indicates that no serious degradation occurs for either signal due to the presence of this noise. Further, the linear slope of the measured data also indicates that the L-band-to-C-band cross strap mode is operating in a linear fashion and is demonstrating no saturation effects due to this noise.

Table 23-3
ATS-6 Return Link Calculations Showing the Predicted Nominal C-band Received C/N_0 at Rosman vs Mobile Terminal L-band EIRP

User Terminal EIRP (dBW)	Watts		
Transmit Propagation and Pointing Loss (dB)			1.0
Transmit Free Space Loss (1659 MHz)			188.6
Satellite G/T (dB/$^\circ$K)			-2.5
Satellite Antenna Gain (dB)			30.8
Boltzman Constant (dBW/Hz-$^\circ$K)			228.6
Satellite Received Signal (dBW)			W-158.8
Satellite Received C/N_0 (dB-Hz)			W+36.5
Satellite Noise Bandwidth (MHz)			40
Satellite Received S/N (dB)			W-39.5
Satellite Total Transmit EIRP with C-band ECH (dBW)[1]			22.5
Assumed W (dBW)	40	30	20
Satellite Received Signal (dBW)	-118.8	-128.8	-138.8
Received Signal-to-Noise Ratio (dB)	0.5	-9.5	-19.5
Limiter Improvement (dB)	0.1	-1.1	-1.1
Received C/N_0 at ATS-6 (dB-Hz)	76.5	66.5	56.5
Transmitted C/N_0 (dB-Hz)	76.6	65.4	55.4
Transmitted Signal-to-Noise Ratio (dB)	+.6	-1.6	-11.6
Signal Degradation Due to Transmitted Noise (dB)	2.9	3.8	11.6
Transmitted Signal EIRP (dBW)	19.6	18.7	10.6
Transmit Free Space Loss (4 GHz)	196.8	196.8	196.8
Propagation and Pointing Loss (dB)	1.0	1.0	1.0
Rosman Receiver Antenna Gain (85') (dB)	58.0	58.0	58.0
Received Total Signal Power (dBW)	-120.2	-121.1	-128.9
Rosman Receiver G/T 85' Dish (dB/$^\circ$K)	40.6	40.6	40.6
Rosman C/N_0 From Ground System Noise (dB-Hz)	110.4	100.4	90.4
Rosman Resultant C/N_0	76.6	65.4	55.4

Notes:
1. This assumes a 4 dB reduction in C-band EIRP due to the presence of a 10 dB pad in the ATS-6 70-MHz IF

23.6 FUTURE PLANS

23.6.1 Routine Operations Checkout

The integrated L-band experiment is scheduled to commence on September 6, 1974 with the first flights of the ESRO Comet aircraft. During the interim period (August and the first week of September) system operations checkout will continue with the checkout of the Santiago Station, the aircraft PLACE avionics, and individual equipment testing for ESRO, TSC, and NAFEC. MARAD will continue
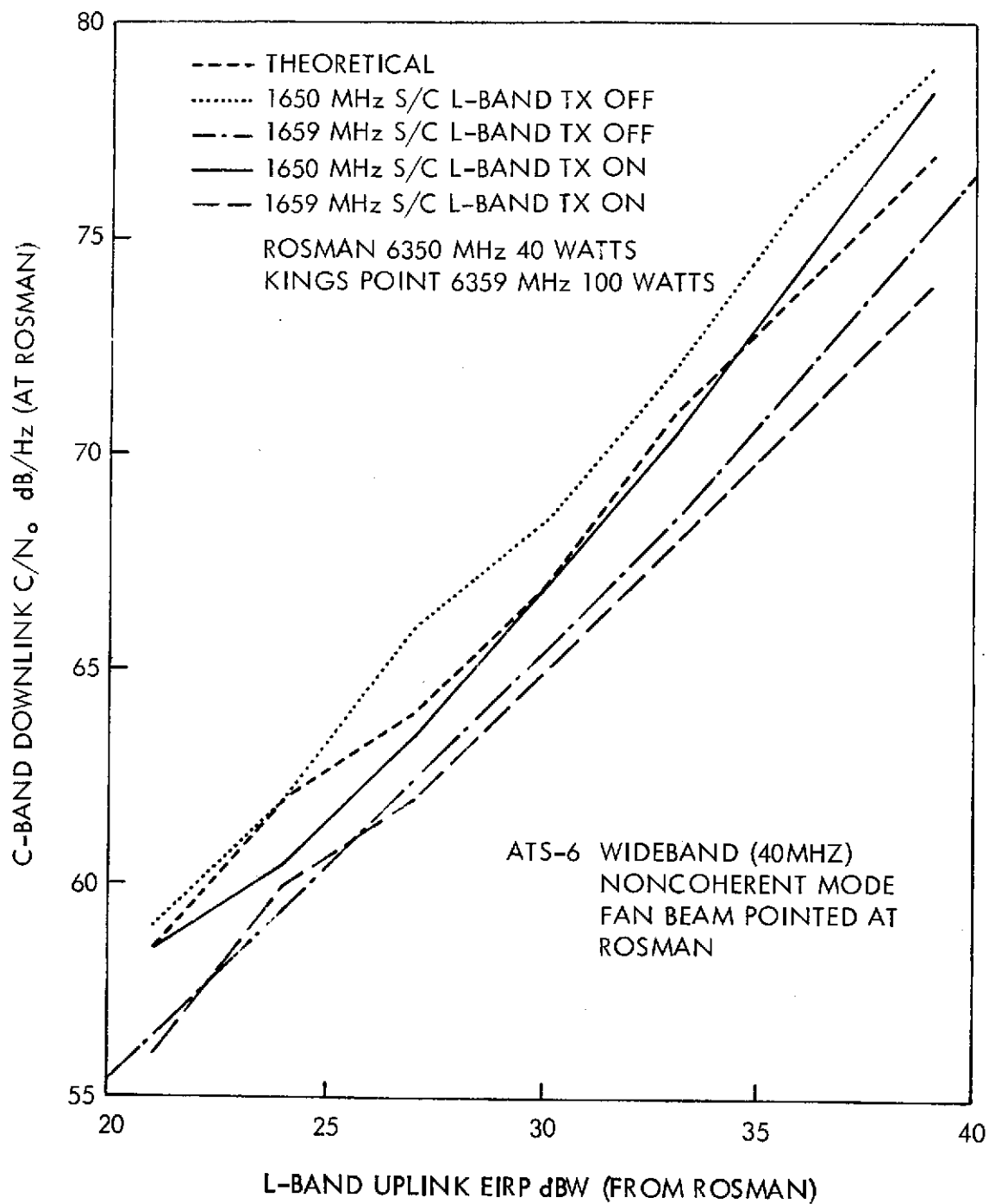
Figure 23.3 Return Link C/N_0 (Data taken 7/19/74)

in the power sharing mode the testing of modems and shipboard units. Bit-error rate data tests and some preliminary voice data tests will be conducted.

The Maritime Ship "American Ace" will sail on August 14, 1974, conducting communication tests underway via the ATS-6 L-band experiment system. This will be the first mobile unit in the system.

23.6.2 Special Tests

ATSOCC has planned a series of special tests in support of the L-band system evaluation. These tests will evaluate the following:

  a. The frequency dependent desensitization of the spacecraft L-band system

  b. Spacecraft frequency stability

  c. The compatibility of experiments; i.e., Beacon, VHRRE

These tests will be conducted when spacecraft time can be made available. The data from test (a) will help to define the characteristics of the spacecraft anomaly discussed in section 1.3.

It is recommended that L-band fan beam antenna pattern measurements be made which will provide spacecraft pointing information needed to optimize sidelobe coverage of the ground stations (Mojave, Santiago, Rosman, and Kings Point) while the fan beam main lobe is illuminating the North Atlantic operating region.

SECTION 24

RADIO BEACON EXPERIMENT
(RBE)

SECTION 24

RADIO BEACON EXPERIMENT
(RBE)

24.1 INTRODUCTION

The 360-MHz and 140-MHz transmitters are operating as predicted; however, the 40-MHz transmitter shows combinations of anomalies which may indicate a poor antenna match. The carrier ALC loop is out of the telemetry range, indicating that it is unable to maintain desired carrier level into the antenna impedance. The engineering model transmitter and the Boulder satellite mock-up are being employed to study the anomalies.

The RBE transmitters and modulation were turned on June 2, 1974. They have remained on almost continuously since then. During this time, ground receiving monitoring has continued from Stanford University, University of Illinois, and the Air Force Cambridge Research Laboratory. Boulder receiving became operational two weeks after the turn-on time.

Evaluation of the extent of successful achievement of the scientific objectives of the experiment is in an early stage. However, at least two new significant physical results have been identified in the preliminary work. The first pertains to the vertical movement of the ionosphere at dawn, and the second to the height at which additional ionization was produced during the recent large solar flare, as determined using the combined group-delay and polarization measurements.

24.2 SCIENTIFIC OBJECTIVES

The radio beacon experiment provides a multifrequency spacecraft-to-ground radio link for investigating particles which affect radio propagation beyond the atmosphere.

24.3 EXPERIMENT DESCRIPTION

The beacon is designed for several types of measurements, principally: Faraday rotation, differential phase (Doppler), phase and amplitude scintillation, and signal amplitude (absorption). The 40-MHz carrier is amplitude stabilized to enable accurate absorption measurements to be made. The mode of operation calls for continuous emission on all frequencies. There is no provision for intermittent operation unless a failure occurs nor for variation of frequencies. The overall design of the beacon is intentionally simple to improve the prospects of continuous operation and to eliminate the need to alert many observers to frequent changes in schedules.

There are three carrier frequencies: 40.0160 MHz, 140.056 MHz and 360.1440 MHz. All radio signals are derived from a common oscillator. Amplitude modulation frequencies are 100 kHz (on the 40-MHz and 360-MHz signals) and 1000 kHz on all three carrier frequencies. The phase reference for the modulation signals is the 100-kHz modulation on the 360.1440-MHz carrier.

All beacon signals are linearly polarized. Since the spacecraft is attitude controlled, it is possible to define the orientation of the emitted polarization. Differential Faraday measurements are possible using carriers and sidebands.

24.4 EXPERIMENT PERFORMANCE EVALUATION

24.4.1 General Summary

This Section covers approximately 2 months of prelaunch activity and 2 months of postlaunch and post radio beacon turn-on activity. During the prelaunch period, the primary activities were reduction of the thermal vacuum test data, program development for both the online and offline computers, and ground antenna construction. In addition, some special tests were carried out using the engineering model transmitter and the satellite mockup to assist in explaining anomalies which were noted in final satellite level testing of the flight transmitter.

The Radio Beacon Experiment transmitter was turned on and left on somewhat earlier in the postlaunch checkout procedure than had been anticipated, and the final installation of feeds and matching adjustments of the ground antennas at Boulder had not been completed. These were completed over the next two weeks and all transmissions were received at close to nominal strengths when the antennas were connected to the receiver. Receiving equipment at Stanford University, University of Illinois, and the Air Force Cambridge Research Laboratories has also been in operation since the turn-on. Receiving systems of the Max-Planck Institute for Aeronomy are in process of installation at Bozeman, Montana; Dallas, Texas; and Elbert, Colorado.

Enough ground data and satellite housekeeping data have now been accumulated to make a preliminary evaluation of the engineering performance of the transmitter and the Boulder receiving system. The transmitter performance at 360 MHz and 140 MHz appears to be close to nominal in EIRP observed on the ground and telemetered forward power. Larger variations in 360 MHz EIRP ($> \pm2$ dB) are being observed as the satellite dish is changed in pointing angle than were expected from the preflight polar diagrams. The reason for this is not known. The 40-MHz carrier EIRP is close to nominal. However the carrier ALC control voltage is out of telemetry range in a negative direction indicating that the impedance seen by the transmitter output stage is incorrect and the

1-MHz side band EIRP is significantly unbalanced indicating a change in transmitter output tuning. Taken together, this seems to indicate that the 40-MHz flight antenna in orbit has a much higher VSWR than that measured in antenna range testing. Measurements are planned using the engineering model transmitter and the Boulder satellite mockup to try to duplicate the observed flight conditions and reestablish a calibration of radiated modulation phase.

The general performance of the Boulder receiving system appears to be very close to predictions and prelaunch measurements. No unexpected difficulties have arisen.

Evaluation of the extent to which the scientific objectives of the overall experiment will be met are in an early stage. Preliminary cross checking of the data for consistency gives satisfactory relative agreement between the group delay and Faraday effect measurements at the two frequencies. Spot checks of plasmaspheric content and ionization transport fluxes give reasonable values. Work to try to establish the validity of the absolute calibration of the system is in progress now. At least two new significant physical results have been identified in the preliminary work so far. The first shows that vertical movement of the ionosphere at dawn is very significant in the interpretation of polarization; however, measurements are questionable. Secondly, the use of the combined group delay and polarization measurements has enabled measurement of the height at which additional ionization was produced during the recent large solar flares. A wealth of data on ionospheric irregularities is clearly available from the 40 MHz data which show unexpectedly great scintillation activity for a midlatitude site. Phenomena such as coherent interference patterns from moving discontinuities which were thought to be rare have been routinely observed, and there is clearly scope for much new scientific interpretation of these new data.

The following sections treat the various topics summarized in this introduction in more detail.

24.4.2 Thermal Vacuum Test Data

Data from the Boulder receiver teletype printout were presented in earlier reports. Some difficulties were encountered in reading the digital tapes due to the discontinuities in recording. These were overcome and a considerable amount of data have been reduced. The biggest difficulty has been the correlation of the telemetry tape data which appear to be somewhat discontinuous.

A particularly convenient period for studying the temperature performance of the transmitter is that from 050:2320 to 051:0400 when the temperature indicated by the oscillator thermister changed from +11°C to 38°C. Computer plots of the modulation phase data are shown in Figures 24-1 through 24-4. Table 24-1 shows
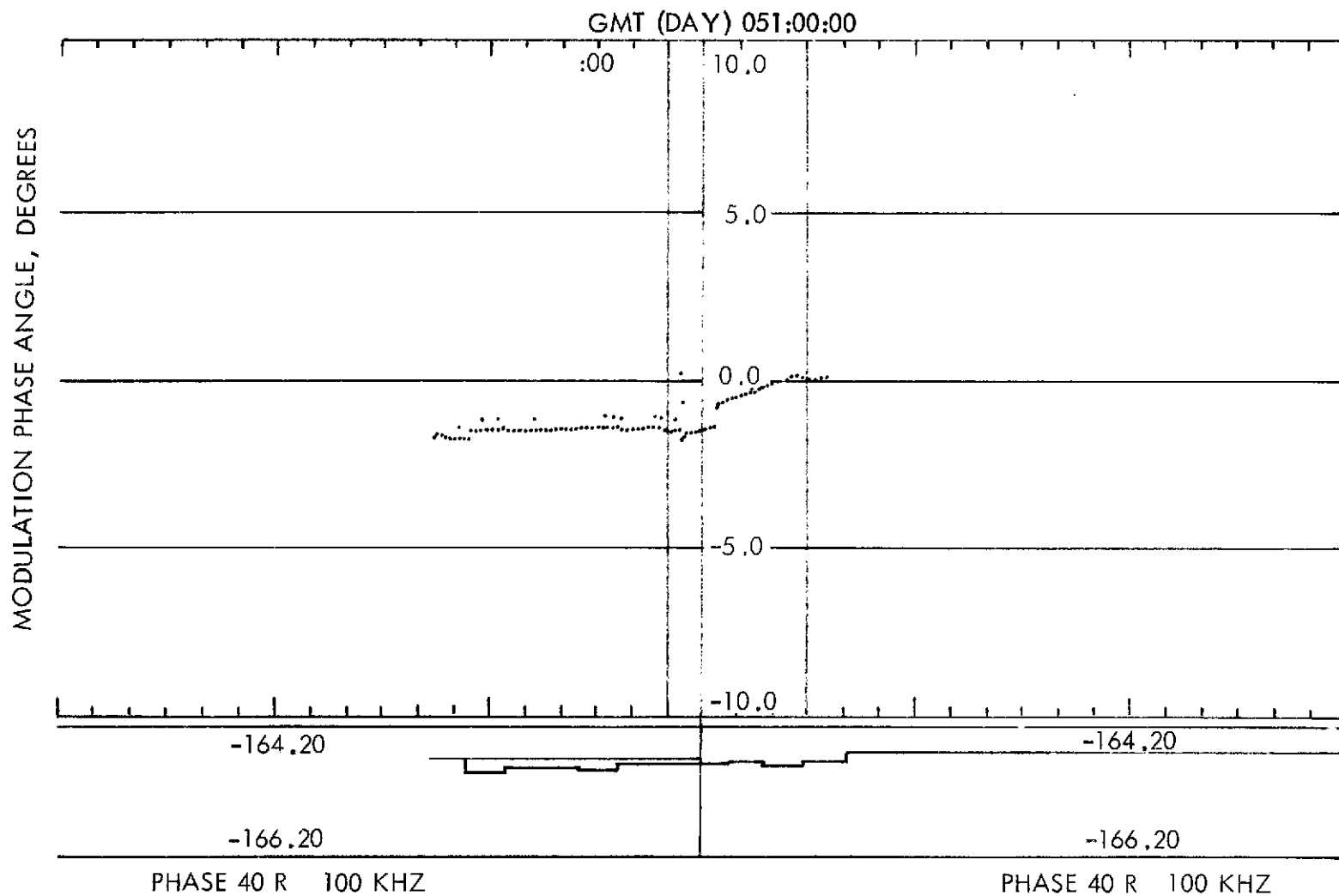
Figure 24-1. Modulation Phase Angle vs Time, Day 051
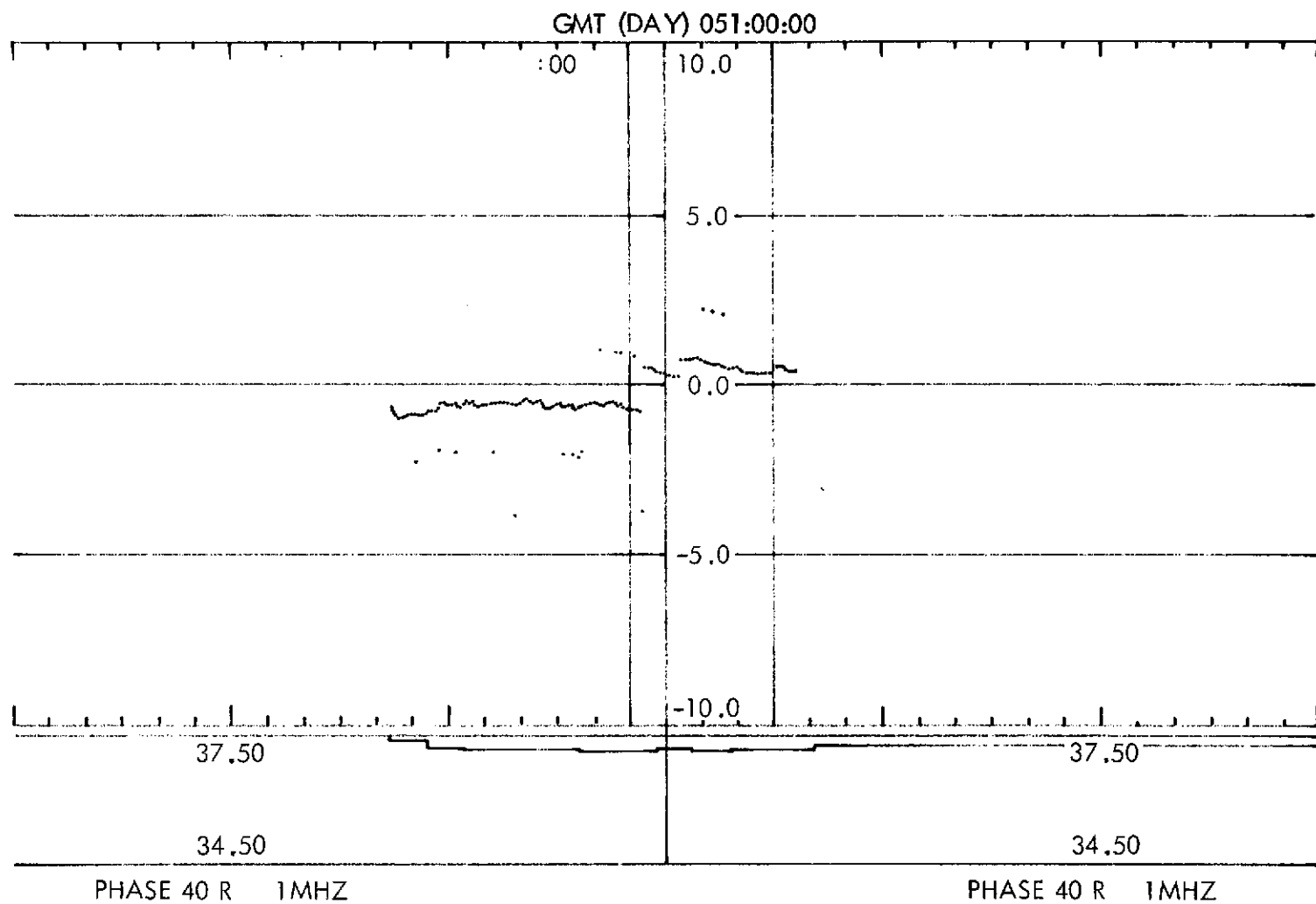(100 KHz Modulation, 160 MHz Beacon)

Figure 24-2. Modulation Phase Angle vs Time, Day 051
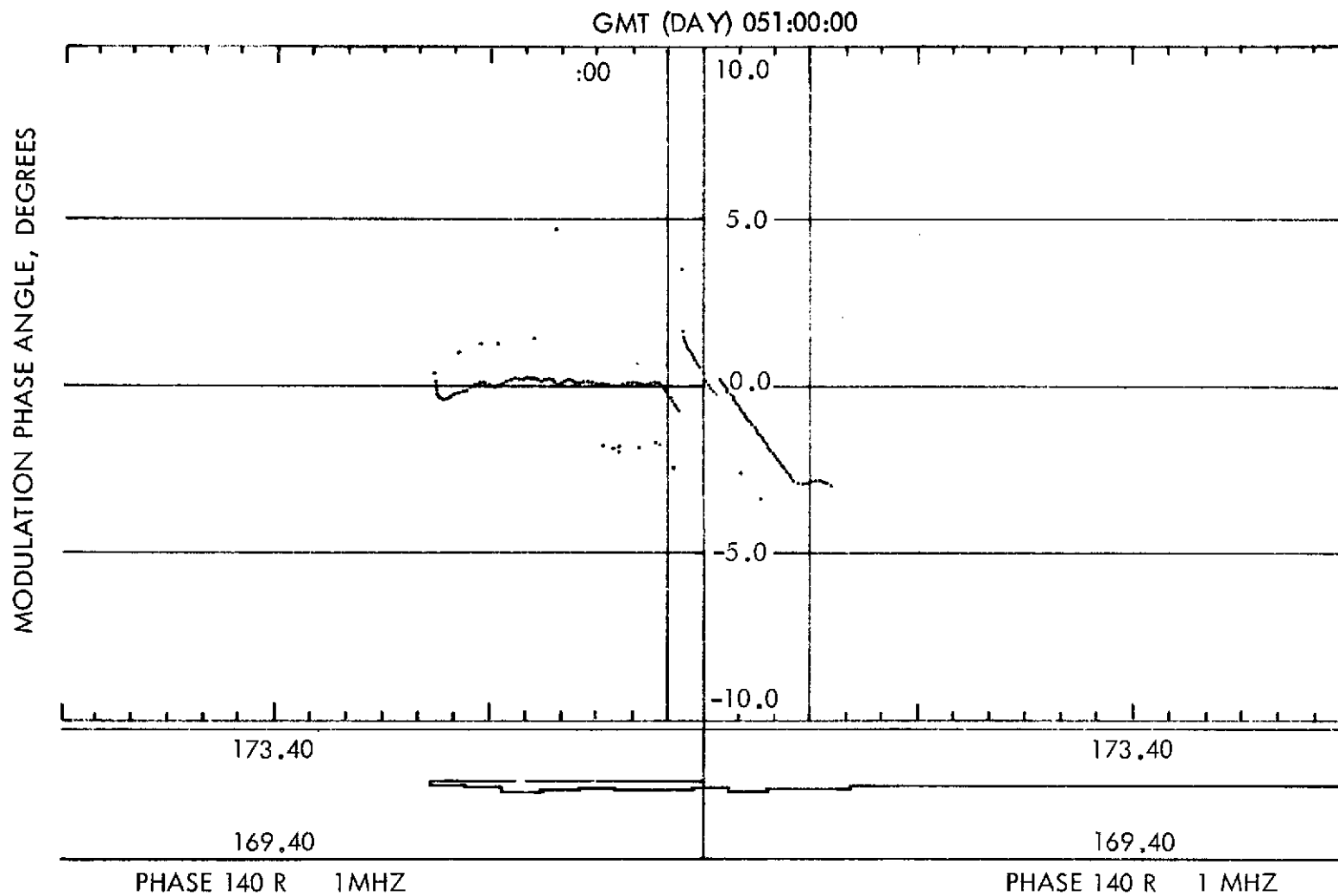(1 MHz Modulation, 40 MHz Beacon)

Figure 24-3. Modulation Phase Angle vs Time, Day 051
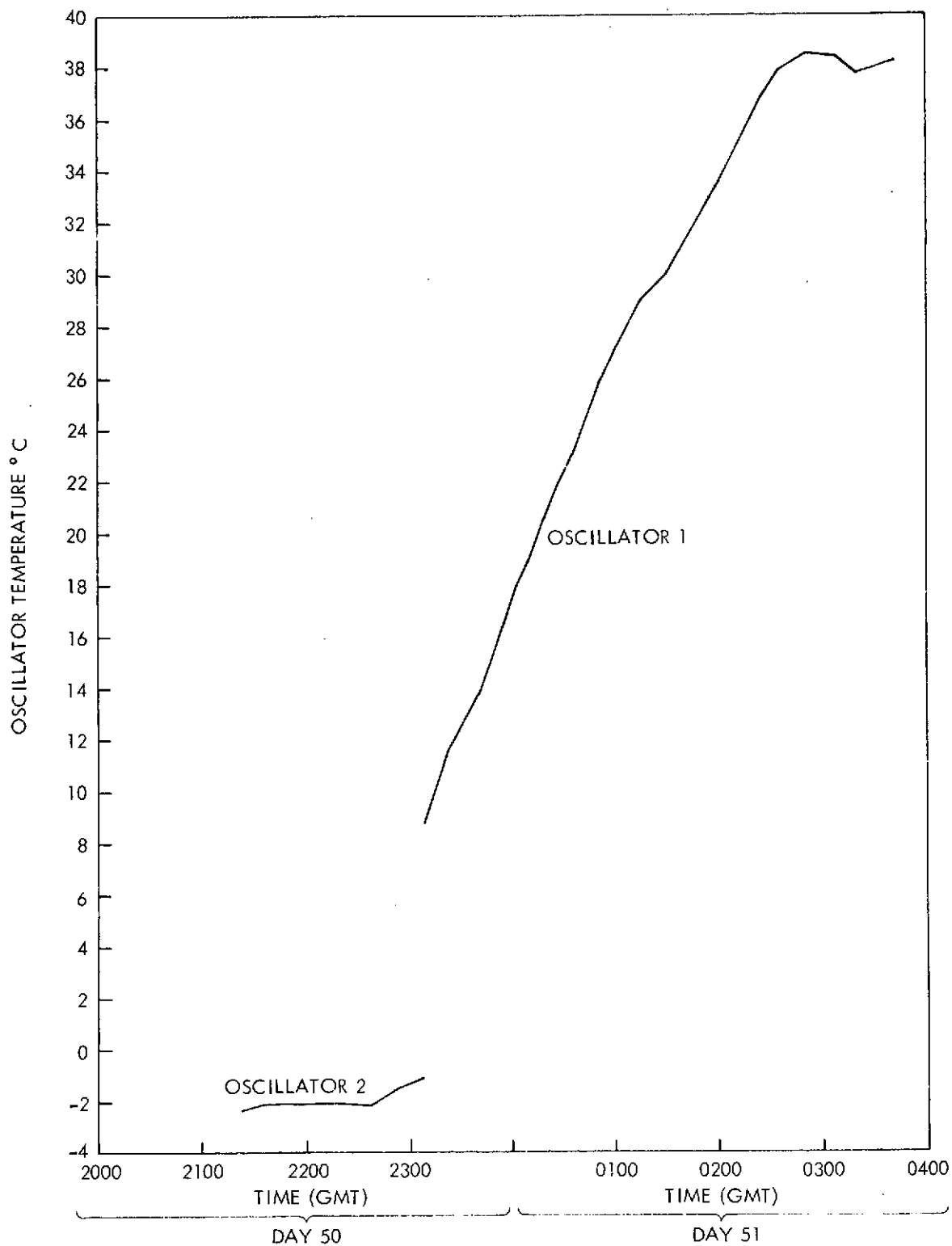(1 MHz Modulation, 160 MHz Beacon)

Figure 24-4. Oscillator Temperatures vs Time, Days 050 and 051

Table 24-1
Thermal Vacuum Test Modulation Phase vs Temperature

Time		Osc. 1 Temp.	TX			CAL.		
			40 100 K	40 1 M	140 1 M	40 100 K	40 1 M	140
1859	Day 50	+2.3°C	-166.4	+38.2	173.8			
2320		+11°C	-166.9	+37.7	+173.2			
2341		+13°C	-166.5	+37.5	+172.2	-163.9	+25.4	-130.8
0002		+17°C	-166.4	+37.3	+171.7			
0023		+20.5°C	-165.6	+38.0	+171.7			
0043		+24.4°C	-165.3	+37.9	+171.2	-163.9	+25.4	-130.8
0105		+27.4°C	-165.2	+37.7	+170.7			
0125		+29.6°C	-165.2	+37.7	+170.1			
0146	Day 51	+31.6°C	-165.0	+37.7	+169.7	-163.9	+25.4	-130.8
0207		+34.6°C	-164.8	+37.6	+169.2			
0228		+37.0°C	-164.7	+37.5	+168.7			
0249		+38.3°C	-164.6	+37.5	+168.6	-164.0	+25.4	-130.8
0310		+38.2°C	-164.7	+37.7	+168.7			
0331		+38.0°C	-164.6	+37.7	+168.6			
0406		?		TX OFF		-163.7	+25.6	-130.5

the numerical data. The discontinuity at ≃ 2310 is due to a change from oscillator 1 to oscillator 2. The reason for the discontinuity at approximately 0030 is not known precisely. It may be related to other discontinuities which appear to be due to slightly intermittent contacts in the coaxial relays in the receiver used to permit changeover between the transmitter and the calibrator. Clearly, the performance of the transmitter into 50-ohm loads is quite satisfactory. Table 24-2 shows spot values of the transmitter modulation phase measured by the receiver over the whole 32 day period. Little or any systematic change is evident.

24.4.3 Preflight Satellite Level Tests

All-up radiating tests of the transmitter into the flight antennas were carried out at Fairchild as part of the overall system compatibility tests. The satellite was placed in a temporary RF anechoic environment using microwave absorbing material. Due to the height of the EVM truss assembly, the radio beacon antennas were within a few feet of the floor of the test area. When radiating tests were made, the 360- and 140-MHz systems performed satisfactorily, but the 40-MHz transmitter showed anomalous behavior. The ALC voltage monitor

Table 24-2

Flight Transmitter, Modulation Phase Overall Thermal Vacuum Test Summary

Time	Osc. #	Pressure	Temp.	40-100 K	40-1 M	140-1 M
057:17:17	1	10^{-6}	23.0°C	-166.2	+36.9	+171.4
057:12:23	1	10^{-6}	21.2°C	-166.2	+36.8	+171.6
050:16:20	2	10^{-6}	+6.5°C	-166.9	+36.6	+172.3
050:17:44	2	10^{-6}	+3.9°C	-166.5	+36.4	+171.5
050:19:28	2	10^{-6}	+3.3°C	-166.5	+36.5	+171.5
049:18:59	1	10^{-6}	+2.3°C	-166.4	+38.2	+173.8
049:14:41	1	10^{-6}	+2.0°C	-166.7	+37.9	+173.7
049:07:08	1	10^{-6}	+3.7°C	-166.6	+37.9	+173.4
047:05:08	1	10^{-6}	-2.1°C(L)	-166.7	+38.3	+173.5
036:15:21	1	ATM	+16.5°C	-166.3	+37.0	+171.5
033:06:25	2	ATM	≈17°C	-166.3	+35.7	+168.9
033:11:21	1	ATM	+17.1°C	-166.4	+37.3	+171.4
025:06:04	1	ATM	+19.2°C	-166.91	+35.1	+169.5

showed a reading of 0.00 indicating a zero or negative voltage. This indicated that the control loop was unable to maintain the carrier output voltage at the set level into the antenna impedance, suggesting that the impedance was significantly different from the nominal 50 ohms. Since no data had been taken previously on the sensitivity to mismatch of the ALC circuit, a series of tests were carried out by SEL on the engineering model transmitter. The ALC loop voltage, the Pin diode control voltage, the power monitor voltage, and the actual total power out and the carrier level measured with the ground receiver were recorded as the output load was varied in magnitude and phase angle. The results obtained are shown in Table 24-3. Using resistive load values only, Figure 24-5 shows that the ALC telemetry voltage goes negative for loads of $\leq$ 31 ohms or a VSWR of 1.6:1. It would not be expected that the ALC voltage would be a simple function of VSWR or of the magnitude of the impedance at the transmitter terminals when this is reactive. The test results give a general indication of the sensitivity however. The specification for the flight antennas calls for the VSWR to be less than 1.5. The values measured on the flight 40 MHz antenna under mockup conditions were < 1.2. Thus the tentative conclusion was that the condition seen in the all-up radiating test was due to the proximity of the floor causing an increased SWR in the 40-MHz antenna. A request was made to move the satellite assembly to increase the spacing between the antenna and the floor, but this was not possible.

A further test was made to check the performance of the engineering model transmitter operating into the Boulder satellite mockup. The significance of results of this test are difficult to evaluate because it was not possible to match

Table 24-3
40 MHz Engineering Model Transmitter Dummy Load Tests

Termination (ohms)	VSWR	Total Power Out (W)	Power Monitor T/M (V)	ALC T/M (V)	Pin Diode Voltage (V)	Received Carrier Level
50	1.0	1.36	4.68	+1.67	.584	1.977
61	1.22	—	4.64	+2.38	.578	1.965
50	1.0	—	4.70	+1.66	.583	1.966
41	1.22 ·	—	4.78	+0.80	.588	1.964
50	1.0	1.36	4.72	+1.64	.582	1.966
25	2.0	—	4.83	−0.56	.604	1.865
50	1.0	1.36	4.75	+1.61	.581	1.958
50 (1+j 0.7)	2.0	—	4.64	3.79	.561	1.968
50	1.0	—	4.76	1.61	.579	1.960

Note: Readings were taken in the sequence shown to allow for thermal drift in the transmitter.
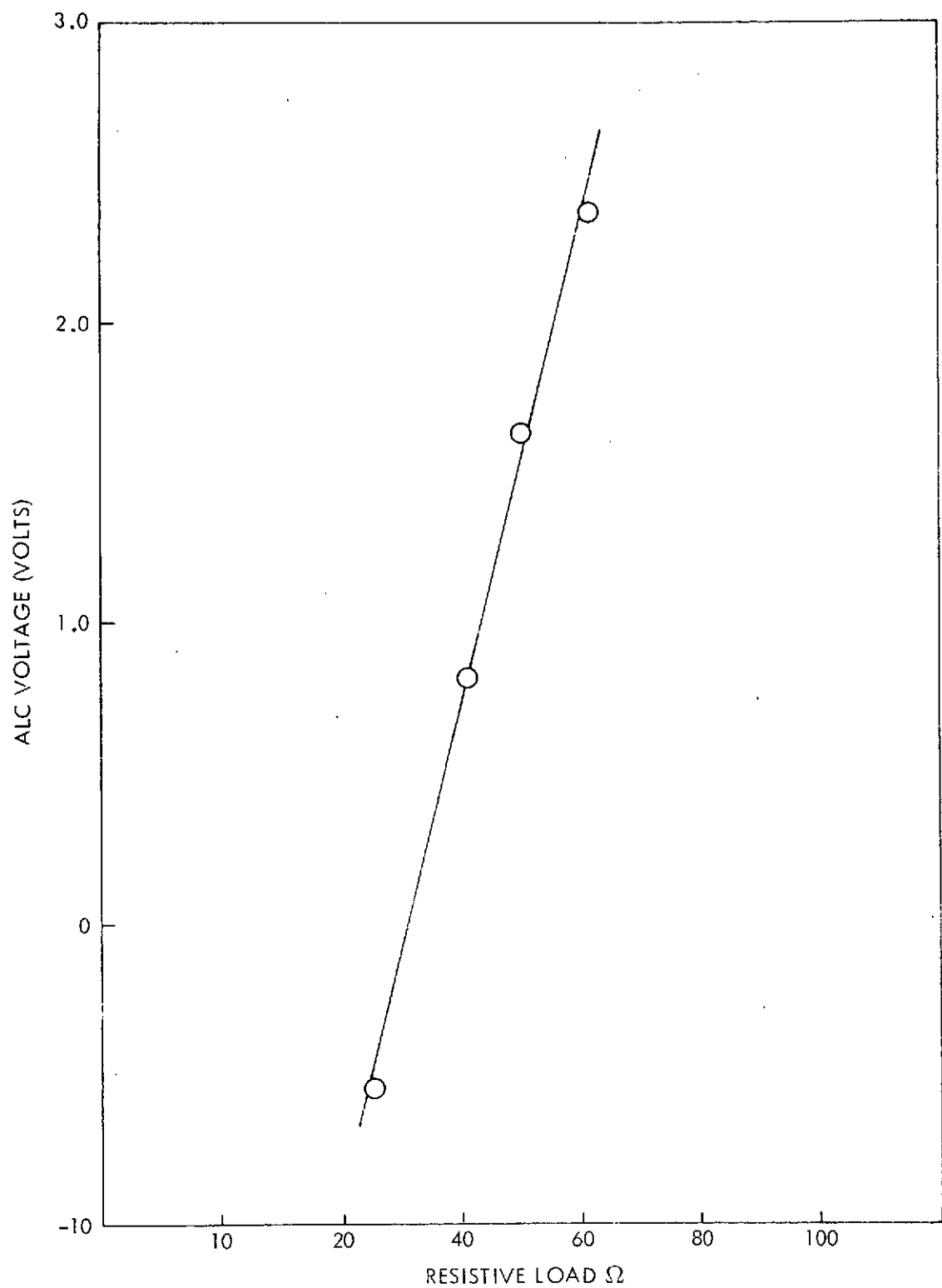
Figure 24-5. 40-MHz ALC Voltage Versus Transmitter Resistive
Load (Engineering Model)

24-11

the 40-MHz mockup antenna to better than 1.6:1 VSWR using the procedure specified for the flight antenna. In addition, any deficiencies in the Boulder mockup of the satellite might have been expected to be of least effect at 40 MHz. The test showed that the ALC voltage also went to zero or slightly negative and the results were relatively insensitive to the exact position of the antenna elements. The 40-MHz power monitor read $\simeq 10\%$ higher in voltage than when terminated in 50 ohms. At the time this test was completed, further satellite level testing of the flight system was impossible.

24.4.4 Boulder Ground Antenna System

Work continued until just before launch to complete the basic antenna reflector structures. The feed structures and matching adjustments were completed in the two weeks following launch. All the basic feeds have a VSWR < 1.2:1 and cross polarization coupling of < 20 dB. Total array VSWR including the power summers is < 1.4:1.

All the antennas are of the Short Backfire type described by Ehrenspeck. This design was chosen because of its favorable properties of low side lobe level, wide bandwidth, and high aperture efficiency. The 40-MHz antenna is a reduced size reflector modified and model tested by the Max-Planck Institute for Aeronomy at Lindau for this application. The 140-MHz antenna is the 4-element and the 360-MHz antenna is the 8-element array described by Ehrenspeck. Figures 24-6 through 24-10 are photographs of the antennas. It is planned to make gain and group delay calibrations by flying the engineering model transmitter through antenna beams. In lieu of these data, the basic properties of the antennas measured by MPI or Ehrenspeck are being used. These are tabulated in Table 24-4.

Table 24-5
Properties of RBE Antennas

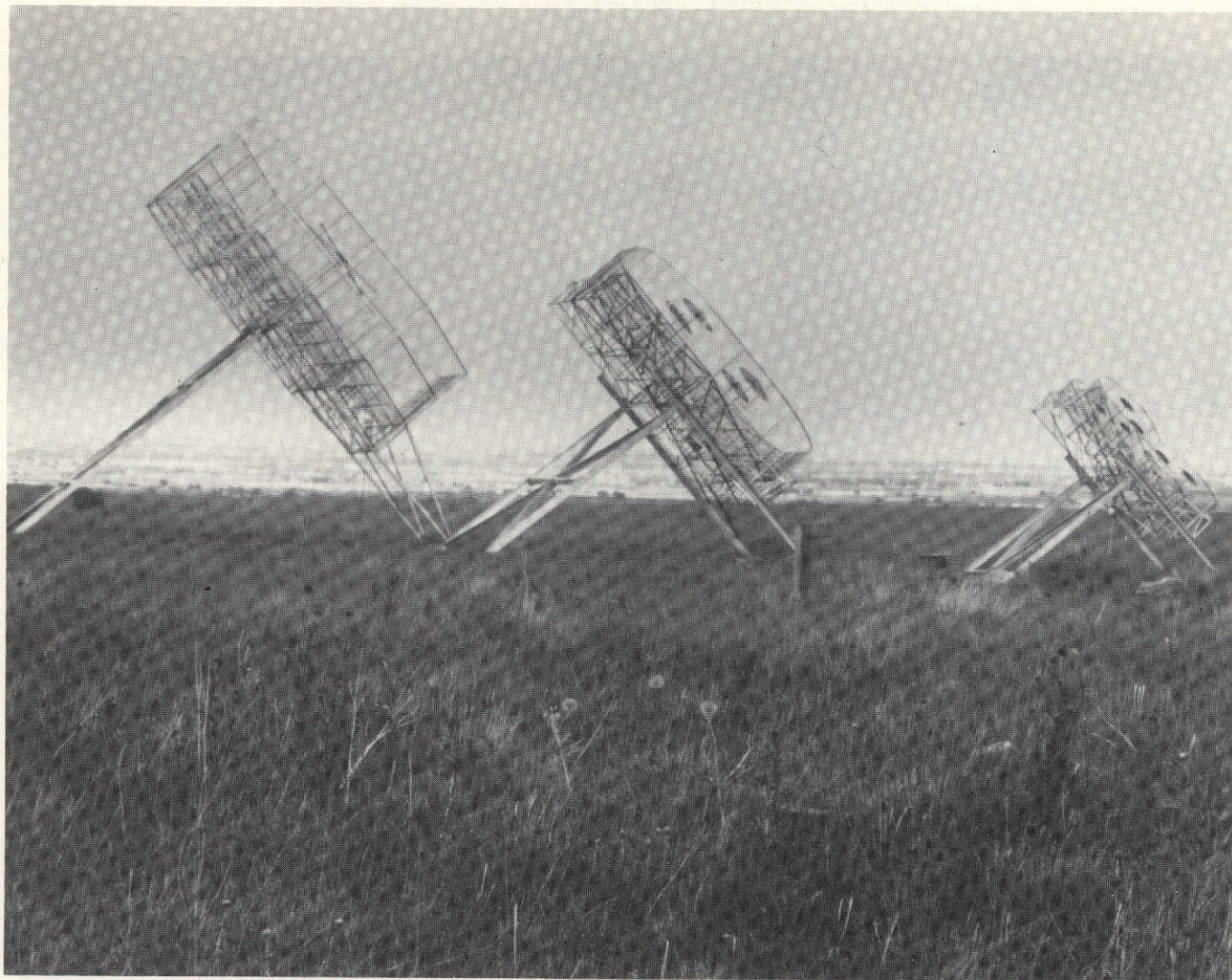| Frequency	Directivity	Beamwidth	First Side Lobe Level	Feed Loss	Assumed Net Gain
40	13 dB	–	-20 dB	1 dB nominal	12 dB
140	19 dB	22°	-18.5 dB	1 dB nominal	18 dB
		←——— Ehrenspeck ———→			
360	22 dB	15°	-17 dB	1 dB nominal	21 dB
		←——— Ehrenspeck ———→			

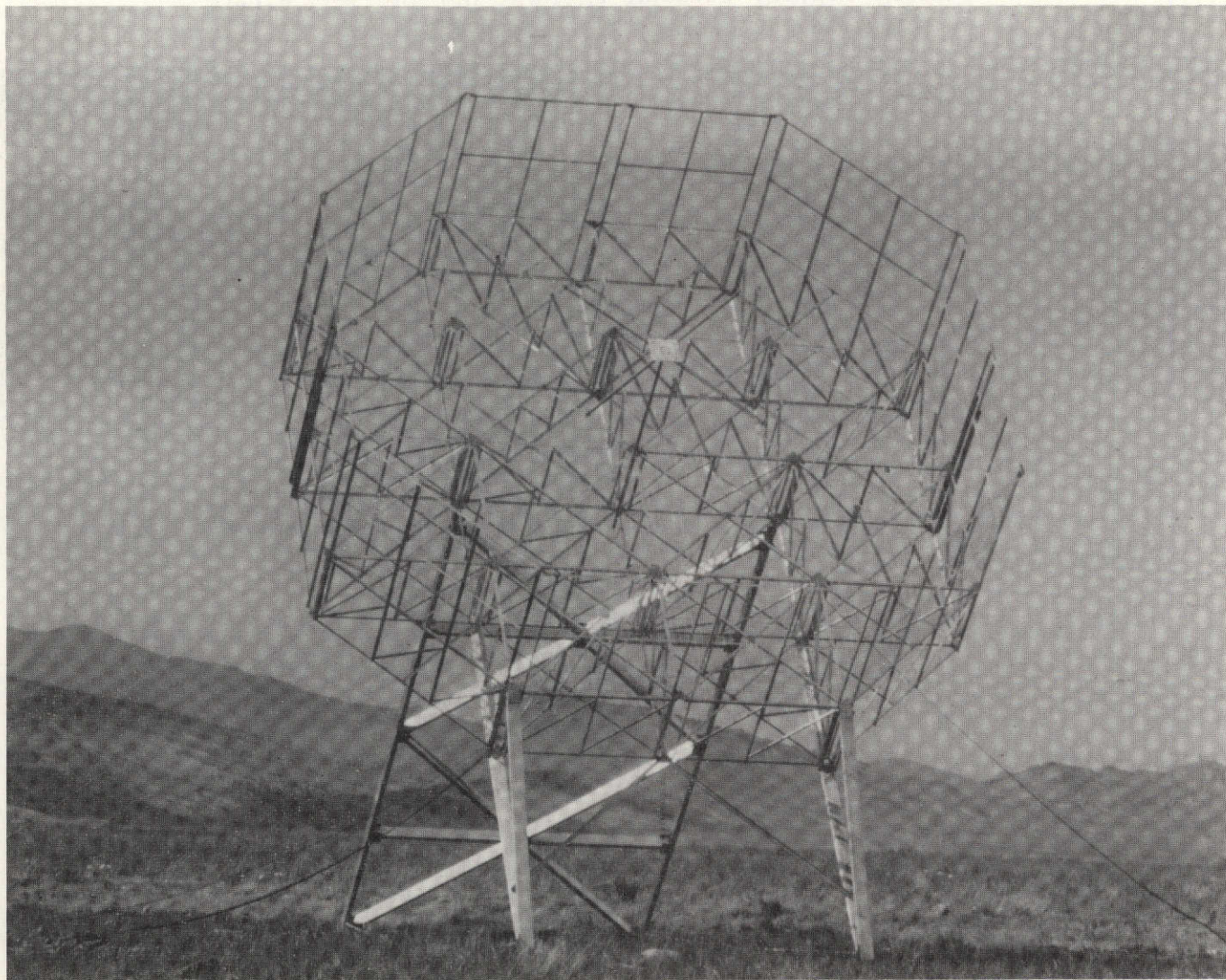Figure 24-6. 40, 140, 360 MHz Antennas, Boulder, Colorado

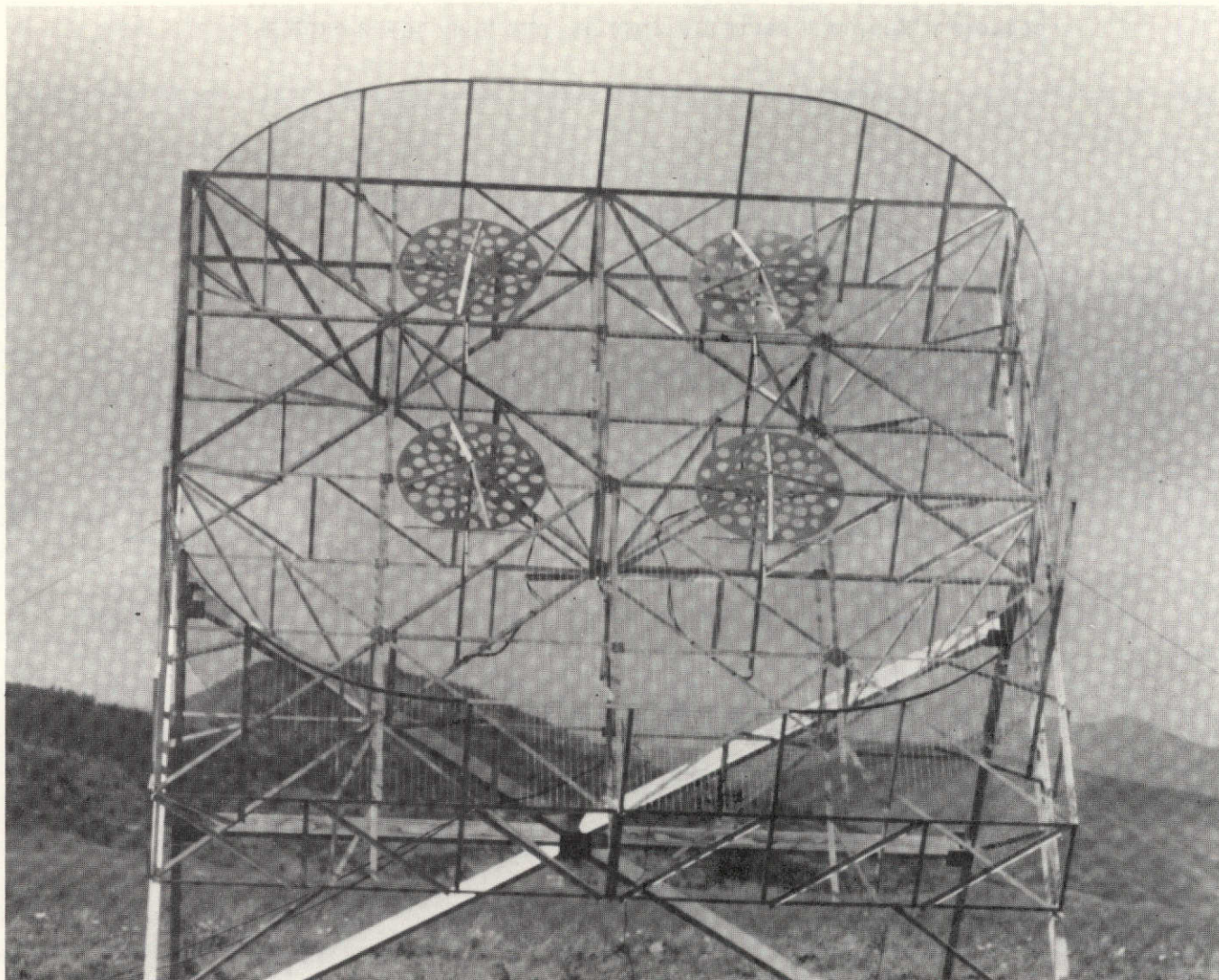Figure 24-7. 40 MHz Antenna, Boulder, Colorado

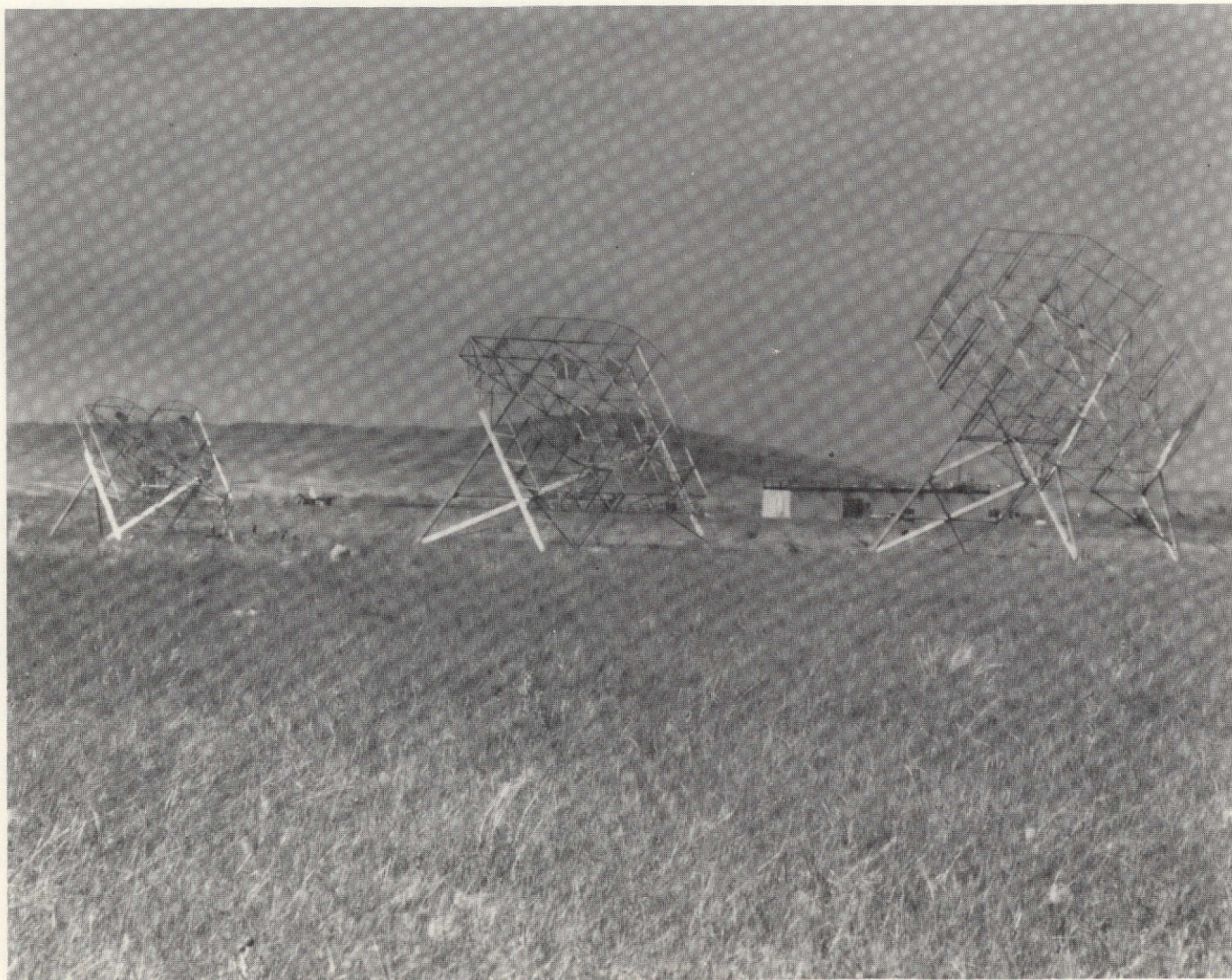Figure 24-8. 140 MHz Antenna, Boulder, Colorado

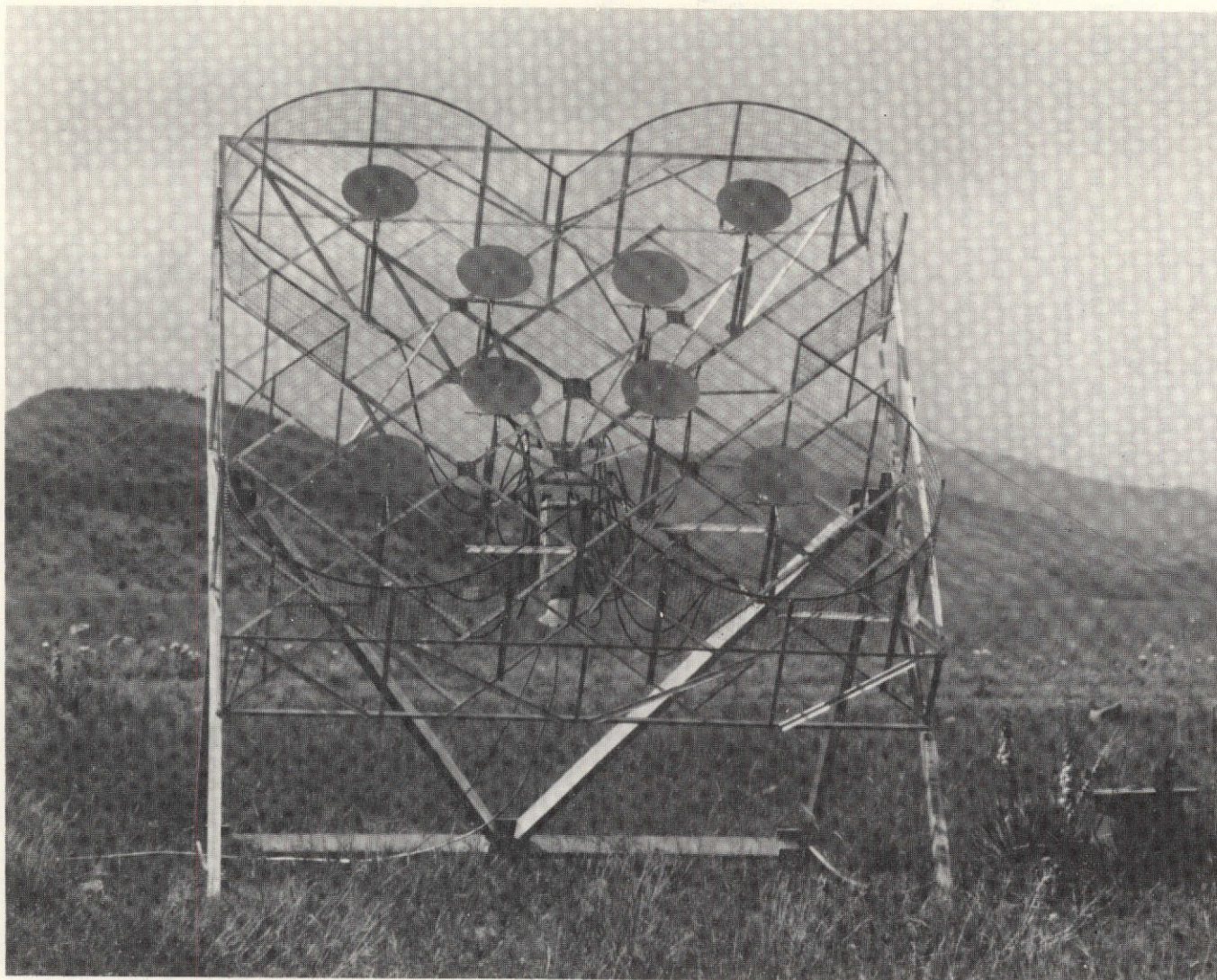Figure 24-9. 360, 140, 40 MHz Antennas, Boulder, Colorado

Figure 24-10. 360 MHz Antenna, Boulder, Colorado

24.4.5 Postlaunch Receiver Evaluation

No basic unexpected problems have arisen with the Boulder ground installation. All signals were received at the expected level as soon as the antenna was connected to the receiver. The carrier phase measuring unit was completed and has been operating satisfactorily. Initial recording was carried out using the online computer software used during the Fairchild thermal vacuum tests. This has now been replaced with the more flexible task oriented system. All the planned online tasks are now operating with the exception of the computer controlled AGC and PLL acquisition task. This is written but has not been debugged. However present operating experience suggests that fixed gain operation and the present simple PLL reset program is satisfactory.

Two unanticipated minor problems have arisen. The 40-MHz carrier PLL is transiently unlocked by spherics during local thunderstorm activity. This has a very minor effect on modulation phase recording but causes discontinuities in the carrier phase. The effect can be considerably mitigated by operating with 3-Hz bandwidth rather than 10 Hz. However this change tends to cause problems during scintillation. It is possible that an improvement can be obtained by signal clipping prior to the IF filters and prior to the phase detector to reduce the energy within the PLL bandwidth. Alternatively, the computer could be programmed to select the 3-Hz bandwidth when spheric, but not scintillation activity, is present. The second problem was an unexpected instability in the calibration of the 140 MHz polarization measurement channel. This appeared to be diurnally related and a thermal effect was suspected. After the preamplifiers had been exonerated, it was noticed that the thermal time constant was very fast, only a few minutes. This suggested that differential expansion of the signal cables was responsible, only 1 part in 1000 mismatch in phase velocity being required to explain the observed variations. This explanation was confirmed and the problem almost completely alleviated by burying the long horizontal cable run from the antenna to the receiver.

A program of receiver performance verification tests has been planned. With the exception of received power calibrations and antenna polarization verifications, these have been postponed until more data have been accumulated from the spacecraft transmitter.

A typical set of quick-look digital plots of data from the system is shown in Figures 24-11 through 24-14.

Figure 24-11. Phase Angle of 100 KHz Modulation
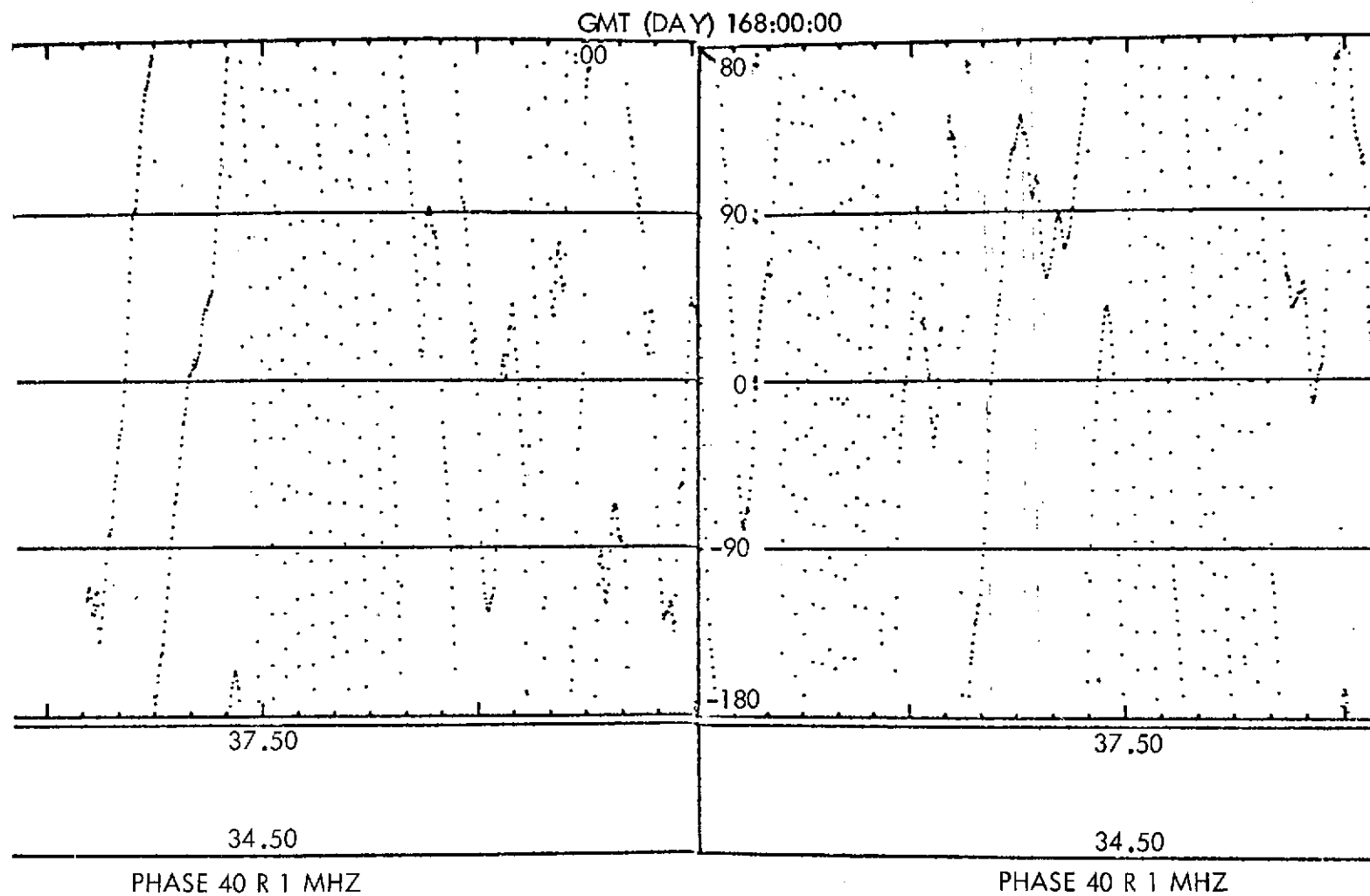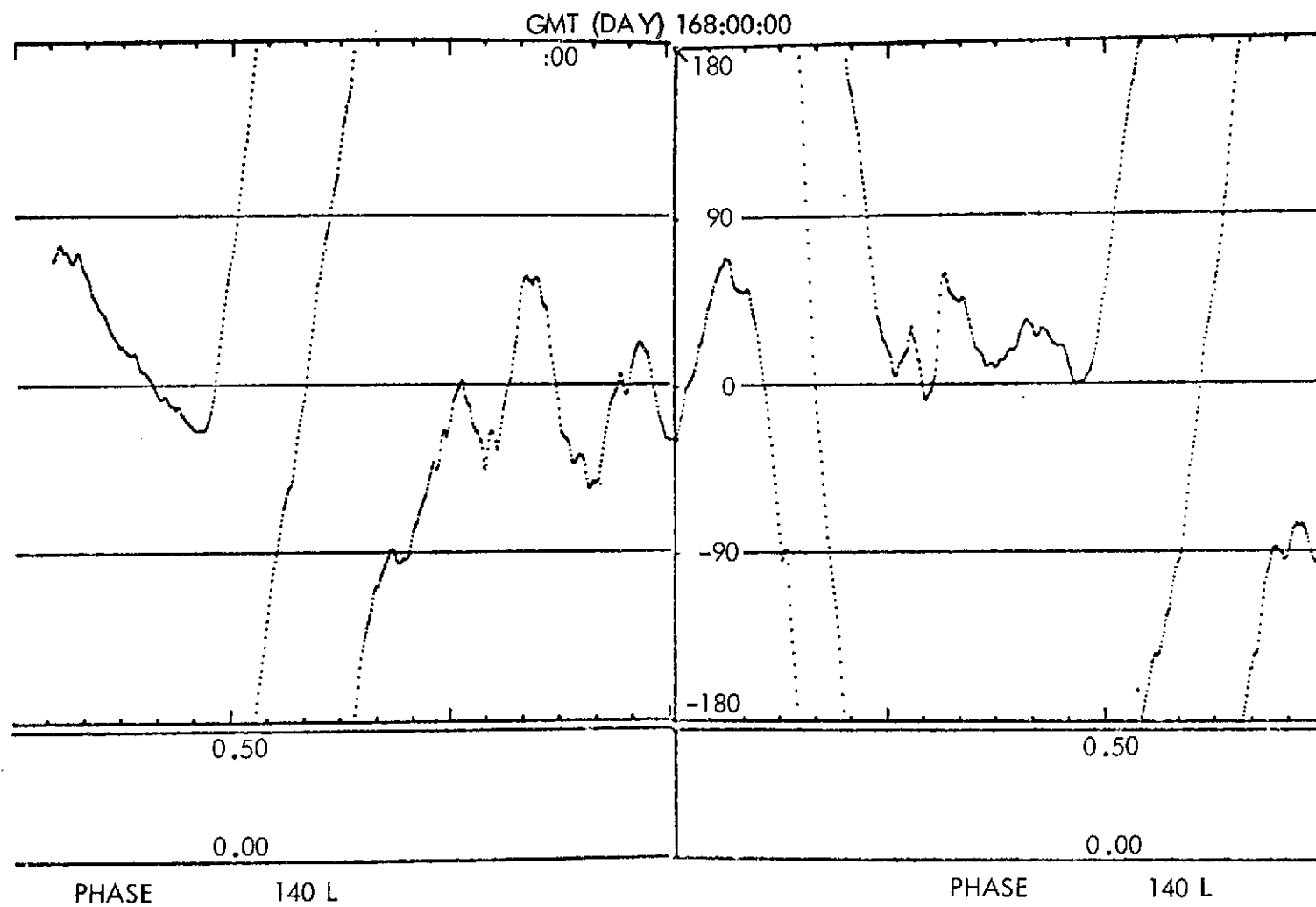on 160 MHz Beacon, Day 168

24-19

GMT (DAY) 168:00:00

Figure 24-12. Phase Angle of 1 MHz Modulation
on 160 MHz Beacon, Day 168

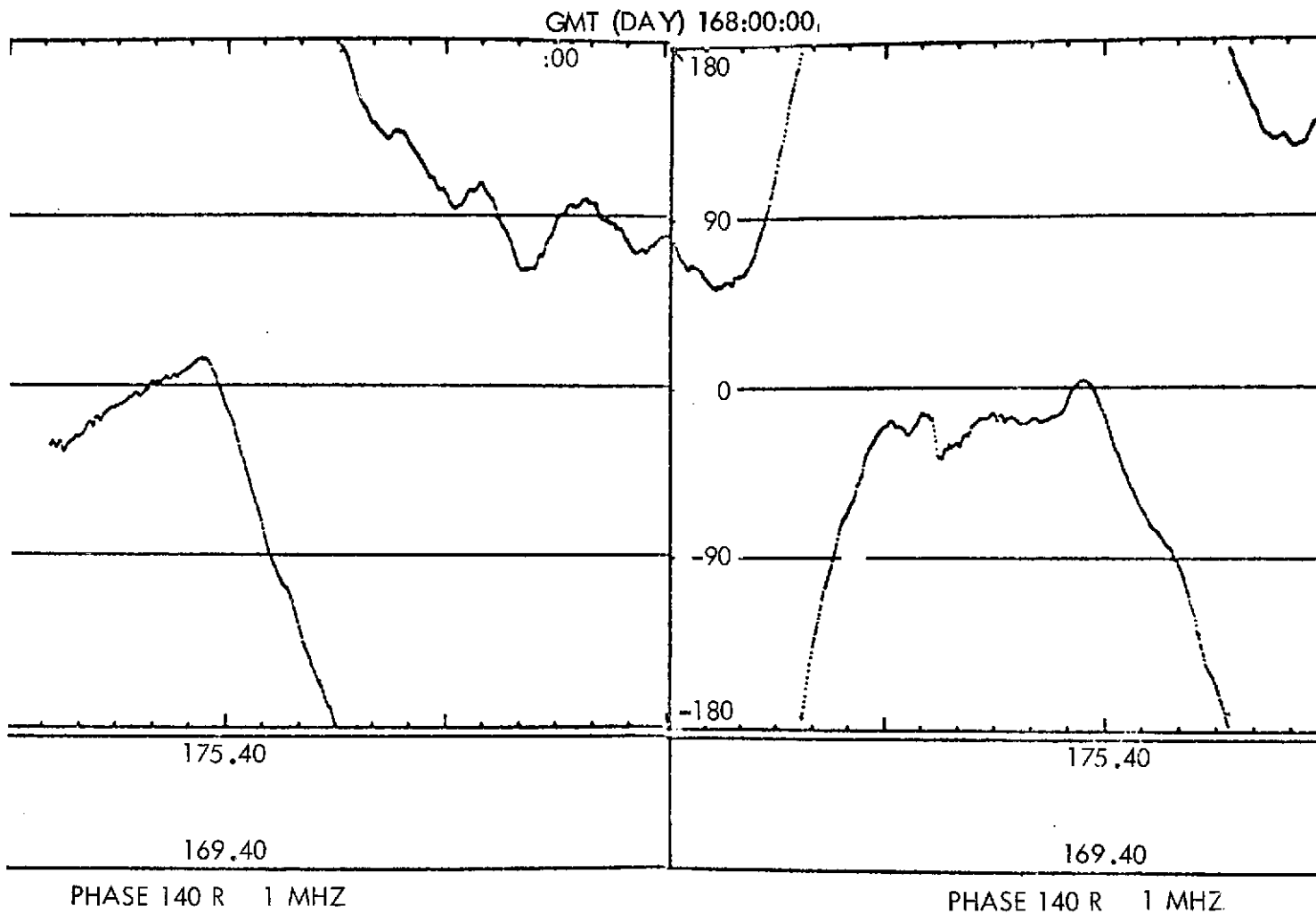Figure 24-13. Phase Angle of 100 KHz Modulation
on 40 MHz Beacon, Day 168

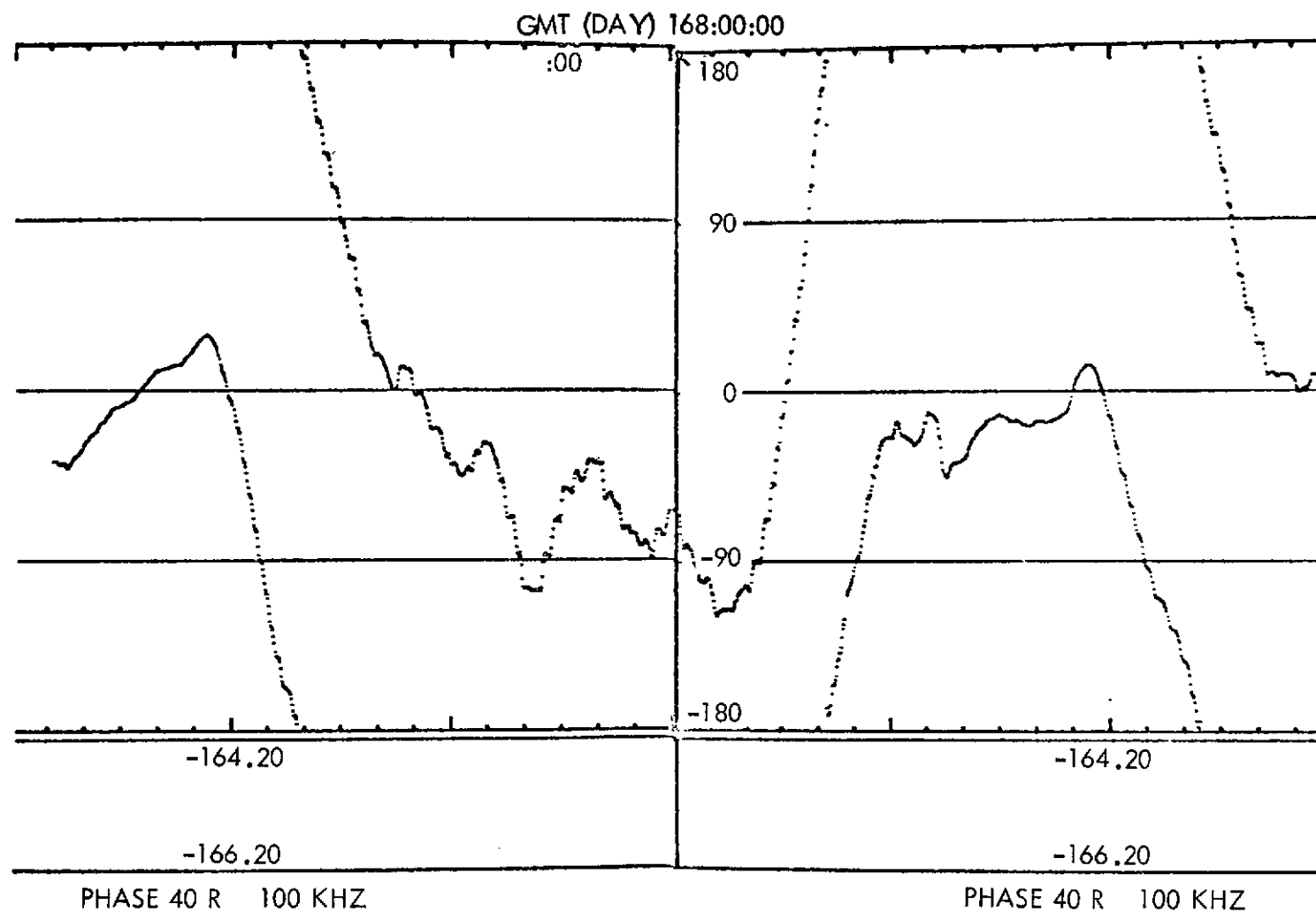GMT (DAY) 168:00:00

Figure 24-14. Phase Angle of 1 MHz Modulation
on 40 MHz Beacon, Day 168

24-22

24.4.6 Transmitter Performance Evaluation

In general the transmitter appears to be functioning well. The housekeeping telemetry values appear to be stable and are not showing any evidence of drift. Measurements by several organizations of EIRP as seen from the ground show good agreement with the preflight predictions. Two anomalies exist.

The condition noted in the prelaunch all-up radiation tests of a mismatch of the 40-MHz antenna has persisted under flight conditions. The ALC loop voltage monitor is showing zero telemetry counts, under normal conditions, and a small reading under modulation-off conditions. Measurements of sideband EIRP on the ground show a significant unbalance in favor of the upper 1-MHz sideband suggesting a reactive load on the transmitter. It is planned to make more measurements using the Boulder satellite mockup and the engineering model transmitter to try to simulate the observed conditions. The loss of the ALC function is not considered a major loss in scientific value; however the condition does call into question the prelaunch modulation phase calibration. A comparison of absolute group delays observed at the two carrier frequencies 140 and 40 MHz, should be completed shortly. If good agreement is obtained, it would considerably increase confidence in the 40-MHz transmission. If agreement is not good, it will be necessary to fall back on rather unsatisfactory hypothesizing to reestablish on calibration zeros. Digital telemetry data from the prelaunch radiating test is not available presently. This will be required for comparison with the engineering model data.

Three reasons for the anomaly seem possible:

   a. The flight antenna developed a fault between prelaunch testing and the flight condition.

   b. The flight antenna on the satellite has always been different to the Philco WDL mockup for impedance matching.

   c. The Philco WDL mockup was in some way incorrect at the time impedance matching was carried out.

In view of the prelaunch condition observed, (a) seems unlikely. In view of the similar behavior of the Boulder 40-MHz mockup and the inability to obtain a correct match by the procedure specified, (c) seems the most likely.

The second anomaly in performance concerns the 360-MHz polar diagram. Much larger changes in ground signal strength have been observed when dish pointing changes have been made than would have been expected from the Philco WDL

prelaunch polar diagrams. A quantitative evaluation has not been started because the digital data tapes containing the dish pointing information have not become available. At Boulder, ±2 dB variations have been observed for quite small maneuvers, such as Rosman to Rocky Mountain West. Other observers have reported ±4 dB for the same maneuver. It appears that the polar diagram may have a much sharper cutoff or lobe structure than anticipated. No operational difficulty due to this has been reported, but a marginal receiver installation could clearly have problems as might an observer considerably distant from the nominal footprint center. (All observations so far have been close to this center.) Fortunately no associated group delay changes have been observed, although AFCRL has reported differential changes in the 1-MHz sideband levels at 360 MHz during maneuvers.

Tables 24-5 through 24-7 contain the preliminary summary of transmitter calibration data, including EIRP, and Figure 24-15 shows location of RBE antennas on ATS-6.

24.4.7 Scientific Studies

24.4.7.1 Introduction – Ionospheric data have been collected fairly continuously from June 16, 1974, to the present, and several interesting events have taken place. In particular, two relatively large solar flare enhancements of total electron content (SITECs) occurred on July 4 (near 1353 GMT, 0653 LST) and on July 5 (near 2141 GMT, 1441 LST). An ionospheric storm occurred on July 4-5.

24.4.7.2 Plasmasphere-Ionosphere Coupling – The modulation phase measurements yield the total content (N_T) between satellite and receiver whereas the Faraday rotation measurements give the electron content N_I up to a height of around 1500 km. The difference gives a measure of the line-of-sight electron content N_P of the plasmasphere

$$N_P = N_T - N_I .$$

The flux F of electrons into or out of the ionosphere in a time t sec is

$$F = \frac{N_P}{t} .$$

Some representative data for the period 0230-1100 GMT on July 4 are:

$$\phi_{40.1} (R) = 585° = 1.625 \text{ cycle}$$

$$\Omega_{140} = 505° = 1.403 \text{ cycle}.$$

Table 24-5
RBE Transmitter Calibration Data

Signal Component	Preflight		Ground Measurements		
	Nominal	Predicted	AFCRL*	U. of Ill.**	SEL Boulder***
40 MHz	+27	+28.8	+26.9		+27
40 MHz 100 kHz USB	+24	+23.8	+23.9		+24.7
40 MHz 100 kHz LSB	+24		+24.9		+24.1
40 MHz 1 MYz USB	+27	+26.8	+29.6		+31.2
40 MHz 1 MHz LSB	+27		+23.7		+26.5
140 MHz	+32	+32.3		+32	+32
140 MHz 1 MHz USB	+26	+26.3			+25.9
140 MHz 1 MHz LSB	+26				+26
360 MHz	+33	+34.9		+35	+33
360 MHz 100 kHz USB	+24	+25.6		+27	+24.1
360 MHz 100 kHz LSB	+24			+26	+22.3
360 MHz 1 MHz USB	+24	+24.7		+25	+22.6
360 MHz 1 MHz LSB	+24			+25	+22.0

*Based on a radiometric measurement calibrated against CASS A source.
**Based on nominal illumination efficiency for a parabolic antenna.
***Based on nominal AFCRL pattern integration gains for SBF array antennas.
Absolute values are ±2 dB. Relative sideband amplitudes are ±0.5 dB.

Table 24-6
Modulation Phase with Respect to 360 MHz

Measurement	Flight Transmitter at 25°C Terminated in 50 Ω	Satellite Antenna Correction	Net
40 MHz 100 kHz USB	-1°	-7°	-8°
40 MHz 1 MHz USB	+12°	+85°	-73°
140 MHz 1 MHz USB	-58°	-5°	-63°

Table 24-7
Polarization Characteristics

Frequency	Polarization Angle (Degrees)	Cross Polarization* (dB)
40 MHz	0°*	> 10
140 MHz	0°	> 22
360 MHz	+22°	> 20

Note:
The polarization angle is measured with respect to the +X spacecraft axis as 0° and +Y as 90° (see Figure 24-16).
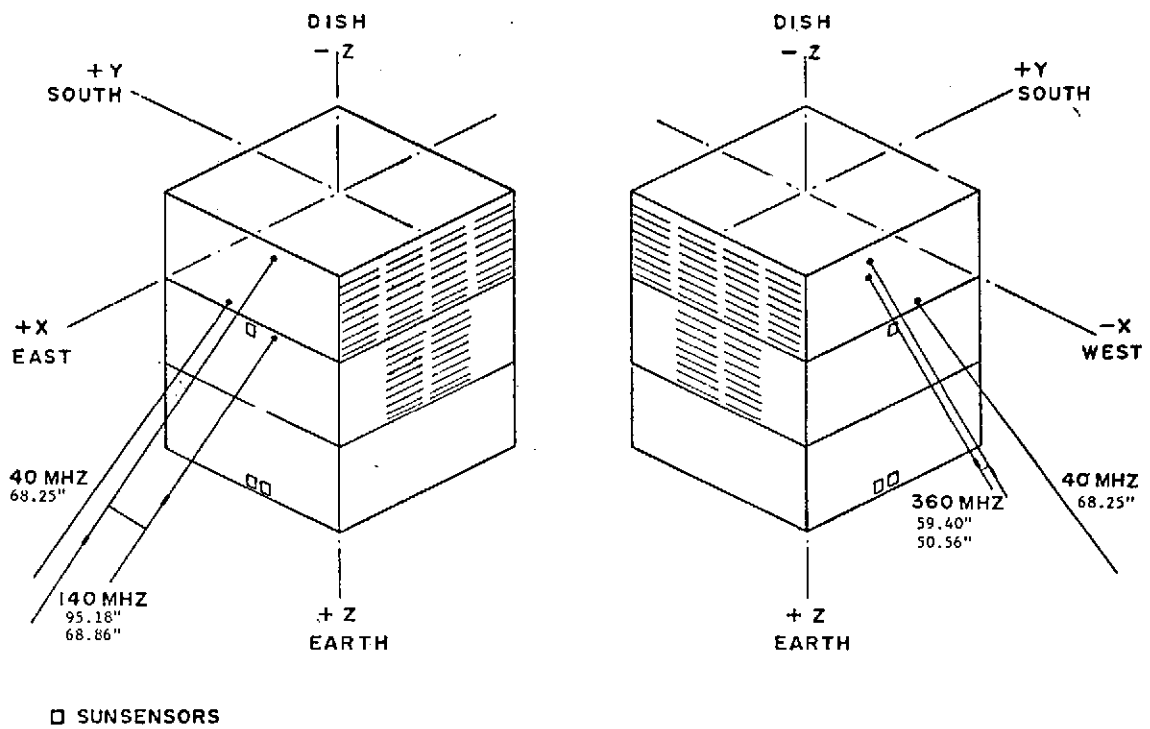
*Measured on scale model.

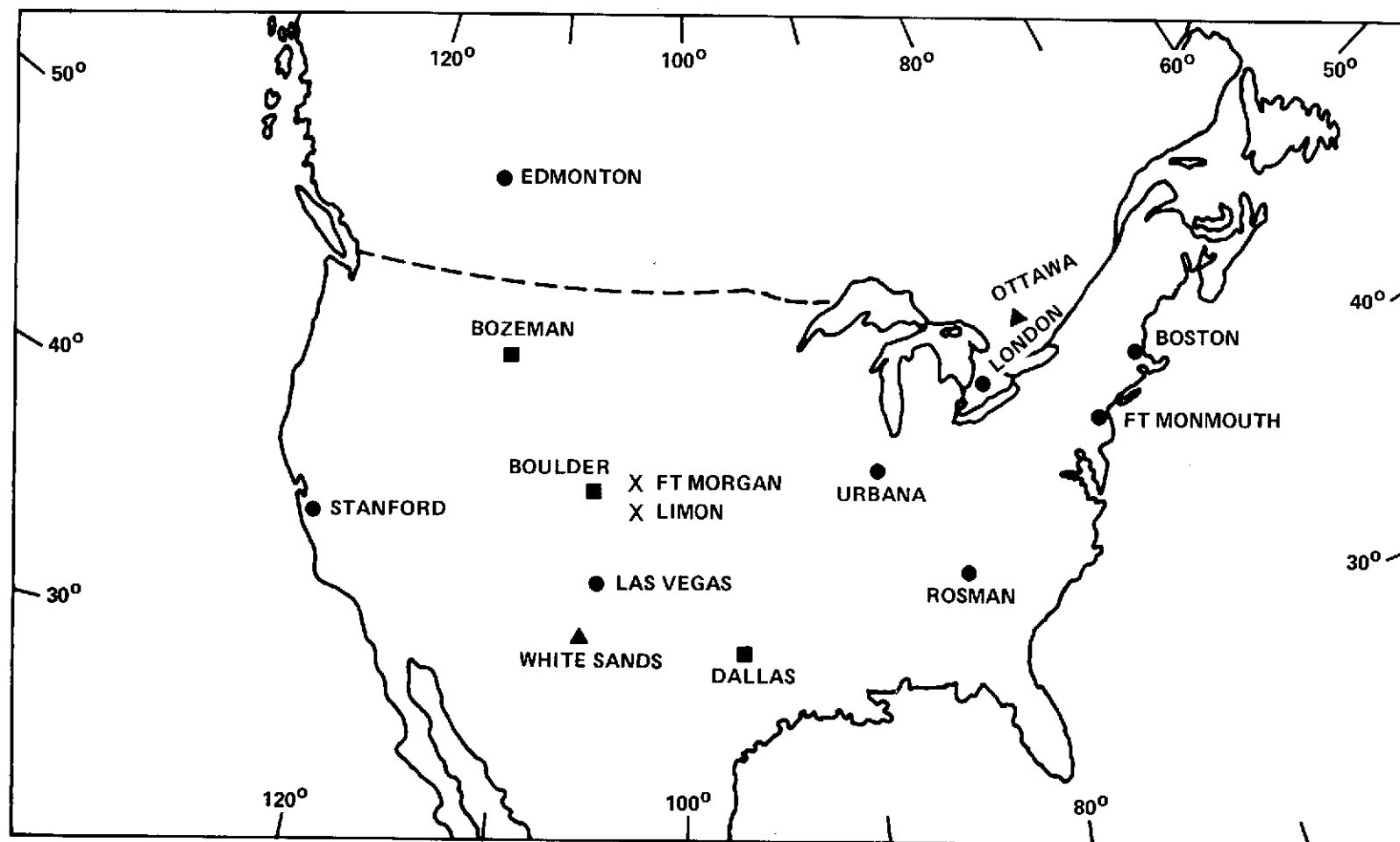Figure 24-15. EVM Layout Showing Communication Subsystem Location

Figure 24-16. Location of Receiving Equipment for the ATS-6
Related Observations

Change in contents are:

$$\Delta N_T = 1.391 \times 10^{17} \ m^{-2}$$

$$\Delta N = 1.302 \times 10^{17} \ m^{-2}.$$

Hence $\Delta N_P = 9 \times 10^{15} \ m^{-2}$ in 8.5 hours, i.e., $F = 3 \times 10^7 \ cm^{-2} \ sec^{-1}$. This value of electron flux is within the range 2 to $4 \times 10^7 \ cm^{-2} \ sec^{-1}$ found for magnetically quiet conditions by other techniques; e.g., whistlers.

24.4.7.3 Sudden Increases of Total Electron Content — Two relatively large SITECs occurred, the first near 1353 GMT on July 4 and the second near 2141 GMT on July 5, both being associated with visible and X-ray flares. These short-lived events provide unique opportunities to study electron production in the ionosphere because the loss and movement terms in the equation of continuity are small. Hence, the integrated production rate Q is given approximately by the time rate of change of N_T.

Measurements of the two enhancements give:

$$\text{July 4: } Q_T = 2 \times 10^{13} \ m^{-2} \ sec^{-1}$$

$$\text{July 5: } Q_T = 6 \times 10^{13} \ m^{-2} \ sec^{-1}.$$

Modulation phase changes for the July 4 flare show that

$$\Delta N_T = 3.483 \times 10^{17} \ m^{-2}.$$

The Faraday rotation measurements can be reconciled with this value provided that the additional plasma is produced at a mean height near 175 km. On the assumption that this occurs over a height range of 200 km and taking the electron density as $2 \times 10^{11} \ m^{-2}$, we find that the fractional increase in electron density is of the order of 60 percent.

24.4.7.4 Amplitude Fluctuations

Short period (≈ 1 min) fluctuations in amplitude have been observed on all frequencies, although they are more common on 40 MHz than on 140 MHz and more on 140 MHz than on 360 MHz. These fluctuations, which can be important in satellite-to-ground communications, are caused by interference between signals transversing slightly different ray paths in an irregular ionosphere. Sometimes, rythmic oscillations build up which end with almost complete signal cancellation even on 360 MHz. Given the height of the irregularities, it is possible to estimate the speed of the responsible irregularities.

SECTION 25

SPACECRAFT ATTITUDE PRECISION POINTING AND

SLEWING ADAPTIVE CONTROL

(SAPPSAC)

SECTION 25

SPACECRAFT ATTITUDE PRECISION POINTING AND
SLEWING ADAPTIVE CONTROL (SAPPSAC)

25.1 INTRODUCTION

A series of slew and hold maneuvers designed to obtain simultaneous spacecraft attitude sensor data was conducted and the data is being processed for sensor calibration data.

The SAPPSAC PDP-11 computer at Rosman has been employed extensively for on-line attitude determination.

SAPPSAC and interferometer tests performed to date have shown that the C-band and VHF command/telemetry links are of high quality.

The SAPPSAC safety position freeze mode, which fixes the target coordinates at the last computer attitude, was successfully demonstrated during one of the slew maneuver attempts when incorrect position entries were made to the SAPPSAC computer.

25.2 SCIENTIFIC OBJECTIVES

The objective of this experiment is to evaluate the feasibility of a real-time computer-controlled ground system for long term attitude control and orbit determination of a geosynchronous spacecraft through an RF command and telemetry link. There are advantages, associated primarily with spacecraft reliability and versatility, if the complicated logic associated with spacecraft control can be ground based so that control operations can be reprogrammed in case of changes in the spacecraft mission or malfunctions during operation. This experiment is expected to provide the data to lay the necessary foundation for the development of future ground based spacecraft control systems which would perform many of the essential functions now performed on board the spacecraft.

25.3 EXPERIMENT DESCRIPTION

Figure 25-1 shows a SAPPSAC schematic illustrating the spacecraft and ground portions of the control system. For this experiment a ground based computer is programmed to put ATS-6 through a series of attitude maneuvers using the spacecraft's radio frequency Interferometer, the Attitude Control System, and the Spacecraft Propulsion System. These include precision pointing to fixed
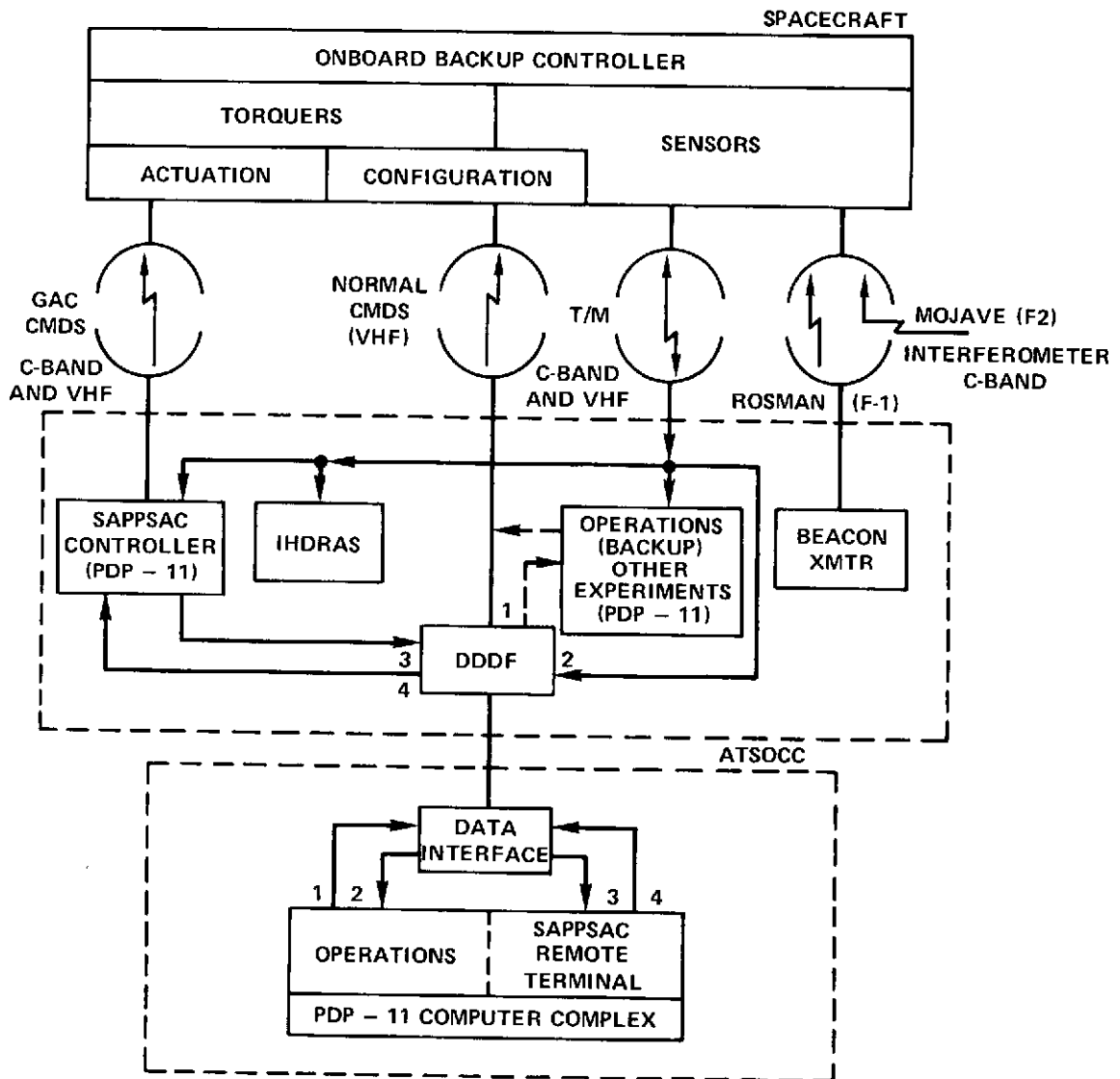
Figure 25-1. SAPPSAC Operations Diagram

targets, slewing between targets, tracking of moving targets, and the generation of prescribed ground tracks.

25.4 EXPERIMENT PERFORMANCE EVALUATION

25.4.1 SAPPSAC Early Evaluation

The Spacecraft Attitude Precision Pointing and Slewing Adaptive Control (SAPPSAC) experiment successfully completed in-orbit operations support for the ATS-6 spacecraft during the first 30 days following launch. The effort included on-line attitude determination at Rosman using the SAPPSAC PDP-11 computer during the first five days of in-orbit checkout. This was followed by subsequent off-line data analysis at GSFC pertaining to preliminary attitude sensor evaluation and interferometer bias determination. The following onboard sensors were evaluated: YIRU, Earth Sensor, Polaris Sensor, and Interferometer. On-line attitude determination using the Earth Sensor and Interferometer successfully tracked the yaw reference maneuver (roll, pitch, and yaw attitudes). Both single station and two station Interferometer tests were performed with the Earth Sensor and near-local vertical conditions. It was found that the 3-axis attitude determination performed using the EAS/F1 Interferometer, ESA/F2 Interferometer, and F1/F2 Interferometer were in agreement to within 0. 02° in roll, 0.06° in pitch, and 0.6° in yaw using zero bias corrections (preflight reference for SAPPSAC). Interferometer receiver/converter biases were measured and used to improve attitude computations. The spread in pitch and roll data was subsequently reduced to better than 0. 035° and less than 0. 4° in yaw. Rosman pointing data revealed that attitude determination using the Polaris 2 sensor produced a bias of about 0. 2° relative to other available combinations using the Earth Sensor and Interferometer. The availability of simultaneous telemetry from the Earth Sensor and two station Interferometer was used in a SAPPSAC algorithm to determine spacecraft orbital position as a function of time. This data was compared with a ranged orbit ephemeris near epoch for an interval of approximately 2 minutes. The following results were obtained:

$$Longitude\ Position\ Error = -2.4 \pm 9\ KM$$
$$Latitude\ Position\ Error\ \ = -0.8 \pm 9\ KM$$
$$Radial\ Position\ Error\ \ \ \ = \ \ \ 0.4 \pm 2\ KM$$

The short span of data reduced gives a 70% confidence level that the means are inside the given bounds. A report summarizing this work was submitted to the ATS-6 Project on 12 July 1974.

25.4.2 ATS-6 SAPPSAC Experiment Flight Test Status

Two SAPPSAC and two Interferometer High Data Rate Acquisition System (IHDRAS) tests have been performed to date. The two SAPPSAC tests showed that the command/telemetry link (used by SAPPSAC) is of high quality.

GAC was commanded using both C-band (on the 85-foot antenna) and VHF with no dropouts or required resyncs. No errors were found in the dwell telemetry. The two IHDRAS tests must be rescheduled due to hardware problems. The Rosman 15-foot antenna was not available, and the Kennedy tape recorder in the IHDRAS hardware malfunctioned.

25.4.3 SAPPSAC Sensor Calibration Test

On Monday, August 19, 1974, the SAPPSAC tested a series of slew and hold maneuvers for ATS-6 designed to obtain simultaneous attitude sensor data over large areas of the Earth's disk. These maneuvers were performed by the onboard DOC controller. This data is being processed to generate calibration corrections which will give consistent attitude determination using the available SAPPSAC sensor combinations.

25.4.4 ATS-6 SAPPSAC Experiment Flight Test Results

On Friday, August 23, 1974, the SAPPSAC experiment was successfully used for on-line attitude control of the ATS-6 spacecraft for a period of approximately 2-1/2 hours. Following initial transfer from onboard DOC control to ground control, SAPPSAC maintained a local vertical pointing mode for 2 hours. During this time the following sensor combinations were briefly selected for control computations; Earth sensor/Polaris 2 sensor, Earth sensor/Rosman interfero-meter (F1), Rosman Interferometer (F1)/Mojave interferometer (F2), and Rosman interferometer (F1)/Polaris sensor. Attitude pointing behavior was found to be stable and nominal for all sensor combinations except Earth sensor/Rosman interferometer (F1), which exhibited a relative yaw bias. This behavior was found to be in agreement with previous SAPPSAC launch support data which indicated that one should expect a relative yaw bias of about 0.25 degree. It was demonstrated that SAPPSAC could hold the spacecraft Z body axis to within 0.04° roll and 0.05° pitch of local vertical, while maintaining bearing within 0.25° of North. Attitude excursions peak-to-peak during the same intervals were 0.02° roll, 0.04° pitch, and 0.07° yaw. This performance was obtained with a control update interval of 2-1/2 minutes which can be decreased to obtain tighter control. During this test SAPPSAC also demonstrated the ability to return to local vertical following a short drift period to introduce attitude errors. Also, during this test ATSOCC experienced two periods where Rosman telemetry was lost due to microwave interference. SAPPSAC provided attitude status

via SCAMA line during the first interruption which lasted approximately 5 minutes. In the second interruption period, ATSOCC maintained telemetry data from the line to Mojave.

Although SAPPSAC functioned in an acceptable manner throughout local vertical hold, several operational problems were encountered. These dealt primarily with triggering of alarms in the ground computer when failure modes did not exist. The causes of such behavior are currently under investigation. No attempt was made during this test to alter screening limits, filter gains, and control parameters in order to improve overall performance.

Following the period of local vertical hold, ATSOCC requested the demonstration of a slew maneuver to reorient the spacecraft Z body axis to -88° longitude and 6° latitude. Due to entering the wrong computer input (-88° longitude and 0° latitude), this maneuver did not proceed as expected; however, the spacecraft did move properly to the commanded coordinates. This was soon found in the output display, and a new entry was attempted. The second attempt (once again in error) gave commanded coordinates of -1.5° longitude and 6° latitude. When it was seen that the spacecraft was accumulating a large pitch error, the decision was made to go to the SAPPSAC position freeze mode which resulted in fixing the target coordinates at the last computed attitude. The spacecraft then proceeded to settle at a longitude of about -74.5° while further diagnostics were performed. The proper target entry was then made and the spacecraft began slewing to -88° longitude and 6° latitude. In the course of this slew, control was transferred back to onboard DOC. This incident clearly revealed the need to improve SAPPSAC procedures for on-line target entry. However, the SAPPSAC safety features precluded any dangerous situation from occurring and return to the expected target was in progress at the time of termination.

On September 23, SAPPSAC successfully demonstrated slewing capability in the vicinity of local vertical. Eight small angle maneuvers were conducted (1° in both pitch and roll angles), followed by individual larger slews of 2° and then 4°. Each maneuver had specified pierce point coordinates (Z Body Axis/Earth Intercept) and maximum body rate limits as commanded by SAPPSAC computer input. A final slew to local vertical was followed by activation of an adaptive feature of the state estimator, which performs identification of un-modelled disturbance torques on each of the three body axes. The adaptive estimator functioned in an excellent manner, as evidenced by slight changes in spacecraft pointing which rapidly converged to within 0.02° latitude and longitude of sub-satellite coordinates obtained from orbit ephemerides. All slewing maneuvers were performed using a 3.5 minute control update, and it was found in all cases that no more than three updates were needed to complete a slew. Maximum latitude overshoot was less than 0.3° which is equivalent to approximately 0.05° in roll angle. Maximum

longitude overshoot reached values as high as 0.8° which is equivalent to approximately 0.13° in pitch angle. It was observed that all easterly slews generated longitudinal undershoots, whereas all westerly slews generated longitudinal overshoots. This was attributed to presence of un-modelled disturbance torques acting in the pitch axis, since the adaptive estimator had not yet been activated.

On September 28, SAPPSAC successfully demonstrated the ability to provide attitude hold during offset pointing to Rosman station. This test, which lasted about 8 hours, provided the first opportunity to assess the attitude stabilization capability using different sensor combinations, different control updates, and adaptive disturbances. It was found that SAPPSAC, when using the ESA/PSA as control sensors in an 8 frame update, has the capability of stabilizing both latitude and longitude to better than 0.035°(p-p) for an interval of more than 15 minutes. This is equivalent to pitch and roll angle stabilization of about 0.005° over this period. Short term stabilization less than 10 minutes indicate better than 0.004° in roll and better than 0.003° in pitch angle. The control center display (ONATT) indicated that SAPPSAC has a pointing accuracy of better than 0.11° latitude and 0.01° longitude. These figures, taken together with the bearing angle accuracy, indicate 3 axis attitude stabilization to better than 0.01° in pitch and roll and 0.02° in yaw. The adaptive estimator was active and successfully tracked changing disturbance torques throughout the test period. SAPPSAC also demonstrated in this test that control can be switched between the ESA/PSA, ESA/F1 Interferometer, and PSA/F1 Interferometer with pointing angle perturbations less than 0.1° latitude and longitude. Using the PSA/Interferometer combination, it was found that for a 10 frame control update, SAPPSAC can achieve stabilization of within 0.02° latitude and longitude of reference intercept coordinates 35.200° latitude and -82.9° longitude. This produces short term pitch and roll angle stabilization better than 0.003°. When controlling with the ESA/F1 Interferometer, it was found that an initial yaw bias of approximately 0.1° was introduced. Further, greater noise was experienced in the yaw axis due to magnification of ESA noise when used to compute yaw. Stabilization in pitch and roll was found to be similar to that obtained using PSA/F1 Interferometer, whereas yaw errors reached 0.05°. Because Interferometer F2 channel was not operational during this test, SAPPSAC was unable to evaluate the remaining sensor combinations. Ability to maintain precise attitude stabilization was, however, seriously degraded when either pitch or roll wheels passed through the tachometer dropout region. This occurred during the test when wheel speeds dropped to about 20 RPM. The tachometer dropout condition produced oscillatory responses in pointing which exceeded 1° (p-p) in latitude and longitude for a short period of time. SAPPSAC was able to maintain control throughout these periods. Following the first such occurrences, several operational refinements were introduced to minimize the attitude disturbances; (1) reduce the control update interval to provide faster response after tach dropout, and (2) fix the adaptive disturbance gains to

zero prior to entering the dropout region. These refinements reduced subsequent oscillations to 0.3°. SAPPSAC also operated without difficulty throughout several periods of sensor anomaly (Polaris hits and interferometer ground transmitter transients). As part of the reliability assessment, SAPPSAC was operated in a mode which removed telemetry inputs from the control computation for a period of about 45 minutes: This simulated a condition where telemetry was lost and control was maintained with predictions from the state model. It was found that attitude errors grew to less than 0.5° in roll, 0.1° in pitch, and 0.4° in yaw. These changes posed no problem in loss of sensor acquisitions and therefore demonstrated that SAPPSAC can operate on its stored math model without telemetry for a duration of more than 1 hour. This should permit adequate time to re-configure ground equipment to restore spacecraft telemetry. Previous tests had shown that without SAPPSAC, GAC commands such as open loop control, could not be maintained for more than 15 minutes without danger of losing PSA or ESA sensor acquisition.

APPENDIX A

THE NOAA/MPI OBSERVATION PROGRAM
FOR
THE ATS-6 RADIO BEACON EXPERIMENT

APPENDIX A

THE NOAA/MPI OBSERVATION PROGRAM FOR THE
ATS-6 RADIO BEACON EXPERIMENT

A-1. INTRODUCTION

The ATS-6 geostationary satellite, to be launched on or about June 1, 1974, has aboard amplitude modulated radio transmitters on frequencies near 40, 140, and 360 MHz for the measurement of the integrated electron content of the ionosphere and plasmasphere. Information on the general properties of the satellite are contained in the ATS-6/7 Handbook (1972) and on the Radio Beacon Experiment by Davies, Grubb, and Fritz (1972).

In June 1972, the National Oceanic and Atmospheric Administration (USA) and the Max-Planck Institute for Aeronomy (Germany, FDR) entered into a cooperative agreement for the operation of radio receivers in the vicinity of Boulder. Similar but separate arrangements have been made between MPI and Montana State University and between MPI and the University of Texas, at Dallas.

On confirmation that the radio beacon transmitters are operational, the MPI will ship their gear to the USA. This should be in July 1974, in readiness for an intensive period of observations lasting about 4 weeks, i.e., covering August 1974, roughly. Actually the receivers will remain in the USA for about 9 months during which time routine observations of the beacon signals will be conducted.

One of the aims of the joint enterprise is to study the equatorward development of the negative phases of ionospheric storms. The satellite technique has several advantages compared with ionosondes for this type of work, for example: firstly, the high time resolution and, secondly, the signals are relatively immune to radio blackout; also the ray path does not suffer large lateral deviations. Unfortunately because of successive delays in launch, the satellite operation will take place at a time of low solar activity when ionospheric storms are infrequent.

Another objective is to study traveling ionospheric disturbances which are of two types: (a) the large scale disturbances associated with ionospheric storms and (2) the medium scale TIDs thought to be generated in the troposphere. In particular, it is hoped to confirm (or deny) the season pattern of TID propagation found by Davies and Jones (1971).

A third objective is to see to what extent it is possible to determine changes in the electron content of the plasmasphere by combining satellite and ground radio data.

It should be borne in mind that the experiments described here will be only part of a larger recording program (see Figure A-1) involving receivers at Edmonton, Alberta; Stanford University, Calif.; Urbana, Illinois; Rosman, North Carolina; London, Ontario; Fort Monmouth, New Jersey; Boston, Massachusetts; and, possibly, several other sites. Indeed, it is possible that some or all of the operators of these receivers will want to cooperate in the intensive recording interval.

A-2. RADIO TECHNIQUE

The basic ATS-6 measurements (see Figure A-2 for illustration) are:

1. <u>Faraday rotation</u> Ω which gives a measure of the ionospheric electron content

$$I = 4.228 \times 10^{-5} \ f^2 \ C\Omega \tag{1}$$

$$C^{-1} = \overline{B_L \ \sec \ \chi} \tag{2}$$

where f is the wave frequency (Hz), B_L is the longitudinal component of the geomagnetic field, and χ is the angle between the radio ray path and the vertical. Because the geomagnetic field strength falls off approximately as the cube of the radius vector, the Faraday rotation technique gives a measure of the integrated electron content (I) up to a height of about 1500 km.

The ambiguity in counting integral numbers of half-rotations is resolved by measuring the differential rotation $\Delta\Omega$ on two closely spaced frequencies f and f + Δf,

$$\frac{\Delta\Omega}{\Omega} = -\frac{2\Delta f}{f} \tag{3}$$

2. <u>Phase dispersion</u> $(d\phi/df)$ gives a measure of the content integral N_T between observer and satellite with only a minor influence of the geomagnetic field. The total content is given by

$$N_T = 7.452 \times 10^6 \ f^2 \ (d\phi/df). \tag{4}$$

3. <u>Angle of arrival</u> departures from the straight line satellite-receiver path gives a measure of the horizontal gradient of total electron content.

4. <u>Transmission</u> from the Navy Navigation Satellite System (NNSS) satellites will be used by Dr. G. Schmidt of MPI to make dispersive Doppler in Boulder. These measurements will enable us to determine whether the holographic technique (e.g., see Schmidt, 1972) is effective at Boulder. At the same time, C. Rufenach (NOAA) will make measurements of amplitude and phase scintillations using ATS-F signals.

Figure A-1. Location of receiving equipment for the ATS-F related observations
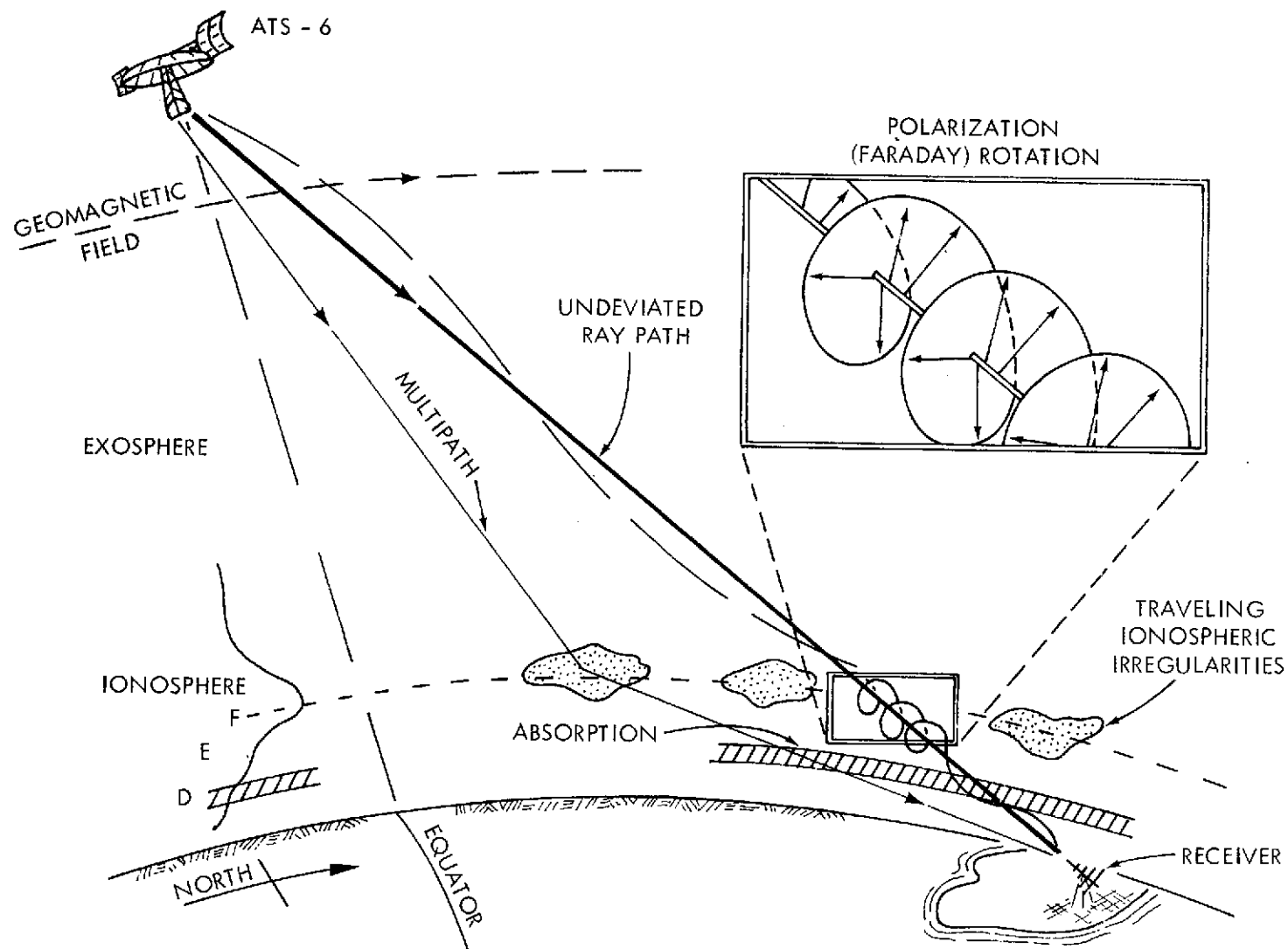
Figure A-2. Geometry of radio ray paths between geostationary satellite and a receiver on the ground

5. Amplitude measurements give a measure of ionospheric (D region) absorption.

6. Additional measurements which may be available in the Boulder vicinity include observations of ionospheric motions and irregularities using the kinesonde (Wright) and airglow (Hernandez).

A-3. OBSERVATIONS

The ATS-6 satellite is expected to spend about a year over the Western Hemisphere (94°W) and then move to 35°E for the Satellite Instructional Television Experiment. In the latter position, the beacon will be available to observers in Europe, Africa, and part of Asia. During the first period, when the satellite is over the Western Hemisphere, the Max-Planck Institute, Lindau, Federal Republic of Germany, will bring several receivers to the USA as part of a cooperative program with the Space Environment Laboratory of the National Oceanic and Atmospheric Administration, Boulder, Colorado.

The MPI will bring over two receivers capable of measuring both phase dispersion and Faraday rotation. These will be located at Montana State University, Bozeman, Montana (Dr. Robert Leo), and at the University of Texas at Dallas (Dr. W. B. Hanson). The NOAA receivers will be located in Boulder, Colorado so that a wide range of latitudes is available for the study of large scale phenomena such as ionospheric storms.

A-4. THE PLASMASPHERIC CONTENT

One of the main objectives of the NOAA/MPI intensive observing program is the determination of the electron content of the plasmasphere. The plasmasphere content between Boulder and ATS-F lies between about 0.1 I by day and 0.5 I by night where I is the ionospheric content. Thus, it is seen that most of the plasma lies in the ionosphere. One measure of the plasmasphere content N_p is the difference between the total content, as measured by phase dispersion, and the ionospheric content I, obtained from Faraday rotation, i.e.,

$$N_p = N_T - I_F.$$ (5)

The difficulty with this approach is that N_p is heavily dependent on the accuracy of I. The measured ionospheric content I_F depends not only on the true content but on height of the ionosphere and its shape. Since much of the ionospheric plasma lies near the F2-layer peak, changes in profile near the peak will tend to determine the measured values of I_F and, hence, N_p.

An alternative method is to measure total electron content using a satellite with a relatively low orbit. The U. S. Navy Navigation Satellite (NNSS) have nearly circular, near polar orbits at approximately 1100 km altitude and radiate radio signals on 150 MHz and 400 MHz. From measurements of the dispersion between these carriers, the total content can be obtained. Some drawbacks of this method are: (a) the tracking of the satellites, (b) the presence of more than one satellite in the antenna beam at a given time, (c) differences between the locations of the ray paths to the geostationary satellite and to the orbiting satellite.

The MPI will locate the necessary NNSS receiving equipment near Boulder and Dr. R. Leitinger of the University of Graz, Austria, will locate a receiver near Las Vegas, New Mexico, about 400 km south of Boulder.

A topside sounder can provide information on the electron profile and content between the satellite orbit and the peak of the F2 layer. Combining bottomside profiles with topside profiles should enable us to determine the content to the height of the sounding satellite. It is hoped that during the period of intensive observation, the ISIS-I and ISIS-II satellites telemetry can be acquired by the Communications Research Centre at Ottawa (Dr. Eldon Warren) when the sounders are heights greater than 1200 km in the vicinity of the ATS-6 to Boulder ray path. Since ISIS-I has an apogee of 3523 km and a perigee of 574 km, there should be plenty of opportunity to observe with that sounder. Also since ISIS-II is in a 1400 km nearly circular orbit, it should provide adquate opportunity.

For the determination of the electron content of the bottomside, we shall rely on interpolation of ionograms at Boulder and at White Sands, New Mexico.

In order to check the effectiveness of these techniques, it would be useful to have available additional profile information such as provided by incoherent scatter sounders (Evans) and plasmaspheric (tube) content from whistler observations (Carpenter and Park).

A-5 TRAVELING IONOSPHERIC DISTURBANCES (TIDs)

TIDs will be monitored using three spaced (Faraday) receivers located at the corners of an approximately equilateral triangle with sides of about 100 km. One of these receivers will be the NOAA computer controlled receiver at Table Mountain near Boulder; the others (1 NOAA, 1 MPI) will be simple Faraday polarimeters and are to be located near Fort Morgan and near Elbert, both in Colorado.

It is planned to transmit the data from the two outlying stations to Table Mountain by radio link where they will be recorded on a single tape thus avoiding timing difficulties at the three sites.